UILU-ENG-98-2004

CIVIL ENGINEERING STUDIES
Transportation Engineering Series No. 97
Illinois Cooperative Highway and Transportation
Series No. 263

ISSN-0197-9191

MECHANISTIC-EMPIRICAL EVALUATION OF THE Mn/ROAD MAINLINE FLEXIBLE PAVEMENT SECTIONS

Report Preparation by

C. Alvarez
M.R. Thompson

Cooperative Evaluation of
Mn/Road Test Results to
Illinois Conditions

Project IHR-535
ILLINOIS COOPERATIVE HIGHWAY AND TRANSPORTATION RESEARCH PROGRAM

A cooperative investigation
conducted by the

TRANSPORTATION RESEARCH LABORATORY
DEPARTMENT OF CIVIL ENGINEERING
ENGINEERING EXPERIMENT STATION
UNIVERSITY OF ILLINOIS AT URBANA-CHAMPAIGN

in cooperation with the

STATE OF ILLINOIS
DEPARTMENT OF TRANSPORTATION
and the
MINNESOTA DEPARTMENT OF TRANSPORTATION
Mn/ROAD RESEARCH PROJECT
and the
U.S. DEPARTMENT OF TRANSPORTATION
FEDERAL HIGHWAY ADMINISTRATION

UNIVERSITY OF ILLINOIS
URBANA, ILLINOIS

JUNE 1998

ACKNOWLEDGMENTS/DISCLAIMERS

This study was sponsored by the Illinois Department of Transportation (IDOT) - Division of Highways as part of IHR-535 (COOPERATIVE EVALUATION OF Mn/ROAD TEST RESULTS TO ILLINOIS CONDITIONS). IHR-535 is a cooperative effort between the Minnesota Department of Transportation (Mn/DOT), the Illinois Department of Transportation (IDOT), and the Department of Civil Engineering - University of Illinois @ Urbana-Champaign to provide broad utilization of the data obtained from the Minnesota Road Research Project (Mn/ROAD). The cooperation is facilitated through a **MEMORANDUM OF UNDERSTANDING** between Mn/DOT and IDOT. The generous cooperation and help of the MnROAD staff is acknowledged; particularly the efforts of George Cochran, Thomas Burnham, David Palmquist, and David Van Deusen.

Technical Report Documentation Page

1. Report No.	2. Government Accession No.	3. Recipient's Catalog No.
FHWA-IL-UI-263		

4. Title and Subtitle	5. Report Date
MECHANISTIC-EMPIRICAL EVALUATION OF THE Mn/ROAD MAINLINE FLEXIBLE PAVEMENT SECTIONS	June 1998
	6. Performing Organization Code
7. Author(s)	8. Performing Organization Report No.
CLARIBEL ALVAREZ - MARSHALL THOMPSON	UILU-ENG-98-2004
9. Performing Organization Name and Address	10. Work Unit (TRAIS)
Department of Civil Engineering Engineering Experiment Station University of Illinois at Urbana-Champaign Urbana, IL 61801-2352	11. Contract or Grant No. IHR - 535
	13. Type of Report and Period Covered Project Report
12. Sponsoring Agency Name and Address	14. Sponsoring Agency Code
Illinois Department of Transportation Bureau of Materials & Physical Research 126 East Ash Street Springfield, IL 62706	

15. Supplementary Notes

The cooperation and help of the Minnesota Department of Transportation and the Mn/ROAD project staff are acknowledged.

16. Abstract

This study utilized Illinois DOT (IDOT) mechanistic-empirical (M-E) technology and Mn/ROAD mainline pavement section data and information to verify/refine/modify IDOT M-E analysis and design concepts and procedures for full-depth asphalt concrete (FDAC) and conventional flexible pavements (CFP). The Mn/ROAD mainline flexible pavements include eleven CFP and three FDAC pavement sections. Four different granular materials were used in the conventional flexible pavements. A fine-grained soil subgrade (R-value of about 12) is present throughout the mainline. Laboratory material testing results, field distress measurements, and FWD test data were used to study pavement deflection response and performance (rutting and asphalt concrete fatigue). The study demonstrated that the IDOT M-E analysis and design procedures for FDAC and CFP sections are adequate. The ILLI-PAVE structural model adequately predicts the pavement responses. The use of bi-linear (arithmetic) subgrade model and the "theta" granular material model ILLI-PAVE inputs closely replicate CFP field FWD deflection responses. The effect of granular material quality on CFP deflection response is very limited. The ILLI-PAVE FWD backcalculation algorithms are adequate for estimating the moduli of asphalt concrete and subgrade soils.

17. Key Words	18. Distribution Statement
Flexible Pavements, Granular Base, Test Roads	No restrictions. This document is available to the public through the National Technical Information Service, Springfield, VA 22161

19. Security Classif. (of this report)	20. Security Classif. (of this page)	21. No. of Pages	22. Price
Unclassified	Unclassified	363	

SUMMARY

The purpose of this study was to use Mn/ROAD mainline flexible pavement data to verify, refine, and modify the Illinois Department of Transportation (IDOT) Mechanistic-Empirical (M-E) based flexible pavement design procedures and concepts. Illinois has used M-E design procedures for the design of full-depth asphalt concrete (FDAC) and conventional flexible pavements (CFP) sections since the late 1980's.

The Mn/ROAD project has 40 test cells that are 500-feet long. The cells represent a wide range of pavements types, with varying combinations of surface, base, subbase, drainage and compaction. Paving materials characterization was addressed through laboratory and field testing programs. Laboratory testing was performed at the University of Illinois, MnDOT and the University of Minnesota. Field characterization of the paving materials was performed through FWD and DCP testing.

The effect of granular material quality on pavement response and performance was assessed through analysis of FWD data. The "Design Time" concept for considering temperature effects on AC modulus fatigue calculations was evaluated. The ILLI-PAVE structural model was validated by comparing measured (sensors) and calculated pavement responses (i.e., strains, deflections, and stresses).

The study demonstrated that the mechanistic-empirical analysis and design procedures for FDAC and CFP sections are adequate. The ILLI-PAVE structural model adequately predicts the pavement responses. The bi-linear (arithmetic) subgrade model and the "theta" granular model closely replicate the field responses. The ILLI-PAVE algorithms are adequate to be utilized in FWD backcalculations. The properties of the layers and pavement responses can be accurately estimated (AC strain, E_{AC}, E_{Ri}).

TABLE OF CONTENTS

LIST OF TABLES

LIST OF FIGURES

FIGURES IN APPENDIX A

FIGURES IN APPENDIX B

FIGURES IN APPENDIX C

FIGURES IN APPENDIX D

FIGURES IN APPENDIX E

LIST OF ACRONYMS

AC	Asphalt Concrete
AREA	Area of Deflection Basin
ATREL	Advanced Transportation Research Engineering Laboratory
AUPP	Area Under Pavement Profile
CBR	California Bearing Ratio
CFP	Conventional Flexible Pavement
DCP	Dynamic Cone Penetrometer
DT	"Design Time"
ESAL	Equivalent Single Axle Load
FDAC	Full Depth Asphalt Concrete
FWD	Falling Weigh Deflectometer
IDOT	Illinois Department of Transportation
ILLI-PAVE	Finite Element Analysis Program for Flexible Pavements
IRI	International Roughness Index
LVR	Low Volume Road
LVDT	Linear Voltage Differential Transducer
M-E	Mechanistic-Empirical
MMAT	Mean Monthly Air Temperature
MMPT	Mean Monthly Pavement Temperature
Mn/ROAD	Minnesota Road Research Project
PK	Pressure gauge (Kulite)
RD	Rut Depth
SSR	Subgrade Stress Ratio
TAI	The Asphalt Institute
U of I	University of Illinois
WIM	Weigh-in-Motion

CHAPTER 1

Introduction

1.1 Introduction

In the United States, as of 1992, there were 2.3 million miles of paved road and 94% are asphalt surfaced (1). Prior to the 1920's the thickness of pavements was based on experience. The same thickness was used for a section of highway regardless of the soil encountered. In the late 1950's and early 1960's performance related equations were developed based on the AASHO Road Test results. These equations are the basis of most of the design procedures currently used in the US. As the understanding of materials behavior and structural modeling developed the trend was to move towards mechanistic-based design procedures to overcome the limitations set by empiricism.

Illinois has used Mechanistic-Empirical (M-E) design procedures for the design of full-depth asphalt concrete (FDAC) and conventional flexible pavements (CFP) sections since the late 1980's. The governing design criteria for conventional flexible pavements is asphalt concrete fatigue and subgrade stress. Subgrade Stress Ratio (SSR) is used for considering subgrade rutting. SSR is the ratio of the deviator stress applied to the unconfined compressive strength of the soil ($SSR = \sigma_D/q_u$). For full-depth pavements the design criteria is tensile strain at the bottom of the asphalt concrete (AC) layer.

The purpose of this study is to use Mn/ROAD mainline flexible pavement data to verify, refine, modify IDOT's M-E based flexible pavement design procedures and concepts.

1.2 Mn/ROAD Research Project

Mn/ROAD consists of two road segments lying parallel to Interstate 94 (I-94) outside Ostego, Minnesota, approximately 40 miles northwest of the Minneapolis-St. Paul metropolitan area. The project has a 3.5-mile mainline roadway carrying interstate traffic, plus a 2.5-mile low-volume loop where controlled truck weight and traffic volume simulate

conditions on rural roads. Mn/ROAD has 40 500-feet long test cells. The cells represent a wide range of pavements types, with varying combinations of surface, base, subbase, drainage and compaction. The mainline cells have only one type of subgrade soil.

The interstate or mainline portion of the facility is divided into two parts: the 5-year and 10-year mainline. These pavement sections were designed for 5-year and 10-year design lives. Figures 1.1 and 1.2 depict the flexible test sections. There are 3 FDAC sections and 11 CFP sections. Four different types of granular materials were used in the mainline flexible pavement sections. Only one type of cohesive subgrade soil is present in the mainline flexible pavement sections. The native soils at the site are primarily silty clay with an average Resistance Value (R) equal to 12. Thin-walled sample data indicate the subgrade soil Liquid Limit (LL) ranges from 28-38, and the Plasticity Index (PI) from 9-17.

The design average daily traffic for this portion of I-94 is 24,200 vehicles with 3,200 classified as heavy commercial vehicles. This traffic translates to 3.2 million equivalent single axle loads (ESAL) for the 5-year sections and 7.2 million ESALs for the 10-year sections. The sections were opened to traffic on the summer of 1994. The Pave Tech Van and visual inspection are utilized to conduct profile and crack surveys. Rut depth (RD) is also measured using a straight edge, dipstick and the Pave Tech Van. Periodically, Falling Weight Deflectometer (FWD) tests are conducted on the Mn/ROAD mainline tests sections to evaluate seasonal changes.

There are approximately 4,500 electronic sensors embedded on the roadway, 1,150 measure pavement responses (i.e., strain, stress, deflection) to dynamic axle loading. The sensors are placed at various levels in the roadway, from the surface into the subgrade. Data flows from these sensors to 26 roadside cabinets, and then to the MnDOT Materials Research Engineering Laboratory in Maplewood, Minnesota, for quality checking and database storage. All data collected at Mn/ROAD are stored on an ORACLE database for retrieval and analysis either locally or over a network system. The University of Illinois collects the data by querying the Oracle database via the Internet.

There are many types of sensors being used at Mn/ROAD: Linear Variable Differential Transformers (LVDT), Strain Gauges and Soil Pressure Gauges. Table 1.1 summarizes the sensors embedded in the mainline Cells, their number and the information collected. These sensors are activated by the passage of heavy vehicles. Information is also collected regarding moisture and temperature conditions in the pavement and subgrade. Extensive information about each passing truck is collected by means of a Weigh-In-Motion Scale (WIM). These data can support the in-depth consideration of the interaction of traffic-environment-materials and can be used to verify/ refine/ modify IDOT's mechanistic-empirical design procedures for full depth and conventional flexible pavements.

1.3 Research Objectives

The primary objective of this study is to utilize Mn/ROAD data and information to further verify, refine, modify IDOT's mechanistic-based flexible pavements analysis and design concepts and procedures.

Three main areas are differentiated in a M-E design procedure: materials characterization, pavement structural modeling, and pavement performance.

Material characterization of the paving materials and subgrade soils is a very important part of mechanistic design. The properties of the paving materials greatly influence pavement performance. This characterization is addressed at Mn/ROAD through laboratory and field testing programs. Laboratory testing of the granular materials used in the mainline test sections was performed at the University of Illinois. Laboratory tests were conducted to determine optimum moisture content, maximum dry density, gradation, shear strength parameters (c, ϕ), resilient modulus (E_R), rutting potential, and moisture susceptibility. Material testing was also performed by MnDOT Laboratory on granular and subgrade materials. The University of Minnesota tested the asphalt concrete utilized in the mainline test sections. Fatigue characterization of the Mn/ROAD mixtures was performed at the U of I - Advanced Transportation Research and Engineering Laboratory (ATREL). Field characterization of the paving materials is performed at Mn/ROAD through periodic FWD and Dynamic Cone Penetrometer (DCP) testing.

SENSOR TYPE	CELLS	NUMBER	DATA COLLECTED
LVDT	1, 17, 22	6	Vertical Deflection
	4, 15	3	(LVDTs are embedded 3 in. from pavement surface)
Strain Gauges:			Horizontal Strains in
LE*	2, 15, 22	3	Asphalt layers
TE*	1, 4, 17, 21	6	
	2, 3, 14, 15, 16, 18,		
	19, 20, 22, and 23	3	
Soil Pressure Gauges:			Vertical Stresses in base,
PG**	1, 17, 22	6	subbase, and subgrade.
PK**	1, 17, 18, 22, 23	1	
	4, 15	3	

* Longitudinal/Transverse Embedment Strain Gauges
** Geokon/Kulite Soil Pressure Cell

Table 1.1. Sensors embedded in Mainline Cells

The other major area is the pavement structural model utilized in the design procedure to estimate stresses, strains, and deflections. ILLI-PAVE is utilized in IDOT's current procedure. Under the scope of this study ILLI-PAVE validation/evaluation is addressed.

A third area of interest is pavement performance. Performance is monitored at Mn/ROAD through rut depth measurements, visual inspection, and the use of the Pave Tech Van.

A detailed list of tasks required to achieve the main objective is presented below:

1. Utilize University of Illinois backcalculation procedure to analyze Mn/ROAD FWD data:

    - Assess the effect of granular material quality on pavement response and performance.
    - Evaluate effect of subgrade properties variability on performance.

2. Evaluate the "Design Time" concept for considering temperature effects on AC modulus fatigue calculations.

3. Evaluate transfer functions utilized in IDOT's flexible pavement design procedures. These functions relate a specific distress or pavement response to the number of load repetitions (N).

    - AC strain (ε_{ac}) - N
    - Rut Depth (RD) - N
    - Subgrade Stress Ratio (SSR) - N

4. Validate/evaluate the ILLI-PAVE structural model by comparing measured and calculated pavement responses (i.e., strains, deflections, and stresses).

5. Evaluate IDOT's flexible pavement design criteria. Consider recent developments.

1.4 Research Approach

Table 1.2 presents some of the data contained in the Mn/ROAD database and its use in achieving the research objectives. Assessing granular material and subgrade variability effects on pavement response and performance requires the use of material testing results along with FWD testing, and performance data. FWD testing is used to monitor the bituminous and granular materials, and subgrade soils properties.

Special FWD testing is performed where pavement response data (i.e., stress, strain, and deflection) is collected simultaneously with the application of the plate load. This provides a good opportunity to compare the measured strains, and deflections with the responses estimated from the structural models. Backcalculation is achieved with ILLI-PAVE based algorithms (2,3,4).

Field calibration of the transfer functions can be attained with the data collected at Mn/ROAD. The WIM measurements along with data obtained from strain gauges, Pave Tech Van and rut depth measurements facilitate the evaluation of the currently utilized performance models. Visual inspections are periodically performed to monitor thermal cracking development.

1.5 Report Outline

Extensive research has been done in the characterization of the different paving materials. Chapter 2 presents a summary of the pertinent literature on the topic of flexible pavement analysis and design. IDOT's current flexible pavement analysis and design procedures are described.

A description of the Mn/ROAD project traffic and vehicles is a very important input in the analysis of the pavement sections. Chapter 3 presents a detailed characterization of the traffic experienced in each cell, the WIM data are discussed and analyzed, and ESAL information for each cell is presented. Chapter 4 presents a summary of the distresses developed in the mainline cells with time and the condition of the cells through November 1997.

Mn/ROAD DATA								
	Material Testing	FWD	WIM	Strain Gauges	Soil Pressure Gauges	LVDT	Rut Depth	Pave Tech Van
Assess granular material and subgrade variability effect	√	√				√	√	√
ILLI-PAVE validation	√	√	√	√	√	√		
Transfer functions	√	√	√	√	√		√	√
"Design Time"	√	√						
Evaluate Design criteria	√	√					√	√

Table 1.2. Research Methodology

A thorough characterization of the pavement materials was performed by Mn/ROAD, MnDOT and the U of I. Chapter 5 discusses and analyzes the laboratory tests performed. Results from field characterization by means of FWD and DCP testing are also presented.

The ILLI-PAVE finite element model was utilized to estimate the pavement responses and these were compared to the field measured results. Chapter 6 presents the results of this evaluation/validation of the structural model using the sensors response. Chapter 7 discusses the performance observed in the mainline cells and relates the performances to the expected behavior based on material characterization and model estimations. The fatigue and rutting behavior for each cell are considered. The conclusion of the study and recommendations of further research are discussed in Chapter 8.

1.6 Summary

Illinois has used Mechanistic-Empirical (M-E) design procedures for the design of full-depth asphalt and conventional flexible pavements since the late 1980's. The primary objective of this study is to utilize Mn/ROAD data and information to further verify/refine/modify IDOT's mechanistic-based flexible pavements analysis and design concepts and procedures. A brief description of the Mn/ROAD research project is presented in this chapter along with the research objectives and approach of the study. An outline of the report is presented.

CHAPTER 2

A Review: M-E Flexible Pavement Design Concepts & Illinois Procedure

2.1 Introduction

Mechanistic-empirical design procedures have been used in Illinois since the late 1980s. The components of a mechanistic-empirical design procedure are presented in Figure 2.1. In this procedure, the pavement materials and subgrade soils are characterized. Field conditions are considered through moisture, temperature, density, and other factors. A structural model is used to calculate the pavement responses (i.e., stress, strain, and deflections) to a standard wheel load, normally 9,000 lb. Transfer functions relate the pavement responses to pavement performance as measured by the type and severity of distress (fatigue, rutting, etc.). The predicted and observed pavement performance frequently do not compare favorably.

The NCHRP 1-26 (6) project indicated a major credibility gap in some current mechanistic-empirical design procedures is the large magnitude of the "shift factors" utilized in various transfer functions. These factors are applied to the mechanistic-empirical predictions of distress to compare more favorably with field observed distress.

2.2 Traffic Considerations

Traffic is a major input in a M-E design procedure. The traffic input for all current flexible pavement design procedures is based on the equivalent single axle load (ESAL). In this method, all loads are converted to the standard 18-kip equivalent single axle load (ESAL) by using equivalency factors. In IDOT's M-E design procedure, the design ESALs are estimated for the average daily traffic (ADT). Minimum design traffic requirements are enforced depending on the classification of the road.

2.3 Material Characterization

The characterization of the paving materials is one of the most important phases in the M-E design procedure. Material properties greatly influence the pavement structure response and behavior.

2.3.1 Asphalt Concrete

The AC layer is directly exposed to the load applications. The AC layer should be resistant to permanent deformation, fatigue, and low temperature cracking and must be durable. The resistance to permanent deformation is addressed by selecting quality aggregates with proper gradation, using an appropriate asphalt cement, and controlling mixture air voids in the mix. Low temperature cracking is important in cold regions and is primarily influenced by the low temperature properties of the asphalt cement (5).

The AC layer is typically characterized as a constant modulus material. The AC modulus (E_{AC}) is influenced by asphalt binder properties, temperature, time of loading, and mixture composition.

AC modulus is significantly influenced by temperature. Thus, AC modulus-temperature effects are incorporated into M-E design procedures. Two approaches have been utilized to establish E_{AC} -Temperature relations. The most popular is estimating E_{AC} based on asphalt binder properties, temperature, time of loading, and mixture composition. The second approach is to characterize "typical" AC mixtures for the temperature ranges of interest. This is done through resilient modulus testing on laboratory samples or field cores. E_{AC} can also be estimated from E_{AC}-split tensile strength relations for "typical" mixes. A recent methodology of "backcalculation" can be utilized to establish E_{AC} - Temperature relations from FWD testing on existing flexible pavements (6).

Asphalt stiffness is required to estimate AC modulus. Asphalt stiffness can be estimated using several procedures (7,8,9). The Bonnaure et al. procedure is utilized in the Shell Pavement Design Manual (10). A statistically based algorithm for estimating AC modulus is utilized in the Asphalt Institute's DAMA pavement analysis and design computer program (11).

Hill et al. (12) utilized field cores to establish E_{AC} - AC split tensile strength relations for two mixtures. Resilient modulus testing was conducted according to ASTM D 4123. The split tensile strength testing was performed at the standard Marshall rate 2 inches/minute. In the NCHRP AAMAS study (13) extensive resilient modulus and split tensile strength testing were conducted. The data were analyzed to establish E_{AC} - AC split tensile strength relations.

AC mean monthly pavement temperatures (MMPT) are estimated based on mean monthly air temperatures (MMAT). The MMPT can then be used to estimate AC modulus from an appropriate AC modulus-temperature relation. The Climatic-Materials-Structural (CMS) model (14,15) has been utilized to estimate the MMPT. CMS includes a one-dimensional forward-finite-difference heat transfer model and an isothermal model that calculates temperature and moisture profiles as a function of time based on pertinent climatic inputs. This model has been found adequate for considering climatic effects in a priori flexible pavement design (6).

A "Design Time" (DT) concept was developed at the University of Illinois to consider the temperature effects on AC stiffness (3,16,17,18,19). The fatigue life of a pavement estimated with the DT AC modulus is equal to the fatigue life estimated based on the monthly AC modulus inputs. This approach is versatile, as it can incorporate different AC modulus-Temperature relations and AC fatigue algorithms.

AC rutting is an important design criteria for flexible pavement design. AC rutting is addressed through material selection and mix design.

Fatigue cracking is another important design criterion. Flexural fatigue is a phenomenon effected by repeated loading stresses smaller than the strength of the material. AC flexural strain depends on wheel loading conditions, thickness of paving material layers, and properties of the various pavement layers and subgrade soil. Fatigue transfer functions relate the number of load repetitions to reach certain pavement "cracking failure" conditions (i.e., crack initiation, 10% area cracking, etc.) to the maximum tensile strain in the asphalt concrete layer. Miner's hypothesis is the most widely used procedure for considering "mixed loading" conditions.

AC fatigue algorithms are commonly given in two forms: "strain-based" and "strain/modulus-based". The "strain-based" relations (20) take the form:

$$N = k(1/\varepsilon)^n$$

The "strain/modulus-based" relations are of the form:

$$N = k(1/\varepsilon)^n(1/E)^m$$

where, N is the number of repetitions to failure, ε is the tensile strain at the bottom of the AC layer, and E is the AC modulus. It is apparent that no unique AC fatigue algorithm can be utilized in a M-E design procedure. However, the general form of the algorithm is evident. Several agencies/research groups have developed fatigue algorithms for use in M-E pavement design procedures.

The Asphalt Institute (TAI) uses a fatigue algorithm based on previous work done by Finn et al (21), and modified to reflect the effect of air void content and asphalt content based on laboratory determined fatigue data developed by Pell and Cooper (22), and Epps (23). The TAI equation is:

$$N = C*18.4(4.32\times10^{-3})(1/\varepsilon)^{3.29}(1/E)^{0.854}$$

where:

N = number of 18 kips-equivalent single axle loads for 20% or greater fatigue cracking.

ε = maximum tensile strain in the AC layer, in/in

E = AC dynamic modulus, psi; and

C = a correction factor equal to: $C = 10^M$

where:

$$M = 4.84\ [(V_b/(V_v + V_b)) - 0.69]$$

in which:

V_b = volume of asphalt, percent

V_v = volume of air voids, percent

The Shell Pavement Design Manual (10) presents a fatigue equation for design purposes. The number of repetitions to failure is calculated from:

$$N = 4.91\times10^{-13} (0.86\ V_v + 1.08)^5 (1/\varepsilon)^5 (1/S_{mix})^{1.8}$$

where:

Vb = volume of asphalt in the mix, %

ε = maximum tensile AC strain, in/in; and

S_{mix} = AC dynamic modulus, ksi

The Illinois Department of Transportation utilizes a strain-based fatigue algorithm in their thickness flexible pavement design procedures (16,24). The fatigue relation was developed for a typical IDOT' Class I AC (dense-graded mixture). The equation is as follows:

$$N = 5\times10^{-6} (1/\varepsilon)^3$$

The equation was established based on considerations of mixture composition factors, split strength characteristics, and field calibration studies (3,16).

The MOBIL procedure (25) uses an AC tensile strain-life relation based on the Nottingham procedure (26). The permissible AC strain for a given life is based on the binder content by volume in the mixture and the initial softening point of the binder. In the development of the Nottingham procedure (22) it was noted that there was a linear relation between k and n in the strain-based algorithm $N = k (1/\varepsilon)^n$. The relation is:

$$n = 0.5 - 0.213 \text{ Log } k.$$

In a recent SHRP study (27), a mix design and analysis system was proposed that accounts for fatigue distress. It relies on laboratory flexural fatigue testing for mix evaluation and incorporates an analysis system for properly interpreting the test results. It recognizes that mix in-situ performance depends on critical interactions between mix properties and in-situ conditions, thus providing sensitivity to mix behavior and to the in-situ traffic, climatic and structural environment.

As part of the SHRP A-003A project, "surrogate fatigue models" were developed to estimate the fatigue response for mixes containing conventional asphalt binders and dense-graded aggregates (27). Guidelines on their applicability were also developed.

The surrogate models are strain and energy based. The surrogate expressions are based on results of controlled-strain flexural fatigue tests of 44 mixes (196 beams) containing a range of asphalt binders and aggregates. The recommended models for use in the surrogate mix analysis system are:

Strain Based:

$N_f = 2.738 \times 10^5 \exp^{0.077VFA} (\varepsilon_o)^{-3.624} (S_o")^{-2.720}$

$R^2 = 0.79$

SEE = 0.776

Energy Based:

$N_f = 2.365 \exp^{0.069VFA} (W_o)^{-1.882}$

$R^2 = 0.76$

SEE = 0.825

where:

N_f = fatigue life;

ε_o = initial strain, in/in;

$S_o"$ = initial flexural loss stiffness ($S_o * \text{Sin}\phi_o$), psi;

S_o = initial flexural stiffness, psi;

W_o = initial dissipated energy per cycle ($\pi/4 * \varepsilon_o * S_o * \sin\phi_o$), psi;

ϕ_o = initial phase angle between applied stress and strain; and

VFA = percent voids filled with asphalt

The SHRP investigators believe that the primary advantage of surrogate models is the elimination of need for extensive laboratory fatigue testing, only mix stiffness and phase angle are needed (loss stiffness, $S_o"$) to use the models. They recommend laboratory fatigue testing when high levels of reliability are required for conventional mixes or for all situations

in which mixes containing modified binders or other than dense aggregate gradations are planned.

The fatigue design and analysis system evaluates the likelihood that the selected mix will resist fatigue cracking in the design pavement under anticipated traffic and temperature. Several differences exist between the laboratory conditions and the field. The laboratory fatigue tests are performed at one temperature and at an accelerated rate. Traffic is represented in design by ESALs in the design lane during the design period. In the field, ESALs accumulate in a mixed temperature environment. Thus, a temperature factor is used in the proposed system to convert the design ESALs to the equivalent ESALs at a single temperature (laboratory conditions). A shift factor is also applied to account for traffic wander, crack propagation rate, construction variability, different frequencies of loading, etc. The variability is accounted for by applying a reliability factor to the design loading before comparisons are made with the laboratory resistance. Under this system a mix is deemed suitable for use in the selected pavement structure to mitigate fatigue cracking when:

$$N \geq (ESALs * TCF*M)/SF$$

where:

N = number of laboratory load repetitions to failure under the anticipated in-situ strain level;

ESALs = the number of equivalent 18 kip single axle load expected in the design lane during the design period;

TCF = temperature conversion factor;

M = reliability multiplier; and

SF = Shift Factor

The temperature conversion factor (TCF) is location specific and depends on the thickness of the AC layer. The procedure used to develop this factor is presented in a study by Deacon et al. (28). The reliability multiplier (M) accounts for the variance in the logarithm of the laboratory fatigue life estimated at the in-situ strain level (under a 9 kip load) and the variance of the estimate of the logarithm of the design ESALs. The variance of laboratory fatigue is attributed to specimen preparation, testing equipment and procedure,

testing program, etc (29,30). Shift factors (SF) ranging between 10 and 14 were recommended based on SHRP A-003A studies. These factors vary as function of the strain level (31).

2.3.2 Granular Layers and Subgrade Soils

Granular base/subbase and subgrade soils are important flexible pavement components. The primary function of the granular base and subbase is to reduce the stresses caused by the repeated wheel load in the underlying layers and minimize rutting in the granular layers. Subgrade soils and granular base resilient moduli are important structural model inputs. These moduli values can be developed from a laboratory testing program, backcalculated from FWD nondestructive testing, predicted from soil/granular material properties (i.e., gradation, PI, clay content, etc.) and/or assigned based on experience with similar soils or granular materials.

Most of the laboratory testing on granular materials and subgrade soils have been repeated load tests. Resilient moduli and permanent deformation behavior can be quantified based on appropriate repeated load testing data. The current AASHTO standard for the test is T 294-94 (32). A SHRP Testing Protocol (P46 Resilient Modulus of Unbound granular Base/Subbase Materials and Subgrade Soils) has been developed.

Triaxial test conditions (generally constant confining pressure) are used for granular materials. Cohesive soils can be tested under triaxial or unconfined compression conditions. Pneumatic and electrohydraulic loading equipment have been utilized. In the P46 procedure, the load duration is 100 msec. and the cycle duration is 1 sec.(60 repetitions per minute). In the T 294 procedure, the load duration is between 100 msec. and 1 sec. and the cycle duration is from 1 to 3 sec. (60 to 20 repetitions per minute).

Specimen deformation is typically measured with either externally or internally mounted LVDTs. Total, resilient, and plastic deformations are recorded (Figure 2.2). The resilient modulus (E_R) is defined as the ratio of the repeated deviator stress (σ_D) to the recoverable axial strain (ε_R).

$E_R = \sigma_D/\varepsilon_R$

where:

E_R = resilient modulus

σ_D = repeated deviator stress

ε_R = recoverable axial strain

The resilient response of granular materials and cohesive soils is stress dependent. Under repeated loading conditions, granular materials present a stress-hardening behavior, while cohesive soils are stress-softening.

The most significant factor influencing the resilient modulus of a cohesive soil is the deviator stress. Two basic stress dependent models relating resilient modulus to deviator stress have been used to characterized the behavior of cohesive soils: the arithmetic model and the semi-log model (Figures 2.3 and 2.4). A "hyperbolic" resilient modulus model has been recently proposed by Boateng-Poku (33) to account for the stress softening behavior.

Extensive resilient testing at the University of Illinois (34) were analyzed based on the arithmetic model. E_{Ri} (resilient modulus at the intersection point), see Figure 2.4, is a good indicator of a soil's resilient behavior. E_{Ri} is typically associated with a repeated deviator stress of about 6 psi.

Many factors influence the resilient response of fined-grained soils. Low plasticity (LL, PI), low group index, high silt content, low clay content, low specific gravity, high organic carbon contents, and high degree of saturation have been found to contribute to low resilient moduli (34). Several studies (35-39) showed that freeze-thaw actions cause a significant increase in resilient deformation (decreased resilient modulus) after only a few repetitions, even if no gross moisture change occurs.

Granular materials also exhibit stress dependent behavior. They "stiffen" as the stress state increases. Several mathematical models have been proposed to characterize this resilient behavior. The "theta" model is the most commonly used model to characterize the behavior of granular materials. The model is:

$E_R = K\theta^n$

where:

E_R = the resilient modulus

$\theta = \sigma_1 + \sigma_2 + \sigma_3$ ($\theta = \sigma_1 + 2\sigma_3$ in triaxial test)

K, n = experimentally derived constants.

The "theta" model has been incorporated in the finite element program ILLI-PAVE. This model is the most widely used in current structural finite element models. A good summary of the resilient behavior models for granular materials is presented in reference (40). Other models include: the Uzan model, the Itani model, the bulk-shear model, the contour model, the University of Texas model, and the University of Texas at Austin model.

Permanent strain-load repetitions relations for granular materials and subgrade soils are typically expressed in terms of permanent strain-log N or log permanent strain-log N relations. The most commonly used model, developed by Monismith (41) is :

$\varepsilon_p = AN^b$

where:

ε_p = permanent strain,

A, b = experimentally determined coefficients, and

N = the number of load repetitions.

Research (42,43) has shown that the "b" term varies between 0.1 and 0.2. The "A" term, on the other hand, is quite variable and is significantly influenced by stress state. Stress state is expressed by:

a) repeated deviator stress (σ_D),

b) principal stress ratio (σ_1/σ_3), and

c) deviator stress ratio $(\sigma_1 - \sigma_3)/\sigma_3$.

Stress ratio, defined as the ratio of repeated stress to ultimate strength, provides a good indication of the rutting potential of the material. Low A terms are noted for reduced stress ratios and large A's for increased stress ratios.

At Ohio State University a permanent strain accumulation model was developed. The model is of the form:

$\varepsilon_p/N = An^m$

The "A" term is highly variable and is influenced by stress state and material, and the "m" term depends on material type. Experimental data (44) indicate that "m" varies within a narrow range for cohesive soils and granular materials. For cohesive soils, a typical "m" is -0.88. For granular materials "m" is around -0.8.

The Ohio State relation can be used in describing rutting progress in all pavement layers. Thompson and Nauman (45) suggested and verified that if all pavement layers (i.e., AC, granular, and subgrade layers) follow the log-log relation then a pavement surface rutting model would be of the same form. A pavement system rutting rate (RR) is obtained by substituting surface rut depth for the permanent strain term. The relation is:

$RR = RD/N = A/N^B$

where:

RR = rutting rate

RD = rut depth, inches

N = number of repeated load applications

A, B = terms developed from field calibration testing data and information.

This model is helpful in analyzing the pavement rutting data for a specific pavement section and estimating future rutting for pavement management system use.

2.4 Design Criteria

The most common M-E flexible pavement design criteria are AC fatigue and pavement rutting. Other criteria also have been utilized. Subgrade strain criteria are used in several mechanistic based flexible pavement design procedures (i.e., Shell, Mobil, TAI, and S. Africa). Stress Ratio criteria have been utilized to try to ensure a stable permanent deformation behavior in the pavement. Thompson and LaGrow (18) use a subgrade stress

ratio criterion (SSR = σ_D/q_u) in Illinois design procedure for conventional flexible pavements.

The South African mechanistic design procedure originally included stress ratio criteria for the granular layers and subgrade soils. A subgrade strain-based criterion was later adopted. A shear failure criterion is considered for granular material in their current procedure (46).

Deflection criteria have been utilized by many agencies for overlay design and estimating future performance. Surface deflection is easy to measure and is a reliable structural response indicator for predicting general performance. At the University of Illinois, pavement deflection is utilized in pavement response algorithms to reliably estimate AC strain, subgrade deviator stress and subgrade stress ratio (2,3).

2.5 IDOT's M-E Pavement Design Procedures

The Illinois Bureau of Local Roads and Streets M-E design procedure for CFP (AC and granular material) and FDAC is based on resilient soil and material testing procedures, the ILLI-PAVE structural model, and design algorithms developed from an extensive ILLI-PAVE database. The distresses considered in the design are asphalt concrete (AC) fatigue and rutting, granular base rutting, and subgrade rutting.

AC rutting is considered by material selection and AC mixture design procedures. AC fatigue is related to the tensile strain at the bottom of the AC layer (ε_{ac}). Granular base rutting is controlled by establishing a minimum thickness of AC surface to limit the stress state in the granular base to a level that will not produce unacceptable rutting. Subgrade rutting potential can be reasonably assessed by maintaining the subgrade stress ratio (SSR) at the pavement structure - subgrade interface to acceptable levels. The "Design Time" concept is utilized to account for the seasonal temperature variation as it affects AC modulus and its resulting effect on AC fatigue.

2.5.1 ILLI-PAVE Structural Model

IDOT's flexible pavement design procedure utilizes ILLI-PAVE-based response algorithms. In the ILLI-PAVE finite element model, the pavement is considered an

axisymmetric solid of revolution. Nonlinear, stress-dependent resilient modulus material models and failure criteria for granular materials and fine-grained soils are incorporated in the ILLI-PAVE finite-element model. The "theta" (θ) model is used for granular materials and a deviator stress dependent bilinear approximation for fine-grained subgrade soils. The principal stresses in the granular materials and fine-grained soil layers are modified at the end of each iteration so that they do not exceed the strength of the materials as defined by the Möhr-Coulomb theory of failure.

2.5.2 Full- Depth Asphalt Concrete Design Algorithms

Design algorithms have been developed from a comprehensive ILLI-PAVE data base for 18-kip axle loads, representative FDAC configurations, materials and subgrade soils (3). The algorithms are as follows:

$$Log(\varepsilon_{AC}) = 5.746 - 1.589*Log(T_{AC}) - 0.774*Log(E_{AC}) - 0.097*Log(E_{Ri})$$

$$Log(DEV) = 2.744 - 1.138*Log(T_{AC}) - 0.515*Log(E_{AC}) + 0.289*Log(E_{Ri})$$

$$Log(D0) = 3.135 + 0.895*Log(T_{AC}) - 0.359*Log(E_{AC}) - 0.287*Log(E_{Ri})$$

$$Log(SSR) = 1.27*Log(D0) - 2.21$$

where:

ε_{AC} = Tensile strain at the bottom of the AC layer, microstrain (10^{-6} in/in)

T_{AC} = Thickness of AC layer, inches

DEV = Subgrade deviator stress, psi

D0 = Surface deflection under center of applied load area, mils (10^{-3} in.)

E_{AC} = Resilient modulus of AC layer, ksi

E_{Ri} = Breakpoint resilient modulus of subgrade, ksi

SSR = subgrade stress ratio ($SSR = \sigma_D/q_u$)

2.5.3 Conventional Flexible Pavement Design Algorithms

Design algorithms have been developed from a comprehensive ILLI-PAVE data base for 18-kip axle loads, representative CFP configurations, materials and subgrade soils (2). The algorithms are as follows:

$$\text{Log}(\varepsilon_{AC}) = 2.9496 + 0.1289*T_{AC} - 0.5195*\text{Log}(T_g)/T_{AC} - 0.0807*(\text{Log}(E_{AC}))*T_{AC} - 0.0408*\text{Log}(E_{Ri})$$

$$\text{Log(DEV)} = 1.7694 - 0.0735*T_{AC} - 0.0222*T_g - 0.2539*\text{Log}(E_{AC}) + 0.0223*\text{Log}(E_{Ri})$$

$$\text{Log(SSR)} = 0.3056 + 0.0560*T_{AC} - 0.0222*T_g - 0.0495*(\text{Log}(E_{AC}))*T_{AC} - 0.4242*\text{Log}(E_{Ri})$$

$$\text{Log(D0)} = 1.9692 + 0.0465*T_{AC} - 0.5637*\text{Log}(T_g)/T_{AC} - 0.0464*\text{Log}(E_{AC})*T_{AC} - 0.2079*\text{Log}(E_{Ri})$$

where:

ε_{AC} = Tensile strain at the bottom of the AC layer, microstrain (10^{-6} in/in)

T_g = Thickness of granular layer, inches

T_{AC} = Thickness of AC layer, inches

DEV = Subgrade deviator stress, psi

SSR = Subgrade stress ratio

D0 = Surface deflection under center of applied load area, mils (10^{-3} in.)

E_{AC} = Resilient modulus of AC layer, ksi

E_{Ri} = Breakpoint resilient modulus of subgrade, ksi

2.5.4 Reliability Considerations in IDOT's Flexible Pavement Design Procedure

Pavement structural response and performance data demonstrate that "pavement life" is not a fixed value, but shows considerable variability. Statistical analyses of Illinois CFP non-destructive testing (NDT) surface deflection data indicate typical coefficient of variation values for the maximum deflection are in the range of 15-35%. A design reliability concept

has been proposed to account for this variability. A "Traffic Multiplier" can be calculated for various levels of design reliability (19).

$MF_R = N/N_R = [1+Z_R (COVDEF/100)]^{3.34}$

where:

MF_R = "Traffic Multiplier" to produce r percent of reliability;

N = Number of 18-kip ESALs to "fatigue failure" for 50% reliability;

N_R = Number of 18-kip ESALs to "fatigue failure" for R% reliability;

COVDEF = Coefficient of Variation (%) for maximum surface deflection;

Z_R = Standard normal deviate for R% reliability;

R = Design reliability level, %

For CFP a coefficient of variation of 25% is recommended. For FDAC a 20% coefficient of variation is used. The following MF_R - design reliability relations are appropriate for CFP and FDAC.

CFP Traffic Multiplier	FDAC Traffic Multiplier	Design Reliability
1	1	50 (average)
2.2	2	85 (intermediate)
3.2	3	95 (high)

2.6 Summary

A brief literature review on the mechanistic-empirical procedures is presented. Models and procedures to characterize the different paving materials are included. The most commonly used design criteria are discussed. The ILLI-PAVE based algorithms used in IDOT's design procedure are presented. IDOT's M-E design procedures for conventional and full depth flexible pavements are described.

CHAPTER 3

Traffic Characterization

3.1 Introduction

Traffic characterization is one of the most important inputs in the design stage of flexible pavements. The Mn/ROAD project is located on one of highest truck volume routes (I-94) in the state of Minnesota. The design average daily traffic for this portion is 24,000 vehicles with 3,200 of these classified as heavy commercial vehicles. The traffic characterization in the project is performed using a Weigh-In-Motion (WIM) system.

3.2 Description of Weigh-in-Motion Equipment

A weigh-in-motion system is located at the beginning of the facility to monitor axle weights. The Weigh-In-Motion is an International Road Dynamics (IRD) system located east of the main Mn/ROAD test sections. WIM consists of four platforms in a sealed frame, four loop detectors, and a microcomputer. The location of the system in shown in Figure 3.1.

Data representing westbound traffic passing over the WIM (including axle weight, spacing, and configuration, and vehicle speed) are collected and stored locally on the WIM PC. This information is then downloaded, via a dial up modem and file download utility, to a PC in the Maplewood Office. These raw data files are processed with the IRD software, transferred to the Network Server and loaded into the central database server on a weekly basis. The raw data files and the processed data files are copied from the central server and stored on CD-ROM.

There is also an axle classification system stationed immediately next to the WIM consisting of induction loops to monitor the types of vehicles corresponding to the axle loads. The scales are configured to weigh the left and right sides of vehicles independently in both the traveling and passing lanes.

3.3 Seasonal Traffic Load Distributions

Three weeks of traffic were collected and analyzed. The dates of traffic collected are: March 15-21, May 15-21 and November 15-21 of 1996. The week of May traffic corresponds to the "Design Time" week of the Mn/ROAD mainline flexible cells. More details on "Design Time" are given in Chapter 7.

Figure 3.2 trough 3.4 present the cumulative distributions of the wheel load in the driving lane for all weeks of traffic analyzed for the 5-year conventional, the full depth, and the 10-year conventional sections(47). Table 3.1 presents the percentiles of the right wheel load distributions. The distributions are very similar for all weeks. Thus, it appears there is no traffic variation throughout the year. This observation validates the typically utilized assumption of evenly distributed ESALs throughout the design period of the pavement.

Percentiles	March 15-21 Wheel Load (kips)	May 15-21 Wheel Load (kips)	November 15-21 Wheel Load (kips)
1	1.2	0.8	1.2
5	1.8	1.4	1.8
10	2.3	1.9	2.3
25	3.5	3.3	3.5
50	5	5.1	5.1
75	7.1	7.1	6.9
90	8.5	8.4	8.2
95	9.0	9.0	8.9
99	10.2	10.2	10.3

Table 3.1. Percentiles of the Right Wheel Load on Driving Lane.

Figure 3.5 shows the distribution of the wheel loads in a week of traffic on the driving lane. A normal curve is superimposed on the histogram. The data does not seem to be normally distributed. A typical axle load and count breakdown (48) for Mn/ROAD is presented in Table 3.2, the data were collected in October of 1994. The configurations of the single and tandem axles are depicted in Figure 3.6.

Axle Group Weight Range, kips.	Single Axle Number	Tandem Axle Number
48-52		13
44-48		58
40-44		387
36-40		2194
32-36		10162
28-32	8	12114
24-28	52	7517
20-24	708	7607
16-20	4649	8504
12-16	6947	9150
8-12	42185	10922
4-8	15484	4342
0-4	12437	647

Table 3.2 Mn/ROAD Typical Axle Load and Count Breakdown (Driving Lane).

3.4 Correlation Between Wheel Load and Strain Distributions

The WIM data collected for the week in May was correlated to strain measurements for the same week. Depending on the location and magnitude of the wheel load, a value may be registered on one, two, or all three of the transverse channels. Each WIM event cannot be paired with the resulting strain. Thus, the quartiles of the sample (week of data) were correlated. This correlation was performed on selected cells. Figure 3.7 shows the correlation between the wheel load and strain samples quartiles. A linear fit and a polynomial fit were performed on the data.

Strain data were collected for four cells. Two full depth sections, Cells 4 and 15 were chosen along with two conventional sections, Cells 17 and 22. Overall, there is a very good correlation between the quartiles of the samples. The coefficient of correlation (R^2) for the linear fit ranges from 0.88 to 0.93. The coefficient of correlation (R^2) for the polynomial fit is better than for the linear fit and is above 0.99 for all cells. Table 3.3 presents the best-fit line constant and slope for the selected cells. The equation is of the form:

$\varepsilon_{ac} = m\,(Load) + b$

where:

ε_{ac} = AC tensile strain, microstrain

m = slope of the line

Load = wheel load, kips.

b = regression coefficient.

Cell Number	m	b	R^2	S.E.E
4	29.39	-45.71	0.93	29.90
15	13.51	-28.76	0.88	17.71
17	21.98	-39.81	0.93	22.09
22	28.94	-35.51	0.93	29.24

Table 3.3. Statistics of Wheel Load and strain quartiles linear correlation.

Table 3.4 presents the results of the constants and coefficient of correlation for the second order polynomial. The equation is of the form:

$\varepsilon_{ac} = a\,(Load)^2 + b\,(Load) + c$

where:

a, b, and c are constants

Load = wheel load, kips.

Cell Number	a	b	c	R^2
4	2.34	-18.49	64.78	0.998
15	2.82	-16.54	72.78	0.994
17	3.87	-23.50	108.88	0.996
22	3.80	-22.95	116.15	0.996

Table 3.4. Statistics of Wheel Load and strain quartiles polynomial correlation.

In the "Design Time" approach the AC strain is estimated using ILLI-PAVE based algorithms. The strain is then used to estimate the expected life. This "Design Time" strain is calculated for a 9-kip wheel load. The strain estimated from the quartile correlation at a 9-kip load does not agree for all cells with the ILLI-PAVE estimated ones for the "Design Time"(Figure 3.8). The ILLI-PAVE estimations assume an "intact" condition of the cells. At the time data were collected, May 15-21, 1996, thermal cracks had appeared on the cells changing the behavior of the system.

Linear correlations were made by Newcomb et al., 1997 (49) between the wheel load (August 1-7) and temperature-corrected strains for several cells. The strains were corrected to a temperature of 25°C (77°F). The relations developed have a very good fit.

3.5 ESAL Calculations on Mainline Cells

The equivalent single axle loads (ESALs) were calculated from the WIM data. The University of Minnesota developed a program to calculate ESALs. The results were

tabulated and included in the Mn/ROAD database. The ESAL information presented here was downloaded from the database.

In the Mn/ROAD procedure, the WIM data collected were evaluated for each week in the traffic period to validate the quality of the data. Close to 35 % of the collected data was found not suitable for use. When the traffic information for a week was not satisfactory, the traffic from the previous week was utilized. The periods of time when the test sections were closed to traffic due to testing were subtracted to obtain the actual applied traffic in the cells. Through June 1 of 1997 the Mn/ROAD cells have been closed to traffic for 21 % of the traffic time (50).

Most design procedures characterize traffic by a fixed traffic approach. In this procedure, the thickness of the pavement is governed by the number of repetitions of a standard vehicle or axle load, usually the 18-kip (80-kN) single axle load. All wheel loads are converted to the standard load by an equivalent axle load factor(EALF). The number of repetitions under each single or multiple axle load is multiplied by its EALF to obtain the equivalent effect based on an 18-kip single axle load. A summation of the equivalent effects of all axle loads during the design period results in an equivalent single axle load (ESAL), which is the single traffic parameter for design purposes.

The EALF depends on the type of pavements, thickness or structural capacity, and the terminal at which the pavement is considered failed. The AASHTO empirical equations were used in estimating the EALF for the Mn/ROAD WIM database. A structural number (SN) was calculated for both driving and passing lanes in each cell. The average AC thickness from ground penetrating radar (GPR) testing was used in the calculation.

Table 3.4 shows the number of repetitions (ESALs) accumulated on the mainline cells through June 1, 1997. There is very little difference in the amount of accumulated ESALs on the cells regardless of the pavement section. Cell 4 has the greater number of ESALs, at 1.496 million and Cell 2 has the smaller number at 1.365 million ESAL. The ESALs in the passing lane are 25 percent of the ESALs accumulated in the driving lane for all cells.

Cell	Driving Lane ESAL (10^6)	Passing Lane ESAL(10^3)
1	1.367	342.10
2	1.365	341.39
3	1.392	349.12
4	1.496	380.24
14	1.439	365.41
15	1.431	365.41
16	1.393	351.74
17	1.395	352.33
18	1.380	348.12
19	1.395	351.74
20	1.399	352.94
21	1.378	345.61
22	1.378	344.49
23	1.320	326.73

Table 3.5. Accumulated ESALs on Mainline Cells.

3.6 Summary

The Mn/ROAD project design average daily traffic is 24,000 vehicles with 3,200 of these classified as heavy commercial vehicles. The Mn/ROAD traffic was characterized with WIM system located at the beginning of the facility to monitor axle weights and an axle classification system stationed immediately next to the WIM.

Three weeks in the year were selected and the WIM information collected. Analysis of the data shows no difference in the cumulative distributions of wheel loads in the driving lane for all weeks of traffic analyzed. Thus, there is no traffic variation throughout the year.

Strain data for four cells were collected during the "Design Time" week. The quartiles of the strain samples were correlated with the quartiles of the wheel load sample. There is a very good correlation between the quartiles of the samples (linear and polynomial fit). The strain estimated from the quartile correlation at a 9-kip load ("Design Time" week) does not agree with the ILLI-PAVE estimated strain values for the "Design Time".

ESAL calculation were performed for each cell in both the driving and passing lane. The accumulated ESALs in the cells ranges from 1.496 million in Cell 4 to 1.365 million in Cell 2. The ESALs in the passing lane are 25 percent of the accumulated ESALs in the driving lane for all cells.

CHAPTER 4

Mainline Sections Distress and Condition

4.1 Introduction

In the mechanistic-empirical design procedures, the different distresses are addressed separately. In the Mn/ROAD project the distress development in each cell has been monitored since the beginning of traffic in the summer of 1994. Thermal cracks, rutting, fatigue cracking and roughness have been measured and are summarized in this chapter. The identification and location of the distresses are very important in the explanation of the behavior/performance of the test sections presented in Chapter 7.

4.2 Rutting

Rutting is one of the failure criteria in a mechanistic-empirical pavement analysis and design procedure. A rut is a surface depression in the wheel paths. Surface rutting is the summation of permanent deformation in the pavement layers and the subgrade.

Cell performance was monitored by measuring rut depth regularly. An aluminum straight edge (6-feet long, 4-inch wide, 1/8-inch thick) was used to measure the rutting in the outer and inner wheel paths of the driving and passing lanes. Two stations in each 500-foot cell were monitored.

The accumulated ESALs on April of 1997 ranged between 1.27 to 1.4 millions. Figures 4.1 and 4.2 present the rut depth in the 5-year mainline CFP sections for the outer and inner wheel path in the driving lane respectively (April 1997). Two bars are presented for each cell, one for each station measured. Cell 2 has the greatest rut depths of the three 5-year sections.

Figures 4.3 and 4.4 show rut depths for the FDAC sections (April 1997). Cell 4 has the greatest rut depth of the FDAC sections. The rut depths for the 10-year mainline CFP sections are presented in Figures 4.5 and 4.6.

Cell 20 and Cell 23 performed the worst of the 10-year cells. These cells have rut depths close to 0.5 inch in both wheel paths of the driving lane. Cell 23 reached high levels of rutting since the beginning of traffic. Most design procedure consider rut depths of 0.5 inch a failure of the section. In October of 1997, rut depths of 0.6 inch were measured in Cell 20.

4.3 Thermal Cracking

Asphalt concrete temperature related cracking develops from two distinctly different mechanisms, low-temperature cracking, and thermal fatigue cracking. The cracking develops from temperature changes, and the interaction with asphalt cement properties.

Thermal cracking is usually addressed in a mechanistic-empirical design procedure through material selection and mixture design. Stiffer asphalt cements are prone to crack due to temperature changes. The Mn/ROAD AC mixtures were constructed with two asphalt cements (AC 20 and Pen 120/150) as discussed in Chapter 1. The AC 20 asphalt cement is not typically utilized in Minnesota because of it high viscosity at low temperature.

As early as February of 1994, thermal cracks were observed on the mainline cells. Ten thermal cracks were located in cells 15-19 (AC 20). The cracks ran the entire width of the pavement including the shoulders. The crack widths ranged from 0.6 inch to 0.38 inch. By May of 1996, the number of cracks had increased significantly. Table 4.1 presents a summary of thermal cracks in the mainline cells as of May of 1996.

In May of 1997, Cells 15 through 19 were spalling at many of the thermal cracks that developed during the winter of 95-96. Spalling was not occurring in the cells with AC of 120/150 penetration.

The crack maps of each cell are presented in Appendix A. Cells 15, 16, 17, 18 and 19 have the worst performance. The AC mixtures in these cells have AC 20 asphalt cement. The cells with the Pen 120/150 cement performed considerably better.

Cell	Number of Cracks	Cracks,ft.	Number of Full Transverse Cracks	Low-Severity, ft.	Med.-Severity, ft.
1	22	345	12	345	0
2	23	469	19	469	0
3	17	368	13	343	25
4	37	479	11	479	0
14	31	487	15	487	0
15	103	963	20	963	0
16	191	1117	3	1069	48
17	99	515	3	442	73
18	68	726	16	630	96
19	204	1024	4	942	82
20	75	434	2	434	0
21	74	457	3	428	29
22	31	479	11	479	0
23	24	429	14	429	0

Table 4.1. Thermal Cracking Mainline Cells.

4.4 Fatigue Cracking

Fatigue cracking is a series of interconnecting cracks caused by the fatigue failure of the asphalt concrete surface under repeated traffic loading. Fatigue cracking appeared earlier than expected in Cells 18 and 19 on the 10-year mainline part of the project. These cells are designed to withstand 7.2 million ESALs and developed fatigue cracking at less than 2 million ESALs.

The crack locations are presented in Figures 4.7 and 4.8. All fatigue cracks have their origin at or very near a thermal crack. The presence of thermal cracks changed the mode of loading and the conditions of the pavements. The layered system, interior loading assumption is less applicable. These previous distresses are believed to be the cause of the fatigue cracks. Thus, the fatigue cracks that occurred in these sections are not representative of the expected fatigue failure in an "intact" pavement section.

4.5 International Roughness Index Measurements

The international roughness index (IRI) is a mathematically-defined summary statistic of the longitudinal profile in the wheel path of a traveled road surface. The index is an average rectified slope statistic computed from the absolute profile elevations. It is representative of the vertical motions induced in moving vehicles for the frequency

bandwidth which affects both the response of the vehicle and the comfort perceived by occupants (51).

The IRI describes a scale of roughness which is zero for a true planar surface. As the roughness of the pavement increases so does the IRI. The critical value for high-type highways has been suggested at 2.0 m/km (126.7 in/mi.).

The Mn/ROAD cells have been monitored (Pave Tech van) for roughness since the paving operation ended in July 1994. Figures 4.9 to 4.22 present the IRI measurents for the driving and passing lanes in each cell. Most cells show an initial high IRI value. The variation of roughness changes during the year. In the spring time higher values are measured, but they decrease during the summer, fall and winter seasons and increase again the following spring. The same trend is observed in both lanes.

Figure 4.23 shows the IRI values for the mainline cells on the latest date in the database, June 1997. The values are fairly close between the driving and the passing lanes. Most cells are close to the 2.0 m/km (126.7 in/mi.) IRI level. A few of the cells have surpassed the value in the critical period (spring).

4.6 Summary

In the Mn/ROAD project the distress development in each cell has been monitored since the beginning of traffic in the summer of 1994. Thermal cracks, rutting, fatigue cracking and roughness have been measured and are summarized in this chapter.

Rutting measurements have been made regularly since the beginning of traffic using a straight edge procedure. Cell 2 has the greatest rutting in the 5-year CPF group. Cell 4 is the worst performer of the FDAC group. In the 10-year group Cell 20 has rut depths of 0.6 inch. Cell 23 of the 10-year group also performed badly. It reached high levels of rutting since the beginning of traffic. These cells have failed according to the commonly used 0.5 inch criteria. These two cells are the worst performers in the mainline.

Significant thermal cracking occurred in the mainline cells. The cells with Pen 120/150 asphalt cement mixtures developed the greatest number of cracks. The extensive

cracking influenced the behavior of the cells, likely instigating fatigue cracking in Cells 18 and 19.

CHAPTER 5

Material Characterization

5.1 Summary of Mn/ROAD Granular Material Testing @ UIUC

5.1.1 Introduction

Granular base and subbase layers are essential components of a flexible pavement. Their function is to reduce the repeated wheel loading related stress state on underlying layers and minimize rutting within the granular layers. These are of particular importance in sections where the AC layer is thin (less than 4 inches).

Six different granular materials were used as base and subbase materials in the flexible sections in the Mn/ROAD project. Only four were used in the mainline portion of the flexible pavement sections (FPS). The material specifications for the four materials are presented in Table 5.1.

Samples of the Mn/ROAD materials were sent to the U of I in the summer of 1994. A detailed characterization of the Mn/ROAD materials was performed at the University of Illinois. The complete study is contained in a Ph.D. thesis by N. Garg (12).The results are summarized below.

5.1.2 Specimen Preparation and Equipment

Cylindrical specimens, 6-inch in diameter and 12-inch in height, were used for rapid shear and repeated load tests. The material was compacted in the mold in five lifts. Target moisture contents and densities were selected based on AASHTO T-99 test results and field construction moisture-density measurements. Compaction was accomplished with a pneumatic vibratory compactor. Specimen density was monitored by measuring the compacted thickness of each lift. The tests were performed under drained conditions.

Aggregate Class	Percent Passing Sieve Size									Plasticity		
	1-1/2"	1"	3/4"	1/2"	3/8"	No. 4	No. 10	No. 40	No. 200	LL	PI min	PI max
CL-3sp	--	--	--	100	95-100	85-100	65-90	30-50	8-15	35 max	0	12
CL-4sp	100	95-100	90-100	--	80-95	70-85	55-70	15-30	5-10	35 max	0	12
CL-5sp	--	100	90-100	--	70-85	55-70	35-55	15-30	3-8	35 max	0	6
CL-6sp	--	100	85-100	--	50-70	30-50	15-30	5-15	0-5	35 max	0	6

Crushing Requirements:

CL-3 sp and CL-4 sp: crushed/fracture particles not allowed

CL-5 sp: 10-15 percent crushed/fractured particles required

CL-6 sp: 100 percent crushed/fractured particles required

Table 5.1 Mn/Road Research Project Base and Subbase Aggregate

Material	Moisture Content %	Dry Density, pcf	Friction Angle (ϕ)	Cohesion (c), psi
CL-3sp	6.8	127.0	44	7
CL-3sp	8.0	128.0	44	7
CL4-sp	7.9	130.0	45	7
CL-4sp	9.4	132.0	31	17
CL5-sp	7.7	139.0	39	8
CL5-sp	6.8	137.0	43	11
CL6-sp	6.3	134.0	47	18
CL6-sp	5.3	133.0	51	14

Table 5.2 Results form Rapid Shear Testing on Mn/ROAD Granular Materials.

An MTS closed-loop electro-hydraulic system, Model 407, was used for testing. The main part of the system consisted of a controller, loading frame, and hydraulic power supply. Two external LVDT's, mounted on the top plate of the triaxial chamber, were used to measure displacements during the resilient modulus tests.

5.1.3 Rapid Shear Testing

Rapid Shear tests were performed at confining pressures of 5-psi, 10-psi, 15-psi, 20-psi, and 30-psi to determine the friction angle 'ϕ', and cohesion 'c' used to define the Möhr-Coulomb failure envelope. The deviator stress was applied at a constant displacement rate of 1.5 inch/second for 12-inch specimens(strain rate 12.5% per second). This corresponds to 5% strain in 400 milliseconds.

The Möhr-Coulomb envelope was determined by regression using the deviator stress and confining pressure. Linear regression was performed to obtain a best fit equation of the form:

$$\sigma_1 = a + b*\sigma_3$$

where σ_1 and σ_3 are the major and minor principal stresses, respectively. Cohesion (c) and angle of internal friction (ϕ) were evaluated as:

$$c = a / (2*\sqrt{b})$$

$$\phi = \sin^{-1} [(b-1)/(b+1)]$$

Conditioned rapid shear tests evaluate the effect of stress history on the shear strength of the material. After the completion of the repeated load resilient modulus sequences, the samples were subjected to a rapid shear test at a confining pressure of 15-psi. Comparisons were made between the peak shear strength of the unconditioned samples and the conditioned ones.

Rapid shear test results are summarized in Table 5.2. Figure 5.1 shows the peak deviator stress attained at a confining pressure of 15-psi for the four granular materials utilized in the mainline sections.

5.1.4 Permanent Deformation Testing

The first part of the repeated loading testing sequence is the conditioning phase. These data are utilized to analyze the rutting potential of the granular material being tested. The specimens were conditioned for 1000 load repetitions at a deviator stress of 45-psi and a confining pressure of 15-psi. Some materials did not withstand this stress state condition. Those were conditioned at a deviator stress of 30-psi and a confining pressure of 15-psi.

Permanent deformation, resilient deformation, and applied deviator stress measurements were made at 1, 10, 50, 100, 500, and 1000 load repetitions. The phenomenological model that relates the log of permanent strain to the log of number of repetitions was used to characterize the rutting potential of the different materials.

$\varepsilon_p\% = AN^b$

where N is the number of load repetitions, b represents the amount of strain (%) accumulated per Log cycle, and A is the antilog of 'a' in:

$\text{Log } \varepsilon_p\% = a + b \text{ Log } N$

Table 5.3 presents the 'A' and 'b' values for the different materials at the different moisture and density levels. Higher 'A' and 'b' values indicate increased rutting potential.

Material	MC, %	Dry Density, pcf	Parameter 'A', %	Parameter 'b'	Stress State psi/psi	R^2
CL-3sp	8.0	127.8	0.516	0.110	45/15	0.99
CL-3sp	6.8	127.3	0.443	0.080	45/15	0.99
CL-4sp	7.9	130.0	0.626	0.240	45/15	0.99
CL-4sp	9.4	132.0	1.001	0.430	30/15	0.99
CL-5sp	7.7	139.0	0.334	0.440	30/15	0.99
CL-5sp	6.8	137.0	0.292	0.350	30/15	0.99
CL-6sp	6.3	134.0	0.151	0.134	45/15	0.99
CL-6sp	6.3	139.0	0.172	0.140	45/15	0.99
CL-6sp	5.4	133.0	0.107	0.155	45/15	0.99
CL-6sp	7.3	131.0	0.276	0.135	45/15	0.99

Table 5.3. Results from Permanent Deformation Testing on Mn/ROAD Granular Materials.

5.1.5 Resilient Modulus Testing

Specimens were subjected to various repeated triaxial stress states less than failure. A haversine load waveform was applied (pulse duration 0.1-second/rest period 0.9 seconds). After conditioning, modulus testing was conducted at the stress states shown in Table 5.4.

The sample was subjected to 100 repetitions at each stress state. If the difference between the 50th and 100th load repetition was more than 5 percent, the sequence was repeated.

Deviator Stress, σ_d, psi	Confining Pressure, σ_3, psi	Number of Load Repetitions
45	15	1000*
10	5	100
15	5	100
20	10	100
30	10	100
30	15	100
45	15	100
45	30	100
60	30	100

* Standard stress state for sample conditioning

Table 5.4. Stress States Utilized during Testing.

Resilient modulus for each stress state was calculated as:

$$E_r = \sigma_d / \varepsilon_r$$

where: E_r = Resilient Modulus, psi

σ_d = Applied Deviator Stress, psi

ε_r = Resilient strain

Resilient modulus test data were used to develop 'K' and 'n' parameters for the K-θ model. Table 5.5 gives 'K' and 'n' values for the materials tested. The following relationship for the Mn/ROAD granular materials (per Rada & Witczak) was established between 'K' and 'n'.

$$\text{Log } K = 3.996 - 0.893*n$$

$$R^2 = 0.81$$

The 'K' and 'n ' relationship obtained by Rada & Witzack and the U of I are presented in Figure 5.2. The results in the Rada & Witzack study came from a broad data base and various testing procedures.

The resilient modulus test data were also used to develop parameters for three(K-θ, UT-Austin, Uzan) granular material resilient modulus models. These models are used to estimate the resilient modulus of granular materials as a function of stress state.

Material	MC,	Dry Density,	THETA Model			UZAN's Model				UT-AUSTIN Model			
Class	%	pcf	K	n	R^2	K3	K4	K5	R^2	N6	N7	N8	R^2
CL-3sp	8.0	128	2012	0.65	0.989	1774	0.88	-0.25	0.996	5574	0.1322	0.4988	0.984
CL-3sp	6.8	127	2707	0.60	0.987	2420	0.81	-0.22	0.993	6922	0.1271	0.4586	0.984
CL4-sp	9.4	132	6490	0.20	0.889	5764	0.42	-0.24	0.943	9925	-0.0534	0.2365	0.995
CL-4sp	7.9	130	2410	0.60	0.939	2033	0.91	-0.34	0.952	6632	0.0610	0.5137	0.903
CL5-sp	6.8	137	3827	0.45	0.883	3181	0.79	-0.37	0.909	8842	-0.0232	0.4445	0.934
CL5-sp	7.7	139	5358	0.32	0.933	4980	0.45	-0.15	0.942	8983	0.0530	0.2565	0.984
CL6-sp	6.3	134	2583	0.64	0.997	2647	0.59	0.05	0.998	5736	0.3047	0.3380	0.993
CL6-sp	5.4	133	2807	0.64	0.997	2737	0.68	-0.05	0.997	6707	0.2442	0.3925	0.992
CL6-sp	7.3	131	3206	0.62	0.996	3225	0.61	0.01	0.996	7121	0.2740	0.3461	0.989
CL6-sp	6.3	139	4597	0.57	0.998	4478	0.62	-0.05	0.999	10049	0.2168	0.3527	0.997

Table 5.5. Resilient Modulus Testing Results on Mn/ROAD Mainline Granular Materials.

K-θ Model

Linear regression was performed to obtain a best fit equation of the form:

$ER = a + n\ Log(\theta)$

where:

θ = the bulk stress ($\sigma_1 + 2\sigma_3$),

σ_1 = major principal stress and

σ_3 = minor principal stress.

This relation is also given as:

$ER = K*\theta^n$

where:

K = the antilog of 'a'

'n' = slope, represents stress sensitivity

Table 5.5 presents the K and n parameters for all the materials tested.

Uzan's Model

Linear regression was performed to obtain the best fit line of the form:

$ER = a\ K4*Log(\theta) + K5*Log(\sigma_d)$

where:

θ = the bulk stress,

σ_d = deviator stress.

The response was transformed into the following model:

$ER = K3*\theta K4*\sigma_d K5$

where:

K3 = antilog of 'a'

K4, K5 = experimentally determined parameters.

The values K3, K4, and K5 for different materials tested are given in Table 5.5.

UT-Austin Model

Linear regression was performed to obtain a best fit equation of the form:

$\text{Log } \varepsilon_a = a + K7*\text{Log}(\sigma_d) + K8*\text{Log}(\sigma_3)$

where:

ε_a = the measured resilient axial strain,

σ_d = the deviator stress,

σ_3 = the minor principal stress.

The response was transformed into the following model:

$\varepsilon_a = N6*(\sigma_d N7)*(\sigma_3 N8)$

where:

N6 = the antilog of 'a'

N7 = 1-K7

N8 = -K8

The values of N6, N7, and N8 are presented in Table 5.5.

The R^2 values for the UT-Austin model were higher than the K-θ model and Uzan's model. The axial strains were calculated from the estimated modulus values for the three models and were compared to the measured axial strains and resilient modulus values. The

axial strain values calculated form the resilient modulus models were in good agreement with the measured axial strain values.

5.1.6 Dynamic Cone Penetrometer Testing

Dynamic Cone Penetrometer (DCP) data are indicative of the shear strength (CBR) of granular materials. Cylindrical specimens (9-inch diameter, 15-inch in height) were prepared and tested in the laboratory. The calibrated lower rod was driven into the material using a 17.6-pound anvil on the upper rod. The DCP was mounted on a guide frame to maintain vertical alignment. Figure 5.3 and Figure 5.4 show the DCP and DCP mounted on a guide frame respectively. The rod penetration after each anvil blow was recorded as inches/blow. This was recorded as the penetration rate (PR). CBR was estimated from PR as follows:

$$\text{Log}_{10}(\text{CBR}) = 0.84 - 1.26^{*} \text{Log}_{10}(\text{PR})$$

The DCP test results show that, in general, a high PR value was obtained for the first several inches of penetration. This is attributed to the lack of overburden or confining stress, and the displacement of material at the surface of the specimen. At greater depths, lower PR values are obtained due to a higher degree of confinement because of overburden. Hence, the PR was evaluated as an average value over the 4-inch portion of the specimen.

Table 5.6 summarizes the results obtained from DCP tests on the four granular materials at various moisture and density levels. For the CL-4sp material, at moisture contents lower than optimum moisture content (OMC), increased density resulted in lower PR value. At moisture contents higher than OMC, the effects due to change in density were not significant. For the other materials (CL-3sp, CL-6sp), PR values increased with increase in moisture content.

The peak shear strength obtained from rapid shear tests were correlated to the PR values obtained from DCP tests for the same moisture/density levels. Shear strengths obtained at a confining pressure of 15-psi gave the best correlation with the PR values. The following relationship was established:

$\sigma_d = 107.86 - 41.05*PR$

$R^2 = 0.63$

SEE = 7.13

The relationship between PR and peak shear strength is shown in Figure 5.5. A correlation was performed between the deviator stress at 2-percent axial strain from rapid shear test at a confining pressure of 15-psi to the penetration rate (PR). The following relation was established:

σ_d@2%strain = 108.04 - 68.03*PR

R2 = 0.71

SEE = 9.92

DCP test results (PR) may be used to get a reasonable estimate of the granular material shear strength.

5.1.7 Summary

Characterization of the four granular materials utilized in the mainline sections was performed at the University of Illinois. A detailed report is presented elsewhere (12). DCP and rapid shear tests were performed to evaluate the shear strength of the materials. Repeated load tests were performed to characterize the resilient modulus and rutting potential of the granular materials.

5.2 Mn/DOT Laboratory Results on Cohesive Subgrade Soils

5.2.1 Introduction

There is only one subgrade soil in the mainline FPS. The native soils at the site are primarily silty clay and the existing topography had no more than 10 to 13-feet of relief prior to construction. The embankments for the mainline track range in height between 0.3 to 10-feet and are constructed on cuts ranging from 0.7 to 2-feet. Laboratory testing on the cohesive soil was performed by MnDOT.

Material	Moisture Content, %	Dry Density pcf.	Penetration Rate inch/blow	CBR, %
CL-3sp	7.4	126	0.23	45
CL-3sp	7.9	127	0.29	33
CL-4sp	6.7	130	0.12	100
CL-4sp	7.3	126	0.41	21
CL-4sp	7.5	126	0.57	14
CL-4sp	7.6	130	0.20	54
CL-4sp	7.9	126	0.57	14
CL-4sp	8.7	130	0.29	33
CL-4sp	9.7	131	0.60	13
CL-4sp	10.4	126	0.59	14
CL-5sp	6.4	129	0.78	9
CL-5sp	7.6	139	0.67	11
CL-5sp	8.4	138	1.03	7
CL-6sp	5.6	137	0.26	38
CL-6sp	6.3	139	0.21	51
CL-6sp	6.8	136	0.33	28
CL-6sp	7.3	130	0.56	14

Table 5.6. Results from DCP Testing on Mn/ROAD Granular Materials.

Date	Sample ID	Test Section	Station	Depth inch	Liquid Limit, %	Plasticity Index, %	Percent Clay	Percent Silt	Specific Gravity	OMC %	Max. Dry Density, pcf	R-Value @ 240 psi
6-25-92	10418A	26	17210	30.00	30	12	15.4	40.4	-	16.5	112	13.30
6-25-92	10419A	27	17775	38.03	37	19	20.4	43.0	-	18.1	108	12.80
6-25-92	10420A	28	18345	33.98	38	19	23.1	40.1	-	16.8	109	13.60
10-22-91	10421A	29	18915	32.99	43	25	25.4	38.5	2.675	17.9	107	13.30
10-22-91	10422A	30	19485	35.04	45	28	28.0	37.7	-	19.1	105	12.00
10-22-91	10423A	31	20055	36.97	37	20	21.9	38.9	-	19.6	105	12.10
10-22-91	10424A	32	20620	30.00	41	23	23.7	36.9	2.665	18.5	105	13.10
6-29-92	10425A	33	6620	35.98	34	16	-	-	-	17.9	109	14.60
6-26-92	10426A	34	7190	30.00	33	14	-	-	-	17.2	110	13.40
6-26-92	10427A	35	7740	30.00	30	11	-	-	-	15.0	111	14.20
				Mean	37	19	22.6	39.4		17.7	108	13.24
				STD	4.97	5.26	3.70	1.88		1.27	2.46	0.77
				COV, %	13.50	28.20	16.38	4.77		7.21	2.28	5.84

OMC : Optimum Moisture Content

Table 5.7. Results of Soil Analyses on Bag Samples.

5.2.2 Laboratory Tests

Subgrade samples were collected by MnDOT at various stages of construction for laboratory testing. Samples were obtained using the Thinwall Shelby Tube (undisturbed) and bulk bag samples (disturbed). The thinwall Shelby tube was 3-inch in diameter and 30-inch in length (sample length = 24-inch). The samples were collected after subgrade completion and before placement of subbase/base layers. The samples were from depths ranging 1-foot to 6-feet under the right outer wheel path at various stations. All bag samples were taken from beneath the centerline of the roadway, near the center of each cell.

Resilient modulus tests (SHRP protocol P 46), and unconfined compression tests (AASHTO T 208) were performed by MnDOT personnel on the undisturbed and disturbed samples (13, 14). Other tests including Atterberg Limits (AASHTO T 90), sieve and hydrometer analysis (AASHTO T 88), Proctor Density tests (AASHTO T 99 and T 180), and Stabilometer (R-value) tests.

Gradation Tests

Sieve and hydrometer analyses were performed following AASHTO T 88. Table 5.7 summarizes the results for the bag samples. The results here are for the LVR sections. These data presented are for the same cohesive soil encountered in the mainline. The percent clay (< 0.002 mm) ranged from 15.4 to 28.0 with an average of 22.6. The percent silt, (< 0.074 mm) ranged from 36.9 to 43.0 with an average of 39.4. The results for the undisturbed samples are presented in Table 5.8. The percent clay ranged from 14.6 to 28.3 with an average of 21.2. The percent silt ranged from 35.8 to 44.5 with an average of 40.5.

Stabilometer Tests

Hveem stabilometer tests were conducted to determine the R-value on the bag samples. The sample depths ranged from 26.8 to 72.7 inches. Table 5.9 presents the results for the mainline sections bag samples. The R-value ranged from 12.4 to 15.9 with an average value of 13.9.

Date	Sample ID	TS	Station	Depth inch	LL %	PI	K1 psi/psi	K2 psi/psi	qu psi	ERi ksi	Bulk Density pcf	Dry Density pcf	MC %	S %	% Clay	% Silt
6/25/92	10051A	26	17215	30.00	30	12	1078	333	21.8	9.5	129	111	15.9	85.1	16.4	39.9
6/25/92	10051B	26	17213	54.02	36	17	1573	484	21.0	13.7	132	113	16.7	95.0	20.9	41.5
6/25/92	10053A	27	17780	38.03	42	23	1660	472	19.0	11.0	133	112	18.1	100.0	21.7	41.5
6/25/92	10053B	27	17780	56.02	48	29	1119	306	18.0	6.6	130	109	19.8	99.8	26.5	40.8
6/26/92	10055A	28	18350	51.97	48	28	1418	384	20.5	8.1	129	107	20.0	96.7	28.3	44.5
6/26/92	10059A	30	19490	53.03	43	24	1171	310	18.9	6.3	132	112	18.1	98.8	26.7	40.7
10/24/91	10061A	31	20060	54.96	37	17	1332	412	12.6	11.8	131	112	17.4	94.5	23.7	37.4
10/24/91	10061B	31	20060	90.94	33	12	1184	420	15.7	20.6	132	115	15.3	90.7	23.0	35.8
6/26/92	10063B	32	20625	60.00	40	22	1673	475	17.7	11.0	133	114	17.2	99.1	22.8	39.7
7/1/92	10065A	33	6625	30.00	37	19	1246	433	36.6	19.1	136	119	14.1	94.2	15.5	38.9
7/1/92	10065B	33	6625	54.02	35	16	1592	447	24.0	10.1	133	113	17.3	98.2	18.7	42.1
7/1/92	10067A	34	7195	35.98	37	18	1468	370	12.9	6.9	131	111	18.2	96.4	21.6	39.5
7/1/92	10067B	34	7195	47.99	30	12	1199	365	31.2	10.0	133	115	15.7	94.0	14.6	41.7
7/1/92	10069A	35	7745	24.02	31	12	911	346	47.2	27.1	137	121	13.1	93.9	15.2	42.2
7/1/92	10069B	35	7745	60.00	38	19	1251	423	25.3	16.6	133	114	16.9	97.0	22.3	40.7
				Mean	38	18	1325	399	22.8	12.5	132	113	16.9		21.2	40.5
				STD	5.63	5.48	222.30	57.15	8.95	5.73	2.18	3.42	1.83		4.19	2.02
				COV, %	14.93	29.73	16.78	14.34	39.19	45.66	1.65	3.02	10.83		19.79	5.00

TS : Test Section
MC : Moisture Content
qu : Unconfined compressive strength
ERi : Subgrade "breakpoint" modulus
LL : Liquid limit
PI : Plasticity Index
S: Degree of Saturation

Table 5.8. Results of Resilient Modulus Tests Near Optimum Moisture from Thinwall Shelby Tube Samples.

Atterberg Limits

Tests were performed on the mainline bag samples to determine the Atterberg Limits. The results are summarized in Table 5.9. The tests were done following AASHTO T 90 procedures. The liquid limit (LL) ranged from 32.5 to 39.0 percent with an average of 36.7.

The plasticity index (PI) ranged from 13.5 to 20.7 with an average of 16.7. The subgrade was classified as an AASHTO A-6 soil (silty-clay, more than 35% passing the 200 sieve, LL-40 maximum, PI-11 minimum).

Unconfined Compressive Strength Test Results

Table 5.10 presents the results for the unconfined compressive strength (q_u) for the bag samples, and Table 5.8 shows the results for the undisturbed samples. The results summarized in this table are for LVR section samples. For the undisturbed samples, q_u ranged from 12.6 to 47.2 psi with a mean of 23.0 psi. The q_u for the disturbed samples ranged from 9.1 psi to 15.3 psi with an average of 12.4 psi.

Resilient Modulus Test Results

Resilient modulus testing was performed on the disturbed and undisturbed samples. The SHRP Protocol P46 was followed. The resilient behavior of the cohesive soil was characterized using the following model;

$$M_R = K_1 \sigma_d^{K2}$$

where:

M_R = the resilient modulus of the soil

σ_d = the deviator stress

K1 and K2 = regression constants.

The values for K1 and K2 were obtained from the Mn/ROAD database. Table 5.8 and 5.10 show the results for the undisturbed and disturbed samples, respectively. For the undisturbed samples, K1 ranged from 911 psi/psi to 1673 psi/psi and K2 ranged 306 psi/psi to 484 psi/psi.

Sample ID	TS	Station	Depth, in.	Liquid Limit, %	Plasticity Index, %	OMC, %	Density, pcf	R-value @ 240 psi
10393A	1	110555	49.80	32.70	14.30	17.30	109.37	13.60
10393B	1	110555	59.76	32.90	19.00	16.80	109.06	-
10394A	2	111115	49.80	35.80	16.50	18.00	106.19	14.50
10395A	3	111675	54.72	36.00	17.20	17.90	107.88	14.10
10396A	4	112280	26.77	32.50	14.20	16.20	110.37	13.10
10406A	14	119165	28.82	34.80	14.30	17.30	107.69	13.00
10406B	14	119165	52.80	37.00	15.70	16.70	109.19	15.40
10407A	15	119715	34.80	33.80	14.30	17.00	109.75	15.10
10407B	15	119770	52.80	33.60	13.50	15.80	109.44	13.80
10408A	16	120310	47.76	36.60	17.00	17.40	109.37	12.40
10408B	16	120205	59.76	35.20	14.50	16.70	107.75	14.60
10409A	17	120860	47.76	35.50	17.30	17.30	107.75	11.90
10410A	18	121430	52.80	32.70	14.00	15.20	112.68	14.10
10410B	18	121430	72.72	39.00	20.40	17.00	105.50	14.60
10411A	19	122000	47.76	58.70	18.50	17.00	109.19	12.60
10411B	19	122000	59.76	38.50	20.70	20.60	103.88	-
10412A	20	122385	47.76	36.80	17.60	17.20	108.75	14.00
10413A	21	123060	48.70	35.70	15.70	17.30	109.19	13.70
10414A	22	123540	43.82	34.80	14.60	18.40	106.88	13.30
10414B	22	123720	55.79	37.70	18.40	17.10	106.94	14.40
10415A	23	124300	39.72	37.20	19.80	18.00	107.69	13.50
10415B	23	124300	57.72	38.80	19.60	17.90	104.94	15.90
			Mean	36.65	16.69	17.28	108.16	13.88
			Stand. Dev.	5.32	2.32	1.05	1.96	1.01
			COV, %	14.51	13.90	6.05	1.81	7.28

Table 5.9. Results of Soil Analyses from Bag Samples (Mainline)

Date	Sample ID	TS	Station	Depth inch	K1 psi/psi	K2 psi/psi	qu psi	ERi ksi	Bulk Density pcf	Dry Density pcf	MC %
6/25/92	10419A	27	17775	38.03	618	207	14.7	7.7	129	111	16.2
6/25/92	10420A	28	18345	33.98	927	313	15.3	12.0	127	109	16.3
10/22/91	10422A	30	19485	35.04	774	228	11.8	5.7	124	104	19.7
6/29/92	10425A	33	6620	35.98	680	212	10.9	6.2	128	109	17.8
6/26/92	10427A	35	7740	30.00	678	230	9.1	9.0	121	106	14.6
				Mean	735	238	12.4	8.1	126	108	16.9
				STD	107.97	38.52	2.33	2.28	2.86	2.54	1.72
				COV, %	14.68	16.21	18.85	27.98	2.27	2.36	10.16

TS : Test Section

MC : Moisture Content

qu : Unconfined compressive strength

ERi : Subgrade "breakpoint" modulus

Table 5.10. Results of Resilient Modulus Tests Near Optimum Moisture from Bag Samples.

For the disturbed samples, K1 ranged from 618 psi/psi to 927 psi/psi and K2 ranged from 207 psi/psi to 313 psi/psi. The E_{Ri} ranged from 6.3 ksi to 27.1 ksi for the undisturbed samples and from 5.7 ksi to 12.0 ksi for the disturbed samples. The results from disturbed samples were always lower than the results for the undisturbed ones.

5.3 Falling Weight Deflectometer (FWD) Testing on Mainline Test Sections

5.3.1 Introduction

FWD testing can be used to evaluate in-situ material properties by backcalculation of the materials properties. The Mn/ROAD FWD is a Dynatest Model 8000. Routine FWD testing on the flexible sections includes deflection testing at 50-foot intervals. Four different transverse sections are being tested. The FWD data files collected from the database contain data from the different stations along a given longitudinal offset from the centerline. The offsets are ± 9.8 and ± 6.5 feet, the positive distances correspond to the passing lane and the negative ones to the driving lane. The greater distances are for the outer wheel path and the other location is between the wheel tracks. During the testing the FWD van and trailer are always pointed westerly. The data in this study represents testing conducted since the beginning of traffic until mid 1996. All of the mainline flexible sections were analyzed.

5.3.2 Asphalt Concrete Thickness Measurements Using Ground Penetrating Radar

The AC thickness variation was considered in the FWD data analysis by using the actual thickness at the test site. The thickness values were obtained from GPR data. A study (57) was performed at Mn/ROAD where the GPR asphalt thickness data were correlated with core data. A statistical analysis of the data showed an R-squared of 0.98. The absolute deviation between radar and core data is 0.24. Data from the pavement thickness survey performed at Mn/ROAD were obtained through querying the ORACLE database via Internet. Table 5.11 contains the summary of the test results for the mainline test cells.

Cell	T_{AC} Target, in	T_{AC} Average, in	Std. Dev.	COV, %
1	5.75	5.894	0.398	6.756
2	5.75	6.094	0.374	6.132
3	5.75	6.263	0.219	3.500
4	8.75	9.082	0.447	4.919
14	10.75	10.931	0.342	3.132
15	10.75	11.105	0.474	4.266
16	7.75	8.012	0.352	4.395
17	7.75	7.925	0.389	4.907
18	7.75	7.907	0.191	2.415
19	7.75	7.915	0.485	6.123
20	7.75	7.747	0.403	5.202
21	7.75	7.724	0.302	3.913
22	7.75	7.855	0.504	6.415

Table 5.11. GPR AC Thickness Results for Mainline FPS.

Figures showing the thickness variation of the AC layer for each of the mainline flexible test sections are presented in Appendix B.

5.3.3 Pavement Temperature

Temperature information is collected with the FWD data at 1/3 of the AC mat depth. The temperature data in the Mn/ROAD database is determined by the BELLS method, which uses readily available information (i.e., time, air temperature, thickness, and AC surface data) to estimate the temperature at 1/3 of the AC mat. BELLS is an acronym for the authors Baltzer, Ertman-Larsen, Lukanen, and Stubstad (58). The BELLS equation is a s follows:

$$T_{1/3} = 8.77 + 0.649*IR + \{\log(d) - 1.5\}\{-0.503*IR + 0.786*(5 - day) + 4.79*\sin(hr - 18)\}$$
$$+ \{\sin(hr - 14)\}\{2.20 + 0.044*IR\}$$

where:

$T_{1/3}$	=	pavement temperature at third-point in AC mat, ^{o}C;
IR	=	infrared surface temperature reading at time of FWD test, ^{o}C;
log	=	base 10 logarithm;
d	=	depth at which mat temperature is to be determined, i.e. total AC mat thickness divided by 3 mm
5-day	=	previous mean 5-day air temperature, sum of 5 highs and 5 lows

		divided by 10, °C
sin	=	sin function in 24 hour clock system, with 2π radians equal to one 24 hour cycle;
hr	=	time of day, in 24 hour system. To use the time-hr function correctly, divide the number of hours in cycle by 24, multiply by 2π, and apply the sin function in radians.

5.3.4 Backcalculation Procedure

ILLI-PAVE based algorithms were utilized to backcalculate the asphalt concrete modulus (E_{AC}) and subgrade soil resilient modulus (E_{Ri}). The routine FWD testing was conducted at different load levels. Only tests at 9,000 lb. (standard wheel load) load level were analyzed.

In this scheme the deflection basin is characterized by D0, D1, D2, D3, AREA, and AUPP (2) as illustrated by Figure 5.6. D0-D3 are surface deflections, in mils., measured under the center of the plate load , at 12, 24 and 36 inch, respectively.

5.3.5 Backcalculation Algorithms

5.3.5.1 Full Depth Sections

The algorithms used to backcalculate the properties of the AC and subgrade layers were specially developed for these cells to increase their sensibility to desired range of thickness. The original algorithms were developed by Gomez et al., 1986 (3). Appendix C contains a detailed description of the algorithm development for the Mn/ROAD sections. The algorithms utilized are given below:

AC Modulus

$$\text{Log}(E_{AC}) = 0.741 - 8.5181 * \text{Log}(D0-D1) + 10.6040 * (D0-D2) - 3.1328 * (D1-D3)$$

$R^2 = 0.99$

SEE = 0.01

Subgrade Modulus

$$E_{Ri} = 25.559 - 5.531* D3 + 0.312 * (D3)^2$$

$R^2 = 0.99$

SEE = 0.47 ksi

5.3.5.2 Conventional Sections

The algorithms utilized for these sections were originally developed by Elliot et al., 1985 (17). In that study the range of thickness used for the base course was less than the thickness of most of the Mn/ROAD conventional test sections. The algorithms are as follows:

AC Modulus

$Log(E_{AC}) = 1.48 + 1.76* Log(AREA/D0) + 0.26*(AREA/T_{AC})$

$R^2 = 0.95$

SEE = 0.11

Subgrade Modulus

$Log(E_{Ri}) = 1.51 - 0.19* D3 + 0.27 * Log(D3)$

$R^2 = 0.99$

SEE = 0.05

The T_{AC} term was obtained from (GPR) measurements. The AREA is a deflection basin parameter in inches and is calculated as:

AREA, in. = 6*[D0 + 2D1 + 2D2 + D3]/D0

To determine the validity of these algorithms for the Mn/ROAD test sections, ILLIPAVE runs were conducted to determine the impact of increased base thickness on the variables included in the algorithms.

Figures 5.7 - 5.10 show the effects due to changes in the inputs for the algorithms with different base thickness. Figures 5.7 and 5.8 present the variation of the (AREA/DO) term for two different values of asphalt concrete modulus. Figures 5.9 and 5.10 depict the change of the ($AREA/T_{AC}$) term also for two different modulus values. There is virtually no change in the AREA/D0 and $AREA/T_{AC}$ terms. It was concluded that the original algorithms were adequate for analyzing the Mn/ROAD sections.

5.3.6 Analysis of Results

The AC layer modulus is greatly influenced by temperature. The Mn/ROAD mixes were tested to determine the resilient modulus at different temperatures. Tests were performed on cores collected before trafficking. These laboratory results were compared with the field backcalculated values.

All mainline flexible sections have the same AC gradation. Different asphalt cements and different compactive efforts were utilized in the design of the AC mixes on the mainline flexible pavement test cells, see Table 5.12.

Asphalt Cement	**AC 120/150**				**AC 20**			
Compaction	75*	50	35	Gyratory	75	50	35	Gyratory
Cells	1, 14, 22	3, 21,23	2, 20	4	15, 17	18	19	16

* Number refers to blows in Marshall Mix Design.
Table 5.12. Summary of Mixes on the Mainline.

The E_{AC} - Temperature relations, backcalculated from FWD tests were plotted to show the variation between cells. For each cell, the backcalculated moduli were plotted and linear regressions were performed to characterize the trends. Figure 5.11 shows the backcalculated relations for all cells where AC 20 was utilized. Figure 5.12 presents the relations for the cells with Pen 120/150 asphalt. There is variation when all are plotted together. Grouping by asphalt cement leads to very condensed plots of the relations, but the binder type effect is not very significant.

No significant influence in AC modulus was observed, even though different compactive efforts were used in the mixture design. In the field all mixes behaved in a similar fashion. Figure 5.13 contains over 5,000 points representing E_{AC} values for all mainline cells. A linear regression performed on all the data rendered the overall E_{AC}-Temperature relation:

$\text{Log } E_{AC} = 3.685 - 0.048 * \text{Temp}$

$R^2 = 0.80$

SEE = 0.18

where:

Temp = is the temperature at which the modulus is required, °C.

To evaluate the FWD results The Asphalt Institute (TAI) equation was used to estimate AC moduli based on mix properties (59). In estimating the asphalt modulus using this algorithm, the in-place properties of the asphalt mix for each cell were utilized. These properties were obtained from the report: "Investigation of Hot Mix Asphalt Mixtures at Mn/ROAD" by Stroup-Gardiner et al., 1996 (60).

The test cores were collected at the time of sensor placement, approximately one month after paving was completed (October, 1992). All cores were obtained before trafficking. The air voids values were determined from the cores. The asphalt contents were extracted from samples obtained during the paving operation. Sieve analyses were performed on the samples after extraction. The average of all the lifts in the core was used in the calculation.

The Asphalt Institute equation for predicting the dynamic modulus is given as:

$|E^*| = 100{,}000 * 10^{\beta 1}$

$\beta_1 = \beta_3 + 0.000005 * \beta_2 - 0.00189 * \beta_2 f^{-1.1}$

$\beta_2 = \beta_4^{0.5} T^{\beta 2}$

$\beta_3 = 0.553833 + 0.028829 (P_{200} f^{-0.1703}) - 0.03476 V_a + 0.070377 \lambda + 0.931757 f^{-0.02774}$

$\beta_4 = 0.483 V_b$

$\beta_5 = 1.3 + 0.49825 \log f$

where:

β_1 to β_5 = constants,

f = the load frequency in Hz,

T = the temperature in °F,

P_{200} = the percentage by weight of the aggregate passing through the No. 200 sieve,

V_V = the volume of air void in %,

λ = the asphalt viscosity at 70 °F in 106 poise, and

V_b = the volume of bitumen in %

The viscosity of the asphalt cement at 70 °F can be estimated by the following equation:

$\lambda = 29{,}508.2\ (P_{77^oF})^{-2.1939}$

in which P_{77^oF} is the penetration at 77°F.

Figure 5.14 shows the TAI values next to the ILLI-PAVE backcalculated overall relation. Resilient moduli obtained at the University of Minnesota laboratory for the cores are also plotted in Figure 5.14. The TAI values and the FWD backcalculated trend show good agreement. The U of MN values tend to be lower at low temperatures.

D0 - Temperature relations were developed for each cell and are presented in Appendix D. A great amount of variability is observed. No overall relation is recommended, and even the ones developed specifically for each cell have large variations. D0 is affected not only by the asphalt concrete modulus, but by subgrade E_{ri}.

AUPP is the area under the pavement profile. The parameter is calculated as follows:

AUPP, in. = ½ (5D0 - 2D1 - 2D2 - D3)

The horizontal strain (ε_{AC}) at the bottom of the AC layer has been correlated with the AUPP term. ILLI-PAVE based algorithms have been developed for full-depth and conventional flexible pavements relating ε_{AC} with AUPP. The algorithms are as follows:

Conventional Sections

$\text{Log}(\varepsilon_{AC}) = 1.00 + 1.01 * \text{Log}(\text{AUPP})$

$R^2 = 0.99$

SEE = 0.03

Full Depth Sections

$\text{Log}(\varepsilon_{AC}) = 1.07 + 0.98 * \text{Log}(\text{AUPP})$

$R^2 = 0.99$

SEE = 0.03

AC fatigue of FPS has been correlated to AC strain. Since AUPP has been correlated with AC strain, a correlation between AUPP to a readily available measurement, maximum deflection (D0) was performed. Figures 5.15 and 5.16 show the D0 - AUPP relation for the conventional sections with an AC thickness of 5.75-inch and 7.75-inch, respectively. Figure 5.17 presents the combined data for sections with both thickness values. The correlation

remains very similar to the other two and the coefficient of correlation is very similar. Figures 5.18 and 5.19 present the D0 - AUPP relation for the full depth sections with AC thickness of 8.75-inch and 10.75-inch. Figure 5.20 shows the results for the combined full depth sections. Again, the overall relation has similar constants and coefficient of correlation (R^2).

Subgrade 'Breakpoint' modulus E_{Ri} was backcalculated from the extensive FWD data using the ILLI-PAVE based algorithms presented above. Figure 5.21 shows the variation in E_{Ri} with time for all cells (1994). Similar results were obtained for the other years. There is a great variation in the moduli for each date. The variation in E_{Ri} is similar for each cell or the combined data of all the cells.

Subgrade stress ratios (SSR) were backcalculated for selected cells. The FDAC and CFP algorithms utilized were presented in Chapter 2. Figure 5.22 presents the SSR results for Cells 1, 4, 14, and 16. Cells 1 and 4 have a 5-year design life. Cells 14 and 16 have a 10-year design life. The SSR for the CFP cells (Cells 1 and 16) is less than 0.1 throughout the year. For the FDAC sections (Cells 4 and 14) , the maximum SSR is 0.25. These values are low, ensuring a "stable" permanent deformation accumulation on the subgrade layer. For the Mn/ROAD test sections, rutting on the subgrade is not a controlling criteria.

5.3.7 Summary

Routine FWD testing was periodically conducted at Mn/ROAD. The data were "downloaded" from the Mn/ROAD database and analyzed. There is no apparent effect due to asphalt cement type or compaction in the E_{AC} - Temperature relations. One relation for all cells characterizes the temperature effect on AC modulus. E_{AC} values were estimated using TAI dynamic modulus predictive equation. These values agree well with the backcalculated ones.

D0 - Temperature trends were not recommended for the cells because of the extensive variability in the data. AUPP - D0 trends were developed and showed a very good correlation. This relation is very important because a good estimate of AC strain can be made from readily available surface deflection values.

SSRs were backcalculated for several cells. The results show that for Mn/ROAD cells subgrade rutting is not a controlling factor. The "thick" AC layer and granular layers in these cells protects the subgrade from high stresses.

5.4 Subgrade Evaluation of MN/Road Research Project Flexible Cells using the Dynamic Cone Penetrometer

Dynamic Cone Penetrometer (DCP) tests were performed on the mainline flexible sections. The mainline flexible sections (CFP and FDAC) have only one subgrade soil. Thus, only three cells were selected to consider the in-situ variation in the subgrade soil. Results for Cells 4, 14, 15 are analyzed below. The tests were performed in 1992 and 1993 before the AC layer was placed.

The DCP used in MN/Road is based on the Central African Standard as modified by the Transvaal Road Department (61). Test results are expressed in terms of the penetration rate (PR), which is defined as the vertical movement of the DCP cone produced by one drop of the sliding weight (in/blow).

The DCP data were downloaded from the Mn/ROAD database. The PR (in/blow) was calculated for each location at different depths. The PR can be correlated with known pavement design parameters. The most common correlation of PR is to CBR. The CBR-PR algorithm used (originally proposed by the South Africans) is widely accepted (54).

Log CBR = 0.84 - 1.26 * Log PR

where:

CBR in (%),and

PR in (in/blow)

Although moisture content and dry density have a great influence on shear strength of fine grained soils, these properties are not taken into account in this relationship since they have been found to have similar influence on both CBR and PR results (62).

5.4.1 Cell 4

DCP testing (driving and passing lane) was performed in the months of June and

August 1992. The results of all the tests during the months of June and August are summarized in Table 5.13 and Table 5.14, respectively. The results for each location are presented in Appendix E. There is a great amount of variability in the CBR values for all depths. The variability is fairly consistent on both sides of the centerline (DL and PL). The distribution of the CBR values for different depths are presented in Figures 5.23 and 5.24.

Depth top	Overall Results			
subg., in	Ave. CBR, %	Standard Dev.	COV, %	Observations
0 - 5	23.19	8.74	37.7	53
5 - 10	13.83	4.33	31.3	40
10 - 15	10.71	3.26	30.4	32
15 - 20	10.45	2.55	24.4	32
20 - 25	10.62	3.51	33.1	33
25 - 30	12.67	4.06	32.0	37
30 - 35	15.45	6.72	43.5	42
35 - 40	16.69	6.74	40.4	52
40 - 45	16.16	7.23	44.7	18

Table 5.13. Summary of DCP testing on Cell 4, June 1992.

Depth top	Overall Results			
subg., in	Ave. CBR, %	Standard Dev.	COV, %	Observations
0 - 5	43.55	17.13	39.3	39
5 - 10	18.79	5.85	31.2	25
10 - 15	11.85	3.21	27.1	21
15 - 20	7.75	4.15	53.6	18
20 - 25	7.92	3.40	42.9	19
25 - 30	10.58	4.05	38.2	22
30 - 35	12.17	7.26	59.7	19
35 - 40	11.52	4.51	39.1	23
40 - 45	9.10	3.08	33.8	15

Table 5.14 Summary of DCP testing on Cell 4, August 1992.

5.4.2 Cell 14

DCP testing was performed in the driving and passing lanes in the months of June and August of 1992 and July of 1993. The results of all tests are included in Appendix E. Tables 5.15 through 5.17 summarize the results on each date. There is a wide variability in the CBR.

Depth top	Overall Results			
subg., in	Ave. CBR, %	Standard Dev.	COV, %	Observations
0 - 5	36.31	16.25	44.8	65
5 - 10	14.38	6.14	42.7	36
10 - 15	10.68	5.73	53.7	32
15 - 20	7.8	1.98	25.4	25
20 - 25	8.95	2.55	28.5	32
25 - 30	11.5	3.21	27.9	35
30 - 35	12.25	4.52	36.9	35
35 - 40	13.74	5.48	39.9	39
40 - 45	11.01	5.52	50.1	32

Table 5.15. Summary of DCP testing on Cell 14, June 1992.

Depth top	Overall Results			
subg., in	Ave. CBR, %	Standard Dev.	COV, %	Observations
0 - 5	43.22	22.93	53.1	30.0
5 - 10	20.06	7.13	35.5	31.0
10 - 15	16.60	12.74	76.7	21.0
15 - 20	11.40	4.10	36.0	22.0
20 - 25	12.80	4.02	31.4	22.0
25 - 30	17.71	16.52	93.3	22.0
30 - 35	15.01	6.73	44.8	24.0
35 - 40	16.44	7.06	42.9	26.0
40 - 45	14.86	5.23	35.2	17.0

Table 5.16. Summary of DCP testing on Cell 14, August 1992.

Depth top	Overall Results			
subg., in	Ave. CBR, %	Standard Dev.	COV, %	Observations
0 - 5	19.64	15.34	78.1	18
5 - 10	9.72	4.76	49.0	19
10 - 15	13.26	7.49	56.5	24
15 - 20	9.74	4.13	42.4	21
20 - 25	12.45	3.47	27.9	27
25 - 30	12.65	4.55	35.9	28
30 - 35	13.62	2.25	16.5	28
35 - 40	13.54	2.71	20.0	28
40 - 45	13.86	3.00	21.6	14

Table 5.17. Summary of DCP testing on Cell 14, July 1993.

The August data show the greatest variation and the variation is considerable at all depths. There is variation of CBR values from one location to the other within the same cell. Figures 5.25 to 5.27 show the distribution of the CBR strength parameter at different ranges of depth.

5.4.3 Cell 15

DCP testing was performed in May, June, and August of 1992. Tables 5.18 through 5.20 present a summary of the results for each test date.

Depth top	Overall Results			
subg., in	Ave. CBR, %	Standard Dev.	COV, %	Observations
0 - 5	9.90	7.16	72.3	17
5 - 10	9.94	4.29	43.2	20
10 - 15	8.03	1.91	23.7	17
15 - 20	10.84	5.10	47.1	20
20 - 25	12.50	4.90	39.2	23
25 - 30	10.81	3.21	29.7	20
30 - 35	13.86	6.89	49.7	19
35 - 40	11.19	3.10	27.7	23
40 - 45	11.27	4.13	36.7	15

Table 5.18. Summary of DCP testing on Cell 15, May 1992.

Depth top	Overall Results			
subg., in	Ave. CBR, %	Standard Dev.	COV, %	Observations
0 - 5	19.60	7.11	36.3	17
5 - 10	9.17	1.66	18.1	10
10 - 15	6.49	3.17	48.8	11
15 - 20	10.96	2.23	20.3	15
20 - 25	14.91	11.05	74.1	15
25 - 30	10.36	3.06	29.5	13
30 - 35	13.86	5.82	42.0	14
35 - 40	10.17	2.32	22.8	15
40 - 45	10.43	2.97	28.5	12

Table 5.19. Summary of DCP testing on Cell 15, June 1992.

Depth top	Overall Results			
subg., in	Ave. CBR, %	Standard Dev.	COV, %	Observations
0 - 5	33.54	11.75	35.0	27
5 - 10	14.54	5.00	34.4	18
10 - 15	8.82	2.54	28.8	15
15 - 20	10.21	2.82	27.6	20
20 - 25	12.85	3.13	24.3	23
25 - 30	9.38	2.34	25.0	18
30 - 35	9.64	2.03	21.1	18
35 - 40	8.87	2.67	30.1	18
40 - 45	8.16	2.43	29.8	12

Table 5.20. Summary of DCP testing on Cell 15, August 1992.

There is significant variation in CBR values from one location to the other within the same cell. The results for each date are presented in Appendix E. Figures 5.28 through 5.30 show the distribution of CBR at different ranges of depth.

5.4.4 Discussion of Results

The data from the various cells show that the upper 5 inches in the subgrade presents a higher variation in CBR values than any other range of depth. This is expected due to moisture changes. At other depth ranges, there is better consistency in the results.

Cells 4 and 14 were tested in the months of June and August of 1992. Results for these dates are comparable. After a year of the first DCP test on Cell 14, there is not notable difference in results. This can be observed by comparing data for June of 1992 with July of 1993. For the month of August of 1992, Cell 14 had somewhat higher results than cells 4 and 15.

5.4.5 Summary

Dynamic cone penetrometer (DCP) tests were performed on the mainline flexible sections. Three cells were selected to consider the in-situ variation in the subgrade soil (Cell 4, 14 and 15). The tests were performed in 1992 and 1993 before the AC layer was placed.

There is a great variability in CBR at all depths for all cells. The data show that the upper 5 inches in the subgrade has a higher variation in CBR values than any other range of depth. At other depth ranges, there is better consistency in the results. The results for different cells tested on the same date are comparable.

5.5 Laboratory Fatigue Testing of Mn/ROAD Asphalt Concrete Mixes @ ATREL

5.5.1 Introduction

The University of Illinois (U of I) is utilizing Mn/Road data to verify/refine/modify IDOT's Mechanistic-Empirical based flexible and rigid pavement analysis and design concepts and procedures. As part of the effort, the U of I - Advanced Transportation

Research and Engineering Laboratory (ATREL) performed fatigue testing on the Mn/ROAD asphalt concrete mixes. Four different mixes were tested.

5.5.2 Description of Mixes

One mix gradation was utilized throughout the project. Four different compaction levels were used in the project, 35, 50, and 75 blows for the Marshall mix designs. An additional mix was designed with the Gyratory compactor (SHRP Level 1). In this study, only 35 and 75 blow (Marshall Mix Design) compactive effort mixes were tested. The asphalt content varied according to the compaction effort used in the mixture design. For the 35 blow mix the asphalt content is 6.4%, and 75 blow compactive effort mixtures have an asphalt content of 5.9%. These values were supplied by University of Minnesota. The mixtures tested were previously prepared at the University of Minnesota and sent to ATREL.

5.5.2.1 Aggregates

The properties of the aggregate sources and their gradation, along with the blending percentages used to prepare the job mix formula are presented in Table 5.21. The table was reproduced from: "Investigation of Hot Mix Asphalt Mixtures at Mn/ROAD - Final Report" (60).

5.5.2.2 Asphalt Cement

Two binder grades, a 120/150 penetration grade and an AC 20 viscosity grade, were utilized for the mixes in this project. The asphalts were supplied by the Koch Refinery in Rosemont, Minnesota. Table 5.22 presents the properties of the two binders and the pertinent specifications.

5.5.3 Description of Fatigue Test

Mixture flexural fatigue characterization was performed per SHRP M009 protocol (AASHTO TP8-94). Under this protocol, a beam sized at 50mm × 60mm (2in × 2.4in) is tested under constant strain haversine loading condition. Failure is designated as the number of repetitions that reduces the initial flexural stiffness by 50 %. The loading frequency is 10

Hz with a haversine load pulse shape and no rest period. The test is performed at a temperature of 20°C ± 0.2°C (68 ± 0.4°F). (*Note:* IDOT's Design Time Temperature for the Mn/ROAD cells ranges between 18 - 20°C (65-69°F).)

Property	Crow River Fines	Crow River Coarse	CA-50	Combined Gradation (Job Mix Formula)
Blending Percentages, %				
Mix Design	74	16	10	100
Construction	66	24	10	100
Bulk Specific Gravity	2.73	2.66	2.62	2.708 (Mix)
Percent Crushed, %	--	61.2	100	2.702 (Field)
Cumulative Percent Passing, %				
¾ inch	100	100	100	100
½ inch	100	75	80	92
3/8 inch	99	53	37	82
No. 4	94	19	4	67
No. 10	82	11	--	57
No. 20	63	8	--	--
No. 40	39	6	--	27
No. 80	10	4	--	--
No. 100	8	3	--	--
No. 200	4.9	2.4	--	--

Table 5.21. Aggregate Properties for Mn/ROAD Asphalt Concrete Test Cells.

Property	Pen 120/150	ASTM D946	AC - 20	ASTM D3381
Viscosity, 60°C(140°F), Poise	846		1,987	2,000±400
Viscosity, 135°C(275°F), cSt	271		397	210 min
Penetration, 25°C(77°F) 0.1mm	130	120 min 150 max	76	40 min
Ductility, 25°C (77°F) 5cm/min	120+		120+	
Flash Point, °C(°F) min	318(605)	218(425) min		232(450) min
Test on Residue from Thin Film Oven Test				
Viscosity, 60°C(140°F), Poise	1,880		4,662	10,000 max
Viscosity, 135°C(275°F), cSt	439		579	
Penetration, 25°C(77°F) 0.1mm	71		45	
Ductility, 25°C (77°F) 5cm/min	120+	100 min	120+	20 min
SUPERPAVE (SHRP) Binder Specifications				
PG Grading	PG 58 -28		PG 58 -22	

Table 5.22. Properties of Asphalt Cements used in the Mn/Road Project.

5.5.4 Equipment

Fatigue testing was performed on an Industrial Process Control (IPC) Beam Fatigue Apparatus (Figure 5.31) (63). This machine is a digitally controlled closed loop servo-pneumatic device with self contained control and data acquisition system (CDAS), providing

complete Proportional, Integral, and Derivative (PID) adjustments and adaptive feedback control during the testing.

The specimen is subjected to 4 point bending with free rotation and horizontal translation of all load and reaction points (Figure 5.32). The spacing between the loading points is 118.5 mm (5.67 in.). The applied force is measured, and the resulting beam deflection is monitored using an on-specimen LVDT. The apparatus operates inside a temperature chamber for temperature control.

5.5.5 Preparation of Specimens

The mixtures were heated to a temperature of 160°C (320°F) and compacted to the target void level using the Rantoul Rolling Wheel Compactor shown in Figure 5.33, which is modeled after the Georgia Tech Compactor. In this scheme, a fixed volume (the steel sample mold 3-inch × 5-inch ×15-inch) is utilized and the amount of material needed to obtain a certain void level is calculated. The sample is compacted until the volume of the material is equal to the volume of the mold.

The bricks were extruded from the mold, stored at room temperature for a week, and the volumetric properties were determined, as shown in Table 5.23. The bricks were then sawed into two beams each for fatigue testing.

Specimen ID	G_{mm}*	G_{mb}	% Air Voids	Ave. % Air Voids	Target % Air Voids**
AC-35-1	2.443	2.275	6.88	6.30	7.00
AC-35-2	2.443	2.300	5.84		
AC-35-3	2.443	2.292	6.19		
AC-75-1	2.443	2.279	6.7	6.72	7.00
AC-75-2	2.443	2.282	6.61		
AC-75-3	2.443	2.275	6.86		
Pen-35-1	2.421	2.239	7.5	7.56	8.50
Pen-35-2	2.421	2.240	7.49		
Pen-35-3	2.421	2.235	7.70		
Pen-75-1	2.421	2.227	8.03	7.78	8.50
Pen-75-2	2.421	2.231	7.81		
Pen-75-3	2.421	2.239	7.51		

*G_{mm} information provided by University of Minnesota
**Established in consultation with Mn/ROAD and University of Minnesota staff.
Table 5.23. Mn/ROAD Beam Properties.

5.5.6 Fatigue Data

Fatigue algorithms for Asphalt Concrete mixes are usually expressed by the following strain-based relation:

$$N = K_1 (1/\varepsilon)^{K_2}$$

where:

N = the number of repetitions to failure

ε = strain at the bottom of AC layer (in laboratory strain at bottom of beam) in in/in

K_1 and K_2 = statistically determined constants.

The constants for the four mixes derived from regression analysis of the laboratory data are presented in Table 5.24.

Mixture	K_1	K_2	R^2
AC-20(35 Blow)	9.600E-13	5.260	0.986
AC-20(75 Blow)	1.692E-12	5.132	0.990
Pen 120/150(35 Blow)	1.784E-11	4.946	0.987
Pen 120/150(75 Blow)	2.366E-10	4.545	0.999

Table 5.24. Material constants and correlation coefficient from controlled-strain fatigue tests.

Flexural moduli are also obtained during the test. The modulus during the first fifty load cycles is representative of the "undamaged" mixture. The flexural moduli are shown in Table 5.25. The moduli recorded for each strain level are presented, along with the average modulus and standard deviation for each mixture.

Mix	Flexural Modulus, MPa	Ave. Flexural Mod., MPa (ksi)	Standard Dev. MPa (ksi)
	4479		
AC - 20 35 Blows	5006	5257 (762)	631 (92)
	5774		
	5767		
	4313		
AC - 20 75 Blows	4939	5270 (764)	791 (115)
	6019		
	5809		
	2322		
Pen 120/150 35 Blows	2433	2679 (388)	381 (55)
	2799		
	3162		
	2387		
Pen 120/150 35 Blows	2775	2619 (380)	205 (30)
	3211		

Table 5.25. Flexural Modulus values for Mn/ROAD mixes tested (21).

5.5.6.1 Dissipated Energy

The dissipated energy per cycle for a beam specimen tested under pulse loading is computed as the area within the stress-strain hysteresis loop. The dissipated energy per cycle decreases with an increasing number of load repetitions in a controlled-strain fatigue test. For the controlled-stress fatigue test, the dissipated energy per cycle increases as the number of repetitions increases. The cumulative dissipated energy to failure for a flexural beam fatigue test is the summation of the area under the curve between dissipated energy and number of cycles. The rate at which the dissipated energy of a material changes is the best indication of the rate of damage being done to the material (64).

For a sinusoidal loading condition, dissipated energy per cycle is given by:

$W_i = \pi * \sigma_i * \varepsilon_i * \sin\phi_i$

where: W_i = dissipated energy at load cycle i.

σ_i = stress amplitude at load cycle i.

ε_i = strain amplitude at load cycle i.

ϕ_i = phase shift between stress and strain at load cycle i.

Researchers have suggested that cumulative dissipated energy is the only factor that predicts fatigue life (Chomton et al., 1972, 26). The relation is usually characterized by:

$$W_N = A\,(N_f)^z$$

where: N_f = fatigue life,

W_N = cumulative dissipated energy to failure (psi), and

A,z = experimentally determined coefficients.

Table 5.26 summarizes the energy based fatigue relations for the four Mn/ROAD mixes.

Mix Type	A	z
AC-20 (35 Blows)	3.6483	0.6561
AC-20 (75 Blows)	3.2496	0.6537
Pen 120/150 (35 Blows)	2.9422	0.6520
Pen 120/150 (75 Blows)	4.9120	0.6056

Table 5.26. 'A' and 'z' parameters (energy based fatigue relations) for Mn/ROAD mixes.

5.5.7 Analysis of Results

Figure 5.34 presents the fatigue relations for the AC-20 mixes and Figure 5.35 the Pen 120/150 mixes. For a given asphalt cement type the slope of the trends are very similar regardless of percent asphalt content, for the same aggregate and gradation.

The laboratory testing shows Pen 120/150 mixes have a better fatigue resistance than the AC-20 mixtures at the same strain level. The difference between the mixes is more pronounced at higher strain levels. Figure 5.36 shows fatigue relations for all the mixes.

The Illinois DOT utilizes a strain-based AC fatigue algorithm (typical dense graded mix) in its thickness design procedure (3). The algorithm is:

$$N = 5\times10^{-6}\,(1/\varepsilon)^{3}$$

Figures 5.37 and 5.38 show the laboratory fatigue trends for the AC-20 and Pen 120/150 mixes and IDOT's fatigue algorithm. This is a conservative relation compared to the laboratory data for the Mn/ROAD mixtures.

A fatigue study of typical Norwegian AC mixes (65), and the FHWA Cost Allocation Study (66), developed relationships between $\text{Log}(K_1)$ and K_2, as shown in Figure 5.39. The K_1 and K_2 values obtained from this laboratory testing are also plotted on Figure 5.39 along with IDOT's fatigue constants. All values plot closely to the Norwegian line, providing a good check on the validity of the fatigue results. Values obtained in a previous Finnish

Technical Research Center (VTT) fatigue study (67) on the Mn/ROAD mixes are also presented in the plot.

5.5.8 Summary

Flexural beam fatigue testing using the SHRP constant strain protocol was conducted on four Mn/ROAD mixes. The results show that Pen 120/150 mixes have a better laboratory fatigue resistance than the AC-20 mixes. The difference decreases at low strain levels. The Mn/ROAD fatigue curves display flatter slopes than IDOT's fatigue algorithm. The Mn/ROAD constants (K_1 and K_2), from U of I testing, compare favorably with Myre's $Log(K_1)$ and K_2 relation.

CHAPTER 6

ILLI-PAVE Structural Model Validation

6.1 Introduction

The ILLI-PAVE finite element structural model has been utilized since the early 1980's. In ILLI-PAVE the pavement is modeled as a three-dimensional half space of a finite solid of revolution (Figure 6.1). By symmetry, the problem can be simplified to a plane radial section. This rectangular half space is then divided into a set of rectangular elements connected at their nodal points (Figure 6.2).

A significant feature in ILLI-PAVE is the ability to incorporate both nonlinear and linear stress-strain behavior of component pavement materials. Seven different material models are available. Möhr-Coulomb failure criteria (cohesion, c; friction angle ϕ) can be specified for the various materials. The load is specified in terms of surface contact pressure and radius of loaded area.

The Mn/ROAD project has more than 4,500 pavement sensors that measure the effects of traffic and the environment on the three-mile test section on Interstate 94 and the 2.5 mile closed loop low volume road (LVR) section. The sensors are placed at various levels in the roadway, from the surface into the subgrade.

Sensors embedded at the bottom of the asphalt surface of the roadway measure the strain induced in the structure due to truck loadings. Sensors embedded in the granular and soil layers under the pavement monitor displacements and pressures from truck loads and environmental conditions such as temperature, moisture content, and frost depth. Data from linear variable differential transducers (LVDT), strain gauges and pressure sensors are analyzed in this chapter and compared to the estimated values obtained using the ILLI-PAVE finite element model.

The sensor response data were collected from special FWD testing performed in sections where pavement response data were collected simultaneously with the application of the plate load. During the tests these sensors collected strains, displacements and subgrade stresses.

6.2 Description of Embedded Gauges

6.2.1 Longitudinal Embedment and Transverse Embedment Strain Gauges

Asphalt concrete horizontal strains have been related to the current fatigue failure criteria used in mechanistic-empirical pavement design procedures. The sensors measure the horizontal strain at the bottom of the asphalt concrete layer. This type of embedment strain gauge consists of electrical resistance strain gauges embedded within a strip of glass-fiber reinforced epoxy, with transverse steel anchors at each end of the strip, to form an H-shape. These gauges are Dynatest PAST-2AC. The gauges can measure up to 1500 microstrain, and are operational in temperature ranging between -30°C to 150°C. The strain gauges have typical service life of 36 months.

A typical AC strain gauge installation consisted of three adjacent gauges spaced 12 inches apart in a transverse direction. The center sensor was placed in the wheel path location. The sensors axis were oriented either in a longitudinal (LE) or transverse (TE) direction. Performance of the gauges had been satisfactory at the time of testing presented here.

6.2.2 Linear Voltage Differential Transducer

There are 119 Schaevitz HCD-500 DT sensors in use throughout the project. Vertical displacement is measured to assess displacements in surface, base, and subgrade materials due to load. The data are used to verify analytical models and to determine failure criteria. The linear variable differential transformer (LVDT) is an electromechanical device that produces an electrical output proportional to the displacement of a separate, moveable core. It consists of a primary coil and two secondary coils spaced on a cylindrical form. A free-moving rod-shaped ferro-magnetic core inside the coil assembly alters the relative coupling of the transformer windings. When the primary coil is energized, voltages are induced in the

secondary coils. The net output of the transducer is the algebraic sum of the magnitude of these two voltages which corresponds to the change in core position or displacement. The DT gauges have a operational temperature range between -18°C and 70°C, the nominal linear range is between -0.5 to 0.5 inch.

The AC installation raised some concerns about the core-hole cap design. Originally, a steel cap was placed to cover the hole but concerns about locally stiffening the pavement and affecting the displacement measurements triggered changes to a flexible cover.

6.2.3 Pressure Gauges

Vertical pressure (PK) data are collected with these sensors. The sensors are small diameter, soil stress cells consisting of a liquid-filled hollow steel cell approximately 50.8mm (2 inches) in diameter and 12.7mm (0.5 inch) thick, with an electrical pressure transducer housed within the cell. The pressure transducer responds to changes in total stress applied to the material in which the cell is embedded. The sensors are Kulite 0234 type. The PK sensors have an operating temperature range between -15°C and 40°C.

6.3 Measured AC Strain Values and Surface Deflections(FWD)

As part of the special FWD testing series, tests were performed on the mainline. The horizontal strain values at the bottom of the AC layer were measured under FWD loading. Also surface deflection information was recorded for each load drop, along with temperature data. Only data for TE gauges were analyzed.

AC strain data were available for Cells 4, 18, 19, 20 and 22. Figure 6.3 shows the pavement sections for these cells. Three FWD load levels (6, 9, and 15 kips) were targeted in each test location and date. The tests for Cell 4 were performed in March of 1994, and April and May of 1996 for all other cells. The location of the strain gauges are summarized in Table 6.1.

Cell Number	Gauge ID	Station	Depth, in
4	TE 02	112225	8.75
18	TE 02	121570	7.75
19	TE 02	121840	7.75
20	TE 02	122660	7.75
22	TE 02	123770	7.75

Table 6.1. Strain Gauge Locations.

6.4 ILLI-PAVE Estimated AC Strain Values and Surface Deflections

ILLI-PAVE runs were performed to estimate AC horizontal strains at the bottom of the layer and surface deflection information. The properties utilized in the ILLI-PAVE runs were obtained as follows. The AC modulus was estimated from the AC Temperature - Modulus relation developed (presented in Chapter 5) from FWD testing. The BELLS temperature information was provided for FDAC Cell 4 but not for the CFP sections. Surface temperature (infra red sensor reading) was recorded for these sections. The AC temperature was then obtained by calculating the MMPT at 1/2 of the mat depth for the section from the MMAT for the time of the testing utilizing the MMPT - MMAT relations presented in Chapter 7. Using this MMPT and the surface temperature, the AC temperature at 1/3 of the mat depth was interpolated. These temperature values were utilized to obtain the AC modulus from the FWD based AC modulus - Temperature relations. The subgrade E_{Ri} value used in ILLI-PAVE was chosen to be the typical value for the time of testing as shown by the extensive FWD testing performed on the sections and presented in Chapter 5. In modeling the granular materials in the conventional sections, the stress dependent models developed in the University of Illinois laboratory (12) were utilized at the laboratory moisture content closest to the field moisture content at the time of testing.

Previously developed ILLI-PAVE based algorithms were used to estimate the AC strains in the CFP and FDAC sections. These algorithms are a function of the Area Under the Pavement Profile (AUPP) as shown in Figure 6.4. The algorithms for the CFP were developed by Thompson et al.(2) and the FDAC algorithms were developed specifically for the Mn/ROAD sections and are presented in Appendix C. The algorithms are as follows:

Conventional Pavements:

$$\text{Log(AC Strain)} = 0.999 + 1.014*\text{Log(AUPP)}$$

Full Depth Pavements:

Log(AC Strain) = 1.073 + 0.980*Log(AUPP)

where:

AC Strain = strain @ bottom of AC layer, microstrain

AUPP = ½*(5*D0-2*D1-2D2-D3)

Backcalculation of AC strain with these algorithms is a versatile approach in that it only requires the readily available surface deflections values and provides a very accurate estimation. The algorithms were based on a series of ILLI-PAVE runs with different sections and materials but at only one load level, the standard 9,000 pounds wheel load.

6.5 Comparison of Estimated (ILLI-PAVE) and Measured AC Strain Values and Basins

The surface deflections measured under each load for the FDAC section (Cell 4) were compared with the ILLI-PAVE estimated deflections. Figure 6.5 shows the deflection values and the equality line. There is good agreement between the measured and the estimated values for the FDAC sections.

Figure 6.6 presents the center deflection (D0) comparison for the CFP sections and Figure 6.7 shows the estimated and measured deflections away from the center of the load (D1, D2, and D3). There is scatter in the plotted values and not very good agreement between field and estimated values in the CFP. The ILLI-PAVE values tend to be higher than the measured values.

The ILLI-PAVE AC strain were plotted against the measured strain from the pavement sensors. Figure 6.8 shows the relation for the FDAC section. There is good agreement between the values. The measured values tend to slightly lower than the ILLI-PAVE estimated values. For the CFP cells, there is very poor agreement as shown in Figure 6.9. The ILLI-PAVE values again tend to be higher than the field measured ones.

The main reason for this discrepancy in the results from the FDAC cell to the CFP cells is the "non-intact" nature of the latter sections. ILLI-PAVE, as all other commonly used pavement structural models assumes continuity of the layers. At the time of testing in

Cell 4 (March 1994) there was no thermal cracking on that section. On the other hand, in April and May of 1996 when the CFP data were collected, significant thermal cracking had occurred and the asphalt concrete layer was then a series of continuous blocks. The thermal cracking present in the mainline sections particularly in the AC 20 cement mixes was very severe and the cracks were very wide. Details on the amount and locations of the cracking were presented in Appendix A.

The AUPP algorithms were used for all FWD tests where measured AC strain values were available, regardless of load level. Comparison of the measured AC strains and the backcalculated strain values using the AUPP algorithm show good agreement between the values. Figure 6.10 a) shows the relation for Cell 4 and Figure 6.10 b) presents the CFP results. Figure 6.11 shows the combined data. The AUPP parameter captures the FWD behavior of the section. The reason the AUPP approach better captures the behavior at a given location is because its geometric nature accounts for all interacting variables, including the effect of the surrounding thermal cracks. Also, the AC thickness utilized in the ILLI-PAVE input files is the target thickness for each cell. The actual AC thickness varies somewhat from station to station within a cell, and there is also aggregate thickness variations. These two factors have an almost insignificant effect on the results compared to the thermal cracks. The results show a good agreement at all load levels, even though the algorithms had originally been developed for 9,000 lb. loads.

The FWD tests included three different load levels in the same location measuring the pavement responses (i.e. AC strain and surface deflections). The different load levels utilized during testing provides an opportunity to study the relationship between percent increase in measured AC strain caused by a given percent increase in load. This increase in strain as result of an increase in load was calculated for each sequence of drops. The strains and load were compared to the base load of 6-kips (lowest load level in the test sequence). The results for the FDAC section are presented in Figure 6.12. For this cell, the increase in strain is greater (equal for some tests) than the increase in load (stress softening). Figures 6.13 through 6.16 present the results for the CFP sections. In the CFP sections, the percent increase in measured strain is consistently lower than the load increase (stress hardening).

The same trend is observed with the surface maximum deflection. This suggests stress hardening effect in these sections and stress softening in the FDAC section.

The ILLI-PAVE outputs for these sections suggest the same trend for the two types of pavements. Figure 6.17 shows the ILLI-PAVE based percent increase in AC strain for an increase in load with different AC modulus (900, 1600, 1800 ksi) for Cell 4. There is a stress softening effect in the strain response at all AC modulus values, the stress softening is increased at low E_{AC} values. The ILLI-PAVE stress softening effect is smaller than that observed in the field. At low E_{AC} values the subgrade effect is accentuated.

Figures 6.18 and 6.19 present the same ILLI-PAVE relation for the CFP Cells 18 and 19. Both cells show a stress hardening effect in the strain response. The stress hardening effect is increased as the AC layer modulus decreases. As the E_{AC} decreases, the granular material "dominates" the behavior and the stress hardening effect is accentuated. Cell 18 has a better quality granular material (CL-6sp) than Cell 19 (CL-3sp) but the difference in the hardening effect is around 2%.

These observations are in agreement with previous extensive research on pavement materials. The cohesive soils present a stress softening behavior that is transferred to the overall pavement behavior in FDAC sections (64). The granular materials stiffen as the stress state increases (stress hardening behavior) which for conventional sections translates to the same trend in pavement responses.

6.6 Measured Total Pavement Displacements, Subgrade Displacements (LVDT) and Surface Deflections(FWD) for Cells 17, 22 and 30

As part of the special testing program, cells with embedded LVDTs were subjected to FWD tests where the sensor responses were collected along with the applied load and surface deflections. Data for mainline Cells 17, 22 and low volume road (LVR) Cell 30 were provided by Mn/ROAD personnel. The center of the load plate was positioned 6 inches away from the LVDT for the tests on Cells 17 and 22. The load was dropped directly over the LVDT for LVR Cell 30.

The LVDTs are embedded at different depths. Figure 6.20 shows the gauge locations. The locations were chosen so that the displacement within the pavement layers could be measured along with the total displacement of the section. The "Within pavement" displacement is the combined displacement in the AC and granular layers. This displacement is measured by an LVDT anchored at the bottom of the base layer. The total pavement displacement is the combined displacement in the AC, granular and subgrade layers up to a depth of 144 inches (LVDT anchorage depth). The two LVDTs in each cell are embedded at different stations. The general information for the tests analyzed in these sections is summarized in Table 6.2.

Cell Number	Date	LVDT 1 Station	LVDT 2 Station	T_{AC} Temp., °F	Sub. MC,%
17	10/11/96	120818	120824	61	22.7
22	10/18/96	123788	123794	61	21.0
30	10/29/96	19442	19448	61	21.0

Table 6.2. Information of Special Testing performed (LVDT sensors).

6.6.1 Cell 17 Testing

The two LVDTs (DT5-within and DT8-total displacement) in this section are located 100 feet apart. Thus, it was necessary to consider the materials properties (i.e, E_{AC}, E_{Ri}) at the two different locations in order to combine the two LVDT measurements. Then, the subgrade displacement can be calculated as the difference between the two LVDT readings.

At each location, three different load levels (three repetitions each) were applied and LVDT values were collected. A major concern of this analysis was determining the validity of the data. There was some concern with the location of the center of the loaded plate. For these tests, the center of the load plate was 6 inches away from the LVDT hole (the edge of the load plate). At this particular location there is a rapid variation in surface deflection, thus any minor offset in the placing of the plate has a significant effect in the measured displacement by the sensor.

The distress maps presented in Appendix A show that at the time of testing, October 11, 1996, significant thermal cracking had occurred in Cell 17. Thermal cracks ran through the core taken during the installation of the sensors, at the exact location of the LVDT.

The first step was comparing the deflection basins of the two LVDT locations. Figures 6.21 through 6.23 show the surface deflection basin for each load level at both locations. For a given location there is very little change from one repetition to the other at the same load level. There is a good match on the surface deflections under the center of the load (D0) and 36 inches away from the load (D3) on the two locations at all load levels. At a distance of 12 and 24 inches from the load (D1 and D2), there is a greater difference at the two locations. The difference in D1 and D2 measurements become greater as the load level increases. Backcalculation of E_{Ri} values at the two locations resulted in very close values. A difference was found on the E_{AC} modulus values between two locations. Backcalculation moduli are presented in Table 6.3.

Location	ERi, ksi	E_{AC}, ksi
LVDT1	14.07	1380
LVDT2	14.78	1900

Table 6.3 Backcalculated properties for Cell 17 locations.

ILLI-PAVE was utilized to estimated the displacement within the pavement layers and the total displacement to a depth of 144 inches. The AC modulus used is the average of the backcalculated values for the two locations and the subgrade E_{Ri} used is the typical value for the time of testing. Figures 6.21 through 6.23 referenced before, show the deflection basins estimated from ILLI-PAVE along with the measured ones. The estimated values are higher than the measured ones.

The LVDT displacements were compared to the ILLI-PAVE estimated values. The subgrade displacements as calculated from the LVDT readings (Difference between total pavement displacement and within pavement displacement) were compared to the ILLI-PAVE estimated values as shown in Figure 6.24. There is very good agreement between the values. The ILLI-PAVE estimated values are 5-15% (0.1-0.25 mils) higher than the measured ones. Figure 6.25 shows the comparison between field measured and estimated total pavement displacement. The ILLI-PAVE values are 15-24% (0.8-1.5 mils) higher than the field values. Figure 6.26 presents the within pavement displacement comparison. The estimated values are 22 - 40 % (0.5-2 mils) greater than the LVDT readings.

The subgrade displacement is calculated by subtracting the two LVDT readings. The subgrade displacement changes very little at different locations at a given depth, thus, the significance of the load plate location is reduced. Greater differences were found on the total and within pavement displacements, the within displacement is the greatest. The location of the plate load and the thermal cracked condition of the pavement section contributed to the differences. The effect is increased for the within pavement measurement. The difference in measured and estimated basins are also likely to be influenced by the distress in the sections.

6.6.2 Cell 22 Testing

The LVDTs in this section are located 100 feet apart. Thus, it was again necessary to consider the properties at the two different locations in order to combine the measurements.

These tests were performed using the same setup as in Cell 17. The center of the loaded plate was placed 6 inches away from the sensor hole. The distress maps presented in Appendix A show that at the time of testing, October 18, 1996, significant thermal cracking had occurred in Cell 22 but to a lesser degree than Cell 17. At the exact location of the LVDT sensors, thermal cracks ran through the cores taken during the installation of the sensors.

The deflection basins of the two different locations were compared at all load levels. Figures 6.27 through 6.29 show the surface deflection basin for each load level at both locations and the ILLI-PAVE estimated values. There is a good match on the surface deflection basin between the two locations and the estimated one at all load levels. Backcalculation of E_{Ri} and E_{AC} values on the two locations resulted in very close values, see table 6.4. These backcalculated values were used in the ILLI-PAVE runs.

Location	ERi, ksi	E_{AC}, ksi
LVDT1	12.56	1115
LVDT2	12.96	1132

Table 6.4 Backcalculated properties for Cell 22 locations.

The LVDT displacements were compared to the ILLI-PAVE estimated values. Figure 6.30 shows the LVDT calculated versus ILLI-PAVE estimated subgrade displacement. There is very good agreement between the values. The differences range from

1-5% (0.05-0.1 mils). Figure 6.31 shows the comparison of field measured (LVDT) and estimated total pavement deflection. The difference between the field and LVDT readings differ from 1-6% (0.1-0.35 mils). Figure 6.32 presents the within pavement displacement comparison, and these values differ by 6-14% (0.15-0.2 mils).

Overall, there is good agreement between the surface basins, as well as the total, within and subgrade displacements at all load levels. Again the subgrade displacements show the least difference between measured and estimated values which may be attributed to little change of the displacement at a given depth moving away from the load, minimizing any plate loading condition variance.

6.6.3 Cell 30 Testing

Cell 30 is a low volume road (LVR) section of the Mn/ROAD project. This was one of the few sections with LVDT data available where special FWD tests were performed. The tests were performed on the outside lane, where the traffic was applied by a five-axle truck trailer weighing 102 kips. The two LVDTs in the section are located 100 feet apart as in Cells 17 and 22.

At each location, three different load levels (three repetitions each) were applied and the LVDT values collected. The center of the loaded plate was applied directly over the LVDT sensor. Distress maps for Cell 30 showed no cracking in the area close to the sensor locations at the time of the testing (October 29, 1996).

Comparison of the surface basins were performed on the two locations. Figures 6.33 through 6.35 show the surface deflection basin for each load level on both sensor locations. For a given location there is variation from one repetition to the other at the same load level. There is great variation between the two locations on the maximum deflection (D0) at all load levels. The difference decreases from D1 to D2 to D3 measurements. Backcalculation of E_{Ri} and E_{AC} modulus resulted in significant variation. The AC modulus shows the greater difference. The values are very low for the time of the year and the temperature at time of testing, see Table 6.5 below.

Location	ERi, ksi	E_{AC}, ksi
LVDT1	13.65	106
LVDT2	19.50	50

Table 6.5 Backcalculated properties for Cell 30 locations.

The temperature was determined to be 61°F. There was no BELLS temperature information available for the tests. The mean monthly air temperature (MMAT) for the time of testing was used in the mean monthly pavement temperature (MMPT) -MMAT relation developed for the cell. The relation is given as:

$$MMPT = (3.88 + 1.308*z) + (1.05 - 0.027*z)*MMAT$$

where:

z = depth at which the temperature is required (1/3 mat thickness), in.; and

MMAT = mean monthly pavement temperature for the location, °F.

Using this temperature in the E_{AC} -Temperature relation from FWD testing of the cells the E_{AC} value should be around 400 ksi. The relation is as follows:

$$Log(E_{AC}) = 3.3804 - 0.0477*Temp\ (°C)$$

$R^2 = 0.89$

Std.= 0.146

ILLI-PAVE was utilized to estimate the displacement within the pavement layers and the total displacement to a depth of 144 inches. The AC modulus used is the value estimated using the modulus -temperature relation for the test temperature. The subgrade ERi used is the typical value for the time of testing. The deflection basin estimated from ILLI-PAVE differs from the measured ones as seen in Figures 6.33 through 6.35 referenced before. The measured D0 (max. deflection)values are higher than the estimated ones. The difference in basin deflections and backcalculated material properties indicates that the two LVDT readings should not be combined, since the two locations are not comparable. The variability in measured deflections and the low backcalculated material properties question the validity of these data. Furthermore, performance data for this cell presented elsewhere (12), shows good performance on this cell. Very limited thermal cracking had appeared at the time of testing and rutting measurements for the cell are around 0.22 inches, casting even more doubt on the surface deflections collected in the tests.

6.7 Measured Subgrade Pressures values on top of Subgrade (Pressure Gauges) for Cell 30

Cell 30 data were obtained from Mn/ROAD personnel. The center of the load plate was placed on top of the pressure gauge located in the outside wheel path. Two other PK gauges measured the pressures 12 inches away on each side as shown on Figure 6.20. The three gauges are at the top of the subgrade. Three load levels were targeted: 5, 9, and 15 kips.

The tests were performed on October 14, 1996, two weeks before the LVDT tests presented in the previous section. FWD files for these tests included BELLS temperature information (61°F). The test temperature is similar to the temperature on the day of the LVDT tests. Backcalculation of E_{Ri} resulted in a value slightly lower than the expected for the time of testing (12 ksi) and E_{AC} modulus very close to the one estimated form the E_{AC} - Temperature relation for this cell and presented in the previous section. Table 6.6 below summarizes the backcalculated material properties.

Location	Station	E_{Ri}, ksi	E_{AC}, ksi
PK2	19432	7.0	350

Table 6.6 Backcalculated properties for Cell 30.

The measured deflection basins were compared at all load levels with the ILLI-PAVE estimated basins obtained using an AC modulus of 400 ksi and a subgrade modulus of 12 ksi. Figures 6.36 through 6.38 show the surface deflection basin for each load level and the ILLI-PAVE estimated values. There is a good match on the measured surface deflection basin for each repetition at all load levels. The measured basins are slightly higher than the estimated deflections but overall, very good agreement was found between basins.

The subgrade pressures recorded by the PK sensors were compared to the ILLI-PAVE pressures. Figure 6.39 shows the field measured and estimated pressure directly under the center of the load pavement deflection. The ILLI-PAVE values differ depending on the load level. Under the center of the load and at the standard load level (80 psi), the difference is 6%. At 55 psi applied pressure, the difference is 30% while at 130 psi, the difference is greatest at 44%.

Figure 6.40 presents the subgrade pressures measured on the two sensors embedded 12 inches away from the center of the load and the ILLI-PAVE estimated values. The difference between the two gauges (PK) measurements ranges between 8-16%. The difference between the average subgrade pressures (12 inches away from center of load) and ILLI-PAVE subgrade stress varies between 5-80%. The smaller variation, 5%, is reported for the greatest applied pressure (130 psi). At a location 12 inches away, the subgrade stress caused by this loading condition is very similar to the subgrade stress (under the center of the load plate) caused by an 9,000 lb. (80 psi) load. For a subgrade stress between 5 and 8 psi the ILLI-PAVE estimated values match the measurements indicating that for the standard load, the maximum subgrade pressure is well accounted for using the subgrade model incorporated in ILLI-PAVE.

Researchers at Mn/ROAD have tried to compare the measured pressures to the estimated pressures using different estimation procedures. Little agreement in comparing the pressure values has been found (86).

6.8 Summary

FWD special testing was performed and data obtained from embedded sensors in the pavement layers were collected and analyzed. Field AC strains, surface deflections and pavement deflections were compared to ILLI-PAVE estimated values. Some of the tests were performed after numerous thermal cracks had appeared. The thermal cracking present in the mainline sections, particularly in the AC 20 mixtures is very severe and the cracks are very wide. These cracks greatly influenced the results.

Very good agreement was found between measured AC strains and ILLI-PAVE values for tests performed on FDAC Cell 4. These tests were done before any thermal cracks had appeared. The ILLI-PAVE results on the CFP cells did not correlate well with the field values. These cells were tested in 1996 after extensive thermal cracks had occurred on the sections.

AC strains estimated with the AUPP algorithm correlated very well with the field values for all cells and tests. The geometric nature of the AUPP term seems to account for all variables interaction including the effect of the surrounding cracks.

The relationship between percent increase in measured strain caused by a given percent increase in load was studied. The increase in strain as a result of an increase in load was calculated for each sequence of drops. Field results encountered a stress hardening effect in the CFP sections and stress softening in the FDAC section.

LVDT data were analyzed for three cells. Some problems were encountered. There was great concern with the tests where the edge of the load plate was over the sensor. At this location the rate of deflection change is very high and any slight difference in load plate placement changes the results. The subgrade deflections present the least difference between measured and ILLI-PAVE estimated values for all cells. The plate loading condition effect is minimized in the subgrade.

The pressure gauge values were compared to ILLI-PAVE estimated values. At a 9 kip load level, there is very good agreement between the field measurement and ILLI-PAVE values. Good agreement was also found with the subgrade pressure measured 12 inches away from the center of the load where the subgrade pressure value is similar to the value obtained under the center of the load caused by a 9 kip load. For all other tests the difference between field and estimated values is very significant, ranging between 30 and 80%.

The field surface deflections had very good agreement with the ILLI-PAVE estimated basin for the PK tests. Results from other researchers at Mn/ROAD have found little agreement in comparing the field subgrade pressure values with different estimation methods.

CHAPTER 7

Performance of Mainline Pavement Sections

7.1 Design Time Calculations for Mn/ROAD Mainline Test Sections

The AC layer is typically characterized as a constant modulus material. AC modulus is significantly influenced by temperature. AC modulus- temperature effects should be considered in a pavement analysis and design procedure. AC mean monthly pavement temperatures (MMPT) are estimated based on mean monthly air temperatures (MMAT). The MMPT can be used to estimate AC modulus from an appropriate AC modulus-temperature relation.

The Climatic-Materials-Structural (CMS) model was utilized to estimate the MMPT (14,15). CMS includes a one-dimensional forward-finite-difference heat transfer model and an isothermal model that calculate temperature and moisture profiles as a function of time based on pertinent climatic inputs. This model has been found adequate for considering climatic effects in a priori flexible pavement design. The required climatic inputs are:

- weekly high / low / average air temperature
- weekly wind speed
- weekly percentage of sunlight
- daily solar radiation

Other pavement system inputs are:

- Number and types of layers
- Thickness of layers
- Thermal and physical properties
- Radiation absorptivity and emmissivity of surface layer

Material	Density,	Moisture,	Thermal Conductivity (BTU/Hr-ft-F)			Heat Capacity (BTU/lb.-F)		
	pcf	%	Unfrozen	Freezing	Frozen	Unfrozen	Freezing	Frozen
Asphalt Concrete*	148	2	0.7	0.7	0.7	0.22	1.44	0.22
Granular Material	147	5	2.18	2.28	2.38	0.21	3.60	0.19
Subgrade Soil	129	17	0.92	1.02	1.13	0.29	10.49	0.22

*Surface short-wave absorptivity for asphalt concrete is 0.85

The climatic data for the Mn/ROAD project were obtained from the National Oceanic and Atmospheric Administration (NOAA) in Asheville, NC. The Minneapolis-St. Paul twin cities data were for 1962 through 1991. Figure 7.1 presents the maximum, minimum and average air temperatures for this location.

Pavement temperatures were calculated using CMS for nodes spaced at one-inch intervals in the AC layer, starting at the surface. Temperatures were calculated six times a day, seven days a week for fifty two weeks. MMPT-MMAT relations were developed for each of the mainline cells. These algorithms are of the form:

$$MMPT(°F) = (A + B*z) + (\{[C + D*z\ ]\ MMAT)$$

where:

A,B,C, and D = regression coefficients

z = depth at which temperature is required, inches

MMPT and MMAT are both in degrees Fahrenheit

Table 7.1 shows the algorithm coefficients for each cell.

7.1.1.1 Design Time

NCHRP 1-26 Phase 2 (68) summarizes some of the procedures utilized to consider the AC modulus-Temperature relation effects. The University of Illinois has established a "Design Time" (DT) concept to consider the temperature and subgrade effects on AC stiffness. The fatigue life of a pavement estimated with the DT AC modulus is equal to the fatigue life estimated based on the monthly AC modulus inputs. This approach can incorporate different AC modulus-Temperature relations and AC fatigue algorithms.

Cell #	A	B	C	D	R^2	SEE
1	3.693	1.234	1.056	-0.026	0.993	1.763
2	3.702	1.232	1.056	-0.026	0.993	1.753
3	3.679	1.221	1.056	-0.025	0.993	1.771
4	3.646	1.192	1.056	-0.025	0.993	1.736
14	3.566	1.151	1.058	-0.024	0.994	1.669
15	3.566	1.151	1.058	-0.024	0.994	1.669
16	3.588	1.172	1.058	-0.024	0.993	1.723
17	3.588	1.172	1.058	-0.024	0.993	1.723
18	3.628	1.188	1.057	-0.025	0.994	1.690
19	3.588	1.172	1.058	-0.024	0.993	1.723
20	3.588	1.172	1.058	-0.024	0.993	1.723
21	3.616	1.182	1.057	-0.025	0.994	1.694
22	3.650	1.196	1.057	-0.025	0.994	1.686

Table 7.1. MMPT - MMAT Algorithms for Mn/ROAD Sections.

The temperature of the AC layer at 1/3 of the depth was utilized to estimate the AC modulus. The AC-Temperature relation used for the Mn/ROAD cells was developed from FWD testing (Chapter 5) and is:

$$\text{Log } E_{AC} = 3.685 - 0.048 * \text{Temp}$$

where:

Temp = is the temperature at which the modulus is required, °C.

E_{AC} = AC modulus, ksi.

The Illinois DOT algorithm was used in calculating the expected life of the section for each month. The Illinois AC fatigue algorithm is:

$$N = 5 * 10^{-6} (1/\varepsilon_{AC})^3$$

Asphalt concrete strains (ε_{AC}) were estimated using ILLI-PAVE algorithms for FDAC (Appendix C) and CFP (2). The algorithms are:

Full-Depth AC Pavements:

$$\text{Log } \varepsilon_{AC} = 5.741 - 1.61 \text{ Log } T_{AC} - 0.759 \text{ Log } E_{AC} - 0.063 \text{ Log } E_{Ri}$$

Conventional Flexible Pavements:

$$\text{Log } \varepsilon_{AC} = 2.9496 + 0.1289 T_{AC} - 0.5195 (\text{Log } T_b)/T_{AC} - 0.0807 (\text{Log } E_{AC}) T_{AC} - 0.0408 \text{Log } E_{Ri}$$

where:

ε_{AC} = AC radial strain, microstrain
T_{AC} = AC thickness, inches
T_b = Granular base thickness, inches
E_{AC} = AC modulus, ksi
E_{ri} = Subgrade resilient modulus, ksi

The cumulative damage due to loading was assumed to follow Miner's cumulative damage model and was estimated by the following relation:

$$N_f = \frac{12}{\left[\sum_{a=1}^{12}\left(\frac{1}{Na}\right)\right]}$$

7.1.1.2 "Design Time" Conditions

In the "Design Time" (DT) calculation , the AC fatigue life, N_f, is estimated. This N_f is associated with an AC modulus and AC strain, for a given pavement section. These values were calculated for all mainline cells. The results are summarized in Table 7.2. The mainline DT air temperatures (DT AT) ranged from 59 to 62°F. The DT pavement temperature (DT PT) ranged from 65 - 69 °F. Figures 7.2 through 7.11 show the "Design Time" for each mainline cell.

From the "Design Time" and its corresponding AC temperature, an E_{AC} value is obtained from the E_{AC}-Temperature relation developed from FWD data. An E_{Ri} value is selected for each cell from the E_{Ri}-Time relation also developed from FWD data.

For all the mainline cells the Design Time E_{Ri} is 10 ksi. For the DT PT of 65°F (18°C) the E_{AC} is 640 ksi. For 67°F (19°C) the E_{AC} is 570 ksi and for 69°F (16°C)E_{AC} is 502 ksi.

Cell #	Weeks from Jan 1st	Date	DT AT, °F	DT PT, °F	E_{AC}, ksi
1	19	15-May	59	65	650
2	19	15-May	59	65	640
3	19	15-May	59	65	640
4	21	27-May	63	69	502
14	21	27-May	63	69	502
15	21	27-May	63	69	502
16	20	21-May	61	67	572
17	20	21-May	61	67	572
18	20	21-May	61	67	572
19	20	21-May	61	67	572
20	20	21-May	61	67	572
21	20	21-May	61	67	572
22	20	21-May	61	67	572
23	20.5	25-May	62	68	542

Table 7.2 "Design Time" Results for Mainline Flexible Cells.

7.1.2 Effect of Asphalt Concrete Thickness on "Design Time"

The asphalt concrete thickness for the CFP sections ranged from 5.75 to 7.75 inches. The thickness ranged from 8.75 to 10.75 inches in the FDAC sections. Two types of binder (AC 20 and Pen 120/150) were utilized in the asphalt concrete mixes. The same thermal properties were assigned to the two binders in CMS.

For the five year cells (Cells 1, 2 and 3) the "Design Time" pavement temperature is 59°F, while the 10 year cells (Cells 16, 17, 18, 19, 20, 21 and 22) have a pavement temperature of 61°F. The FDAC cells do not present a difference in the estimated pavement temperature between the five year (Cell 4)and the ten year (Cells 14 and 15) cells even though a 2 inch AC thickness difference exists between the two different design lives.

"Design Time" results from Cells 1 and 2 were compared to those of Cells 16, 17, 19 and 20. These sections have similar granular material thickness and a 2 inch AC thickness difference. This thickness difference results in a 2 degree Fahrenheit difference in both DT air and pavement temperatures and a week in the DT date, from May 15 to May 21. This validates previous research, NCHRP 1-26 Phase 2 (43), in which the DT temperature was found to be fairly insensitive to pavement section.

7.1.3 Effect of Granular Material Thickness on Design Time

Four different types of granular materials were used in the Mn/ROAD mainline CFP sections. The granular materials thermal properties were kept constant during the CMS modeling, thus AC thickness was the only difference in the input.

The five year CFP cells have granular base thickness that vary from 32 to 37 inches with the same asphalt concrete thickness of 5.75 inches. There was no effect due to granular layer thickness. The ten year CFP have granular layers ranging from 18 to 28 inches with the 7.75 inch asphalt concrete layer. Again, there was no difference in the estimated "Design Time" pavement temperature or date as a result of granular layer thickness variation. These results are consistent with the NCHRP results. As the asphalt concrete thickness increases the effect of the granular layer thickness is decreased.

7.2 Conventional Flexible Pavement Sections

7.2.1 Fatigue Behavior

Asphalt concrete fatigue cracking, AC thermal cracking and pavement surface rutting are the flexible pavement distress modes considered in flexible pavement analysis and design procedures.

The fatigue behavior of the Mn/ROAD mixtures were investigated in the laboratory and the results are presented in Chapter 4. The fatigue tests were performed at 20°C (68°F), very close to the "Design Time" pavement temperature of the Mn/ROAD CFP sections (65-69 °F). No fatigue failure was expected at the time of this report due to the structure of the test sections and the amount of traffic experienced to date.

Figure 7.12 presents the expected life of the CFP cells estimated using IDOT's fatigue algorithm. This algorithm has been shown to be very conservative for Illinois conditions. Figure 7.13 shows the expected life of the CFP cells as predicted using the AC fatigue algorithms developed from laboratory mixture testing at ATREL. The life estimated using these laboratory algorithms has not been field calibrated and can only provide a mean of ranking the mixes and the expected order of failure.

The five year CFP cells have an IDOT estimated life of 1.2 million ESAL. The traffic experienced by those cells is already greater than that number (1.4 million ESAL), but as was mentioned above IDOT's algorithm is very conservative.

Numerous thermal cracks have appeared in the CFP cells. The most affected cells are those where the AC 20 binder type was used. These cracks change the pavement system behavior. The layered system, interior loading assumption is less applicable. As a result, any fatigue failure encountered in the field while load related, is not the expected fatigue mode in a "intact" CFP section.

Fatigue cracking appeared on Cells 18 and 19 at 1.4 million ESALs. These cells were designed to withstand at least the design traffic of 7.2 million ESALs in 10 years. Both sections have an asphalt concrete thickness of 7.75 inches and granular layer thickness of 18 inches in Cell 18 (CL-6sp & CL-3sp) and 28 inches in Cell 19 (CL-3sp). Both cells have AC 20 binder type in the asphalt concrete mixes and severe thermal cracking is present on the cells. Figure 7.14 and 7.15 present the distress maps as of December 1997 for both cells and the location of the fatigue cracks. All the fatigue cracks originate from a previously developed thermal crack. However, fatigue failure does not appear in the vicinity of every thermal crack. This points to the thermal cracks as the source of the deterioration of the pavement structure. Cells 1, 2 and 3 have a "weaker" structure and no fatigue cracking is evident. These cells all have Pen120/150 binder and fewer thermal cracks have occurred.

No definitive conclusion can be made on the fatigue performance of these sections. The cells with Pen 120/150 binder still provide an opportunity to observe the fatigue development on an "intact" section. Cells with AC 20 binder are not a good source of information for evaluating the fatigue failure mode expected on CFP because of the extensive thermal cracking.

7.2.2 Effect of Thermal Cracking on Pavement Response and Performance

Thermal cracking occurred on the mainline cells. The cells with AC 20 cement presented more extensive cracking than the cells with Pen 120/150 cement. Detail on the location and degree of cracking on each cell was presented in Chapter 4.

The main concern with the appearance of thermal cracking in the pavement sections is the change in the continuity of the AC layer and the loading condition. The interior loading condition does not apply for an extensively cracked pavement. In a "non-intact" section the pavement responses (i.e., deflection, stress and strain) approach the edge loading condition.

In the development of high strength stabilized base (HSSB) thickness design procedure (69) the "interior" flexural stress is increased by 50% to estimate the stress expected after the occurrence on transverse cracks. A similar analysis was performed to study the influence of the thermal cracks on pavement response and behavior.

A series of ILLI-SLAB runs were performed to quantify the increase in stress and strain in the AC layer. ILLI-PAVE runs were performed with AC modulus ranging from 500 - 1800 ksi, to simulate the range of temperatures experienced on the pavement throughout the year. The models developed from laboratory testing on the granular materials and subgrade soils were utilized as inputs. Laboratory results were presented in Chapter 5.

ILLI-SLAB runs were performed under interior loading condition and an "equivalent k" (modulus of subgrade reaction) was established by matching the deflection basin obtained from the program to the ILLI-PAVE basin.

The typical pavement section analyzed had a 7.75 in. AC layer and an "equivalent k" of 250 psi/in. After matching the basins, an edge loading condition analysis was performed using ILLI-SLAB (same E_{AC} and k) to quantify the increase in horizontal stress at the bottom of the AC layer. The increase from interior to edge stress ranged from 64 to 83 % for the E_{AC} modulus range of 500 to 1800 ksi respectively. This increase in AC stress translates in an equal increase in AC strain(elastic theory). The decrease in fatigue life of a section is given by:

$[\varepsilon_{AC}\ (edge) / \varepsilon_{AC}\ (interior)]^n$

where:

ε_{AC} (edge) = AC horizontal strain for "interior" loading condition

ε_{AC} (interior) = AC horizontal strain for "edge" loading condition

n = exponent of the strain-based fatigue algorithm

For IDOT's fatigue algorithm (n = 3) the life of the pavement is decreased by 4.5 and 6.1 times for an increase in stress of 64% and 83%, respectively.

These findings suggest that the fatigue cracking that occurred prematurely in Cells 18 and 19 on the mainline is attributable to a large increase in AC strain due to the "non intact" condition of these cells. The AC strain increased from the value for interior loading to edge loading condition.

7.2.3 Rutting Behavior

Rutting is one of the distress modes considered in flexible pavement design. In IDOT's mechanistic-empirical design procedure rutting in the AC layer is addressed by material selection and mix design procedures. Rutting in the granular layers is avoided by establishing a minimum AC thickness. Subgrade rutting is controlled by limiting the subgrade stress ratio (SSR) at the subgrade-structure interface.

The cells on the mainline portion of the project have a "thick" asphalt concrete layer and granular layer and thus subgrade rutting is expected to be minimum. For the CFP cells subgrade stress ratios (SSR) were backcalculated from FWD data (the results were presented in Chapter 5). The SSR in the CFP sections were always below 0.1. This low SSR eliminates "unstable" rutting behavior in the subgrade soils.

Rut depths were measured for all cells using a straight edge, dipstick, and the PaveTech Van. Only the straight edge data were analyzed in this report. Rut depths were collected in both the driving and the passing lanes and the inner and outer wheel path of each. There is a difference in rutting between the driving and passing lanes caused by the difference in traffic. The outer wheel path rutting in the driving lane is greater than in the inner wheel path for the majority of the cases. The ruts in the outer wheel path in the CFP sections are 10% - 50% larger than in the inner wheel path.

Table 7.3 summarizes the in-place properties of the asphalt concrete layer for the mainline cells.

Figure 7.16 presents the rut depth accumulation with traffic for the five year CFP cells (Cells 1, 2 and 3). Cell 2 shows greater rutting when compared to Cells 1 and 3. This cell has a granular layer thickness of 32 inches with 5.75 inches of asphalt concrete. Cells 1 and 3 had very similar air voids at the time of placement. On the other hand, Cell 2 had half of the air voids of the other two cells. The difference in mixture air voids seems to be the source of rutting difference. All three cells have a very similar asphalt cement content and the same asphalt cement type (Pen 120/150).

Cell	Air Voids, %	AC%	P200, %	Asphalt Type
1	6.4	5.3	4.7	Pen 120/150
2	3.6	5.8	4.9	Pen 120/150
3	6.9	5.6	4.7	Pen 120/150
4	6.8	5.3	4.7	Pen 120/150
14	6.0	5.3	4.3	Pen 120/150
15	6.3	5.4	4.4	AC 20
16	8.2	5.1	4.6	AC 20
17	7.7	10.2	4.2	AC 20
18	5.6	5.8	4.4	AC 20
19	6.5	6.1	5.0	AC 20
20	6.3	6.1	4.8	Pen 120/150
21	5.3	5.9	4.8	Pen 120/150
22	6.5	5.4	4.3	Pen 120/150
23	8.0	5.6	4.5	Pen 120/150

Table 7.3. In-Place Asphalt Concrete Properties for Mainline Cells.

The ten year mainline cells provided an opportunity to observe the effect of granular material thickness and asphalt cement type on rut depth accumulation. Figure 7.17 shows the rut depth accumulation with traffic for the ten year CFP cells. A "head-on" comparison was made between Cells 19 and 20 where the only difference is asphalt cement type. Cell 20 has Pen 120/150 cement and Cell 19 an AC 20 binder. As expected, the section with the lower viscosity asphalt developed greater rutting than its higher viscosity counter part. Comparison of the asphalt cement content shows no difference between the two, Cell 19 has a binder content of 6.1% and Cell 20 also has 6.1%. The in-place voids are around the same level, 6.45% for Cell 19 and 6.25% for Cell 20. There is a 60% difference between the measured rut depths in the two cells. This difference is consistently 50% or higher since the summer of 1995.

Another "head-on" comparison was made between Cells 18 and 22. Cell 18 has 21 inches of granular material [12 inches(CL6-sp) and 9 inches (CL3-sp)]. Cell 22 has 18 inches of CL6-sp granular material thickness. CL6-sp granular material type is encountered in the first 12 inches of the granular layer in both cells and the granular layer is protected by 7.75 inches of AC which ensures low stresses in the granular material. Thus, the rutting can be mostly attributed to the AC layer. These cells also present a high difference in accumulated rut depth, 20 % in the last measurement and 40% in the summer 1995 measurements. There is a difference in the rutting behavior of the mixes because of the asphalt cement type. The effect seems very exaggerated in Cell 20. It is believed that the difference encountered while comparing Cells 18 and 22 is more reasonable and that other factors played a role in Cell 20 rutting performance.

The granular material thickness did not have a clear effect on rutting behavior. Cells 21 and 22 both have Pen 120/150 binder but different granular materials thickness (Cell 21: 23 in. Cl5-sp, and Cell 22: 18 in. CL6-sp). The thicker section (Cell 21) shows a 20% greater rut accumulation than Cell 22. The granular material in Cell 21 is CL5-sp. This material showed poor permanent deformation behavior during the characterization performed at the University of Illinois and summarized in Chapter 4. CL5-sp was the only granular material in the mainline sections that did not withstand the same conditioning procedure imposed on the other three materials. It is the worst of the four granular materials.

Several mechanistic-based distress models for rutting have been proposed. These permanent accumulation models have been developed based on repeated load testing procedures. A phenomenological model relating the log of permanent strain to the log number of load repetitions has been proposed for asphalt concrete, granular materials and subgrade soils (70).

$$\text{Log } \varepsilon_p = a + b \text{ Log } N$$

or $\varepsilon_p = AN^b$

where:

ε_p = permanent strain

a & b = experimentally determined factors

A = antilog of "a"

All the paving materials (AC, granular base/subbase) and the subgrade soils follow the Log ε_p -Log N phenomenological model. Thompson and Nauman (45)showed that a phenomenological surface rutting model is of the same form.

Log RD = a' + b Log N

where:

RD = Rut Depth, inches

N = number of repeated load applications

a', b = terms developed from field calibration testing data and information.

The Mn/ROAD CFP data were analyzed. The parameters (a' and b) and coefficient of correlation were determined and are presented in Table 7.4 for all CFP cells.

		Inner Wheel Path			Outer Wheel Path		
Cell	**Station**	a'	b	R^2	a'	b	R^2
1	1104	-3.605	0.447	0.75	-4.108	0.549	0.80
	1105	-3.067	0.358	0.67	-3.021	0.367	0.86
2	1112	-5.060	0.713	0.88	-4.408	0.644	0.97
	1113	-3.746	0.502	0.87	-3.901	0.554	0.94
3	1118	-3.057	0.353	0.73	-4.937	0.697	0.96
	1119	-3.057	0.353	0.73	-3.032	0.383	0.85
16	1202	-2.576	0.295	0.71	-4.093	0.491	0.74
	1203	-2.727	0.324	0.74	-3.993	0.480	0.81
17	1209	-3.271	0.428	0.73	-2.809	0.304	0.74
	1210	-4.222	0.585	0.90	-4.620	0.611	0.93
18	1213	-3.843	0.505	0.70	-4.617	0.611	0.93
	1214	-3.984	0.529	0.75	-4.617	0.611	0.93
19	1219	-3.302	0.434	0.71	-4.382	0.567	0.90
	1220	-3.032	0.382	0.74	-4.108	0.576	0.86
20	1224	-6.440	1.001	0.85	-5.379	0.792	0.77
	1225	-5.167	0.794	0.85	-4.401	0.638	0.76
21	1231	-3.648	0.499	0.75	-3.204	0.378	0.70
	1232	-3.746	0.517	0.75	-3.204	0.378	0.70
22	1236	-3.257	0.429	0.79	-2.872	0.351	0.74
	1237	-2.572	0.387	0.73	-3.115	0.400	0.84

Table 7.4 Summary of Log RD - Log N parameters for Mn/ROAD CFP Cells.

The parameters were determined for the inner and outer wheel path of the driving lane and in two station in each cell. All relations show significant ($\alpha = 0.05$) coefficient of correlations. The model captures the rutting behavior. Cell 20 developed very larger rut depths and does not seem to have a "stable" rutting behavior compared to the other 10-year

cells. The "a' " and "b" parameters for this cell are the highest for both the inner and outer wheel path. Cell 2 developed large rut depths. For this cell the " a' " and "b" parameters are also large.

Cell 20 and Cell 23 have reached 0.5 inch (failure in most design procedures) due to rutting at the current applied traffic. The ten year cells were design for 7.2 million ESAL and the five year cells for 3.2 million ESAL. The vertical line in Figures 7.16 and 7.17 indicates the ESALs accumulated at the end of February of 1996 in the 5 and 10-year CFP cells. Most of the thermal cracking developed after this date. No effect is apparent in the rutting accumulation as a result of the thermal cracks that developed on these sections.

7.2.4 South African Criteria for Granular Material Rutting

The South African Mechanistic Design Method (SAMDM) considers rutting by limiting the applied shear stress. Granular materials exhibit deformation due to densification and gradual shear under repeated loading. Maree (71) developed the concept of the "safety factor" against shear failure for granular materials used in the SAMDM.

The safety factor was developed from Möhr-Coulomb theory of static loading and represents the ratio of the material shear strength divided by the applied stress causing shear. It is defined as:

$$F = (\sigma_3 \phi_{term} + c_{term})/(\sigma_1 - \sigma_3)$$

where:

$$\phi_{term} = \sigma_3[K(\tan^2(45+\phi/2) - 1]$$

$$c_{term} = 2KC \tan^2(45+\phi/2)$$

σ_1 and σ_3 = major and minor principle stresses at a point in the granular layer.

C = cohesion

ϕ = angle of internal friction

K = constant = 0.65 for saturated conditions

0.80 for moderate moisture conditions and

0.95 for normal moisture conditions

Safety factors smaller than 1 imply that the shear stress exceeds the shear strength and that rapid shear failure will occur for the static load case. If the safety factor is larger than 1, deformation may accumulate gradually with increasing load applications. The rate of deformation is controlled by the magnitude of the safety factor against shear(46).

Transfer functions have been proposed relating the safety factor (F) to number of load repetitions (N). The relation for a high reliability road is given by (72):

$$N = 10^{(2.6051*F = 4.4801)}$$

Safety of factors against shear failure were calculated for the LVR sections (12). The safety of factors were well above 1 for cells with AC layer greater than 5 inches. The lowest safety factors occurred in the summer when AC modulus is minimum. The mainline cells have AC thickness ranging from 5.75 to 7.75 inches, ensuring low stresses on the granular materials.

7.2.5 Effect of Granular Material Quality on Pavement Response

In CFP with thick AC layer, the properties of the granular materials does not significantly influence the measured responses (deflection and AC strain). The controlling factors are the thickness and modulus of the AC layer and the thickness of granular layers.

The Mn/ROAD data are appropriate for considering the effect of granular material quality on pavement responses. The project has several cells with similar pavement sections but different aggregate material type with only one type of subgrade soil. The mainline portion of the facility is divided into two parts: the 5-year and 10-year design life mainline cells.

The three CFP sections of the 5-year design part, Cells 1 through 3 were grouped into Set 1, since they all have the same AC thickness and similar aggregate material depth. The cells in Set 1 have different granular material type. In the 10-year portion, two additional sets

were formed for the purpose of the evaluation of granular material type effect on pavement response. Set 2 includes Cells 16, 17, 19 and 20. All cells in Set 2 have the same granular material. Set 3 includes Cells 18, 21 and 22.

FWD test data were analyzed for each set. The FWD tests, in each set, were performed on the same day, only minutes apart from each other to assure little temperature change. Surface deflections, load and temperature were collected for each test.

To evaluate the effect of material type in the pavement deflections it is necessary to isolate material type as the only variable in the set. This was achieved by adjusting the field deflection to a set of conditions common to all cells in a set. The procedure utilized is outlined below:

- Select a date where all cells in set were tested. Choose from the test the load level close to 9 kip (standard wheel load). Normalize deflections to 9 kip.
- Backcalculate the asphalt concrete modulus (E_{AC}) and subgrade modulus (E_{Ri}) using ILLI-PAVE based algorithms for CFP for all tests and all cells. (These algorithms were presented in Chapter 5.)
- Calculate $D0'_{ij}$, where i is the number of cells in the set and j is the number of samples in a test date in a given cell. The properties used to obtain each value are the properties backcalculated from FWD and the actual thickness of the layers as measured by GPR.
- Calculate D0". The properties utilized in the algorithm are the overall average property of each material. That is average E_{AC} and E_{Ri} for all tests and all cells in a set. The average AC thickness and average granular material thickness is used. This value is a constant.
- Calculated the ratio $D0"/D0'_{ij}$ for each test drop.
- Calculate the adjusted maximum deflection, $D0^*_{ij}$, by multiplying the ratio $(D0"/D0'_{ij})$ by the measured deflections for each FWD drop.

- Calculate $\bar{D0}^*_i$, the mean maximum deflection for each cell. These mean deflections, one for each cell, are now comparable values.

Four different test dates were chosen: April 25, May 10, May 23 and June 21 of 1994. On these dates, all the cells were "intact" and no thermal cracking or any other significant distresses were present.

Pairwise comparison were performed on the adjusted mean deflections ($\bar{D0}^*_i$) for each set and each test date. The Tukey procedure was utilized to perform the paired comparisons. In this procedure a Tukey W is calculated and if the difference between two means is greater than W, then the hypothesis of equality of means is rejected.

$$W = q_{\alpha(t,df)}\sqrt{(MSW/n)}$$

where:

q is the Studentized range which is the sample distribution of the sample range divided by the estimated standard deviation. The distribution of the Studentized range depends on the number of means being compared (t), the degrees of freedom for the error (within) means square or MSW (df), and the significance level α.

Table 7.5 summarizes the Set 1 results. In the following tables (Tables 7.5 - 7.7), the vertical lines to the left of the mean adjusted maximum deflections groups the means for which the hypothesis of equal means is not rejected.

For Set 1 there was no significant ($\alpha = 0.05$) difference among the means ($\bar{D0}^*$) for testing performed on April 25, 1994. For tests done on May 10, there was no significant difference between means for Cells 2 and 3 of the set, but Cell 1 was different. In testing done on May 23 and June 21, the means for Cells 1 and 2 were not significantly different from each other but the mean for Cell 3 was different from Cells 1 and 2. Figures 7.18 through 7.21 present the mean adjusted maximum deflection ($\bar{D0}^*$) for the three cells. The maximum difference between the adjusted values is less than a mil. The difference at any testing date is less than 5% indicating little effect of granular material quality on pavement responses.

	Test Date: April 25, 1994		
Cell Number	**Mean Adjusted Max. Deflection, mils**	**Standard Dev.**	**Observations**
Cell 1	11.46	0.18	27
Cell 2	11.37	0.26	30
Cell 3	11.38	0.28	30
	Test Date: May 10, 1994		
Cell 1	14.41	0.15	30
Cell 2	14.20	0.22	24
Cell 3	14.03	0.33	30
	Test Date: May 23, 1994		
Cell 1	15.04	0.15	30
Cell 2	14.93	0.26	30
Cell 3	14.53	0.36	30
	Test Date: June 21, 1994		
Cell 1	18.61	0.26	30
Cell 2	18.62	0.37	30
Cell 3	17.76	0.46	30

Table 7.5. Set 1 Maximum Deflection Adjustment Procedure Results.

Table 7.6 presents the results for Set 2. Comparison of the maximum mean deflection on Set 2 shows the same result for all test dates. Cell 16, 17 and 19 means are not significantly different from each other whereas Cell 20 mean is significantly different from the others. Figures 7.22 through 7.25 show the mean adjusted maximum deflection ($\bar{D}0^*$) for the four cells. Cell 20 has a Pen 120/150 cement type, the other cells have AC 20 binder. There was a consistent difference of around 30% in backcalculated AC modulus between Cells 16,17 and 19 and Cell 20. This was accounted for in the adjustment procedure. The difference in adjusted maximum deflection was for all cases less than 0.75 mil or 6%.

Table 7.7 presents the results for Set 3. Cells 21 and 22 have Pen 120/150 asphalt cement and Cell 18 has AC 20 binder. In Set 3, the mean deflection for Cells 21 and 22 are not significantly different from each other on all tests dates. The mean deflection ($\bar{D}0^*$) on Cell 18 is different from the other two. The maximum difference in mean deflections was 1.2 mil (May 23, 1994) or 9%. Figures 7.26 through 7.29 show the mean adjusted maximum deflection ($\bar{D}0^*$) for the three cells.

	Test Date: April 25, 1994		
Cell Number	**Mean Adjusted Max. Deflection**	**Standard Dev.**	**Observations**
Cell 16	8.60	0.29	30
Cell 17	8.53	0.25	30
Cell 19	8.38	0.47	30
Cell 20	8.11	0.12	30
	Test Date: May 10, 1994		
Cell 16	9.22	0.28	27
Cell 17	9.20	0.23	30
Cell 19	9.05	0.49	30
Cell 20	8.78	0.15	30
	Test Date: May 23, 1994		
Cell 16	12.41	0.28	30
Cell 17	12.34	0.22	30
Cell 19	12.16	0.41	30
Cell 20	11.75	0.12	30
	Test Date: June 21, 1994		
Cell 16	12.38	0.27	30
Cell 17	12.40	0.21	30
Cell 19	12.25	0.44	30
Cell 20	11.76	0.15	30

Table 7.6. Set 2 Maximum Deflection Adjustment Procedure Results.

	Test Date: April 25, 1994		
Cell Number	**Mean Adjusted Max. Deflection**	**Standard Dev.**	**Observations**
Cell 18	9.35	0.30	30
Cell 21	8.28	0.14	30
Cell 22	8.34	0.44	30
	Test Date: May 10, 1994		
Cell 18	9.59	0.27	30
Cell 21	8.70	0.15	30
Cell 22	8.81	0.49	30
	Test Date: May 23, 1994		
Cell 18	13.23	0.28	30
Cell 21	11.69	0.15	30
Cell 22	12.06	0.34	30
	Test Date: June 21, 1994		
Cell 18	12.97	0.25	30
Cell 21	11.42	0.15	30
Cell 22	11.86	0.35	30

Table 7.7. Set 3 Maximum Deflection Adjustment Procedure Results.

Some mean deflections are statistically different from others in a set. The difference between the statistically different means ranged from 5 to 10% (0.2 to 1.2 mil). This difference is of little significance for practical engineering purposes.

7.2.6 Effect of Granular Material Quality on Pavement Performance

The AC thickness in the CFP cells ranges from 5.75 to 7.75 inches. This "thick" layer substantially reduces the stress state in the granular material and minimizes the subgrade stress. For these conditions the effect of granular material quality of the on performance is reduced.

The granular materials utilized in the mainline conventional sections are: CL-3sp, CL-4sp, CL-5sp and CL-6sp. The materials are ranked, best to worst, as follows (based on laboratory testing, see Chapter 5):

CL-6sp → CL-3sp → CL-4sp → CL-5sp

The rut depth discussion presented in a previous section showed Cell 21 with CL-5sp base material, shows a worse rutting performance when compared with Cell 22 that has the same asphalt concrete properties but CL-6sp granular material. Cells 1 and 3 have the same asphalt concrete properties (air voids, binder type and content). Cell 3 has CL-5sp in its first 4 inches of granular layer and when compared with Cell 1 that has only CL-4sp material, Cell 3 shows greater rut depth at the time of the last measurement.

There is an effect of aggregate material quality on performance if a material has low shear strength properties. Average to good material properties will not significantly influence the performance of the sections for "thick" AC layers. The granular material quality effect is diminished as the AC thickness increases.

7.3 Full-Depth Flexible Pavement

7.3.1 Fatigue Behavior

There are three FDAC sections in the Mn/ROAD mainline. Cell 4 design life is five years and cells 14 and 15 were designed to last ten years. Pen 120/150 and AC 20 binder types were incorporated in the FDAC sections. For these cells the expected AC strain is low due to the thickness of their AC layer. The fatigue behavior of the Mn/ROAD mixtures, as mentioned before, are investigated in the laboratory and the results are presented in Chapter 5. Again, no fatigue failure was expected at the time of this report due to the structure of the test sections and the amount of traffic experienced to date.

Figure 7.30 presents the expected life of the FDAC mainline cells estimated using IDOT's fatigue algorithm. Figure 7.31 shows the expected life of the FDAC cells as predicted using the algorithms developed from Mn/ROAD mixture testing at ATREL. The life estimated using these laboratory algorithms has not been field calibrated and only provides a mean of ranking the mixtures.

Extensive thermal cracks have occurred in the FDAC cells. The most affected is Cell 15 (AC 20 binder). The thermal cracks impact the pavement system behavior. The layered system, interior loading assumption is less applicable under these "new" conditions. No fatigue failure had occurred on the FDAC sections at the time of this report.

Cells 4 and 14 (Pen 120/150 binder) still provide a good source of data to observe the fatigue failure development on an "intact" section. Cell 15 (AC 20 binder) is not expected to be a good source of information on the fatigue mode expected of FDAC pavements due to the extensive thermal cracking experienced on this cell.

7.3.2 Rutting Behavior

The mainline FDAC cells have an AC layer thickness that ranges from 8.75 to 10.75 inches. This "thick" layer ensures a low subgrade stress ratio (SSR), thus subgrade rutting potential is low. For the FDAC the SSRs were backcalculated and were presented in Chapter 5. The SSRs for in the mainline FDAC sections ranged between 0.1 to 0.25.

Figure 7.32 presents the rut depth accumulation with traffic for the FDAC sections. Table 7.3, presented in the rutting section of the CFP cells, presents the in-place properties of the AC layer for the FDAC cells.

Rut measurements were collected in both the driving and the passing lanes and the inner and outer wheel path of each. There is significant difference in rutting between the driving and passing lanes. Rutting in the outer wheel path of the driving lane is greater than in the inner wheel path for the majority of the cases. The outer wheel path ruts are 12% - 35% larger than the inner wheel path ruts.

Cell 4 shows the greatest rutting. This cell has the thinnest AC layer. The ten year mainline FDAC cells provide an opportunity to observe the effect of asphalt cement type on rut depth accumulation. A "head-on" comparison was made between Cells 14 and 15 where the only difference is asphalt cement type. Cell 14 has Pen 120/150 asphalt and Cell 15 AC 20 binder. As expected, the section with the lower viscosity asphalt developed greater rutting than its higher viscosity counter part. Comparison of the asphalt cement content shows no difference between the two, Cell 14 has an asphalt binder content of 5.34% and Cell 15 has 5.44% (Table 7.3). The in-place voids were around the same level, 6.04% for Cell 14 and 6.26% for Cell 15. There is a 15% difference between the measured ruts in both cells. There is a significant difference in the rutting behavior of the mixes because of the asphalt cement type.

The phenomenological model relating Log RD to Log N was used to evaluate the FDAC data. The Log RD - Log N parameters (a' and b) and coefficient of correlation were determined and are presented in Table 7.8. The parameters were determined for the inner and outer wheel path of the driving lane in two station in each cell.

		Inner Wheel Path			**Outer Wheel Path**		
Cell	**Station**	a'	b	R^2	a'	b	R^2
4	1124	-4.744	0.675	0.82	-3.253	0.465	0.96
	1125	-3.417	0.461	0.86	-2.580	0.355	0.96
14	1190	-3.653	0.480	0.85	-4.231	0.585	0.90
	1191	-4.701	0.675	0.88	-4.195	0.578	0.93
15	1197	-3.626	0.460	0.73	-3.994	0.530	0.75
	1198	-3.820	0.497	0.72	-3.949	0.520	0.77

Table 7.8. Summary of Log RD - Log N relation parameters for FDAC Mainline Cells

All relations show significant ($\alpha = 0.05$) coefficient of correlations. The model to captures the rutting behavior. The vertical line in Figure 7.32 indicates the ESALs accumulated at the end of February of 1996. Most of the thermal cracking developed after this date. No effect is apparent on the rut depth accumulation as a result of the thermal cracks that developed on these sections.

7.4 Summary

The "Design Time"(DT) scheme is utilized to account for the AC modulus - temperature effects. The DT date is mid-to-late May. DT pavement temperatures range from 65 to 69°F and the AC modulus range from 500 -640 ksi. The DT subgrade E_{Ri} isestimated at 10 ksi. The DT temperature is fairly insensitive to AC and granular layer thickness.

Fatigue cracking has developed in CFP Cells 18 and 19. These cracks originated at thermal crack sites. The cells with Pen 120/150 binder still provide an opportunity to observe the fatigue development on an "intact" section. Cells with AC 20 binder are not "intact". The fatigue data for these sections are of limited value in studying the fatigue failure mode of an "intact" section.

The phenomenological model relating rut depth to number of repetitions to failure (Log RD - Log N) was applied to the Mn/ROAD flexible mainline cells. The model captures the rutting behavior. Cell 20 developed the larger ruts of all cells. The "a' " and "b" parameters are greatest for this cell. Asphalt cement type has a significant effect in rut accumulation. Cells with Pen 120/150 binder (lower viscosity) developed larger ruts than cells with AC 20 binder (higher viscosity).

There is not a significant effect of granular material quality on pavement response. The maximum adjusted deflections of cells with different granular material types showed a difference of 5% to 10% (0.2 to 1.2 mil). This difference is of no engineering significance for practical purposes.

The material quality effect on pavement performance is quantified by rut depth measurements. The effect is minimized in these test sections due to the "thick" AC layer protecting the granular material. The performance of "thinner" sections is significantly affected by granular material quality.

CHAPTER 8

Summary, Conclusions and Recommendations

8.1 Review

The purpose of this study was to use Mn/ROAD mainline flexible pavement data to verify, refine, and modify IDOT's M-E based flexible pavement design procedures and concepts. Illinois has used Mechanistic-Empirical (M-E) design procedures for the design of full-depth asphalt concrete (FDAC) and conventional flexible pavements (CFP) sections since the late 1980's. The governing design criteria for CFP is asphalt concrete fatigue and subgrade stress. Subgrade Stress Ratio (SSR) is used for considering subgrade rutting. SSR is the ratio of the deviator stress applied to the unconfined compressive strength of the soil (SSR = $\sigma D/Qu$). For Full-Depth pavements the design criteria is tensile strain at the bottom of the asphalt concrete (AC) layer.

Paving materials characterization was addressed through laboratory and field testing programs. Laboratory testing of the granular materials used in the Mn/ROAD mainline test sections was performed at the University of Illinois. Laboratory tests were conducted to determine optimum moisture content, maximum dry density, gradation, shear strength parameters (c, ϕ), resilient modulus (E_R), rutting potential, and moisture susceptibility. Material testing was also performed by MnDOT Laboratory on granular and subgrade materials. The University of Minnesota tested the asphalt concrete utilized in the mainline test sections. Fatigue characterization of the Mn/ROAD mixtures was performed at the U of I - Advanced Transportation Research and Engineering Laboratory (ATREL). Field characterization of the paving materials was performed through FWD and DCP testing.

The effect of granular material quality on pavement response and performance was assessed through analysis of FWD data. The "Design Time" concept for considering temperature effects on AC modulus fatigue calculations was evaluated. The ILLI-PAVE

structural model was validated by comparing measured (sensors) and calculated pavement responses (i.e., strains, deflections, and stresses).

8.2 Summary

The following specific conclusions were drawn from the study:

1. Analysis of the weigh-in-motion (WIM) data showed no difference in the cumulative distribution of wheel loads in the driving lane throughout the year. The standard 18-kip axle load used in design, corresponds to the 95 percentile of the distribution.

2. Characterization of the paving materials can be adequately accomplished using FWD testing. The variation of the properties throughout the year are quantified with FWD testing. The temperature effects in the AC layer, and moisture and freeze-thaw conditions in the subgrade soils are captured through FWD testing.

3. FWD based AC modulus - Temperature relation is in good agreement with The Asphalt Institute (TAI) estimated values.

4. FWD tests showed very good correlation between the AUPP parameter and the center deflection (D0). The ILLI-PAVE strain - AUPP algorithms result in a very good estimate of AC strain for FDAC and CFP sections. The algorithm produces good estimates for "intact" and "non intact" sections. They can be used at various load levels. The AUPP captures the FWD behavior of the sections and accounts for the effect of surrounding cracks.

5. ILLI-PAVE AC strain values relate well with field measured values (strain gauges) if the test section is "intact". That is, no extensive cracking is present.

6. Field strain and load measurements, showed a stress softening effect on the FDAC sections. For a given load increase the resulting AC strain increase was greater in the FDAC sections. The effect was increased at low AC modulus values. The field observations are comparable to ILLI-PAVE results. The field data showed a more pronounced stress softening effect.

7. Field strain and load measurements showed a stress hardening effect in the CFP sections. For a given load increase, the resulting AC strain increase was smaller in the CFP sections. The effect was increased at low AC modulus values. The field observations are comparable to ILLI-PAVE results. The field data showed a more pronounced stress softening effect. There is little difference in stress hardening between the granular material types.

8. ILLI-PAVE estimated and FWD measured basins of "intact" sections correlate very well.

9. Subgrade displacement measurements (LVDT) correlate well with the ILLI-PAVE estimated values. Total pavement displacements measured with LVDT also showed good agreement with the ILLI-PAVE values. The within pavement deflections (LVDT) showed differ form the ILLI-PAVE estimated values. The placement of the edge of load over the sensor is apparently the source of error.

10. The subgrade stress values measured in the field (PK sensor) compare favorably with ILLI-PAVE estimated values in the range of 4-8 psi. At other stress ranges, the difference between measured and estimated is large.

11. Evaluation of pressure gauges performance and development of better installation techniques should be addressed.

12. "Design Time" Pavement and Air Temperatures are fairly insensitive to AC thickness in already "thick" sections. Aggregate material thickness has little effect on the temperatures. A two inch increase in AC thickness results in a 2°F increase in DT pavement temperature.

13. IDOT's fatigue algorithm is very conservative. The 5-year CFP sections have not failed under fatigue, in contrast to IDOT's fatigue algorithm estimate.

14. The asphalt cement type influences the rutting behavior of the flexible sections. A 20% difference was found in rutting between cells with the same section and different asphalt cements. Cells with the low asphalt cement (viscosity Pen 120/150) resulted in higher rut depths than cells with AC 20 asphalt cement.

15. The rutting behavior of the flexible cells can be modeled with the phenomenological Log RD - Log N relation. Good correlations were obtained for all the flexible cells in both the inner and outer wheel paths of the driving lane.

16. Extensive thermal cracking occurred in the AC 20 cells. The occurrence of thermal cracking did not affect rutting development on the Mn/ROAD flexible sections. The International Roughness Index (IRI) was not significantly affected by the cracks either.

17. Granular material quality has little effect on pavement response in "thick" CFP sections. The average difference in center deflection between cells with different granular materials is less than 1 mil or 5%.

18. Granular material quality influences the rutting behavior on CFPs. The influence is limited in "thick" sections. The difference is encountered only between poor shear strength materials and average to good materials. The effect is negligible between average and good shear strength materials.

19. Thermal cracking development significantly influenced the fatigue life of the flexible pavement sections. "Non intact" sections in the Mn/ROAD project do not provide a good source of information for evaluating the fatigue failure mode expected of an "intact" section.

20. Based on Mn/ROAD data evaluation and analyses, it was concluded that the present M-E design procedure used by IDOT in FDAC and CFP pavements is adequate.

8.3 Conclusions

The study demonstrated that the Illinois Department of Transportation mechanistic-empirical analysis and design procedures for FDAC and CFP sections are adequate. The ILLI-PAVE structural model adequately predicts the pavement responses. The bi-linear (arithmetic) subgrade model and the "theta" model closely replicate the field responses. The ILLI-PAVE algorithms are adequate to be utilized in FWD backcalculations. The properties of the layers and pavement responses can be accurately estimated (AC strain, E_{AC}, E_{Ri}).

The ILLI-PAVE model can only analyze the interior loading condition on a section. This was a limitation on the evaluation of thermal cracked sections. Supplemental analyses are needed to consider the impact of thermal cracks on flexible pavement response and performance. A structural model with 3-D capability would be more appropriate in addressing this issue.

Analyses of the Mn/ROAD sections indicate that IDOT's AC fatigue algorithm is very conservative. Continued AC fatigue algorithm refinement is needed.

8.4 Recommendations for Future Work

Mn/ROAD project should continue to be monitored. The cells with Pen 120/150 asphalt cement can be used to evaluate fatigue development and to calibrate the existent fatigue algorithms. All cells should be monitored to evaluate rutting behavior.

Effort should placed in trying to relate the laboratory fatigue life to the field observed life. "Shift factors" need to be developed.

At this time, the accuracy of the pressure gauges (PK) is not known. This issue should be addressed.

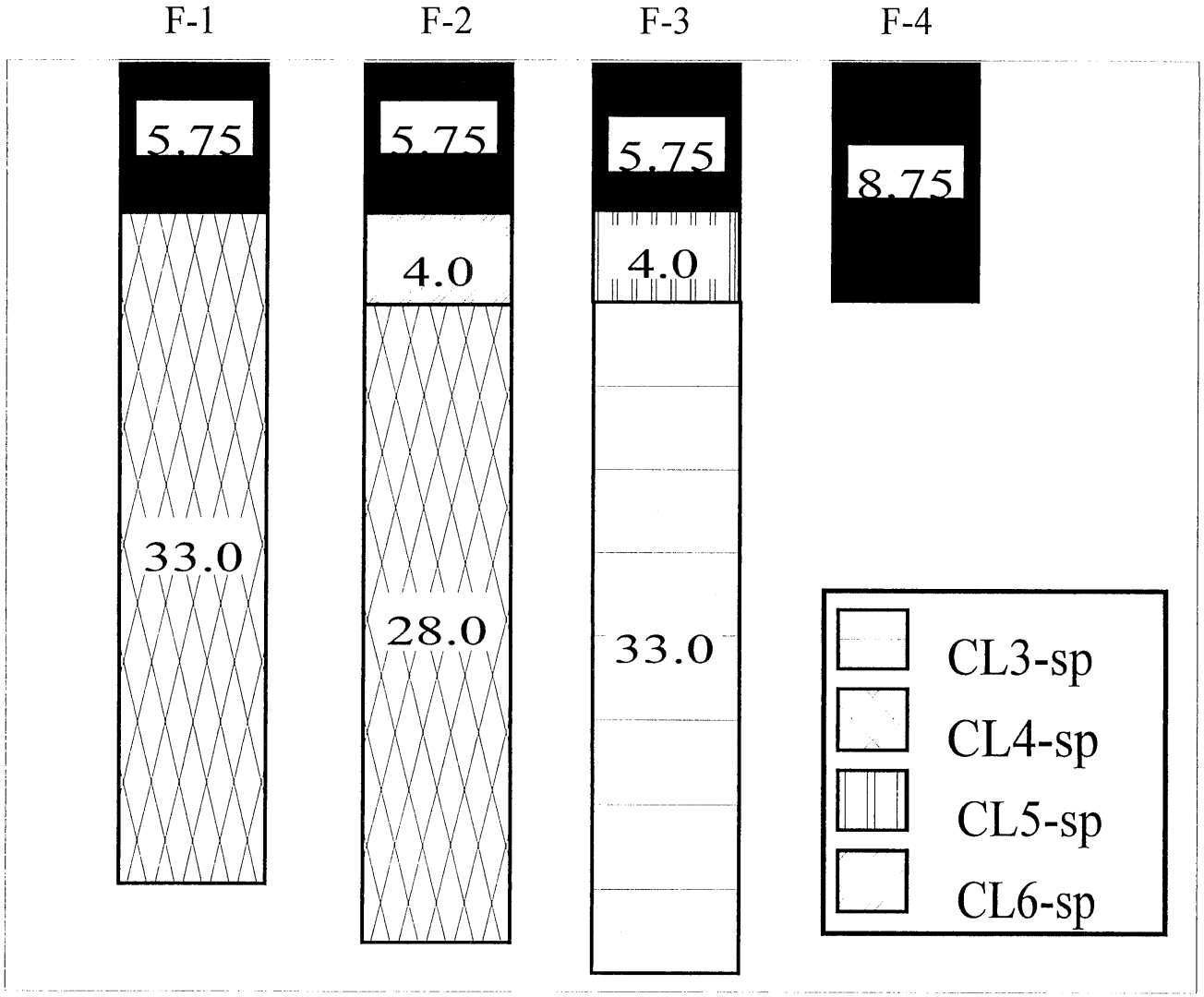

Figure 1.1. 5 Year Mainline Flexible Pavement Sections.

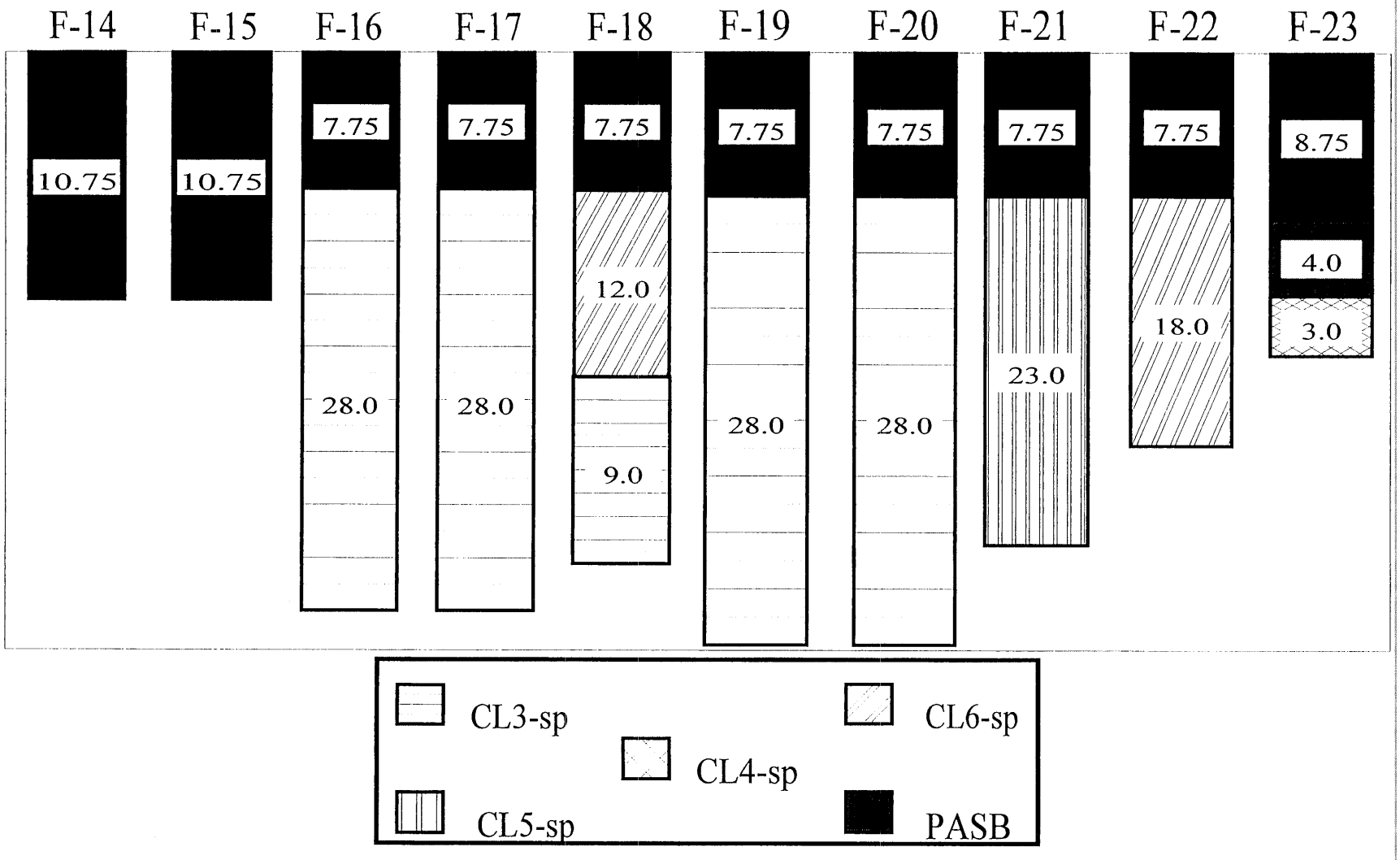

Figure 1.2. 10 Year Mainline Flexible Pavement Sections.

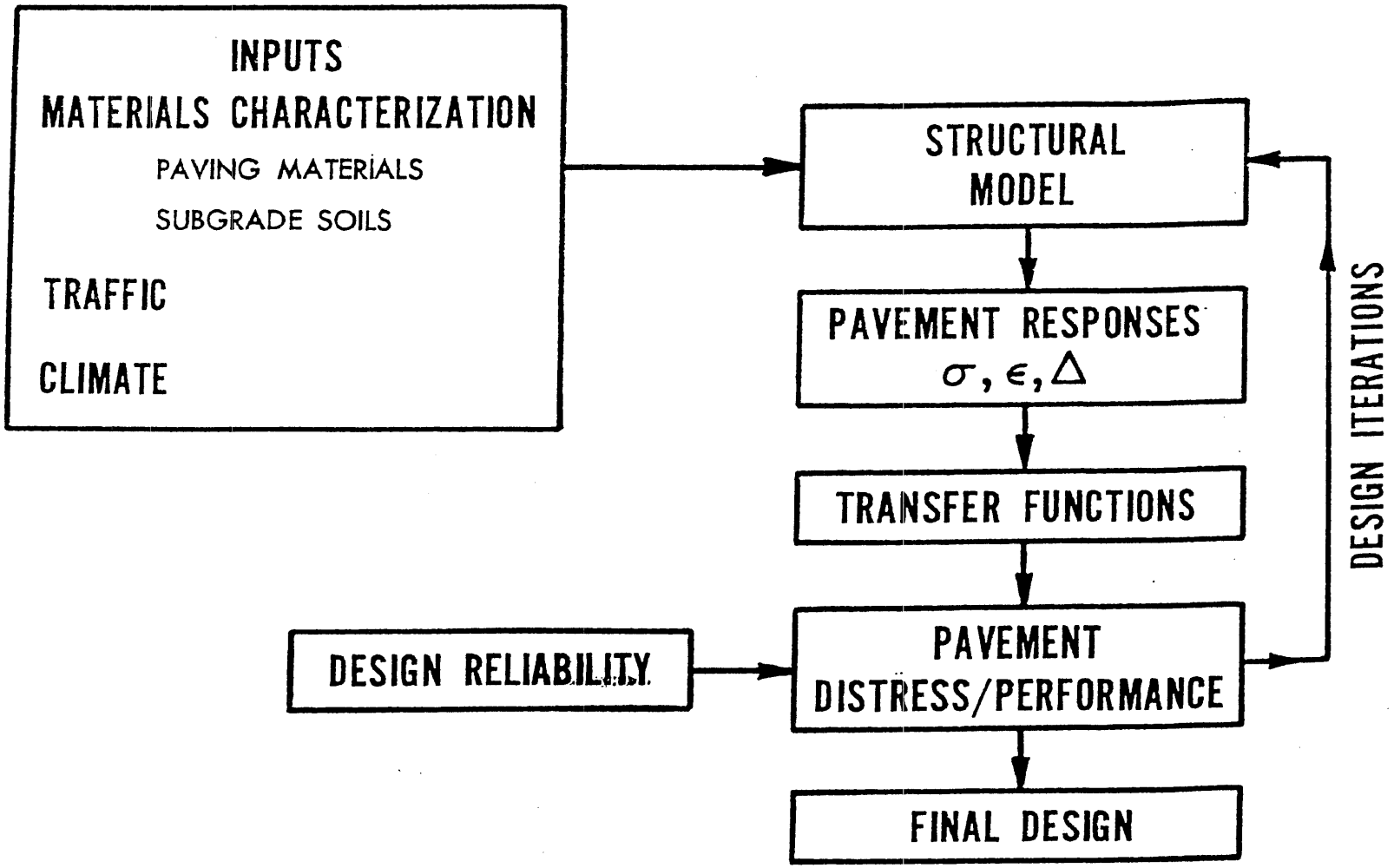

Figure 2.1. Components of a Mechanistic-Empirical Design Procedure

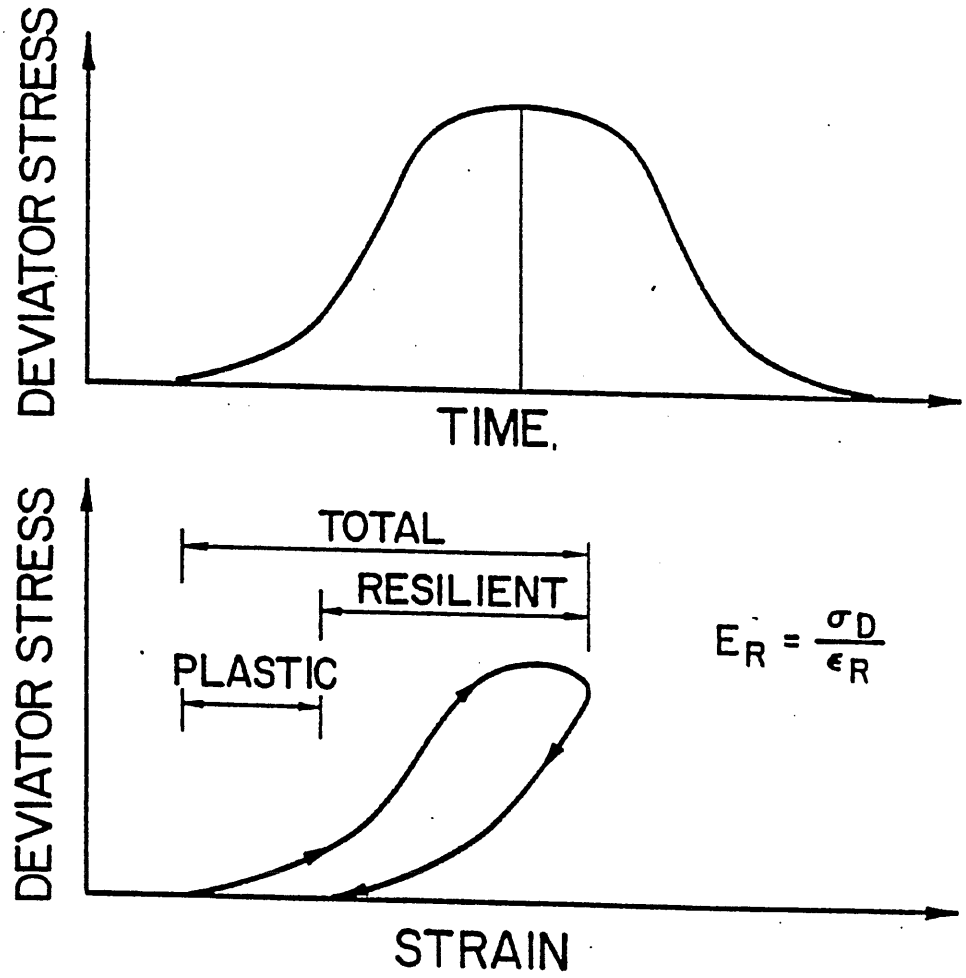

Figure 2.2. Repeated Load Testing Concepts.

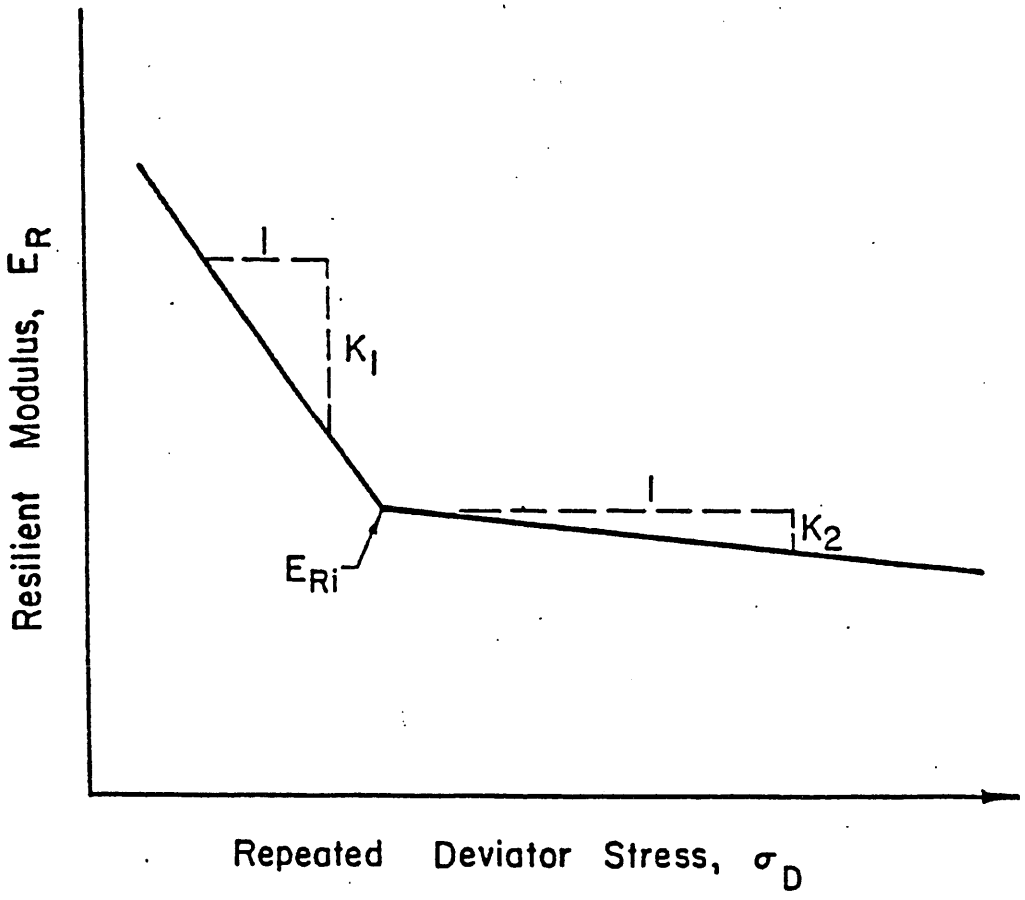

Figure 2.3. Arithmetic Model for Stress Dependent Resilient Behavior of Fine-Grained Soils.

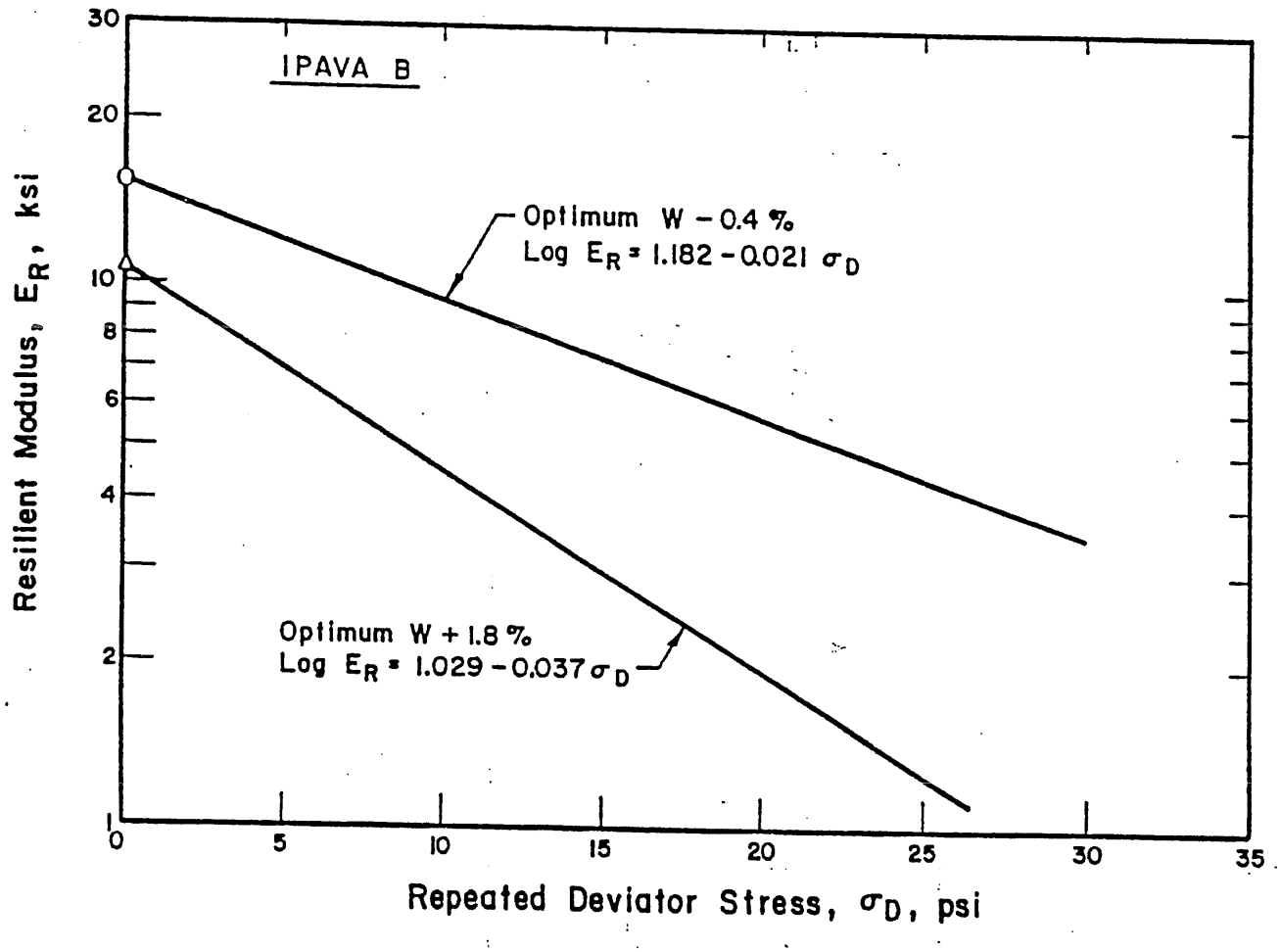

Figure 2.4. Semi-Log Model for Stress Dependent Resilient Behavior of a Fine-Grained Soil.

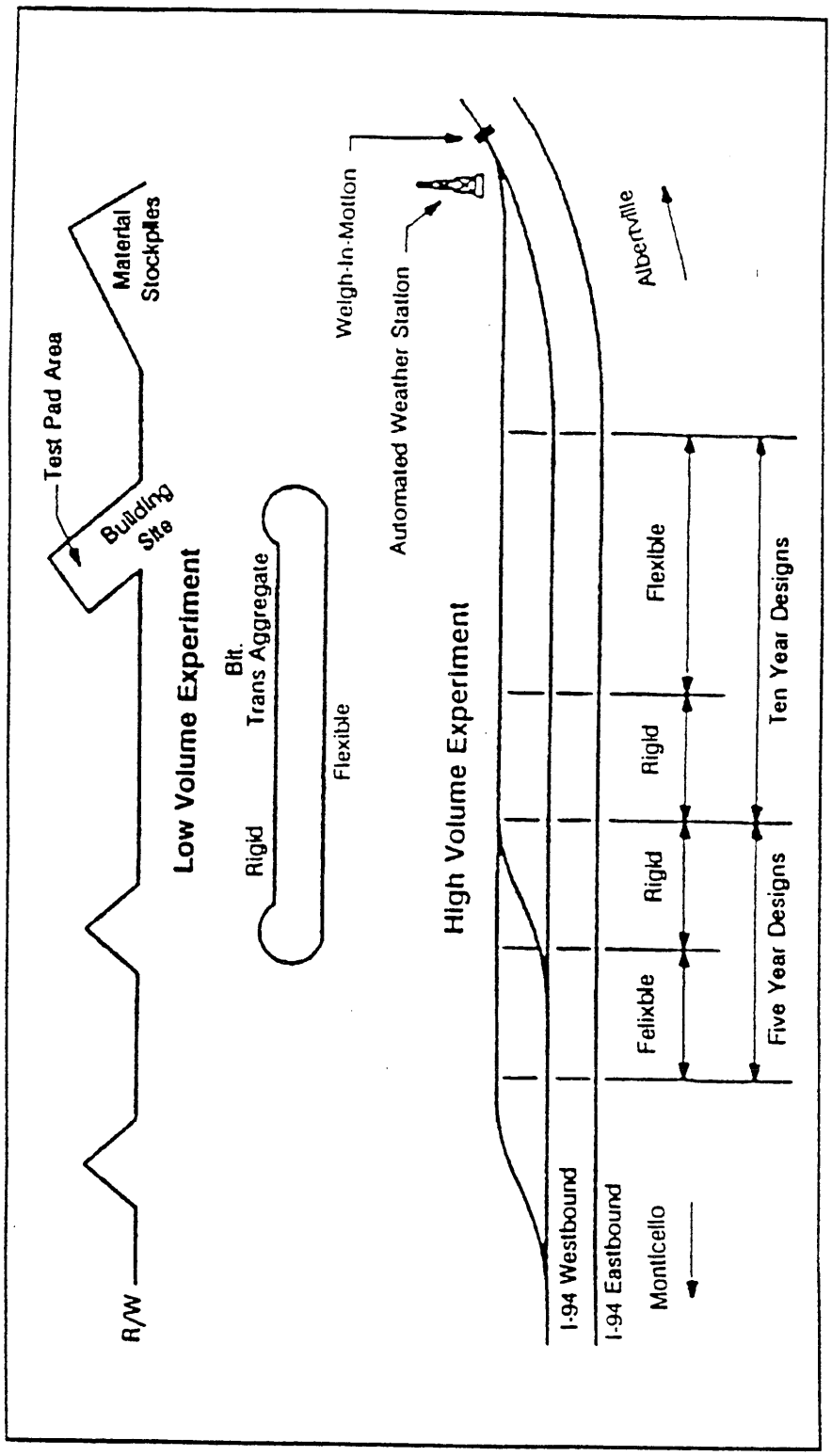

Figure 3.1. Minnesota Road Research Project.

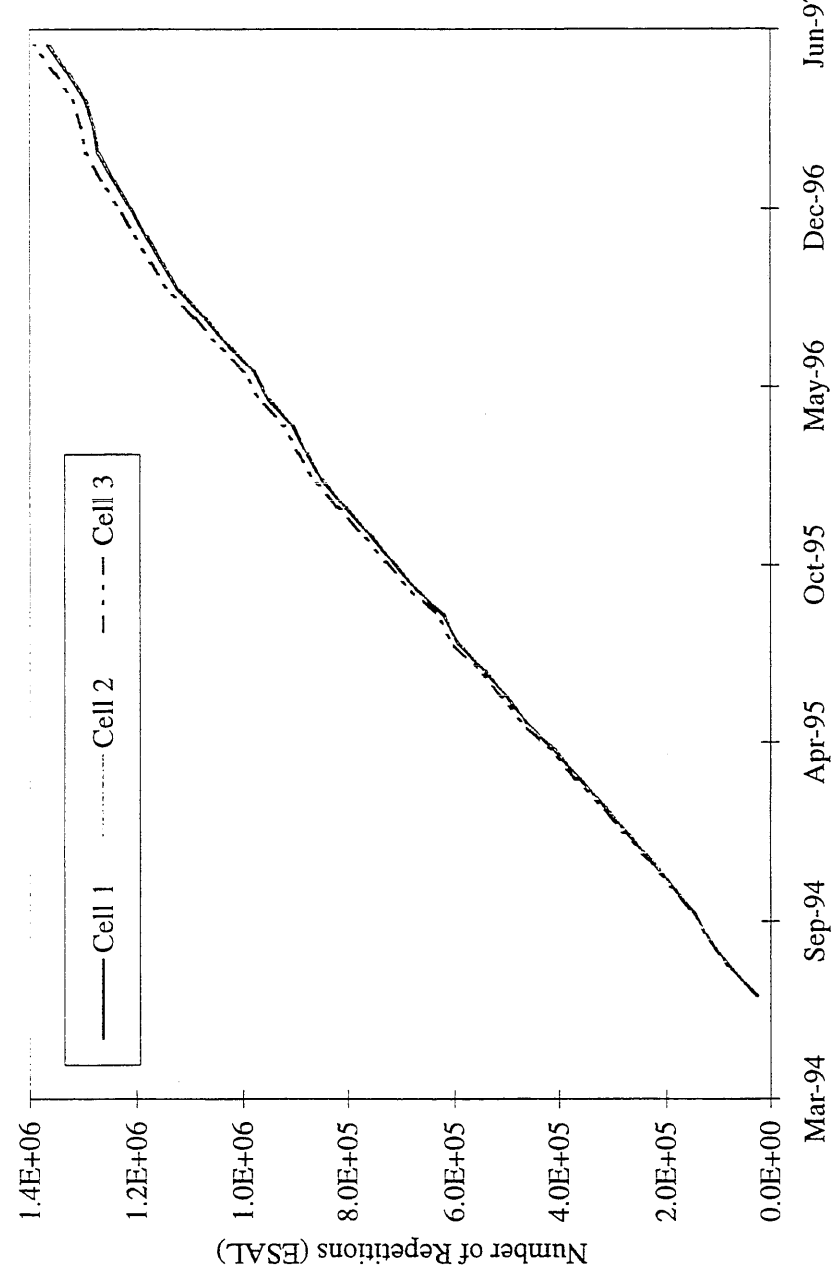

Figure 3.2. ESAL Accumulation for 5-year Mainline Conventional Sections (Driving Lane).

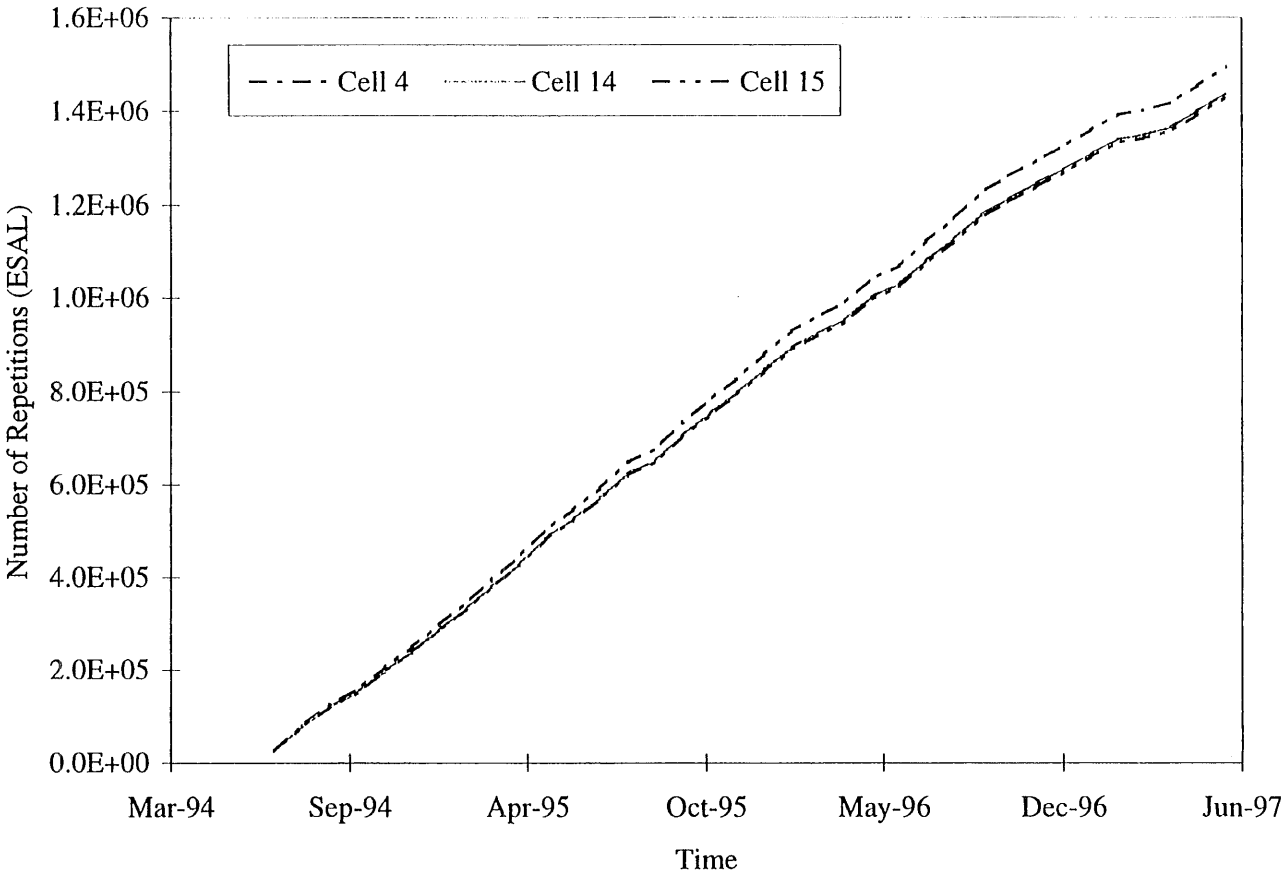

Figure 3.3. ESAL Accumulation for Full Depth Mainline Sections (Driving Lane).

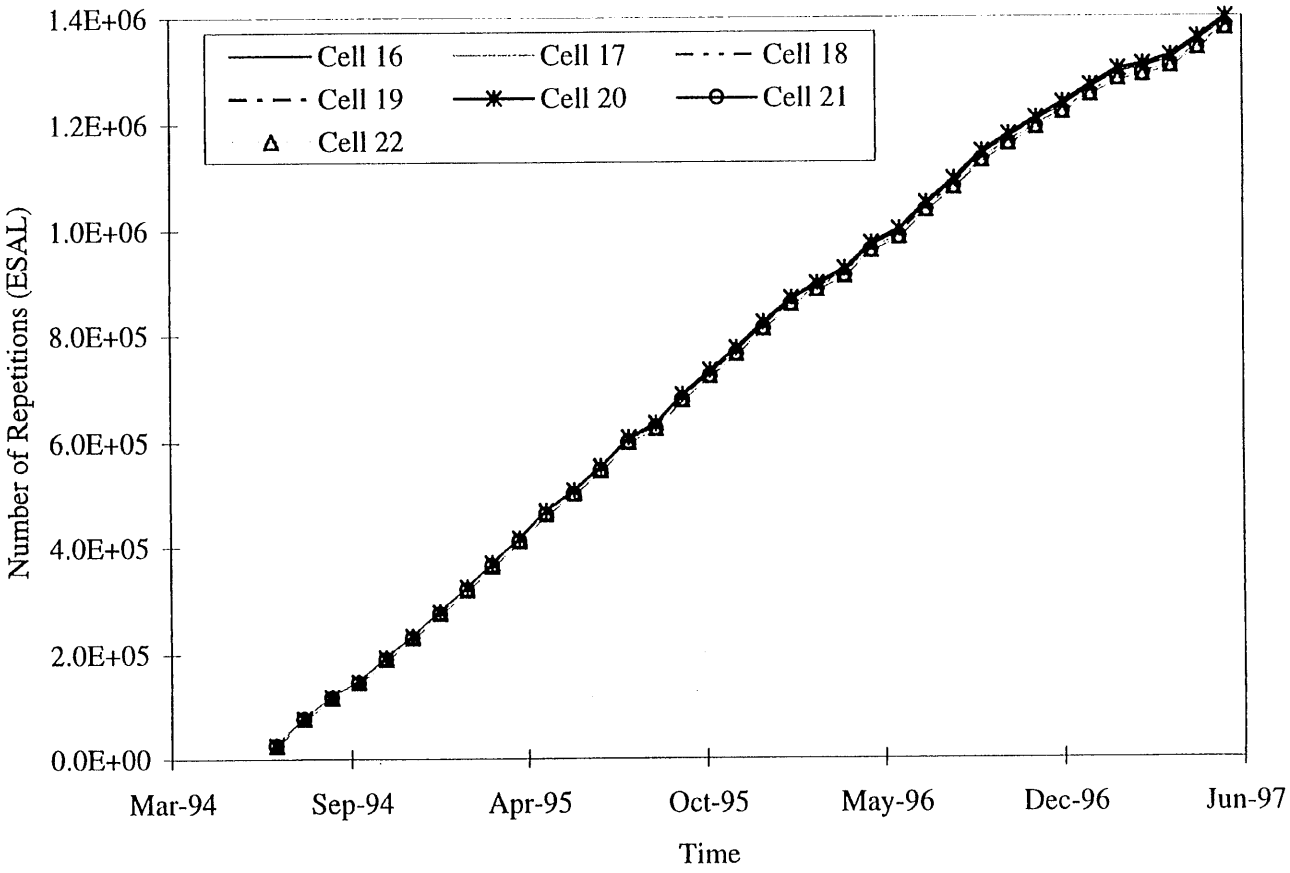

Figure 3.4. ESAL Accumulation for 10-year Mainline Conventional Sections (Driving Lane).

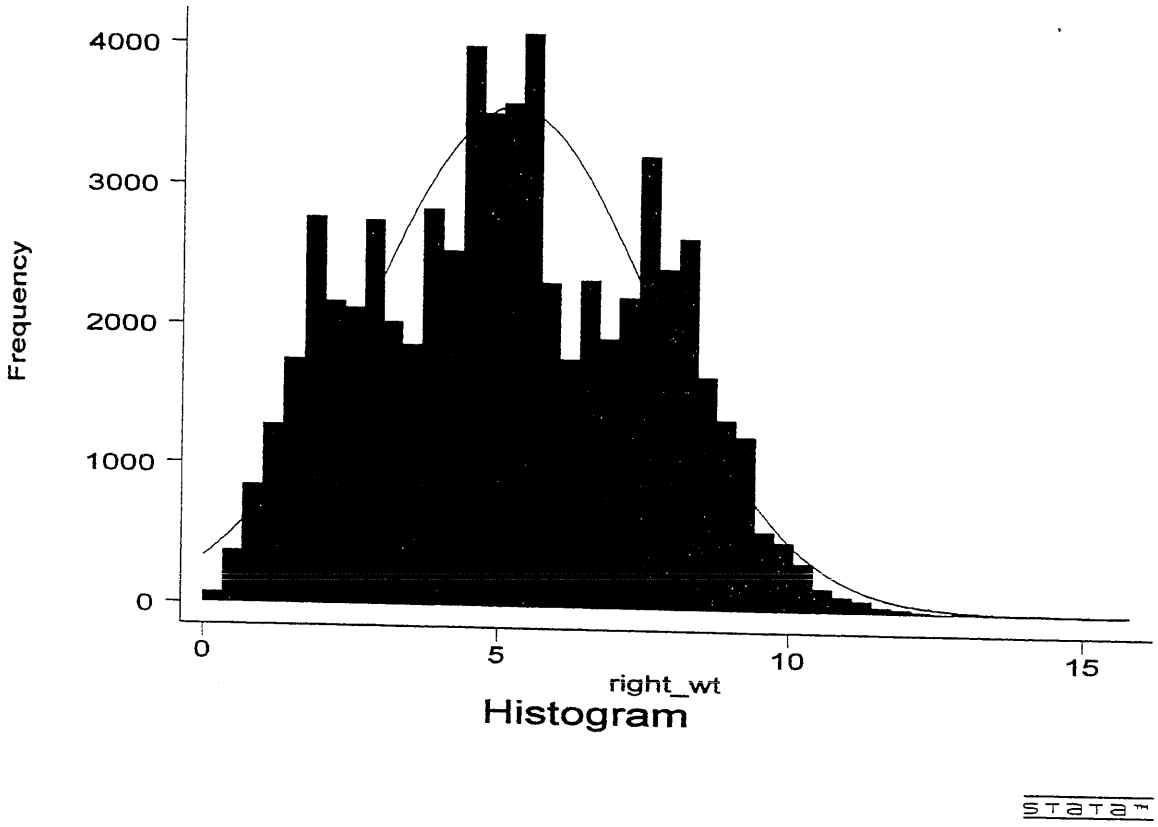

Figure 3.5. Histogram of Wheel Load (Design Time week).

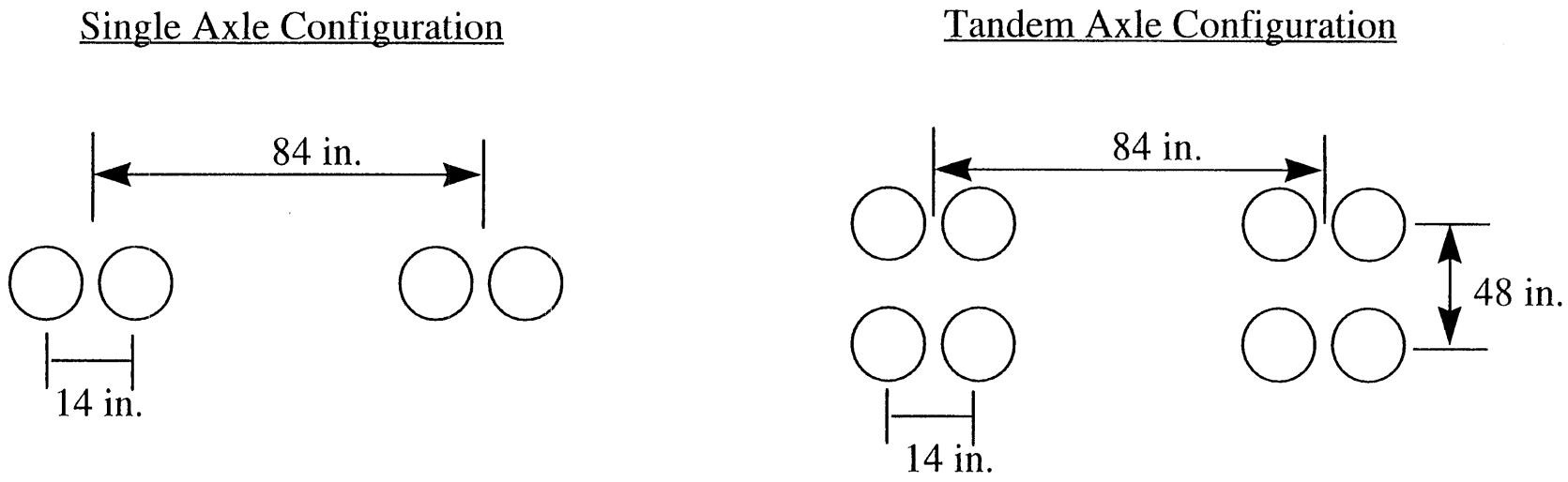

•Tire Pressure = 100 psi

Figure 3.6 - Tractor-Trailer Axle Wheel Configuration for Mainline Road Sections.

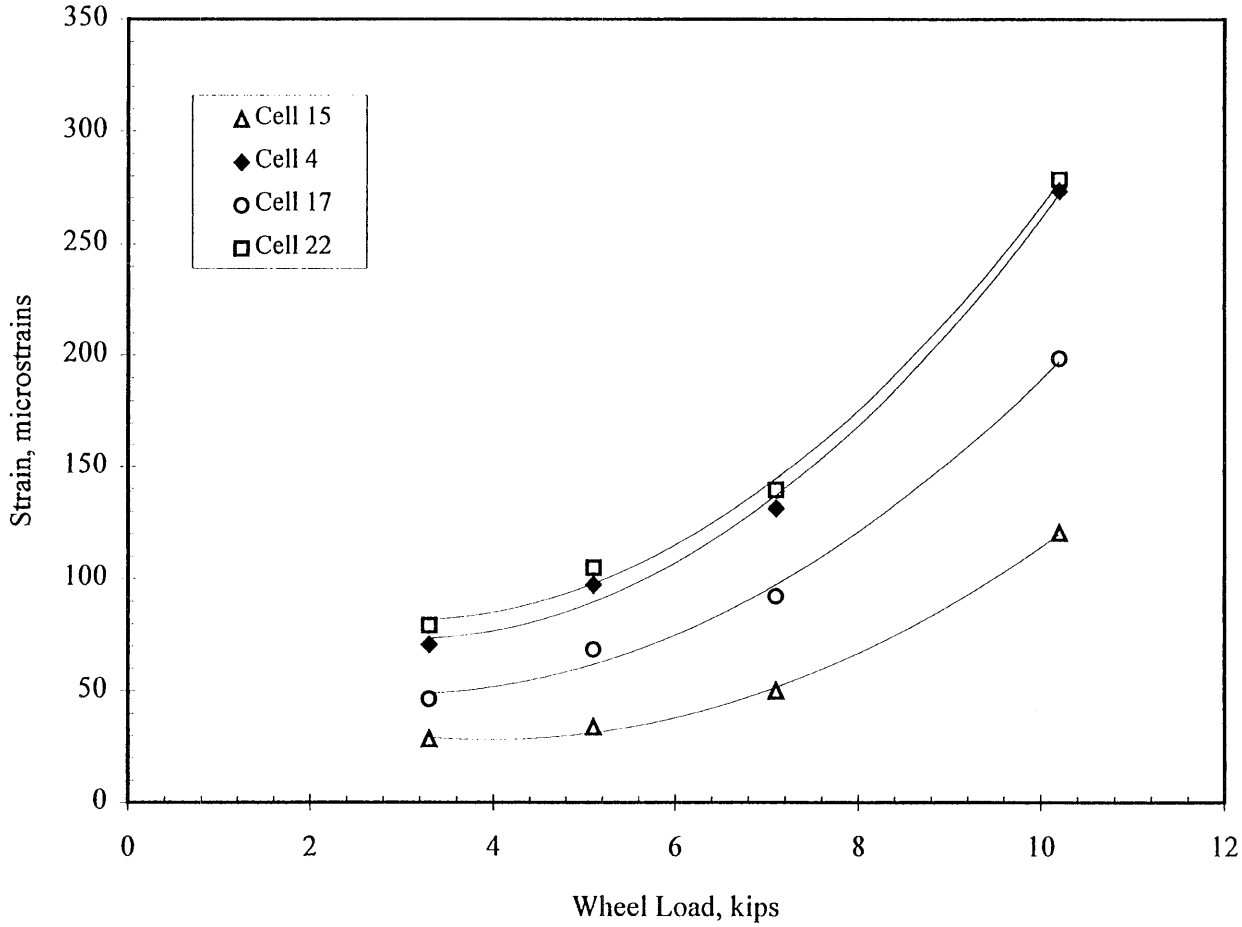

Figure 3.7. Correlation for Wheel Load and Strain Percentiles ("Design Time" Week)

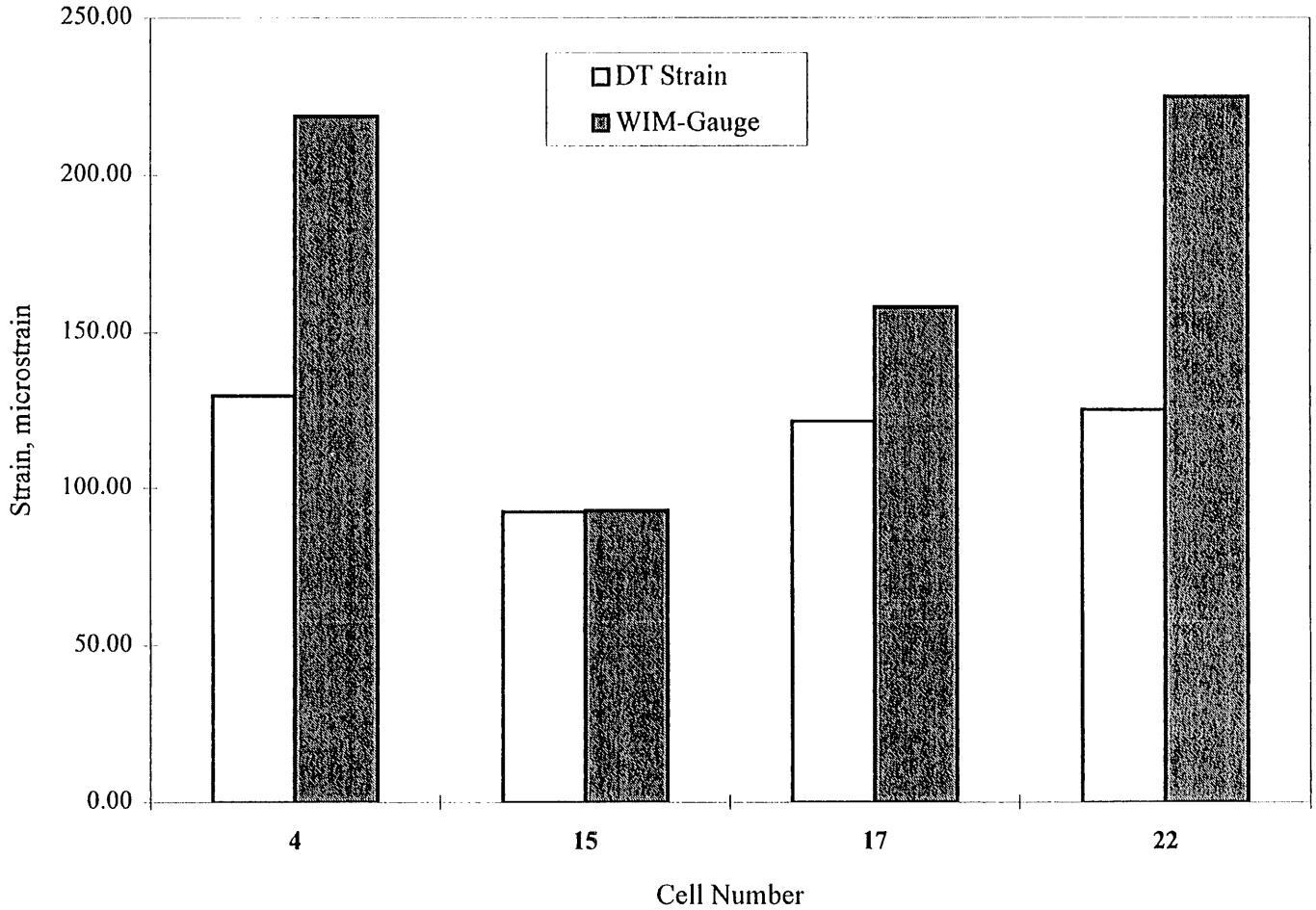

Figure 3.8. Comparison of "Design Time" and WIM-Gauge Relation Strain.

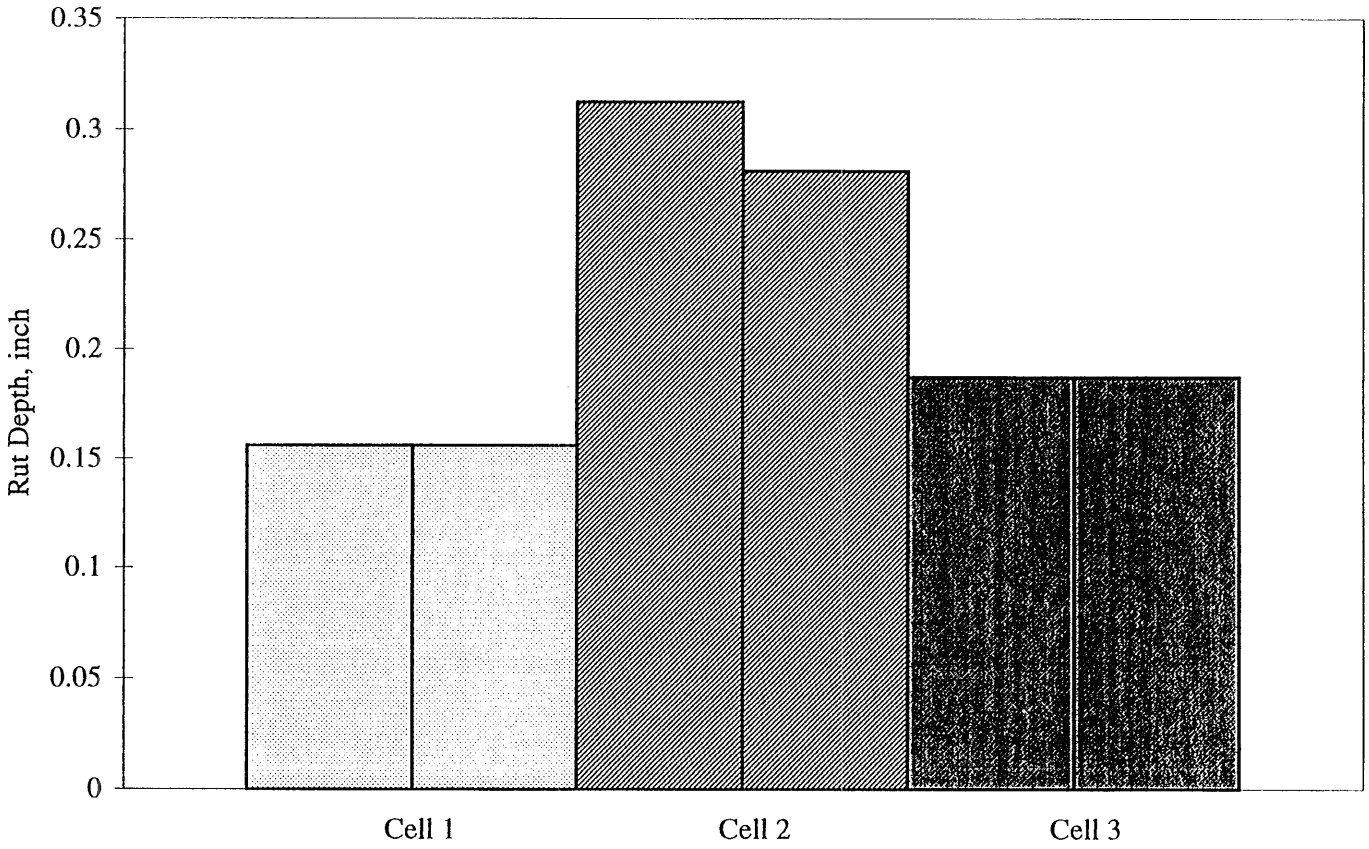

Figure 4. 1. Rut Depth on 5-Year Mainline Cells Outer Wheel Path (4/1/97)

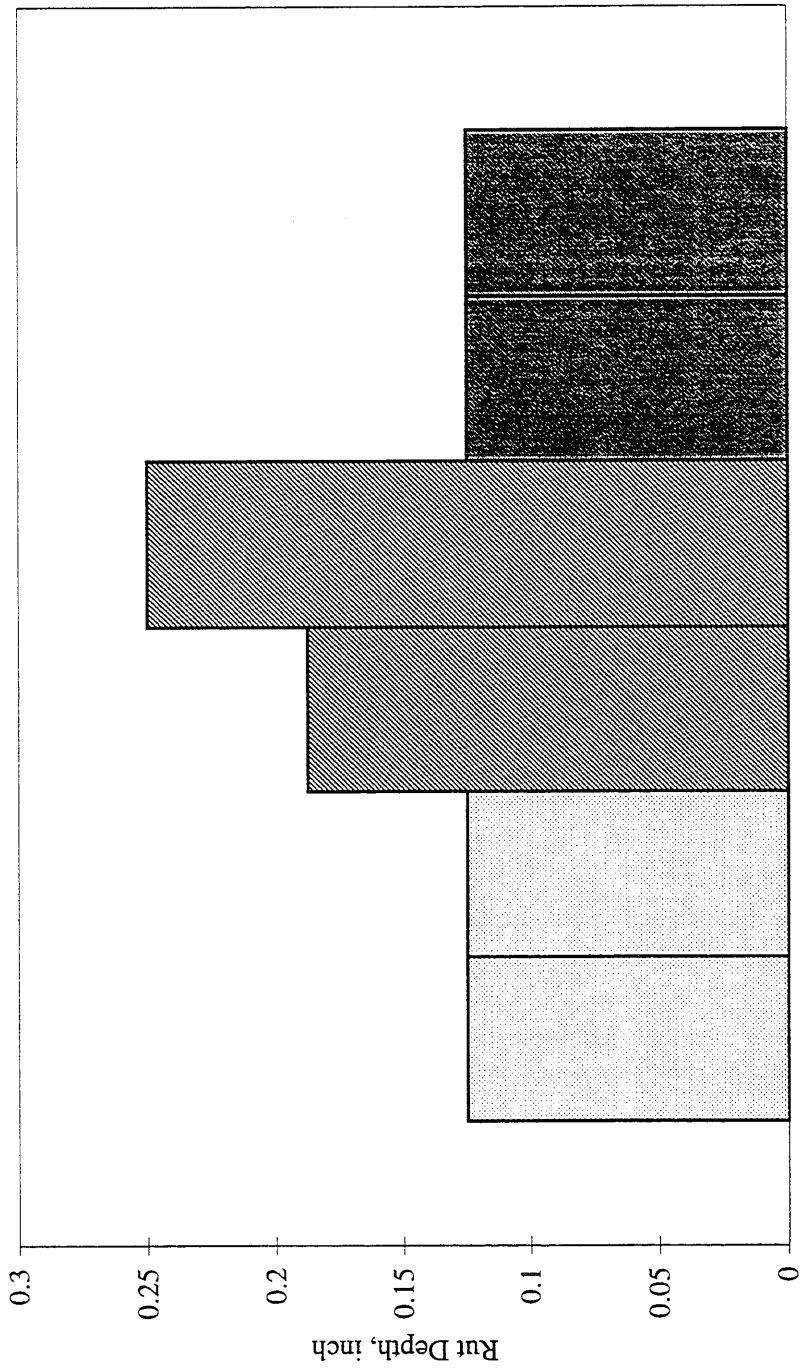

Figure 4. 2 Rut Depth on 5-Year Mainline Cells Inner Wheel Path (4/1/97).

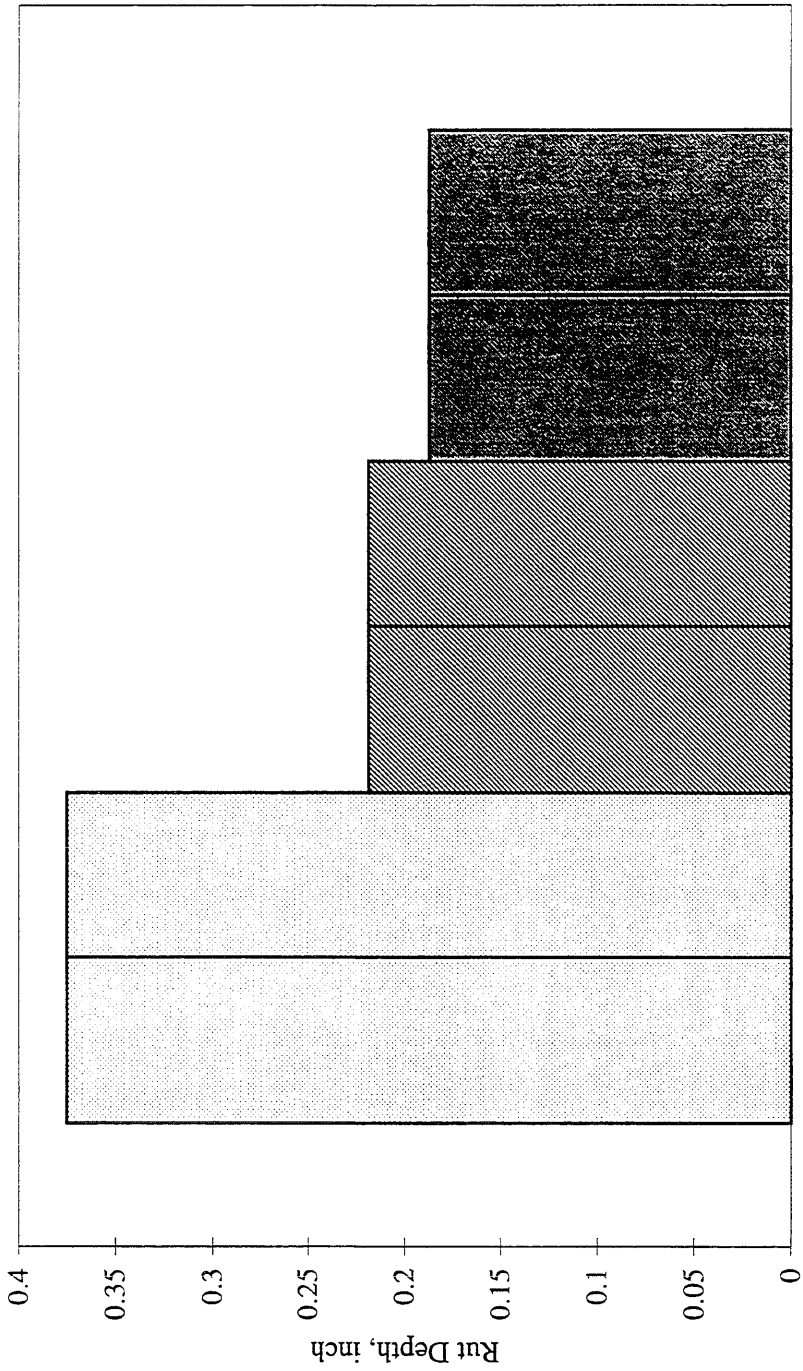

Figure 4.3. Rut Depth on Full Depth Mainline Cells Outer Wheel Path (4/1/97).

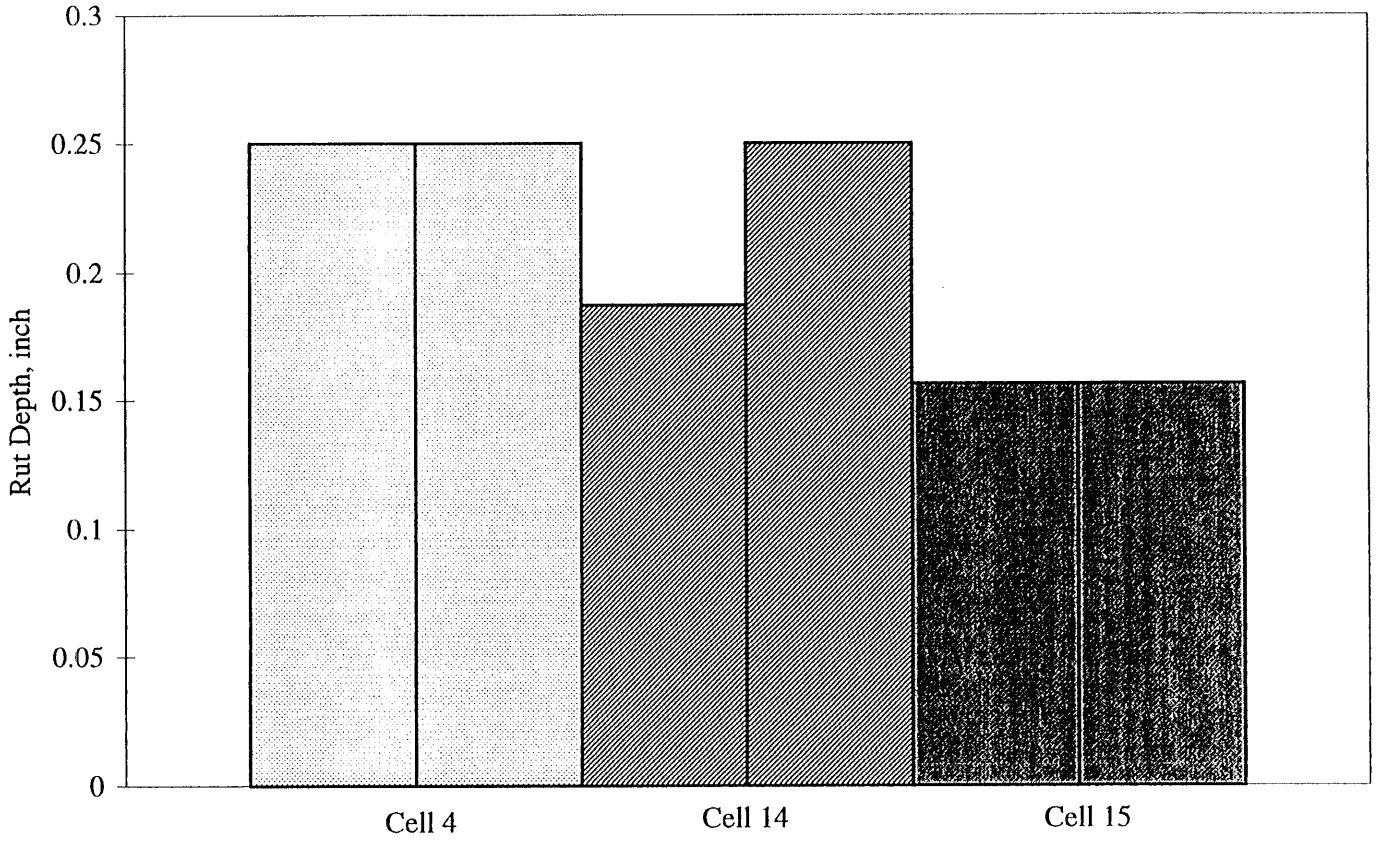

Figure 4.4. Rut Depth on Full Depth Mainline Cells Inner Wheel Path (4/1/97).

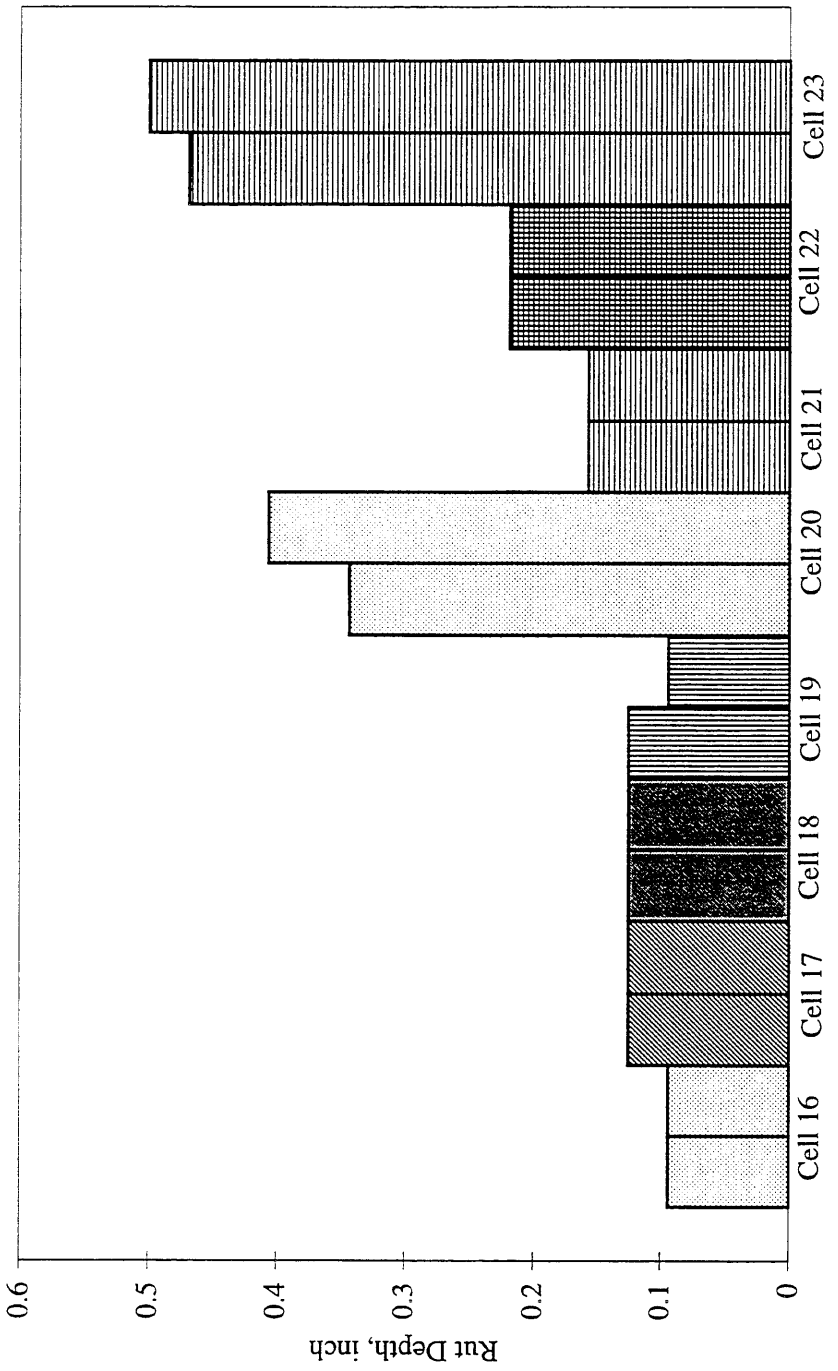

Figure 4.5 Rut Depth on 10-year Mainline Cells Outer Wheel Path (4/1/97).

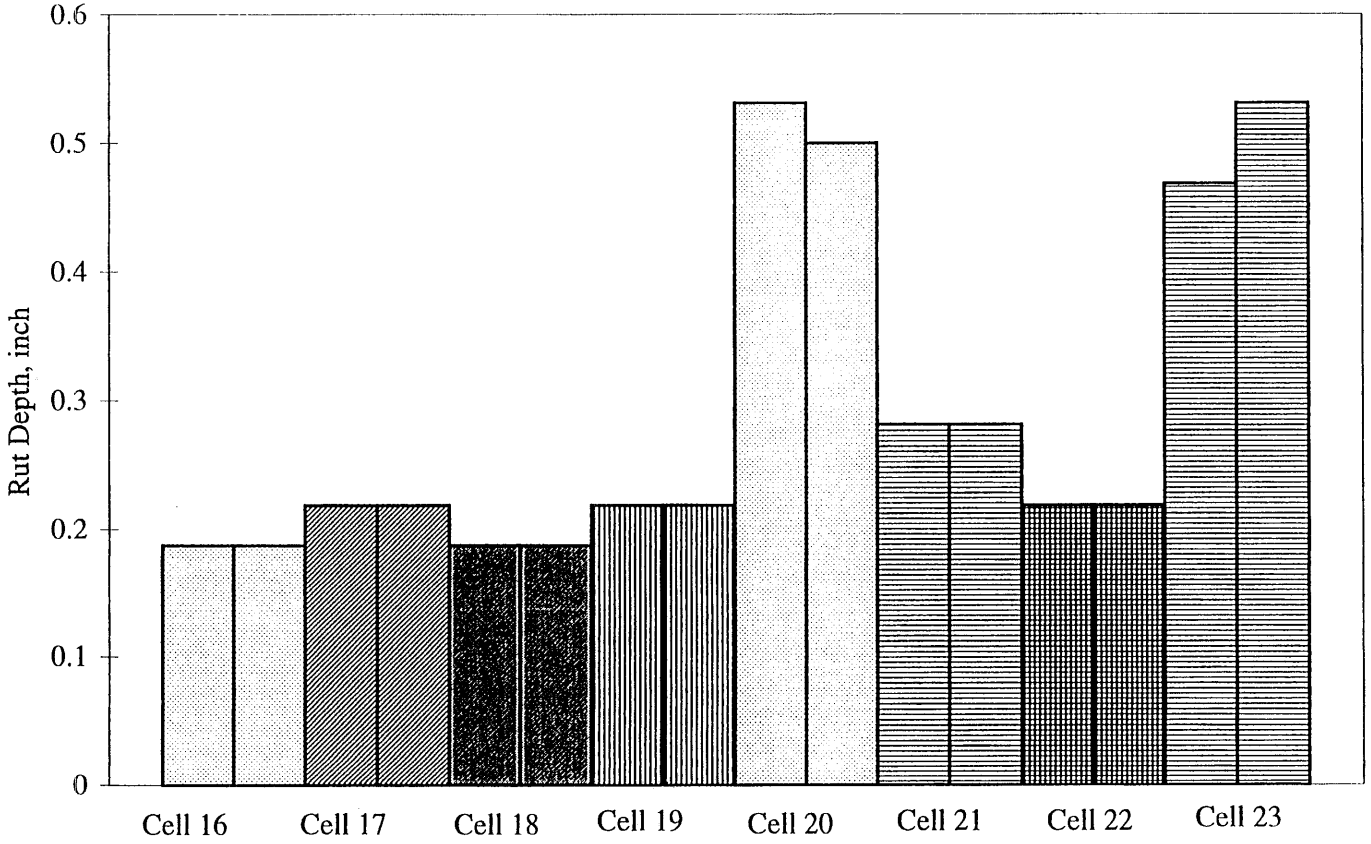

Figure 4.6 Rut Depth on 10-Year Mainline Cells Inner Wheel Path (4/1/97).

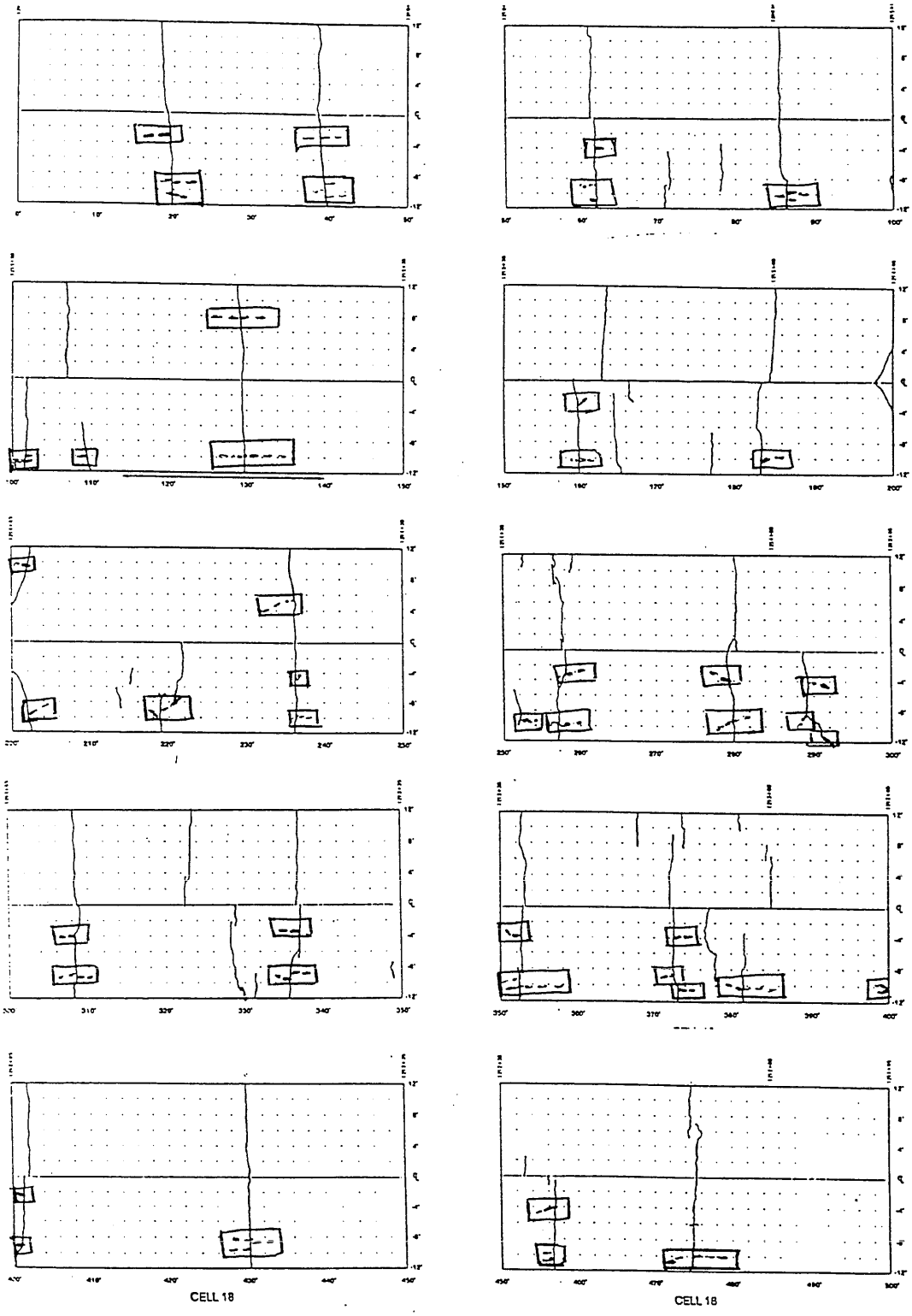

Figure 4.7. Fatigue Cracking Locations on Cell 18.

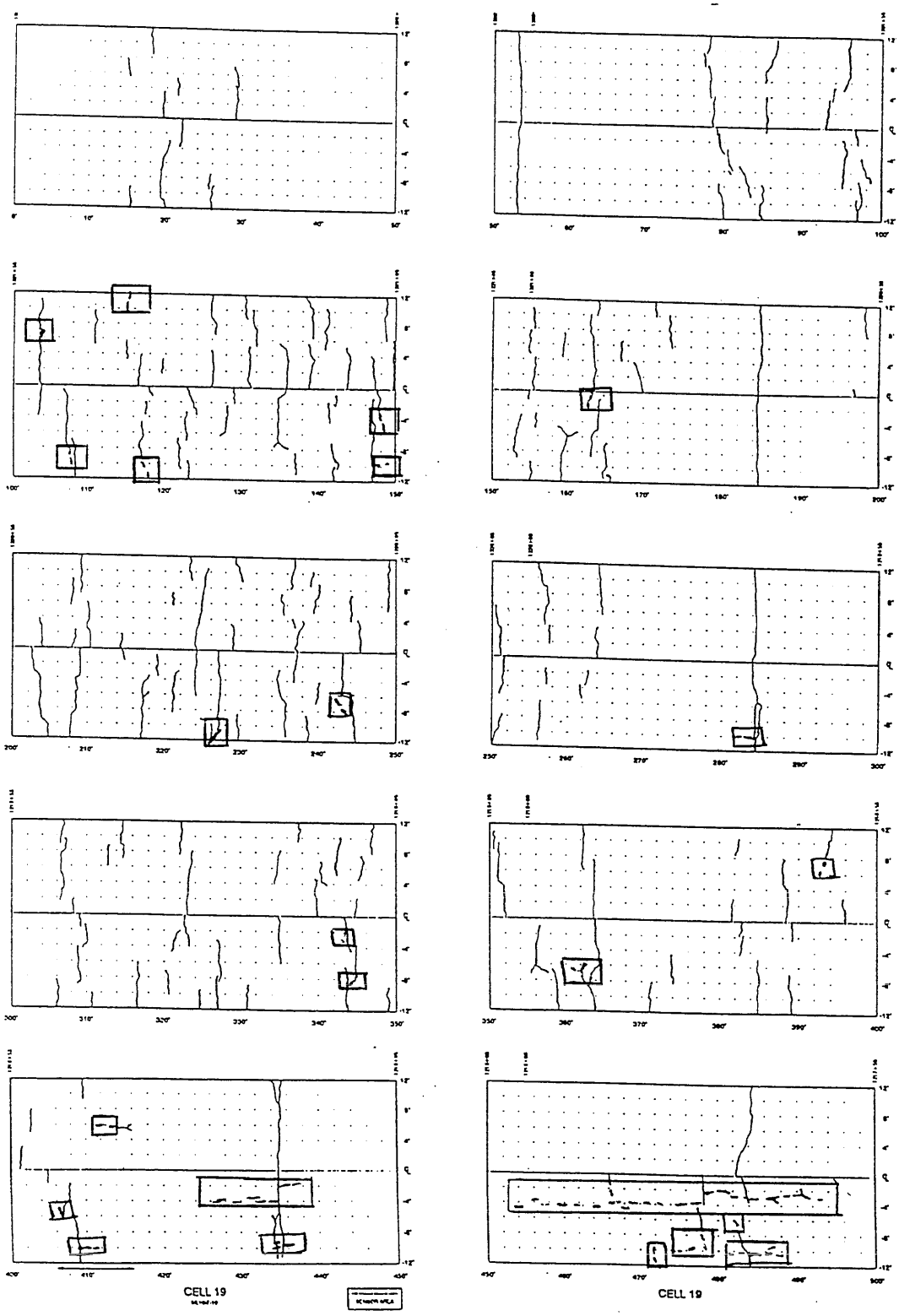

Figure 4.8. Fatigue Cracking Locations on Cell 19.

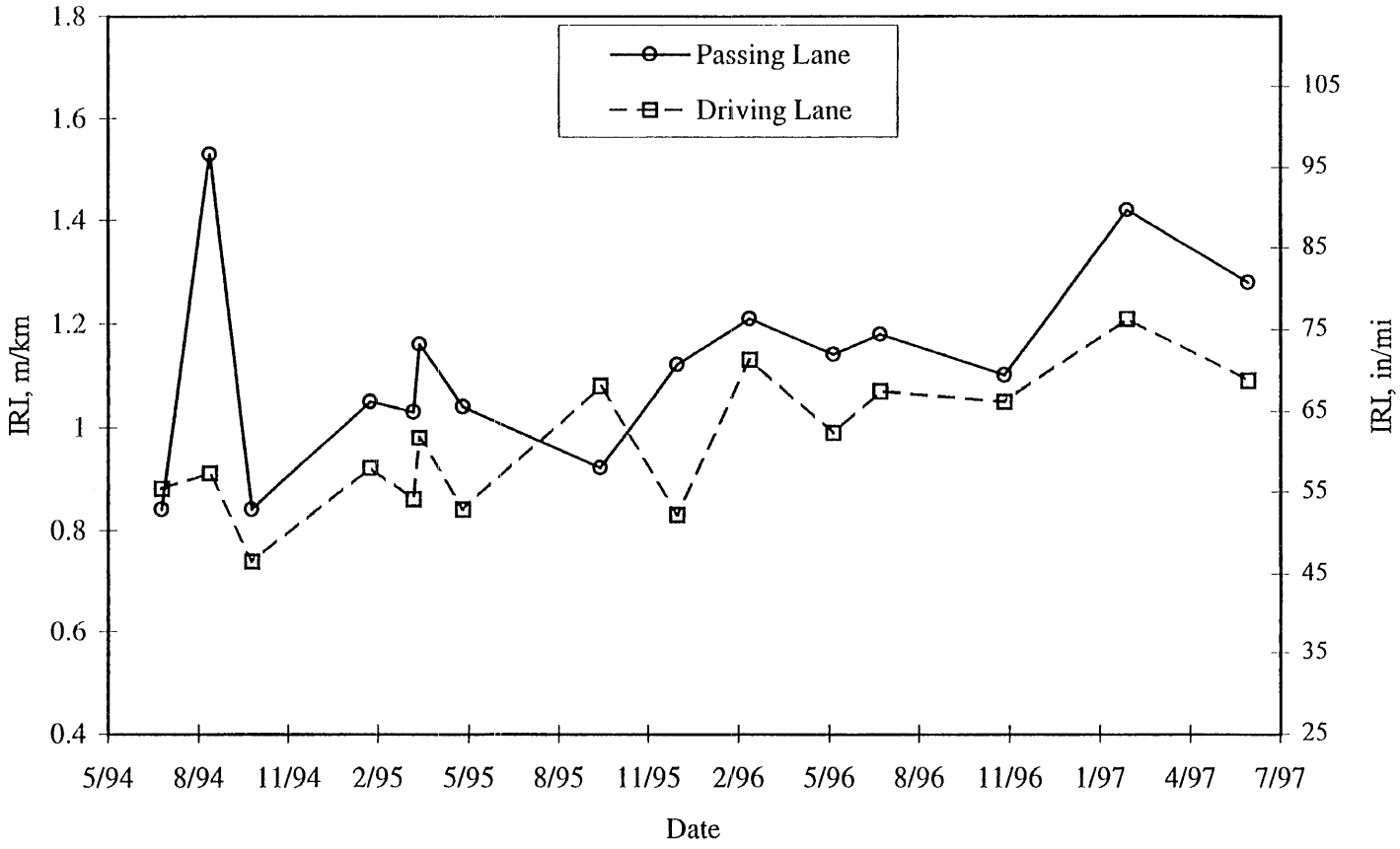

Figure 4.9. IRI Measurements for Cell 1.

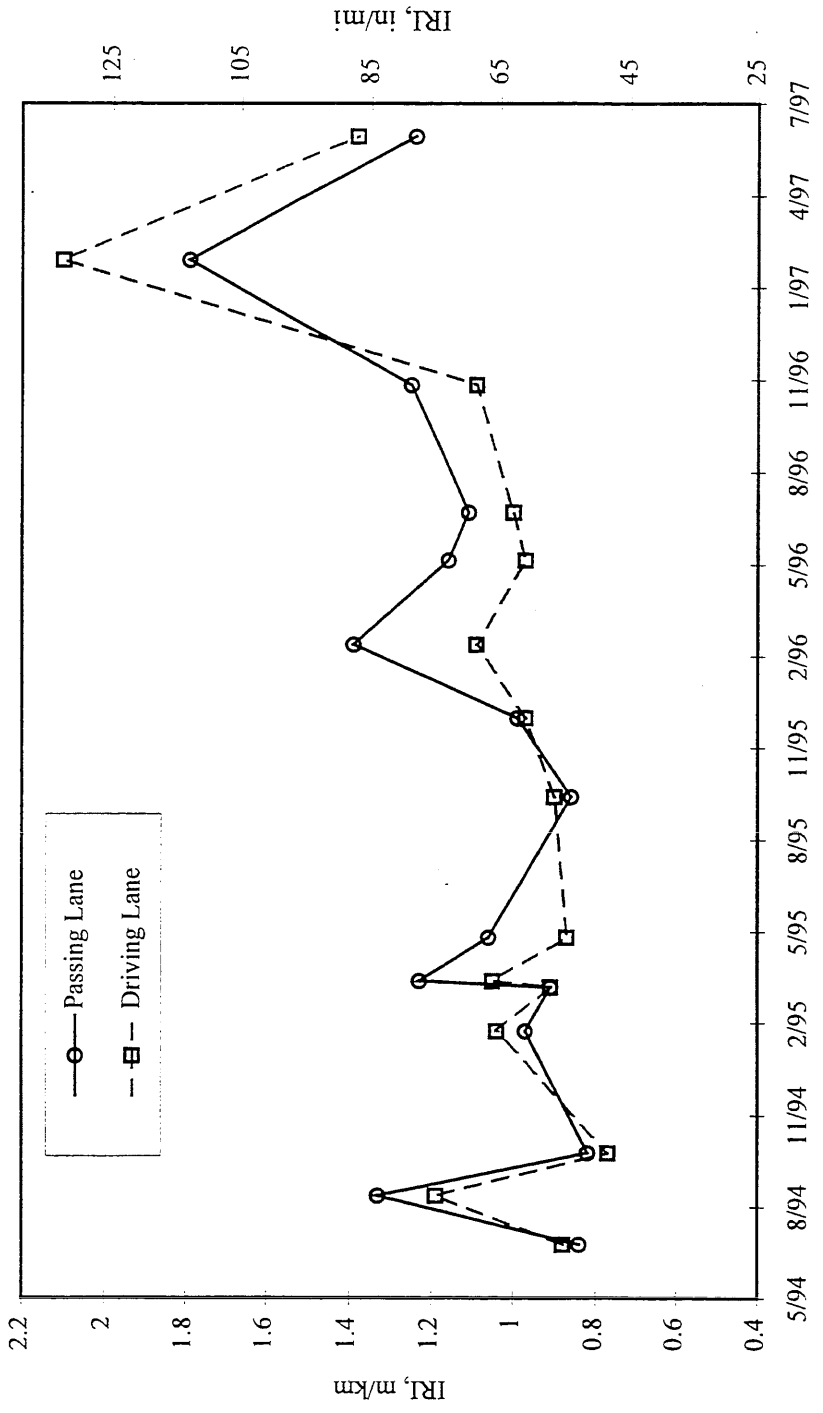

Figure 4.10. IRI Measurements for Cell 2.

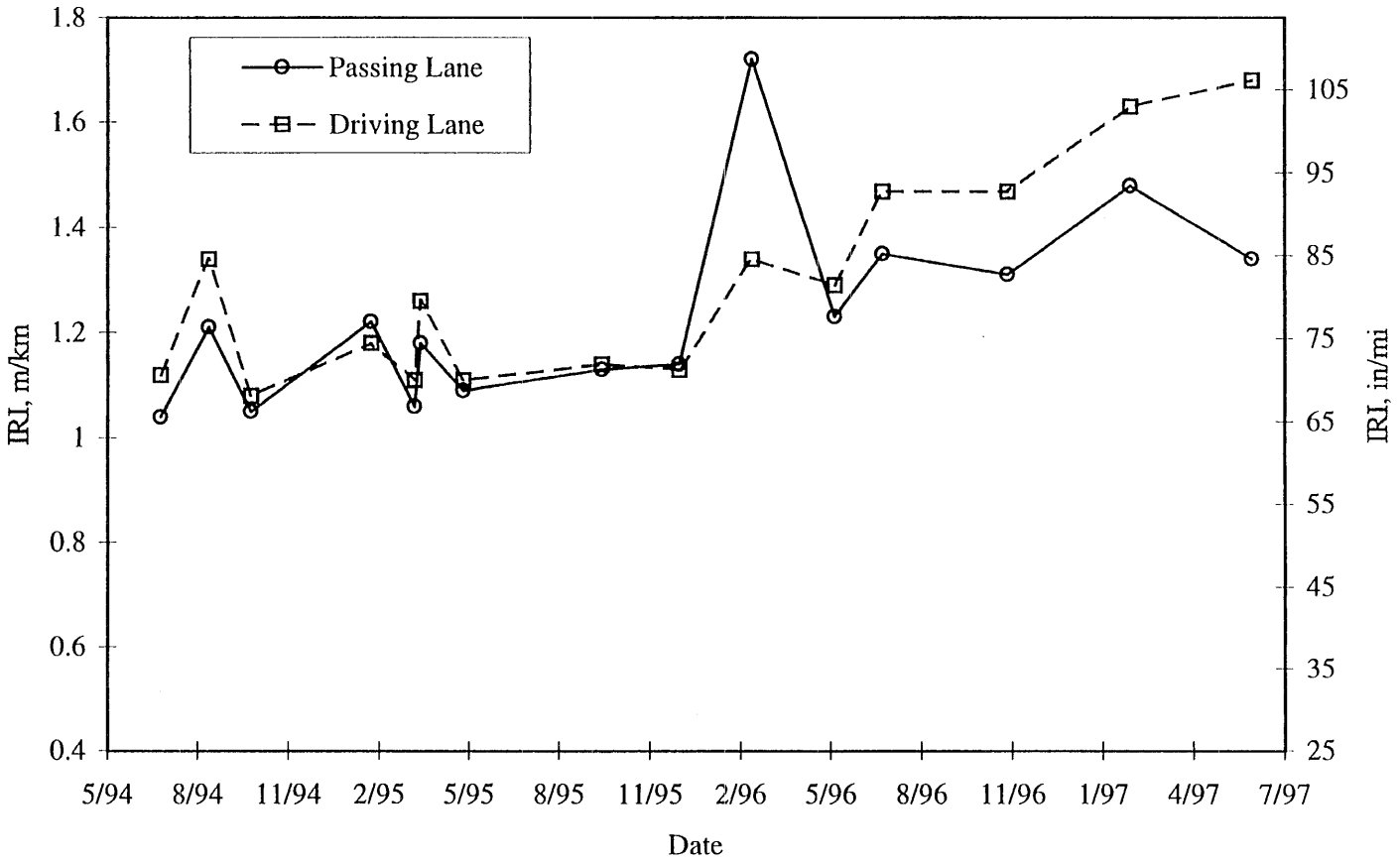

Figure 4.11. IRI Measurements for Cell 3.

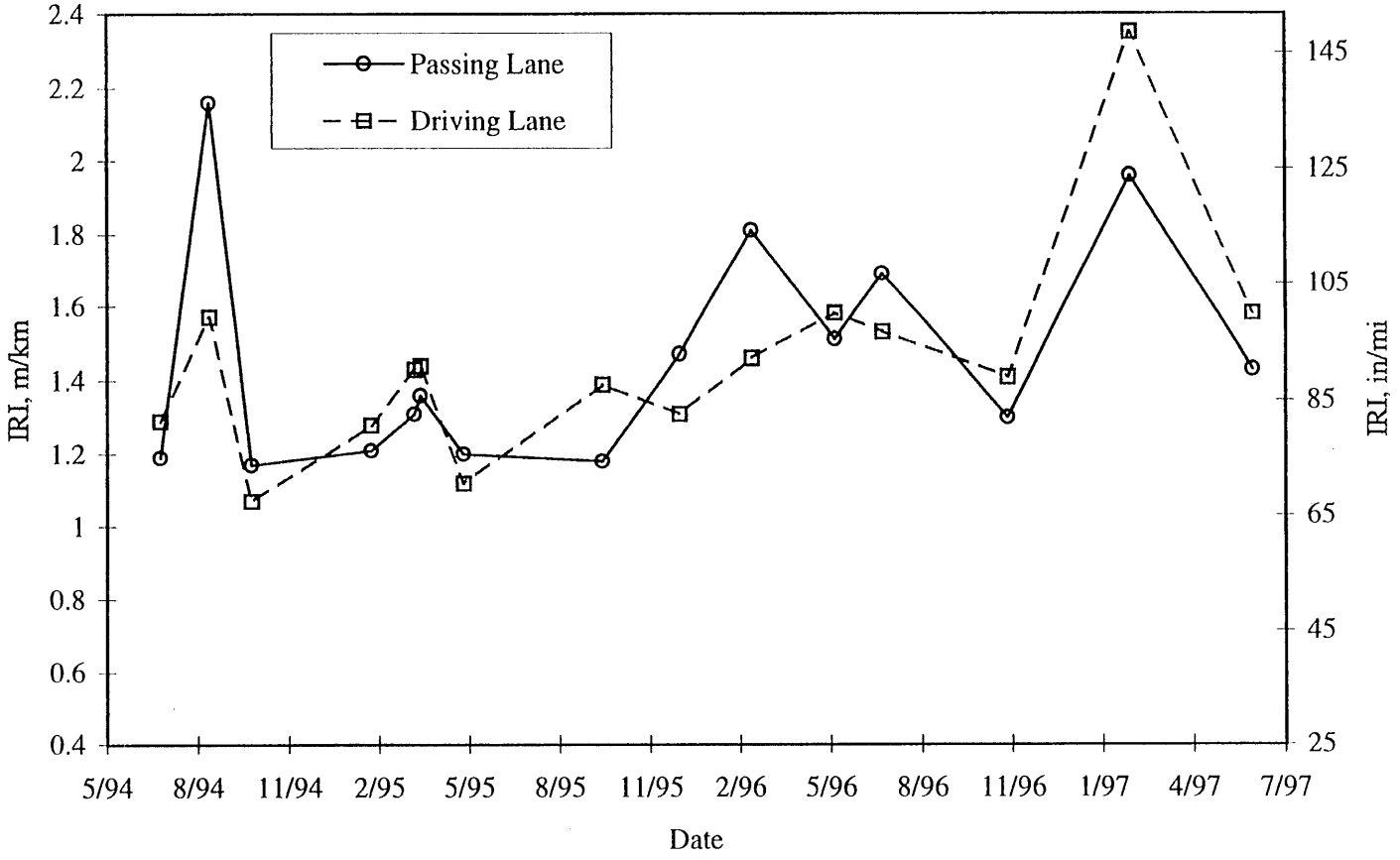

Figure 4.12. IRI Measurements for Cell 4.

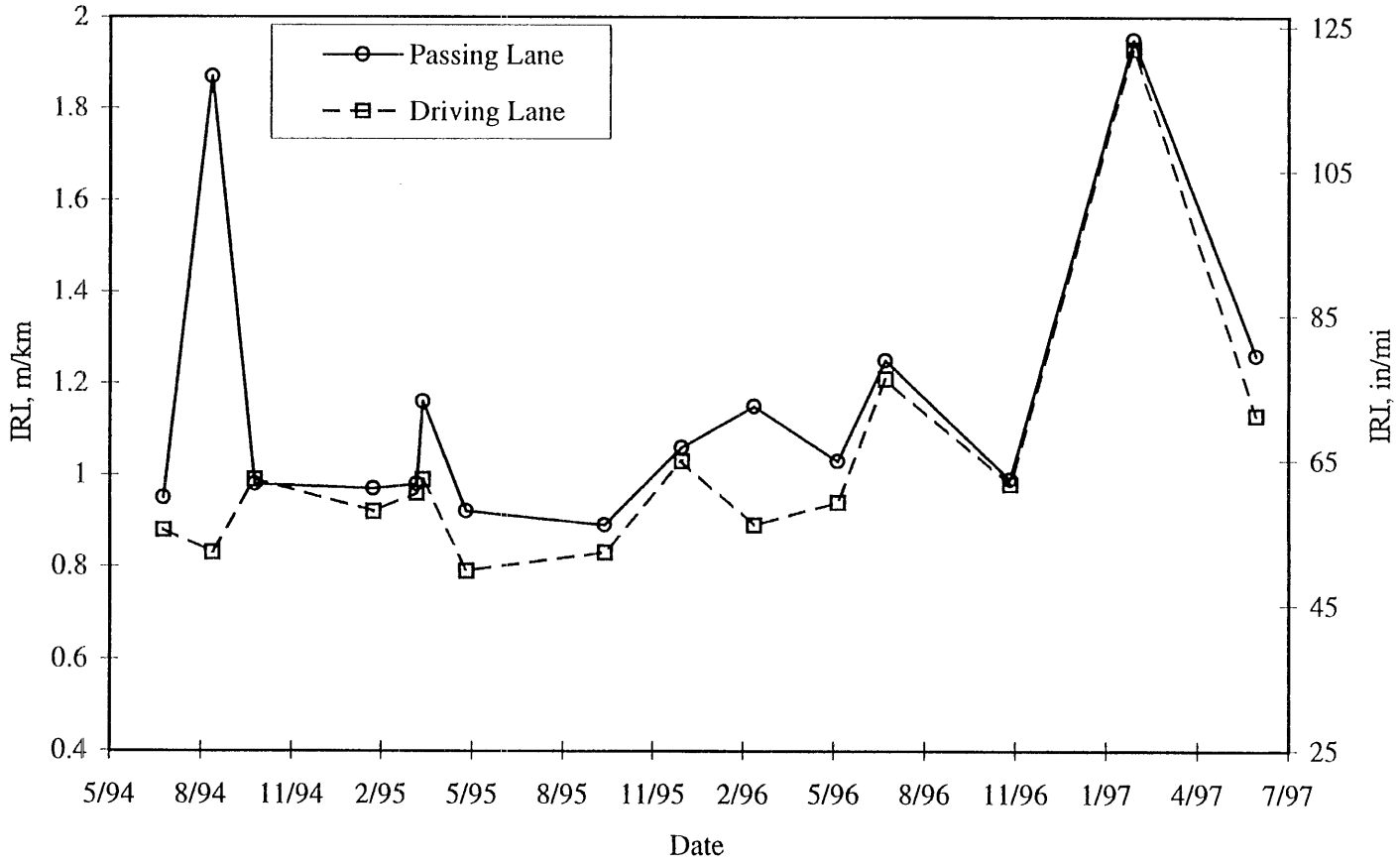

Figure 4.13. IRI Measurements for Cell 14.

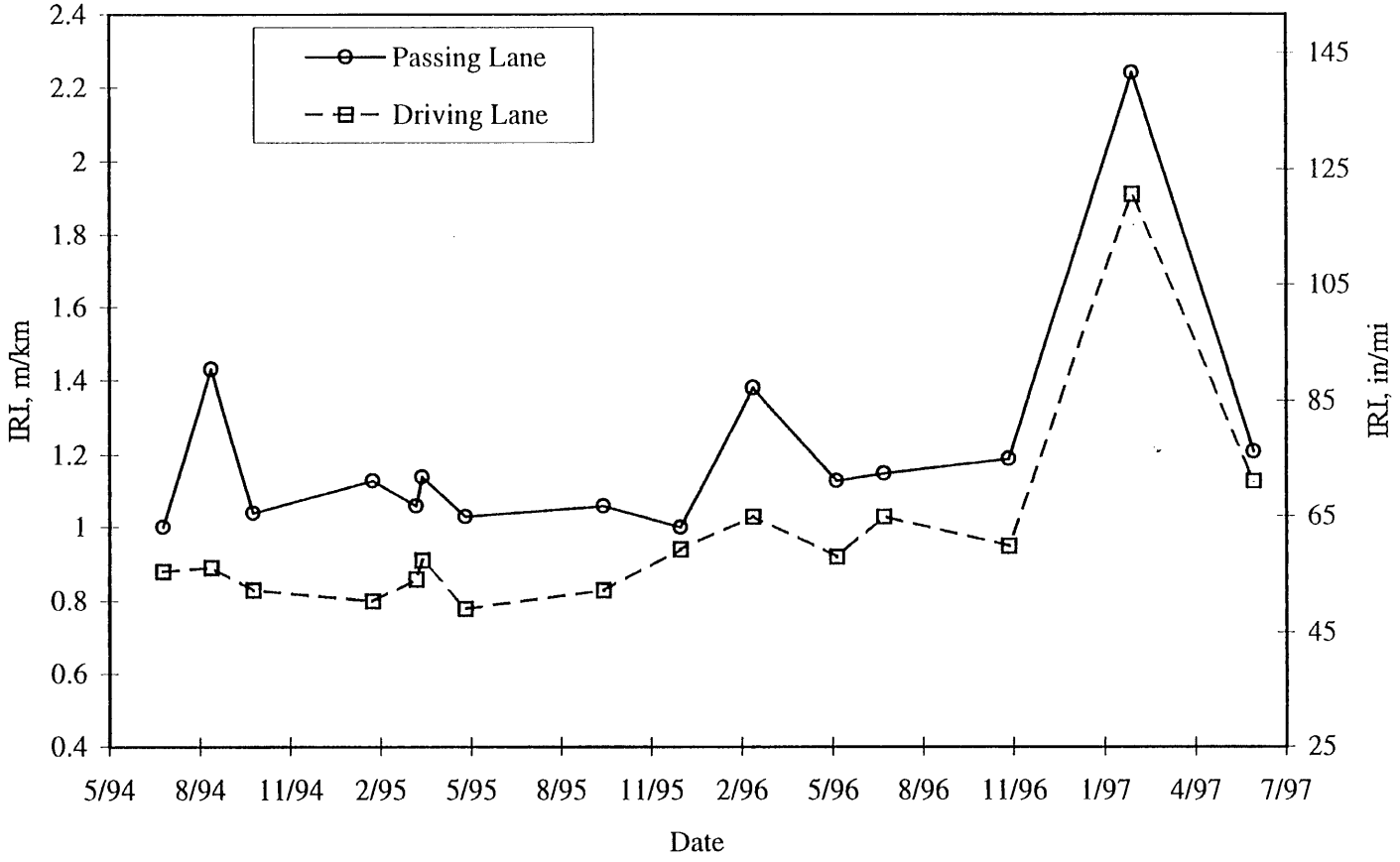

Figure 4.14. IRI Measurements for Cell 15.

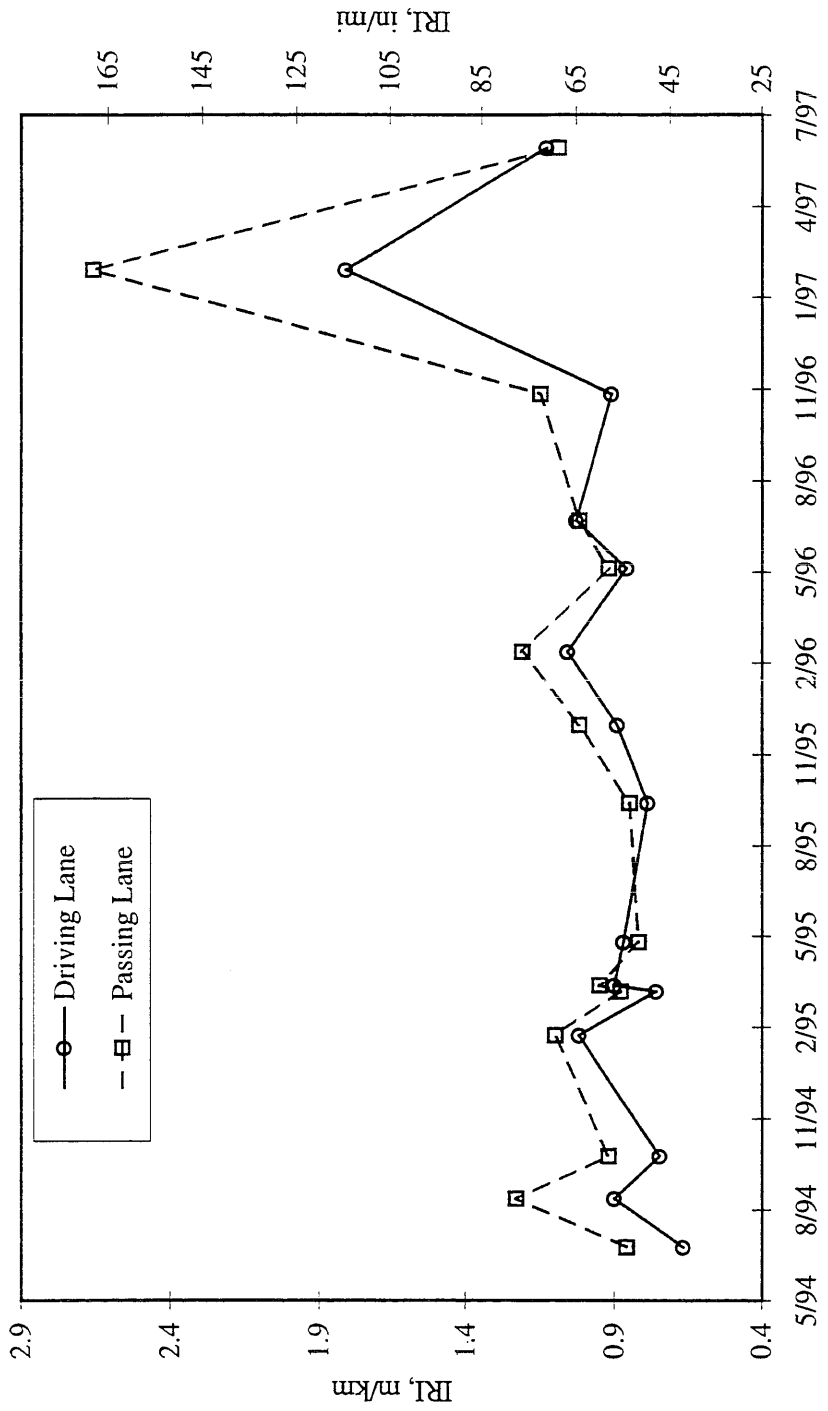

Figure 4.15. IRI Measurements for Cell 16.

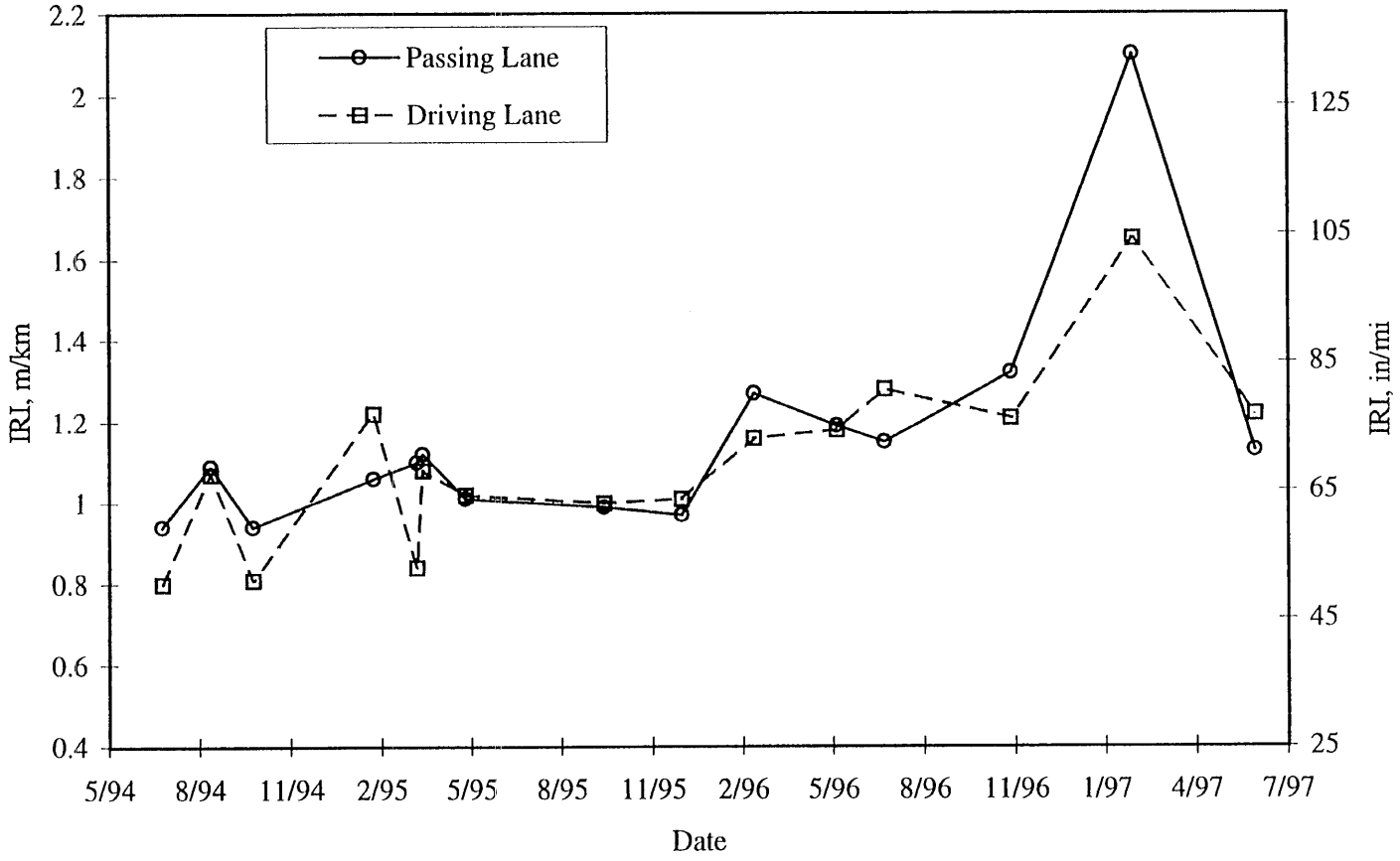

Figure 4.16. IRI Measurements for Cell 17.

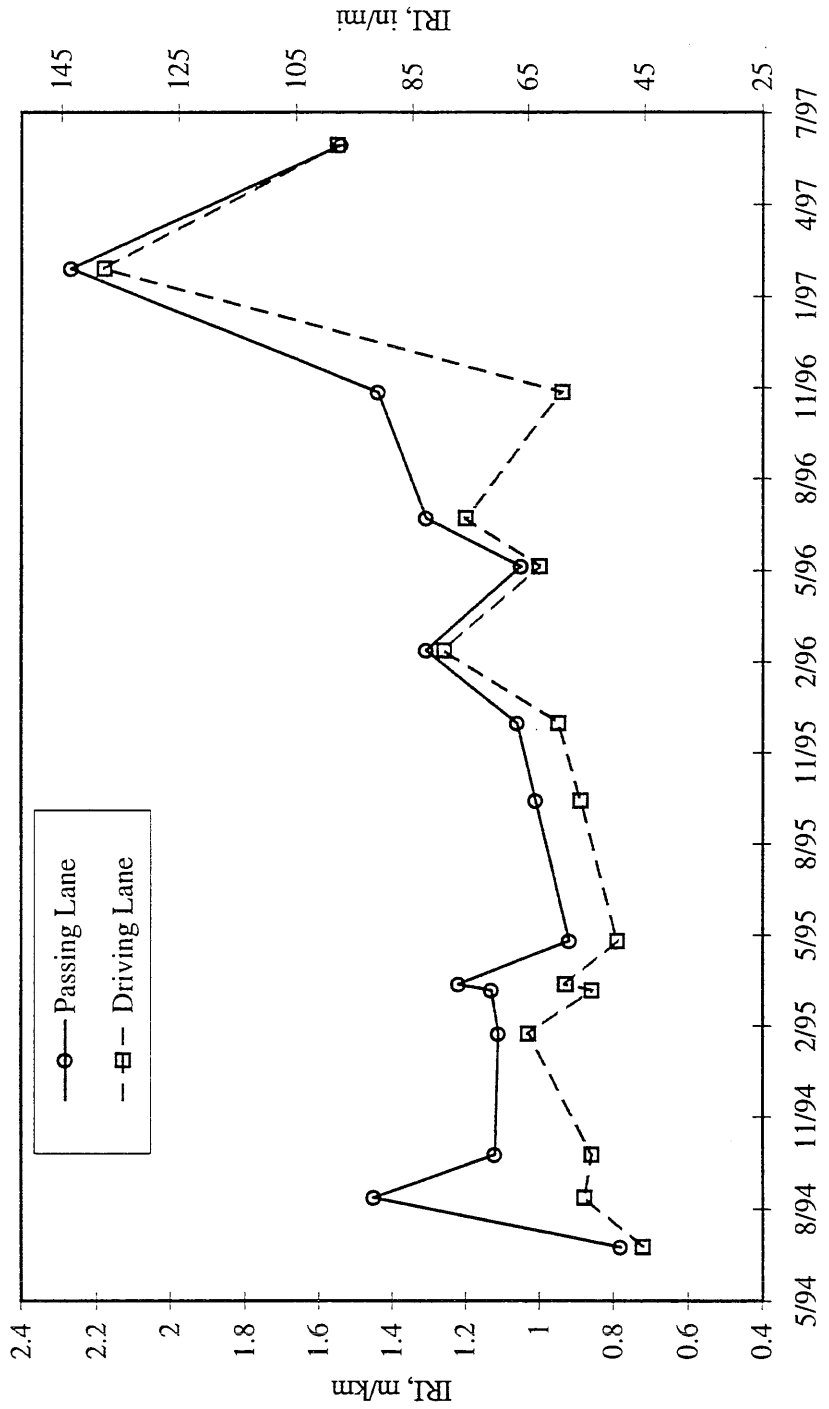

Figure 4.17. IRI Measurements for Cell 18.

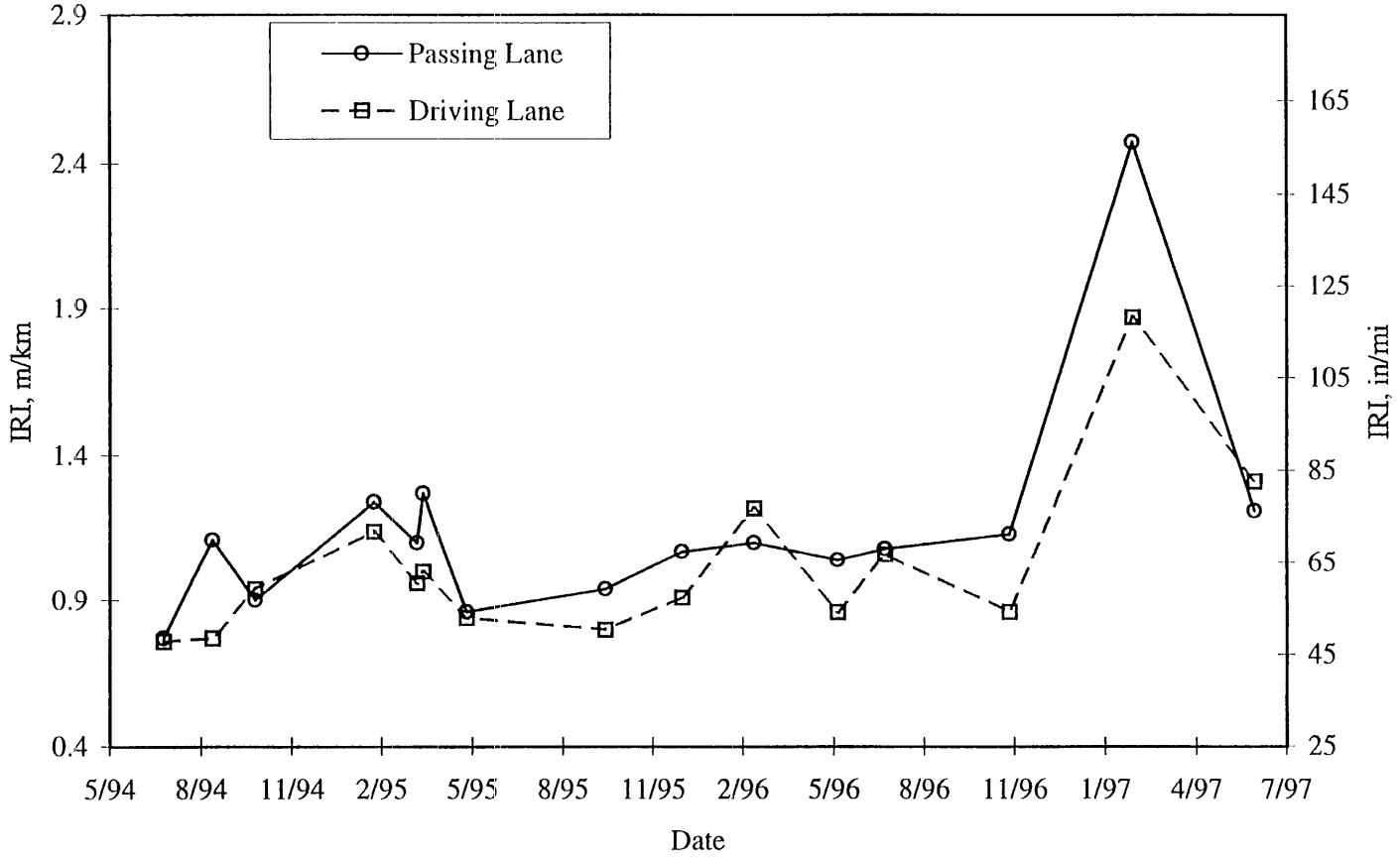

Figure 4.18. IRI Measurements for Cell 19.

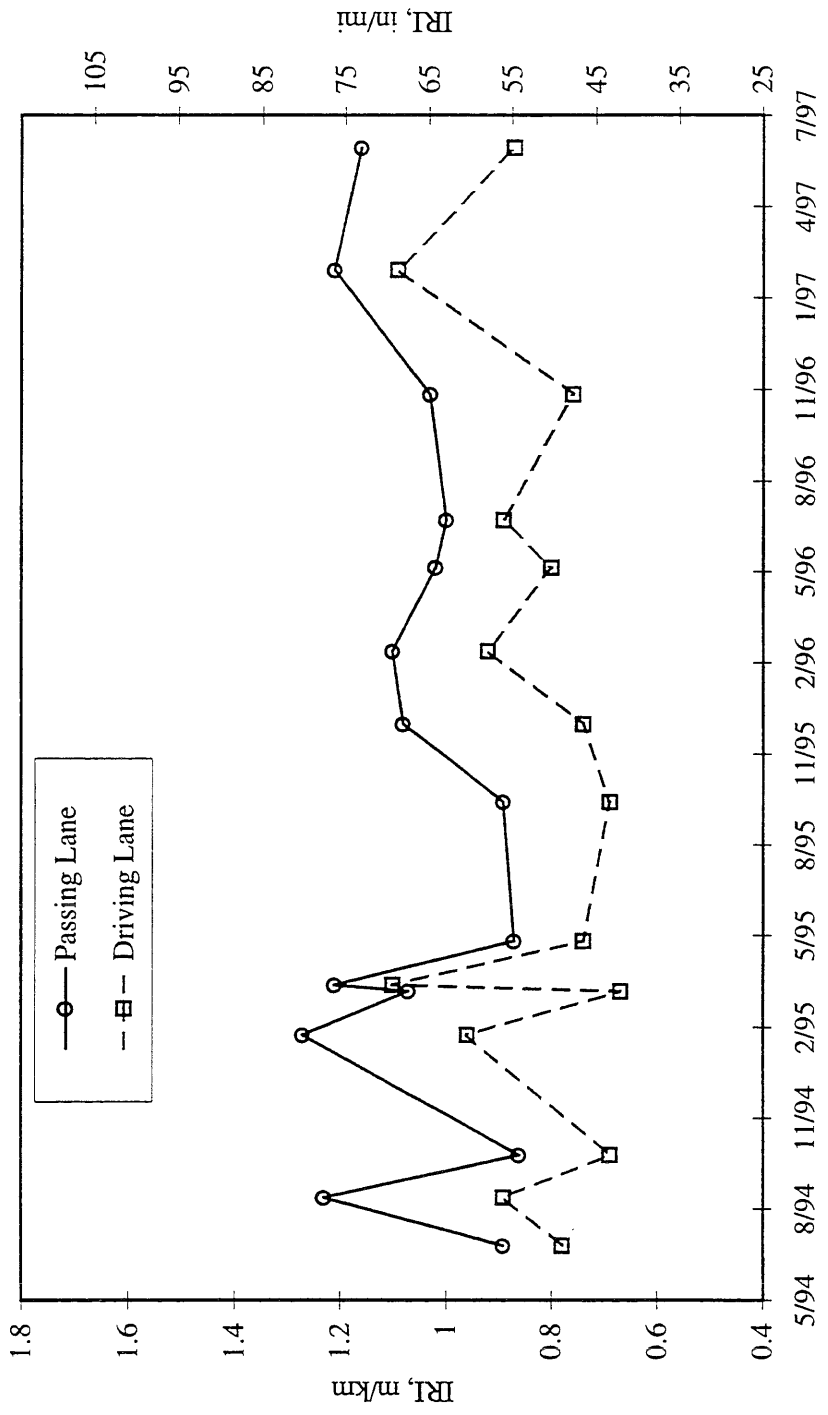

Figure 4.19. IRI Measurements for Cell 20.

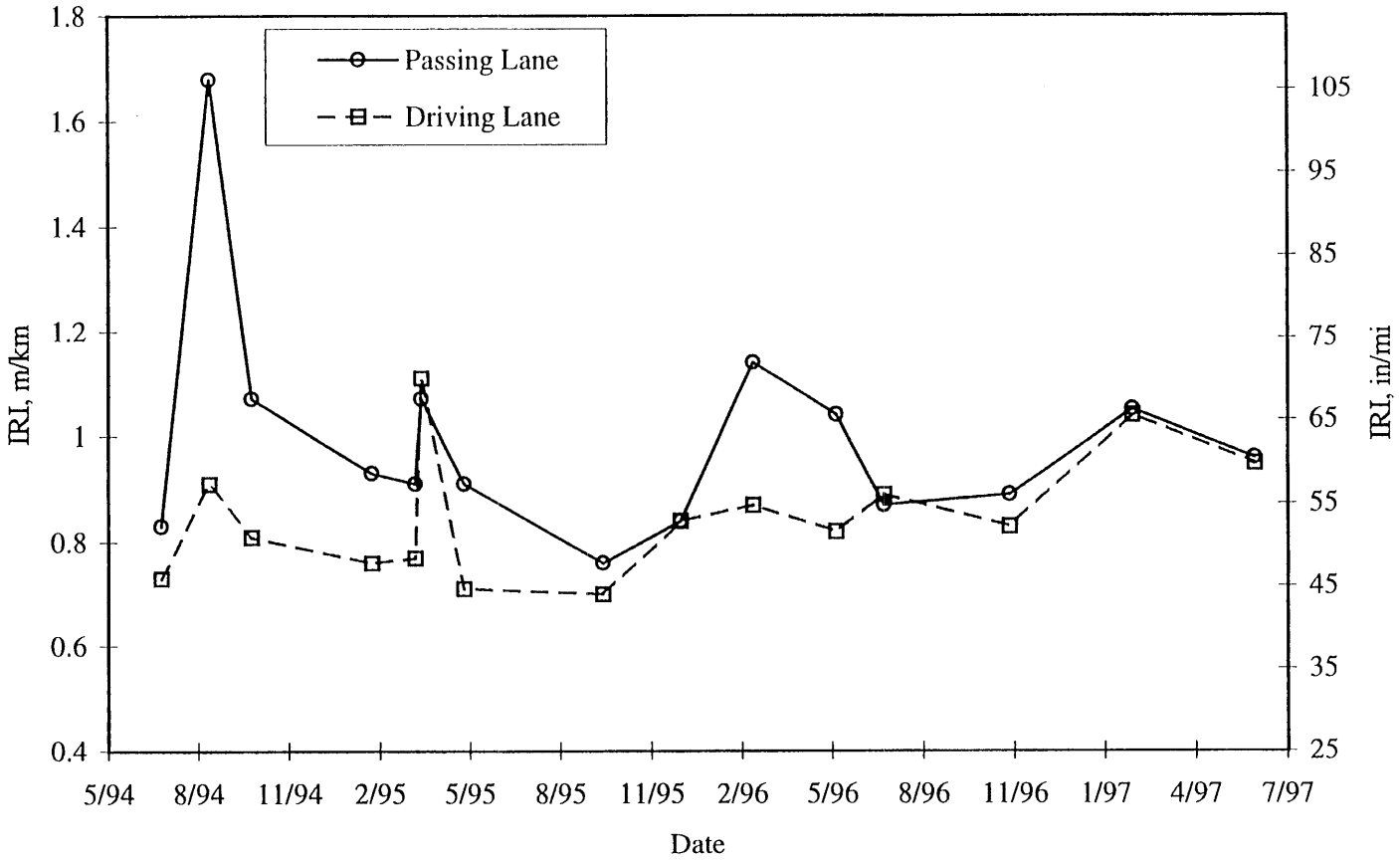

Figure 4.20. IRI Measurements for Cell 21.

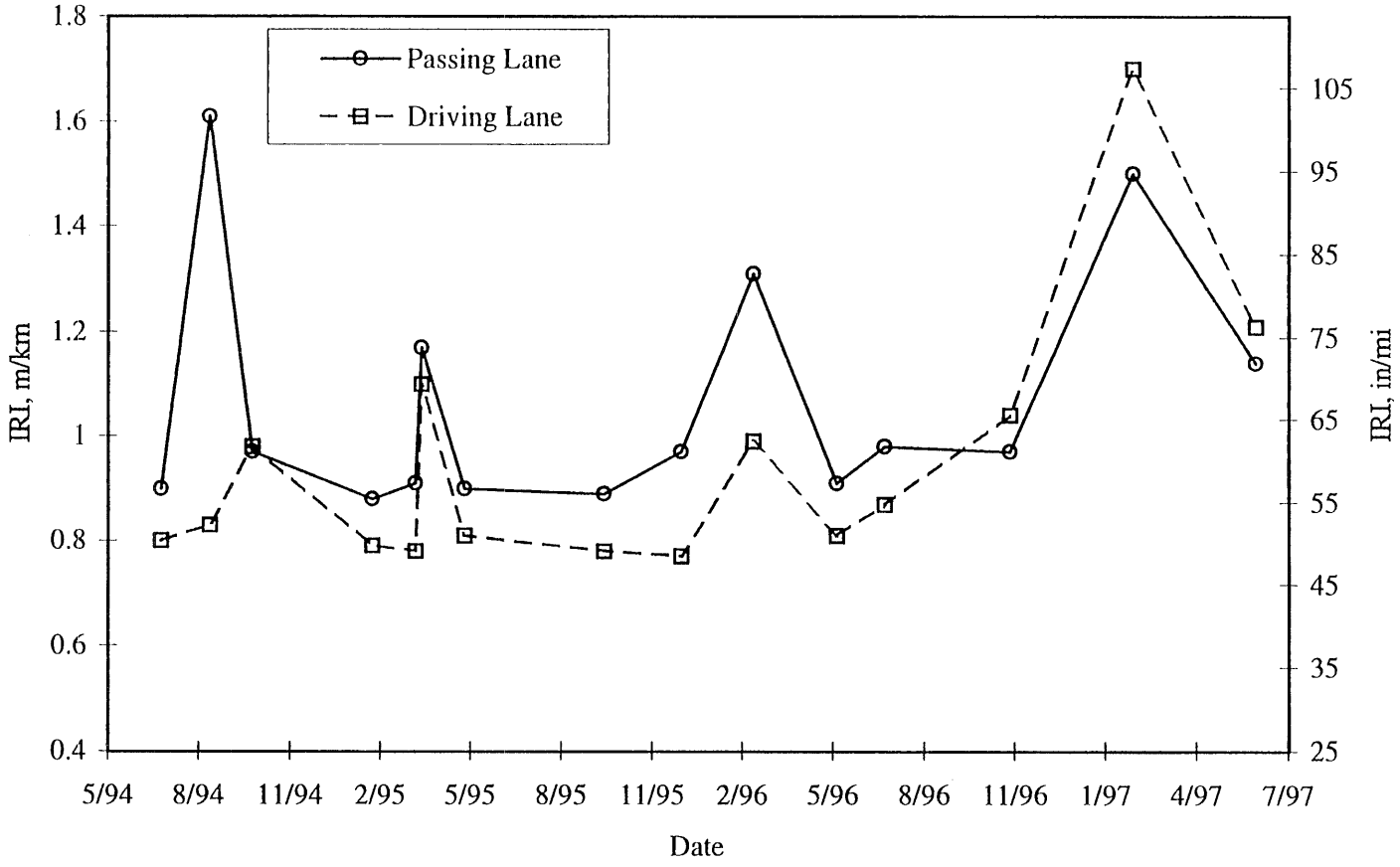

Figure 4.21. IRI Measurements for Cell 22.

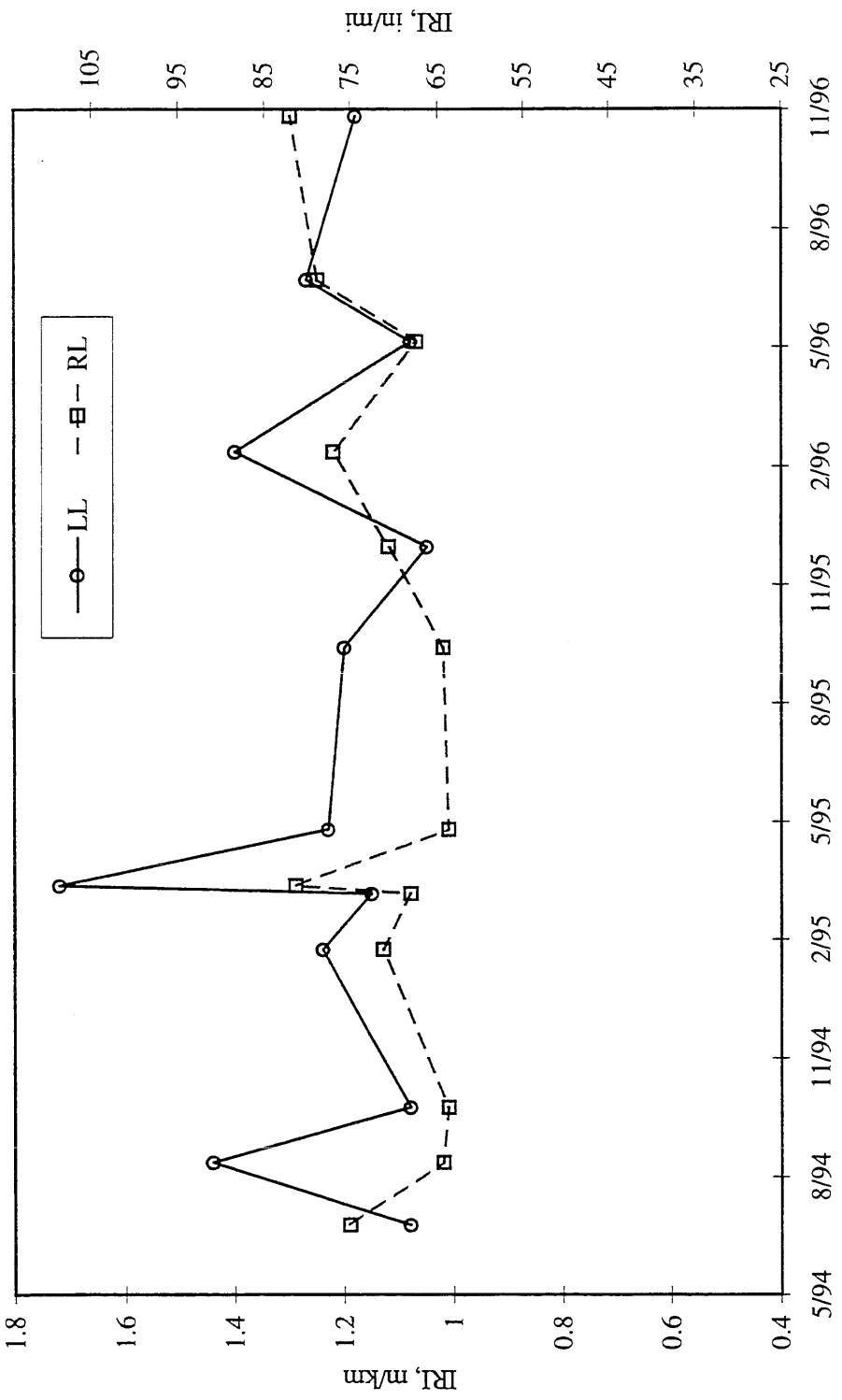

Figure 4.22. IRI Measurements for Cell 23.

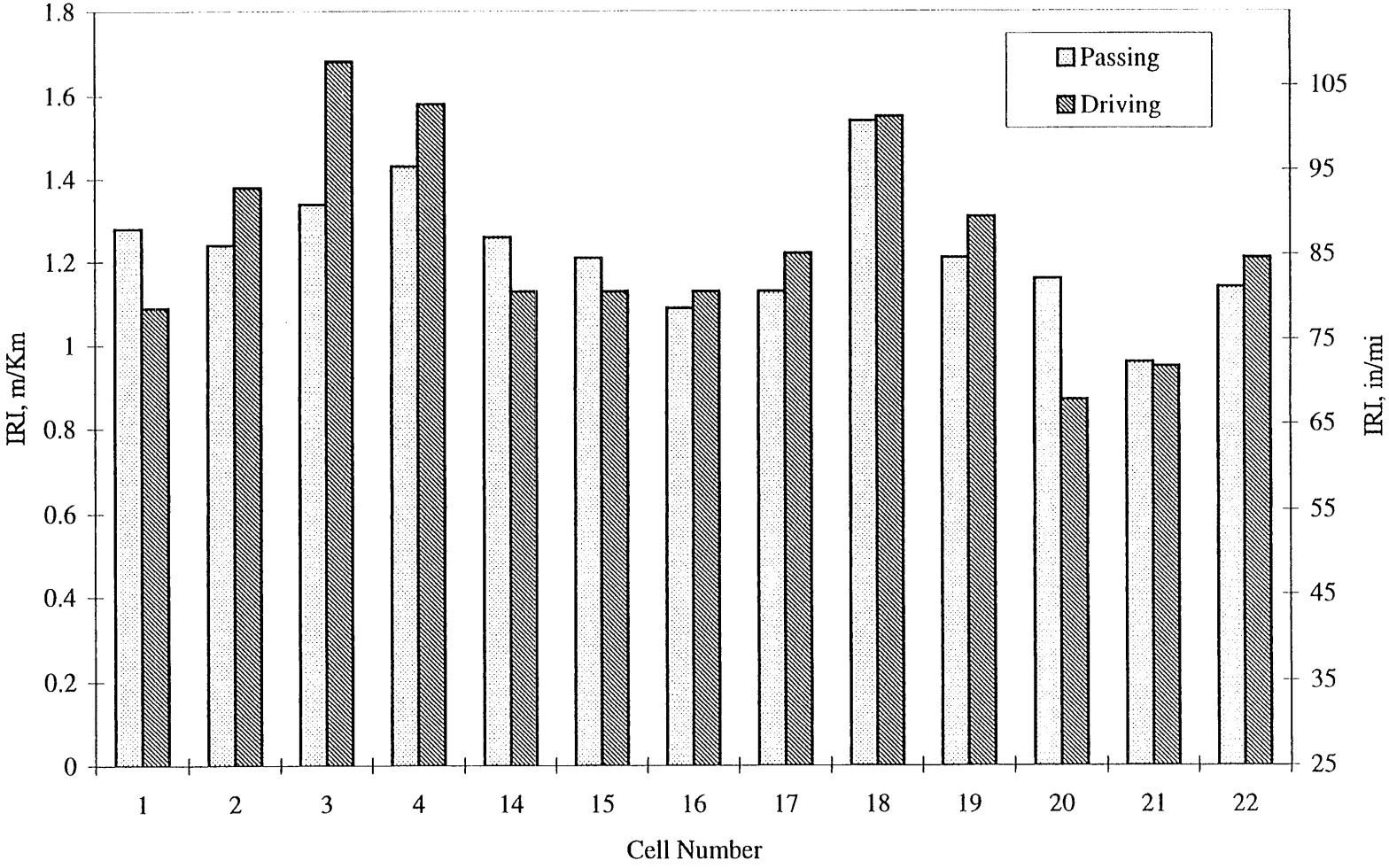

Figure 4.23. Mainline Cells IRI Values for June 27, 1997.

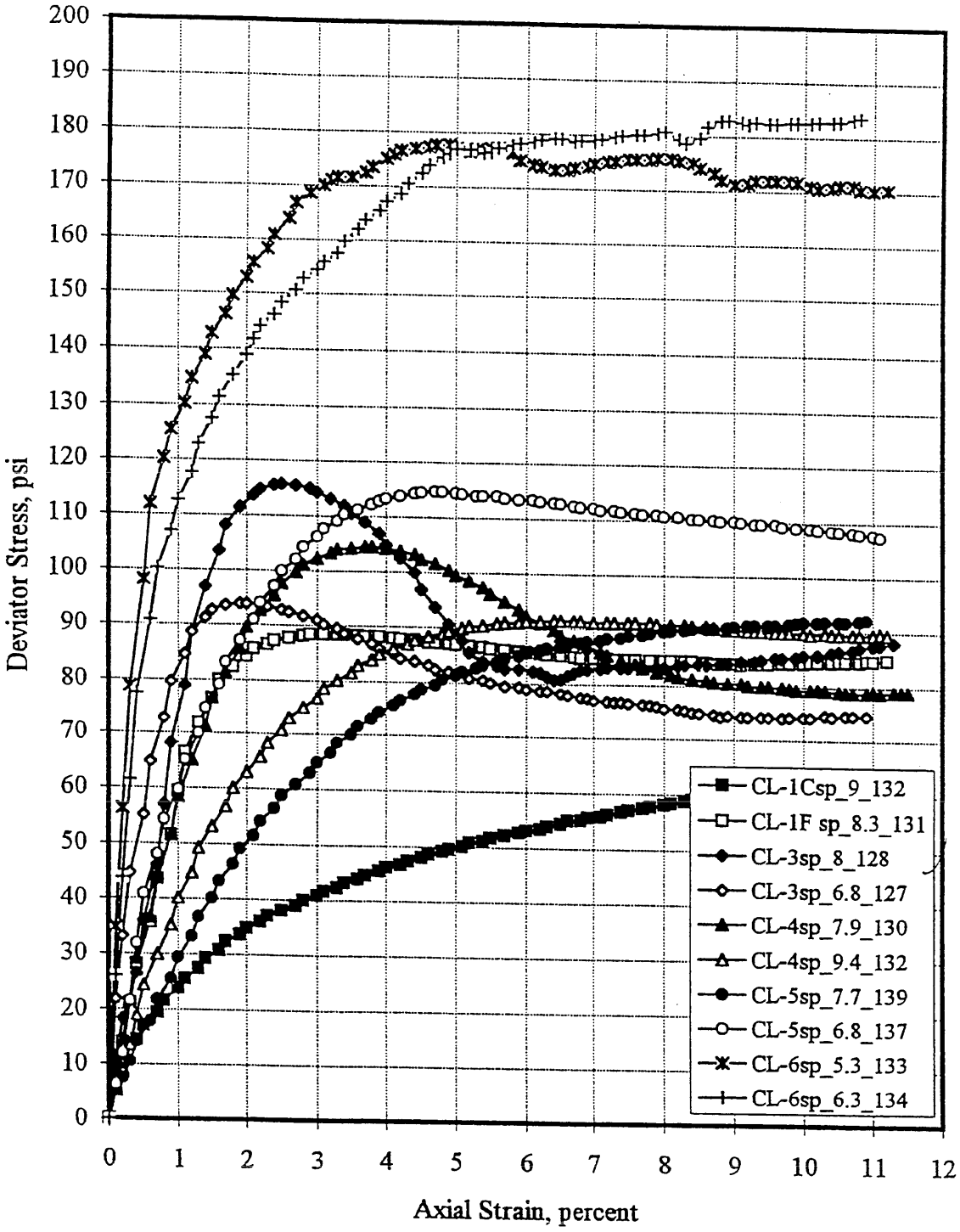

Figure 5.1. Rapid Shear Test Results for Confining pressure of 15 psi.

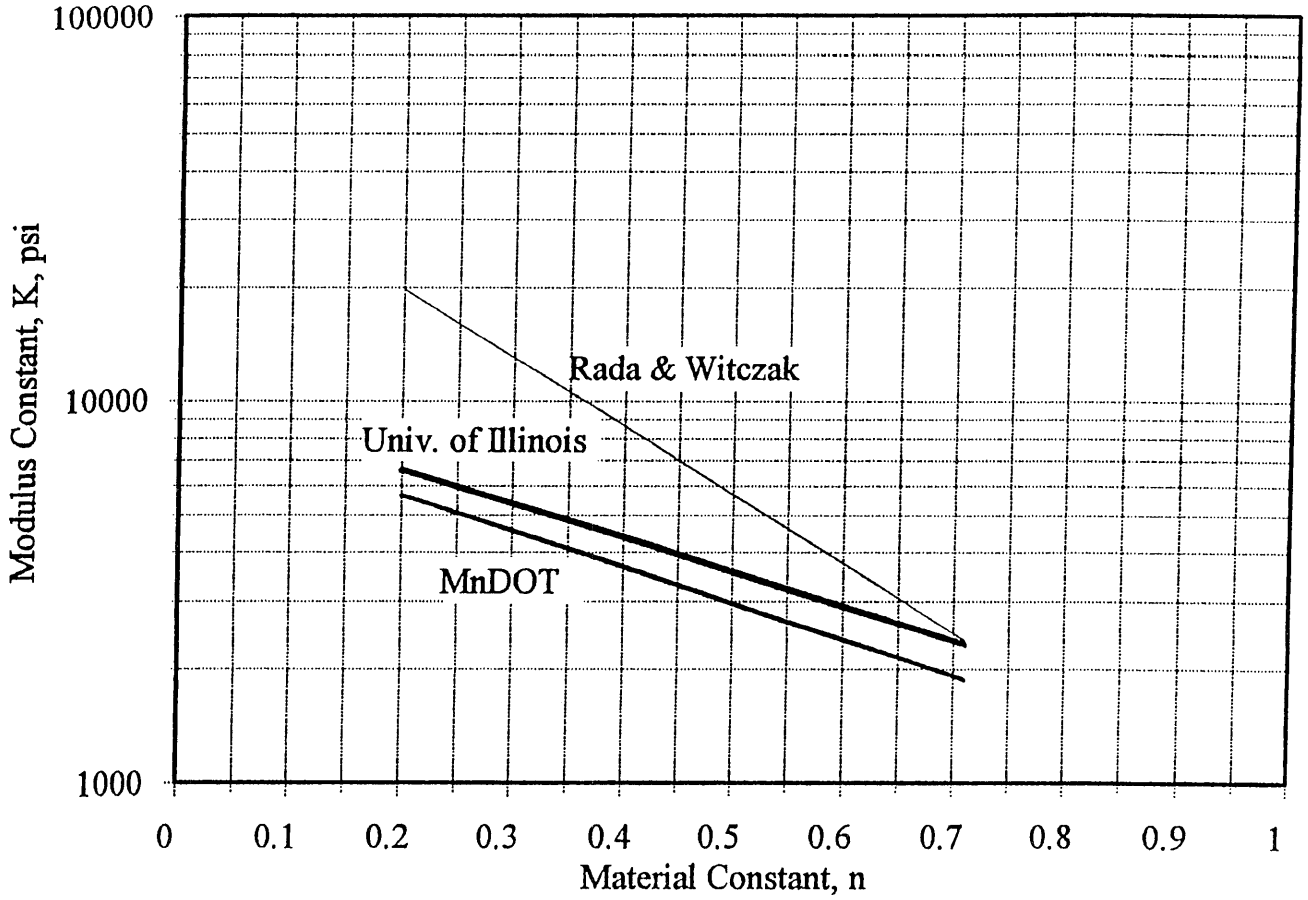

Figure 5.2. Relationship Between Resilient Modulus parameters K and n.

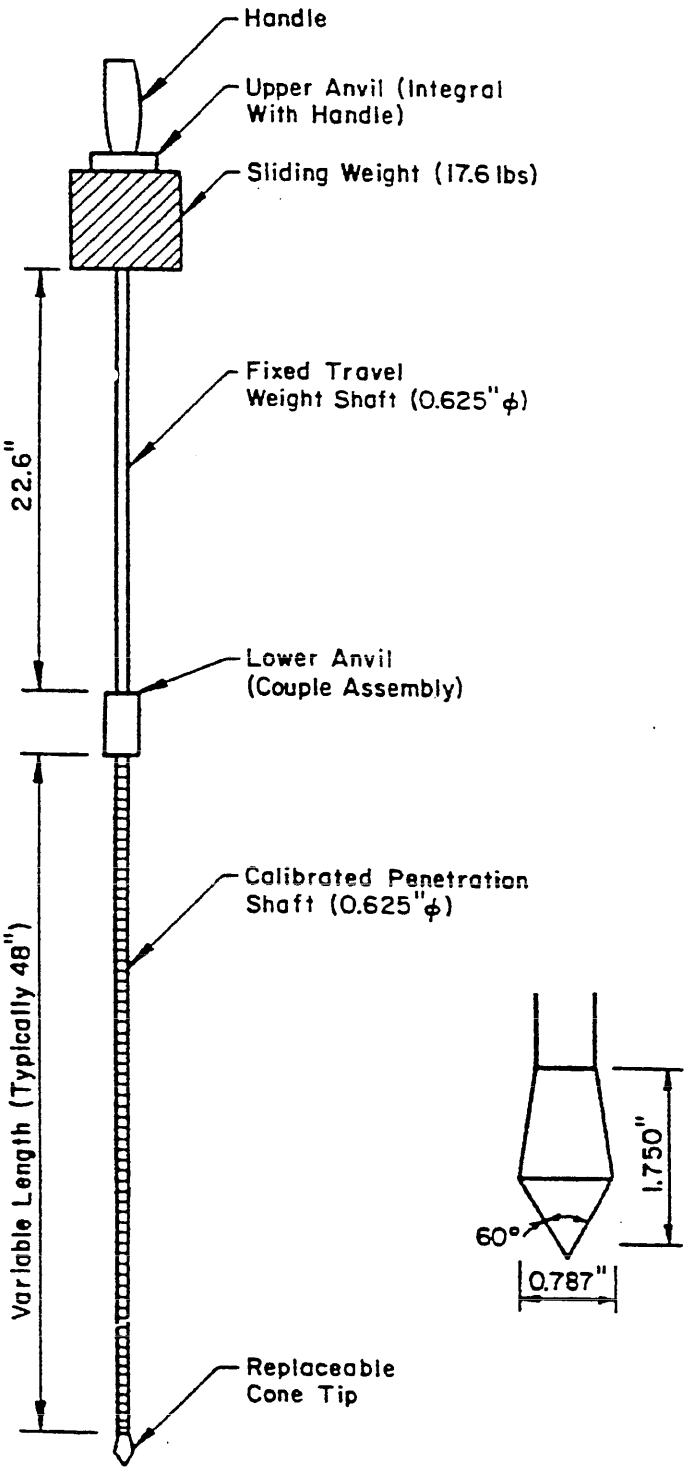

Figure 5.3. Dynamic Cone Penetrometer (DCP).

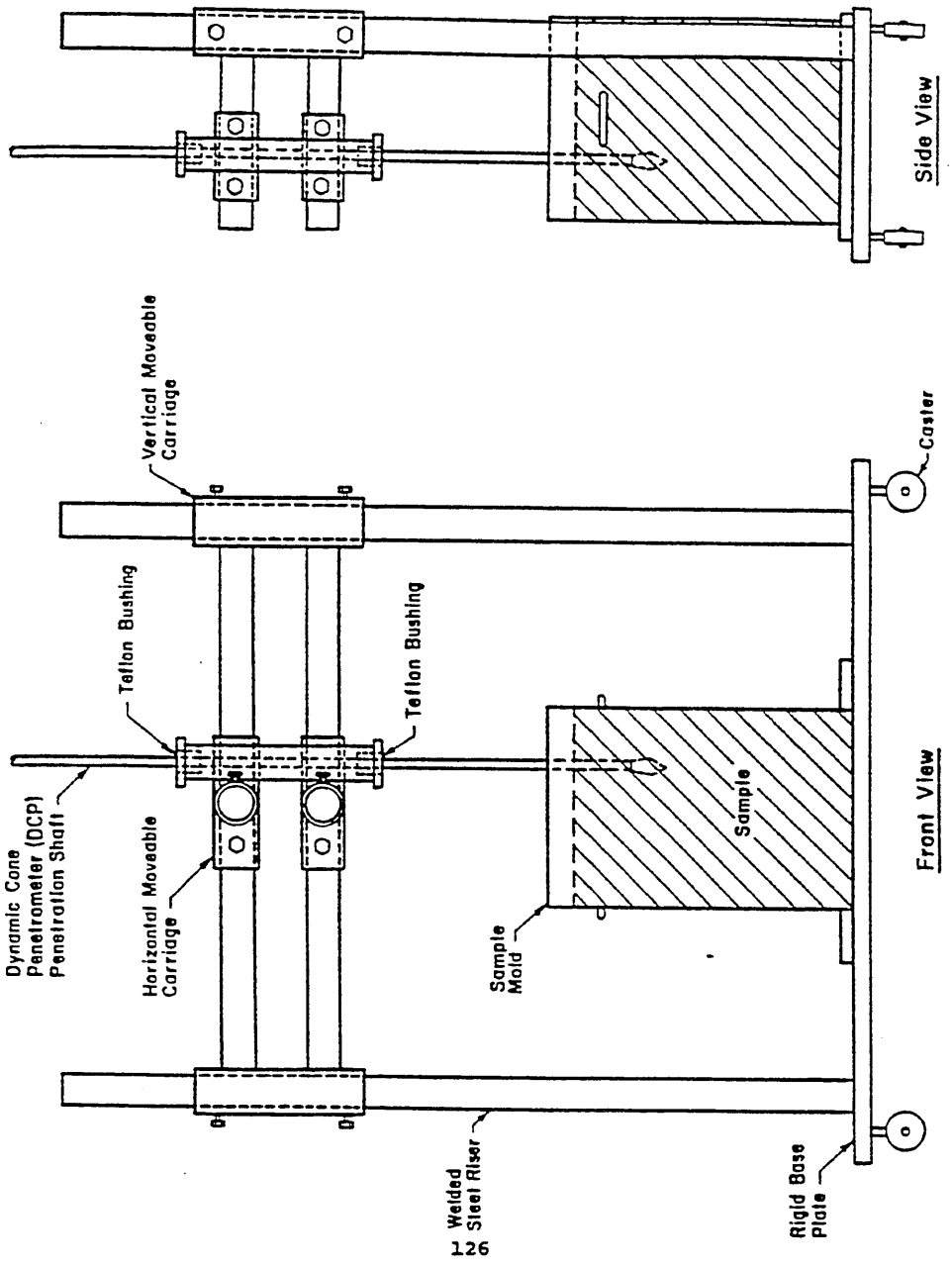

Figure 5.4. Dynamic Cone Penetrometer (DCP) Alignment Device.

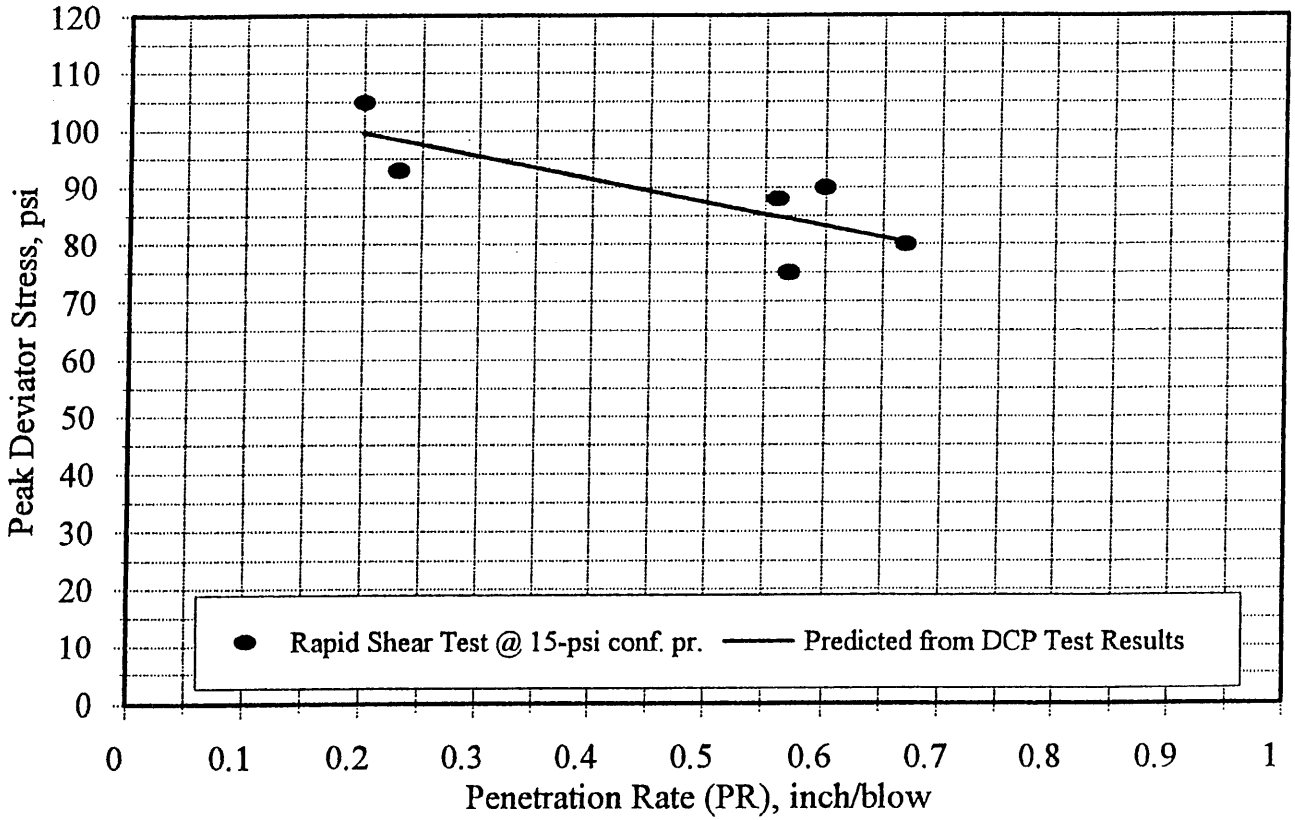

Figure 5.5. Peak Deviator Stress/ Penetration Rate Relationship.

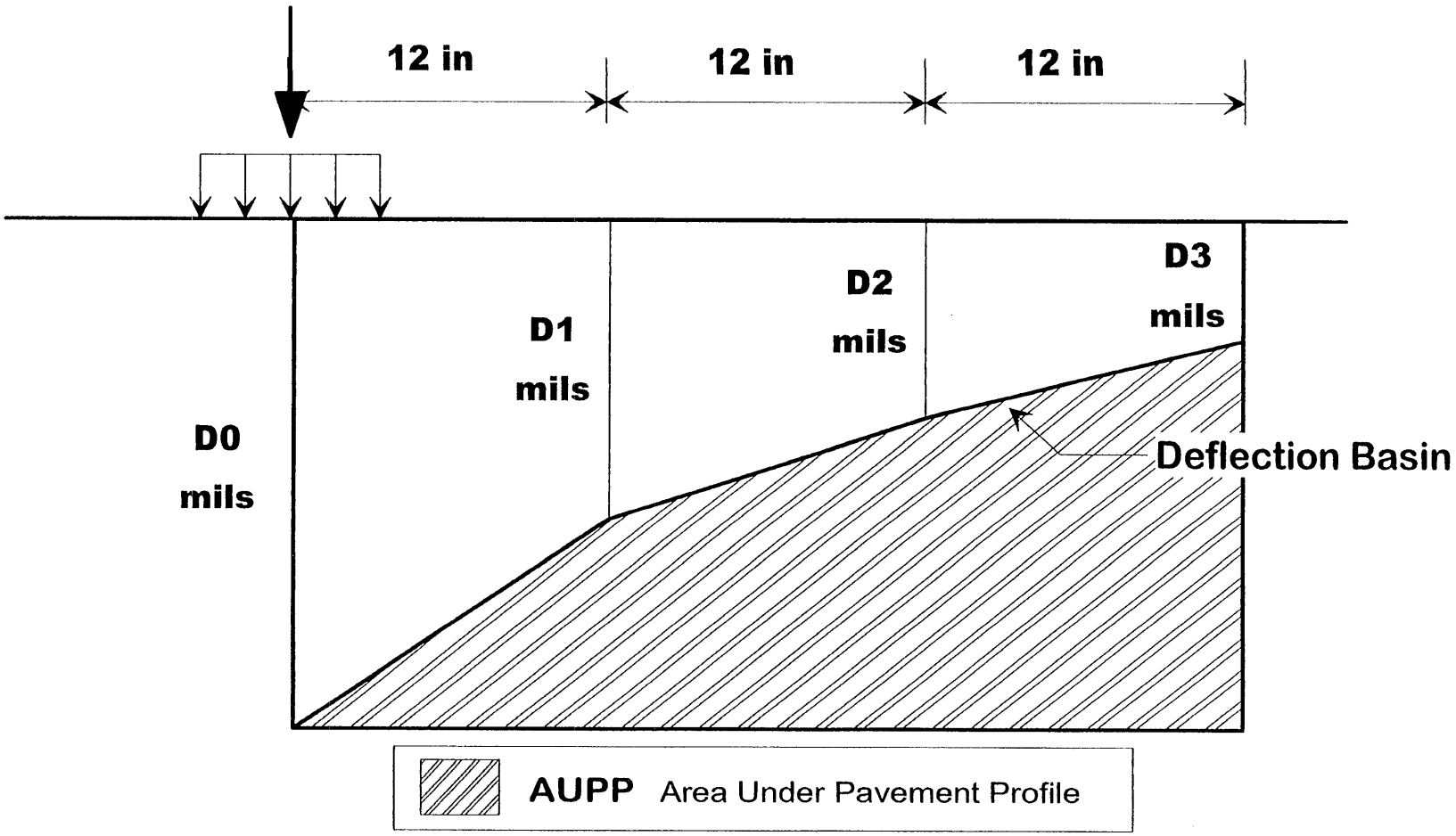

Figure 5.6. Deflection Basin and Area under Pavement Profile

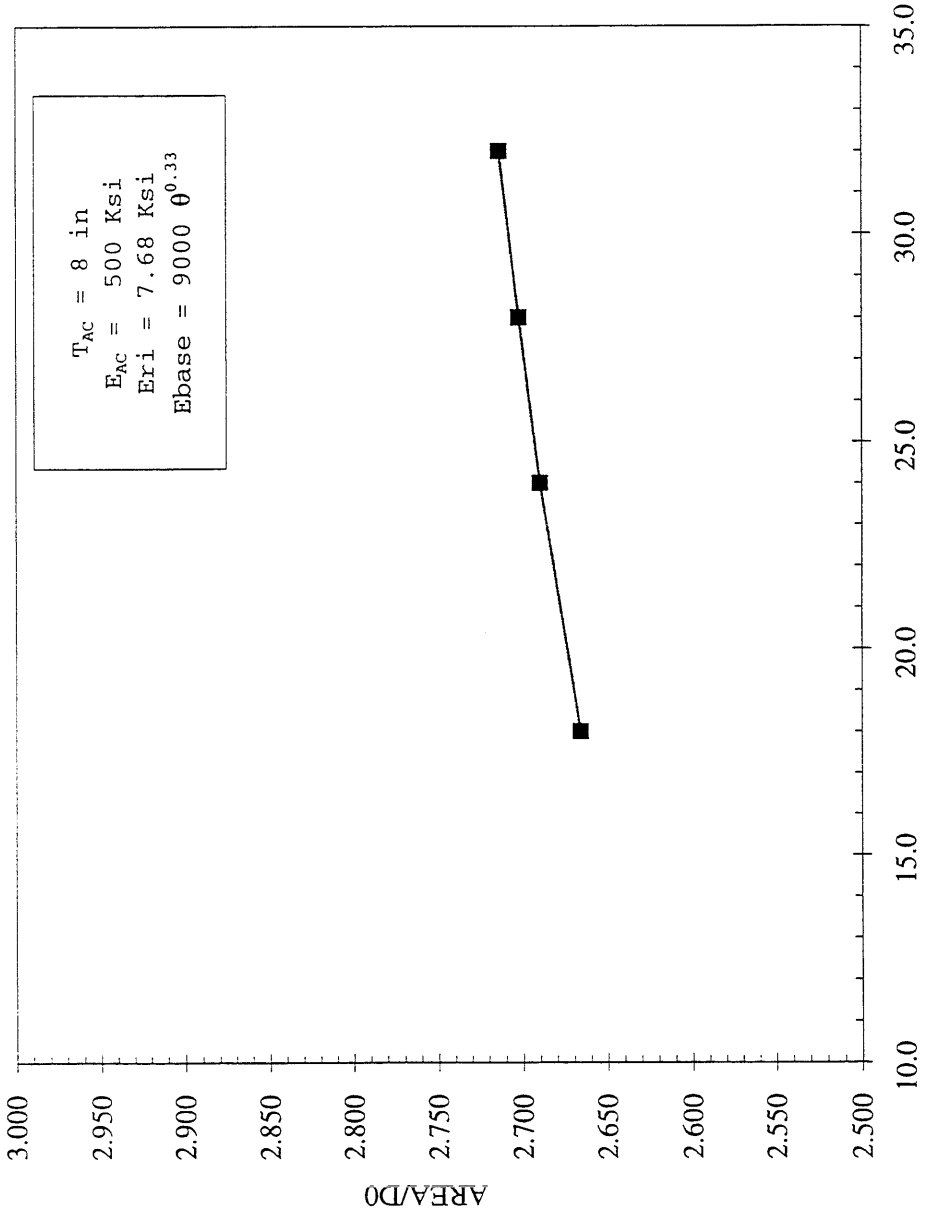

Figure 5.7. Variation of (AREA/D0) with Base Thickness.

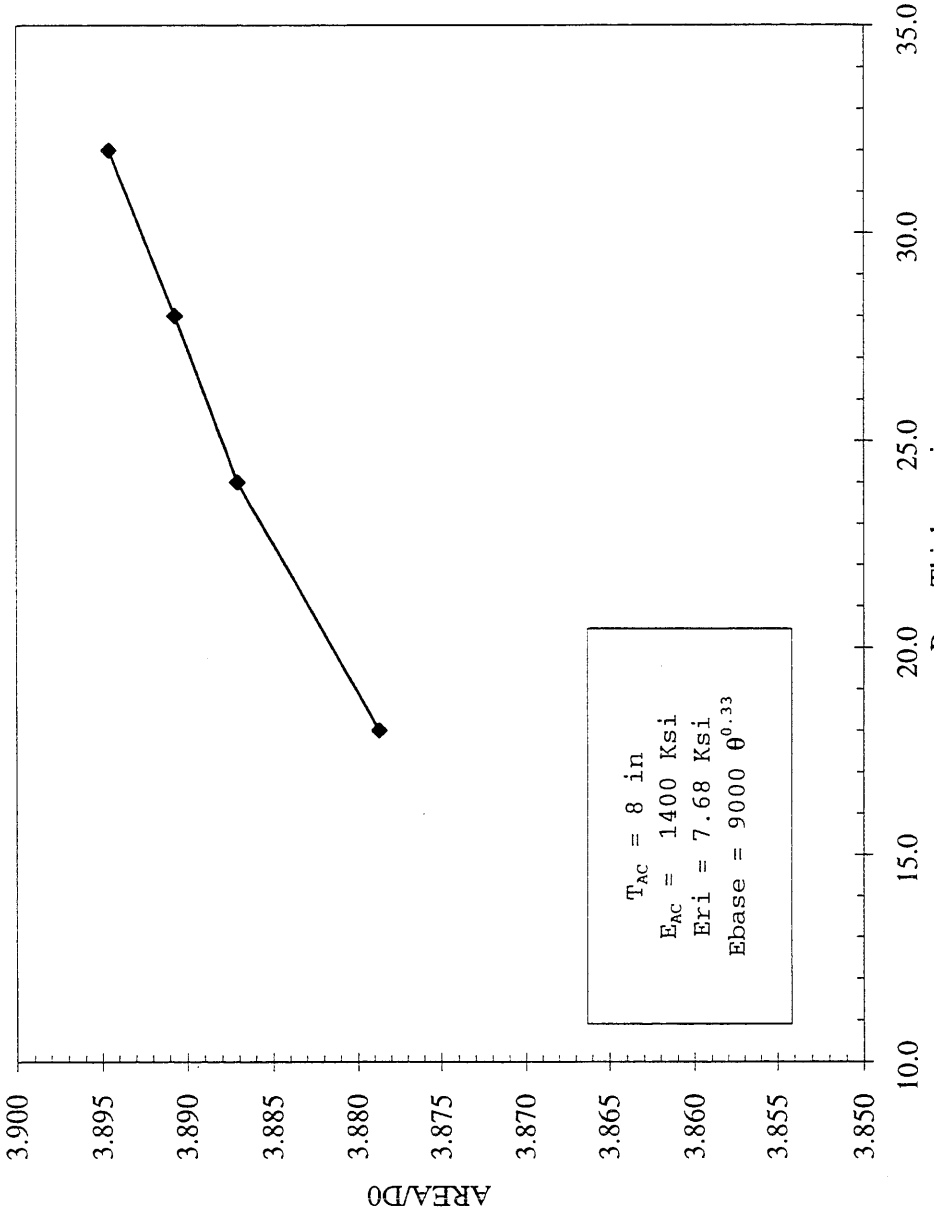

Figure 5.8. Variation of (AREA/D0) with Base Thickness.

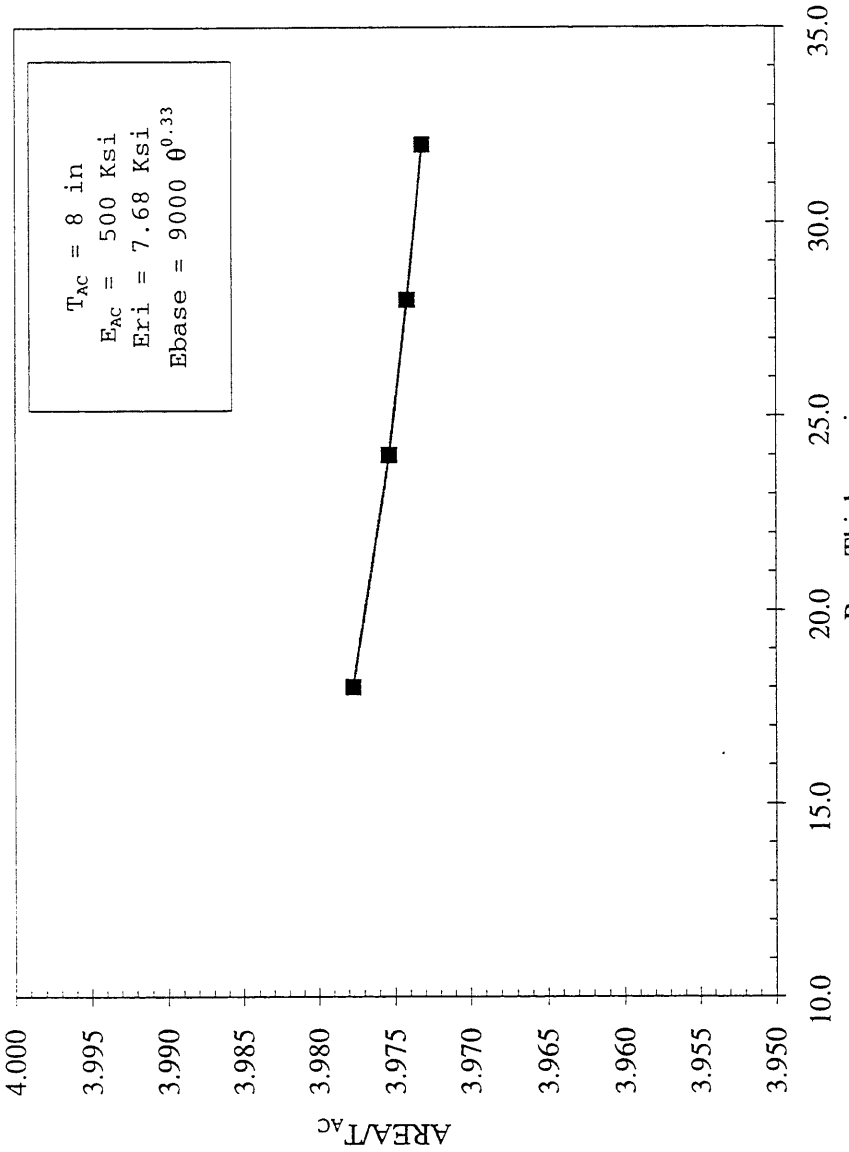

Figure 5.9. Variation of (AREA/TAC) with Base Thickness.

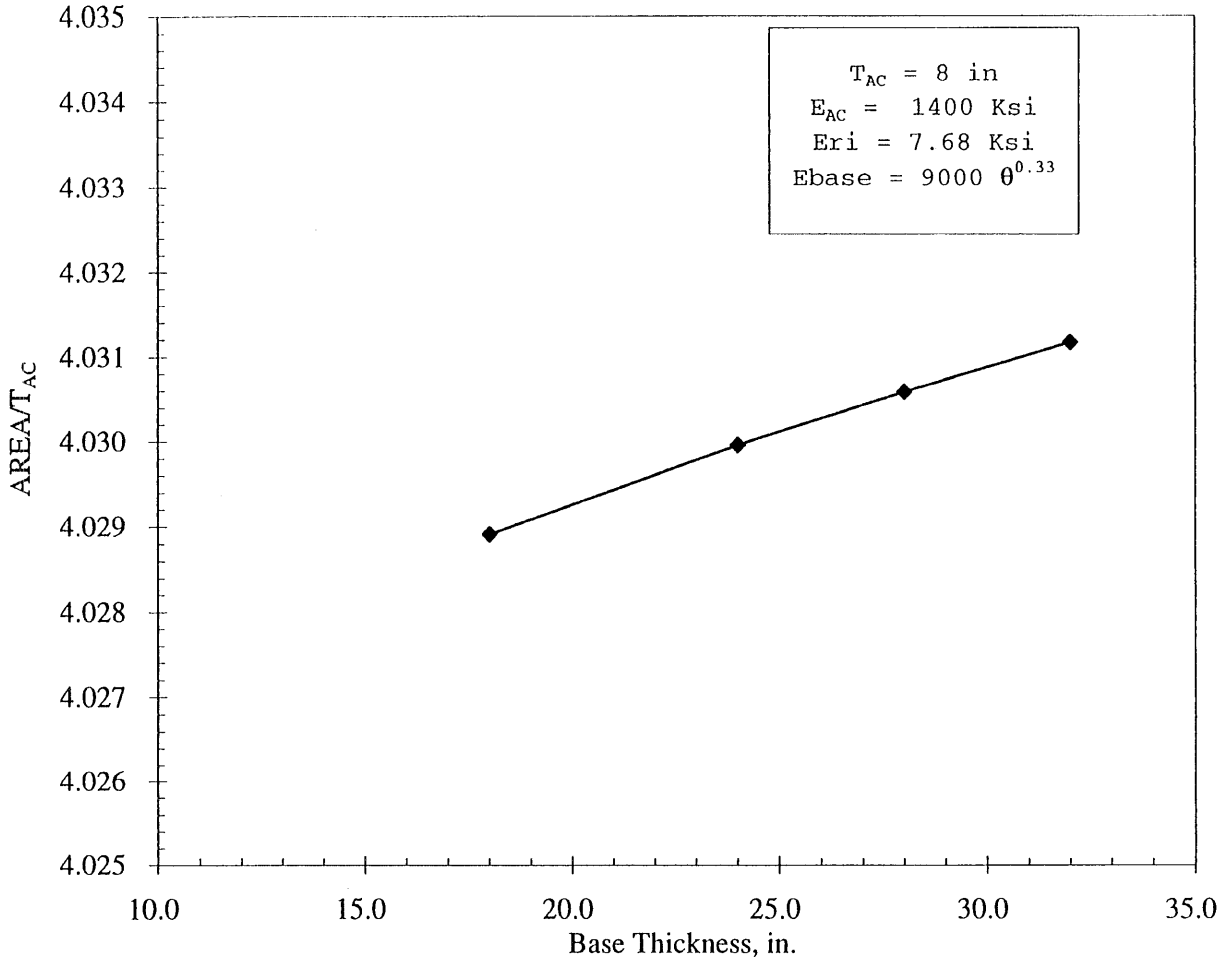

Figure 5.10. Variation of (AREA/TAC) with Base Thickness.

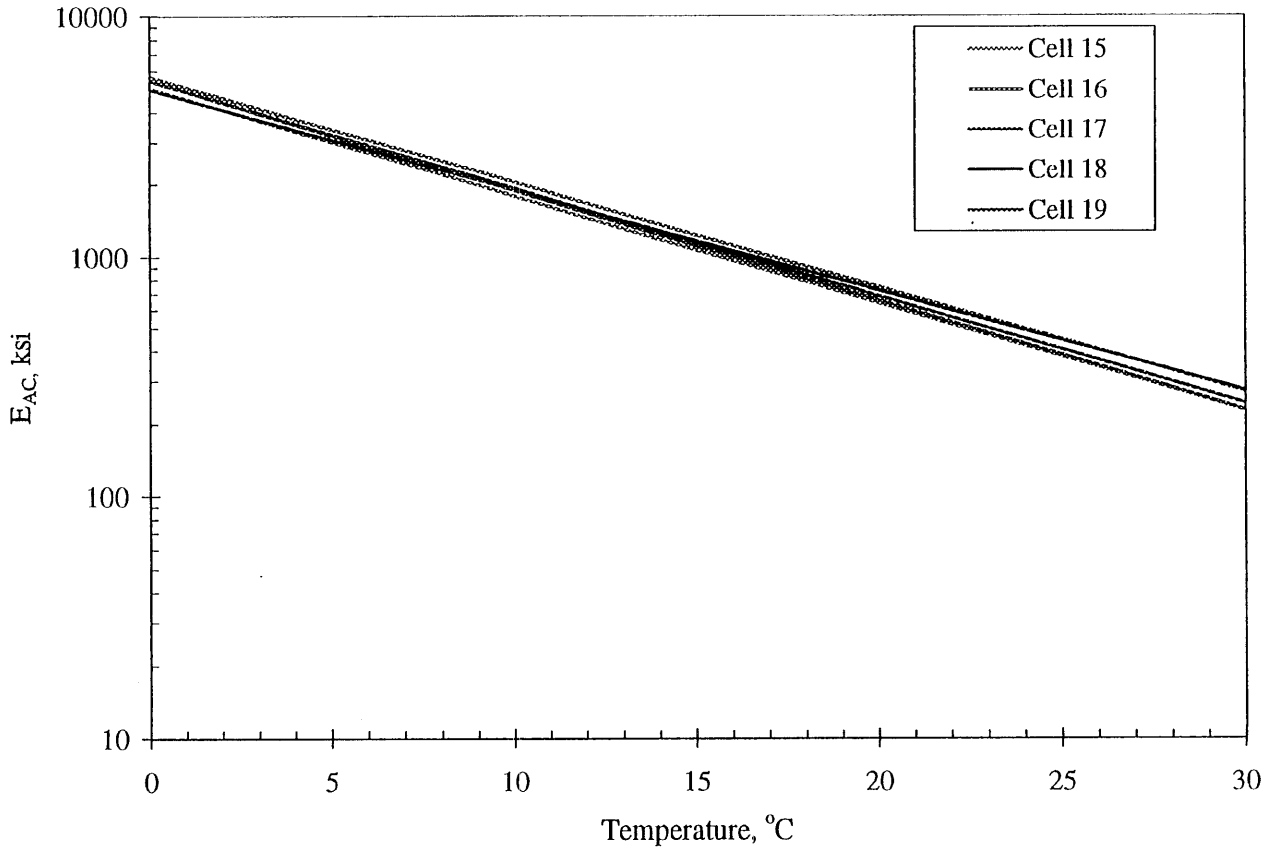

Figure 5.11 E_{AC} -Temperature Relations for AC 20 Sections

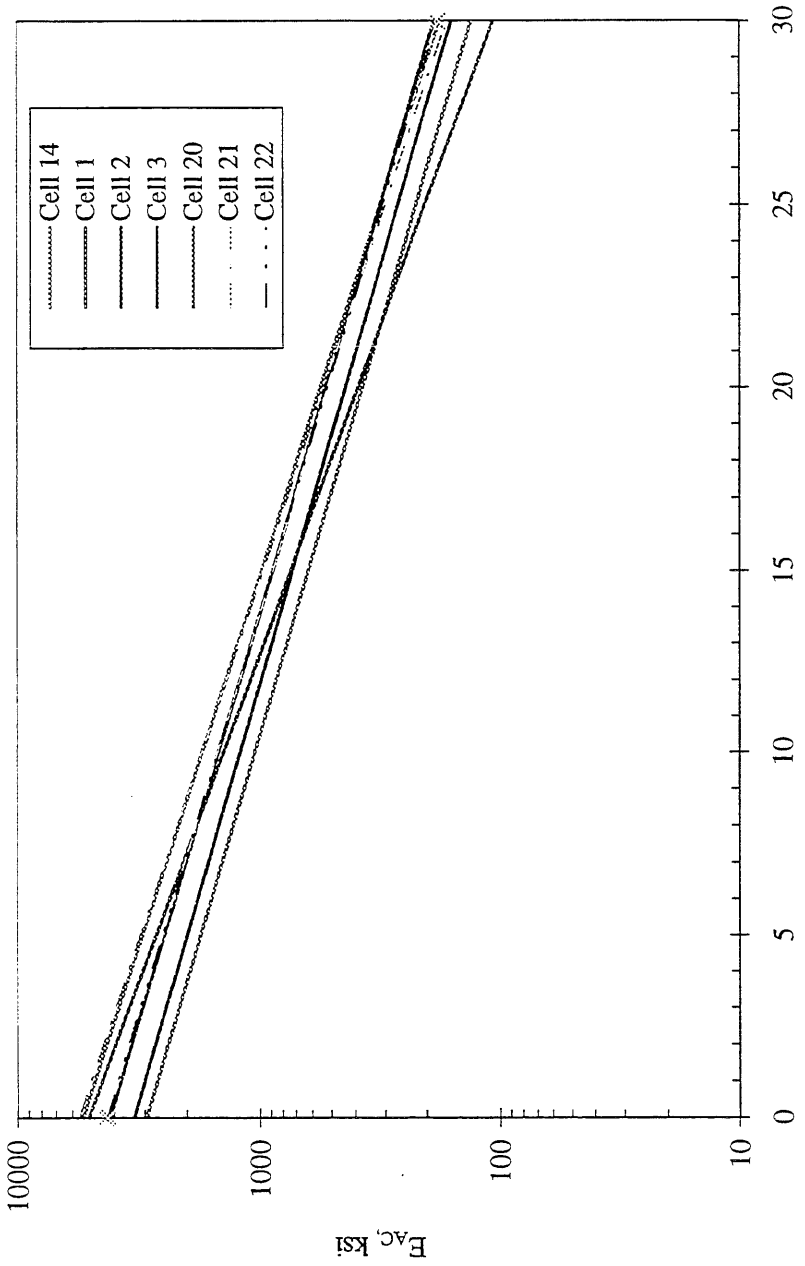

Figure 5.12 E_{AC} -Temperature Relations for Pen 120/150 Sections.

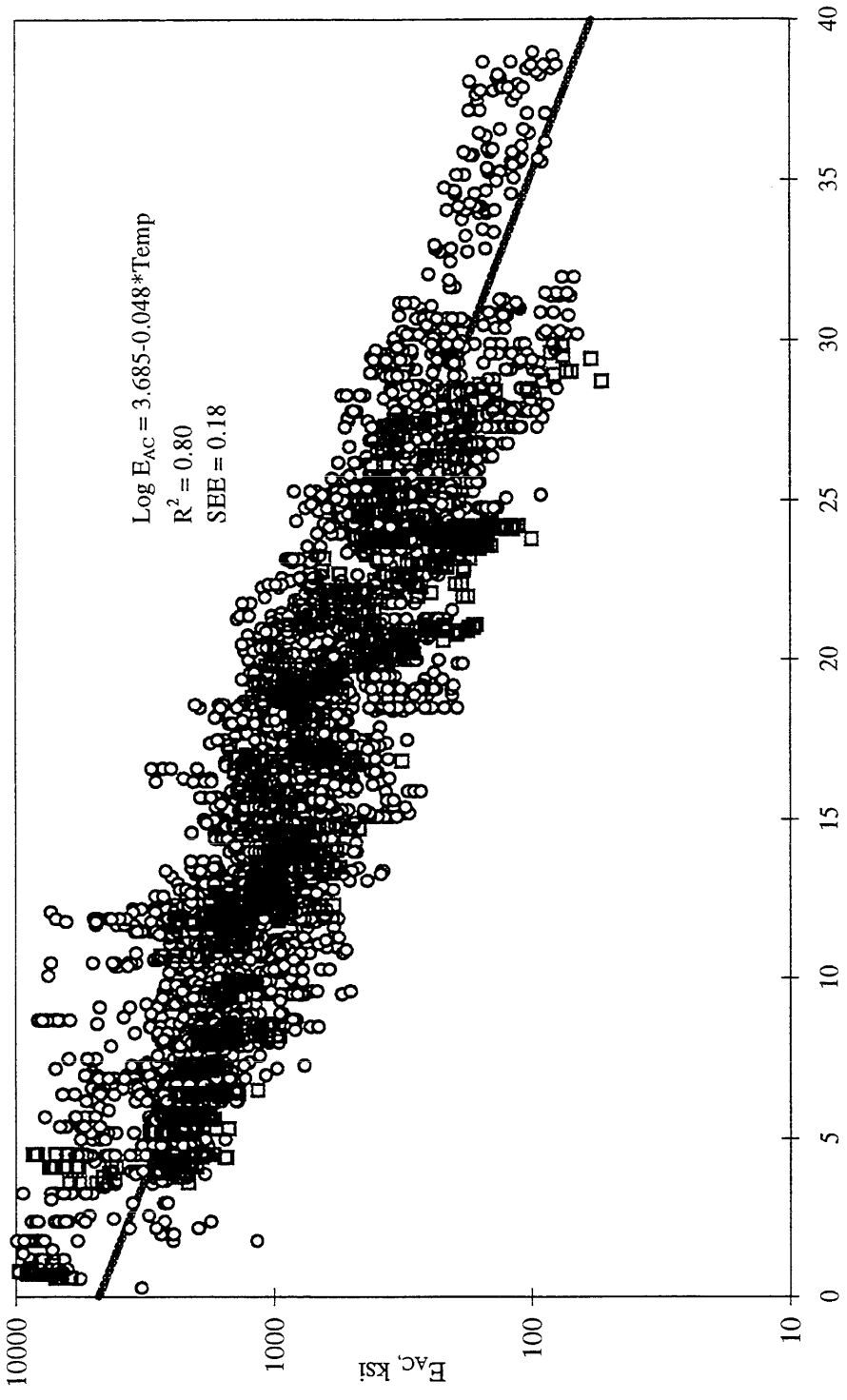

Figure 5.13. E_{AC} - Temperature Relation from FWD Results on Mainline Sections

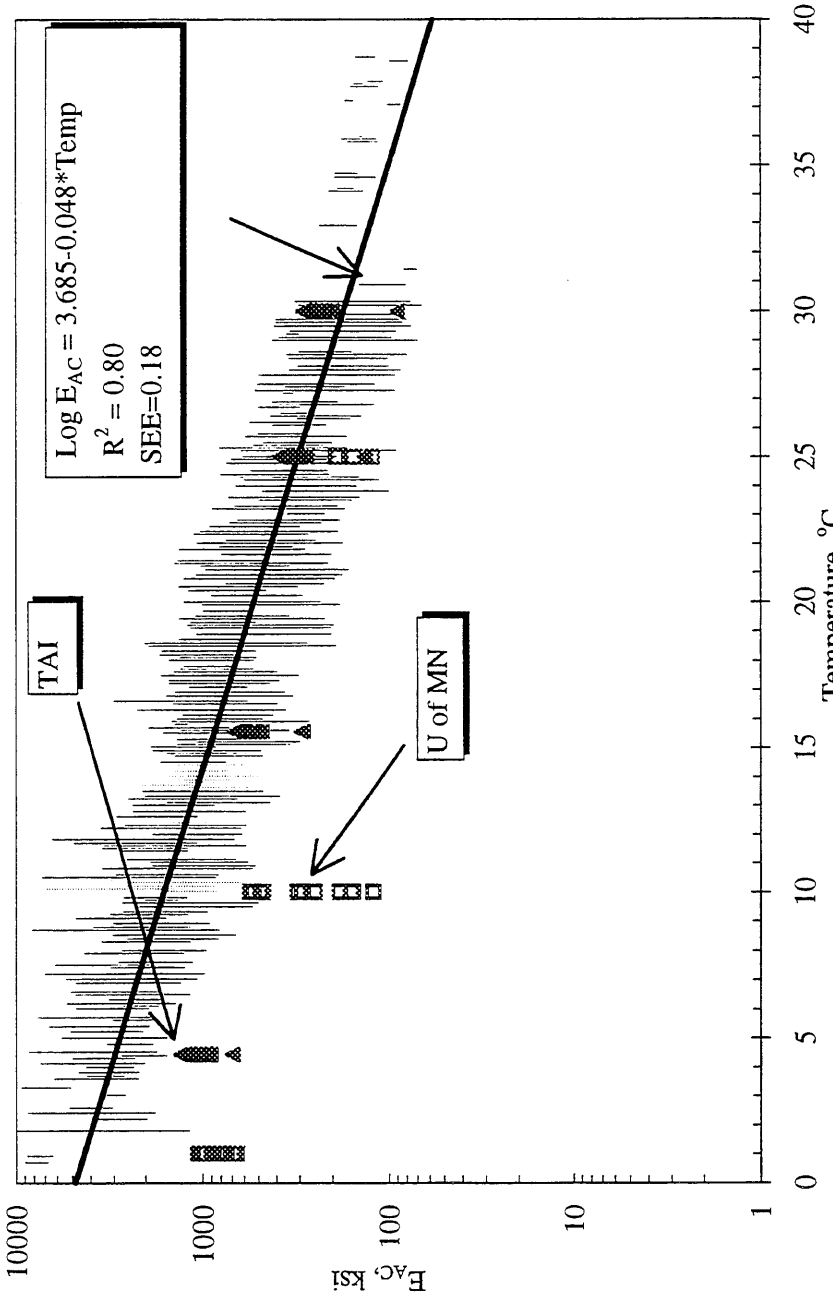

Figure 5.14. E_{AC} - Temperature Relation Mainline Cells

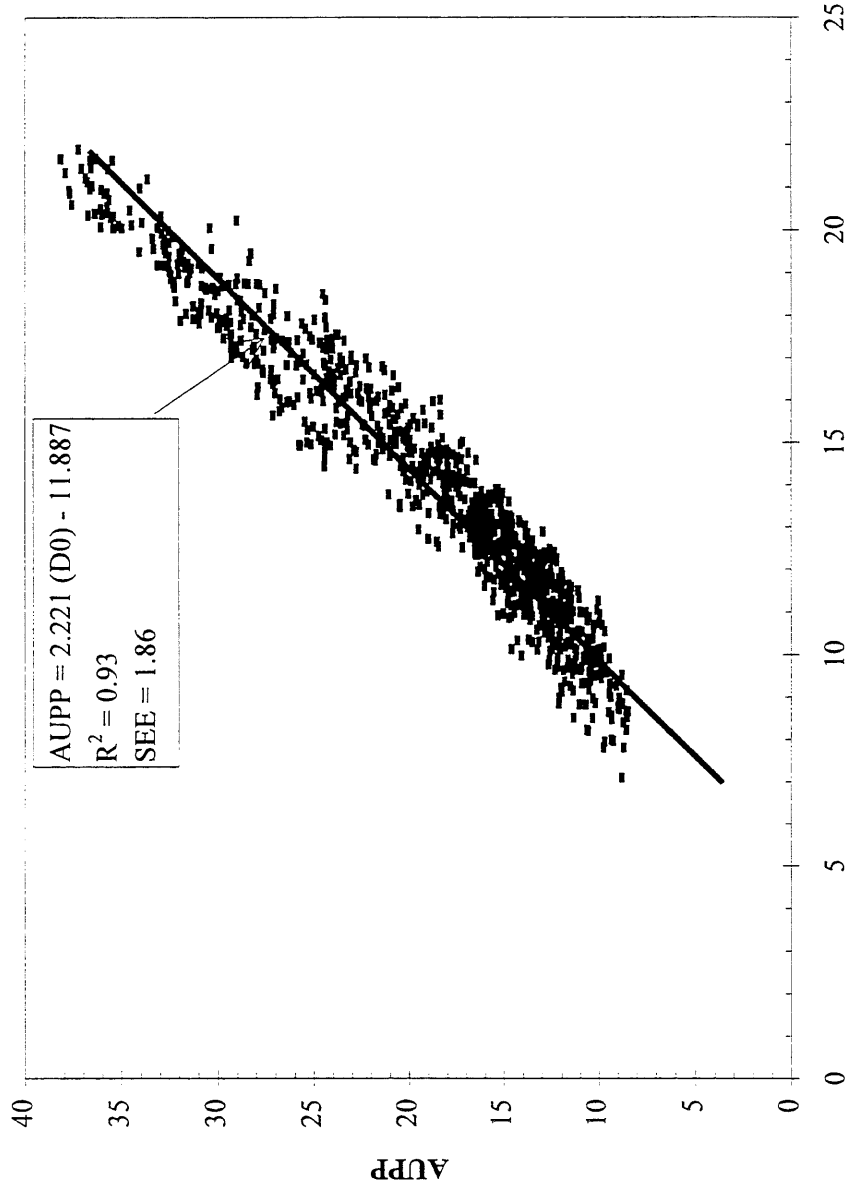

Figure 5.15. AUPP-Center Load Deflection (D0) Relation for T_{AC} = 5.75 in. Sections.

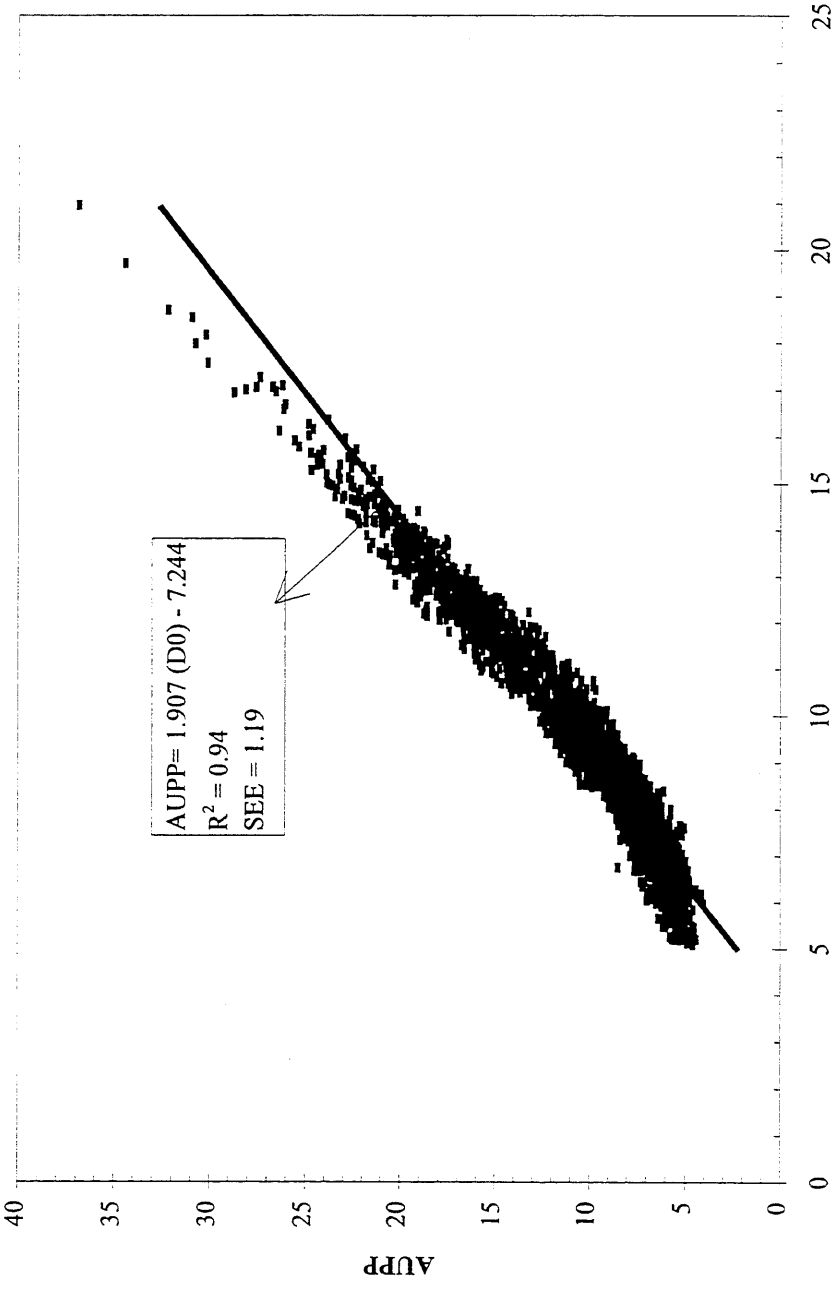

Figure 5.16. AUPP-Center Load Deflection (D0) Relation for T_{AC} = 7.75 in. Sections.

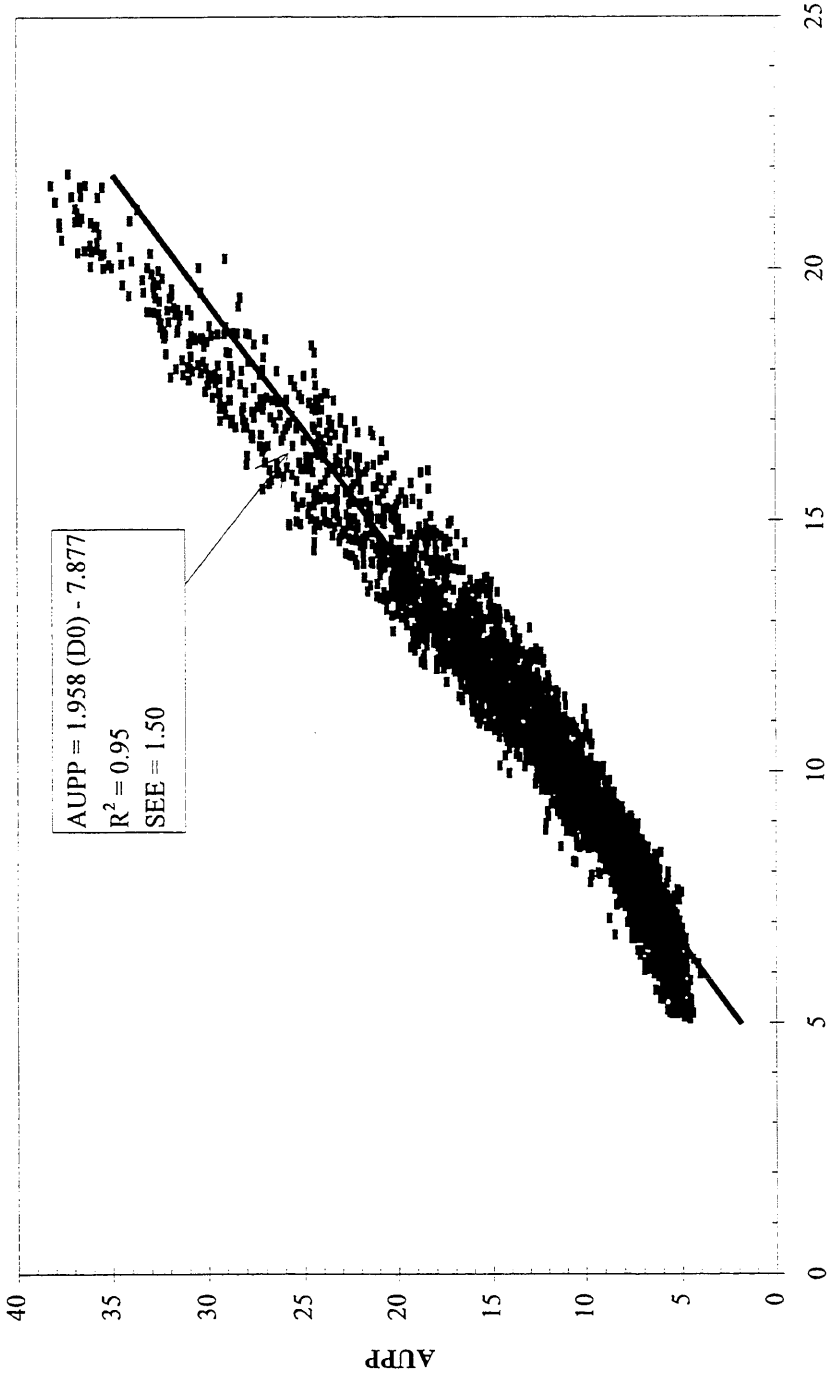

Figure 5.17. AUPP-Center Load Deflection (D0) Relation for All Conventional Sections.

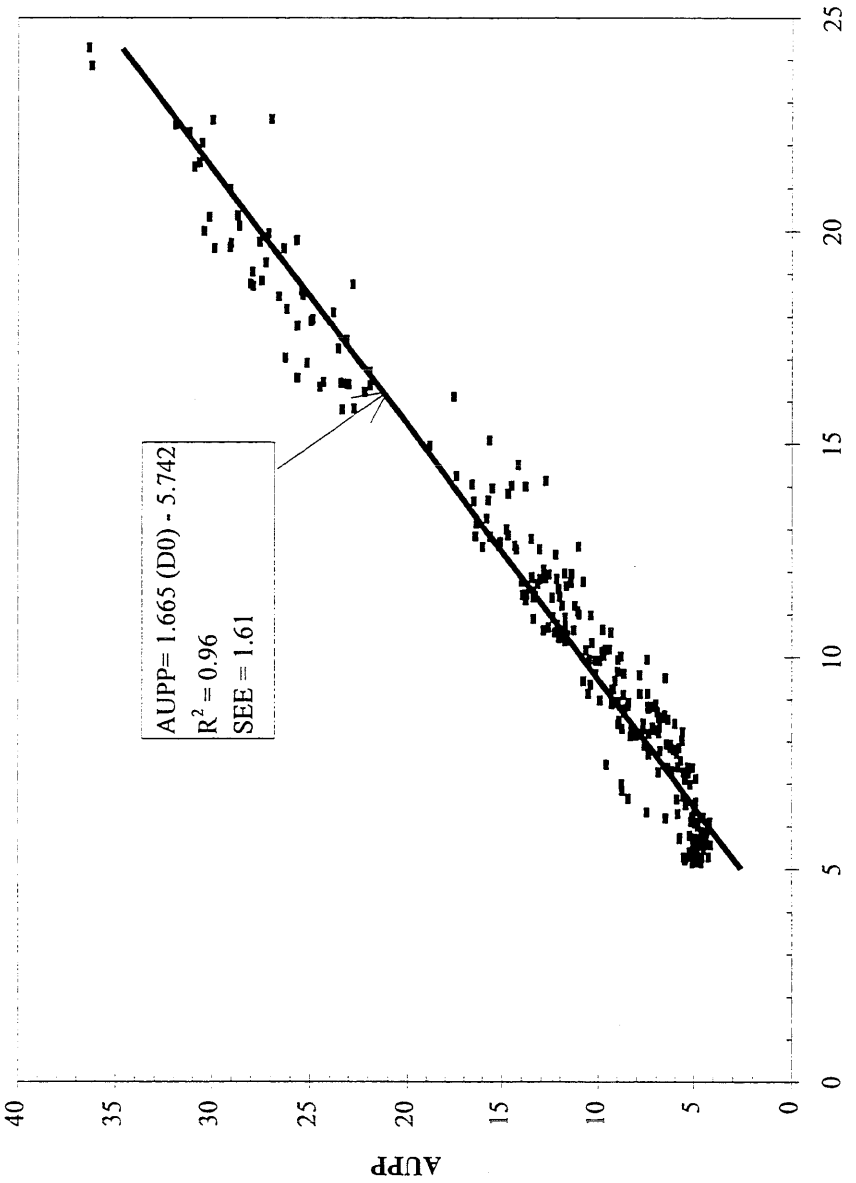

Figure 5.18. AUPP-Center Load Deflection (D0) Relation for Full Depth Cell 4 (T_{AC} = 8.75 in.).

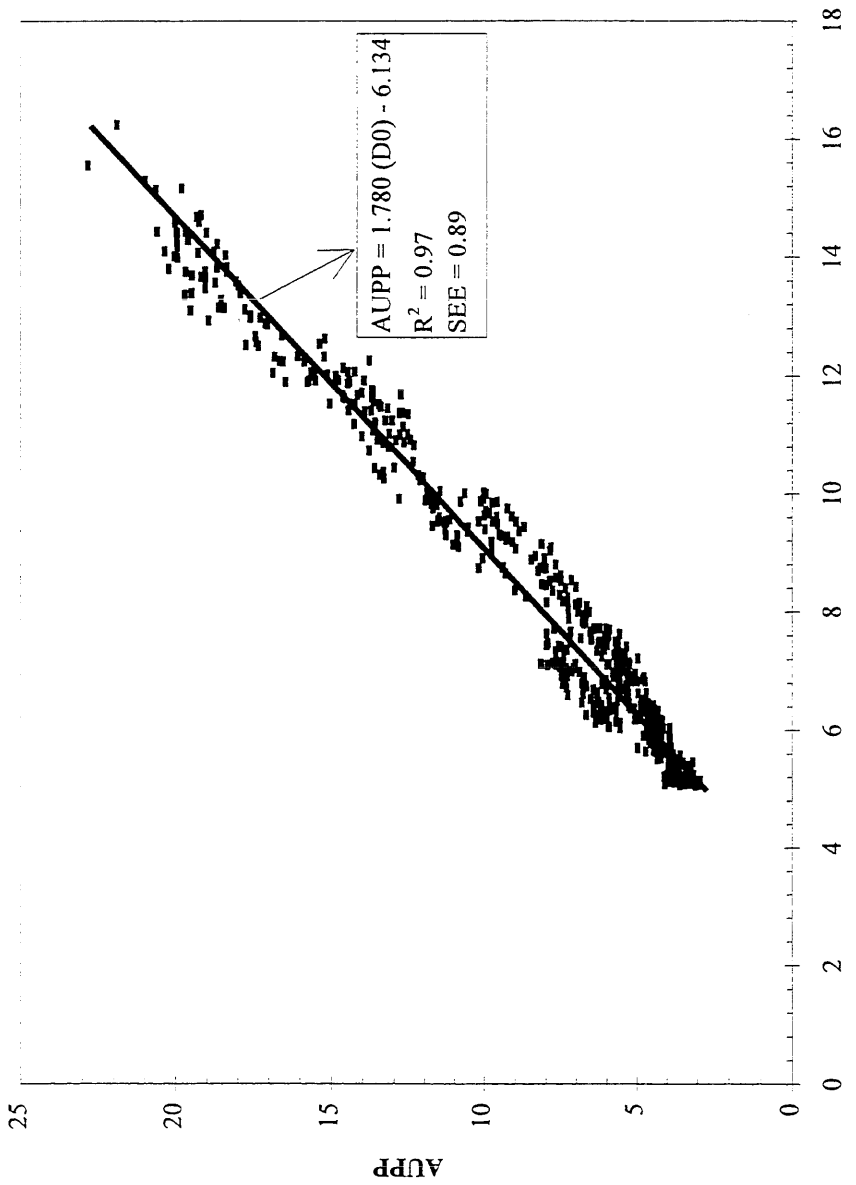

Figure 5.19. AUPP-Center Load Deflection (D0) for Full Depth Cells 14 & 15 (T_{AC} = 10.75 in.)

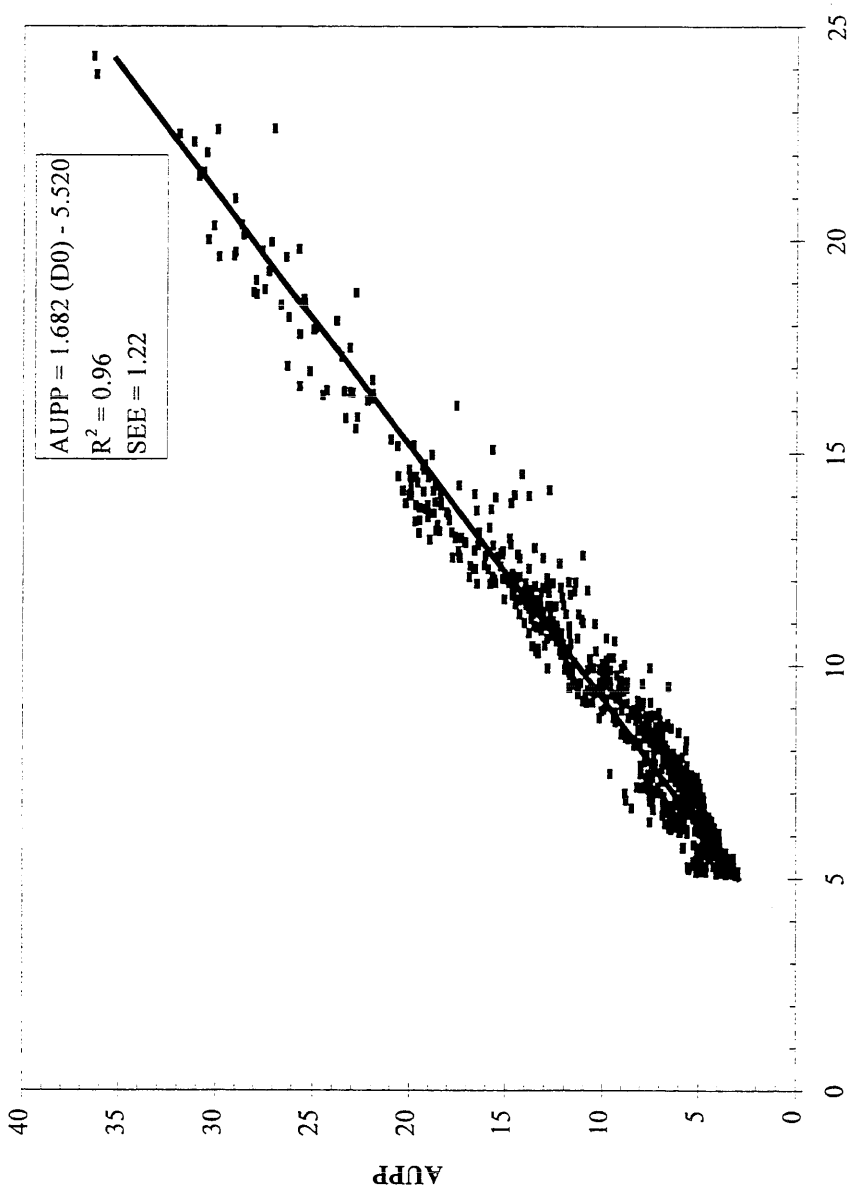

Figure 5.20. AUPP-Center Load Deflection (D0) Relation for Full Depth Mainline Sections.

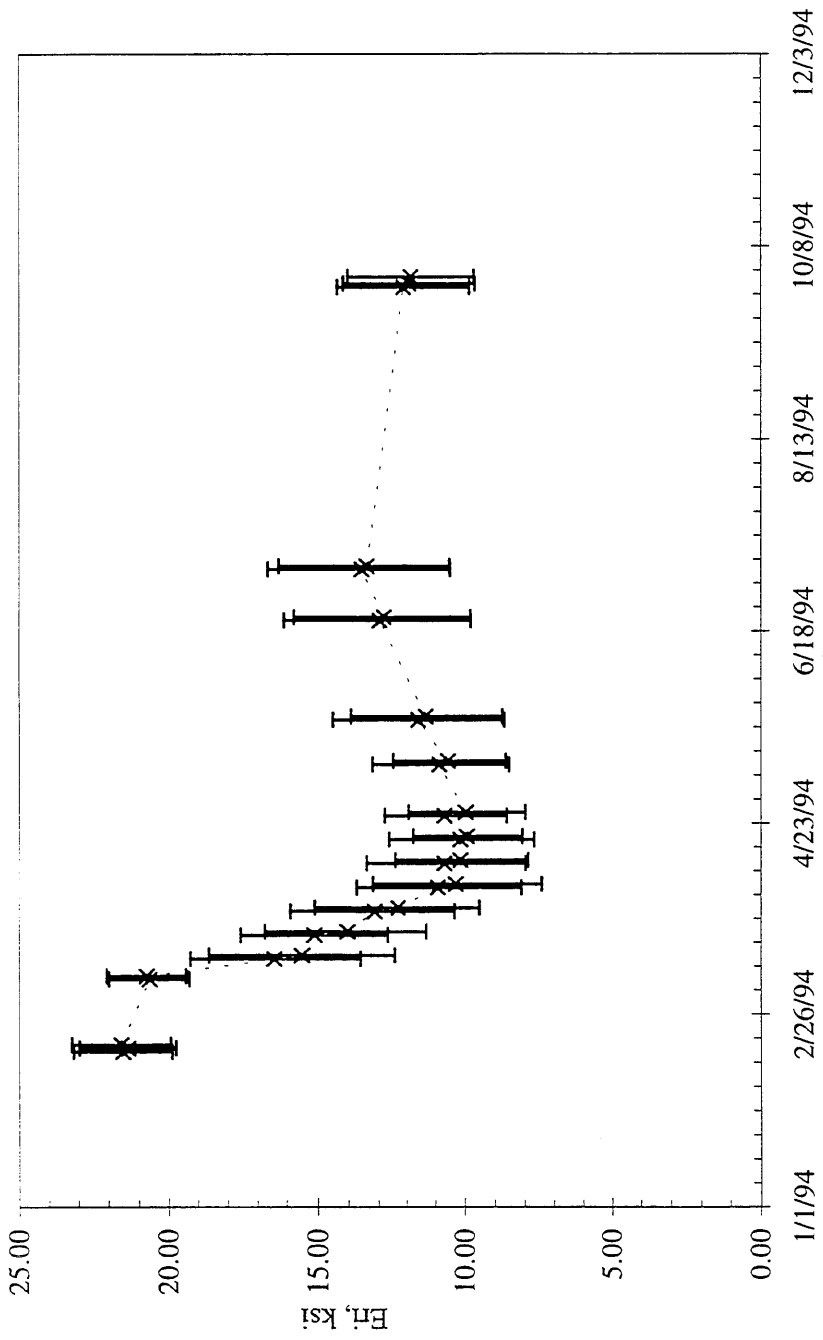

Figure 5.21. Variation of Backcalculated E_{RI} with Time for all Mainline Cells.

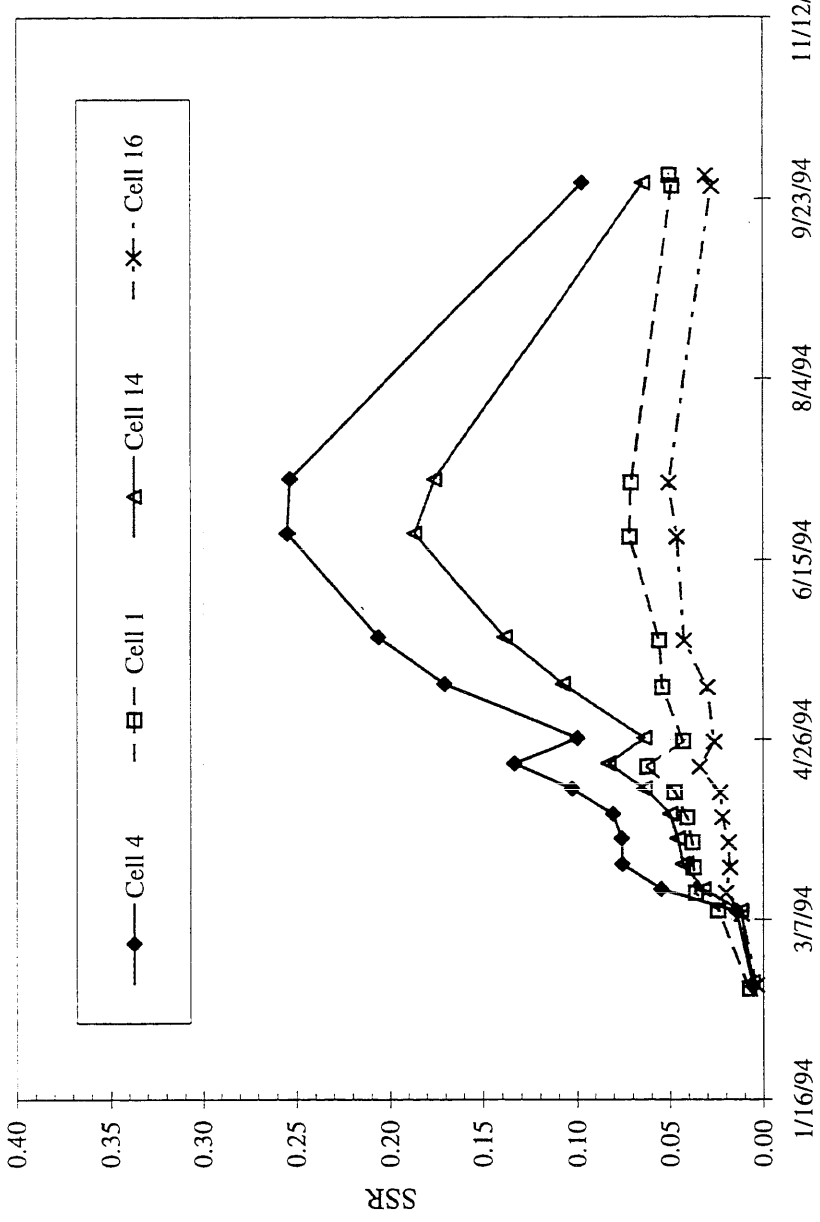

Figure 5.22 Backcalculated Subgrade Stress Ratio(SSR) for Selected Mainline Cells.

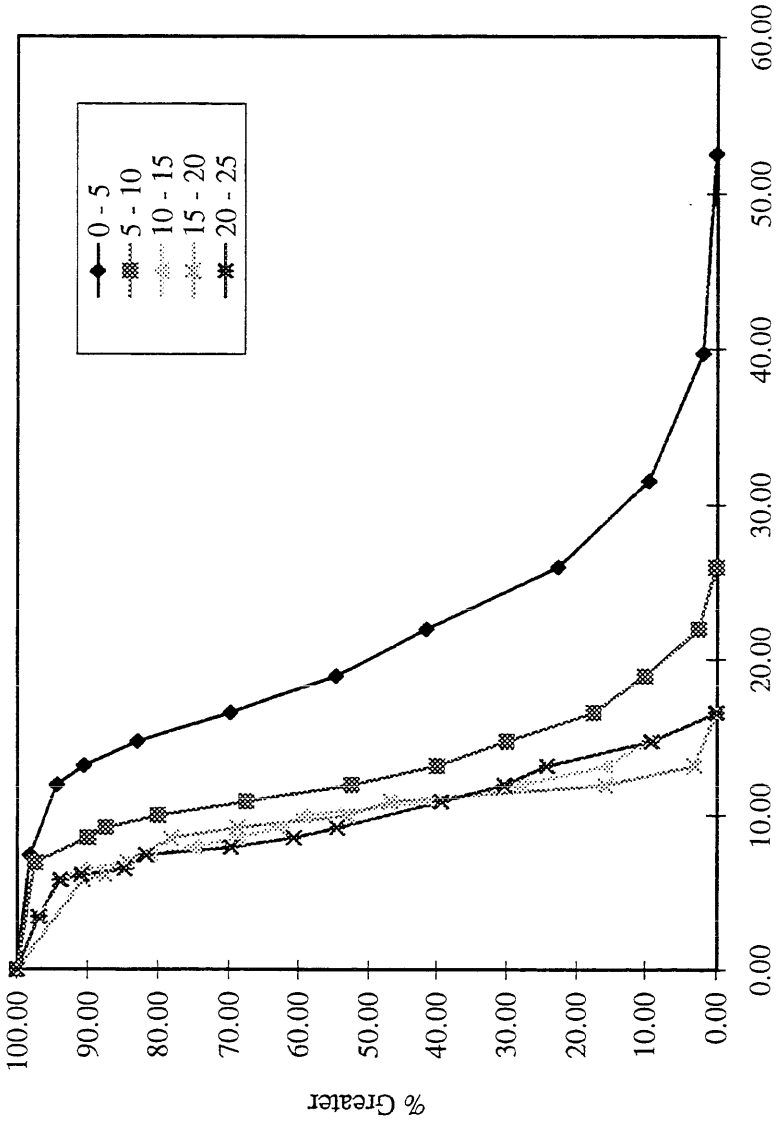

Figure 5.23 a) CBR Distribution with Depth for Cell 4, June 1992.

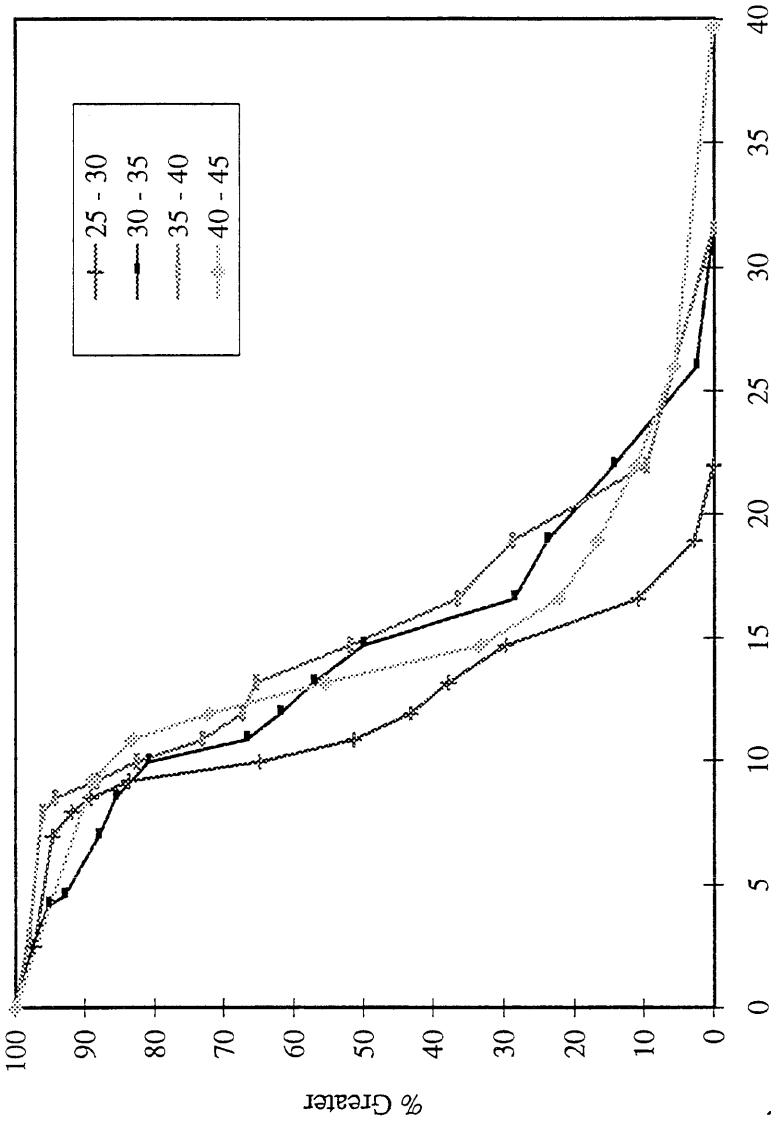

Figure 5.23 b) CBR Distribution with Depth for Cell 4, June 1992.

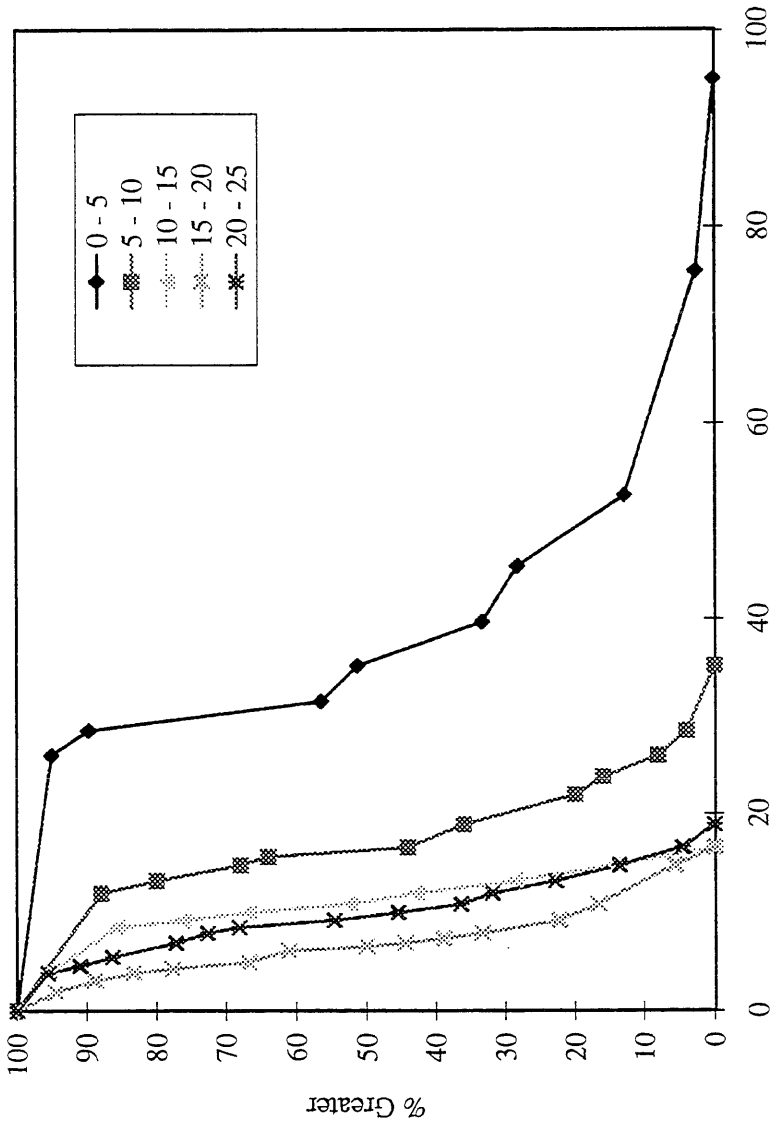

Figure 5.24 a) CBR Distribution with Depth for Cell 4, August 1992 .

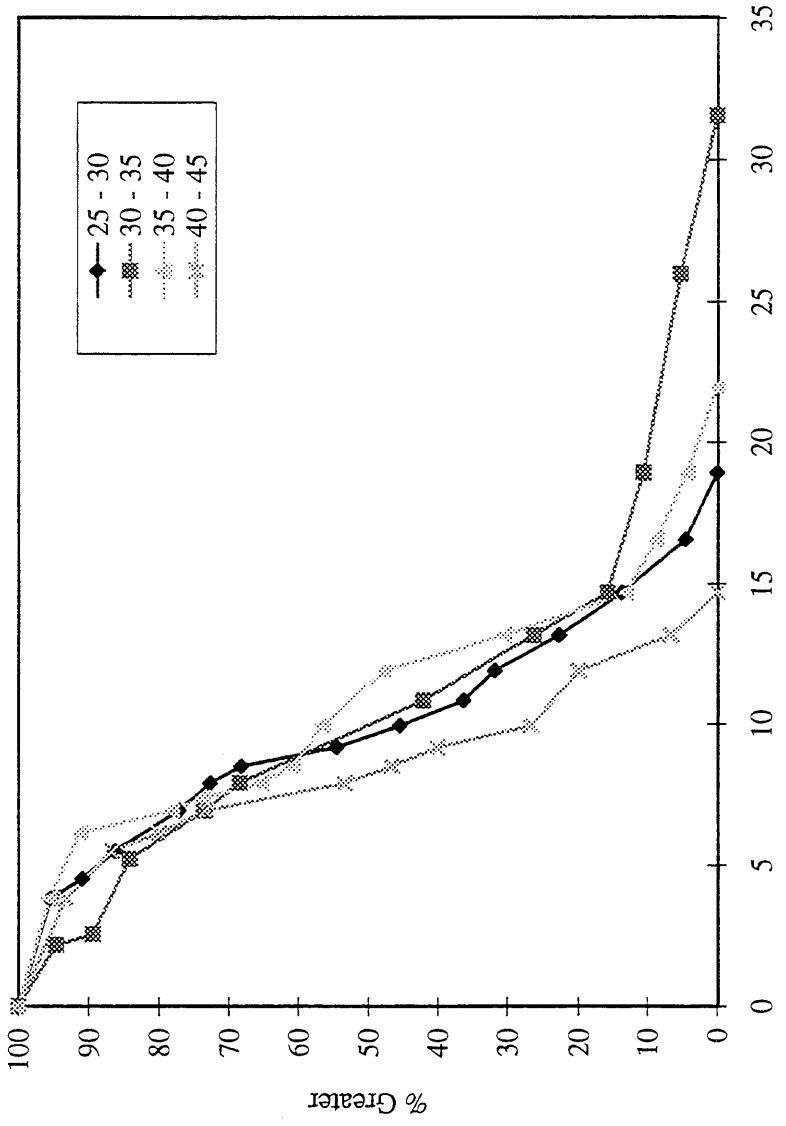

Figure5.24 b) CBR Distribution with Depth for Cell 4, August 1992.

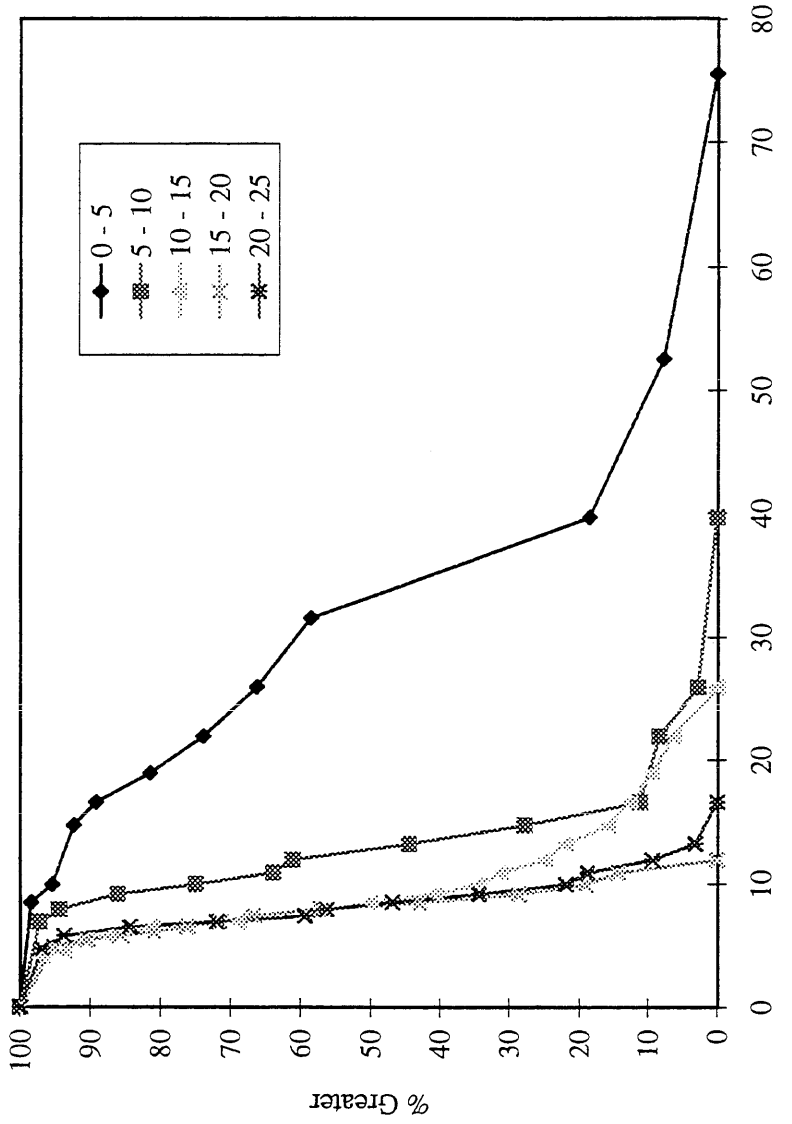

Figure 5.25 a) CBR Distribution with Depth for Cell 14, June 1992.

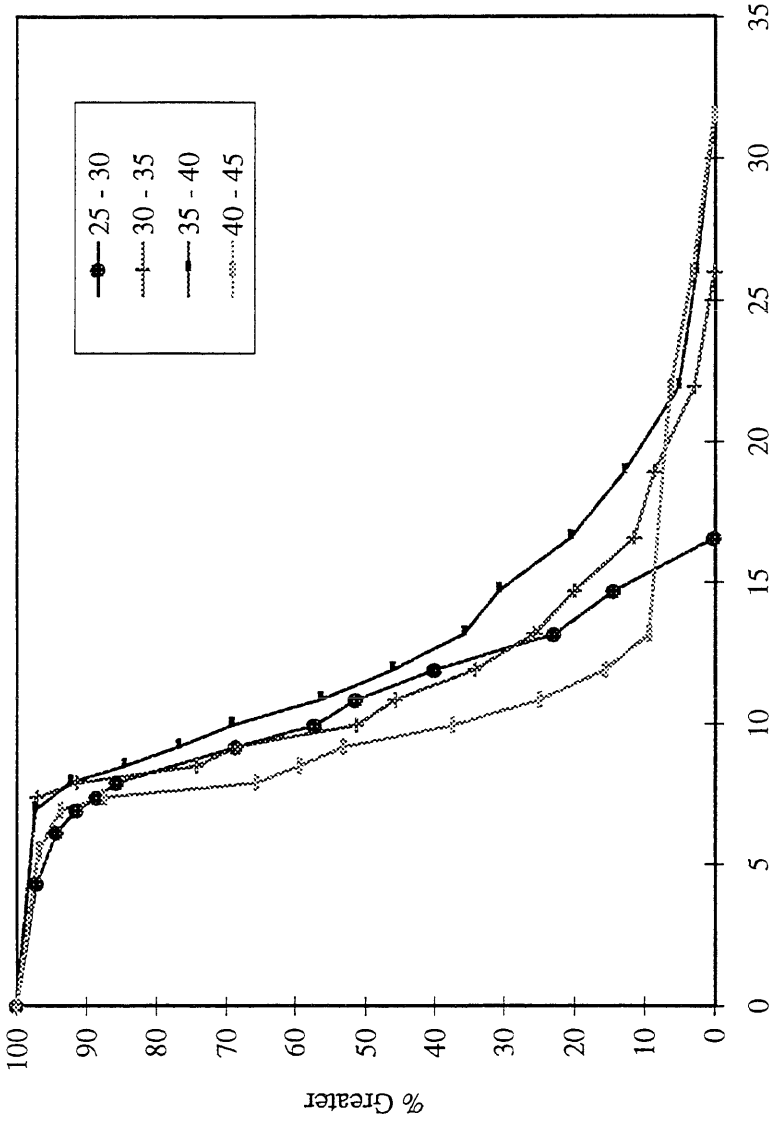

Figure 5.25 b) CBR Distribution with Depth for Cell 14, June 1992.

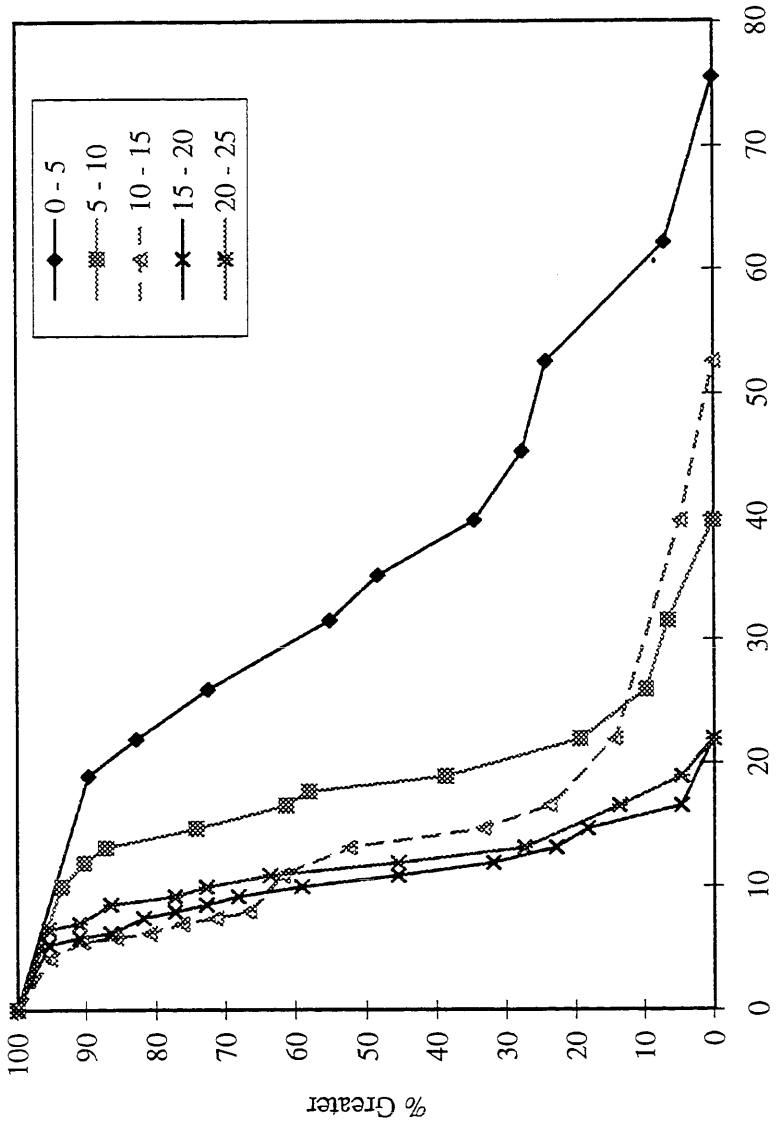

Figure 5.26 a) CBR Distribution with Depth for Cell 14, August 1992.

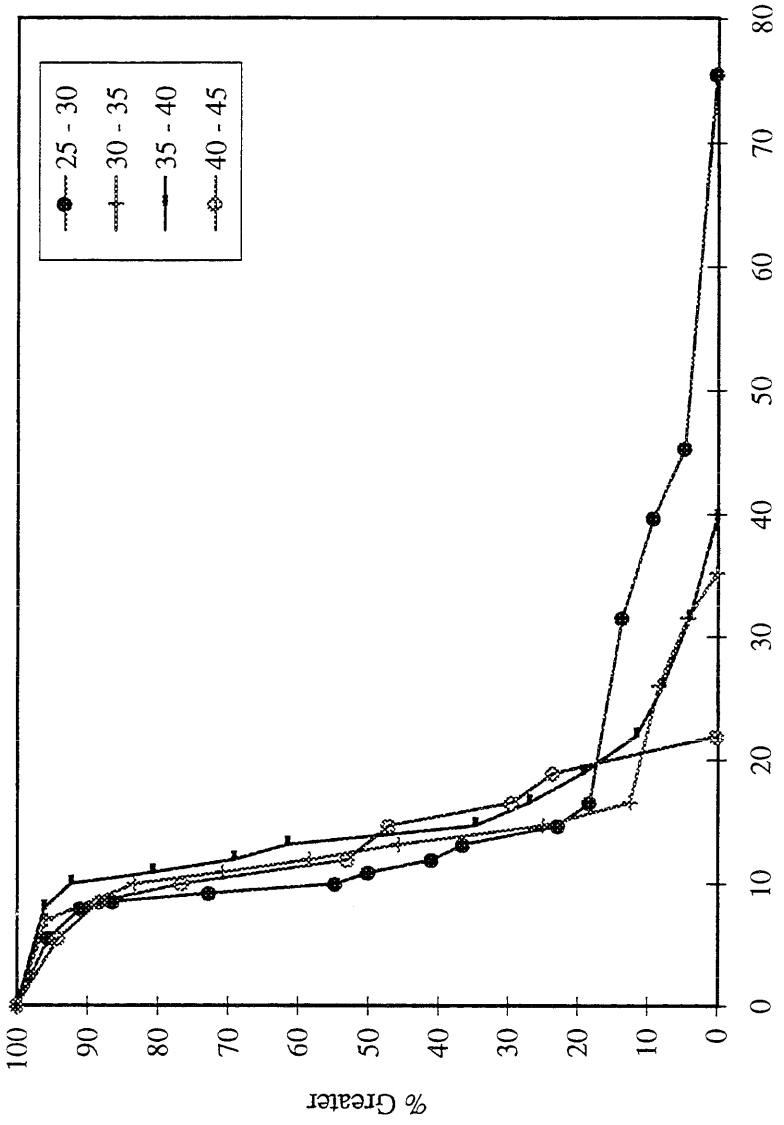

Figure 5.26 b) CBR Distribution with Depth for Cell 14, August 1992.

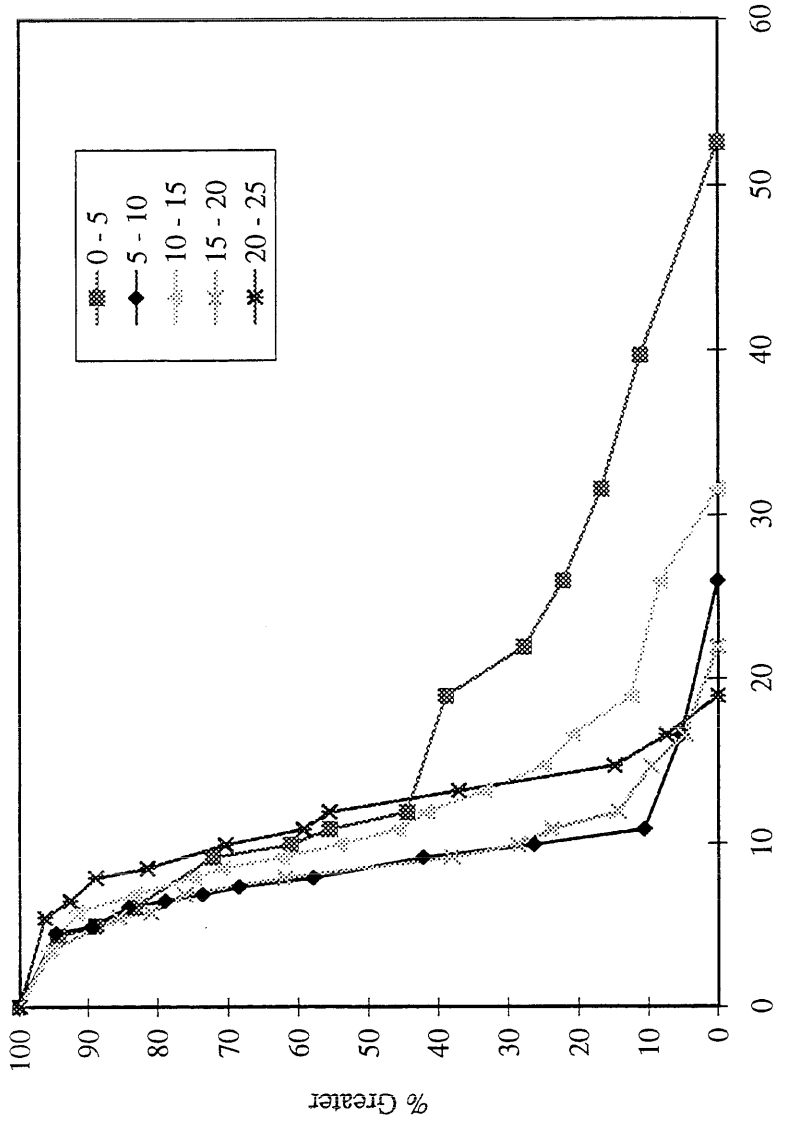

Figure 5.27 a) CBR Distribution with Depth for Cell 14, July 1993.

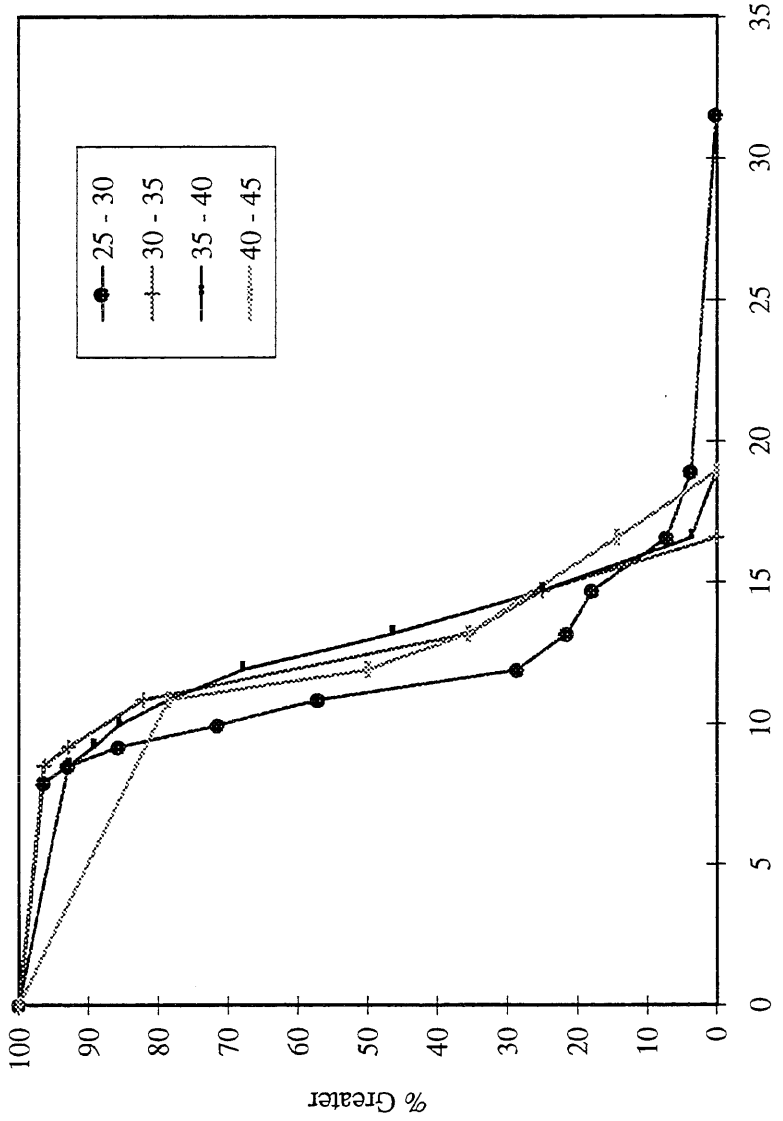

Figure 5.27 b) CBR Distribution with Depth for Cell 14, July 1993.

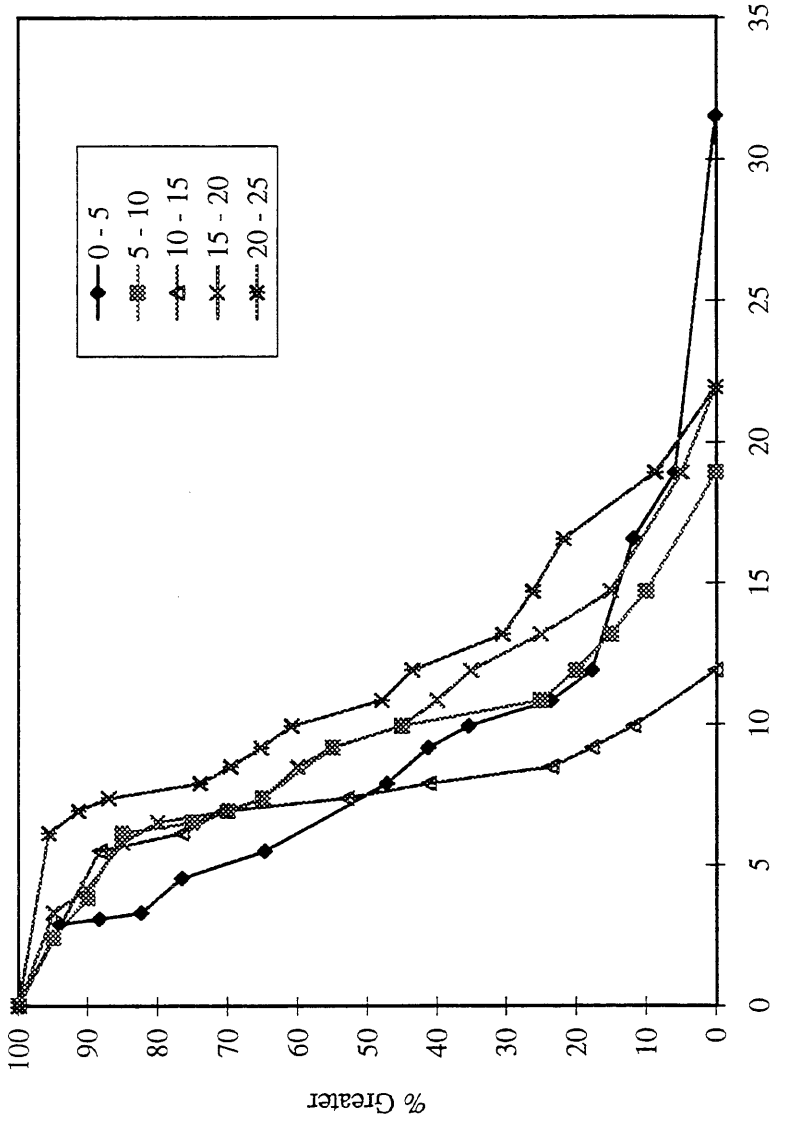

Figure 5.28 a) CBR Distribution with Depth for Cell 15, May 1992.

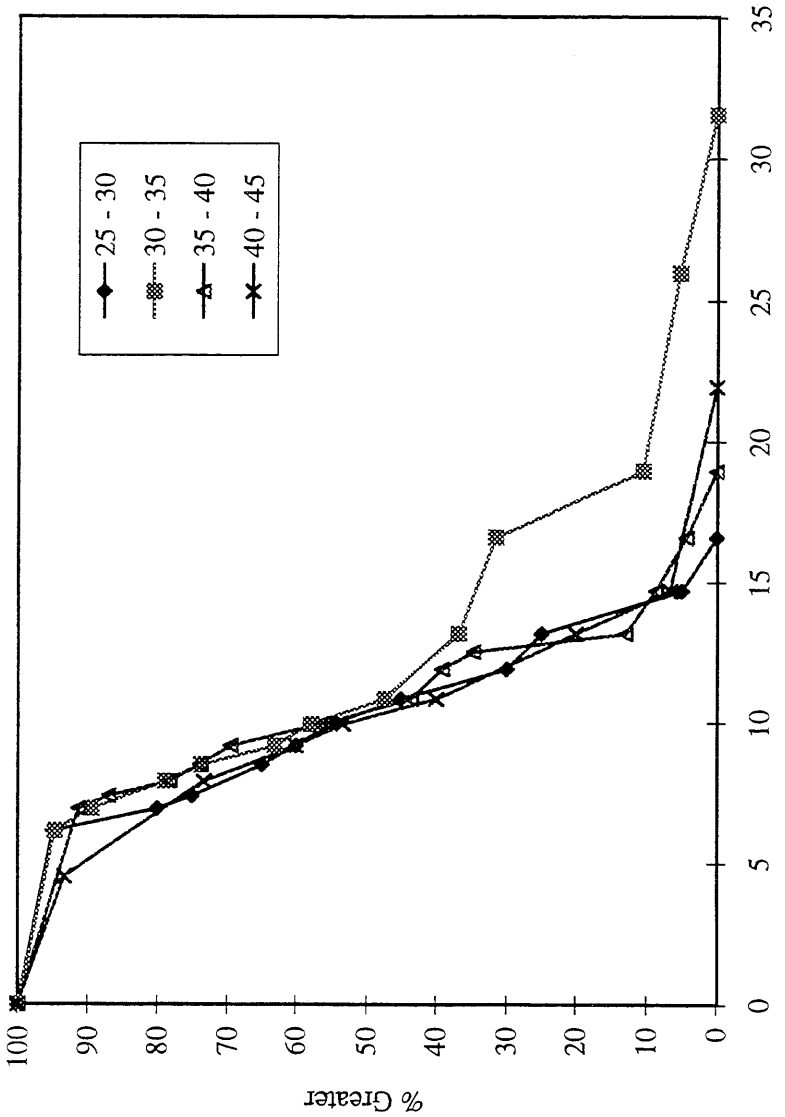

Figure 5.28 b) CBR Distribution with Depth for Cell 15, May 1992.

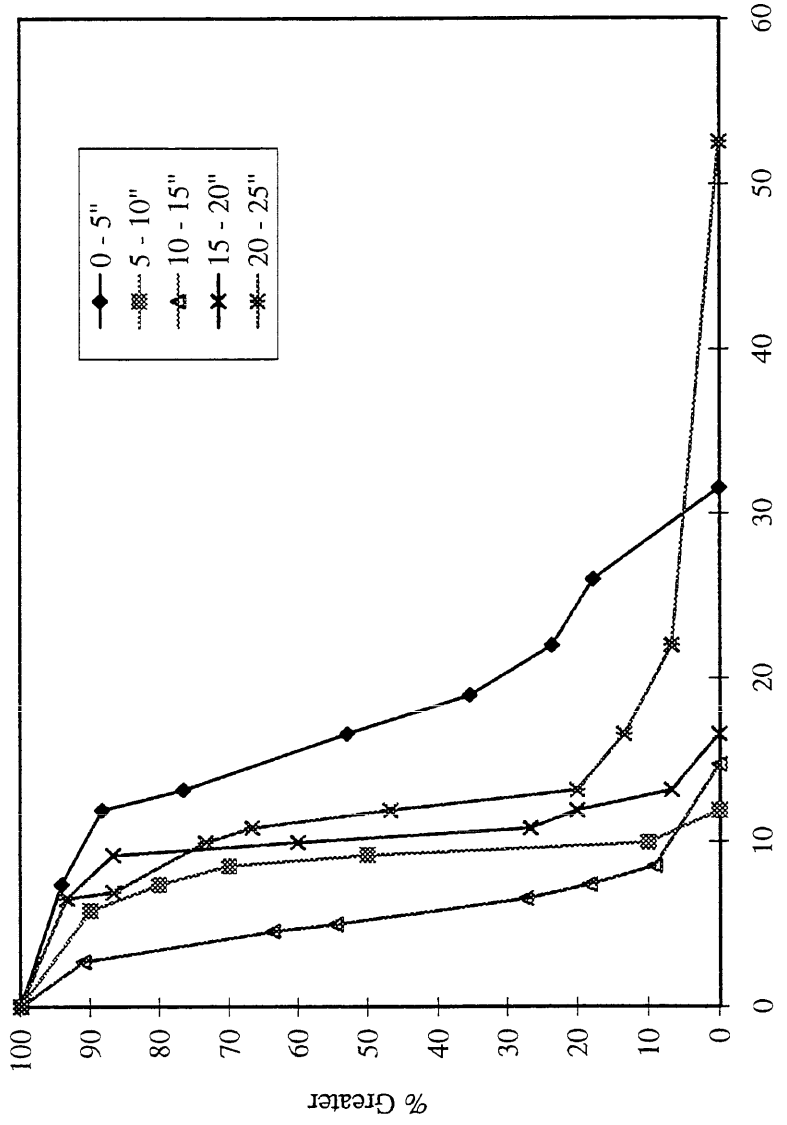

Figure 5.29 a) CBR Distribution with Depth for Cell 15, June 1992.

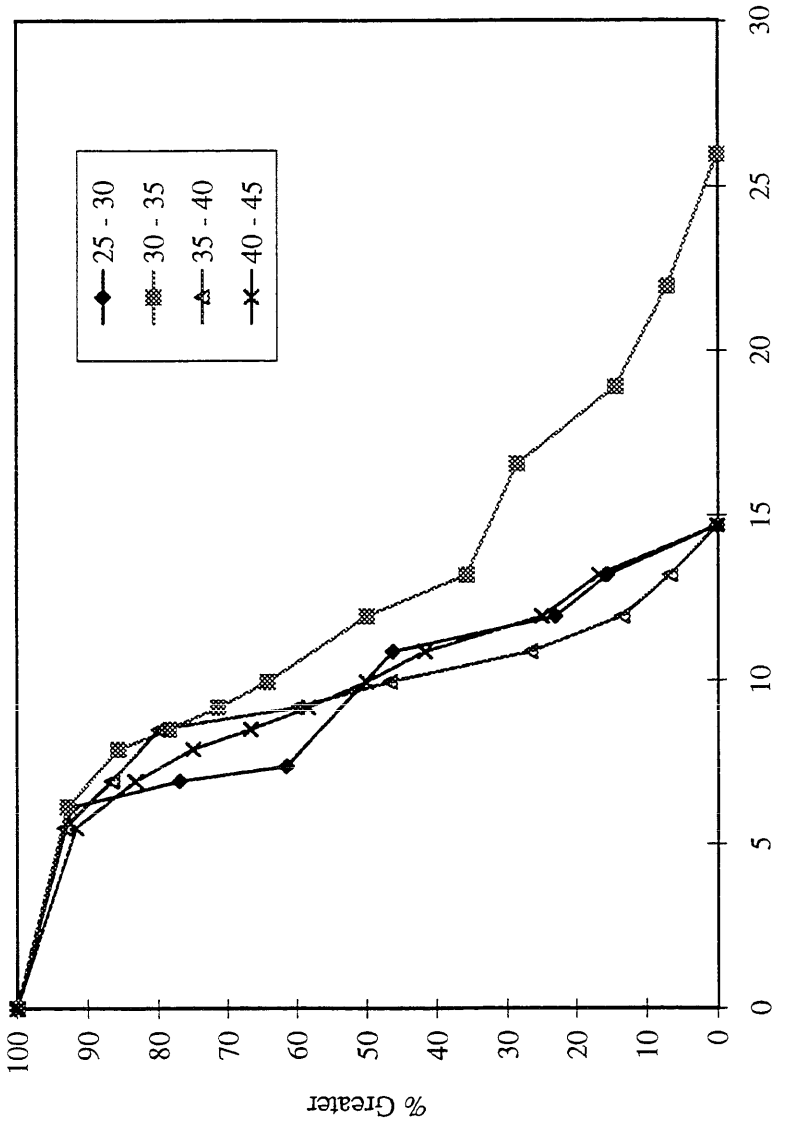

Figure 5.29 b) CBR Distribution with Depth for Cell 15, June 1992.

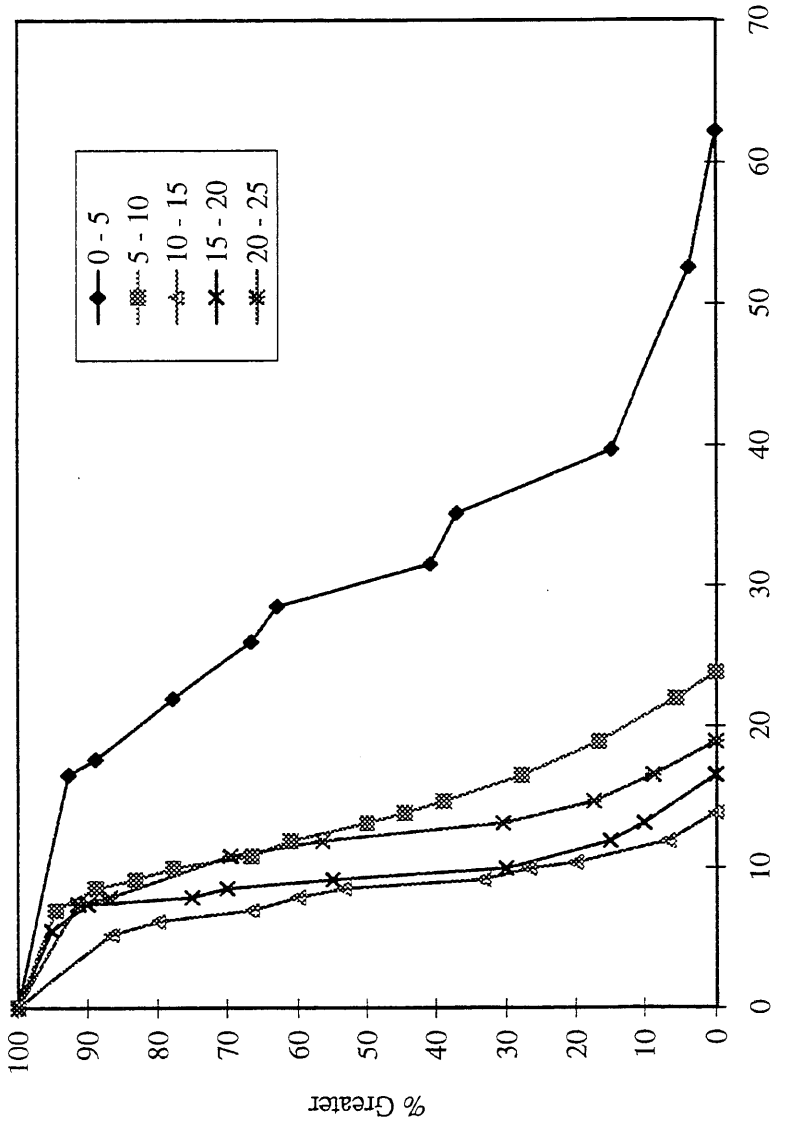

Figure 5.30 a) CBR Distribution with Depth for Cell 15, August 1992.

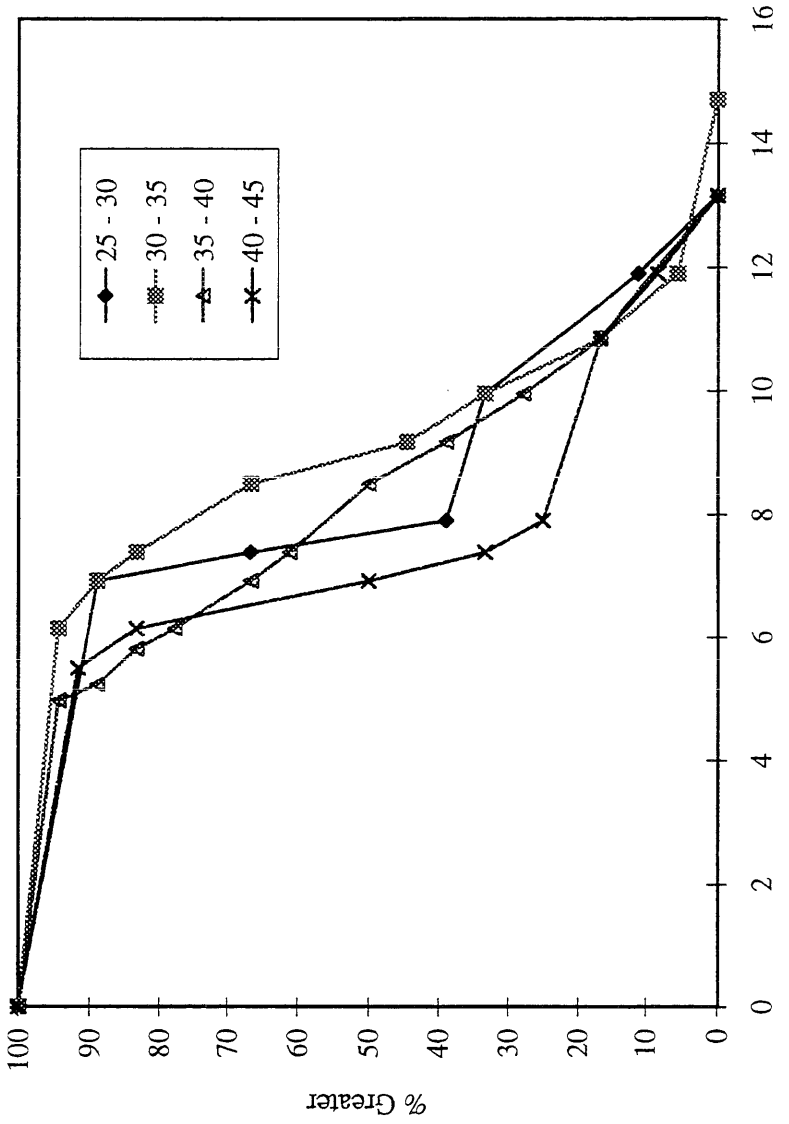

Figure 5.30 b) CBR Distribution with Depth for Cell 15, August 1992.

Figure 5.31. IPC Beam Fatigue Apparatus.

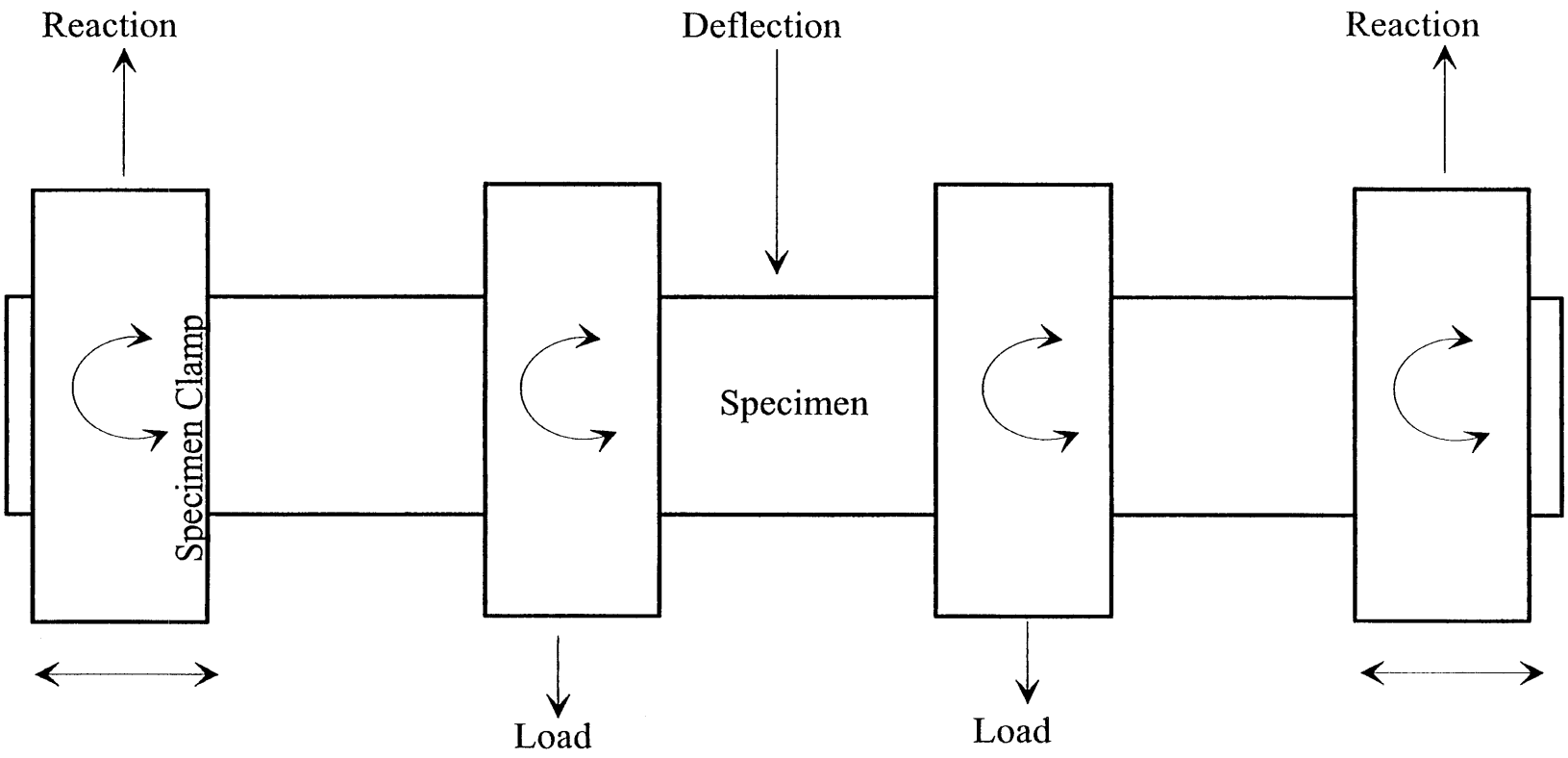

Figure 5.32. Loading Characteristics of the Beam Fatigue Apparatus

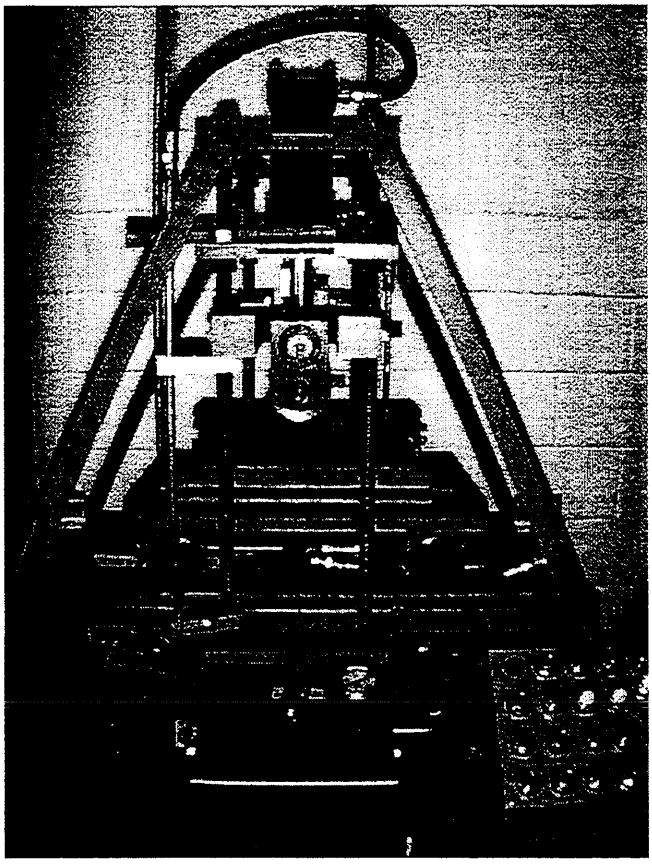

Figure 5.33. Rantoul Wheel Compactor.

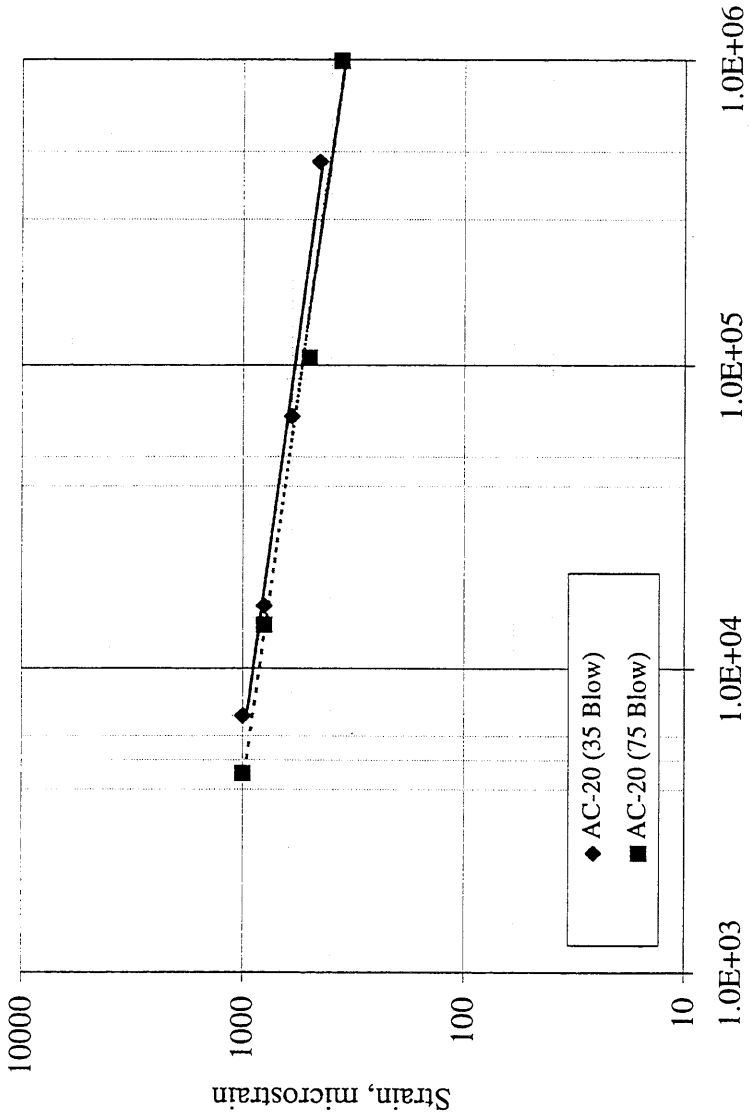

Figure 5.34. Fatigue Relations for AC-20 Mixes.

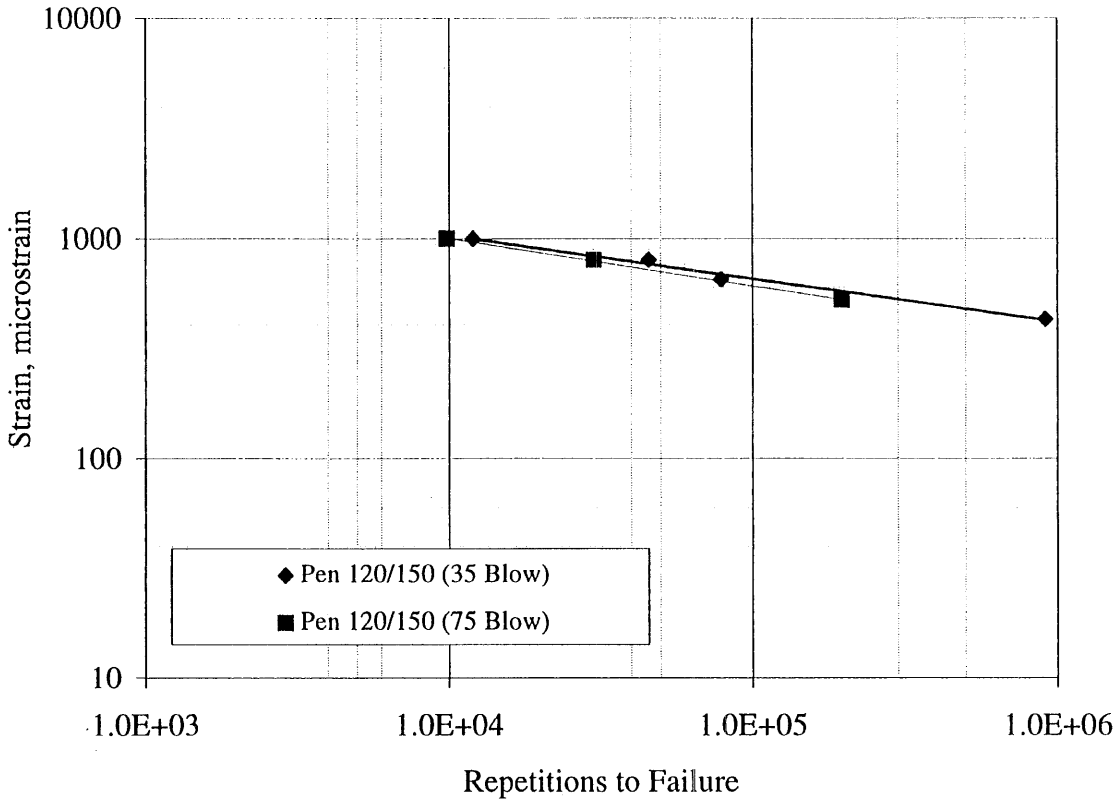

Figure 5.35. Fatigue Relations for Pen 120/150 Mixes.

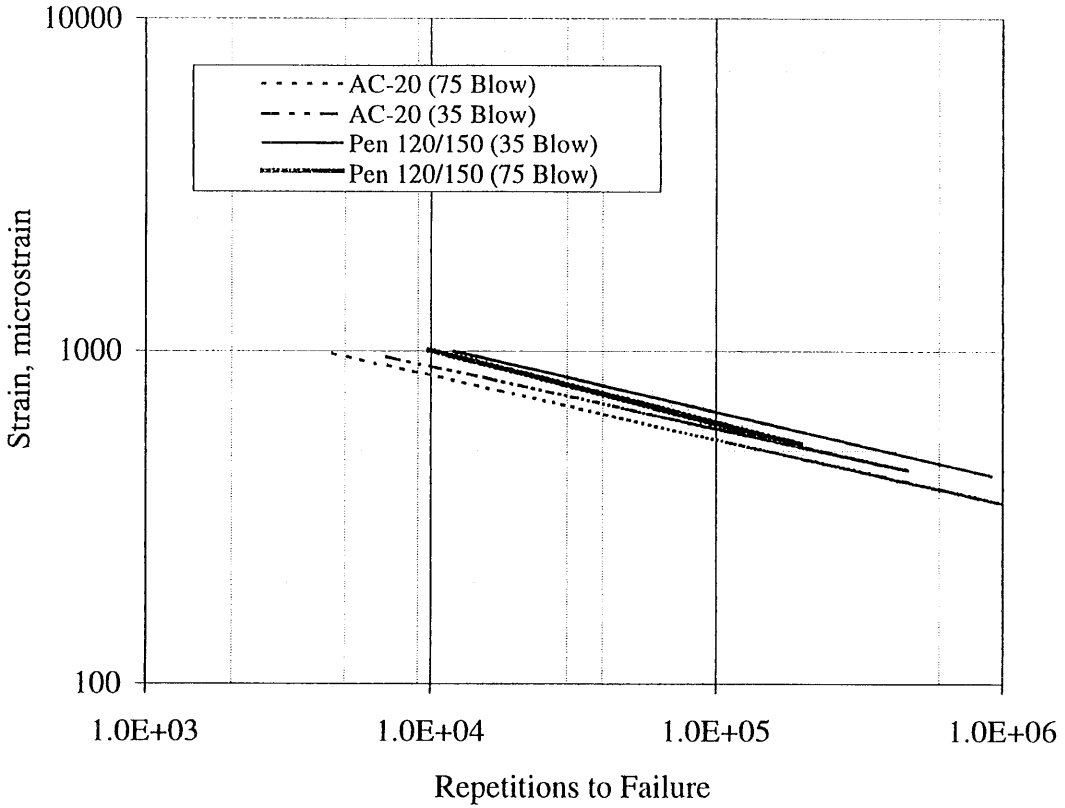

Figure 5.36. Fatigue Relations for Mn/ROAD Mixes.

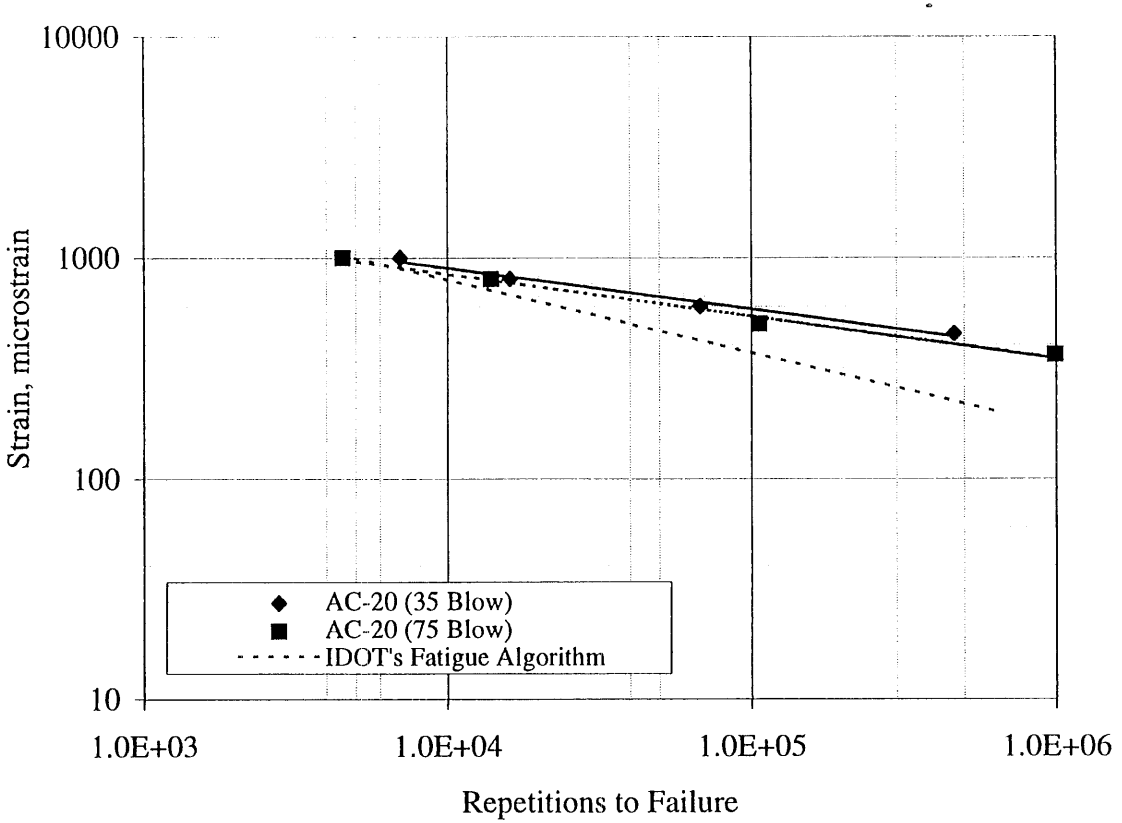

Figure 5.37. Comparison of Mn/ROAD AC-20 Mixes and IDOT's Algorithm

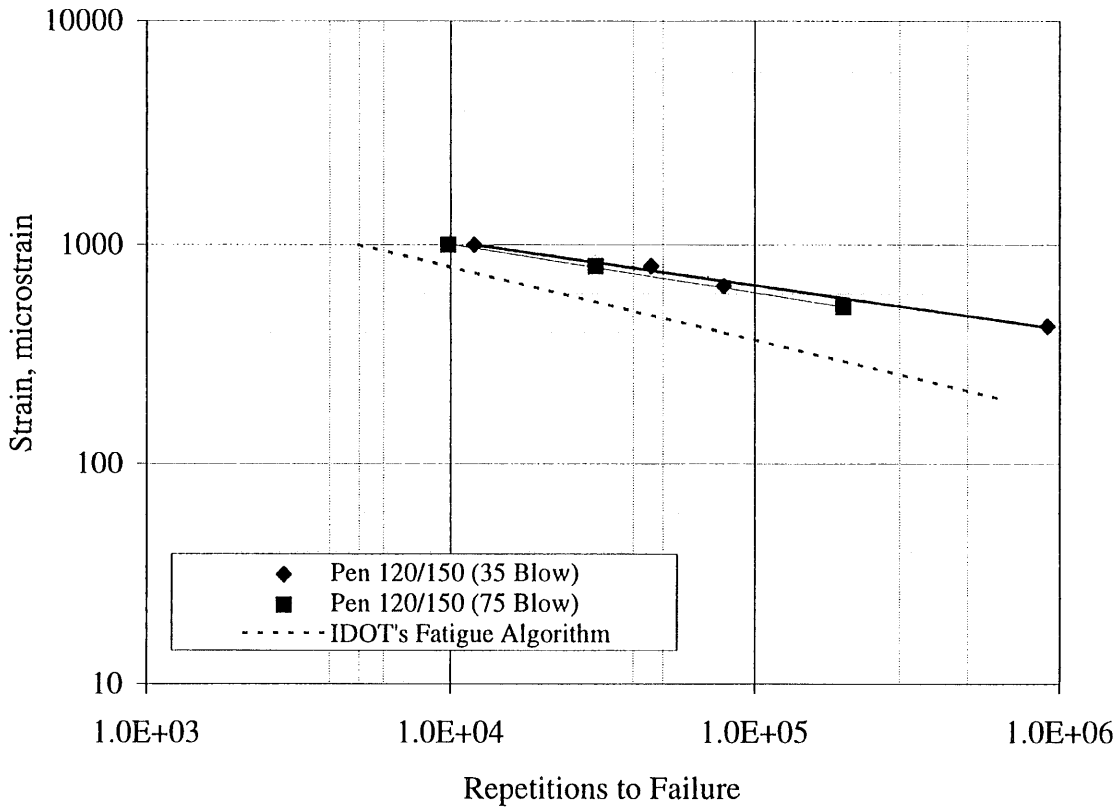

Figure 5.38. Comparison of Mn/ROAD Pen 120/150 Mixes and IDOT's Algorithm

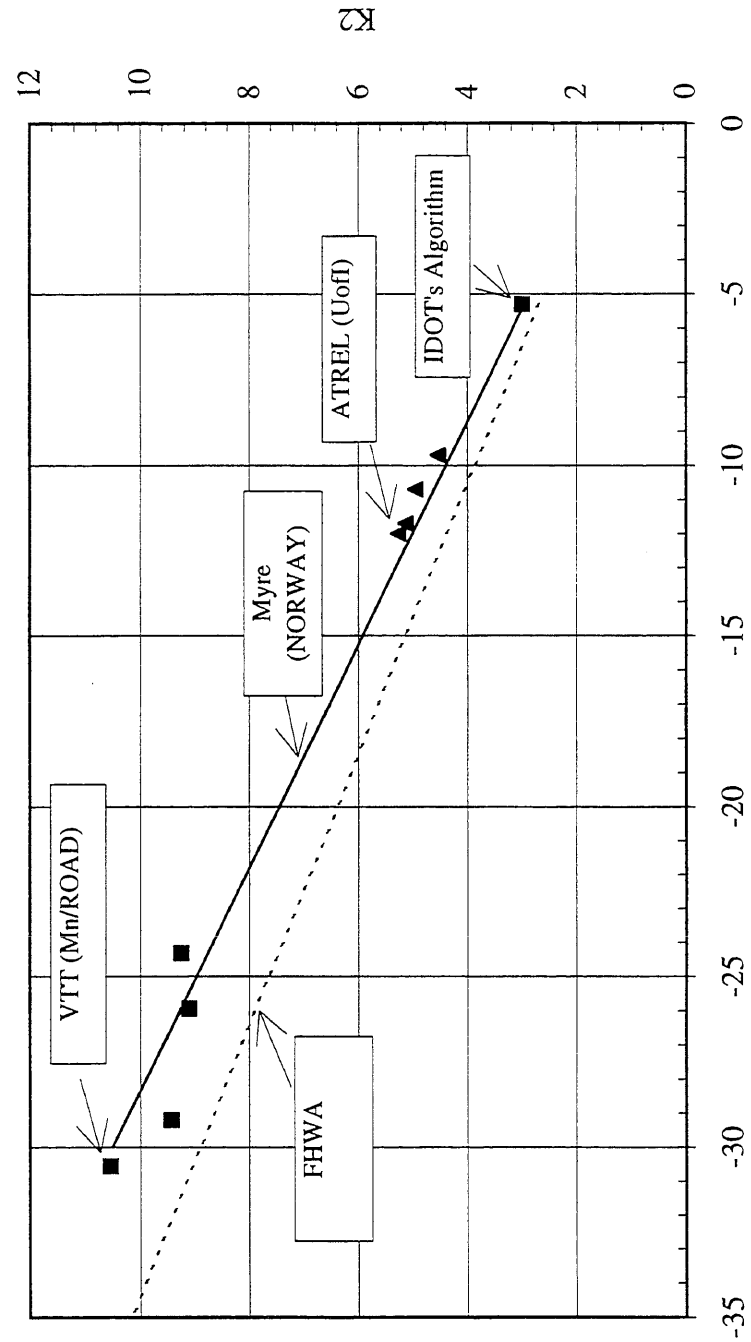

Figure 5.39. K1 -K2 Relations for AC Fatigue.

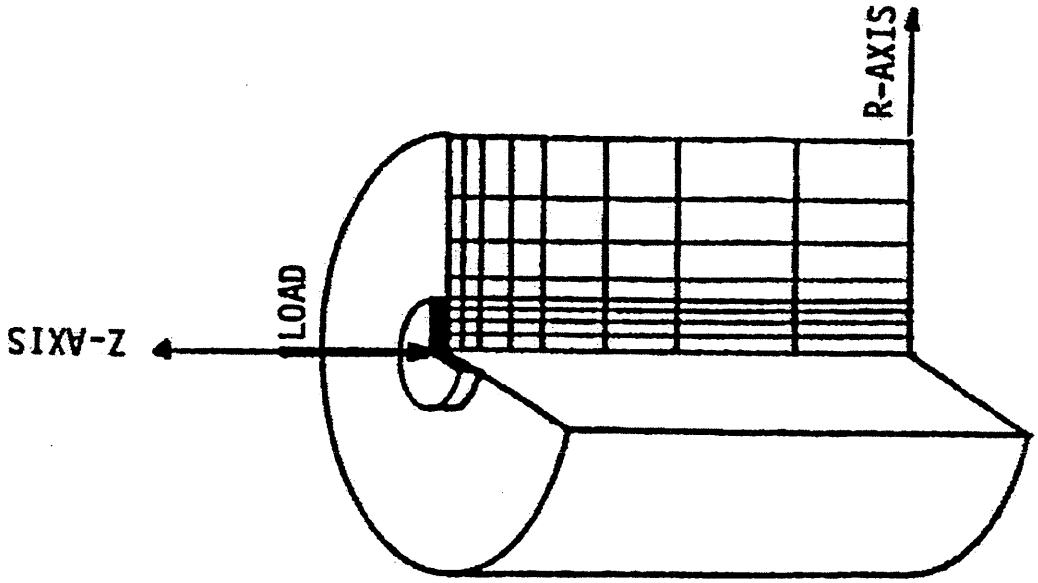

Figure 6.1. Cylindrical Pavement Configuration

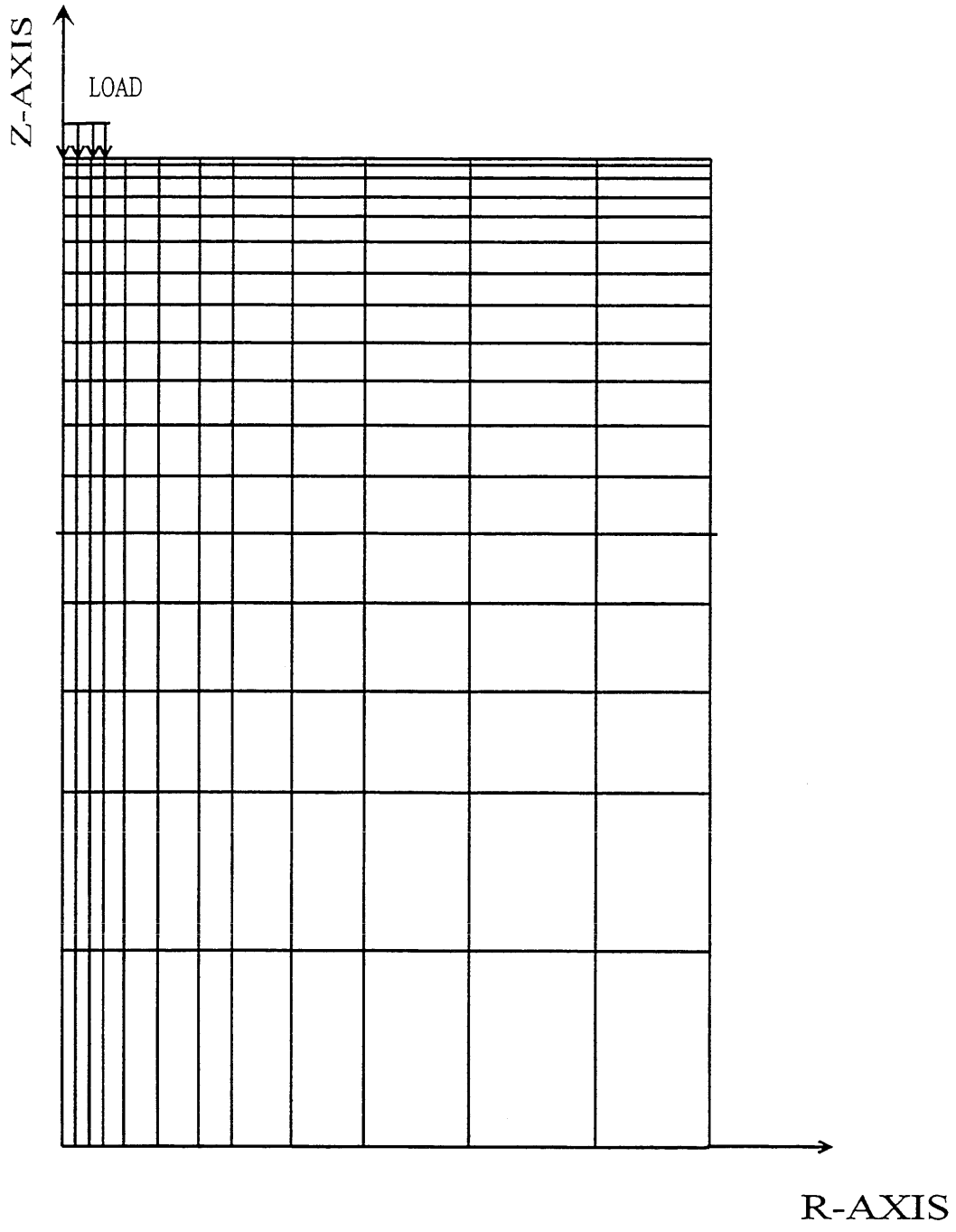

Figure 6.2. Rectangular Half Space of Axisymmetric Solid.

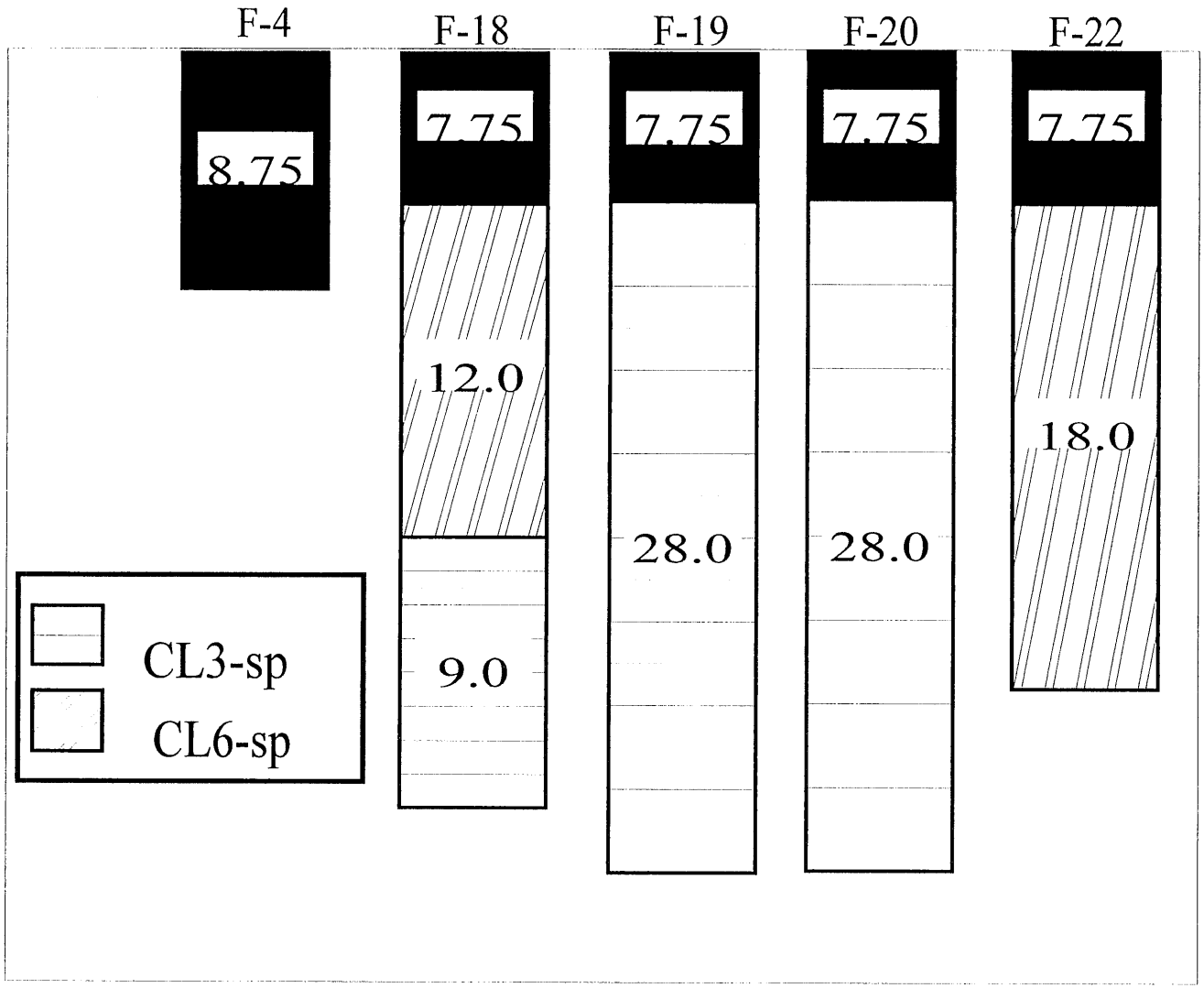

Figure 6.3. Mainline Cells with Embedded Sensors.

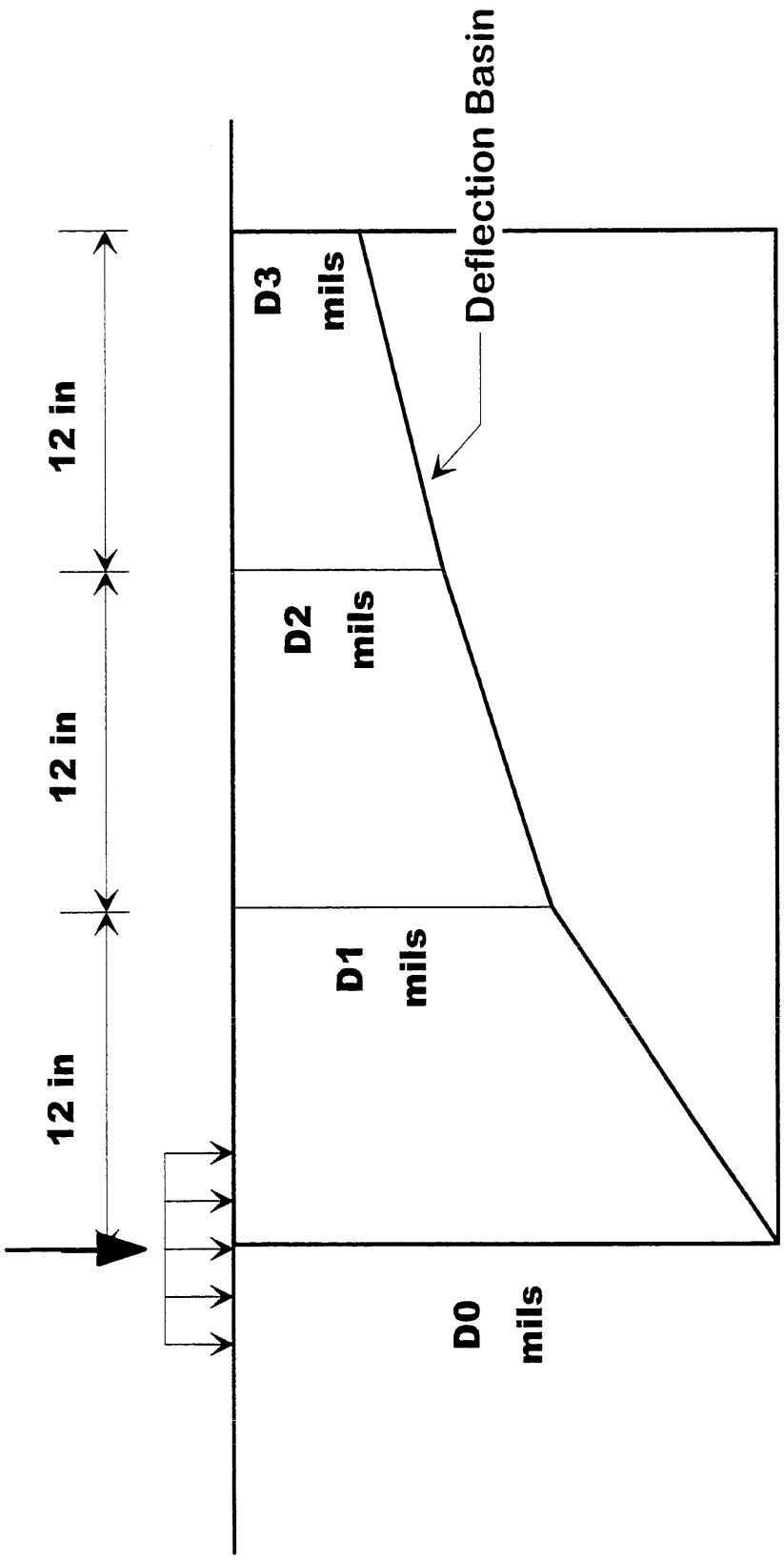

Figure 6.4. Deflection Basin and Area under Pavement Profile

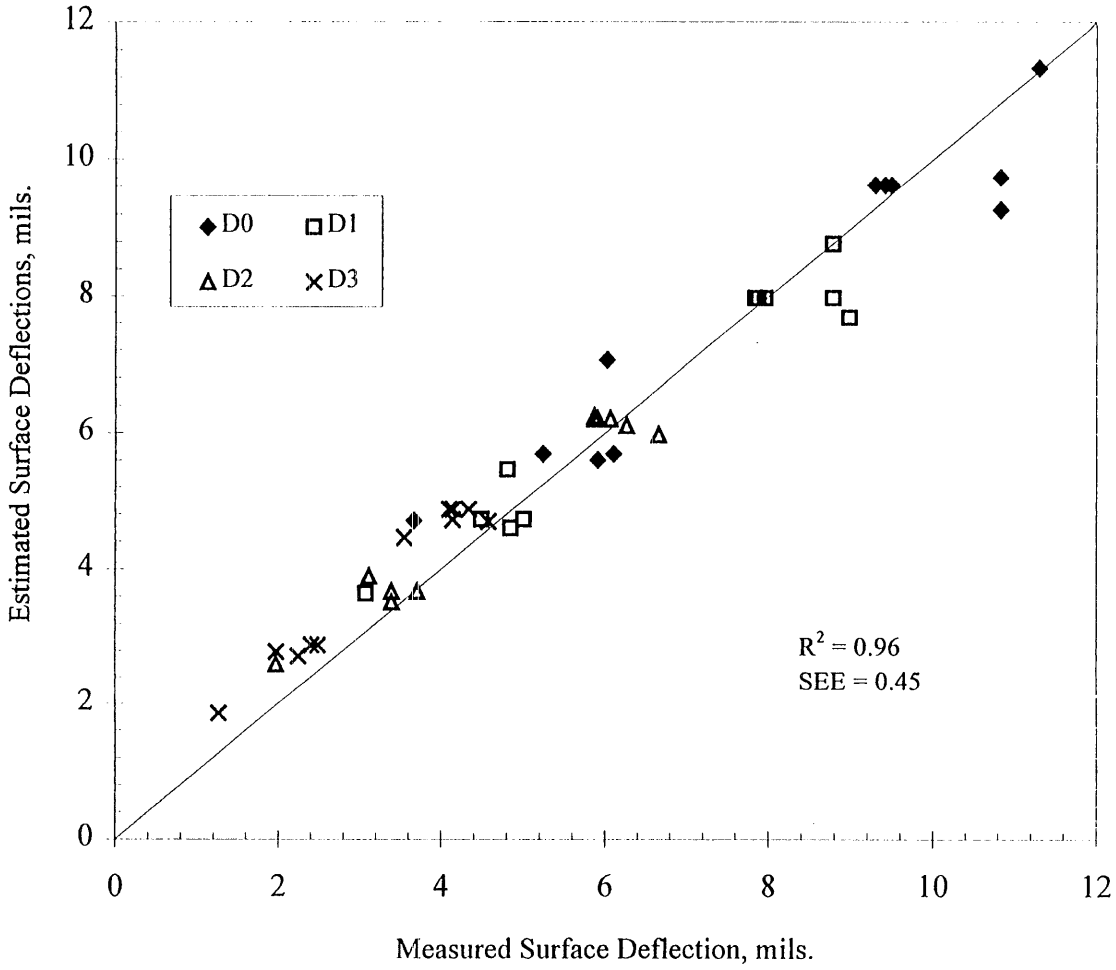

Figure 6.5. Measured versus Estimated Surface Deflections for FDAC Cell 4.

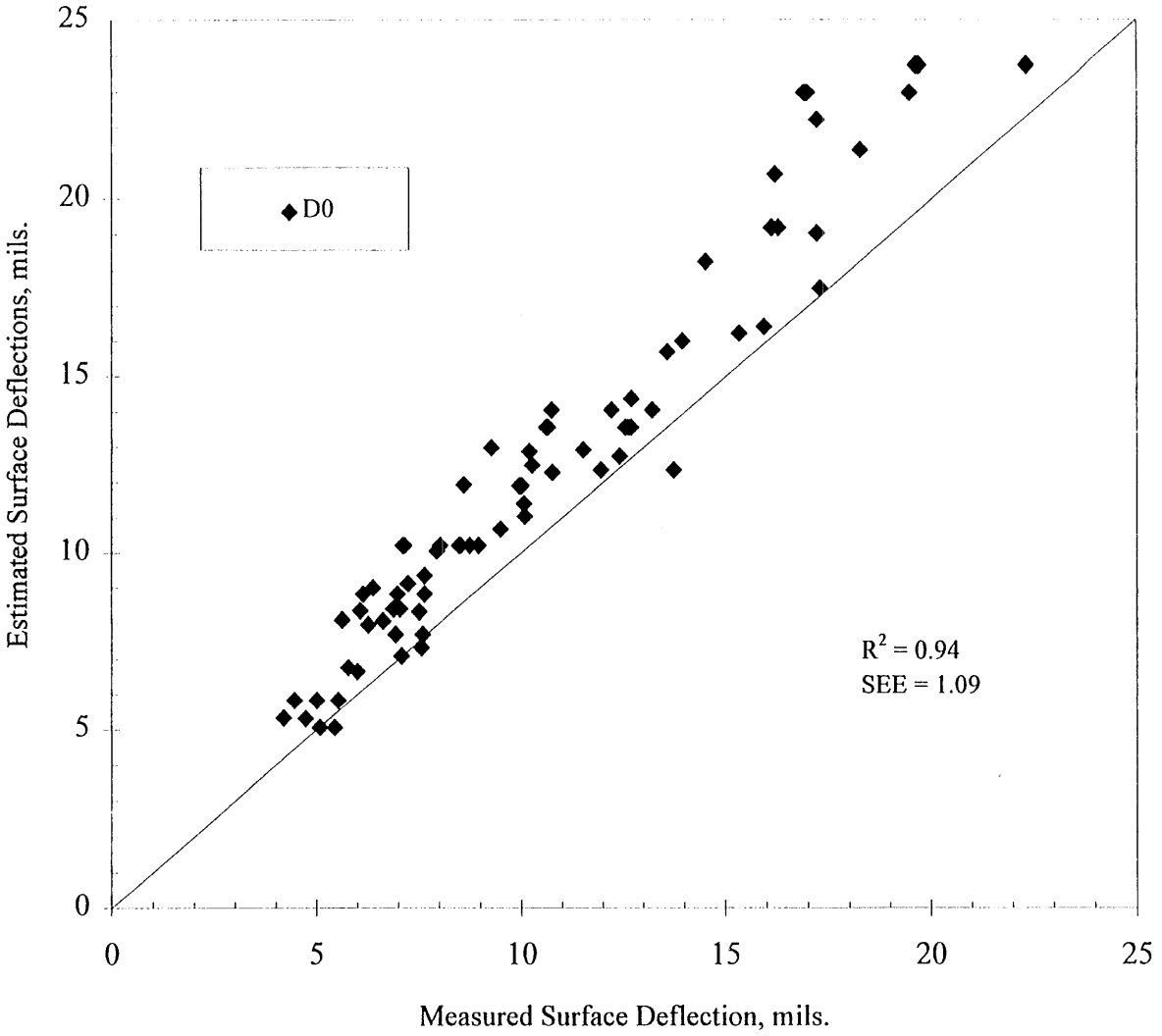

Figure 6.6. Measured versus Estimated Center Deflection for CFP Sections.

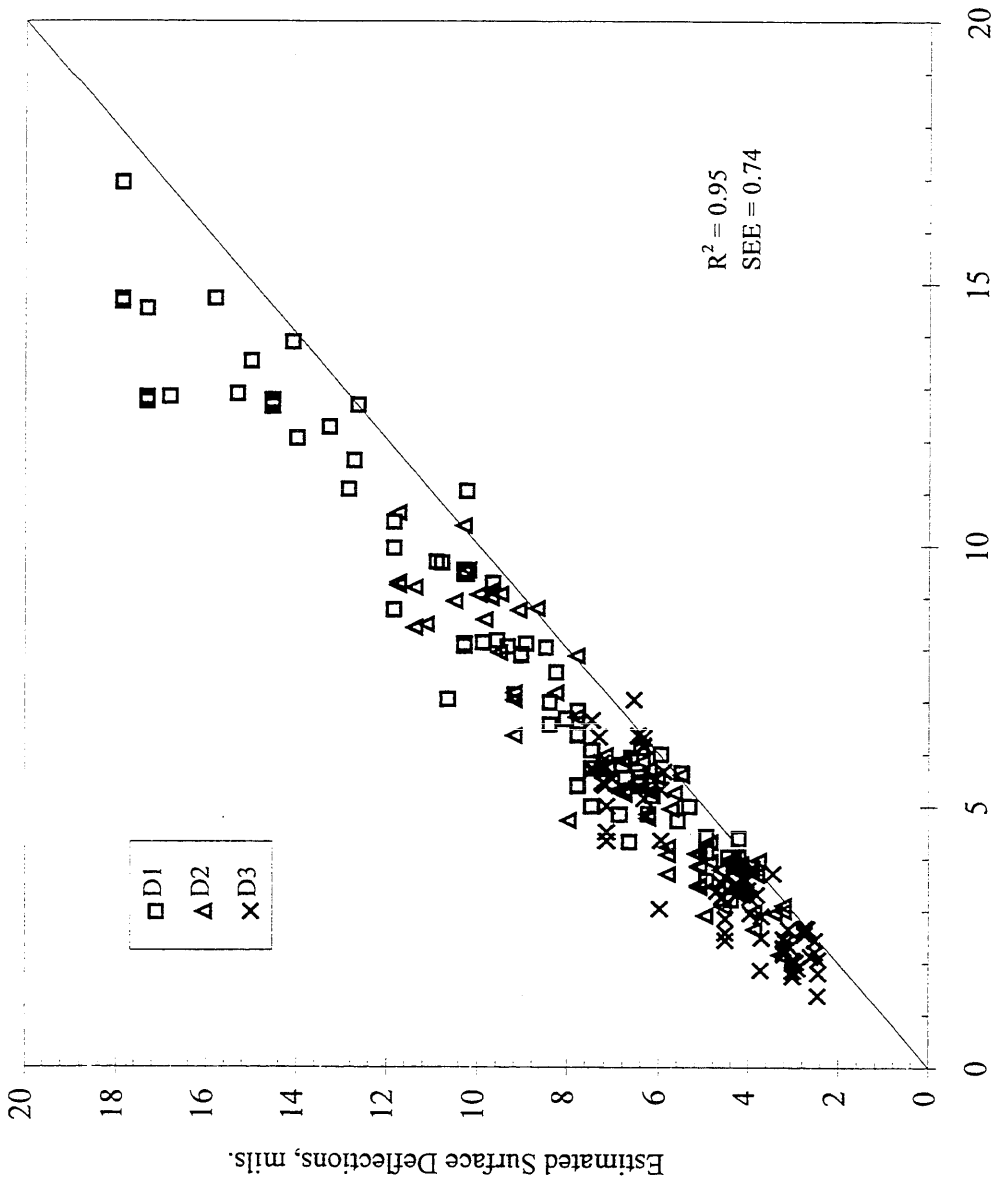

Figure 6.7. Measured versus Estimated Surface Deflections for CFP Sections.

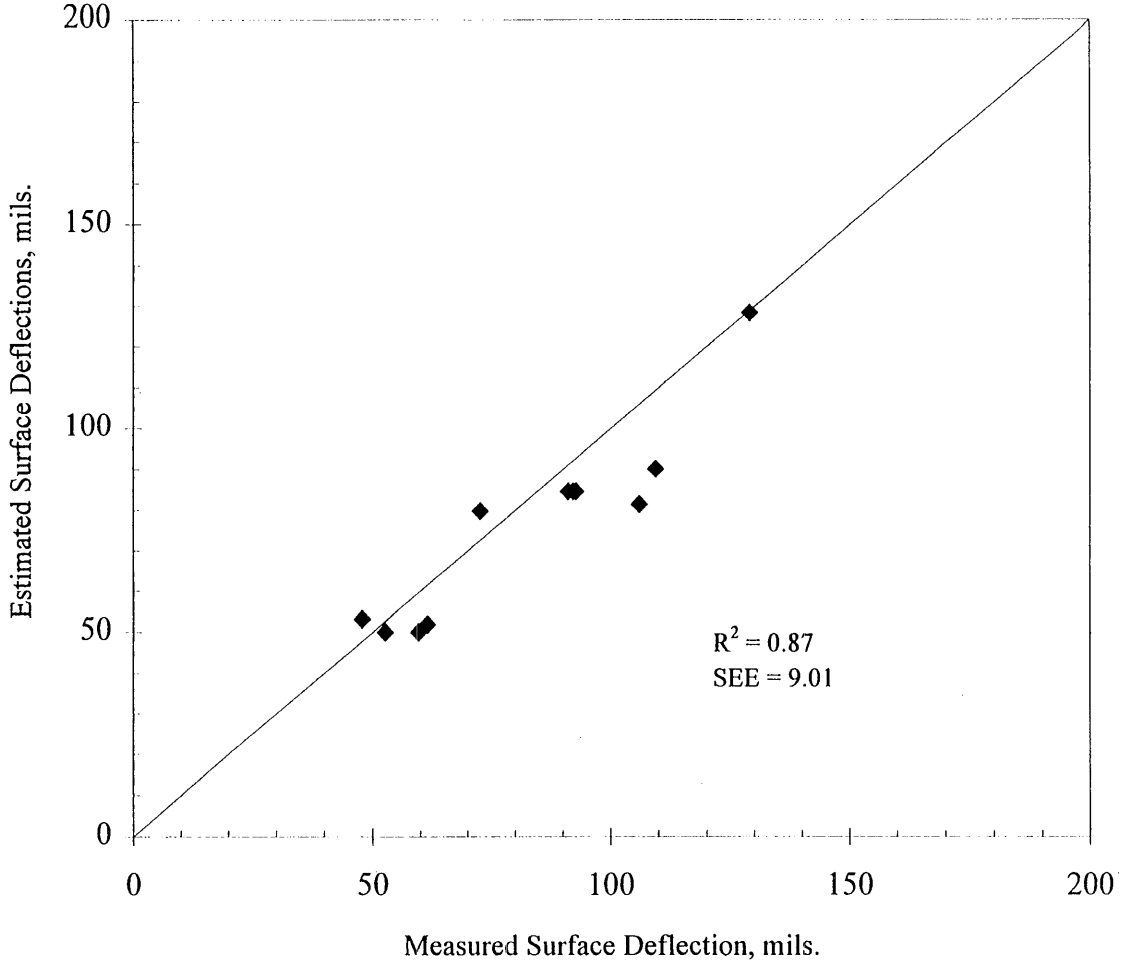

Figure 6.8. Comparison of Measured versus ILLI-PAVE Estimated Strain for Cell 4.

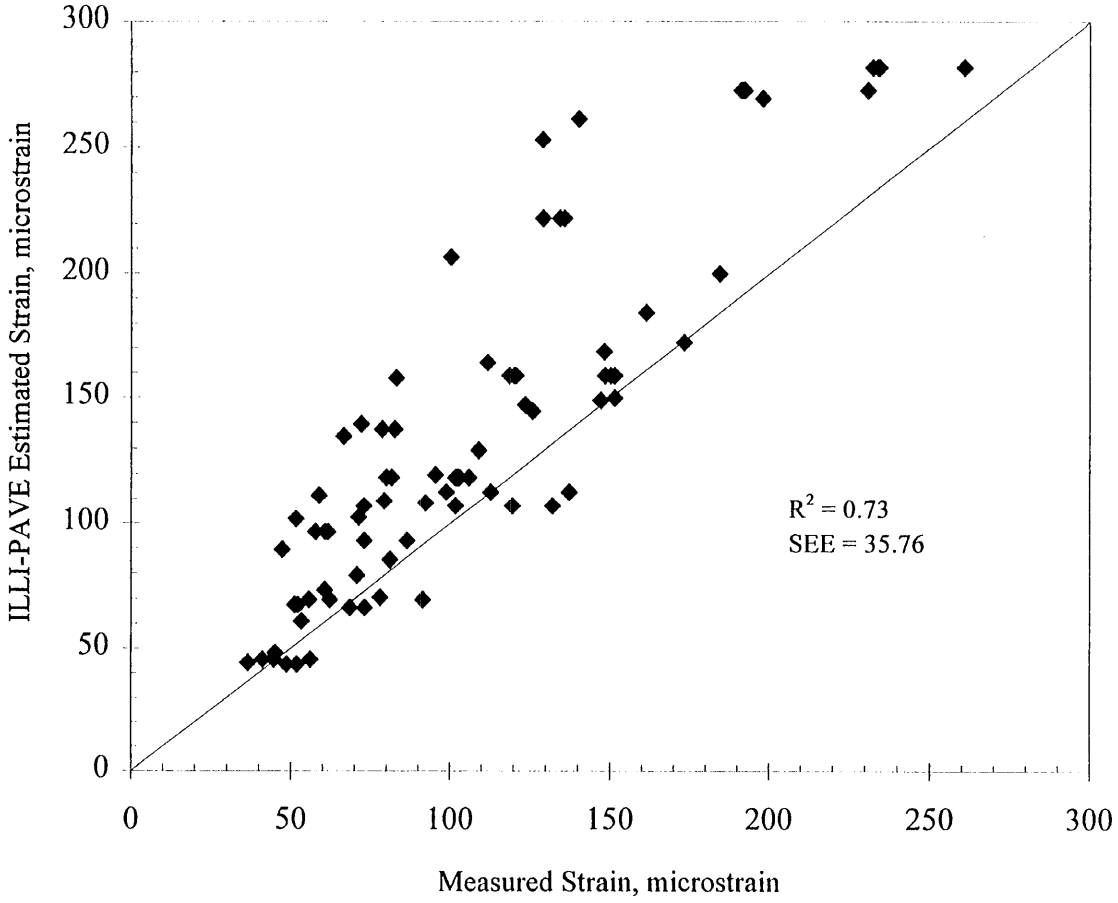

Figure 6.9. Measured versus ILLI-PAVE Estimated Strain for CFP Sections.

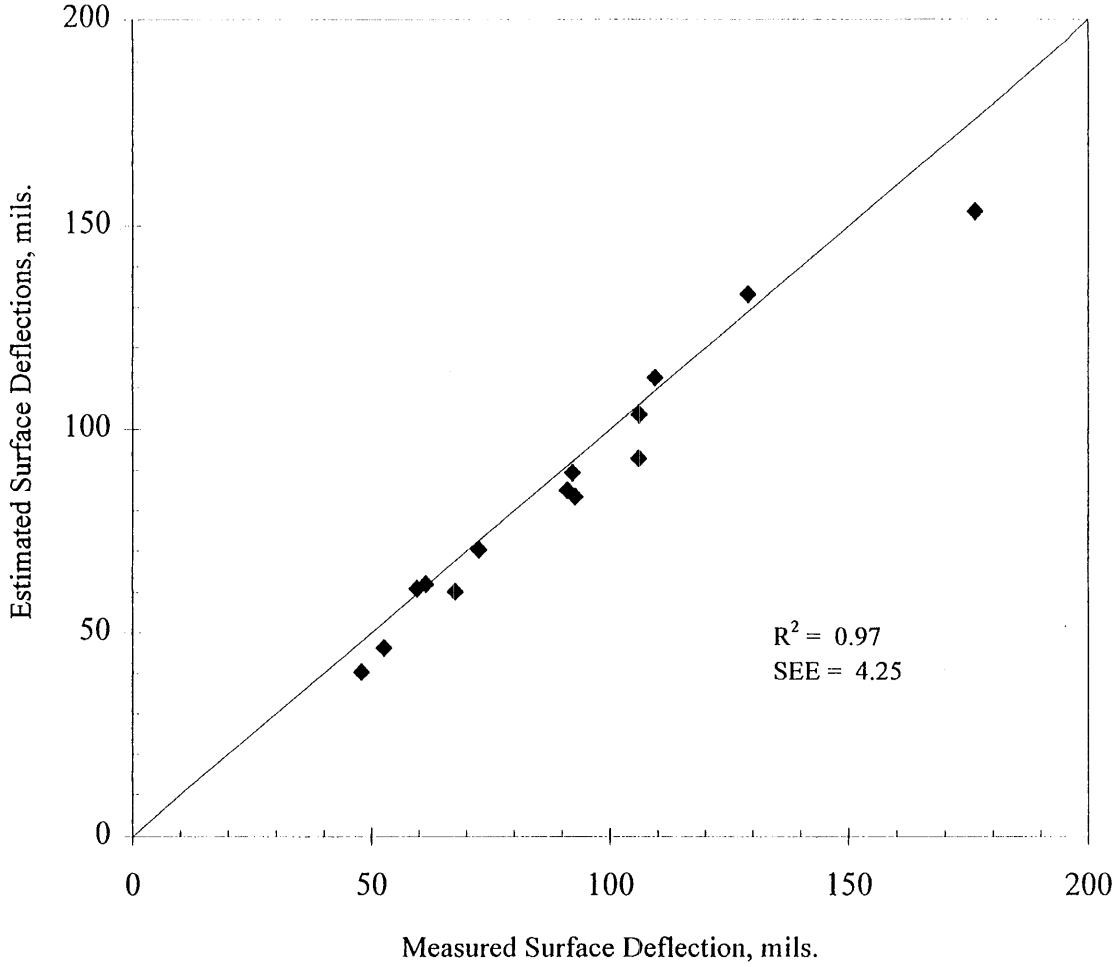

Figure 6.10 a) Comparison of Measured versus AUPP Estimated Horizontal Strain for Cell 4.

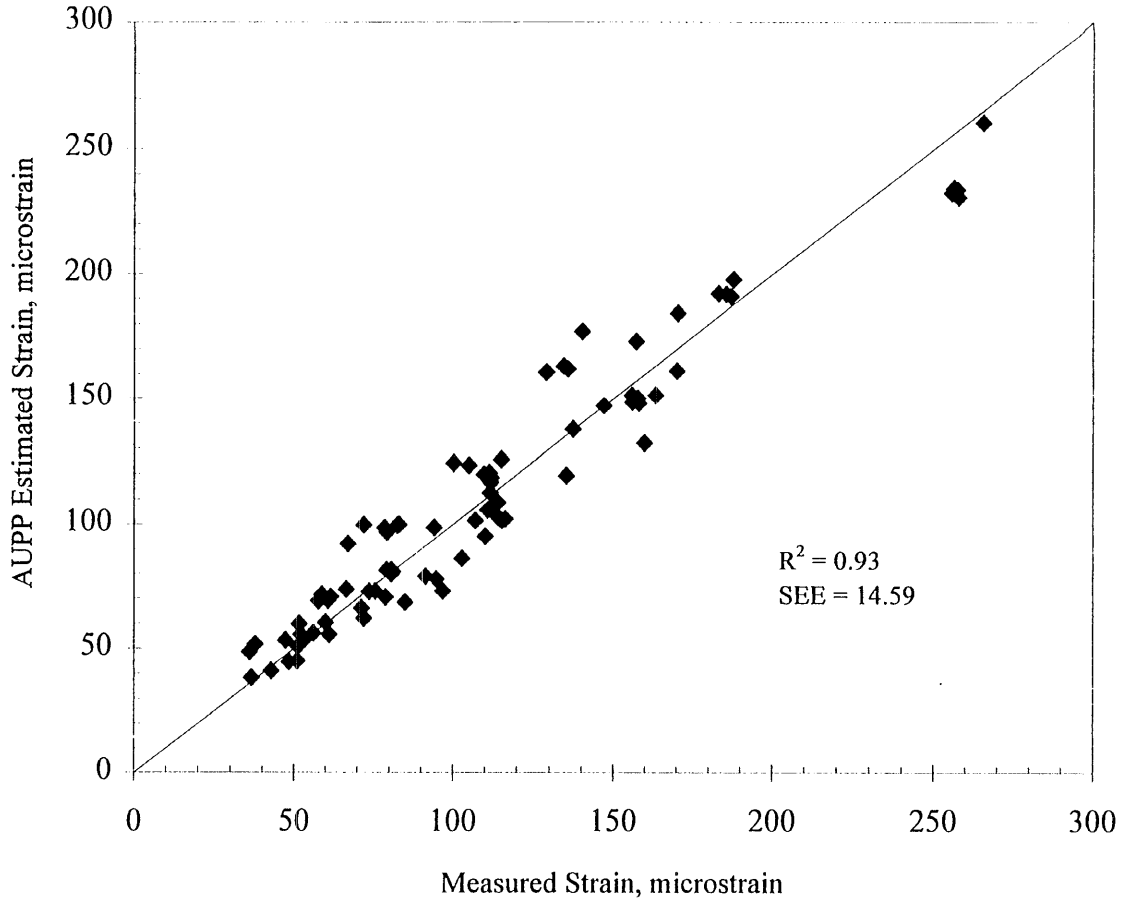

Figure 6.10 b) Comparison of Measured versus AUPP Estimated Horizontal Strain for CFP Sections.

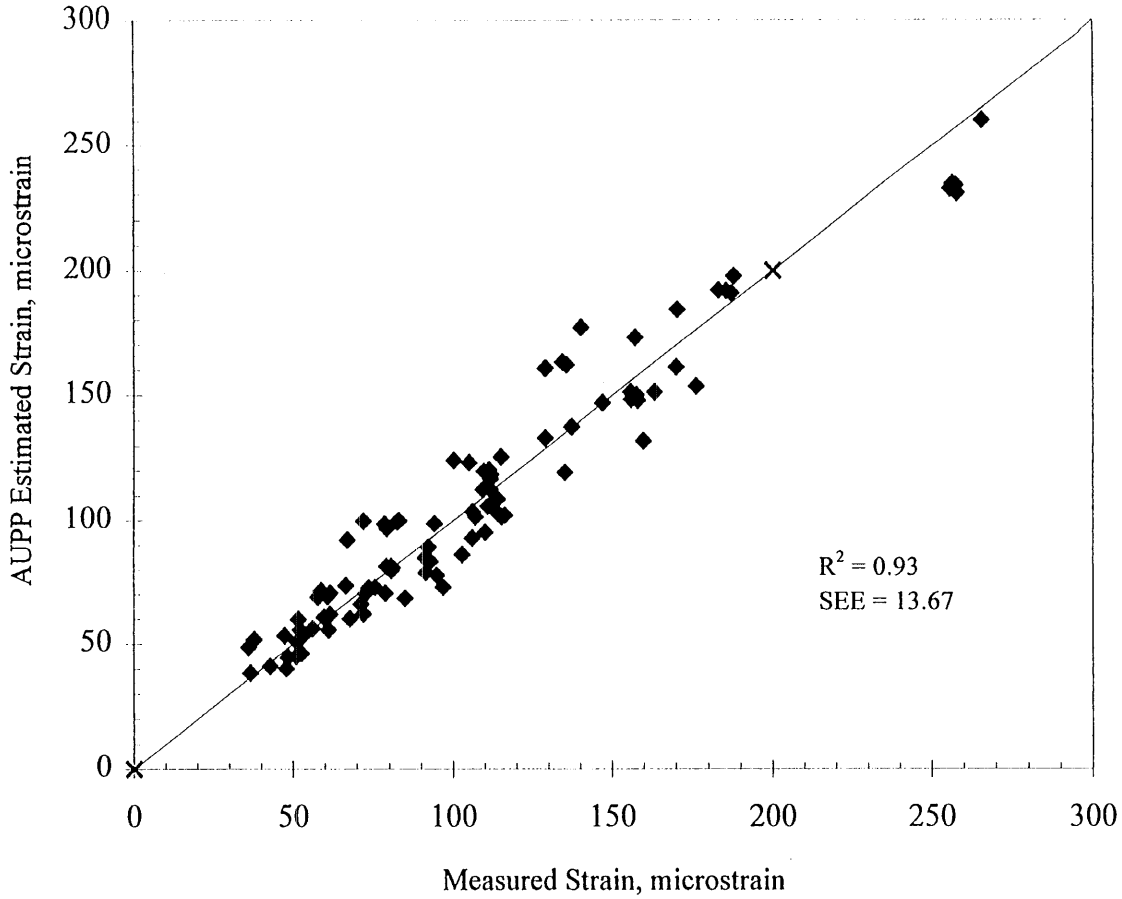

Figure 6.11. Comparison of Measured versus AUPP Estimated Horizontal Strain for all Cells.

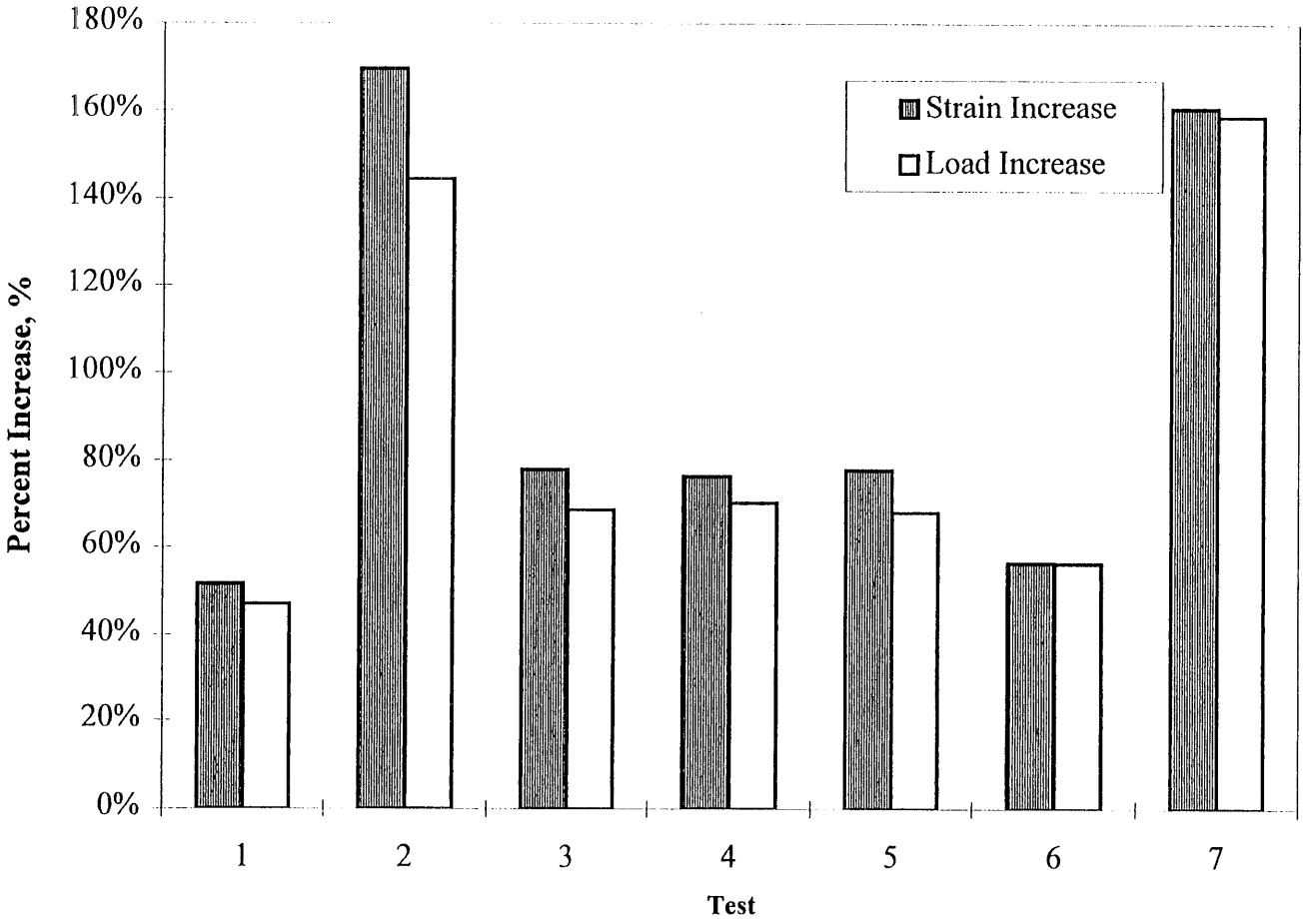

Figure 6.12. Comparison of AC Strain Increase caused by Load Increase for Cell 4.

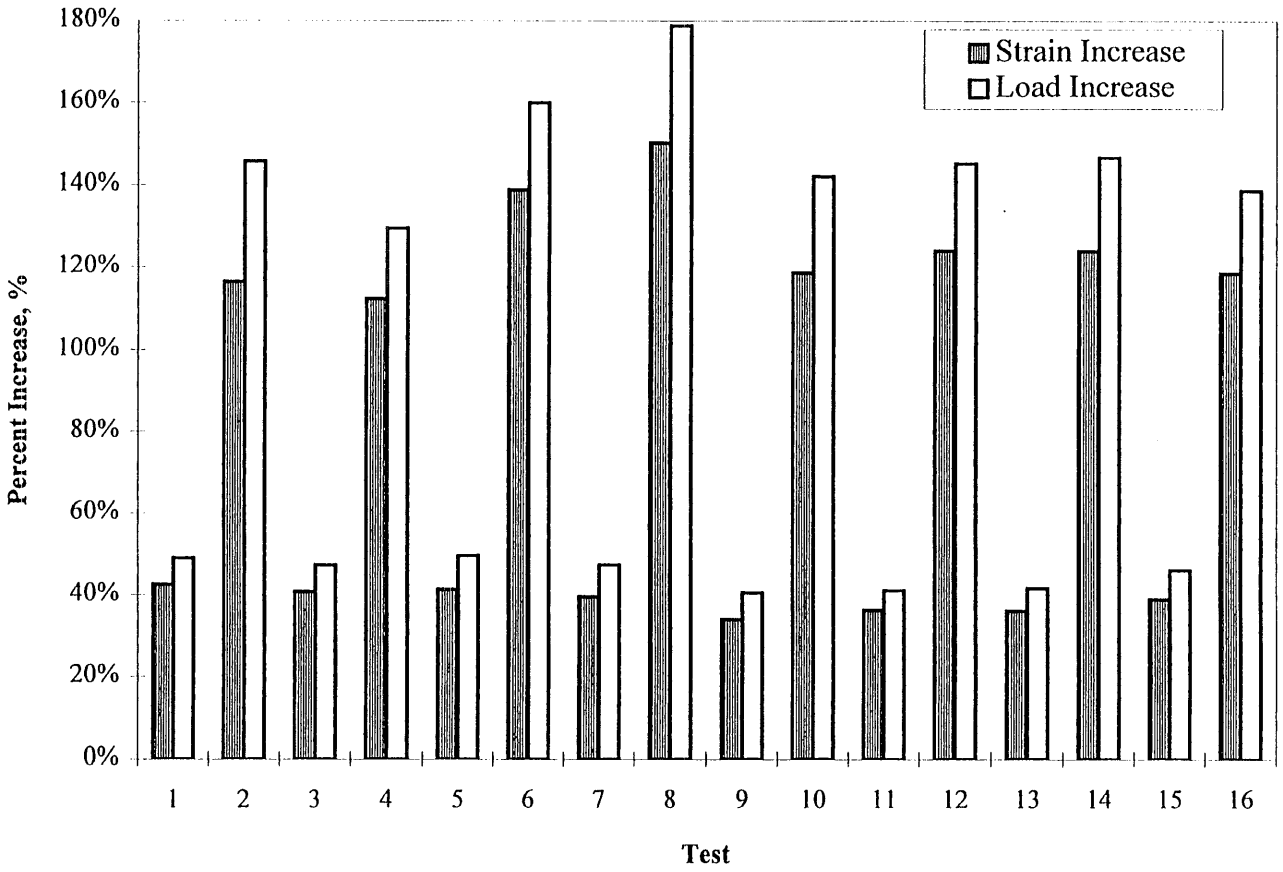

Figure 6.13. Comparison of AC Strain Increase caused by Load Increase for Cell 18.

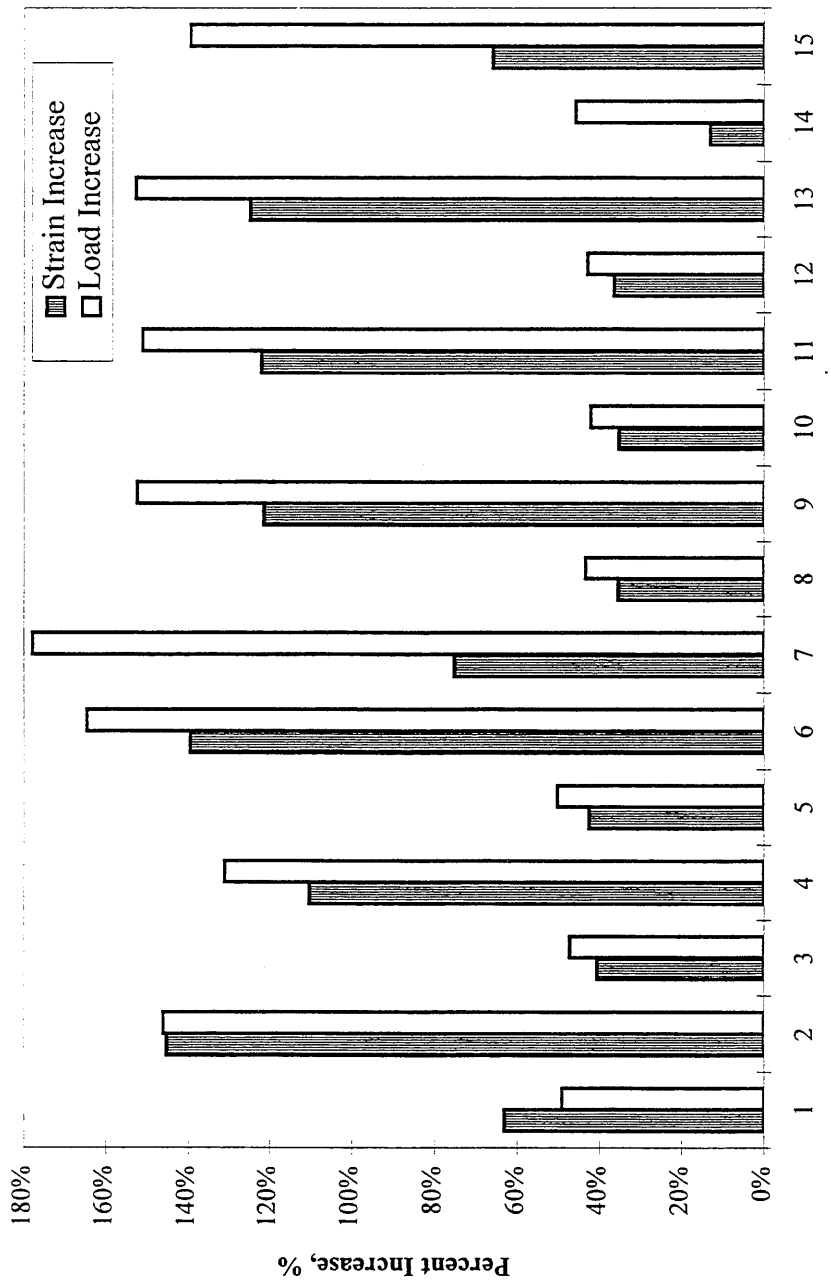

Figure 6.14. Comparison of AC Strain Increase caused by Load Increase for Cell 19.

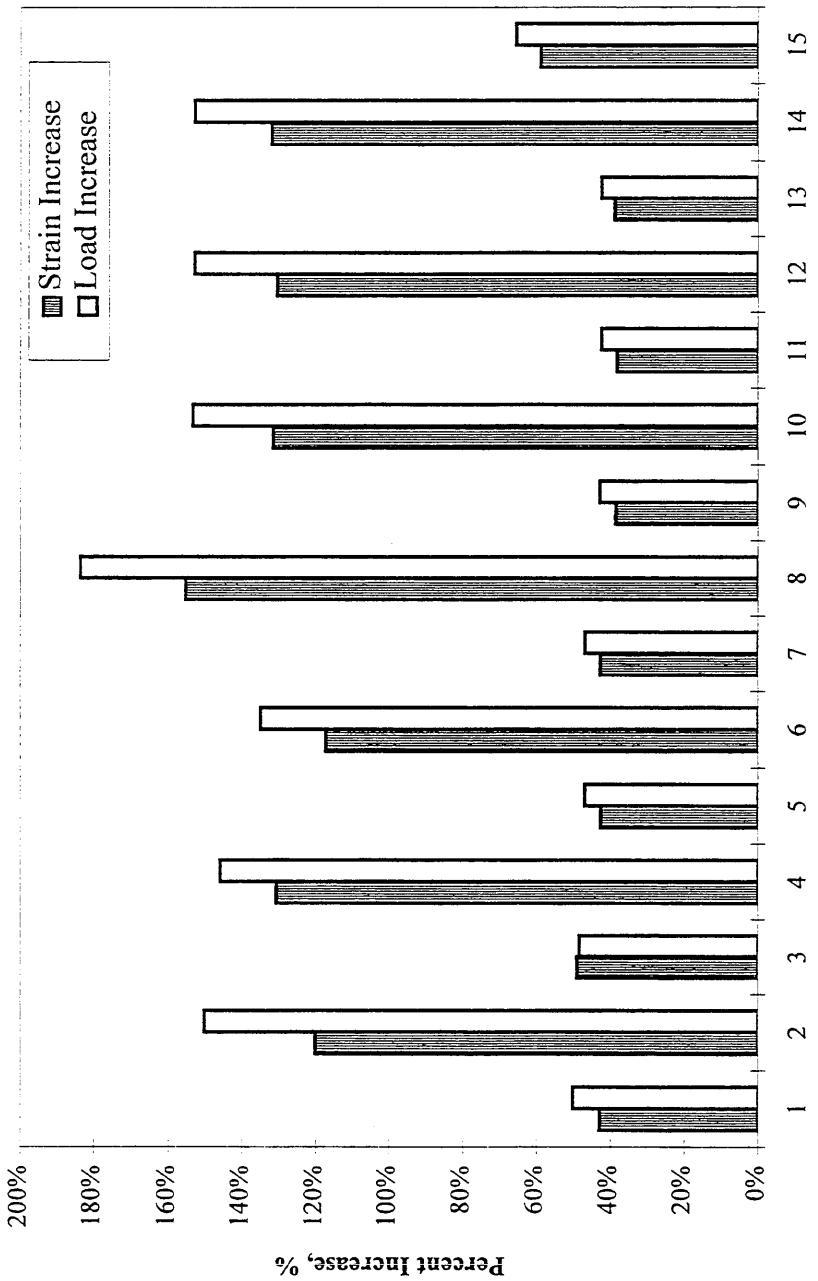

Figure 6.15. Comparison of AC Strain Increase caused by Load Increase for Cell 20.

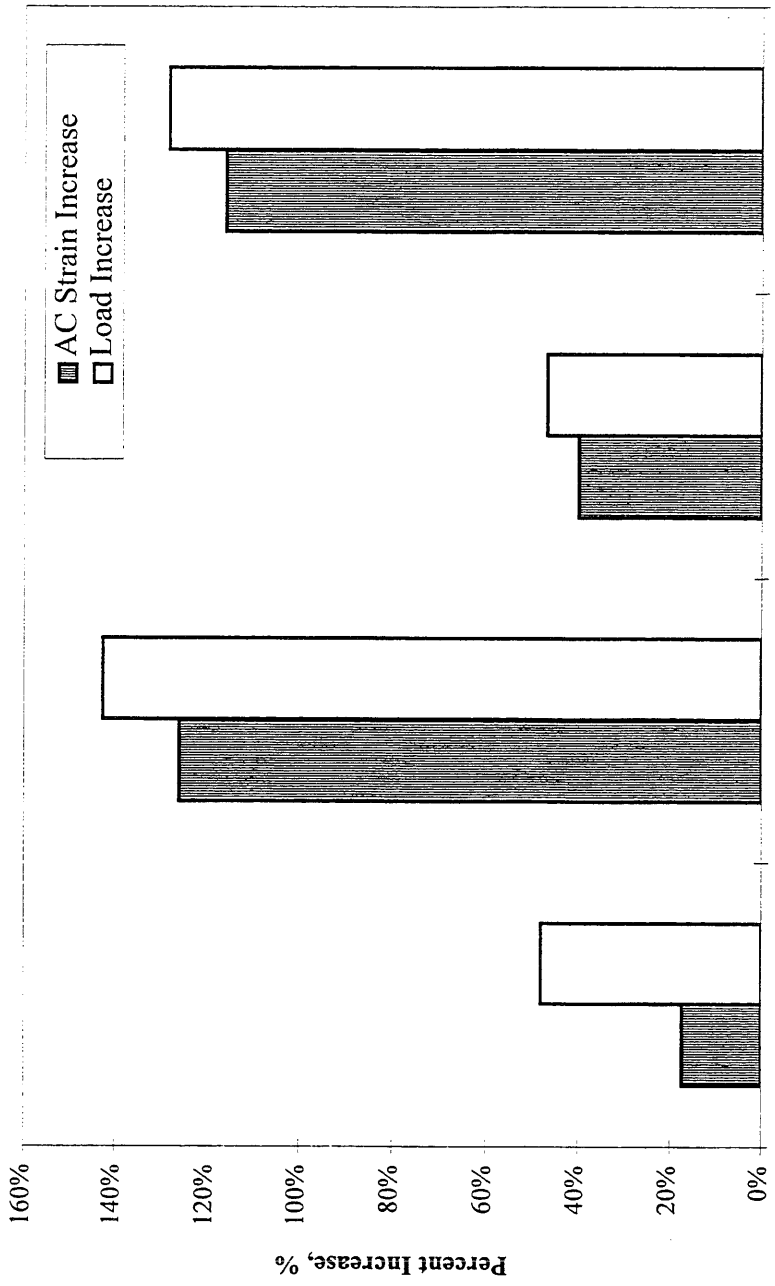

Figure 6.16. Comparison of AC Strain Increase caused by Load Increase for Cell 22.

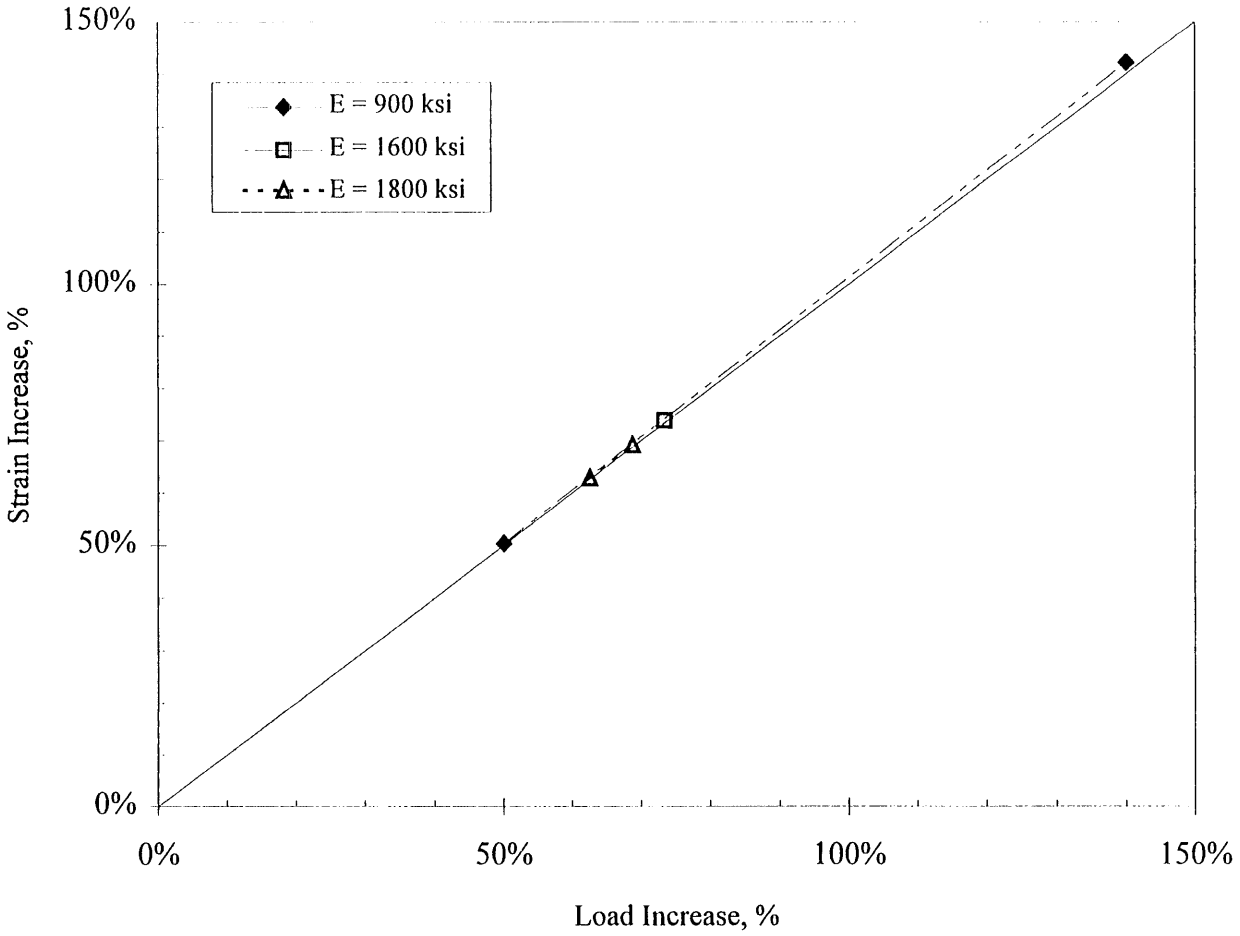

Figure 6.17. ILLI-PAVE Based AC Strain -Load Increase Relation for Cell 4.

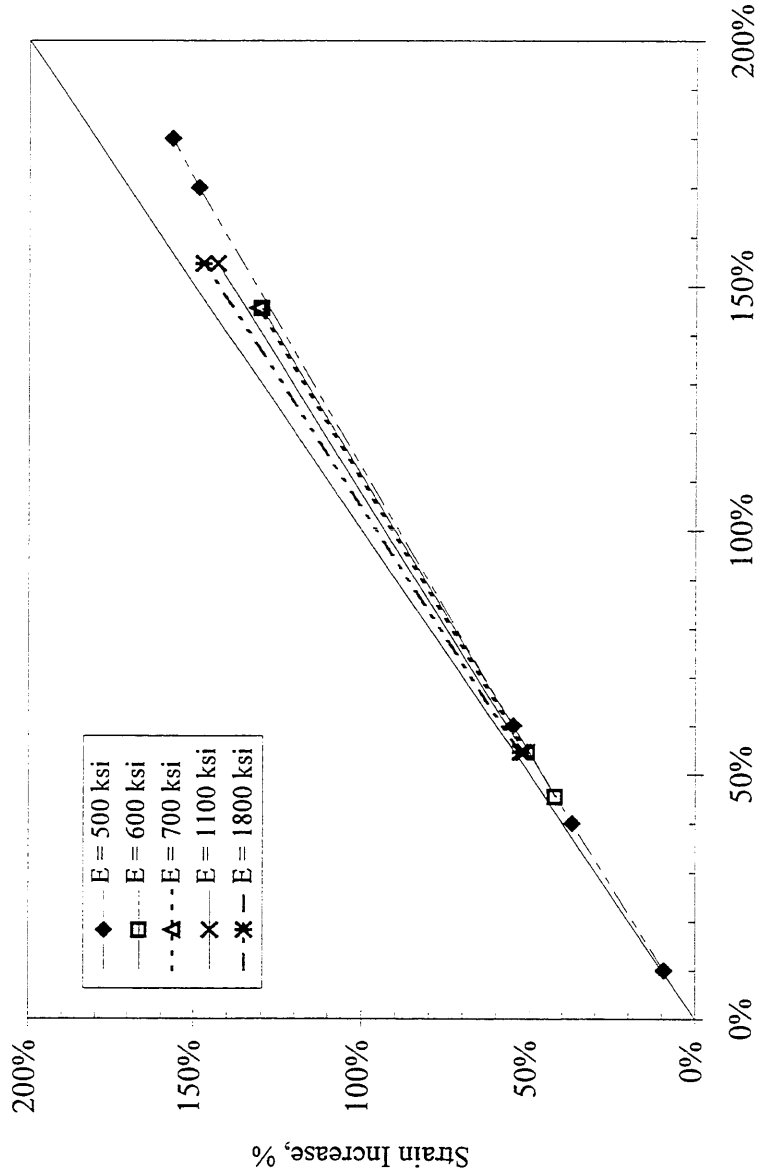

Figure 6.18. ILLI-PAVE Based AC Strain -Load Increase Relation for Cell 18.

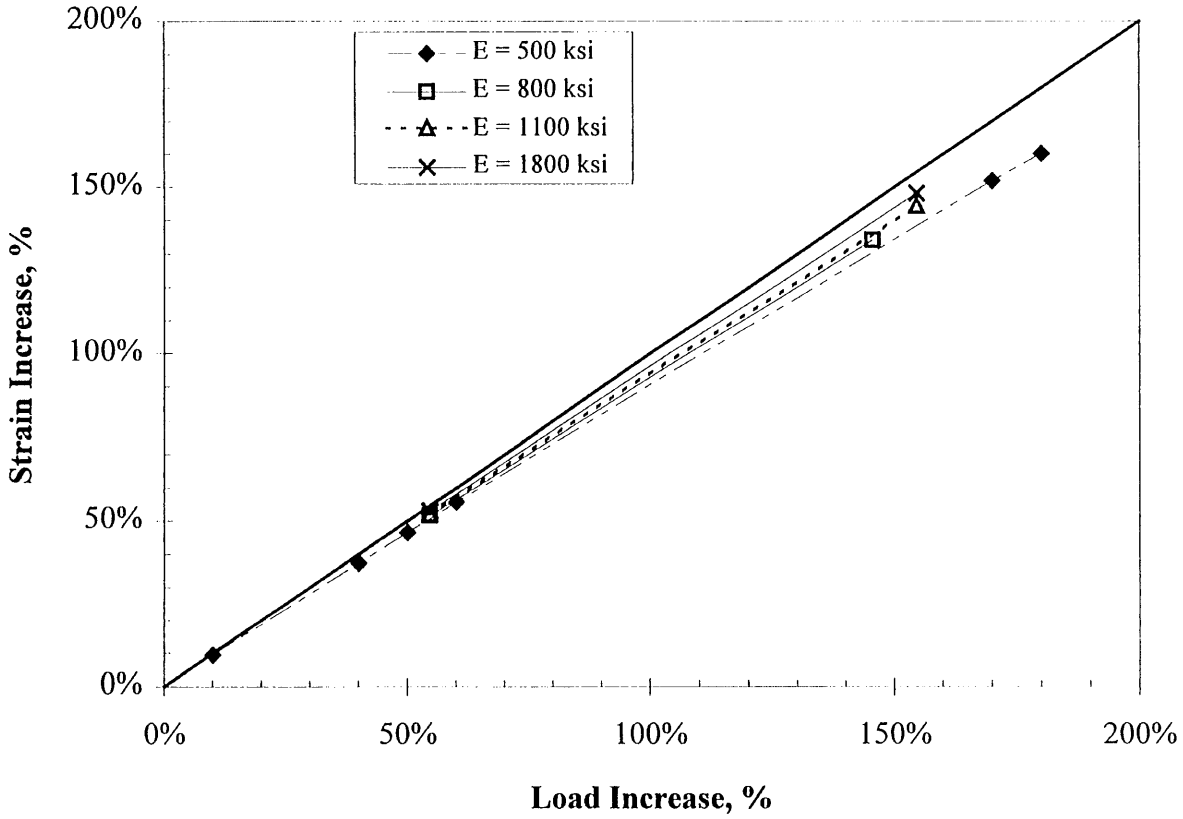

Figure 6.19. ILLI-PAVE Based AC Strain -Load Increase for Cell 19.

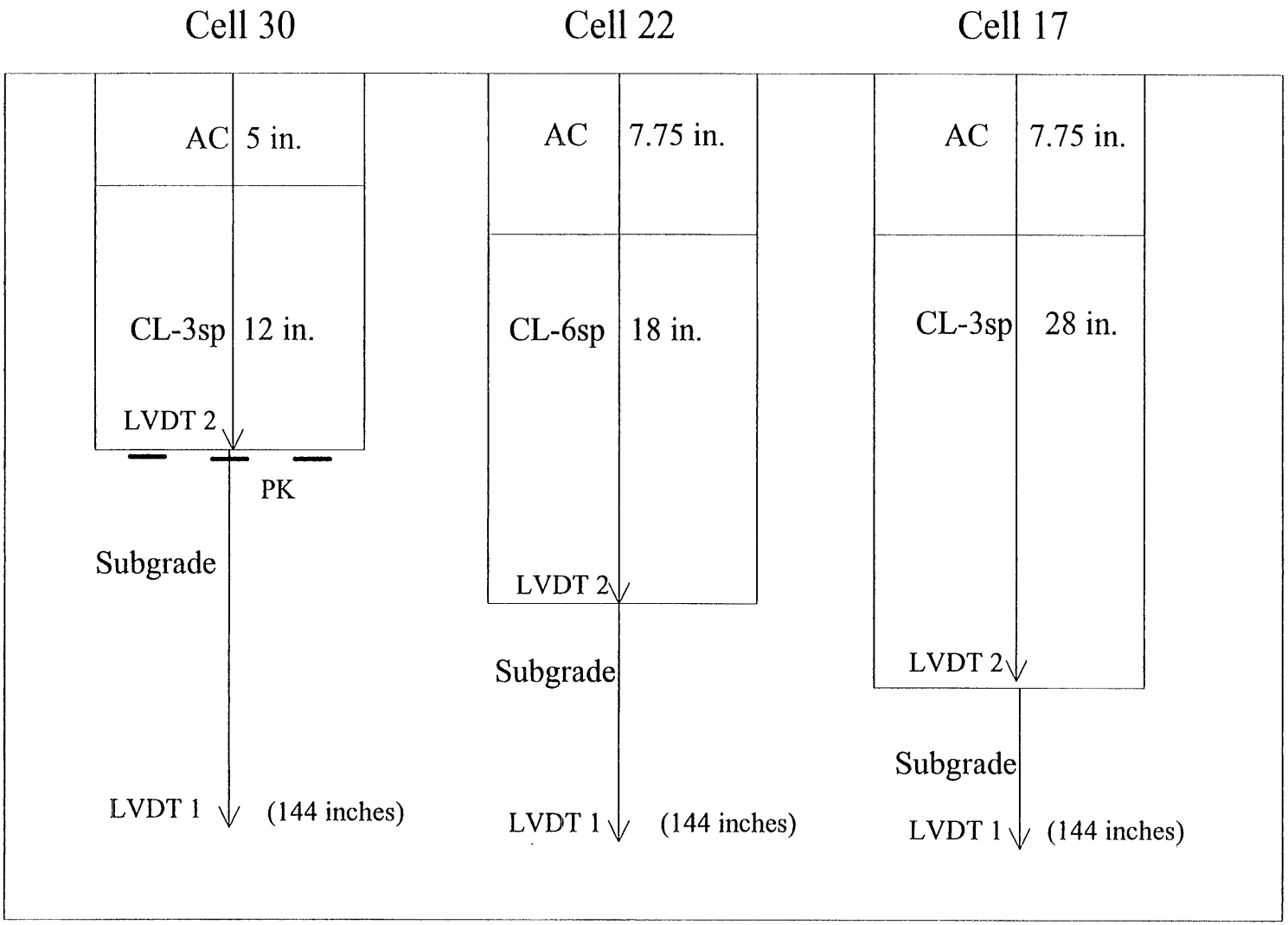

Figure 6.20. Schematic Representation of Cells Tested.

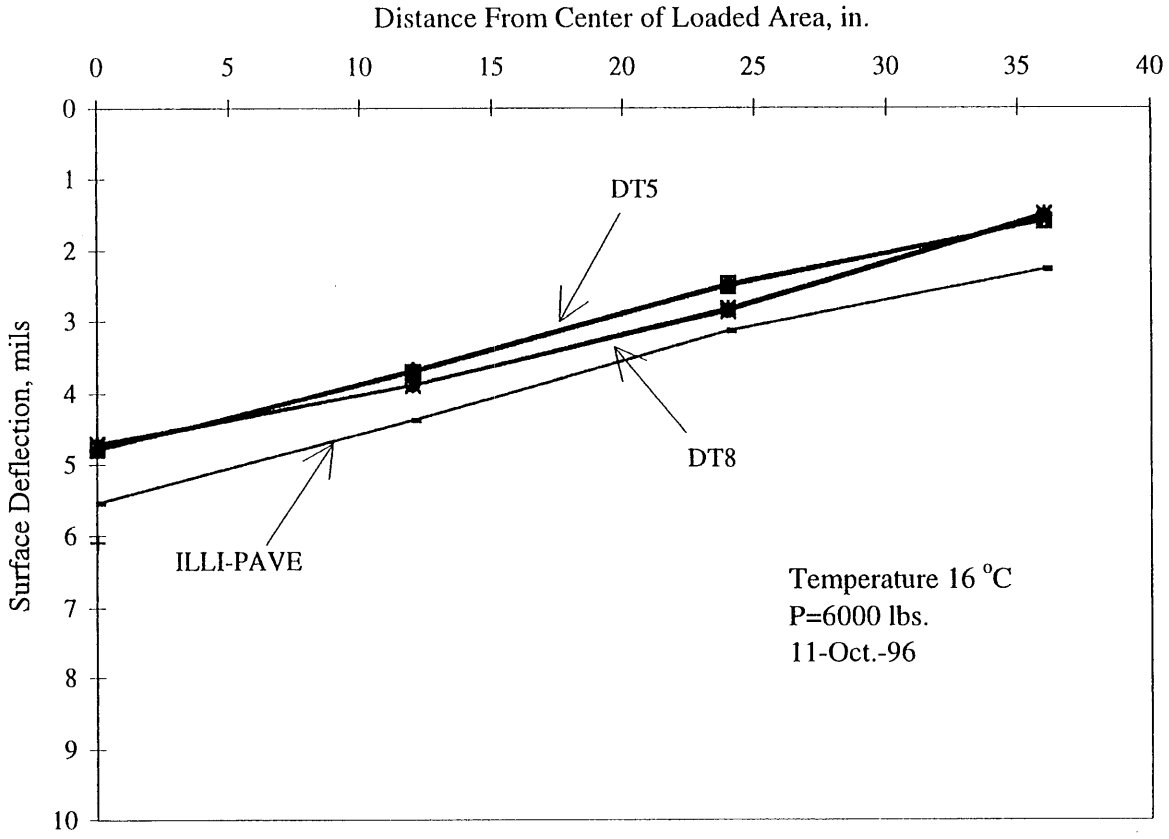

Figure 6.21. Deflection Basin Comparison for LVDT Testing on Cell 17.

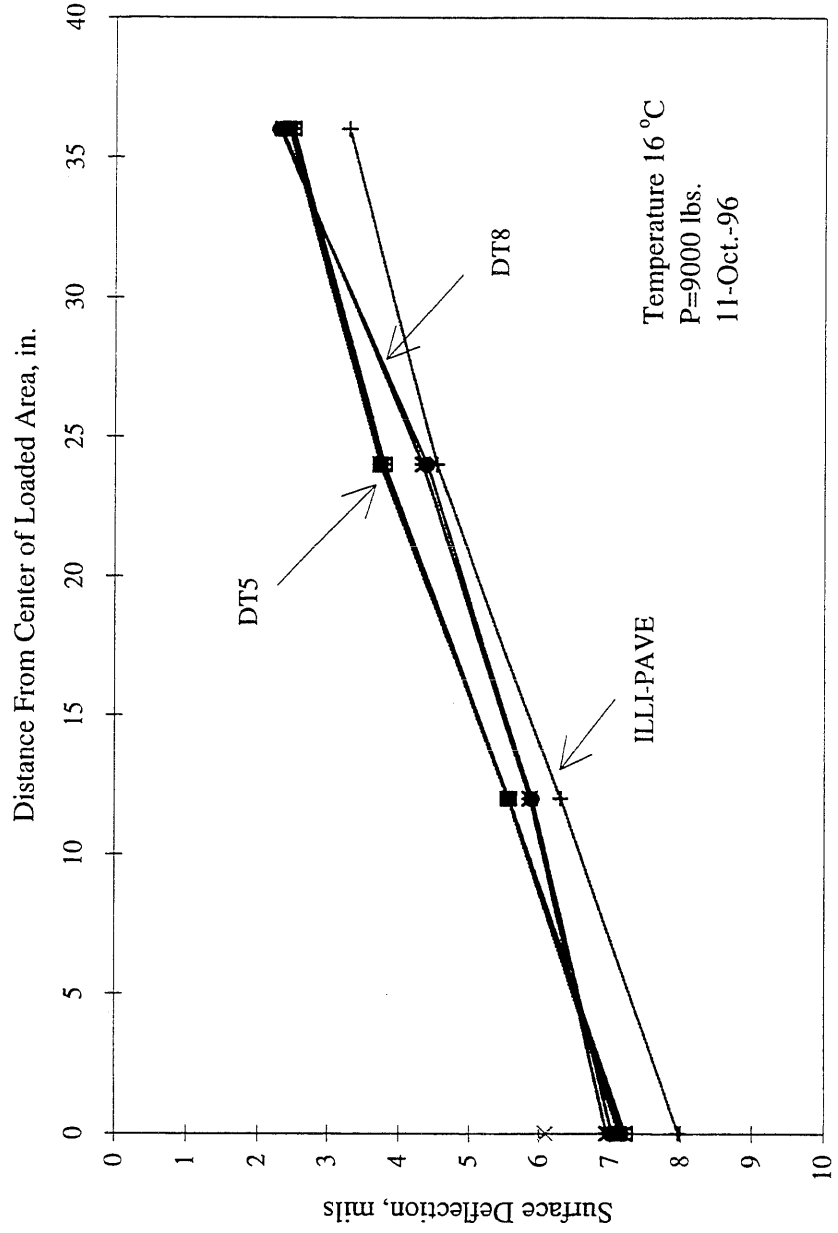

Figure 6.22. Deflection Basin Comparison for LVDT Testing on Cell 17

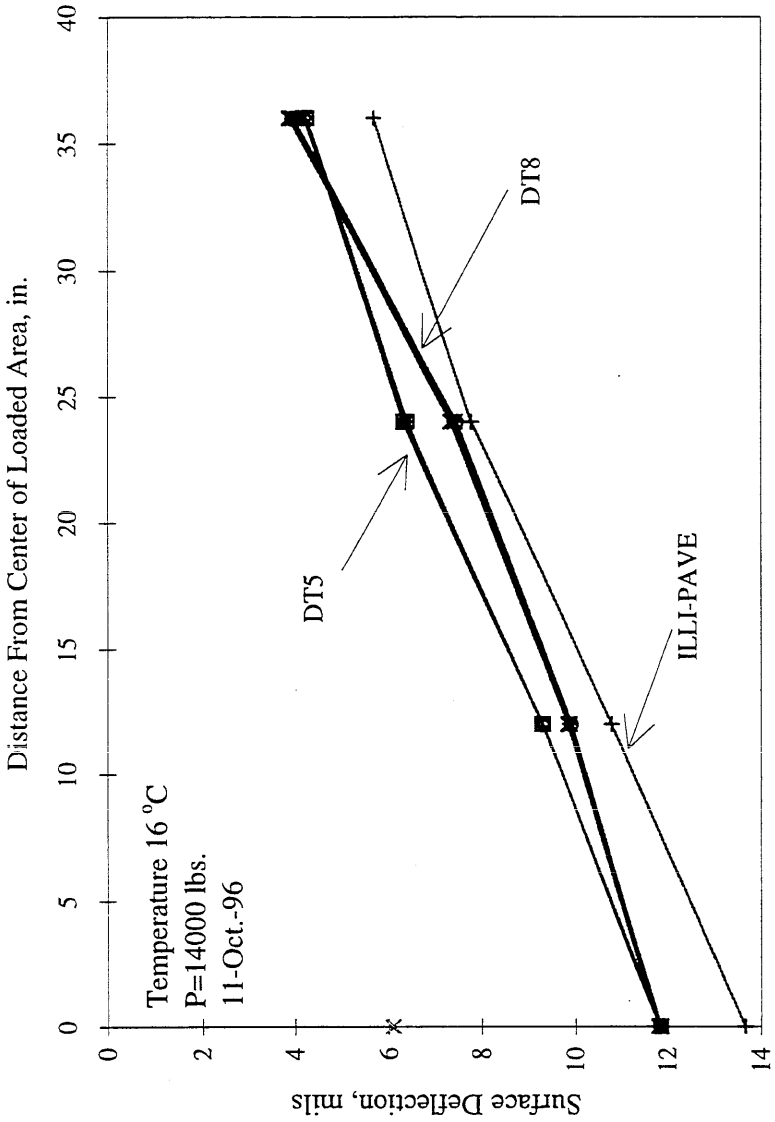

Figure 6.23. Deflection Basin Comparison for LVDT Testing on Cell 17.

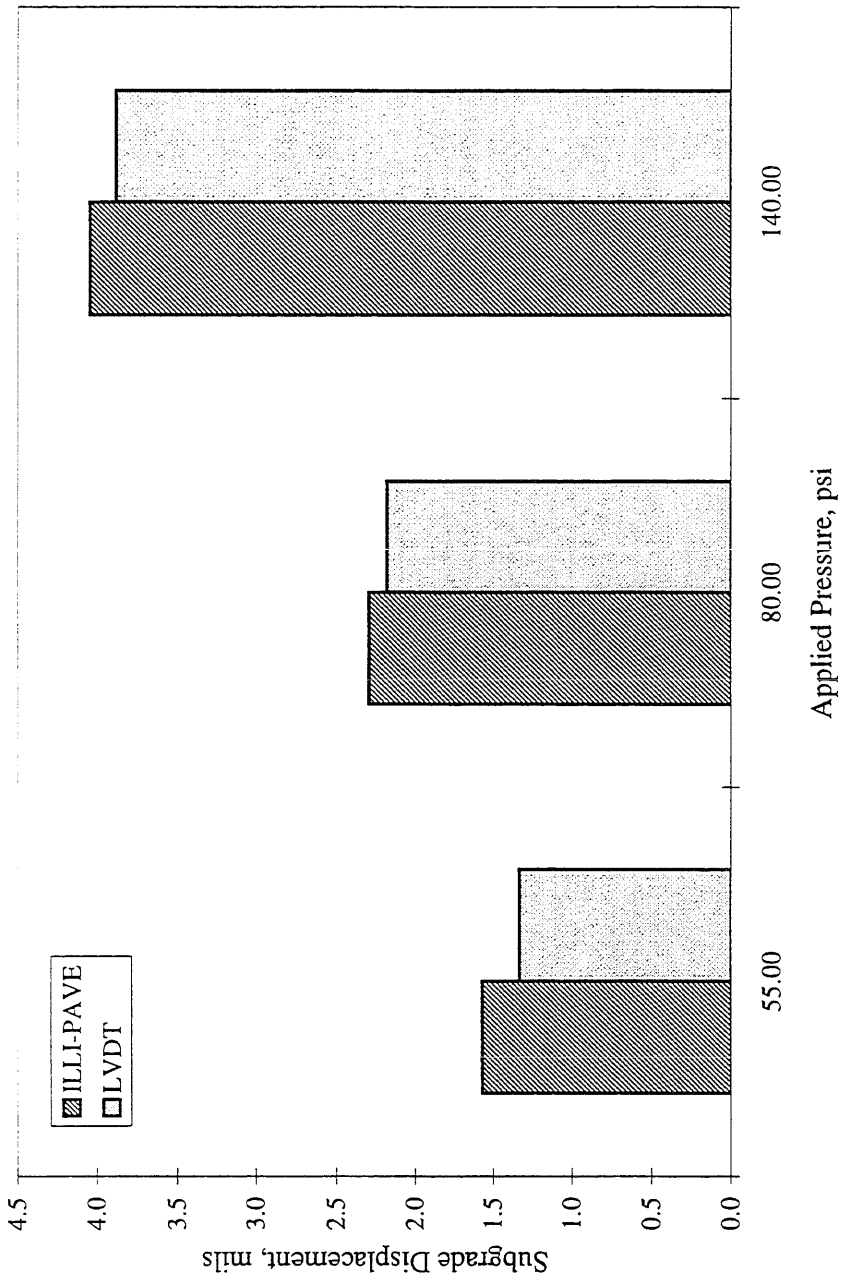

Figure 6.24. Comparison of Field and Estimated Subgrade Displacement for Cell 17.

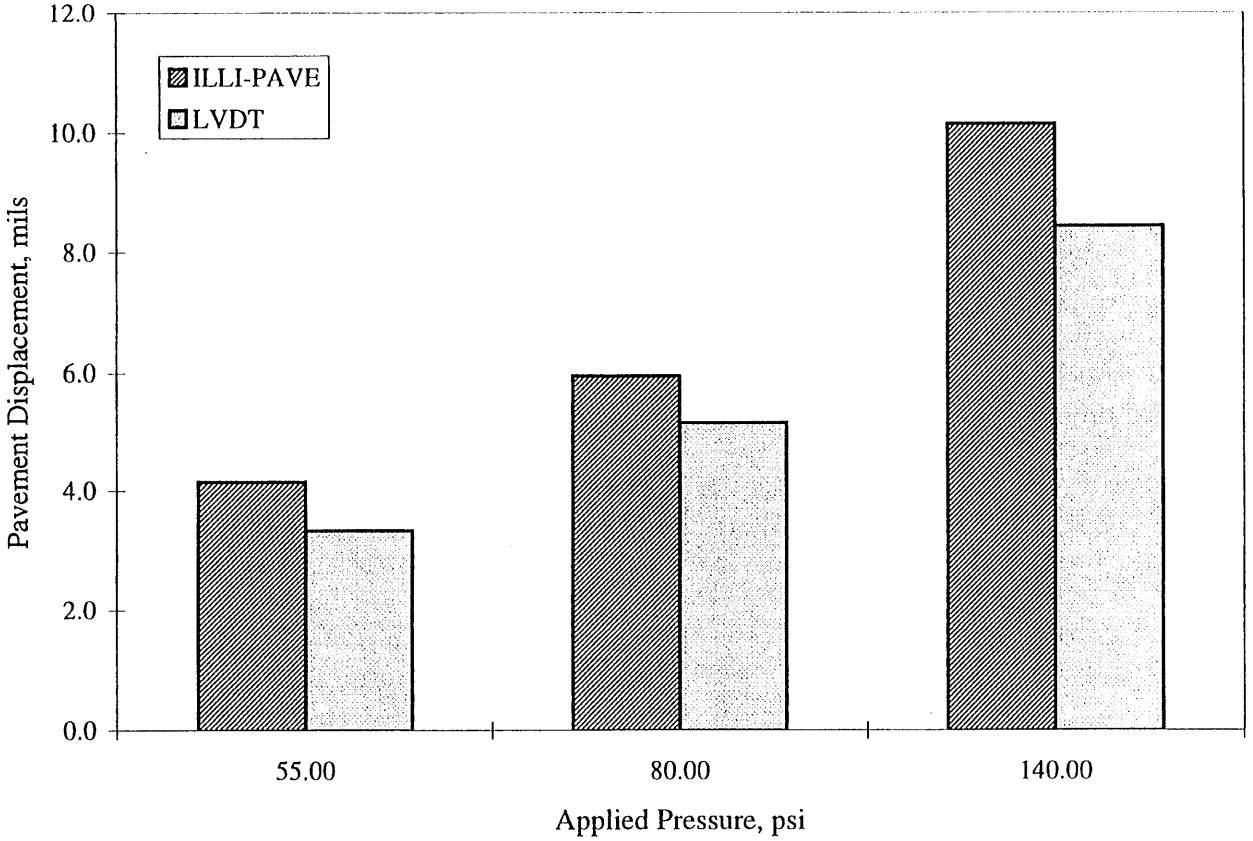

Figure 6.25. Comparison of Field and Estimated Total Pavement Displacement for Cell 17.

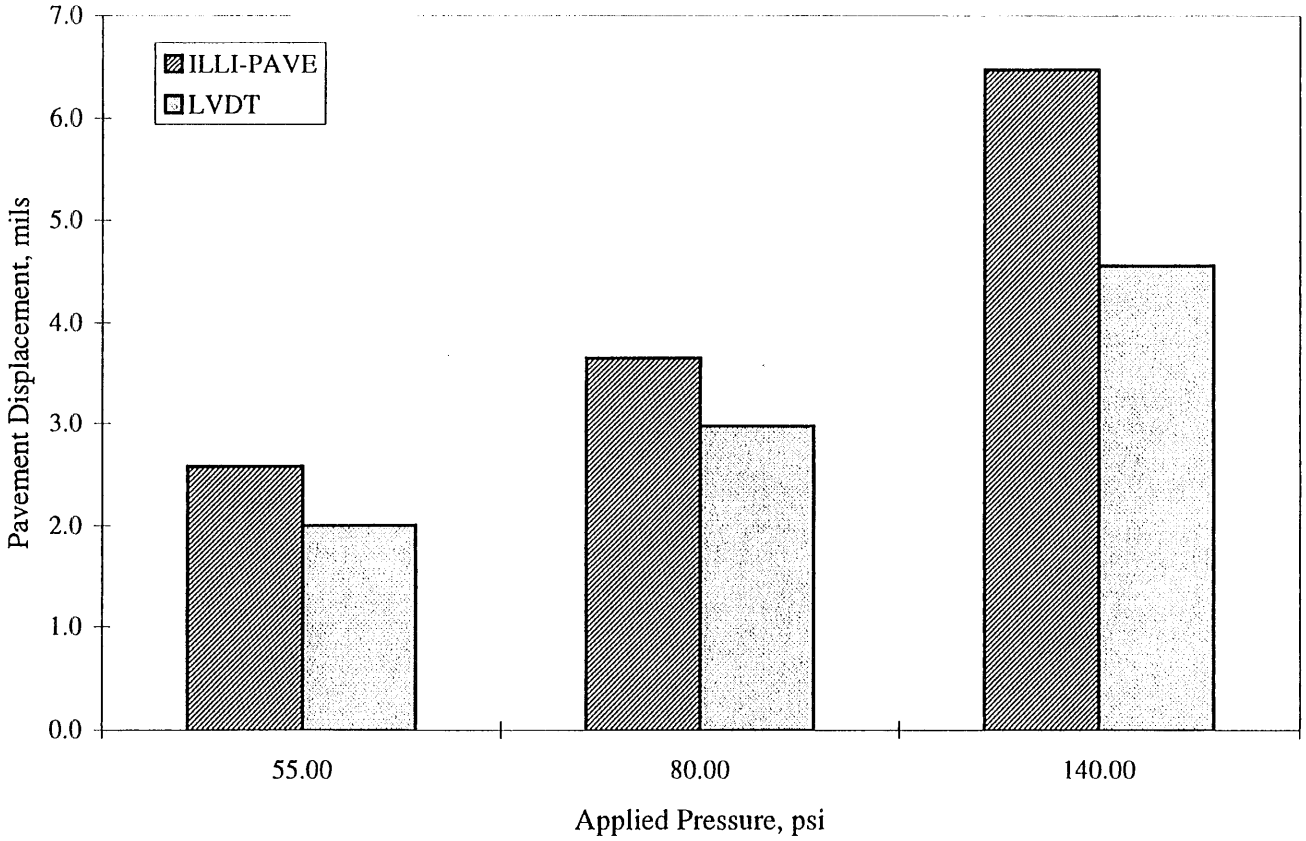

Figure 6.26. Comparison of Field and Estimated Within Pavement Displacement for Cell 17.

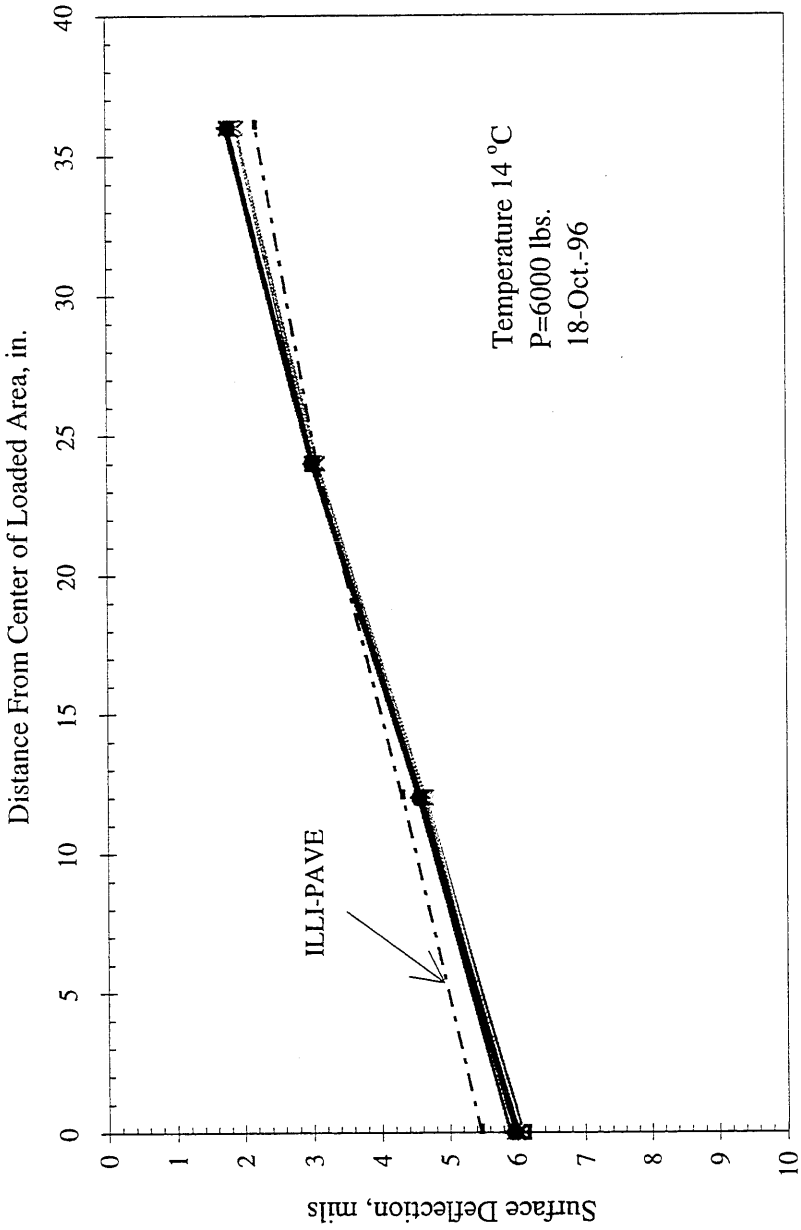

Figure 6.27. Deflection Basin Comparison for LVDT Testing on Cell 22.

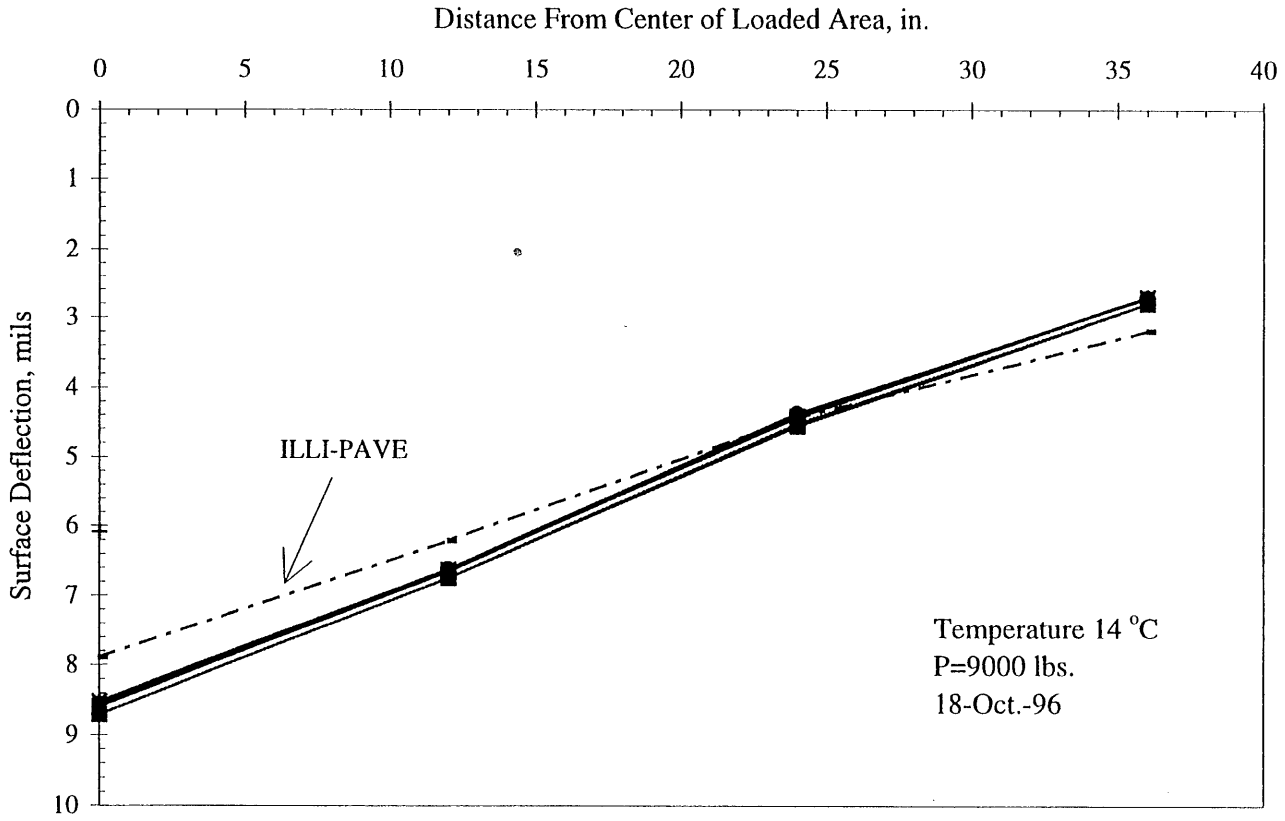

Figure 6.28. Deflection Basin Comparison for LVDT Testing on Cell 22.

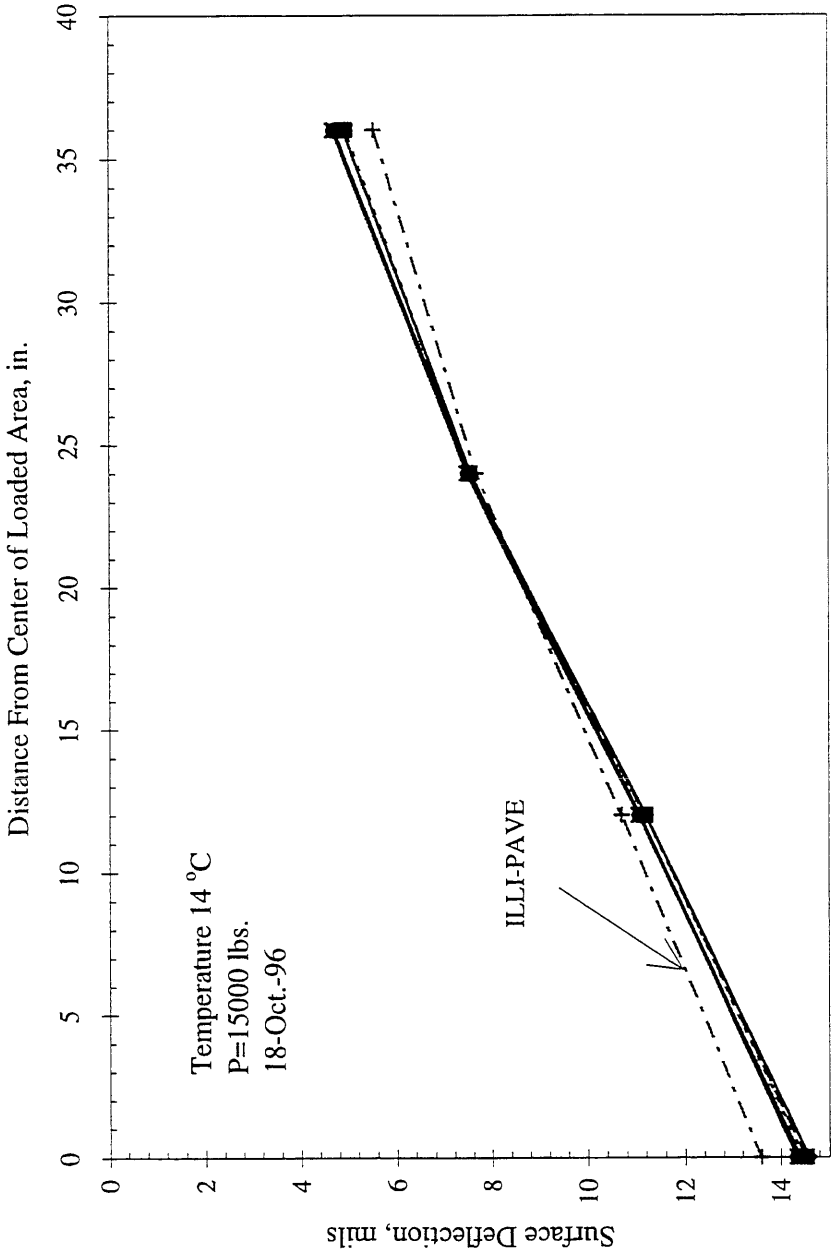

Figure 6.29. Deflection Basin Comparison for LVDT Testing on Cell 22.

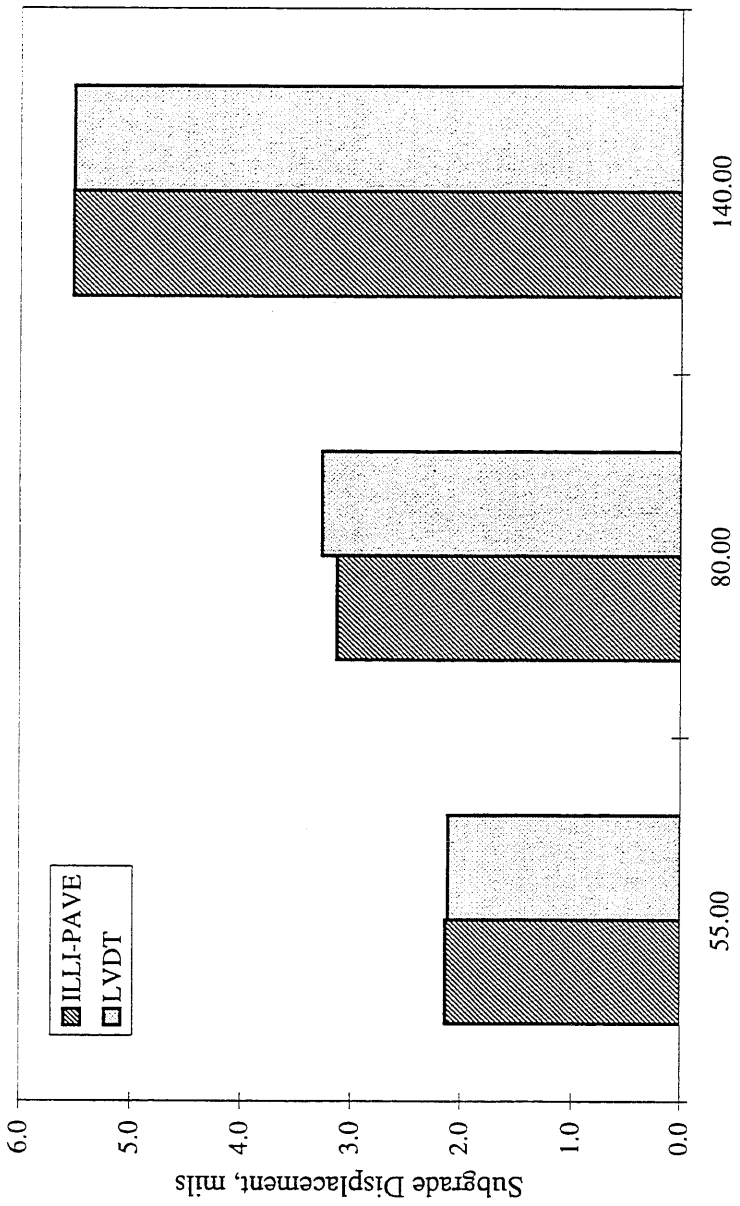

Figure 6.30. Comparison of Field and Estimated Subgrade Displacement for Cell 22.

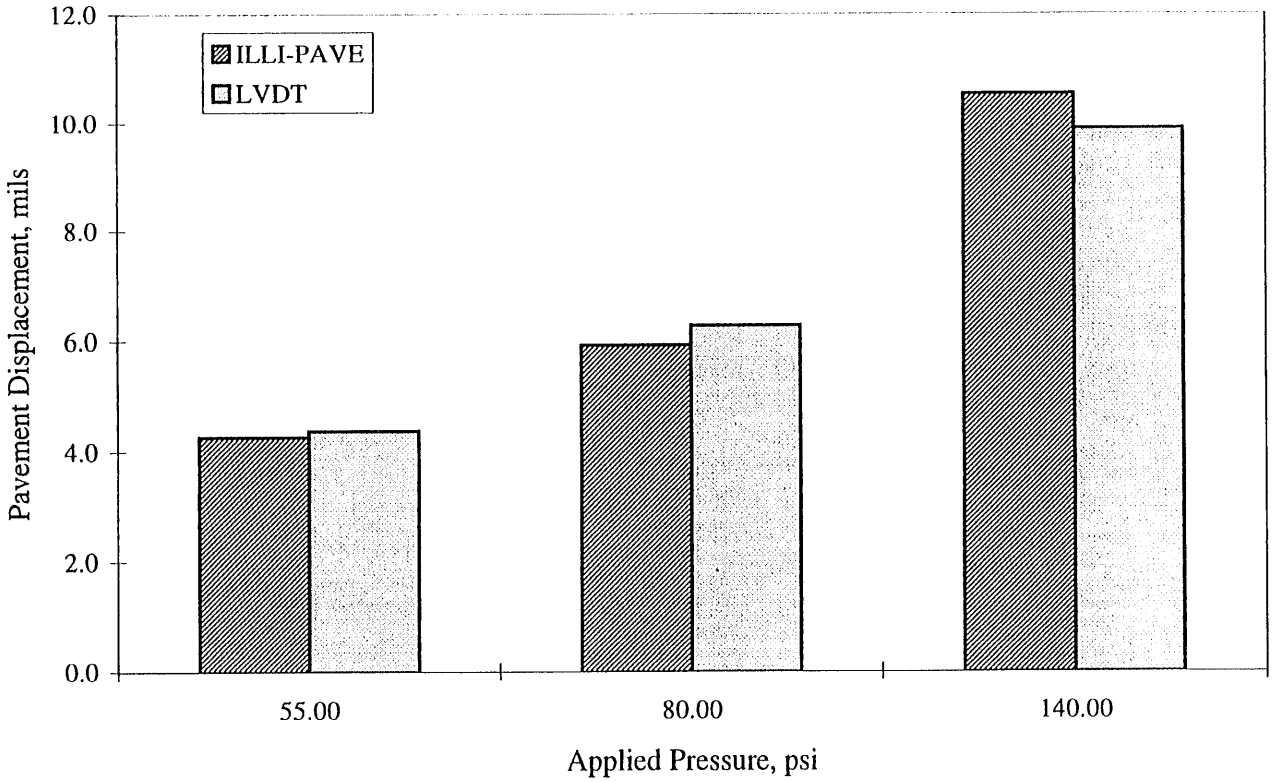

Figure 6.31. Comparison of Field and Estimated Total Pavement Displacement for Cell 22.

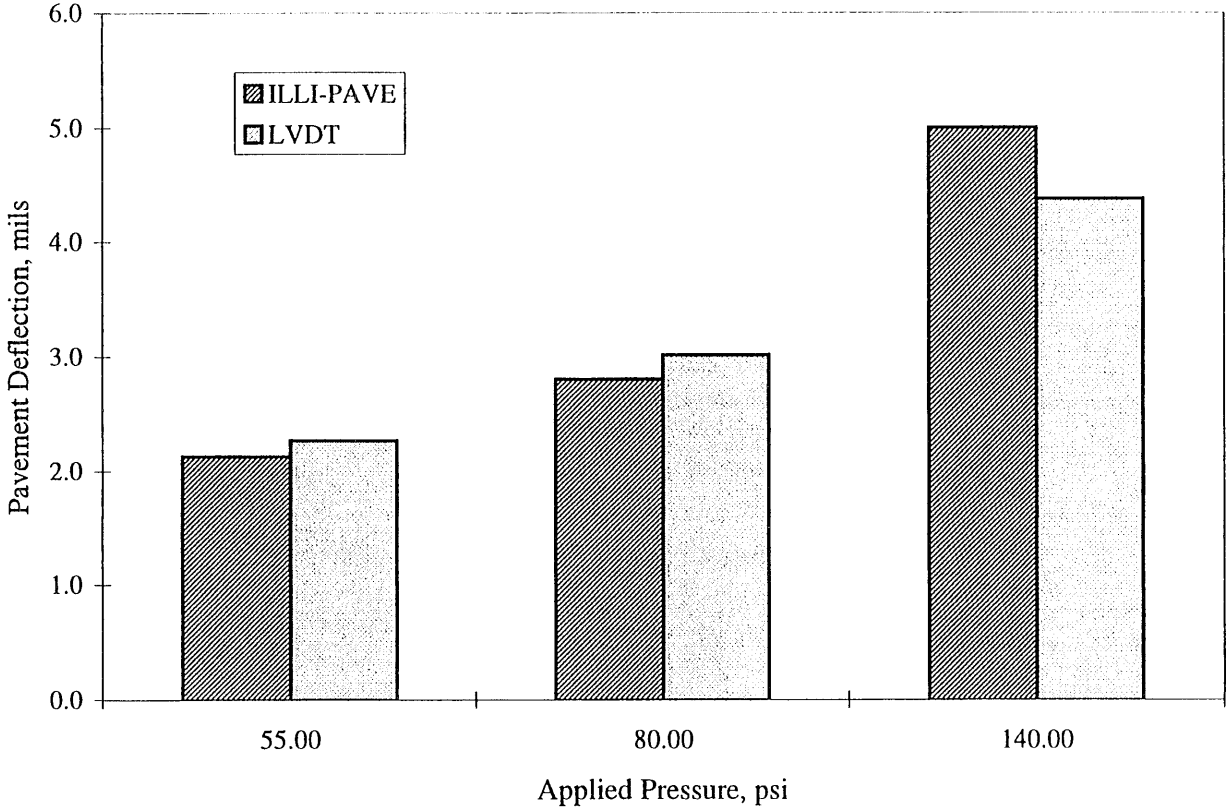

Figure 6.32. Comparison of Field and Estimated Within Pavement Displacement for Cell 22.

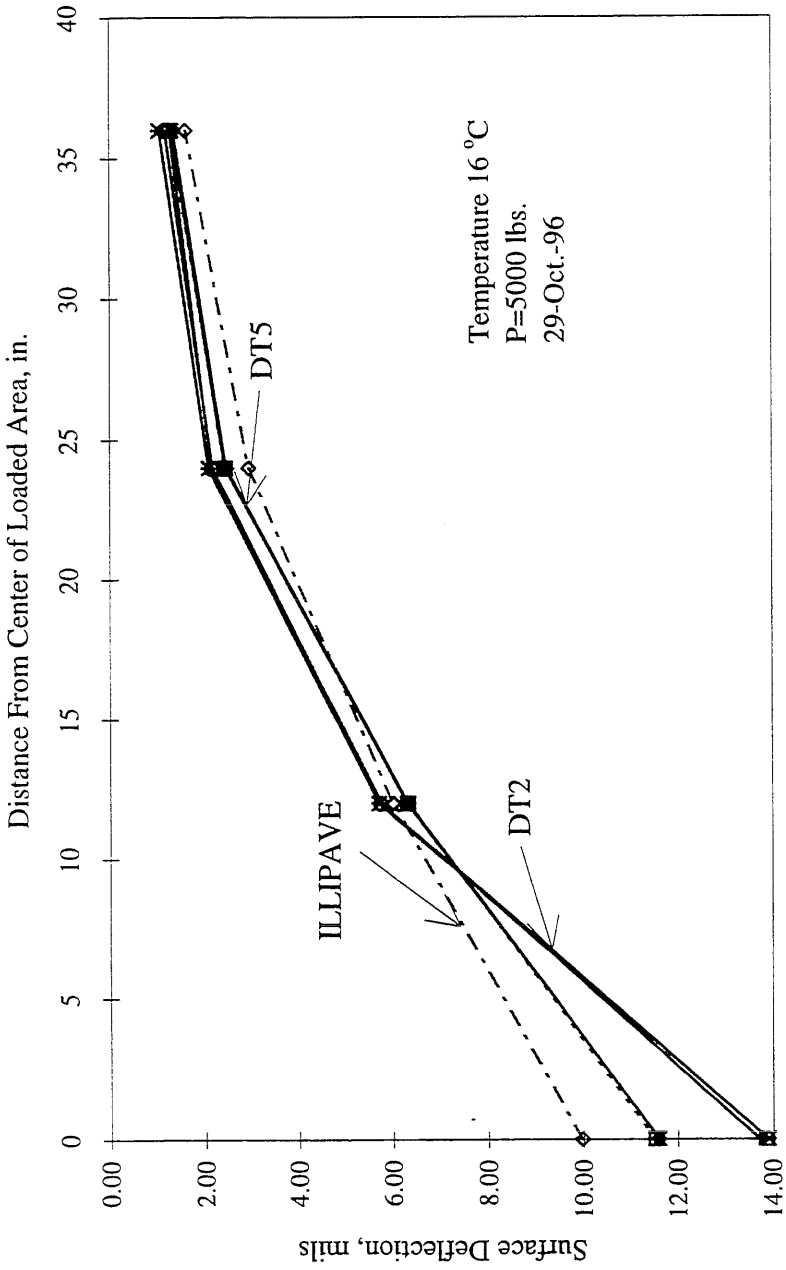

Figure 6.33. Deflection Basin Comparison for LVDT Testing on Cell 30.

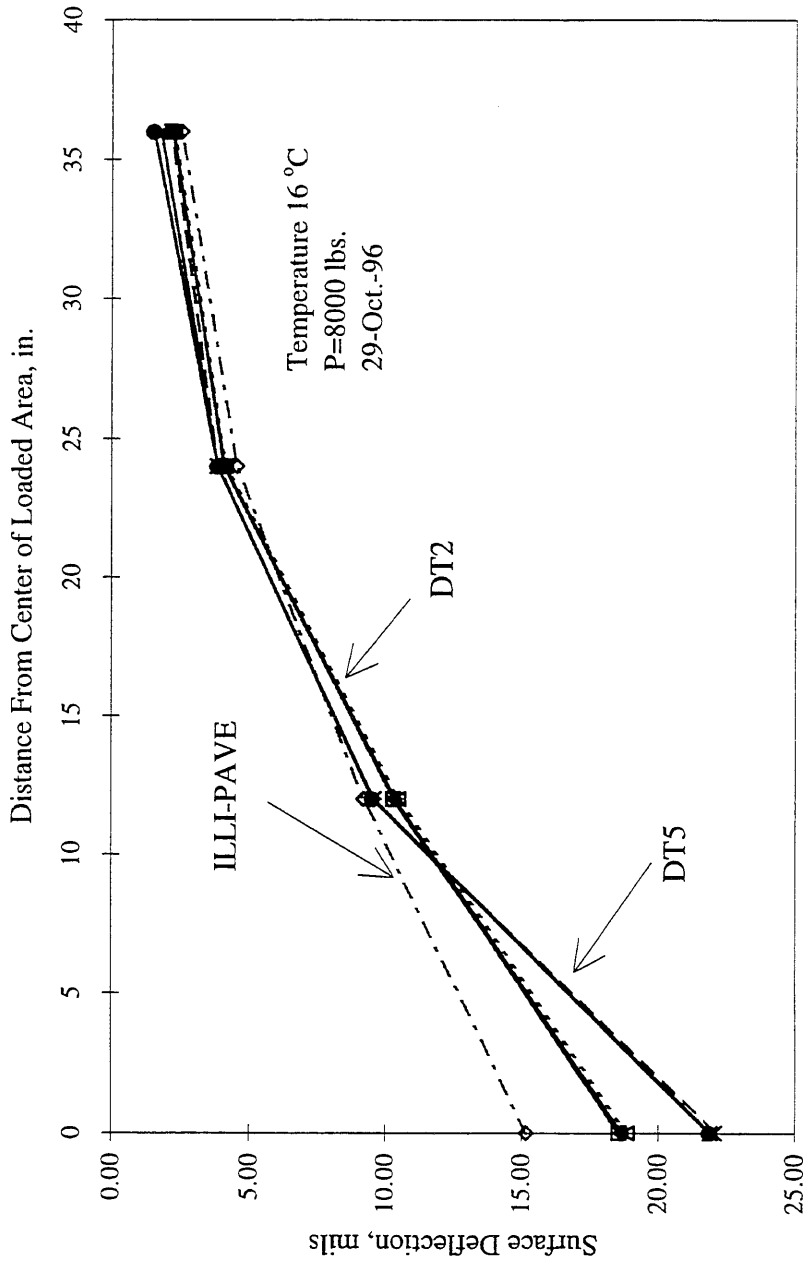

Figure 6.34. Deflection Basin Comparison for LVDT Testing on Cell 30.

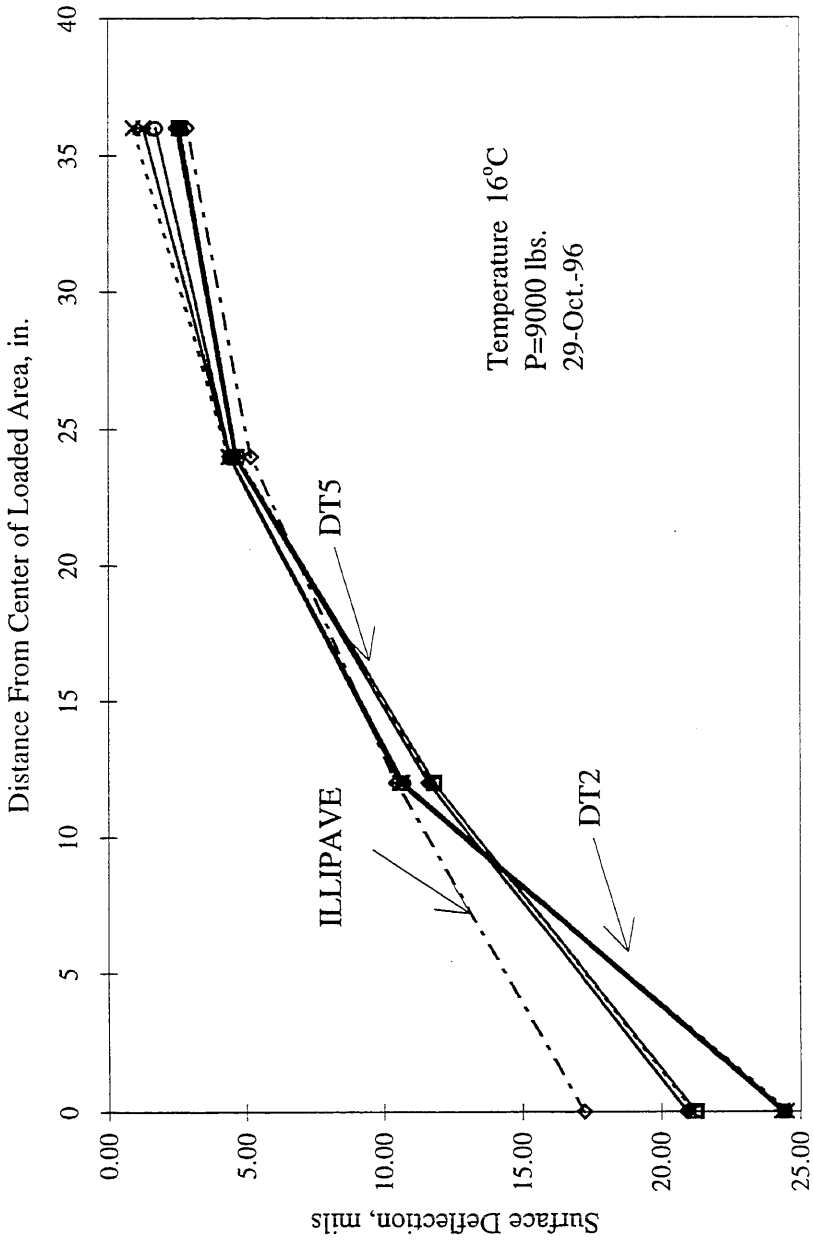

Figure 6.35. Deflection Basin Comparison for LVDT Testing on Cell 30.

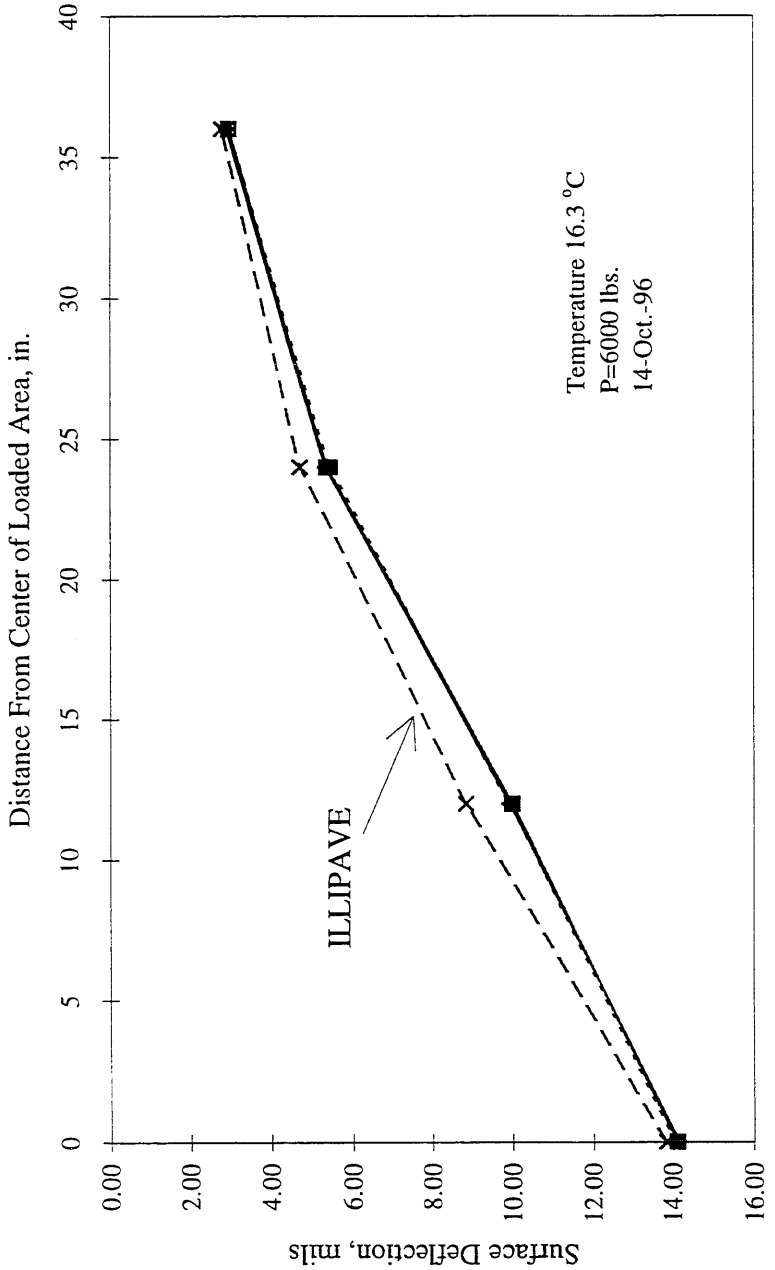

Figure 6.36. Deflection Basin Comparison for Special Testing on LVR Cell 30.

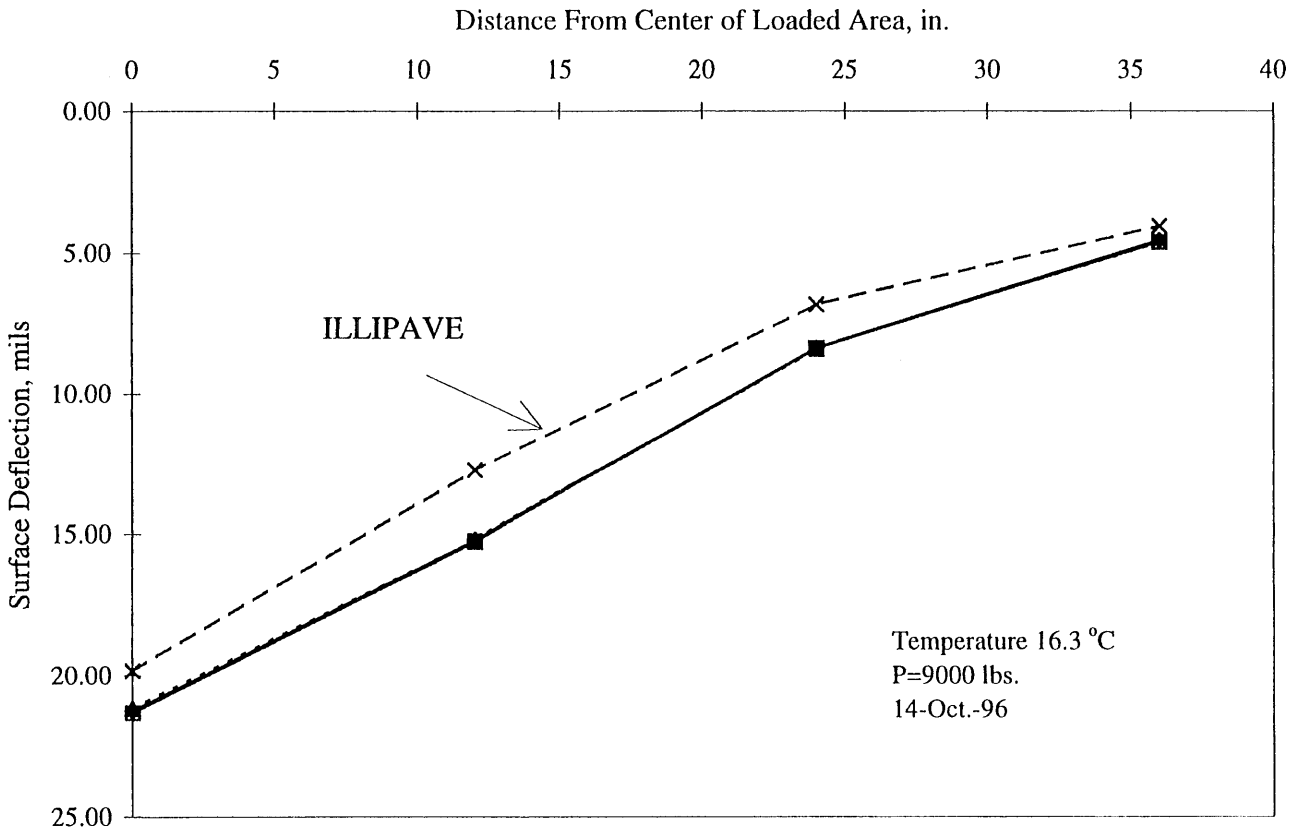

Figure 6.37. Deflection Basin Comparison for Special Testing on LVR Cell 30.

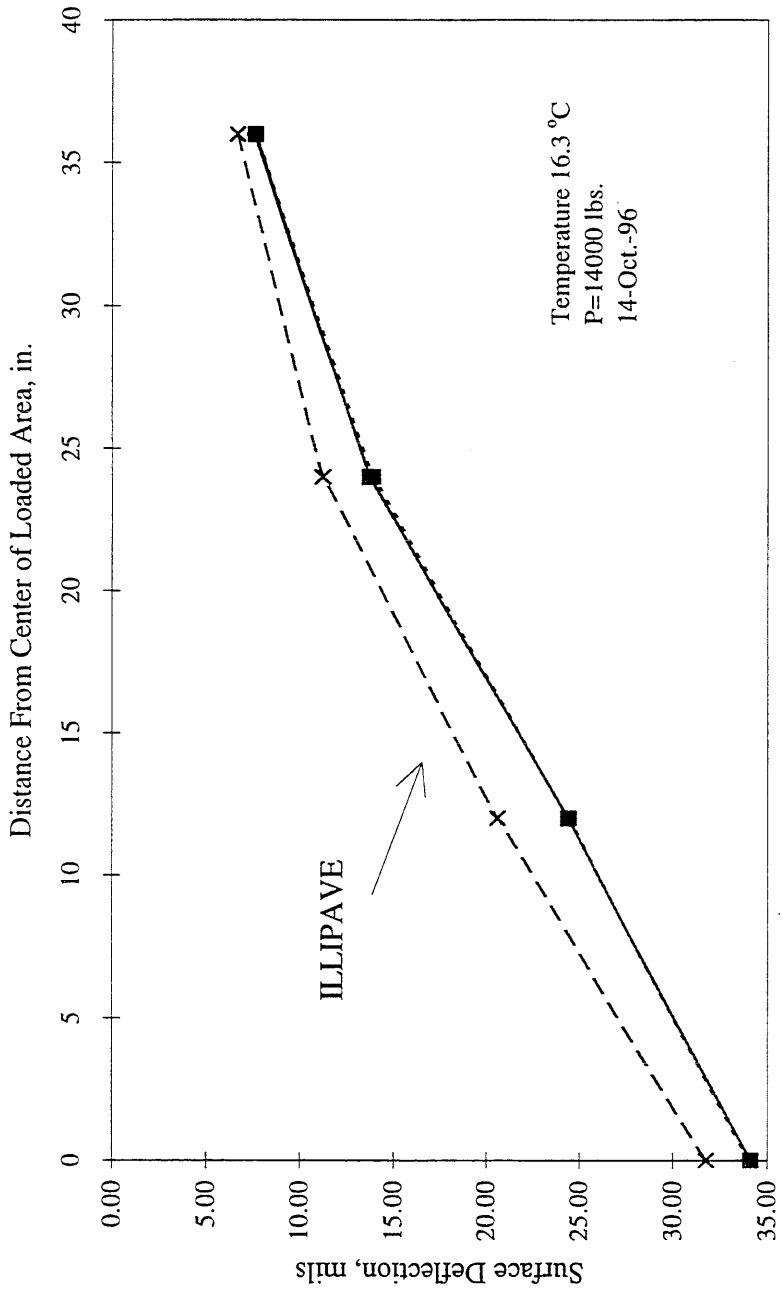

Figure 6.38. Deflection Basin Comparison for Special Testing on LVR Cell 30.

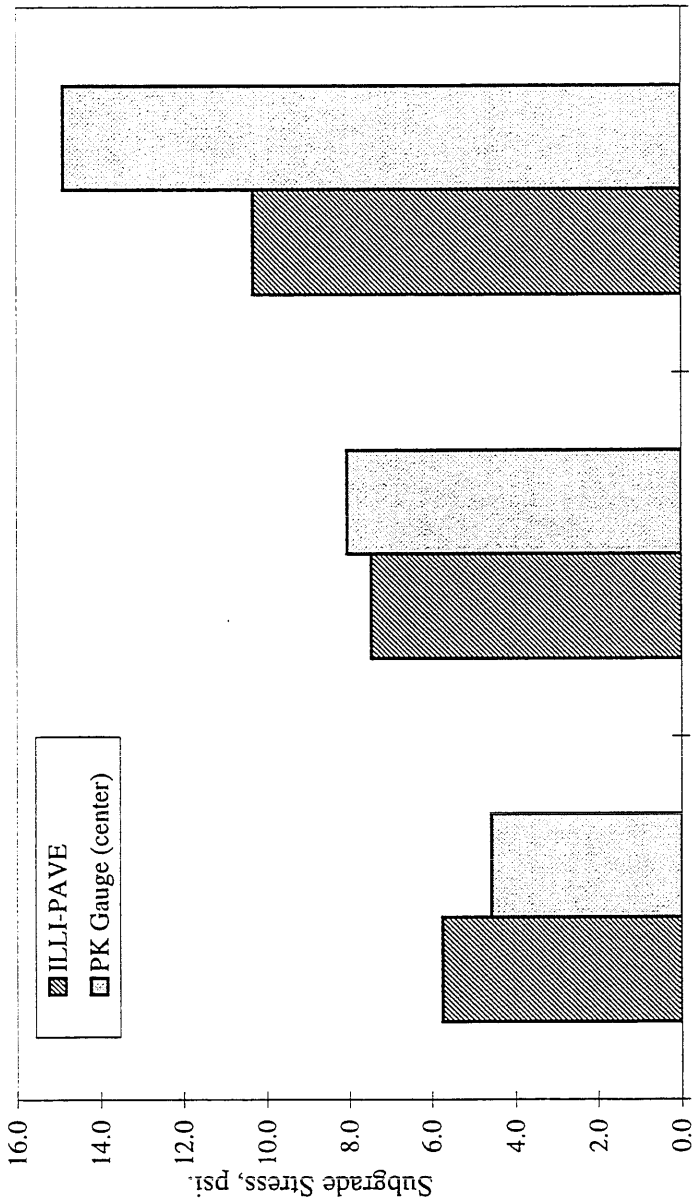

Figure 6.39. Comparison of Field and Estimated Subgrade Stress on Cell 30.

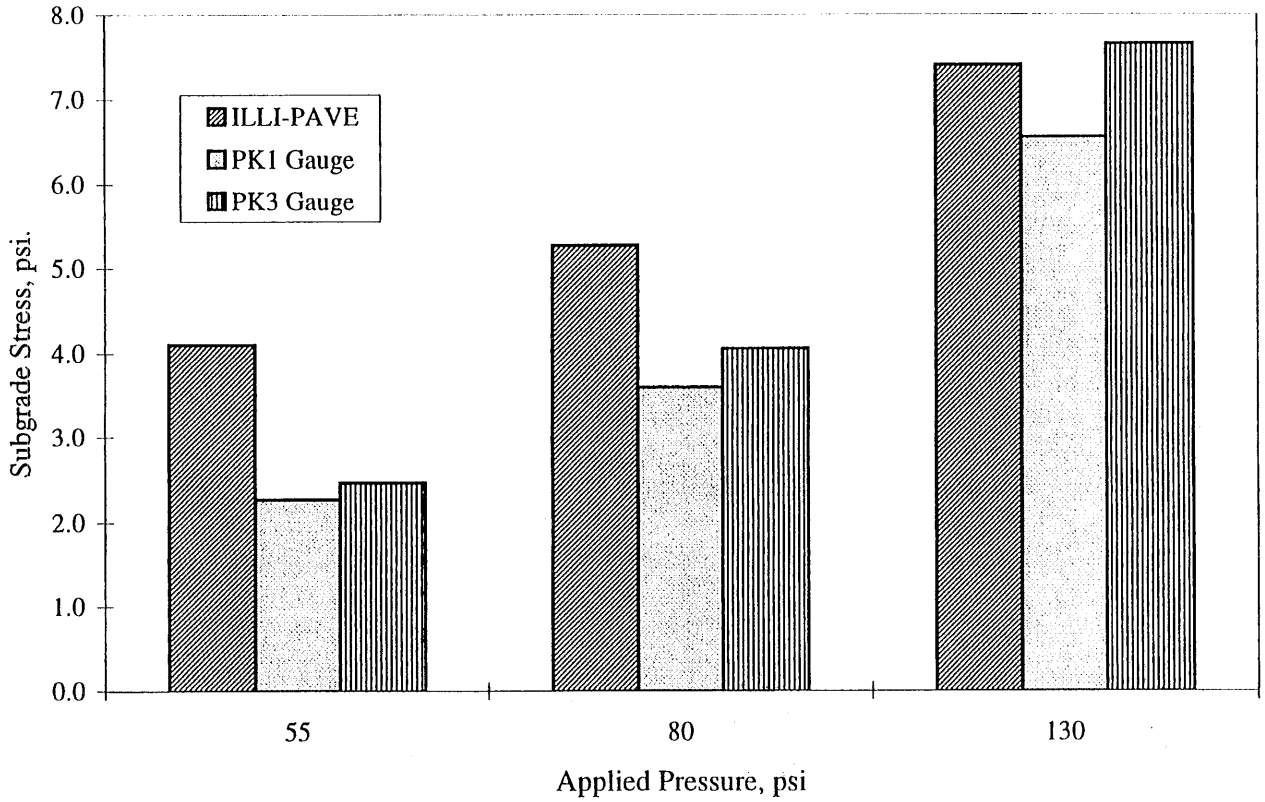

Figure 6.40. Comparison of Field and Estimated Subgrade Stress (12 inches away from load) on Cell 30.

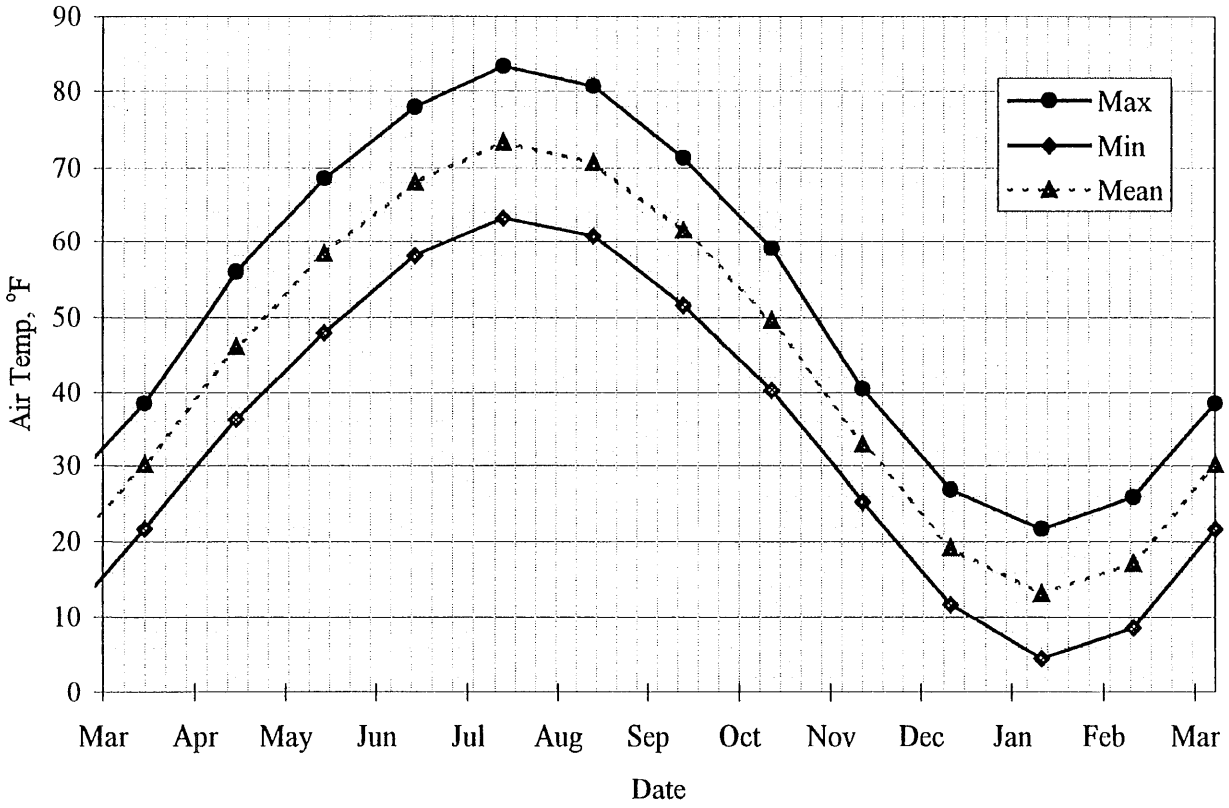

Figure 7.1. Average Air Temperatures (1962-1991) for Minneapolis, MN

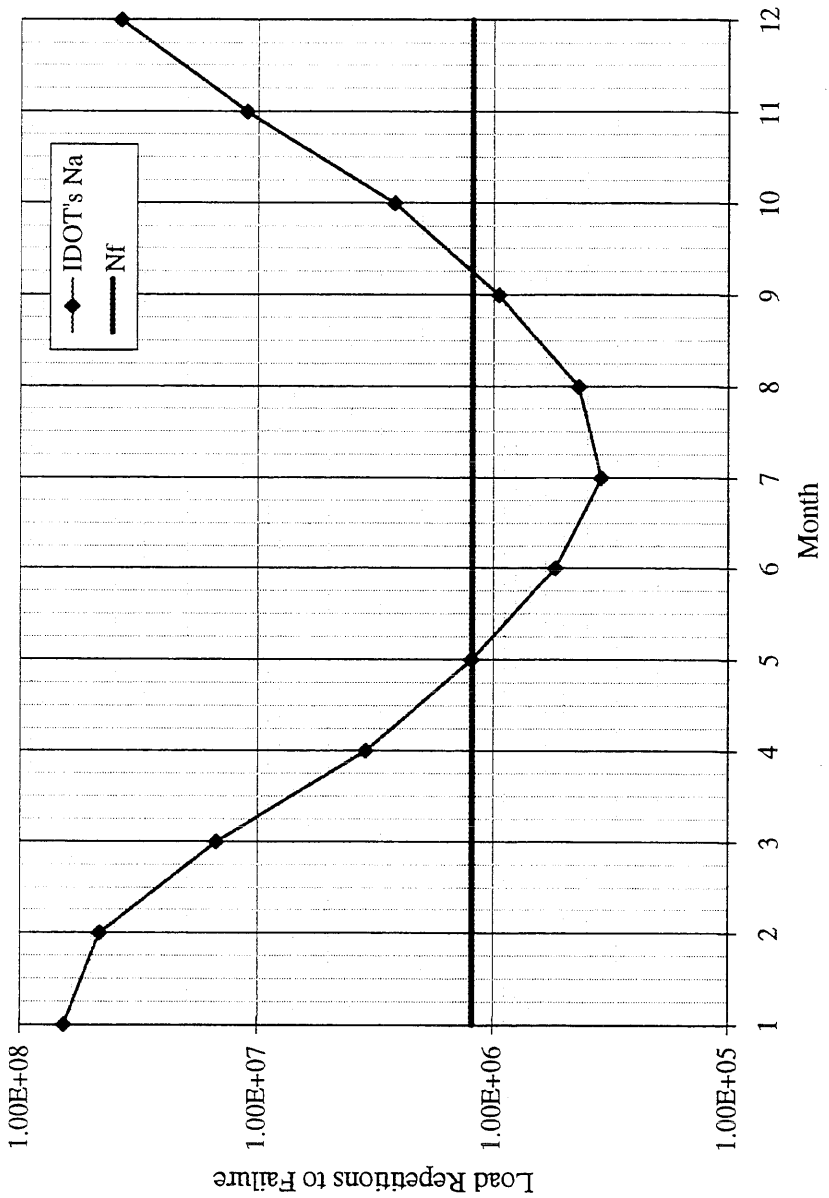

Figure 7.2 Design Time Relation for Mainline Cell 1 (5.75 in. AC, 33 in. CL-4sp).

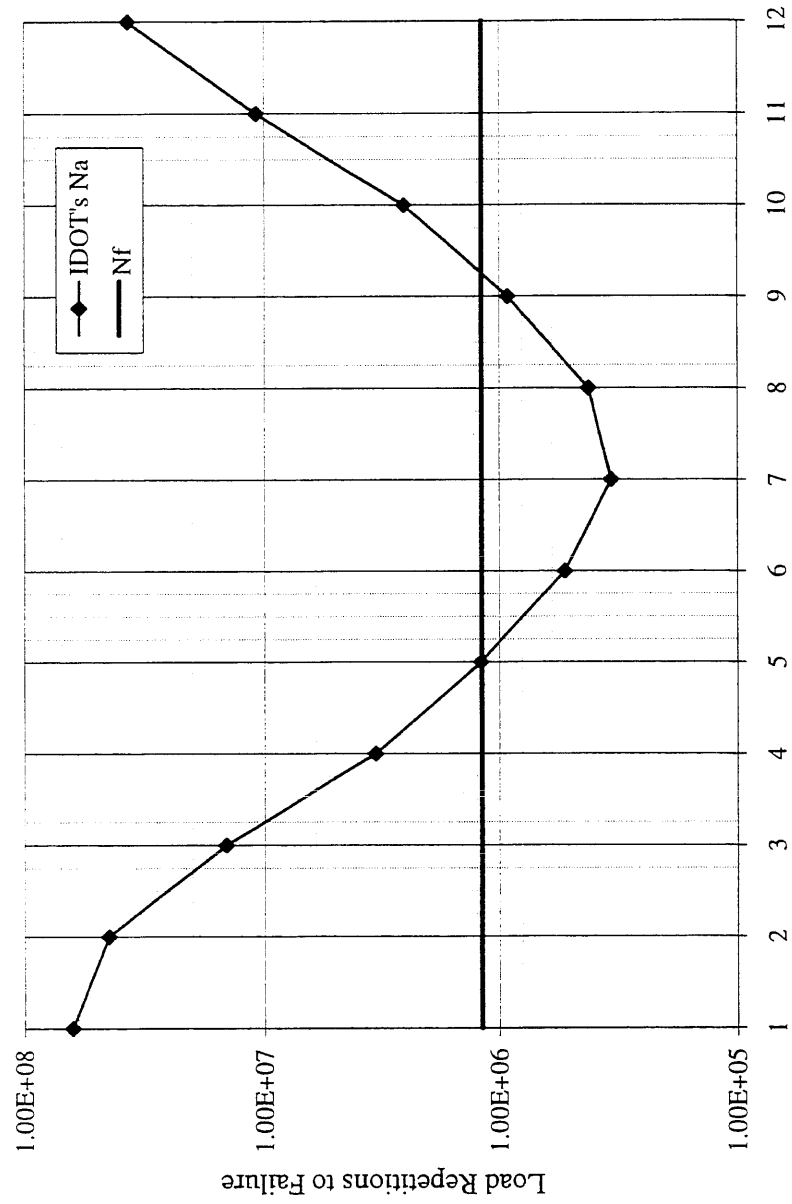

Figure 7.3 Design Time Relation for Mainline Cell 2 (5.75 in. AC, 4 in. CL-4sp, & 28 in. CL-6sp).

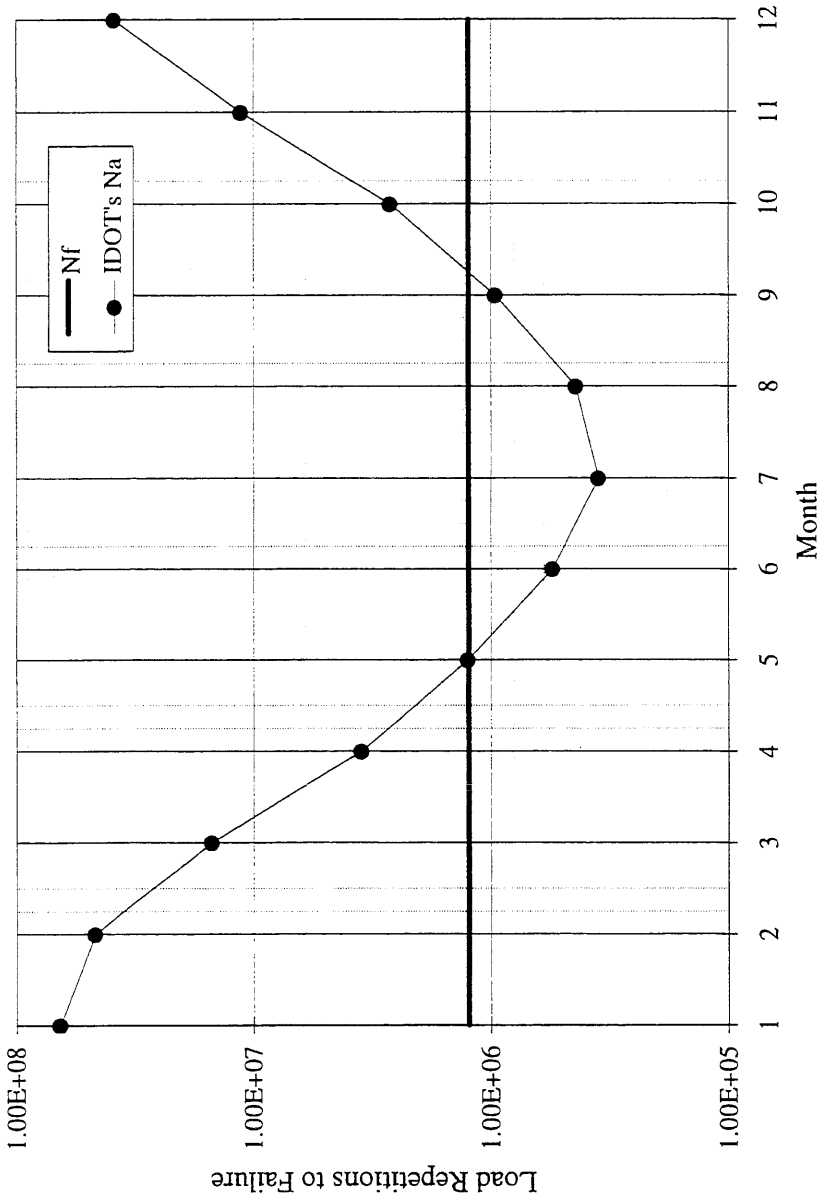

Figure 7.4 Design Time Relation for Mainline Cell 3 (5.75 in. AC, 4 in. CL-5sp, & 33 in. CL-3sp).

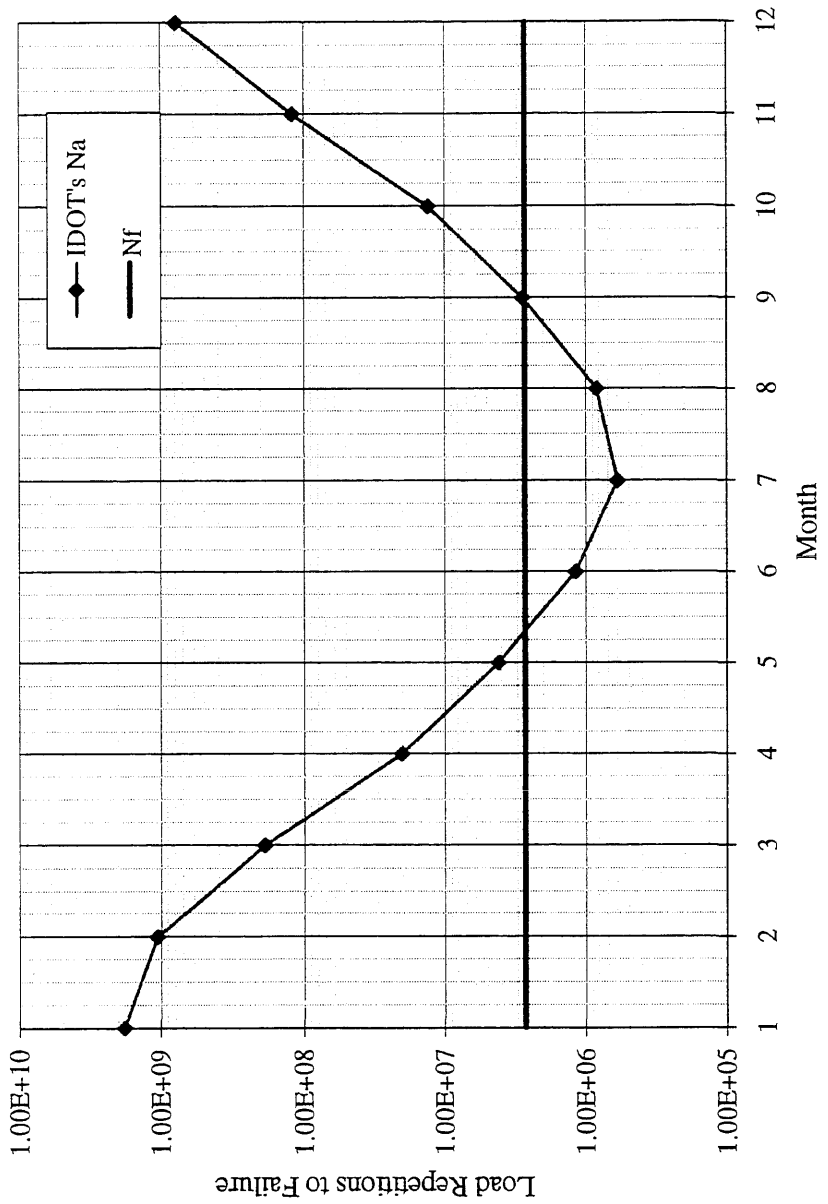

Figure 7.5 Design Time Relation for Mainline Cell 4 (8.75 in. AC over Subgrade).

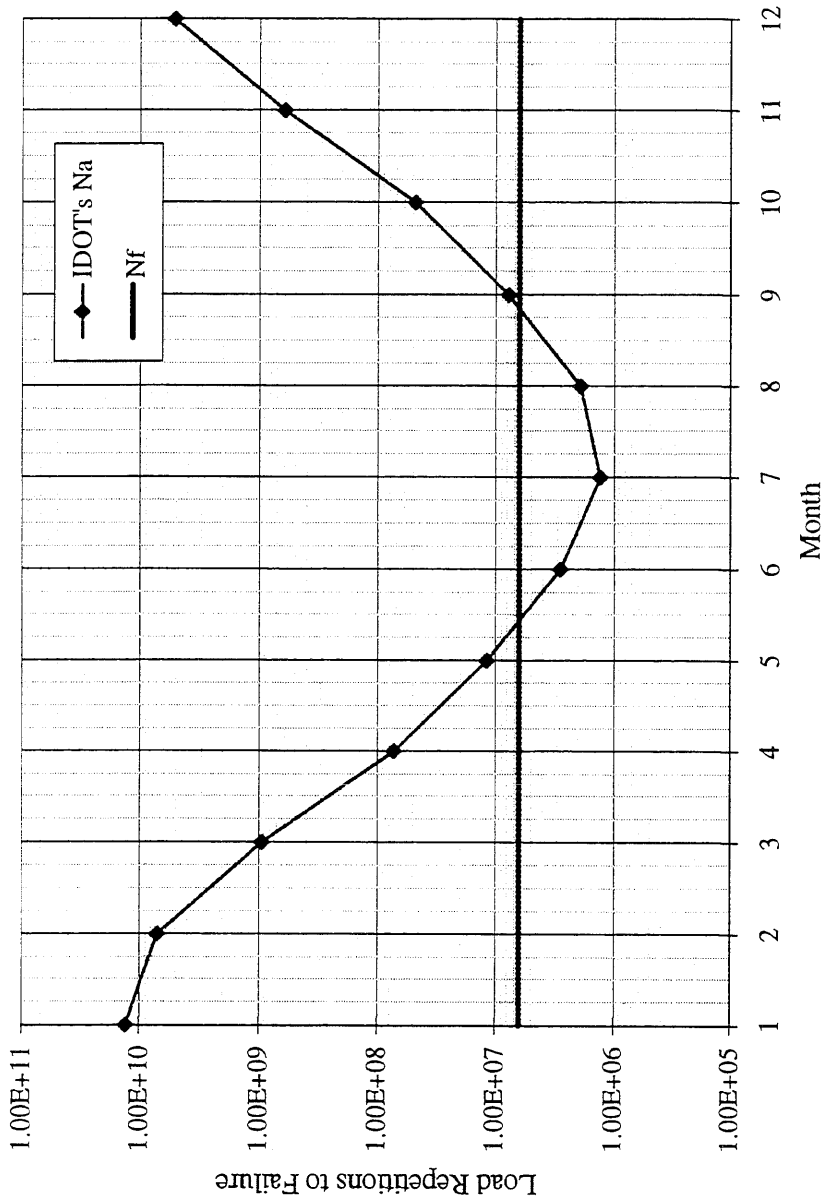

Figure 7.6 Design Time Relation for Mainline Cells 14 and 15 (10.75 in. AC over Subgrade).

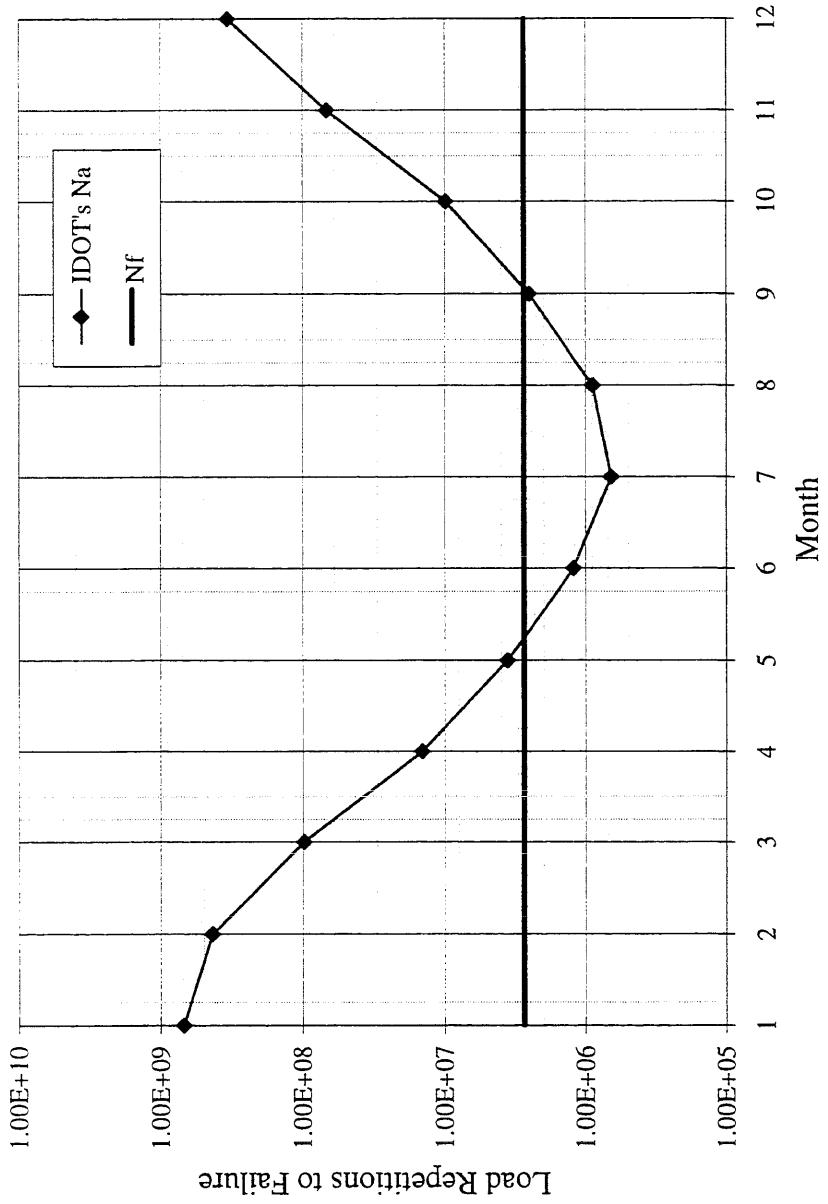

Figure 7.7 Design Time Relation for Mainline Cells 16, 17, 19 and 20 (7.75 in. AC, 28 in.CL-3sp).

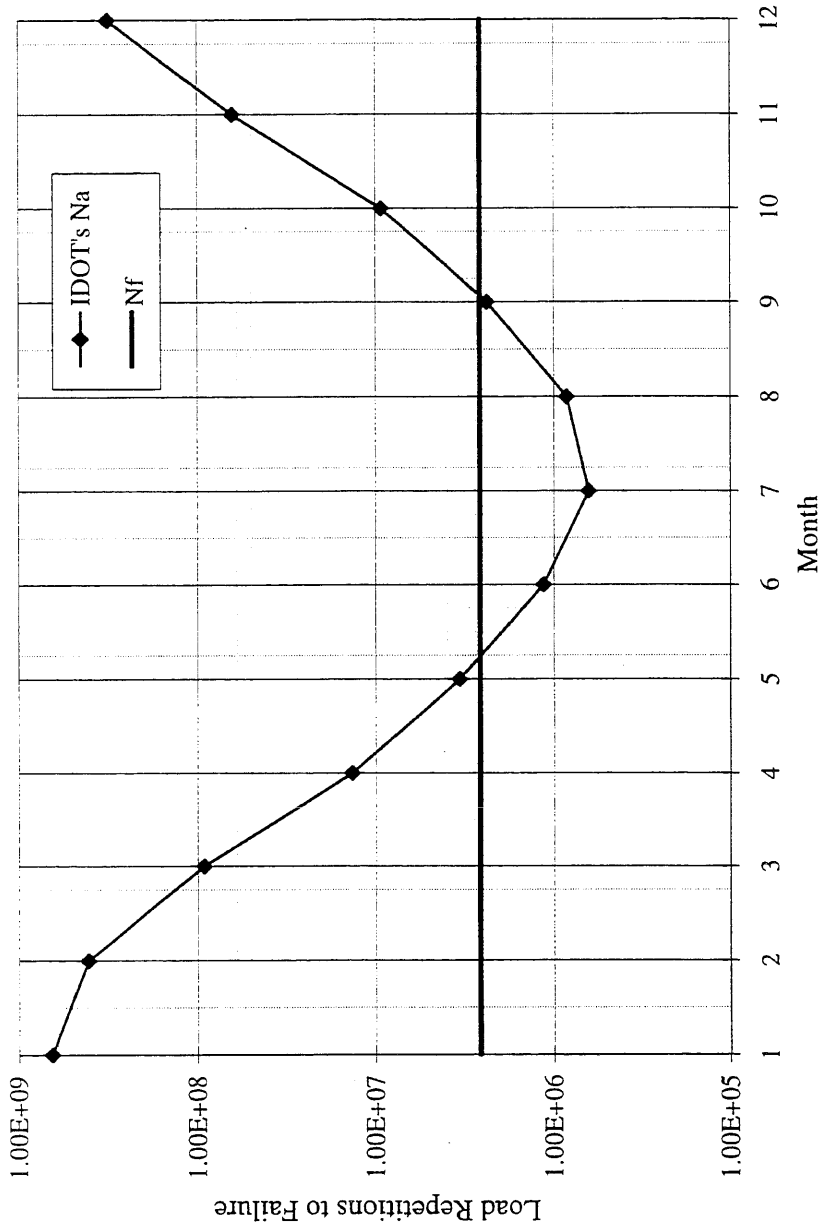

Figure 7.8 Design Time Relation for Mainline Cell 18 (7.75 in. AC, 12 in.CL-6sp & 9 in. CL-3sp).

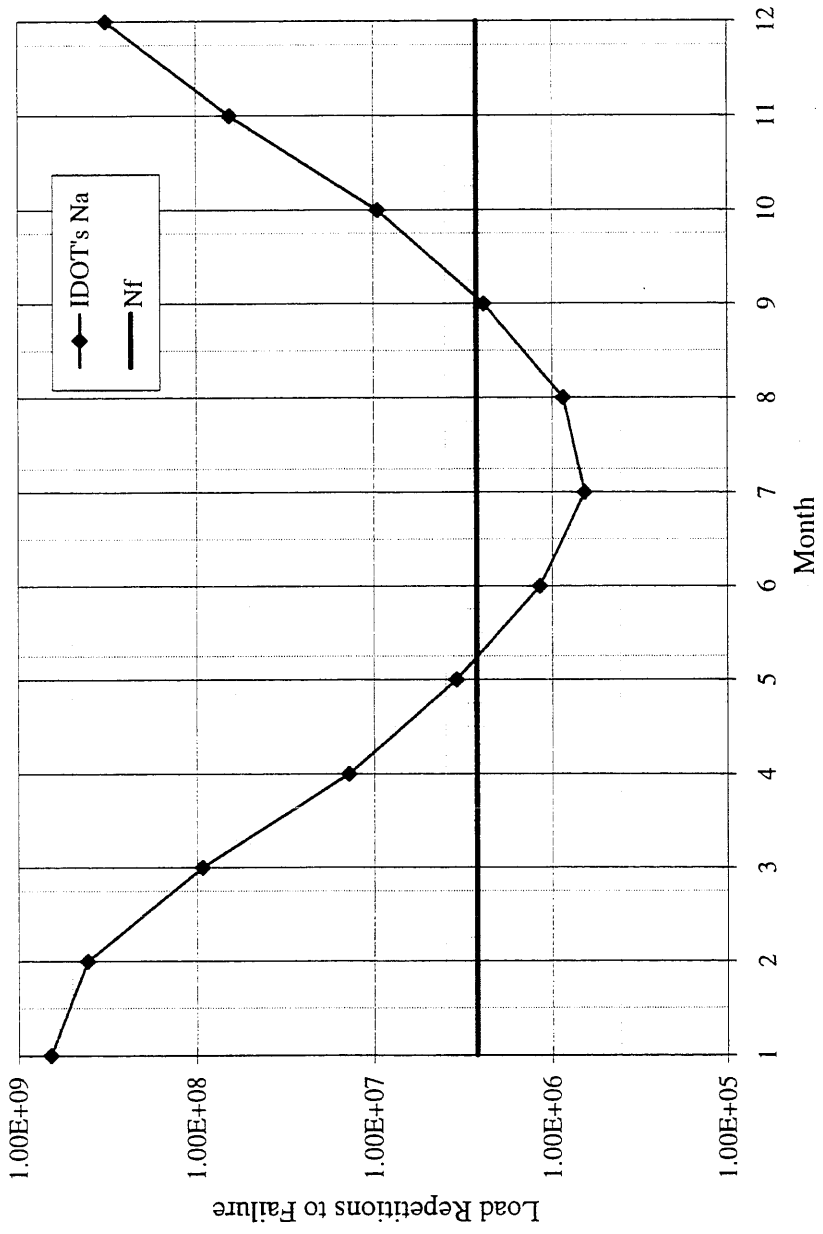

Figure 7.9 Design Time Relation for Mainline Cell 21 (7.75 in. AC, 23 in. CL-5sp).

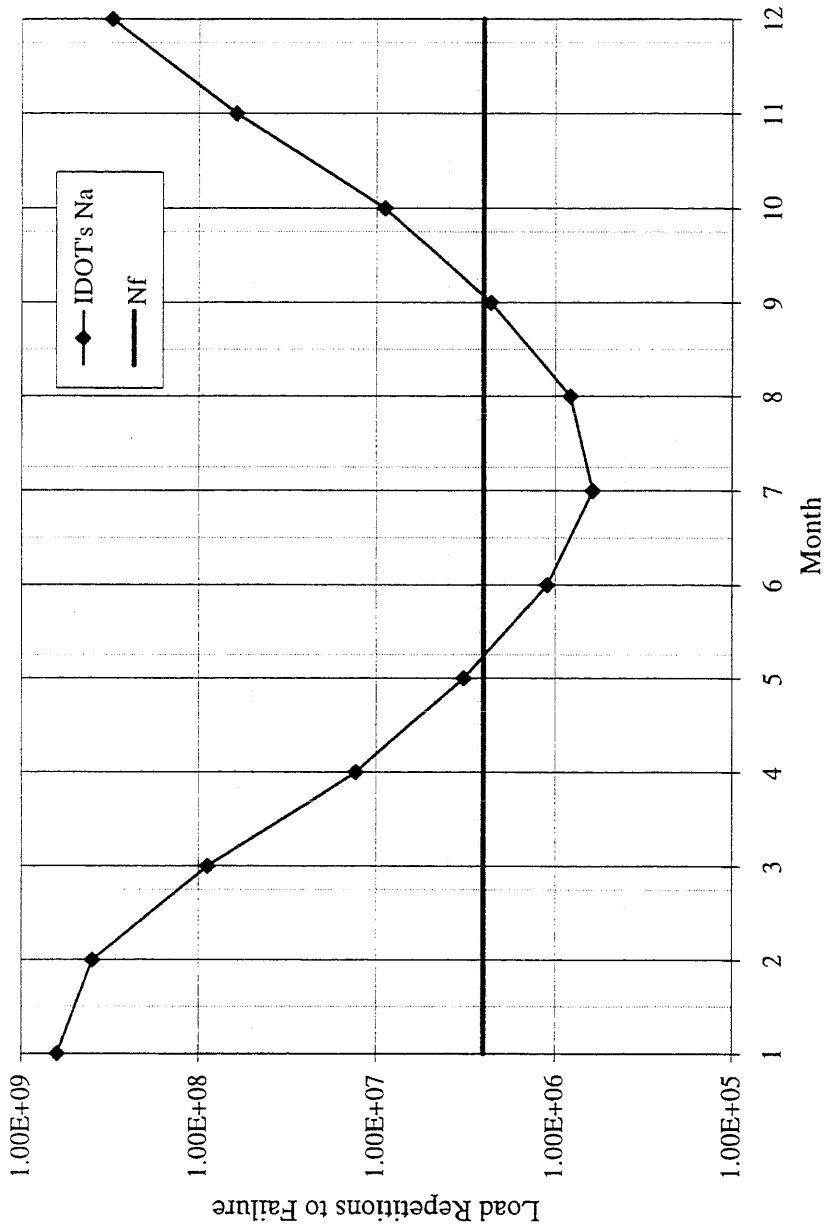

Figure 7.10 Design Time Relation for Mainline Cell 22 (7.75 in. AC, 18 in. CL-6sp).

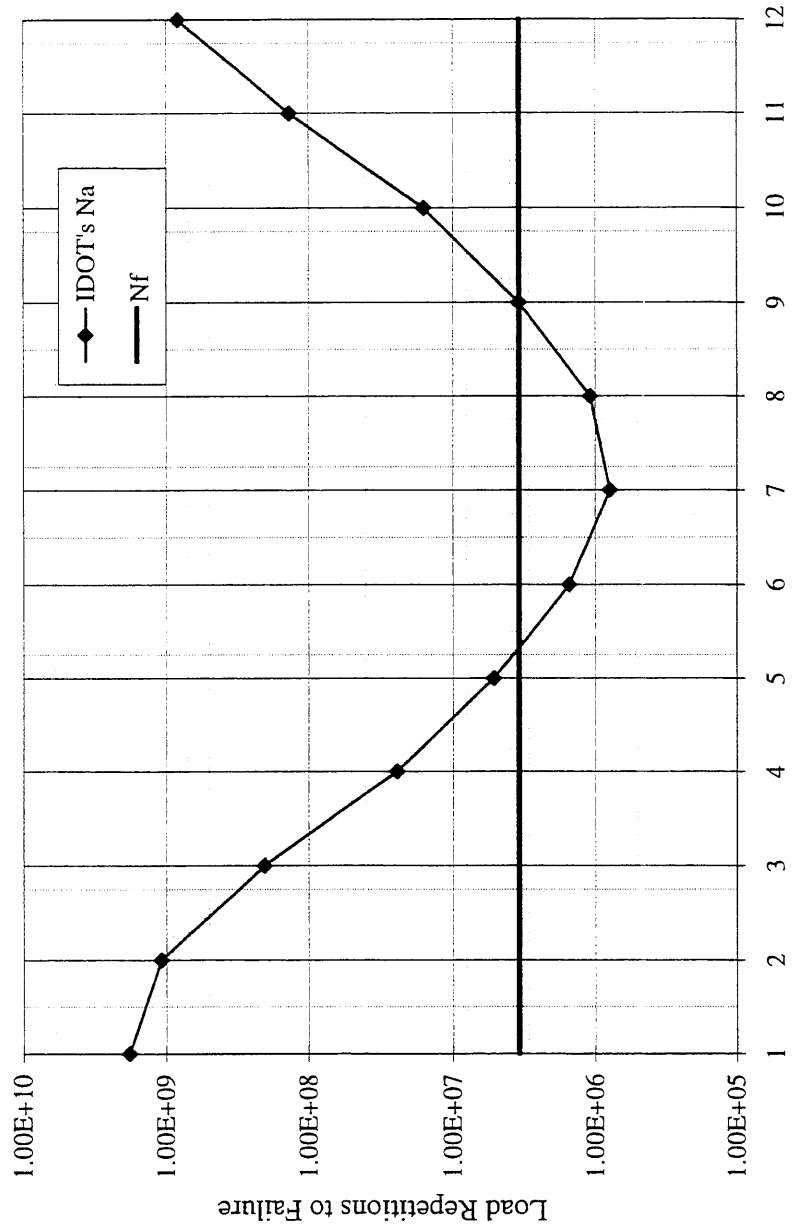

Figure 7.11 Design Time Relation for Mainline Cell 23 (8.75 in. AC, 4 in. PASB & 3 in. CL-4sp).

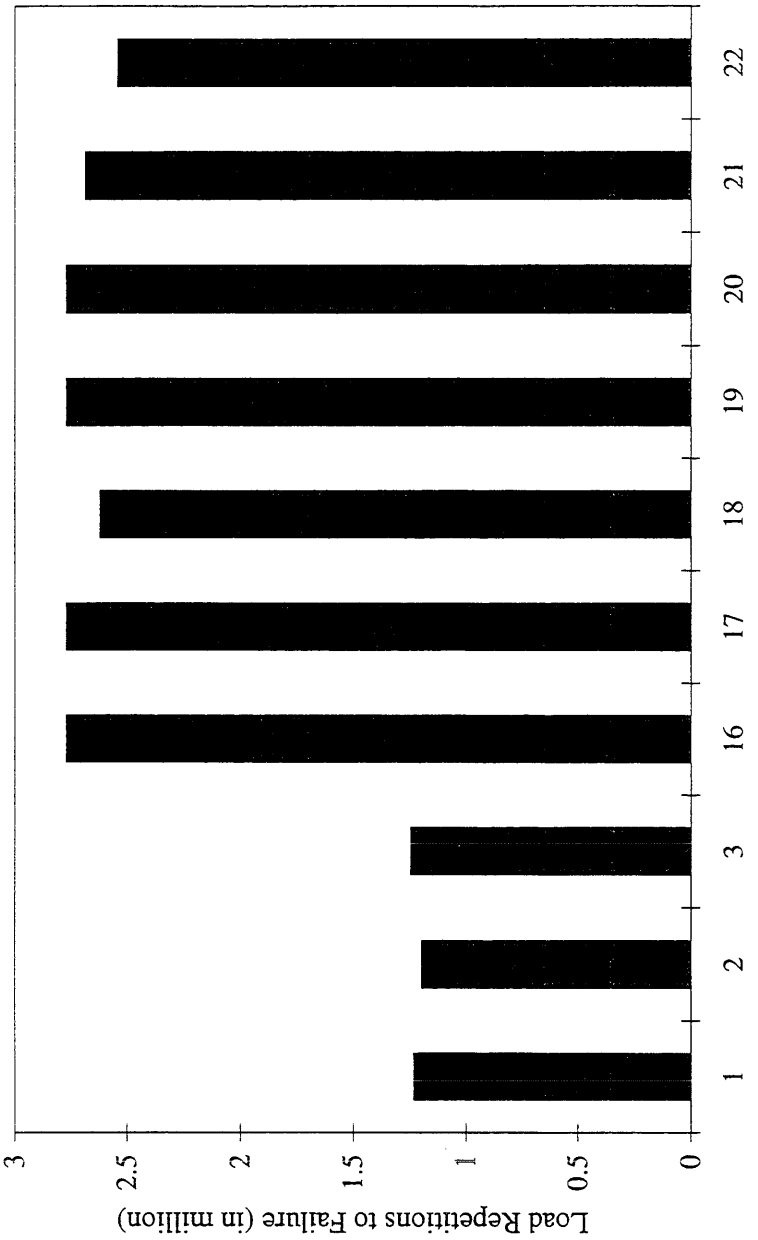

Figure 7.12 Estimated Fatigue Life on Mainline CFP Cells (IDOT's Algorithm).

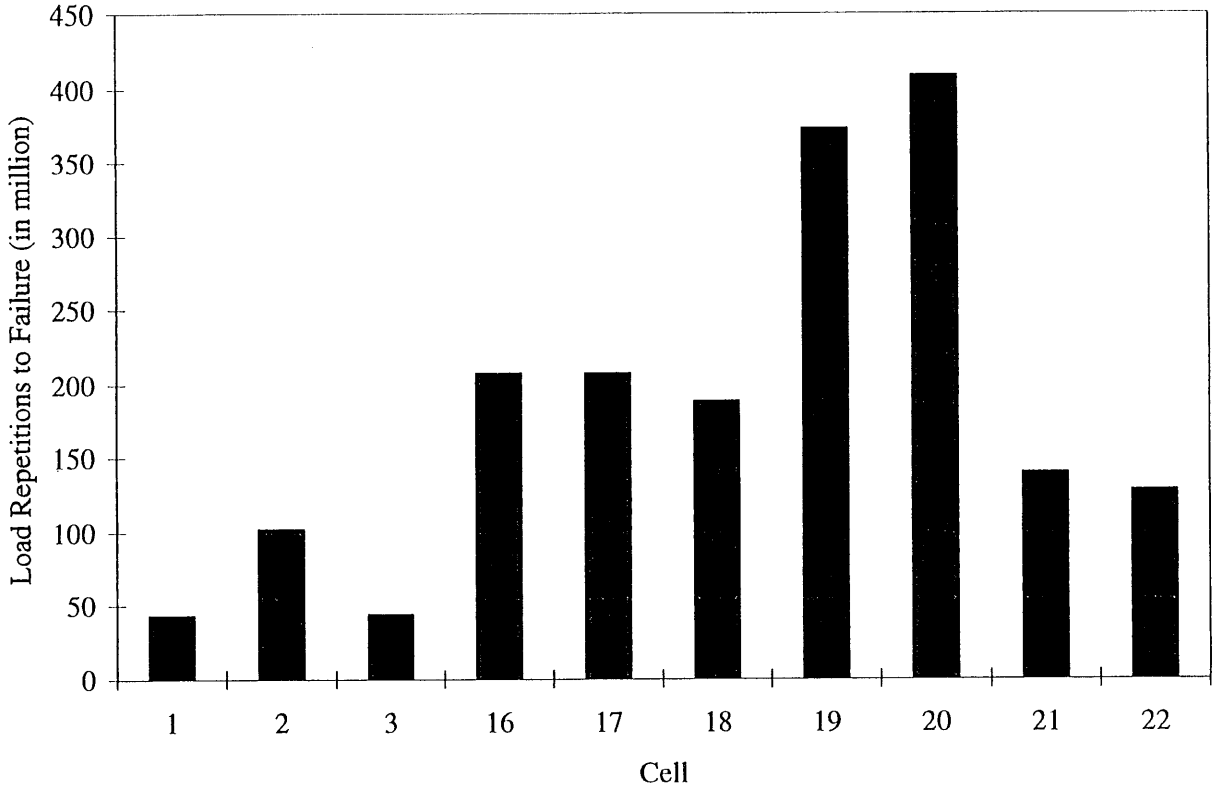

Figure 7.13 Estimated Fatigue Life on Mainline CFP Cells (Laboratory Algorithm).

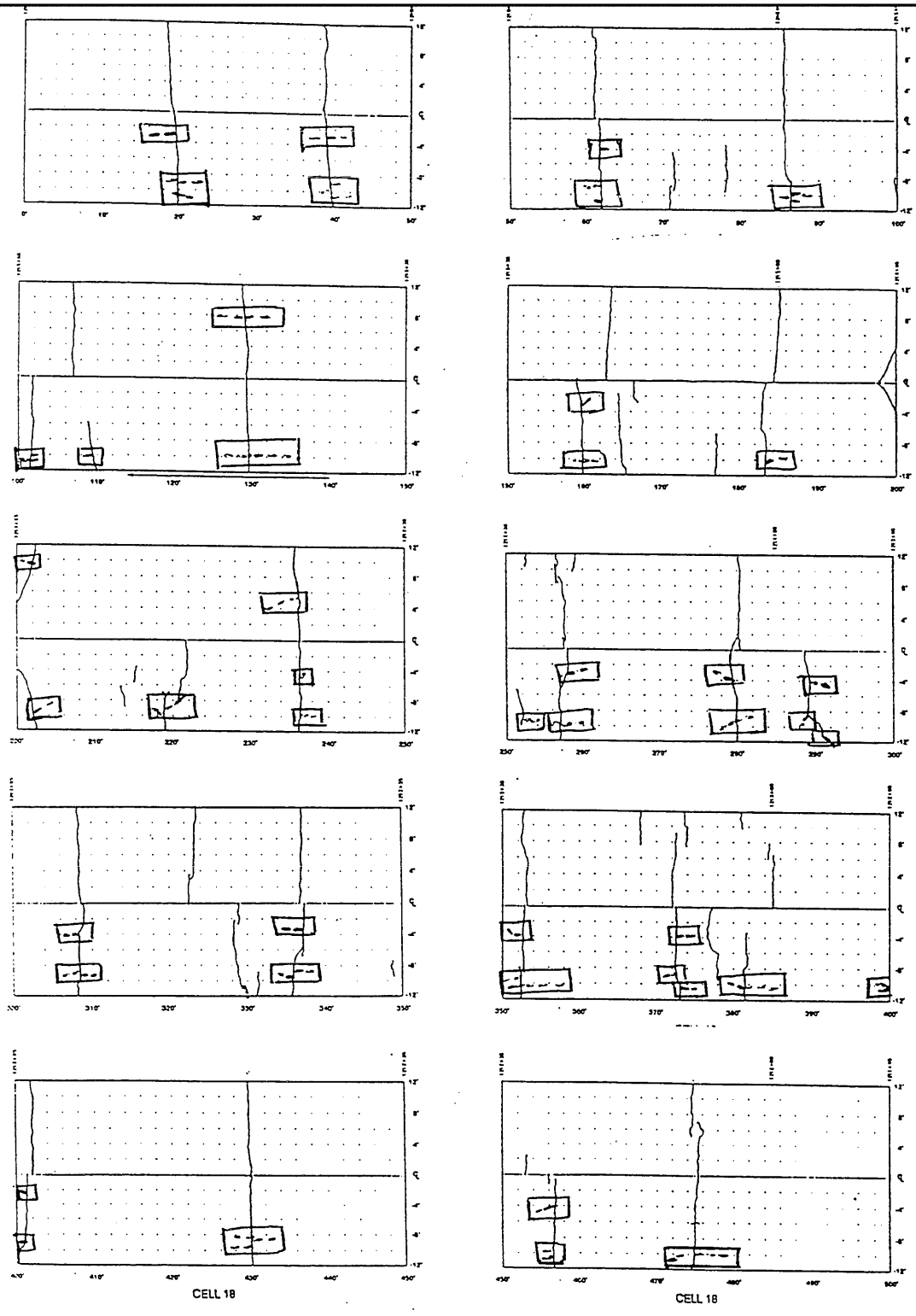

Figure 7.14. Fatigue Cracking on Cell 18.

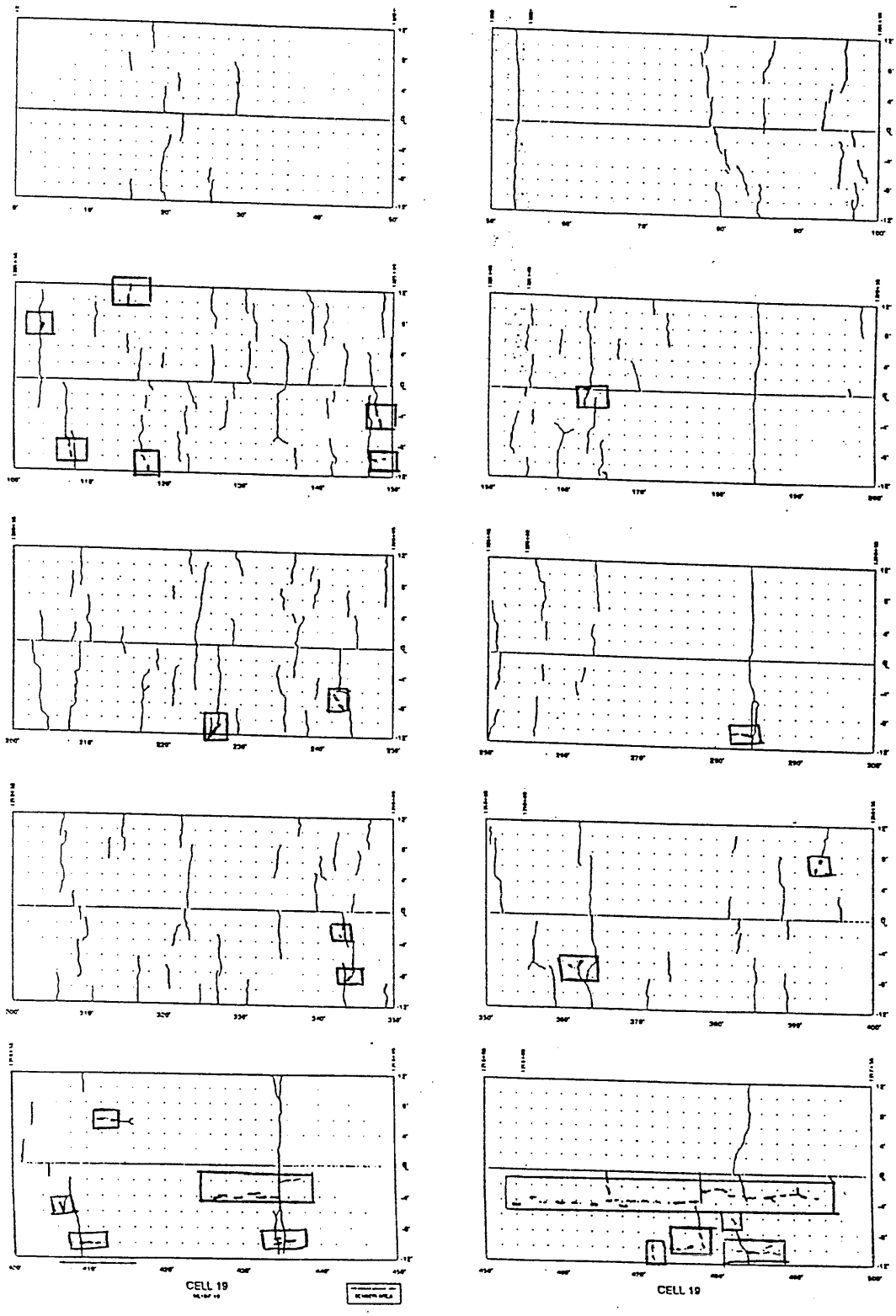

Figure 7.15. Fatigue Cracking on Cell 19.

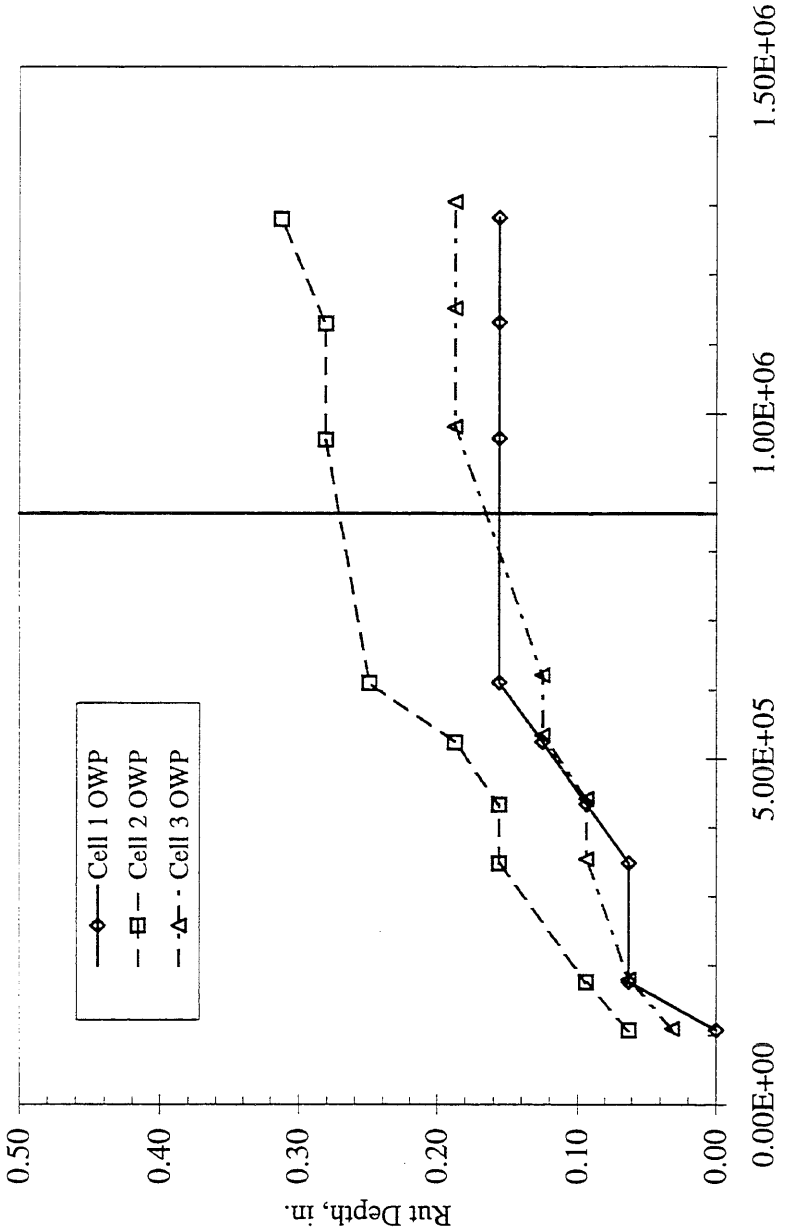

Figure 7.16. Rut Accumulation on Five-Year Mainline CFP Sections.

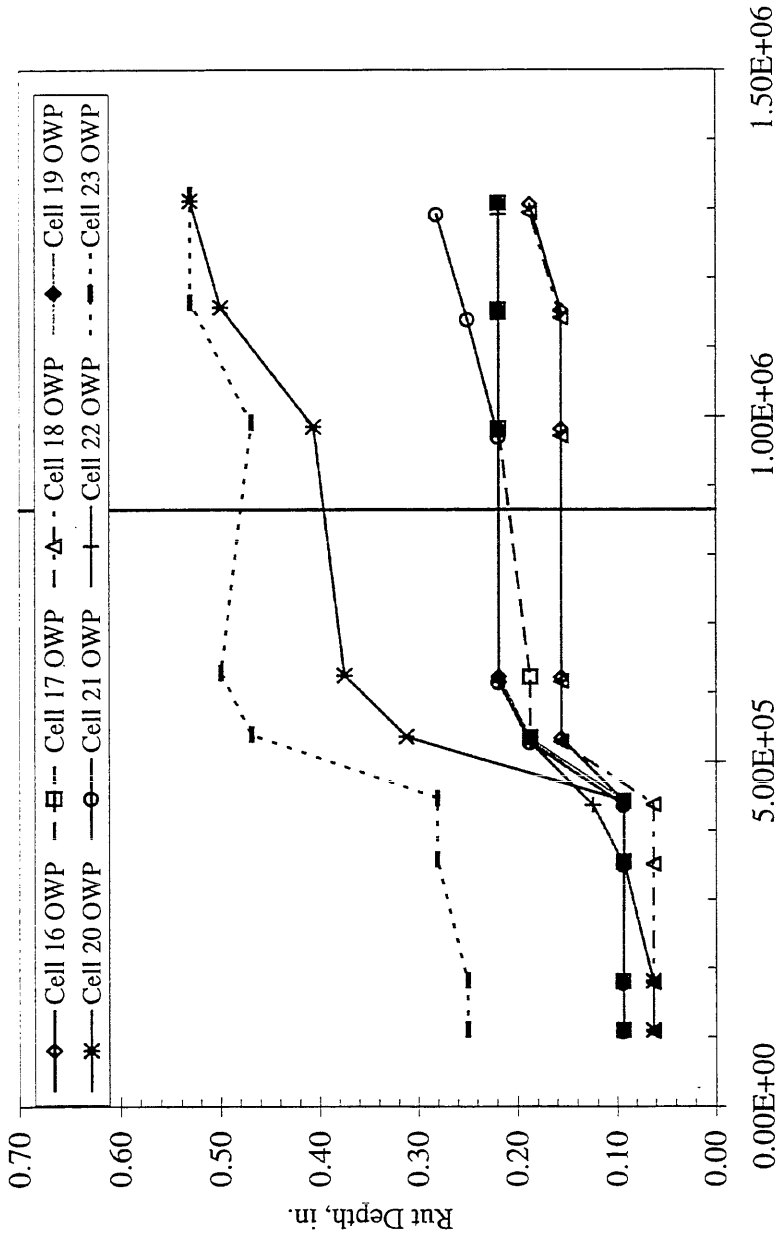

Figure 7.17. Rut Accumulation on Ten-Year Mainline CFP Sections.

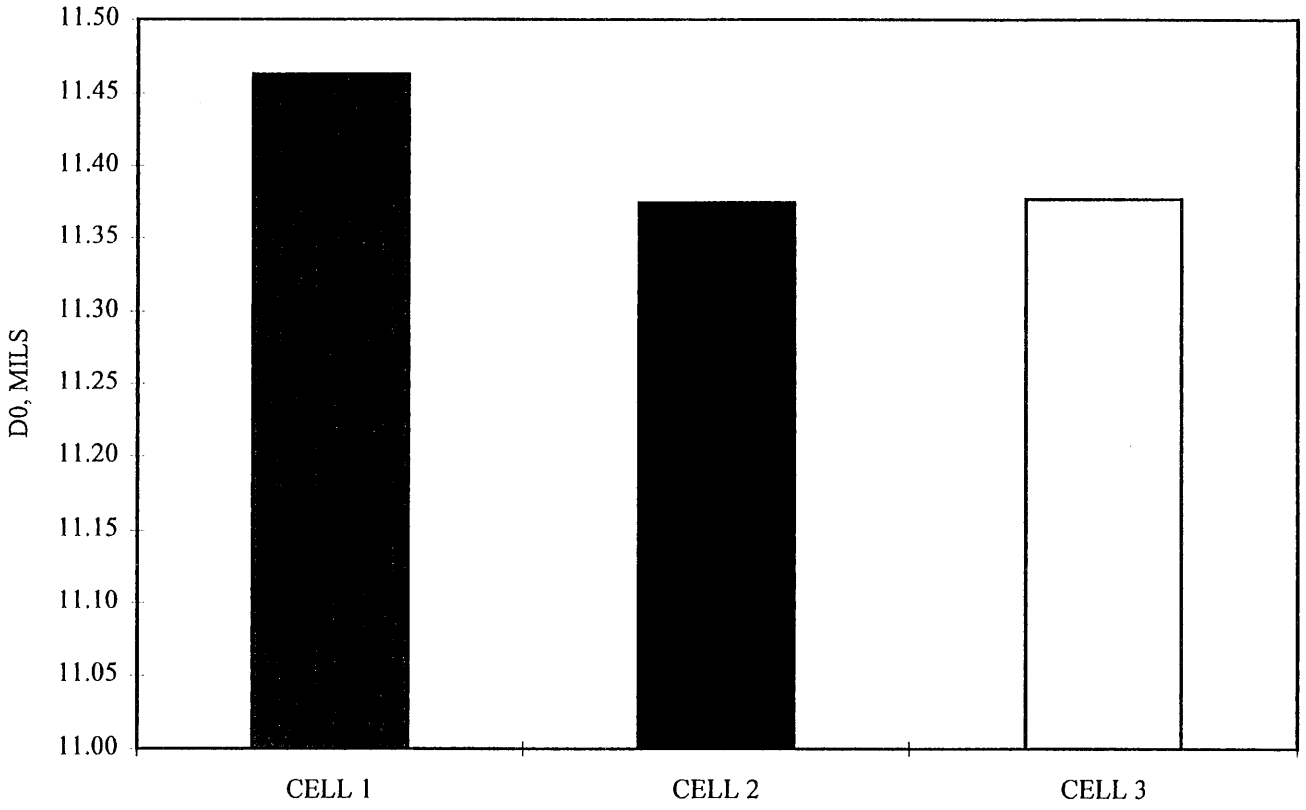

Figure 7.18. Comparison of Adjusted Maximum Deflections (April 25,1994).

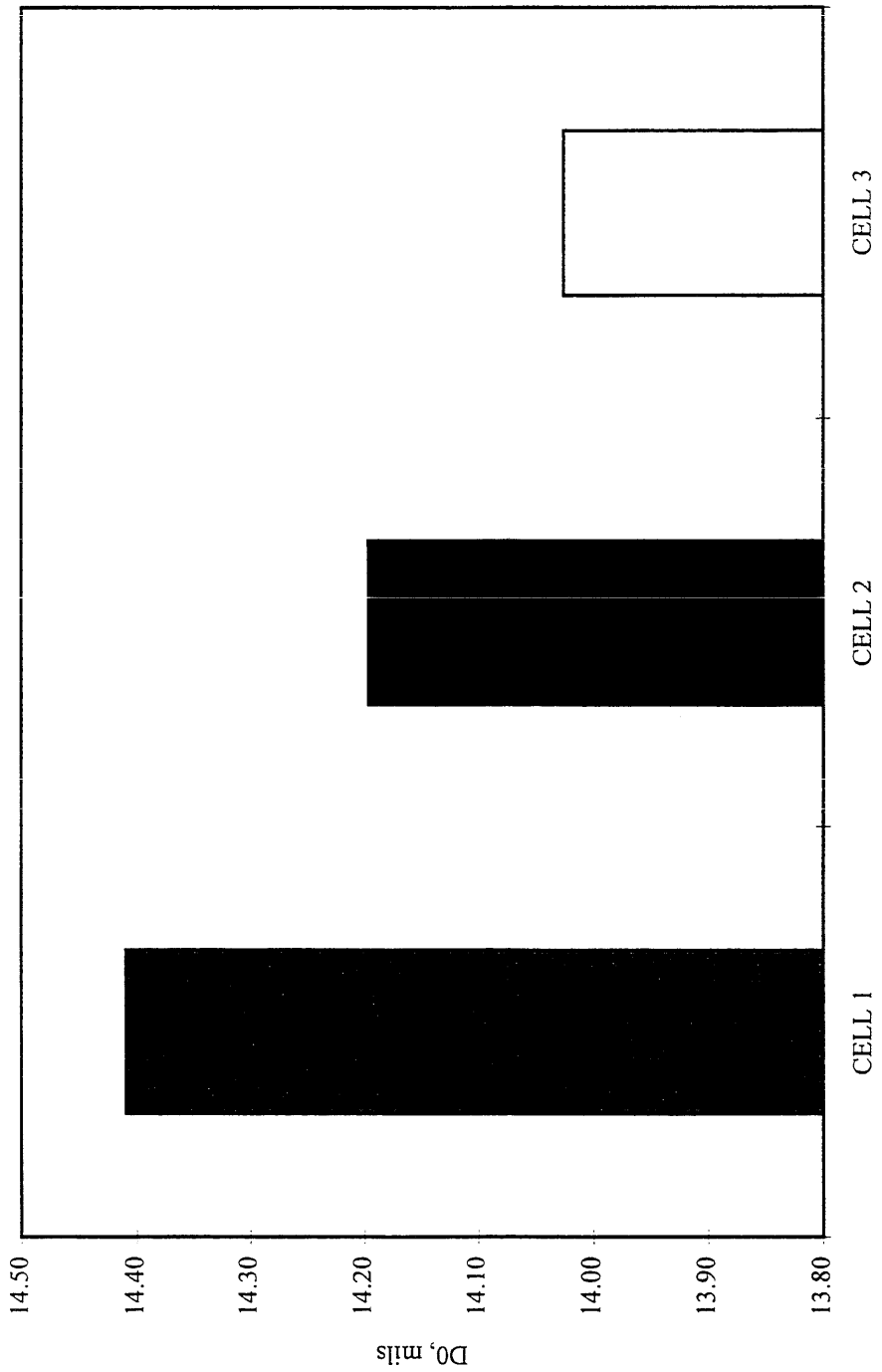

Figure 7.19. Comparison of Adjusted Maximum Deflections (May 10,1994).

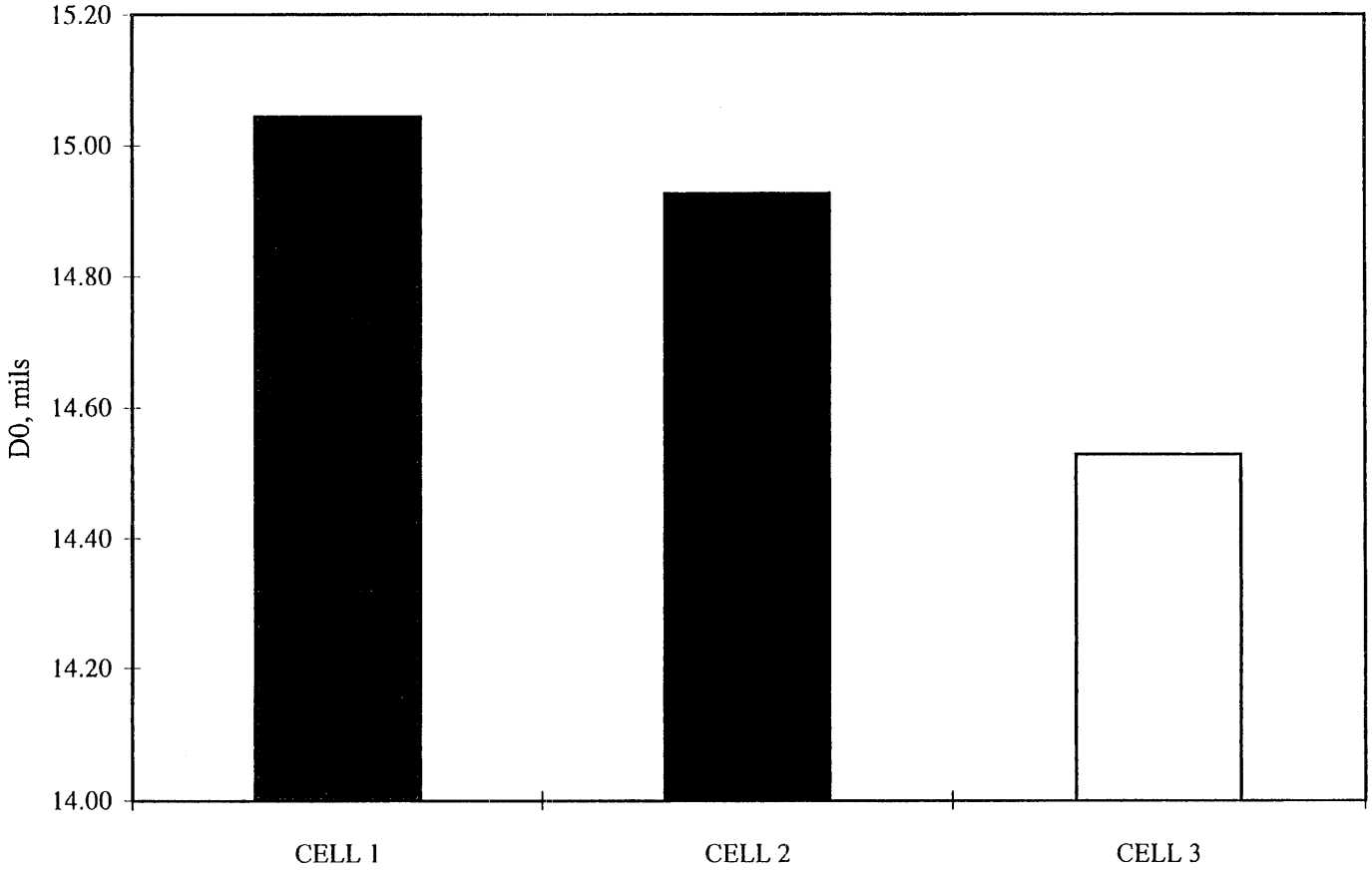

Figure 7.20. Comparison of Adjusted Maximum Deflections (May 23,1994).

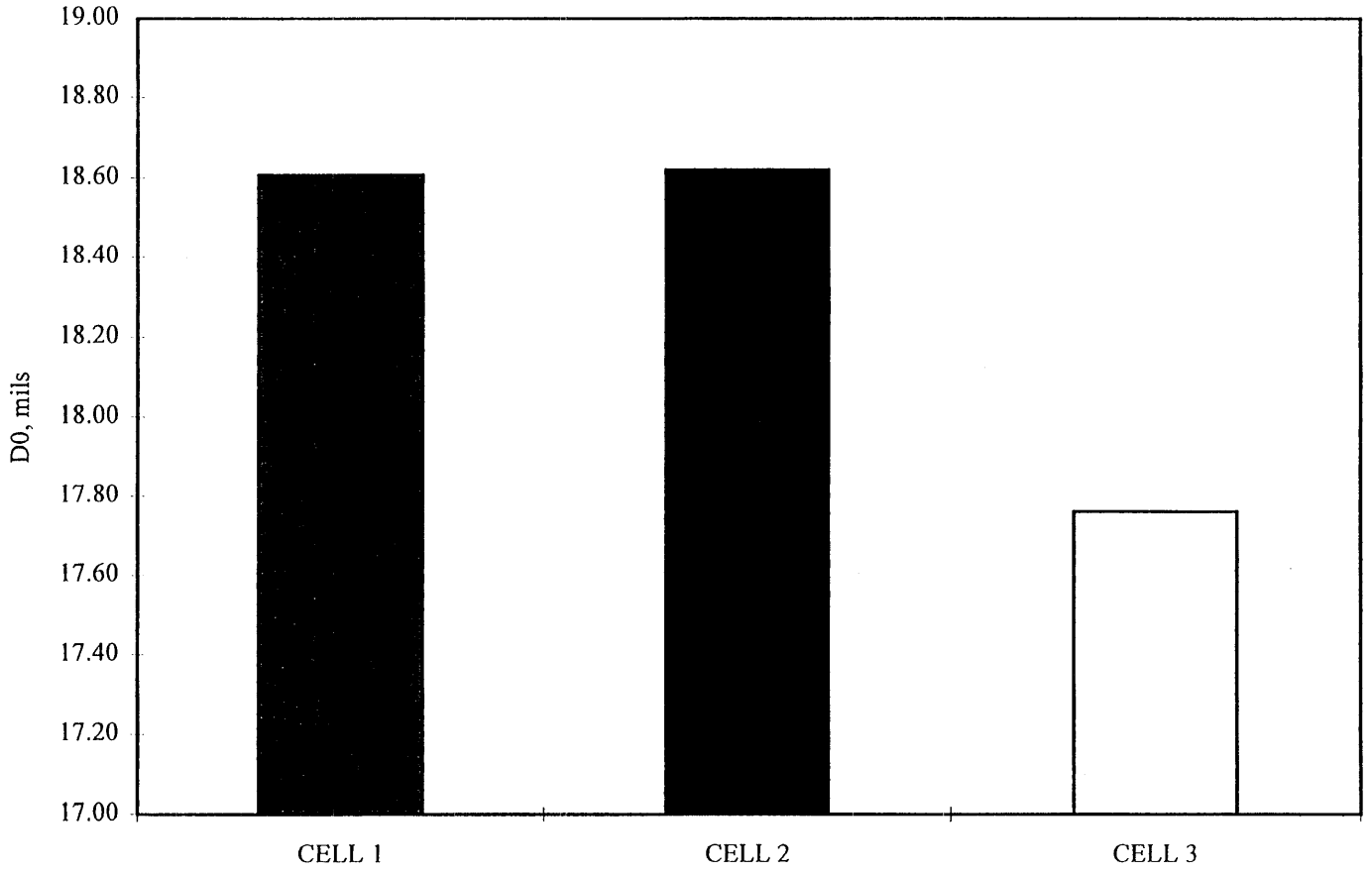

Figure 7.21. Comparison of Adjusted Maximum Deflections (June 21,1994).

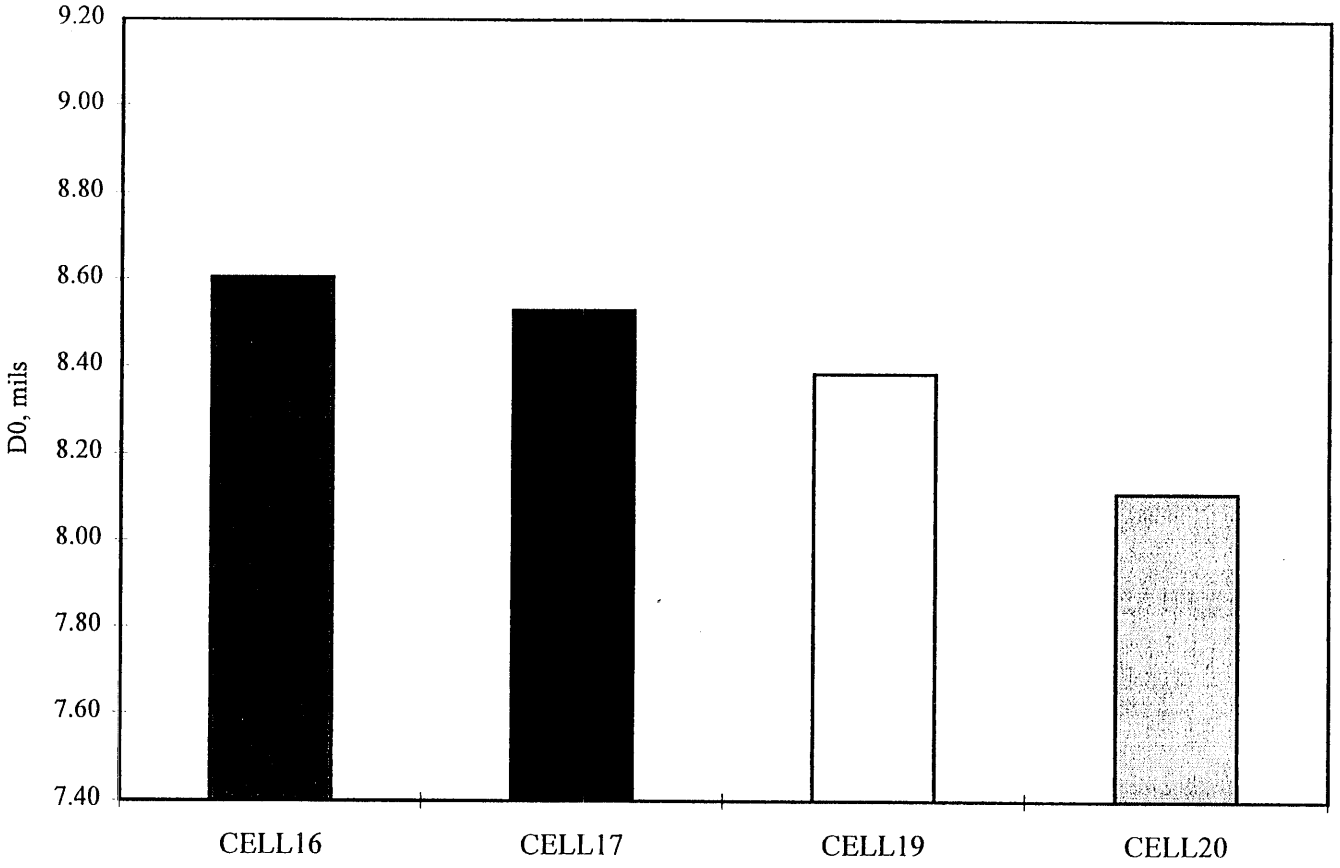

Figure 7.22. Comparison of Adjusted Maximum Deflections (April 25, 1994).

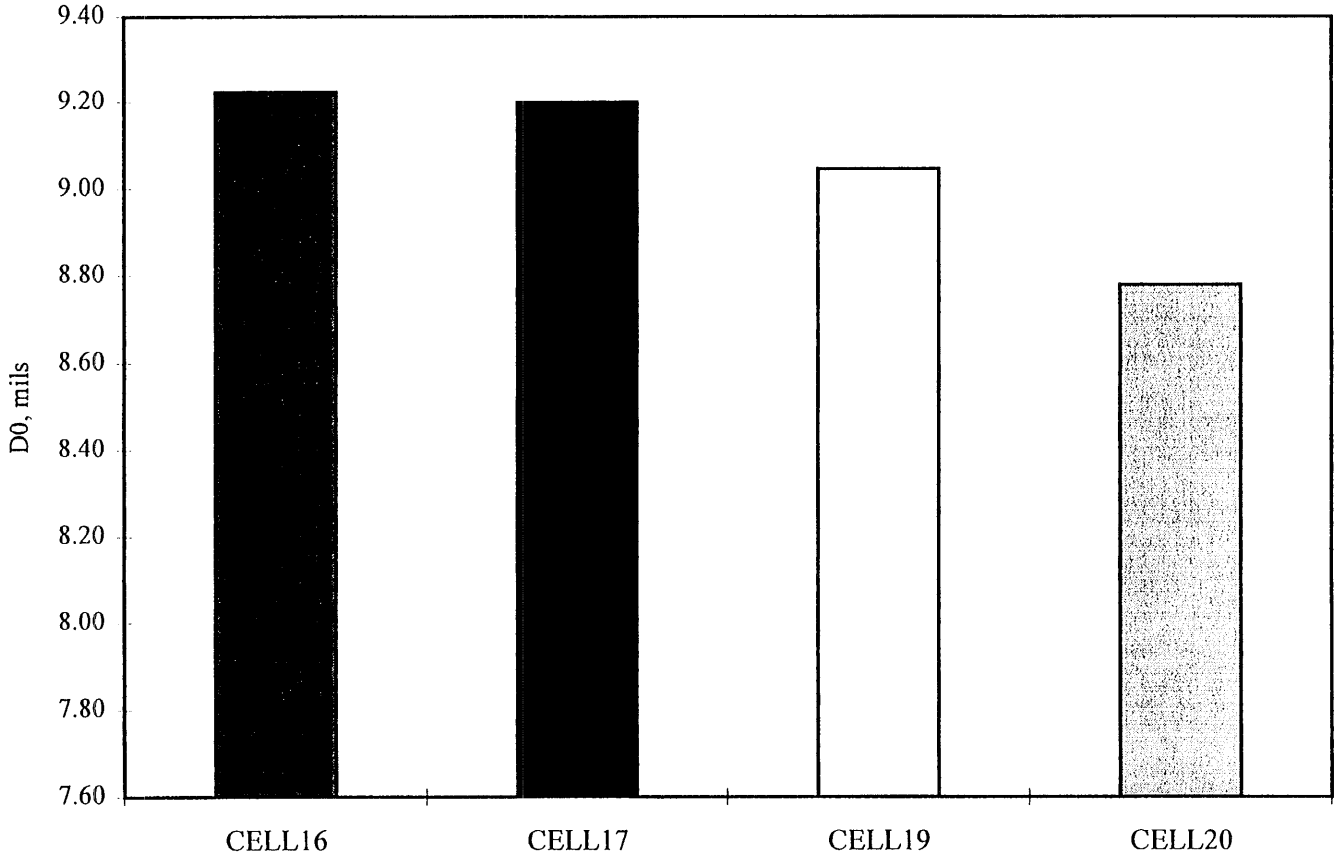

Figure 7.23. Comparison of Adjusted Maximum Deflections (May 10, 1994).

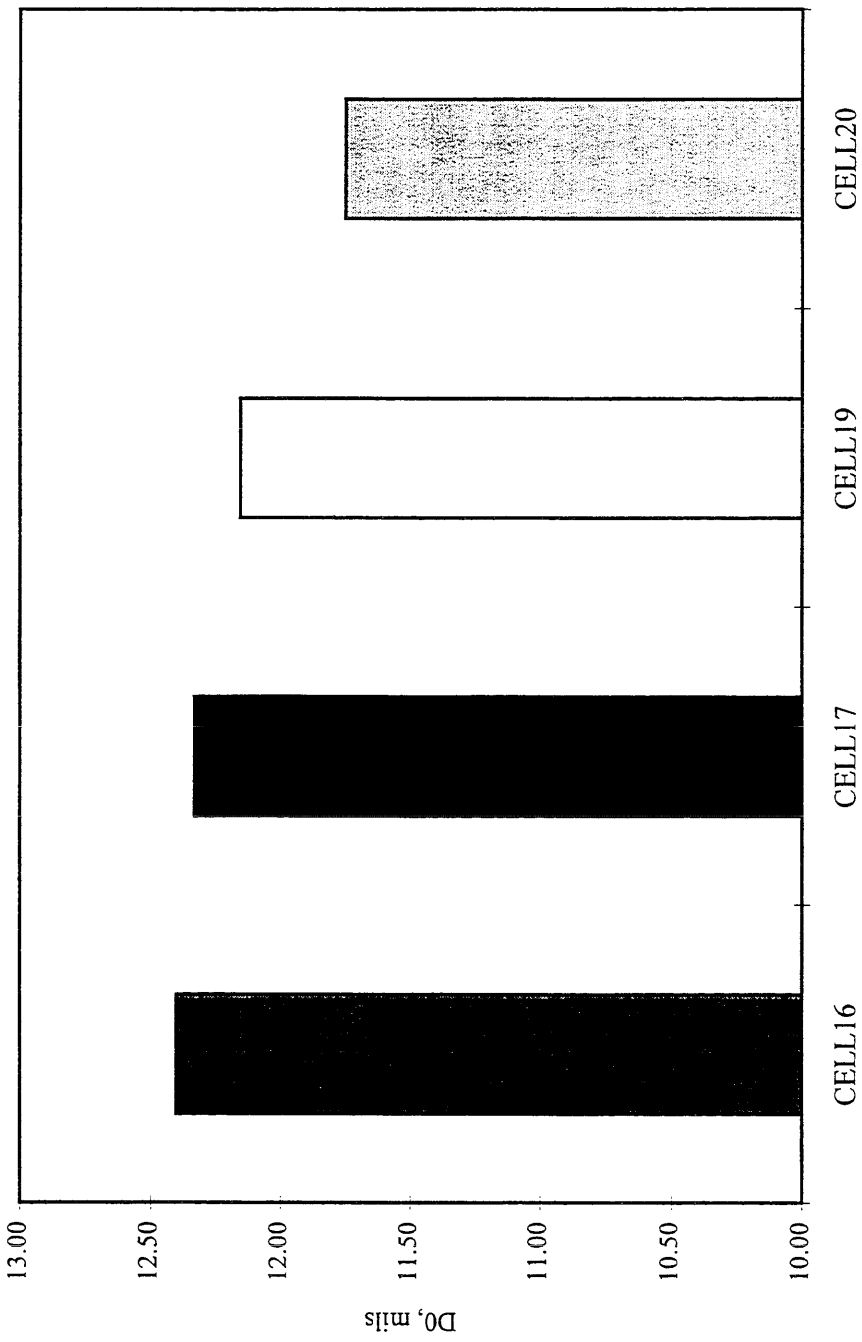

Figure 7.24. Comparison of Adjusted Maximum Deflections (May 23, 1994).

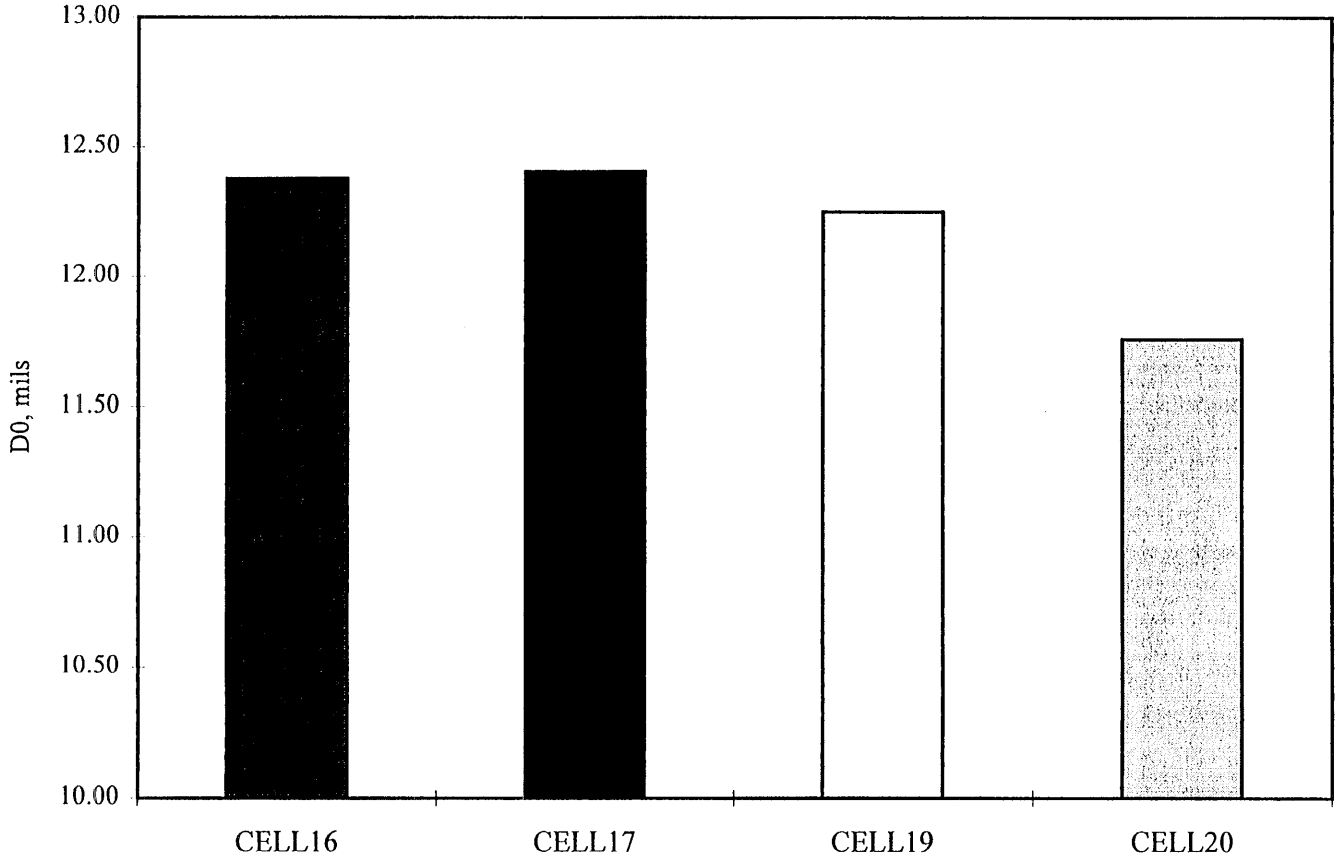

Figure 7.25. Comparison of Adjusted Maximum Deflections (June 21, 1994).

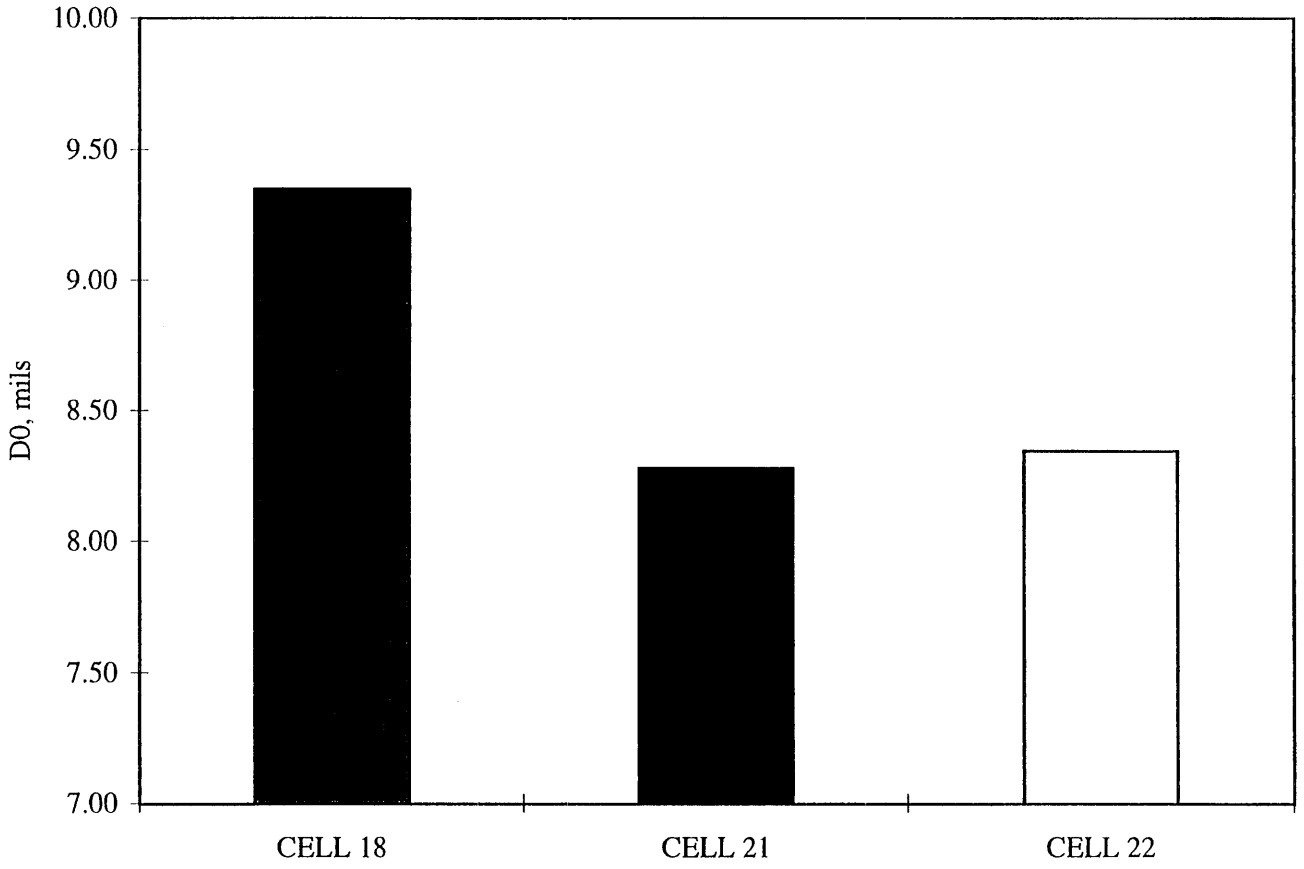

Figure 7.26. Comparison of Adjusted Maximum Deflections (April 25, 1994).

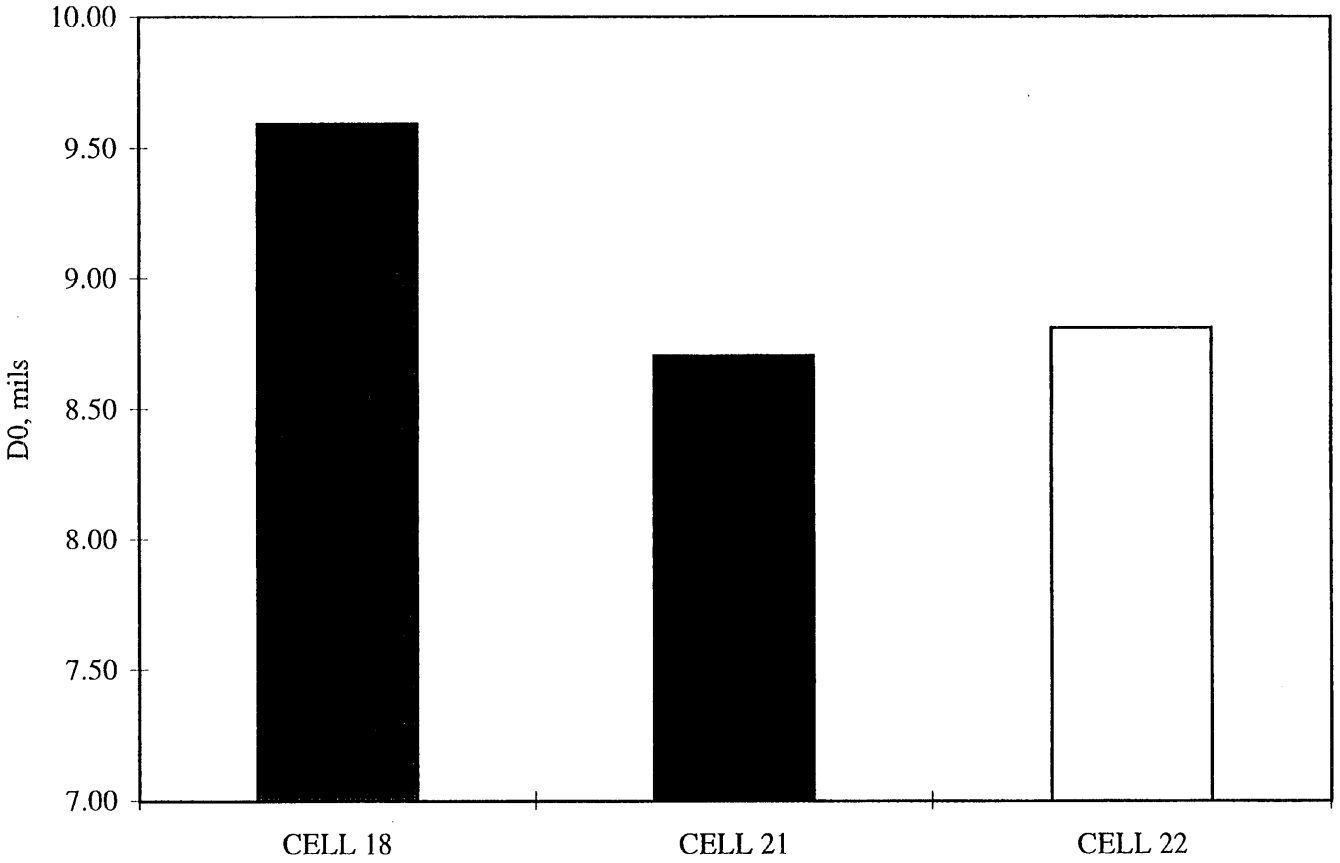

Figure 7.27. Comparison of Adjusted Maximum Deflections (May 10, 1994).

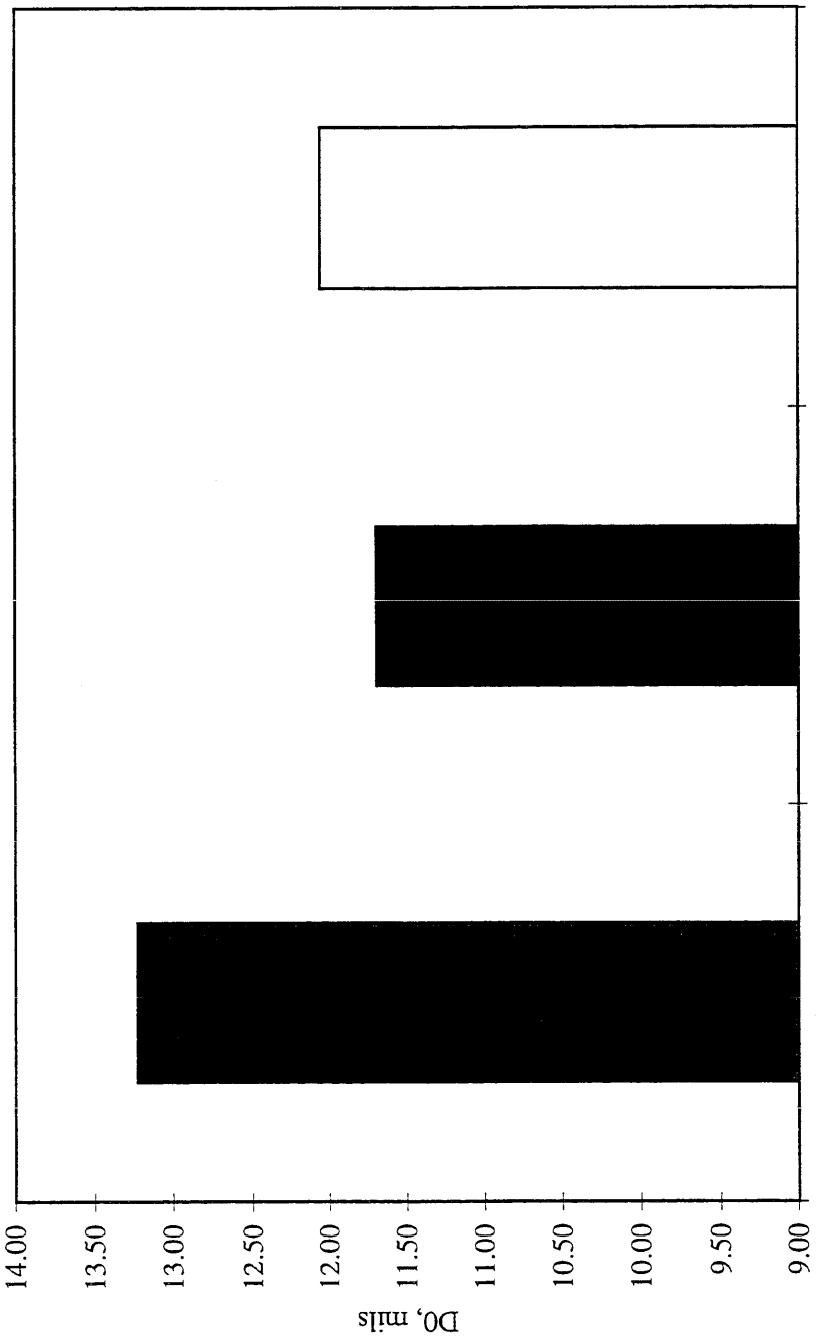

Figure 7.28. Comparison of Adjusted Maximum Deflections (May 23, 1994).

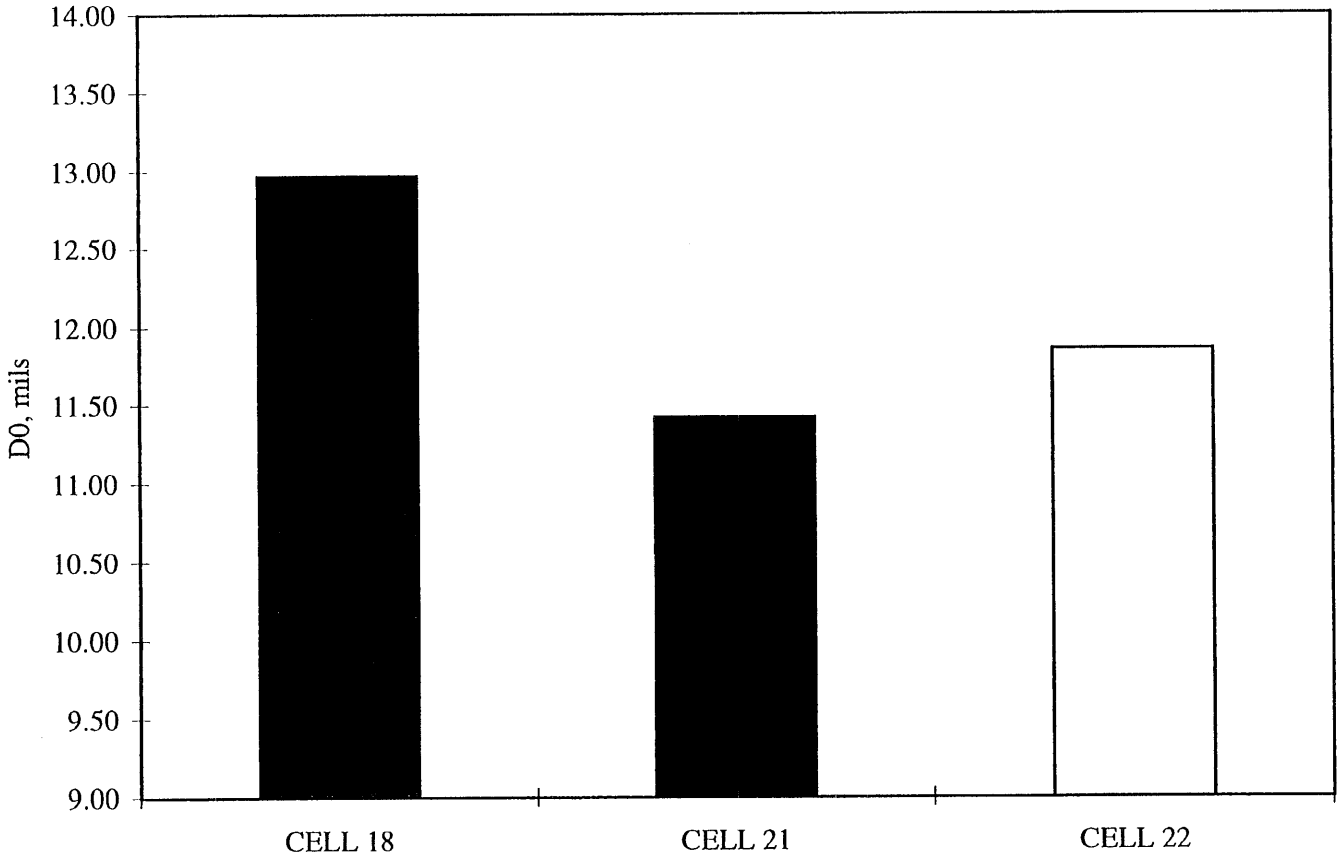

Figure 7.29. Comparison of Adjusted Maximum Deflections (June 21, 1994).

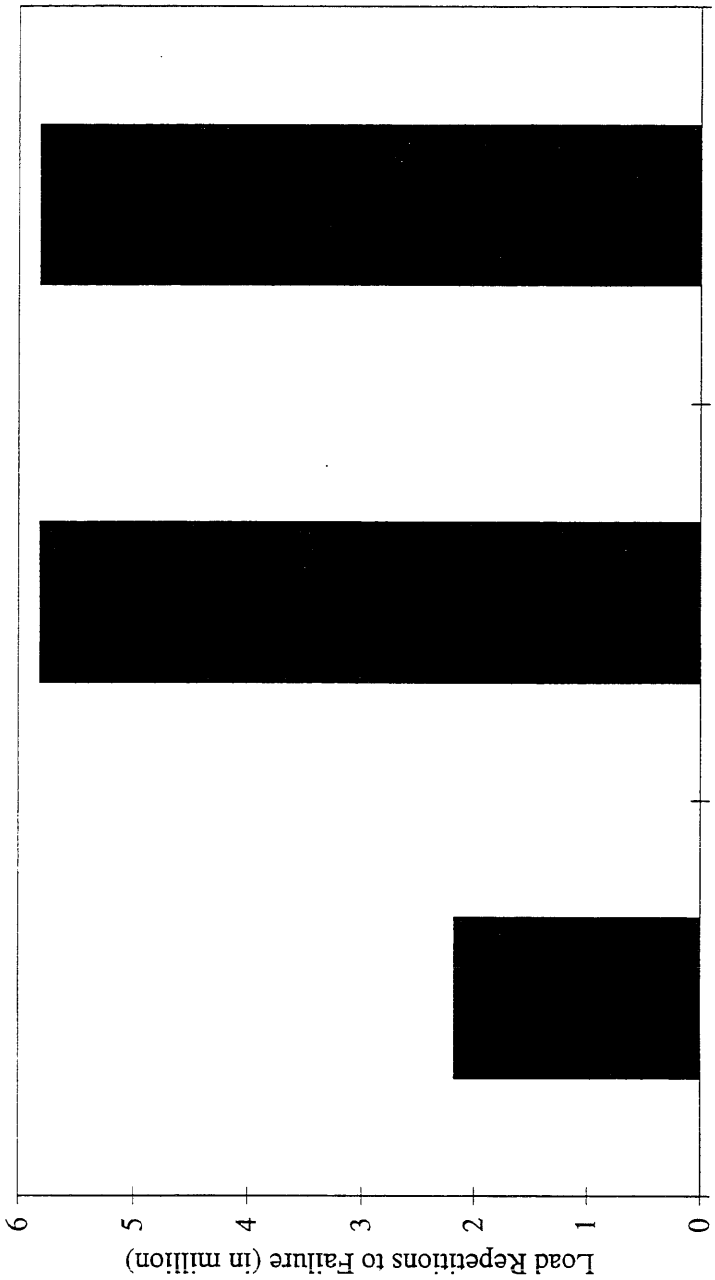

Figure 7.30 Estimated Fatigue Life on Mainline FDAC Cells (IDOT's Algorithm).

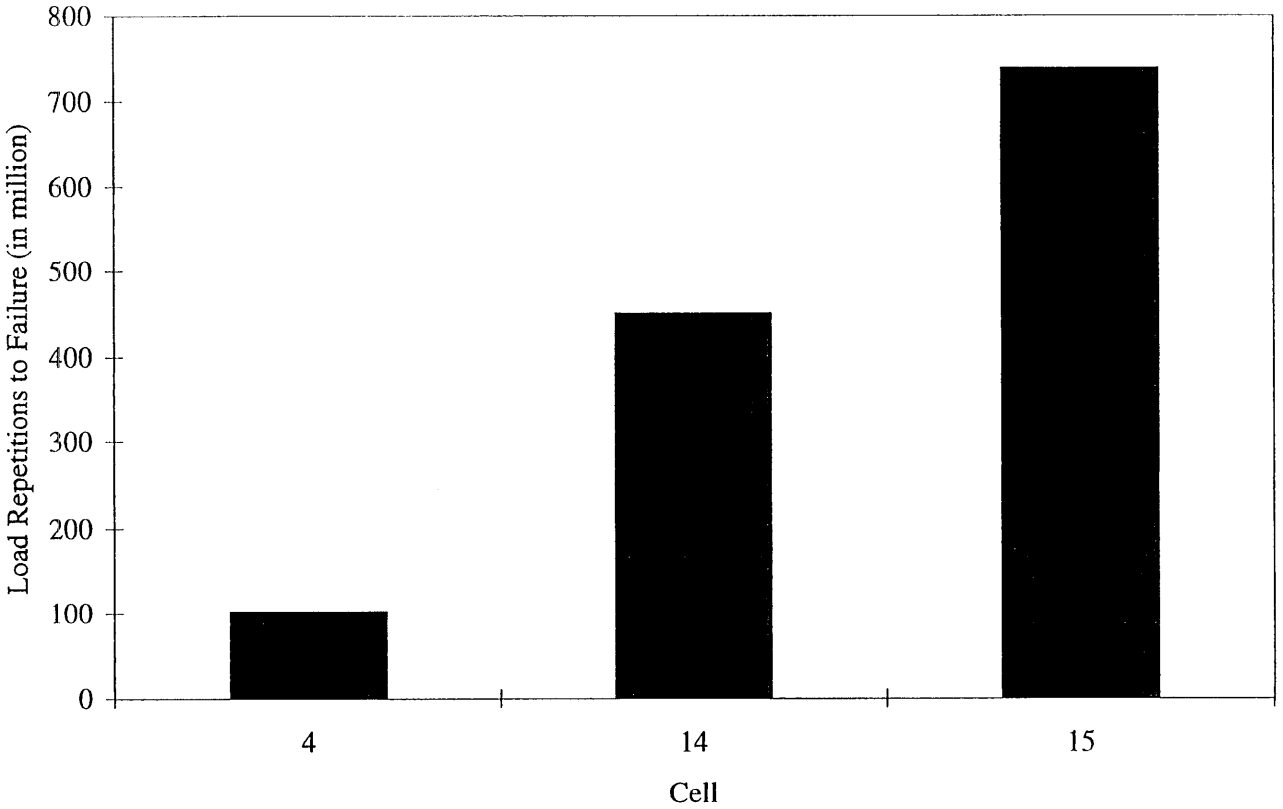

Figure 7.31 Estimated Fatigue Life on Mainline FDAC Cells (Laboratory Algorithm).

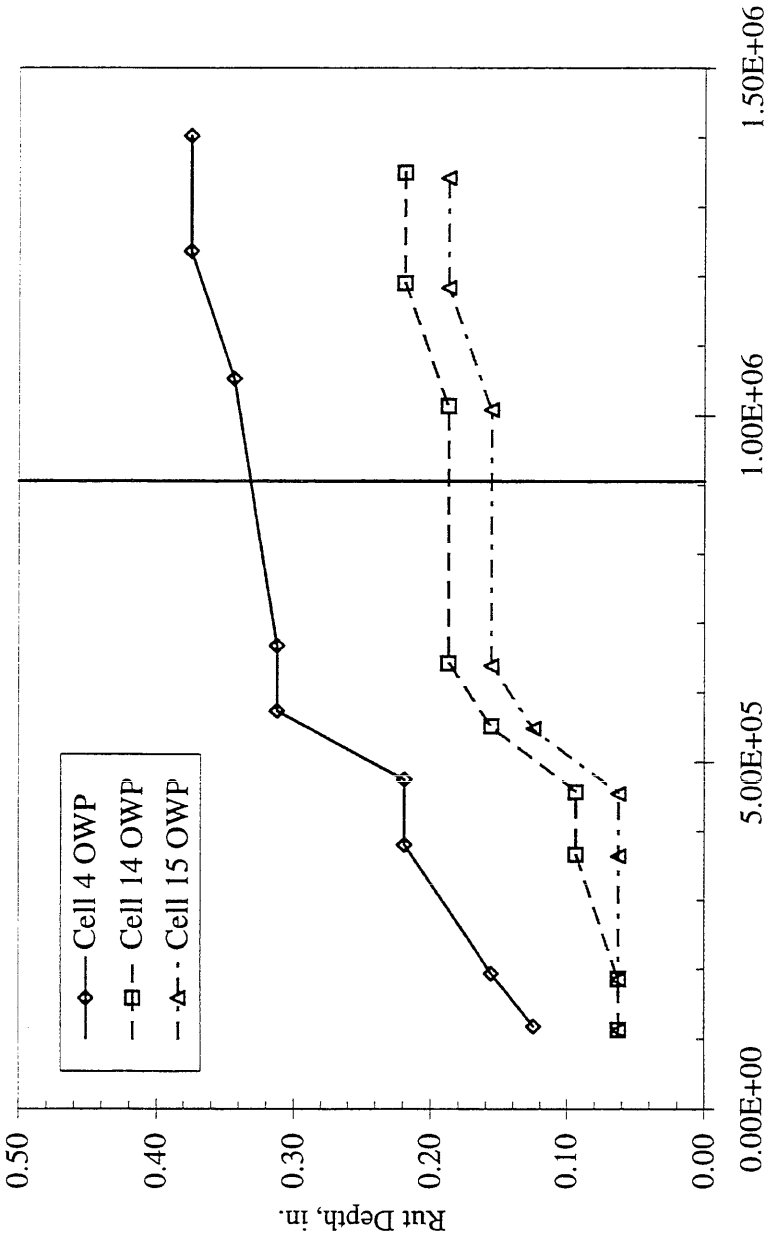

Figure 7.32. Rut Accumulation on FDAC Sections.

Appendix A

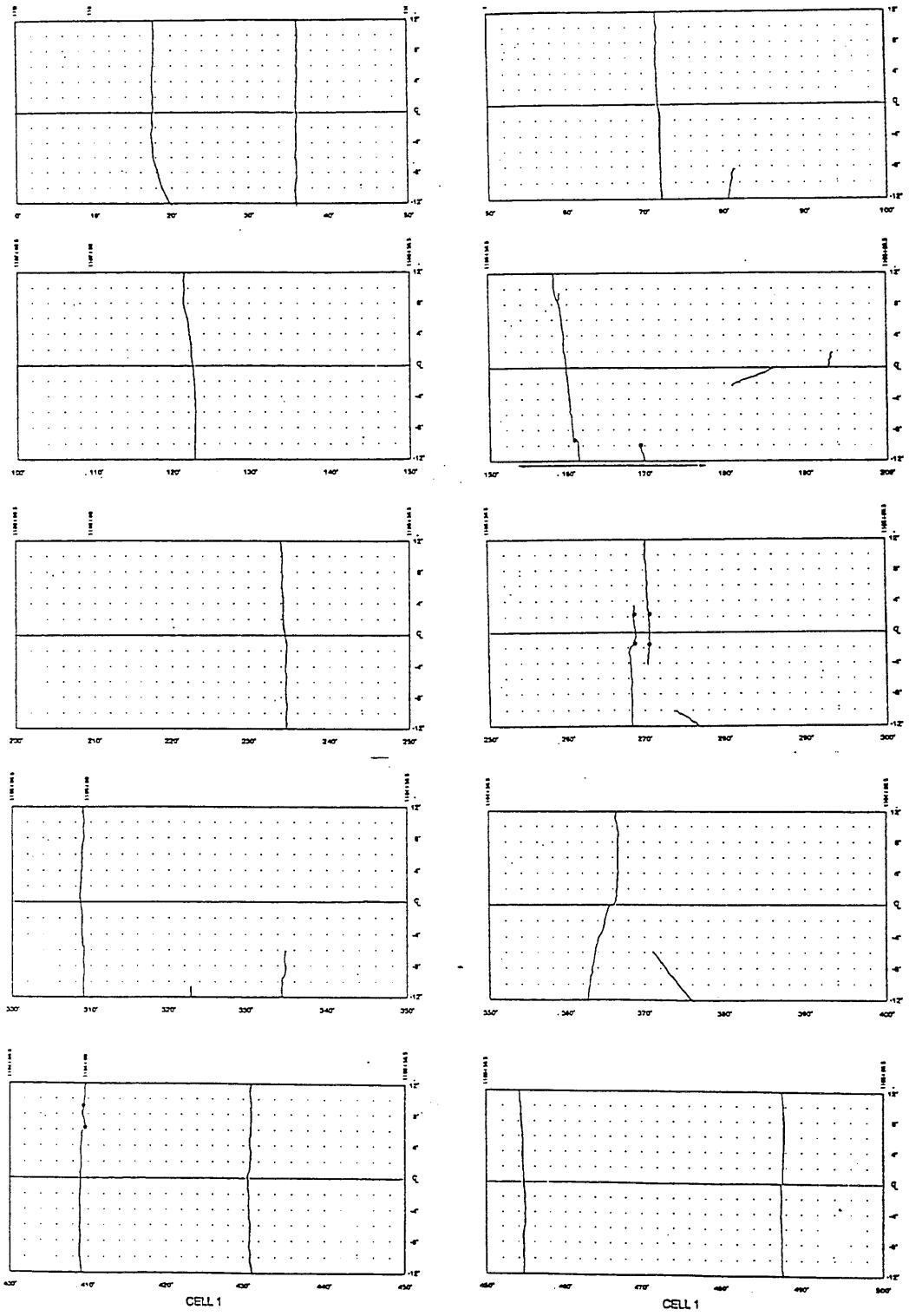

Figure A.1. Thermal Cracking on Cell 1.

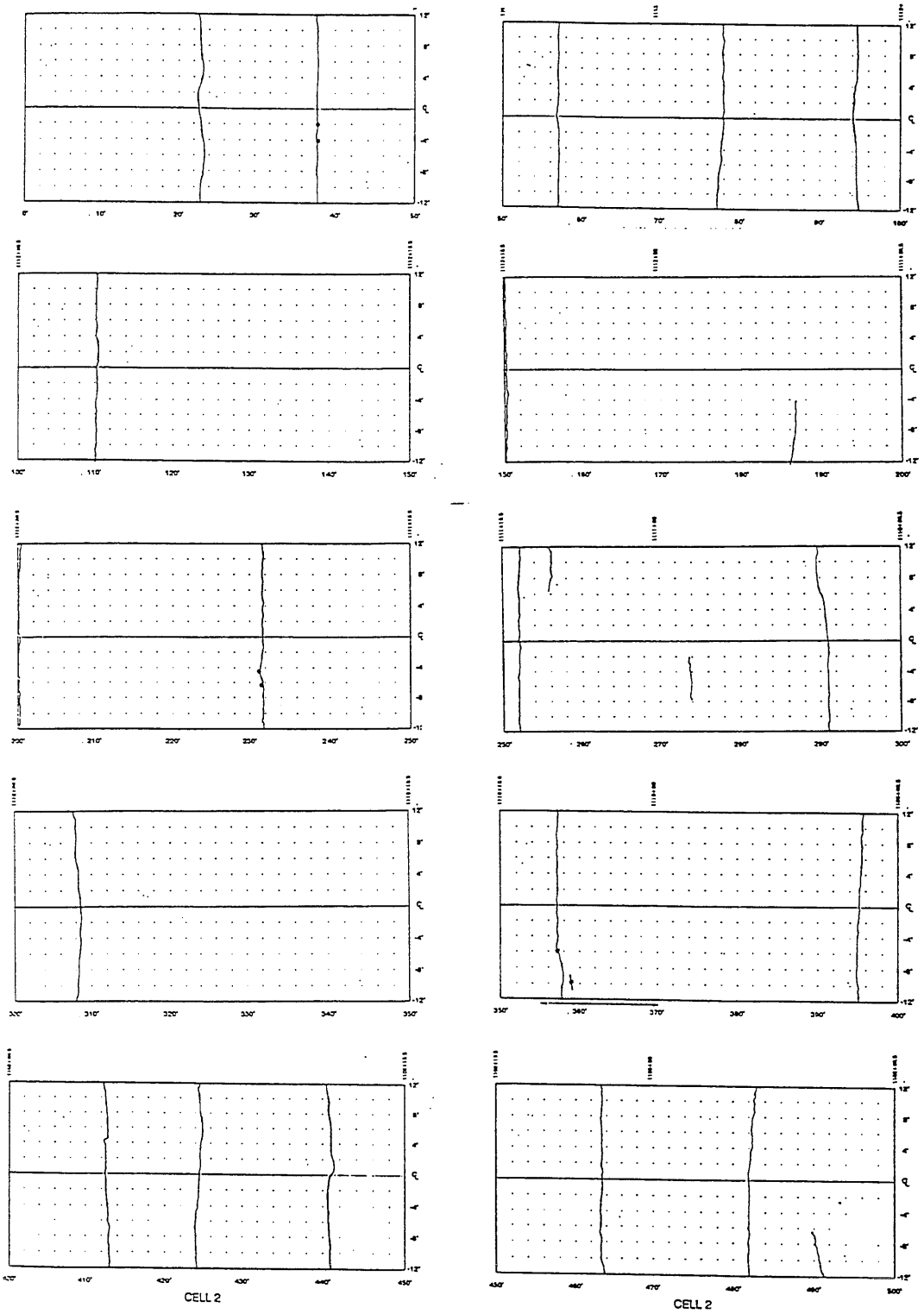

Figure A.2. Thermal Cracking on Cell 2.

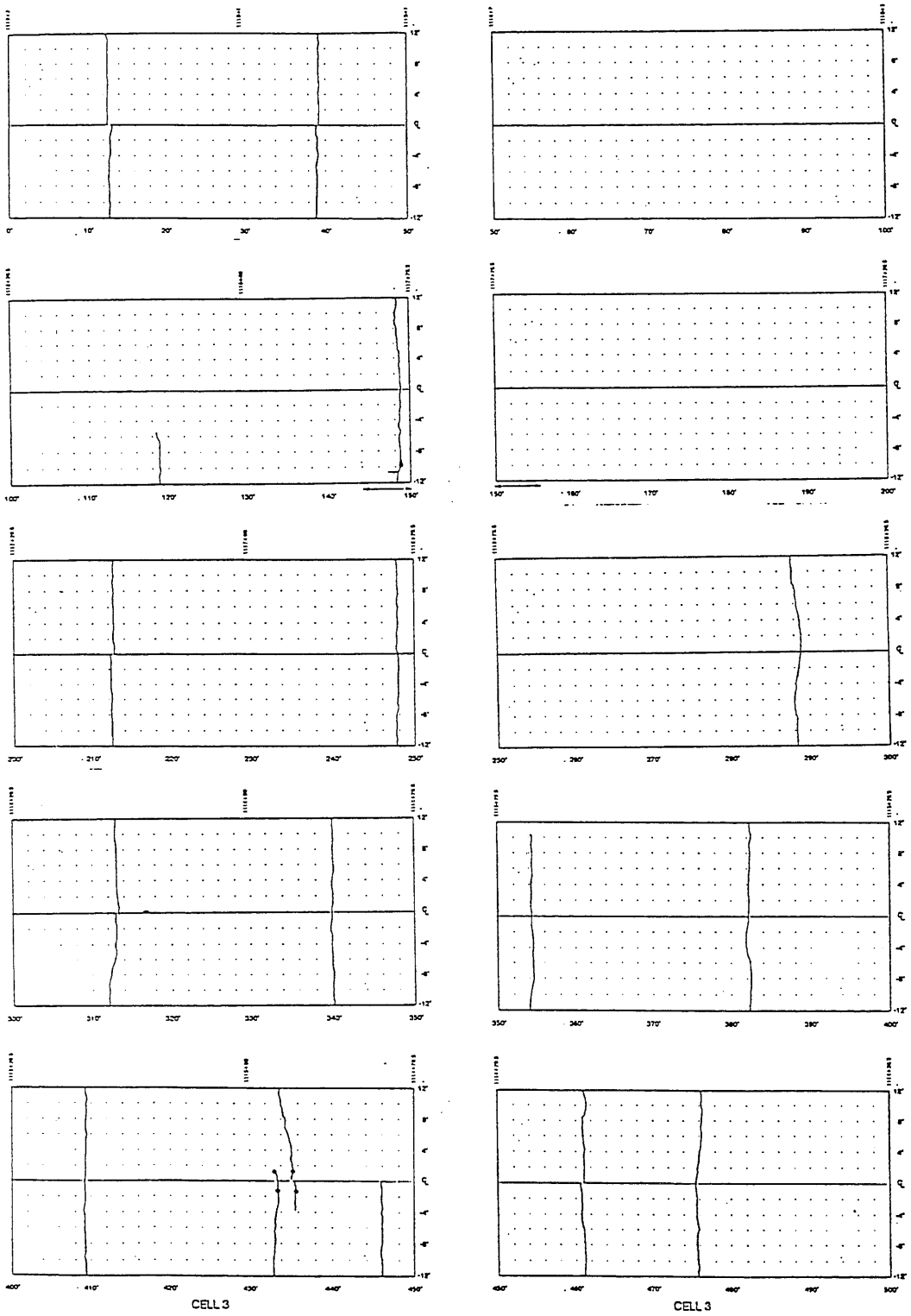

Figure A.3. Thermal Cracking on Cell 3.

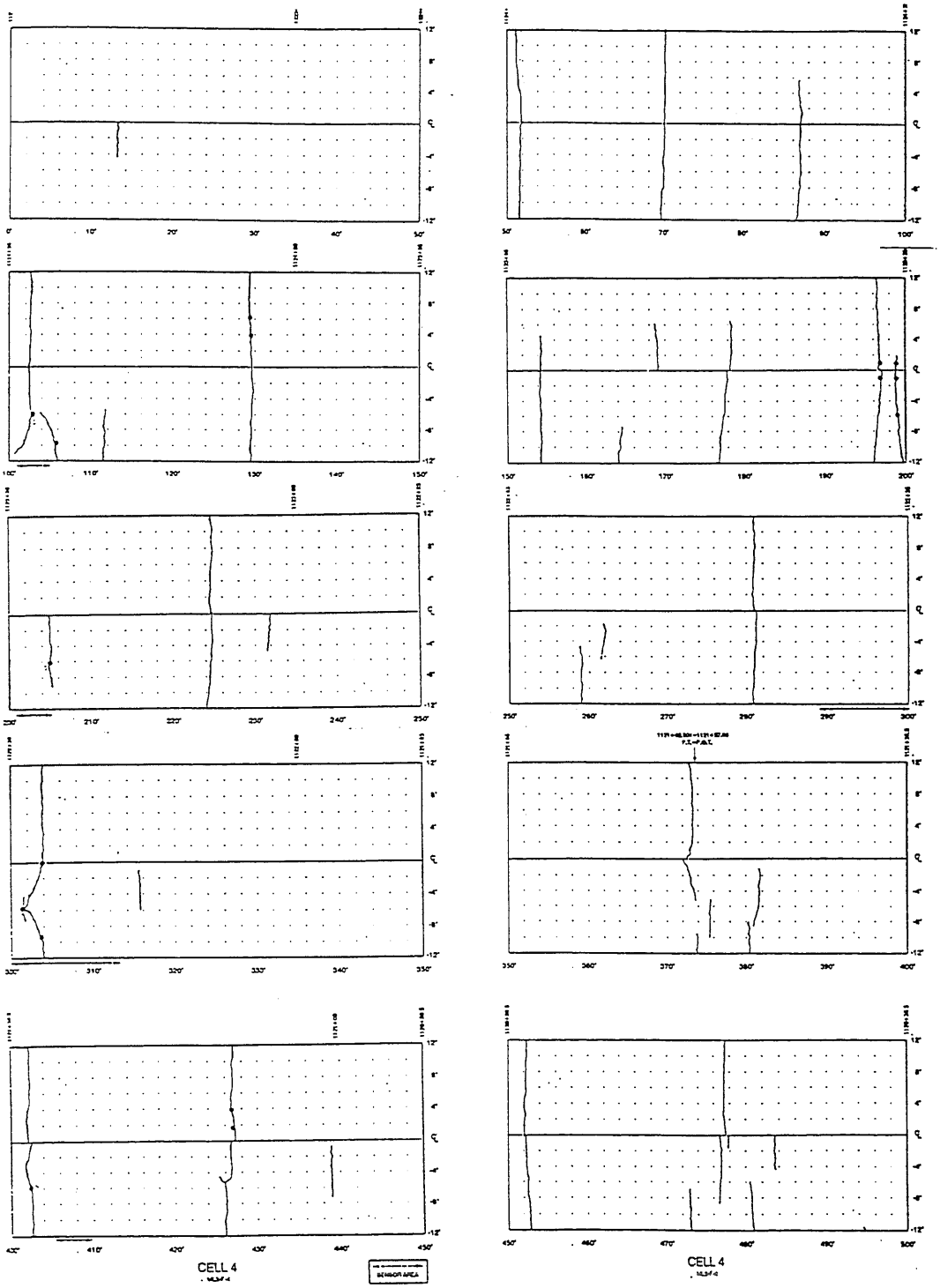

Figure A.4. Thermal Cracking on Cell 4.

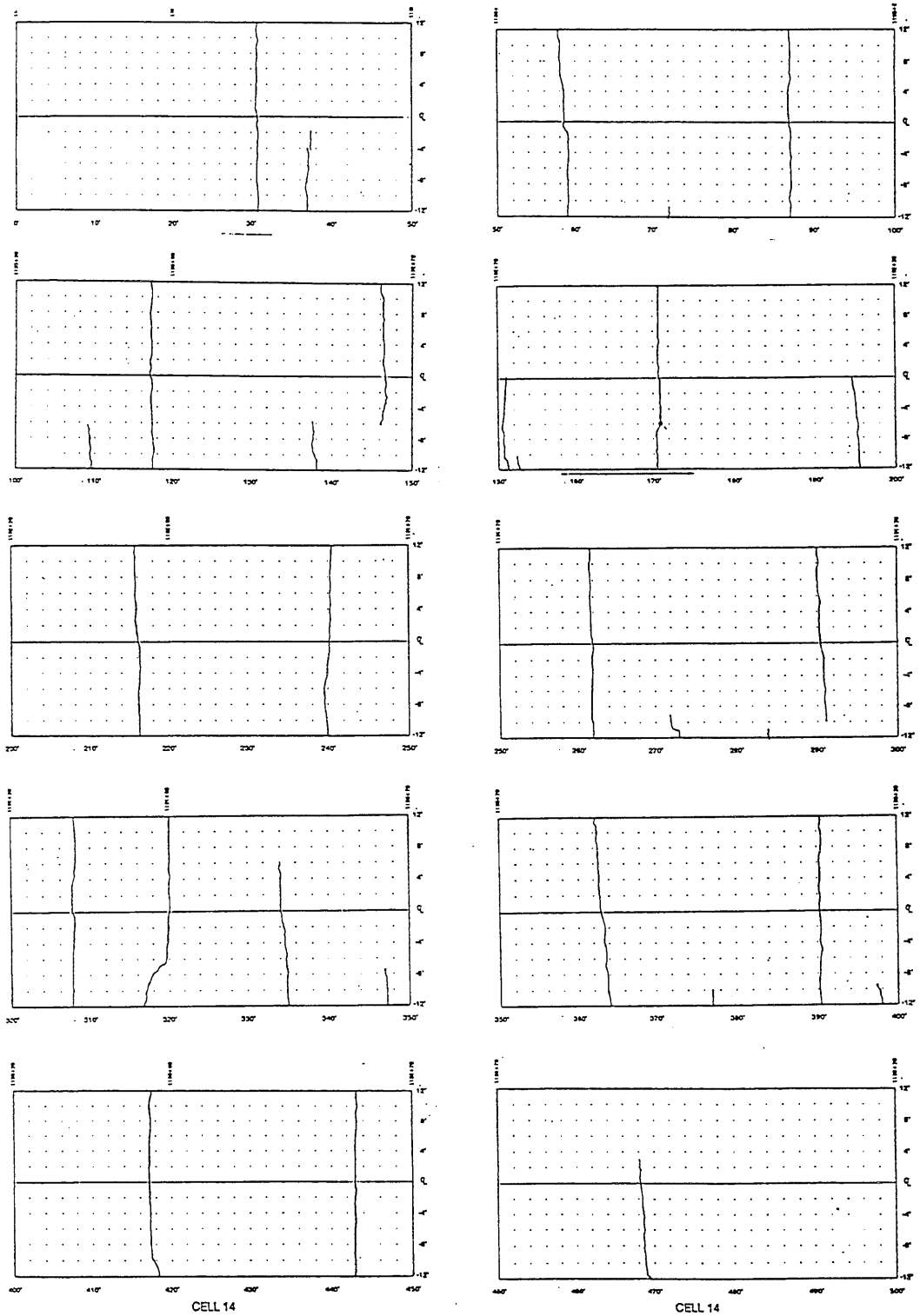

Figure A.5. Thermal Cracking on Cell 14.

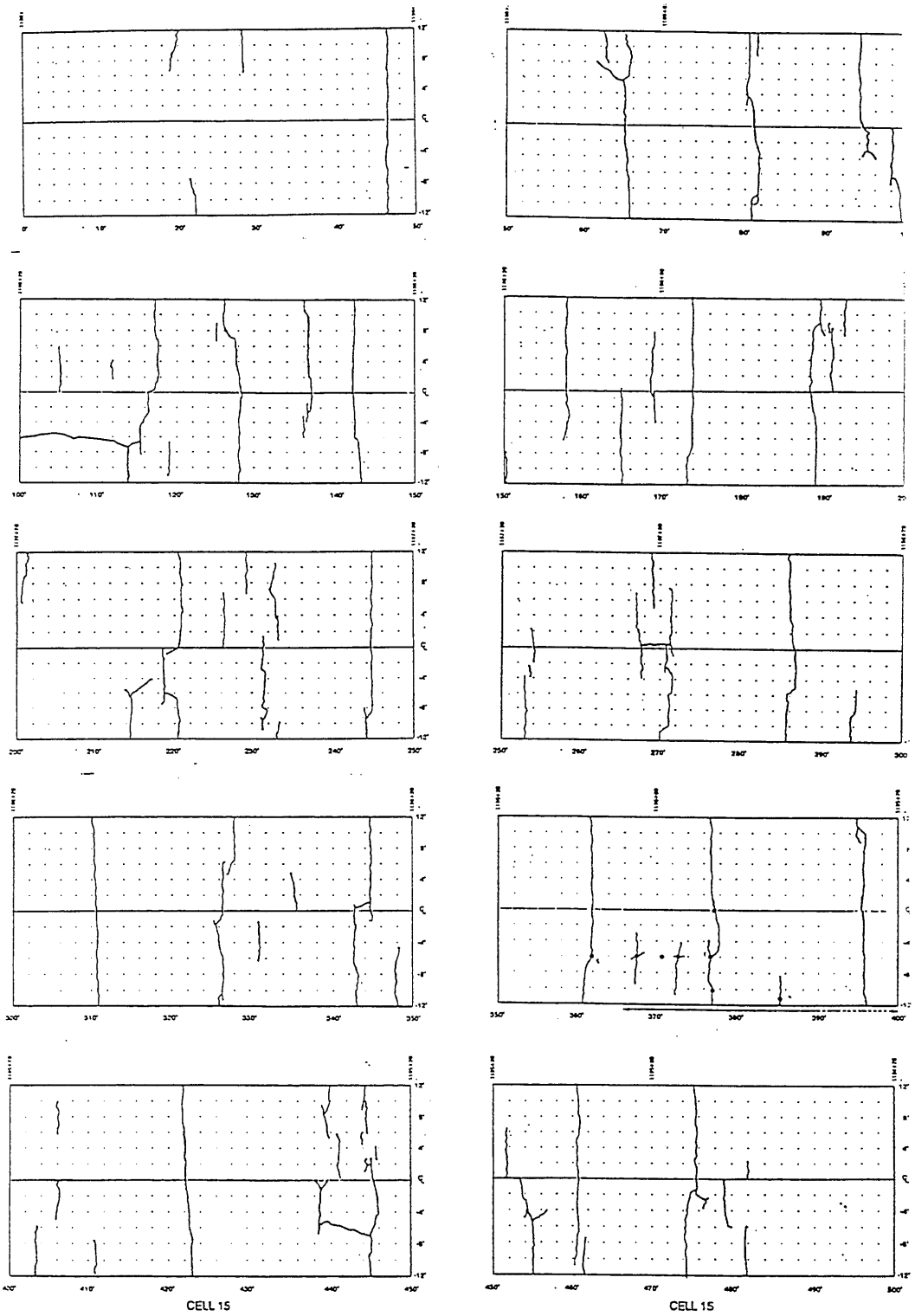

Figure A.6. Thermal Cracking on Cell 15.

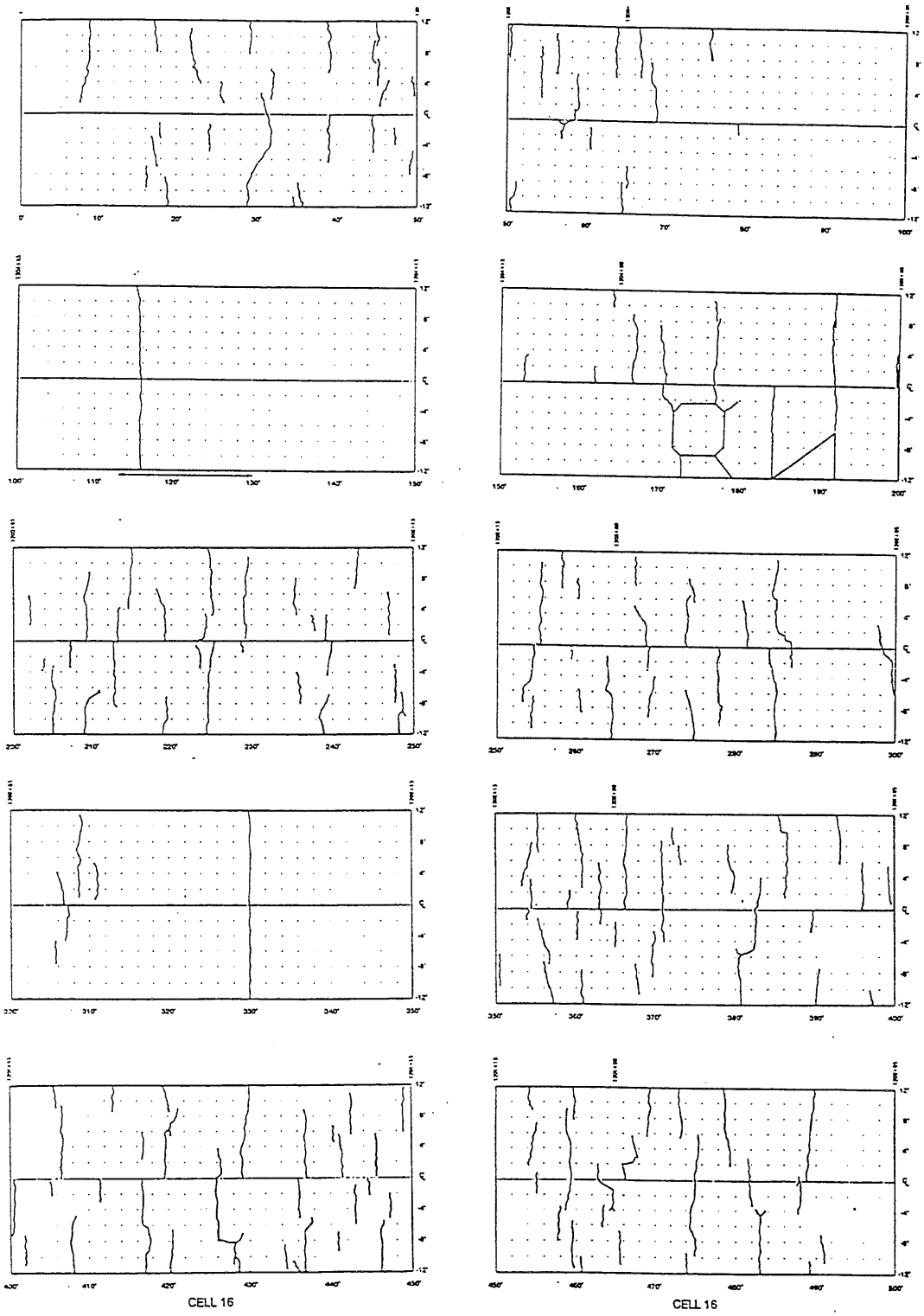

Figure A.7. Thermal Cracking on Cell 16.

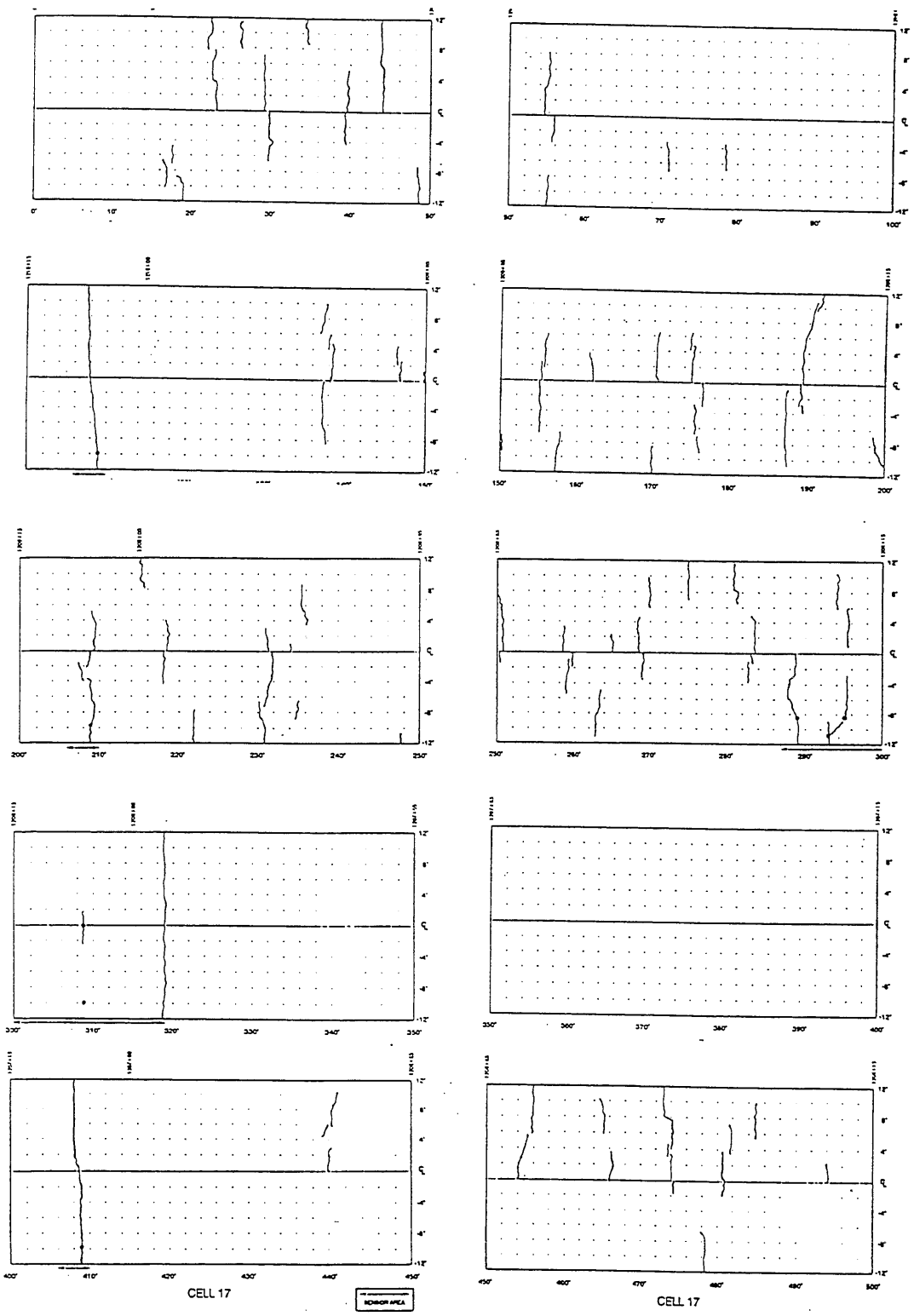

Figure A.8. Thermal Cracking on Cell 17.

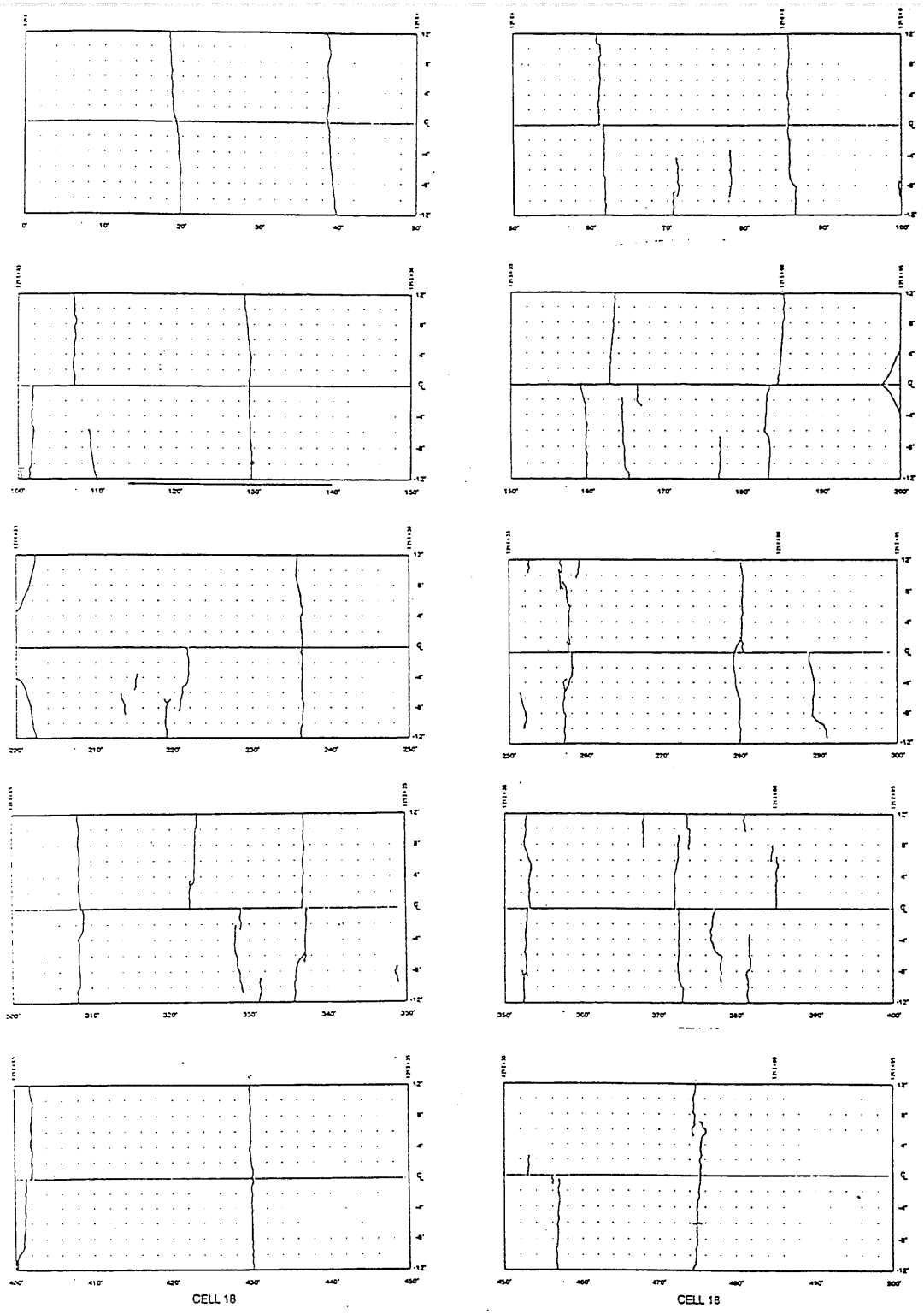

Figure A.9. Thermal Cracking on Cell 18.

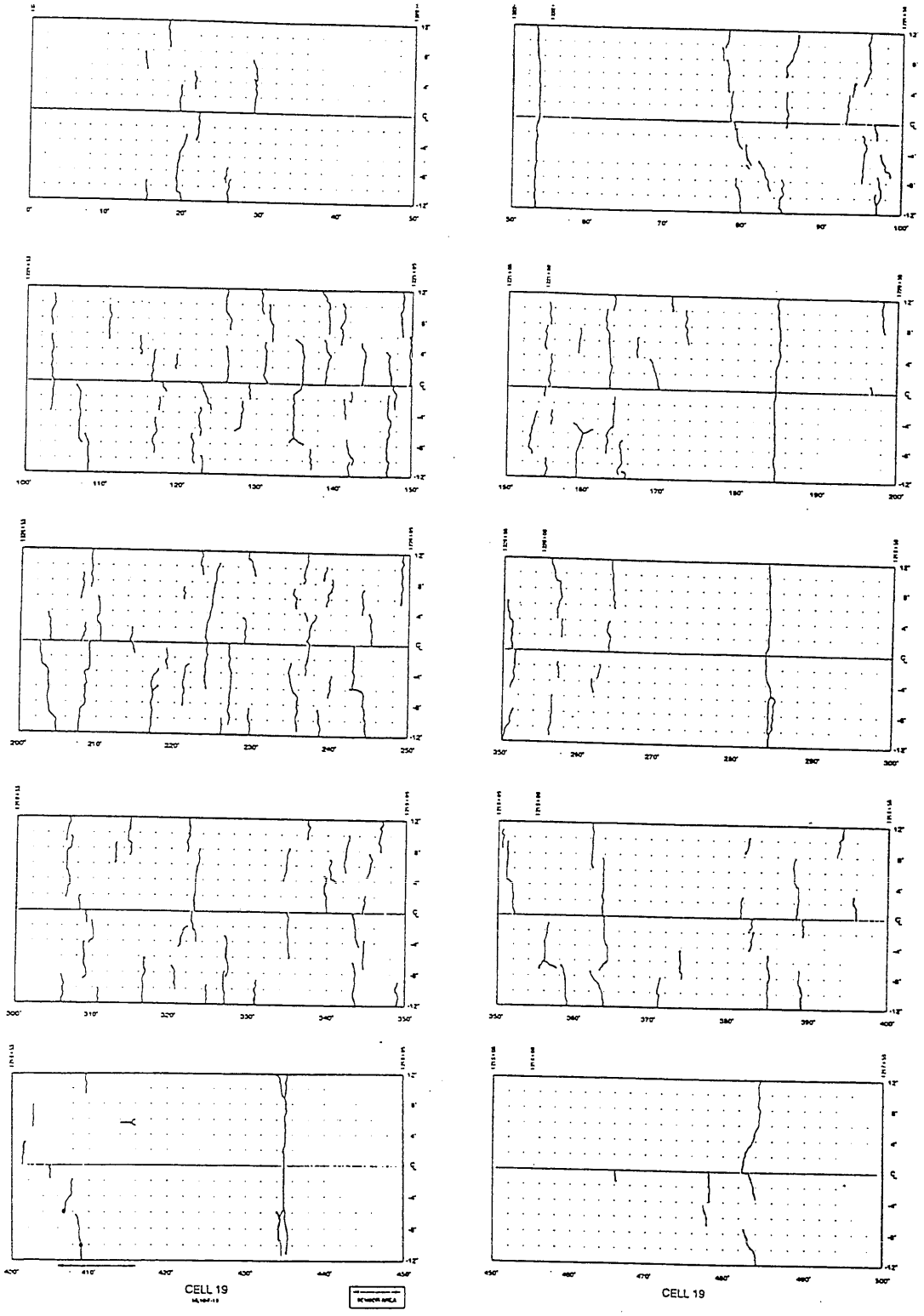

Figure A.10. Thermal Cracking on Cell 19.

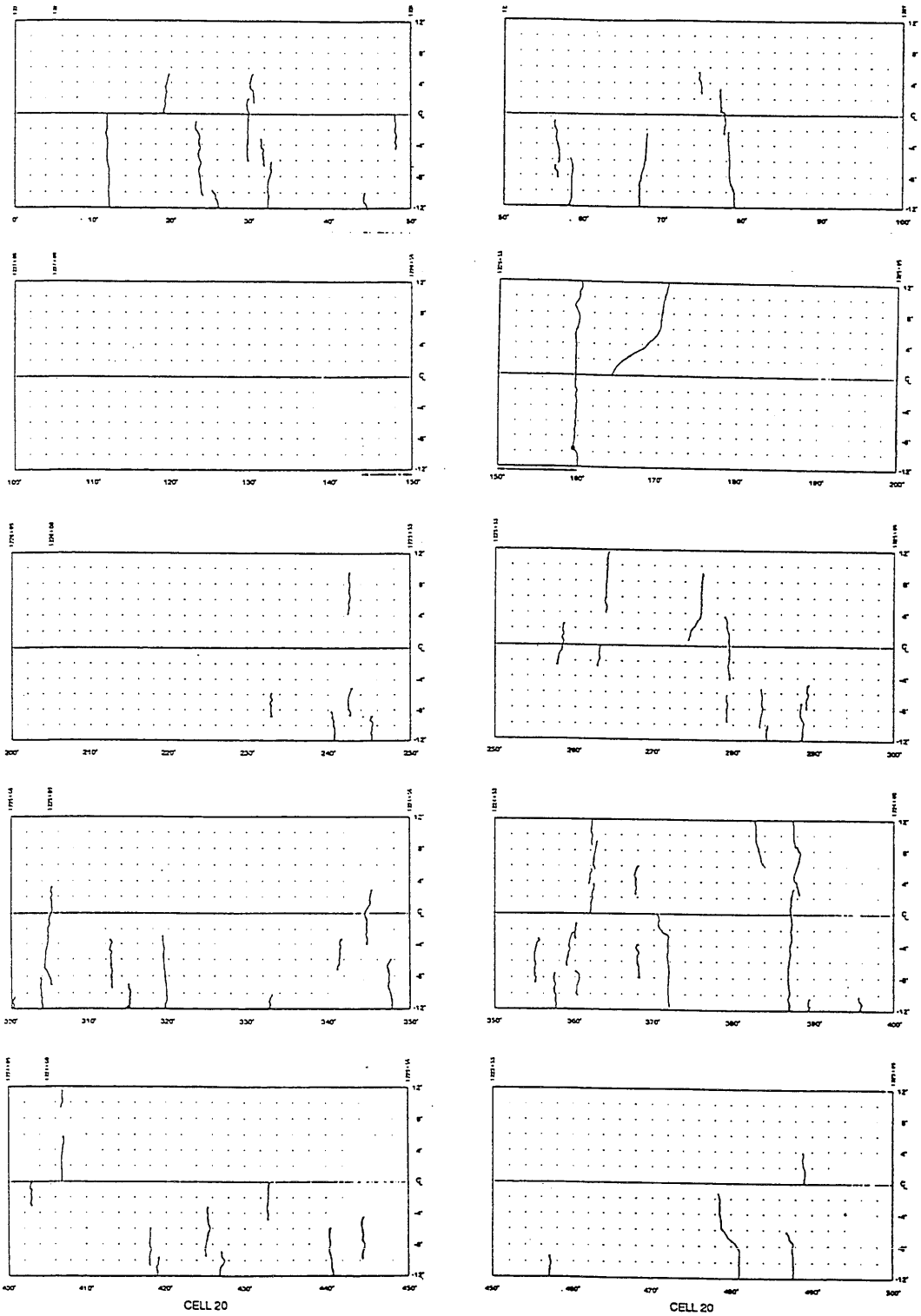

Figure A.11. Thermal Cracking on Cell 20.

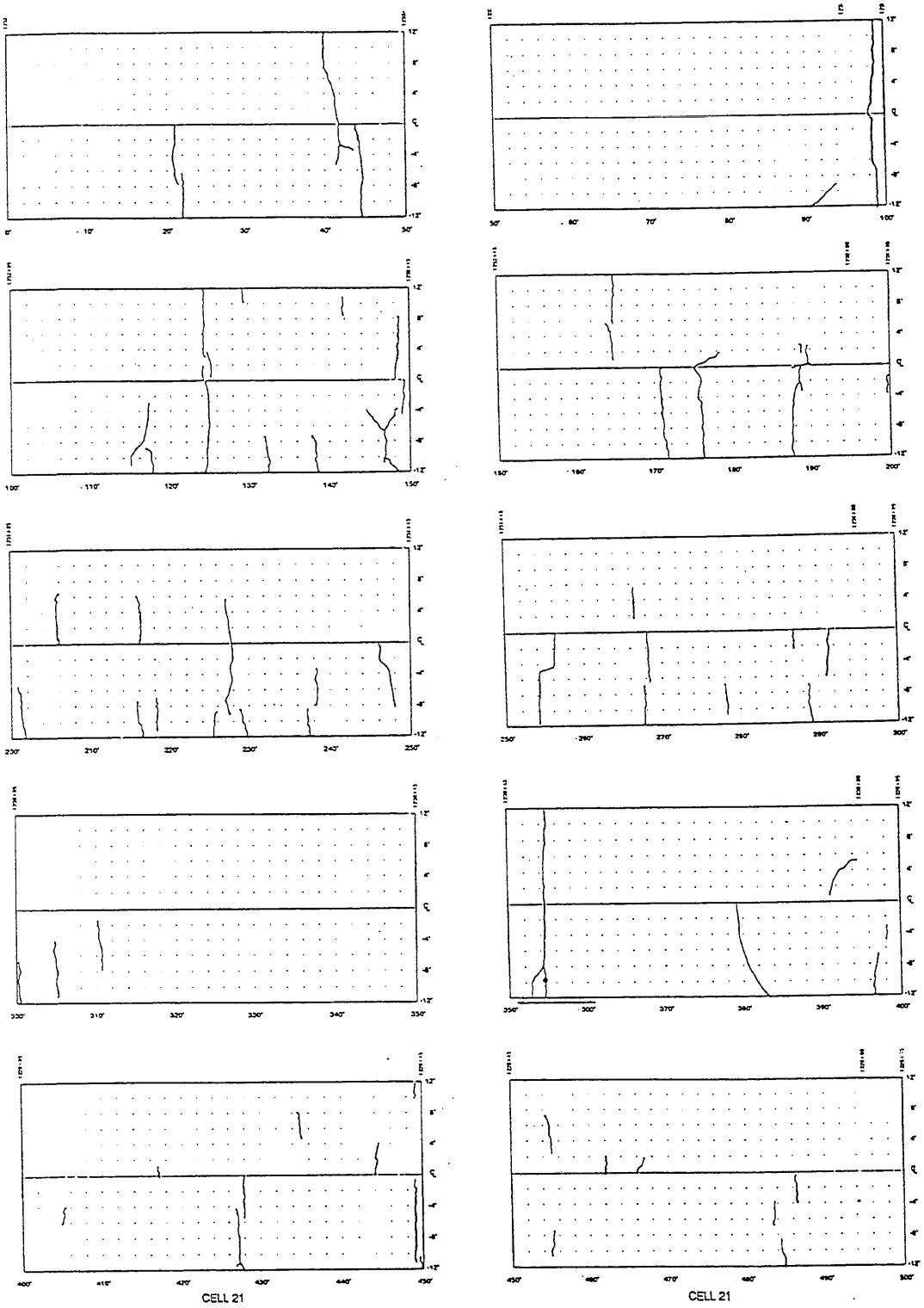

Figure A.12. Thermal Cracking on Cell 21.

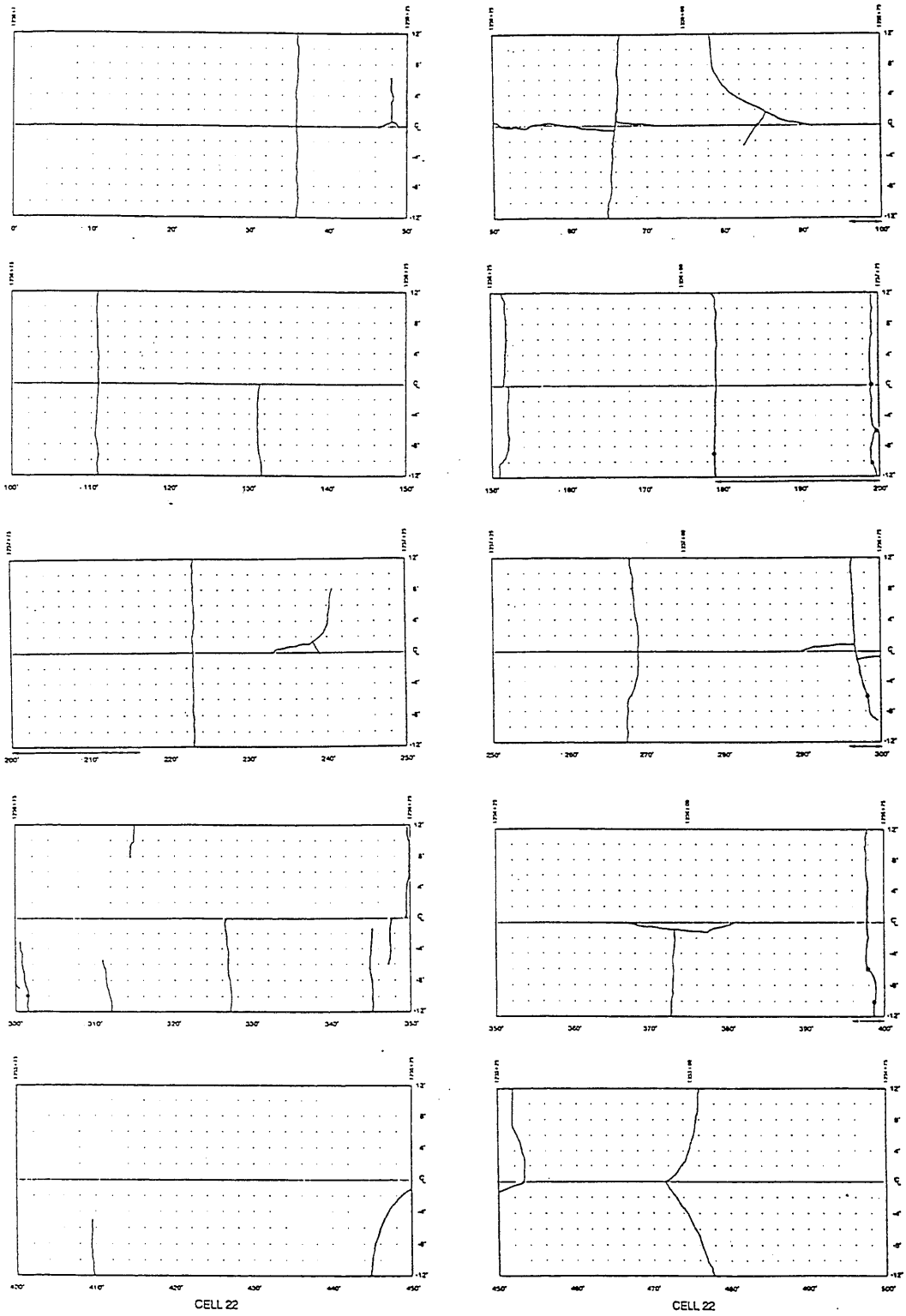

Figure A.13. Thermal Cracking on Cell 22.

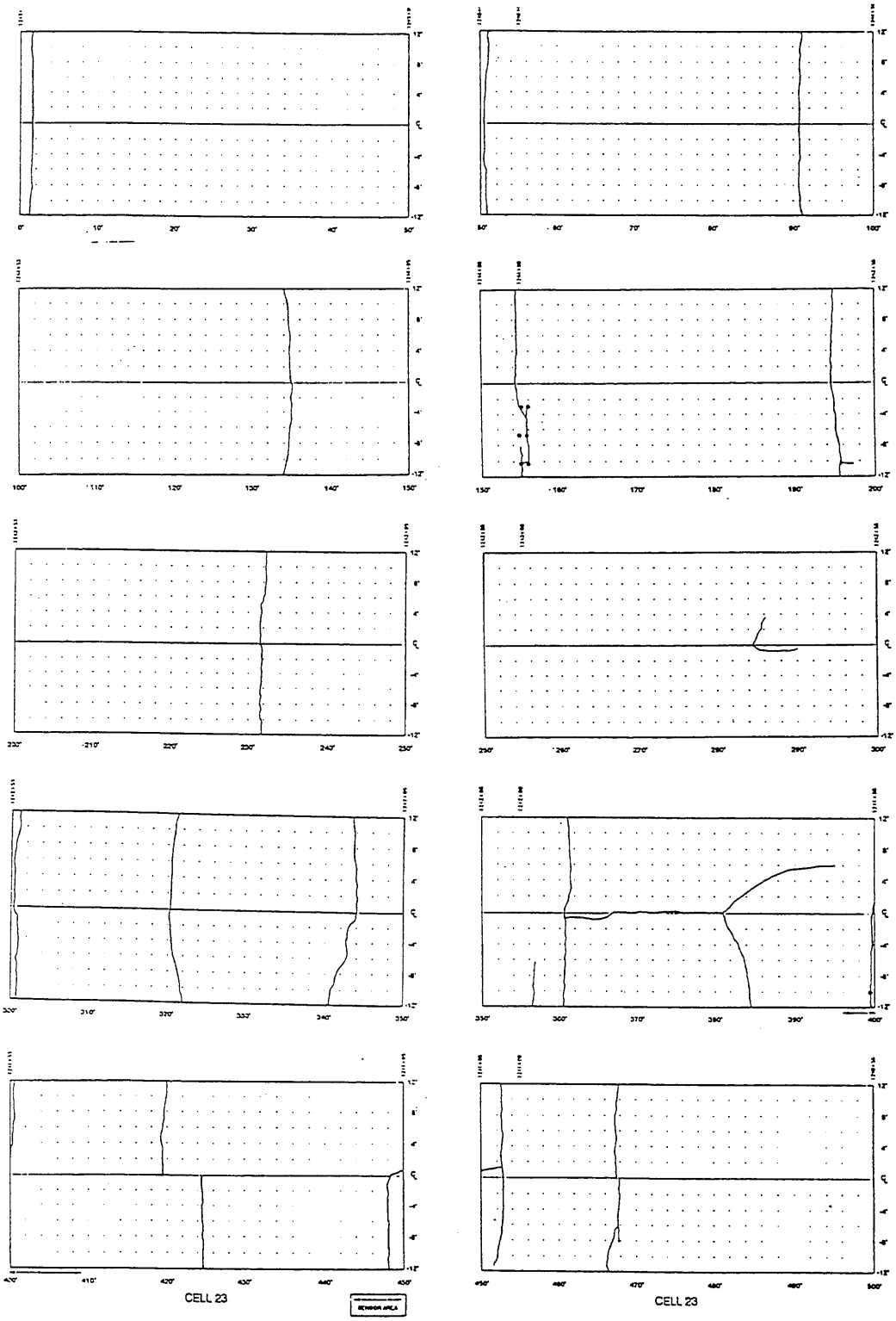

Figure A.14. Thermal Cracking on Cell 23.

Appendix B

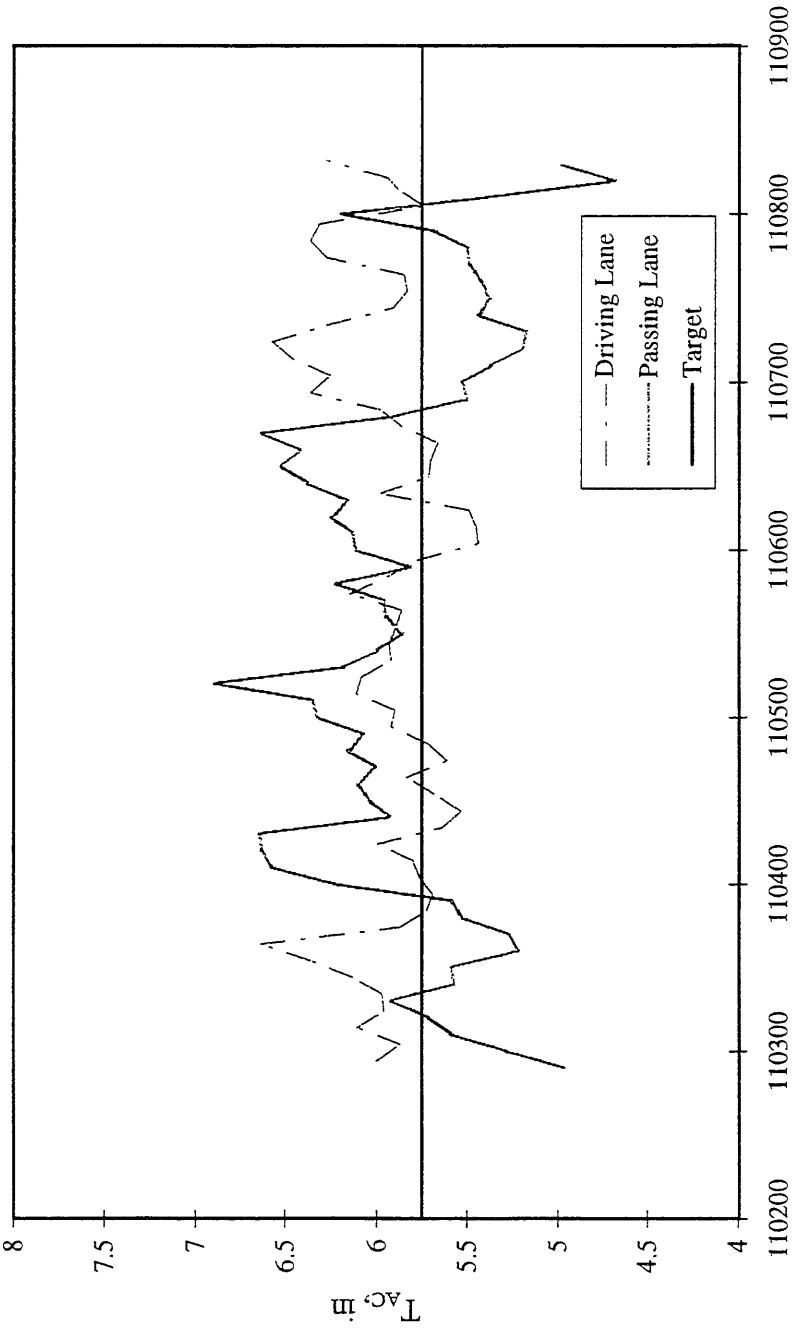

Figure B.1. AC thickness Variation for Cell 1

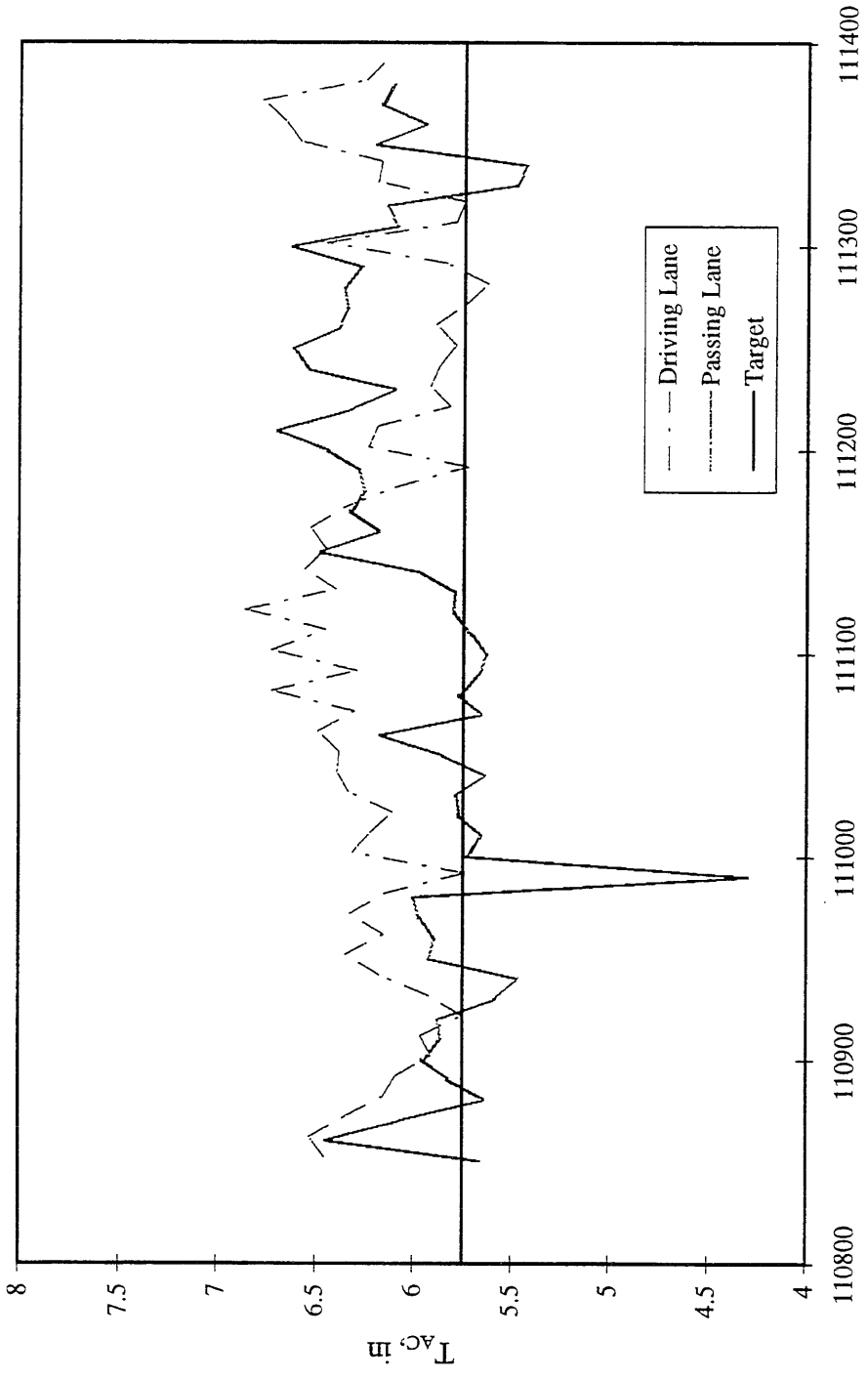

Figure B.2. AC thickness Variation for Cell 2

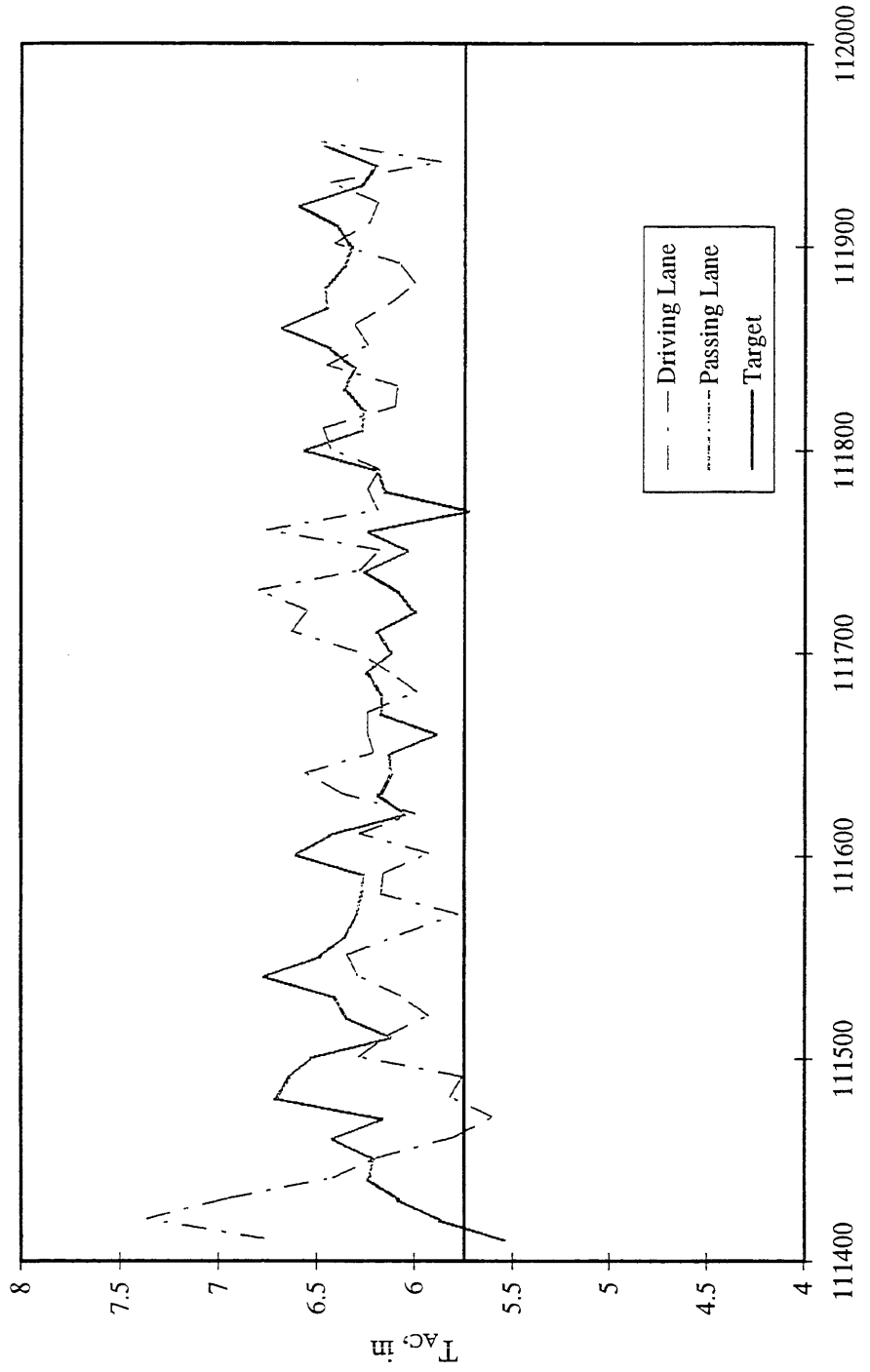

Figure B.3. AC thickness Variation for Cell 3

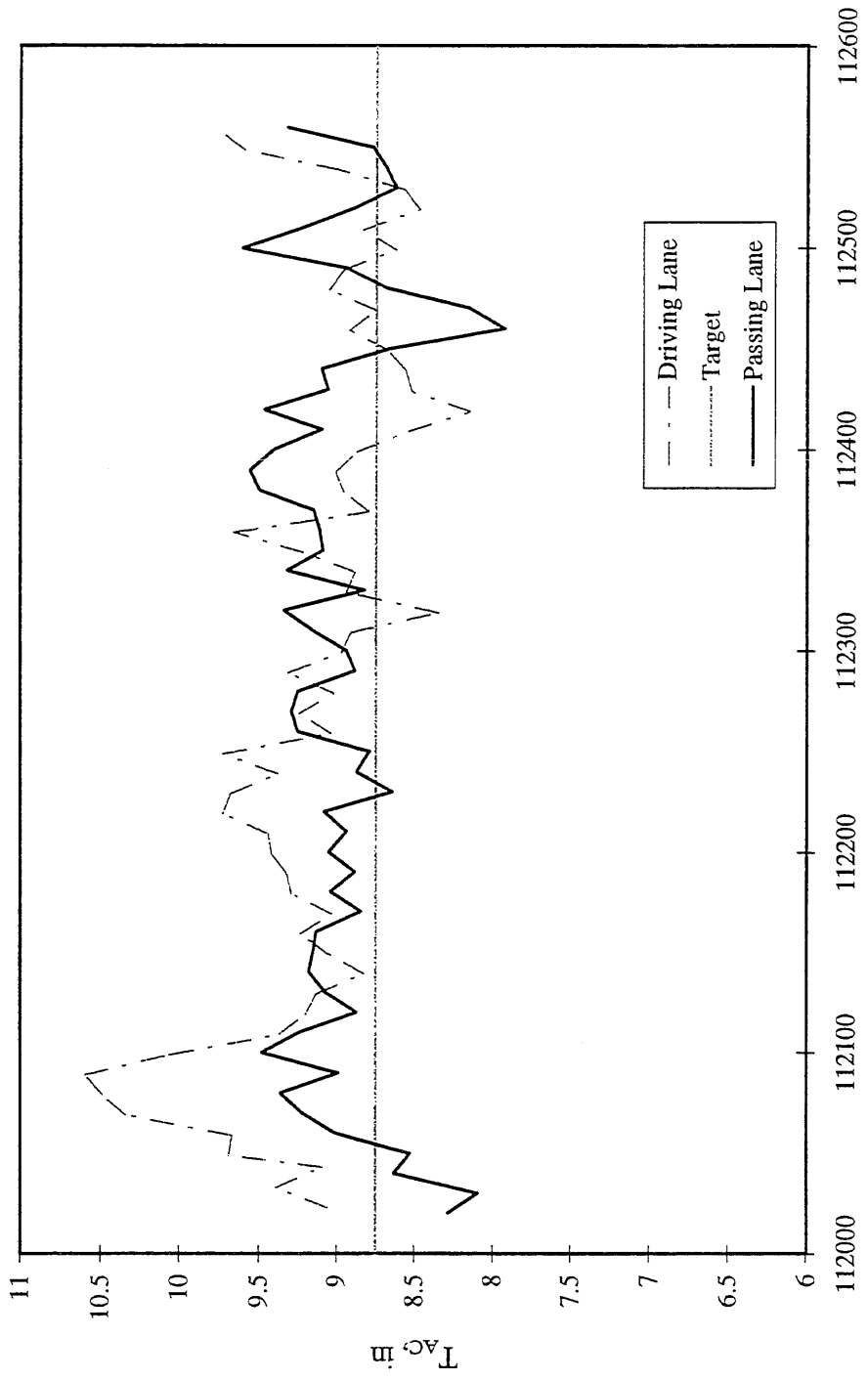

Figure B.4. AC thickness Variation for Cell 4

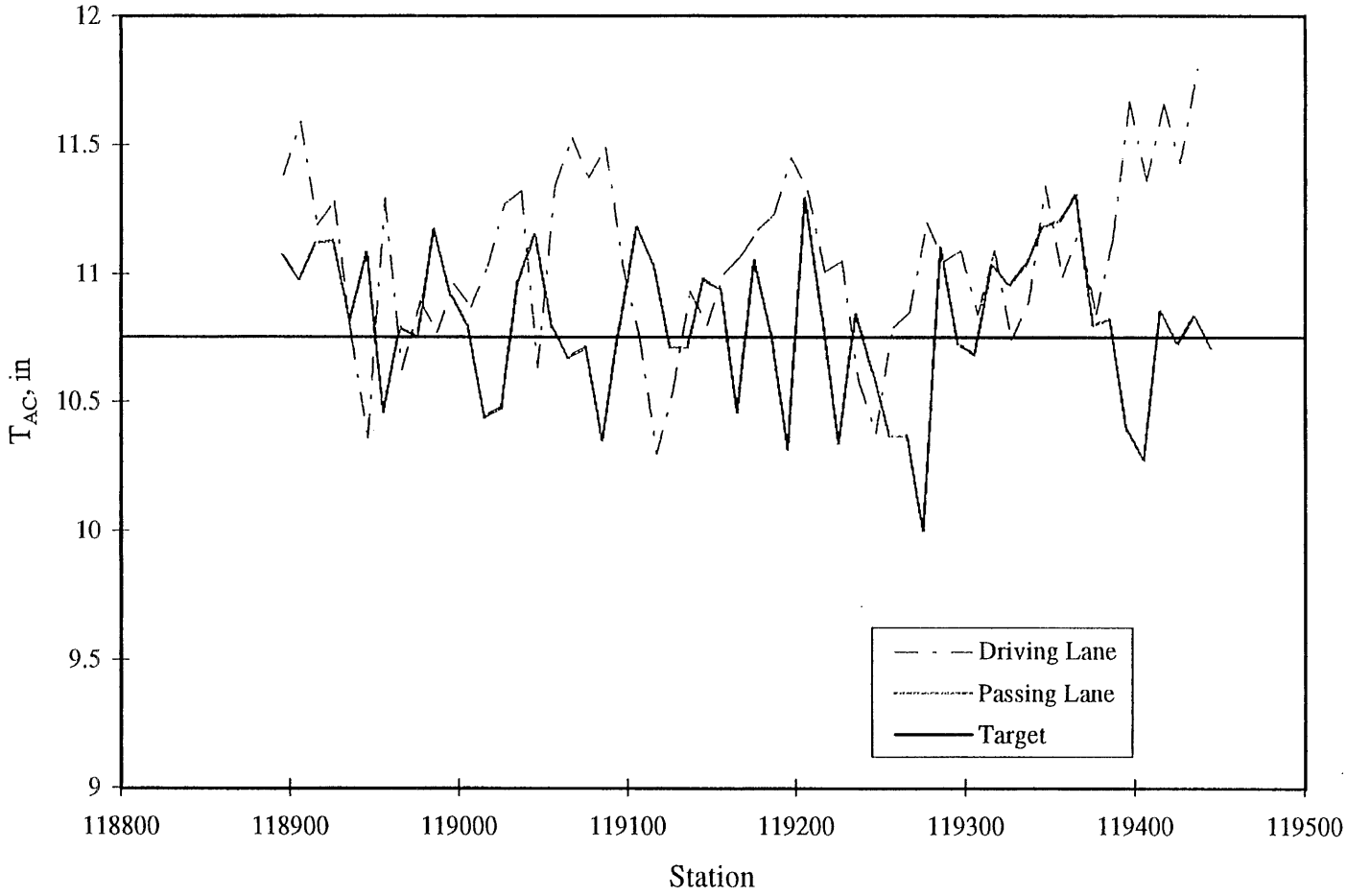

Figure B.5. AC thickness Variation for Cell 14

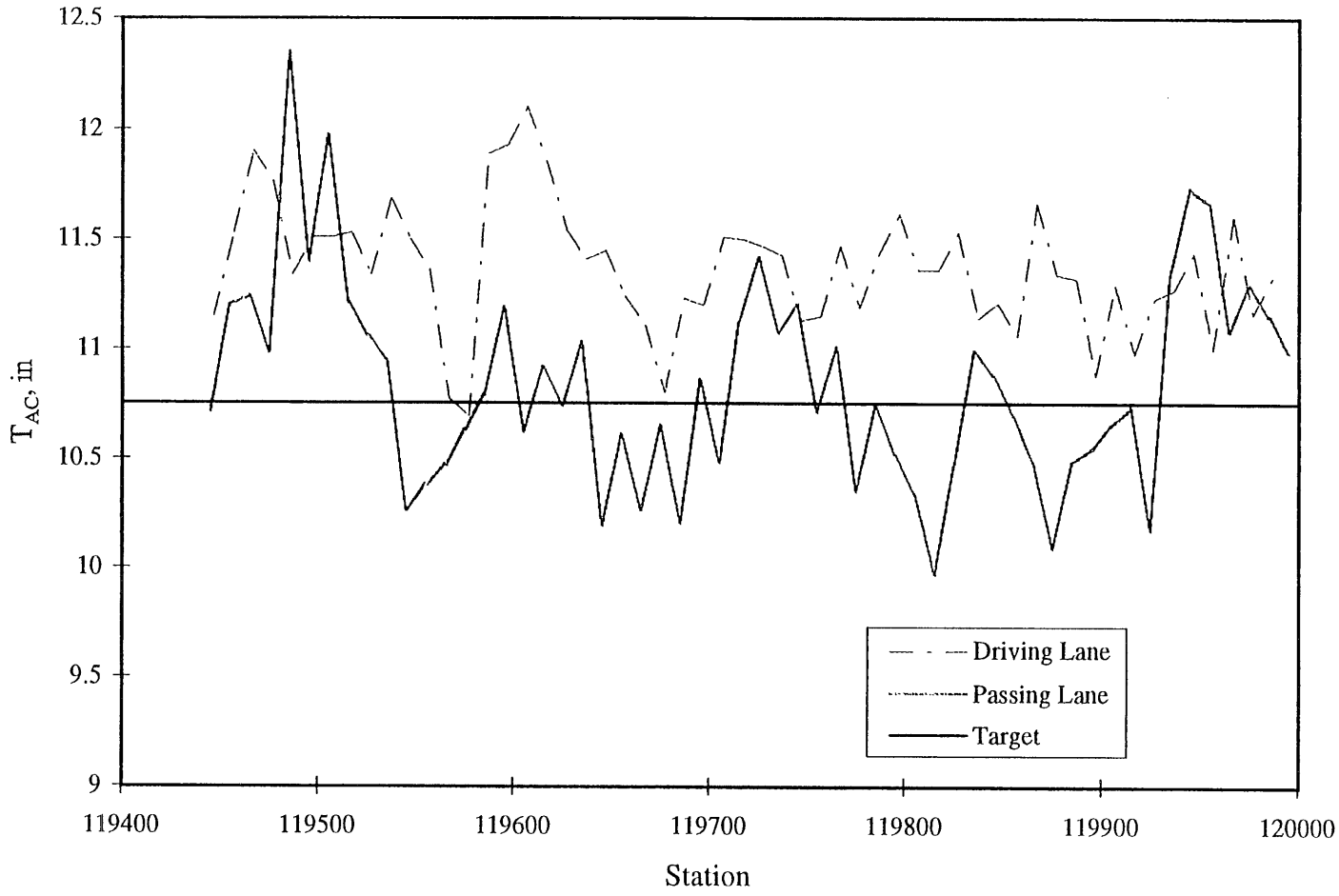

Figure B.6. AC thickness Variation for Cell 15

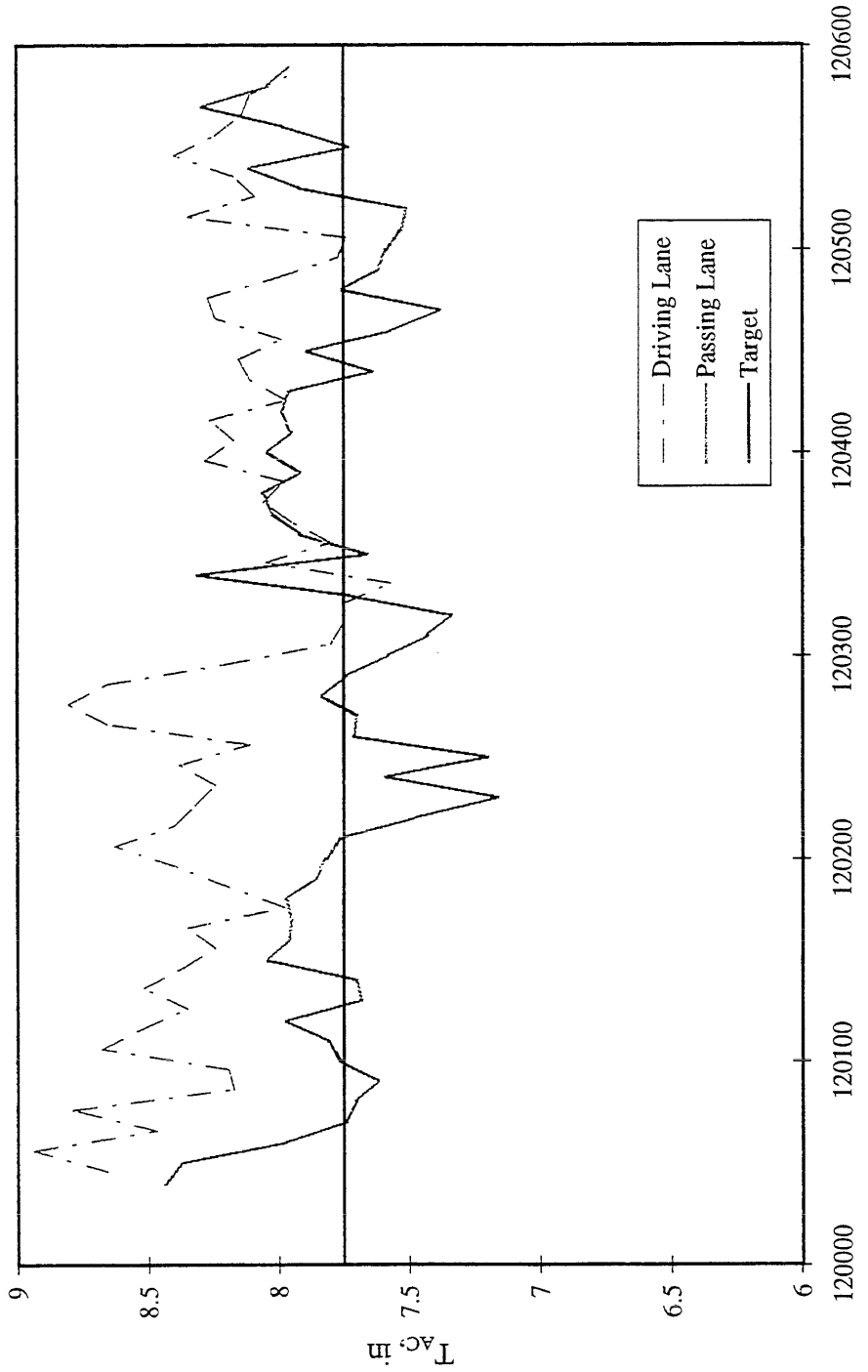

Figure B.7. AC Thickness Variation for Cell 16

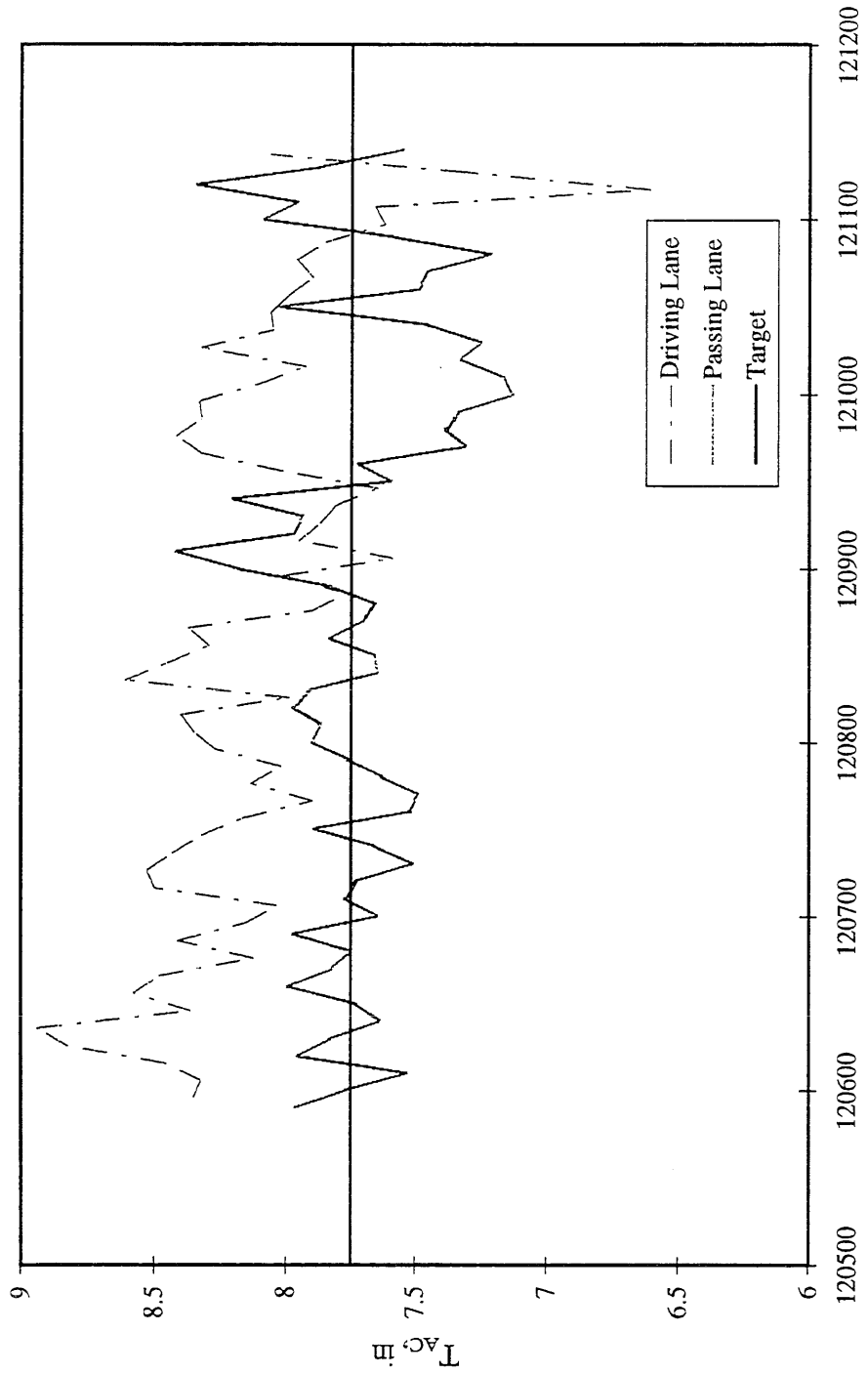

Figure B.8. AC Thickness Variation for Cell 17

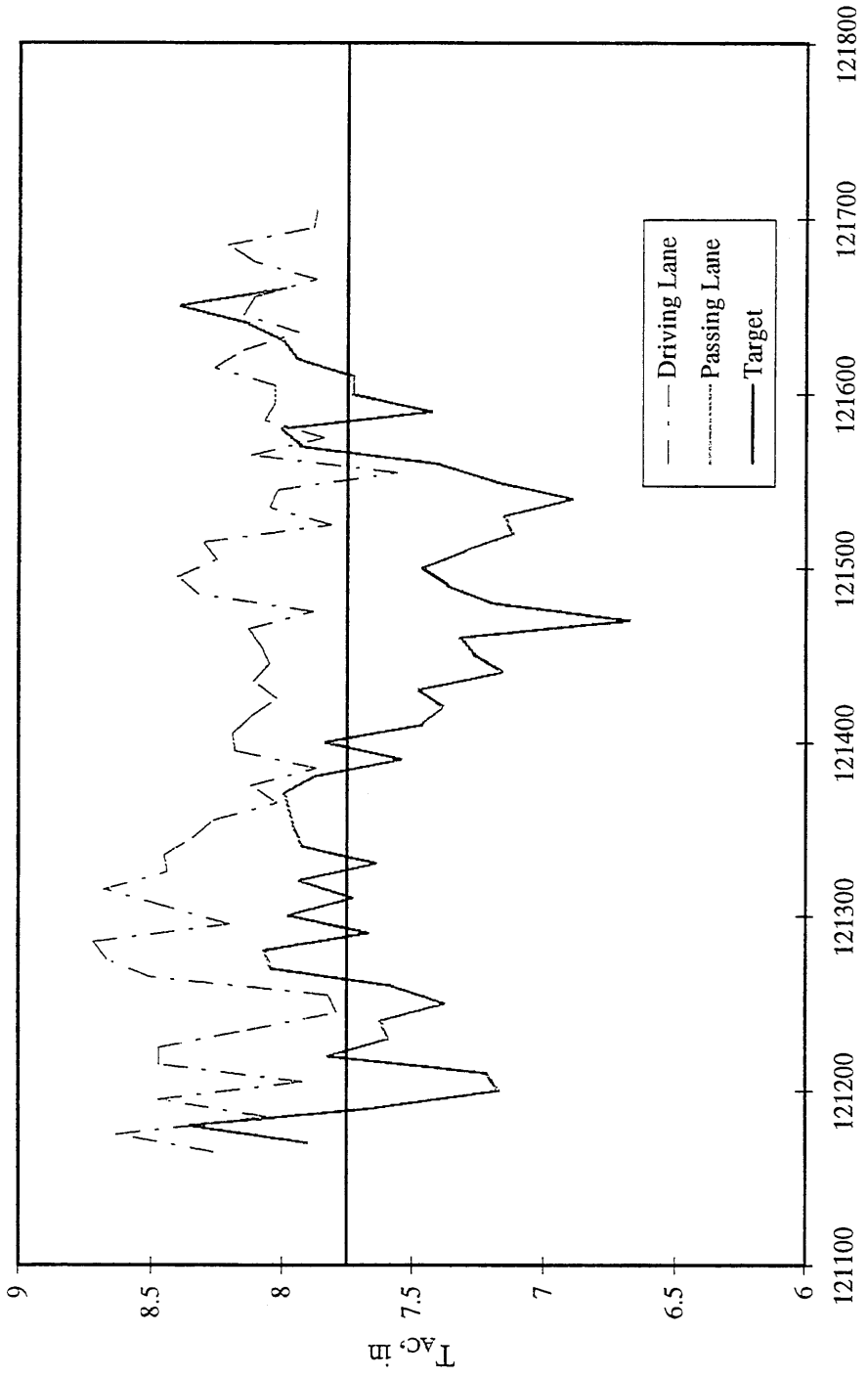

Figure B.9. AC Thickness Variation for Cell 18

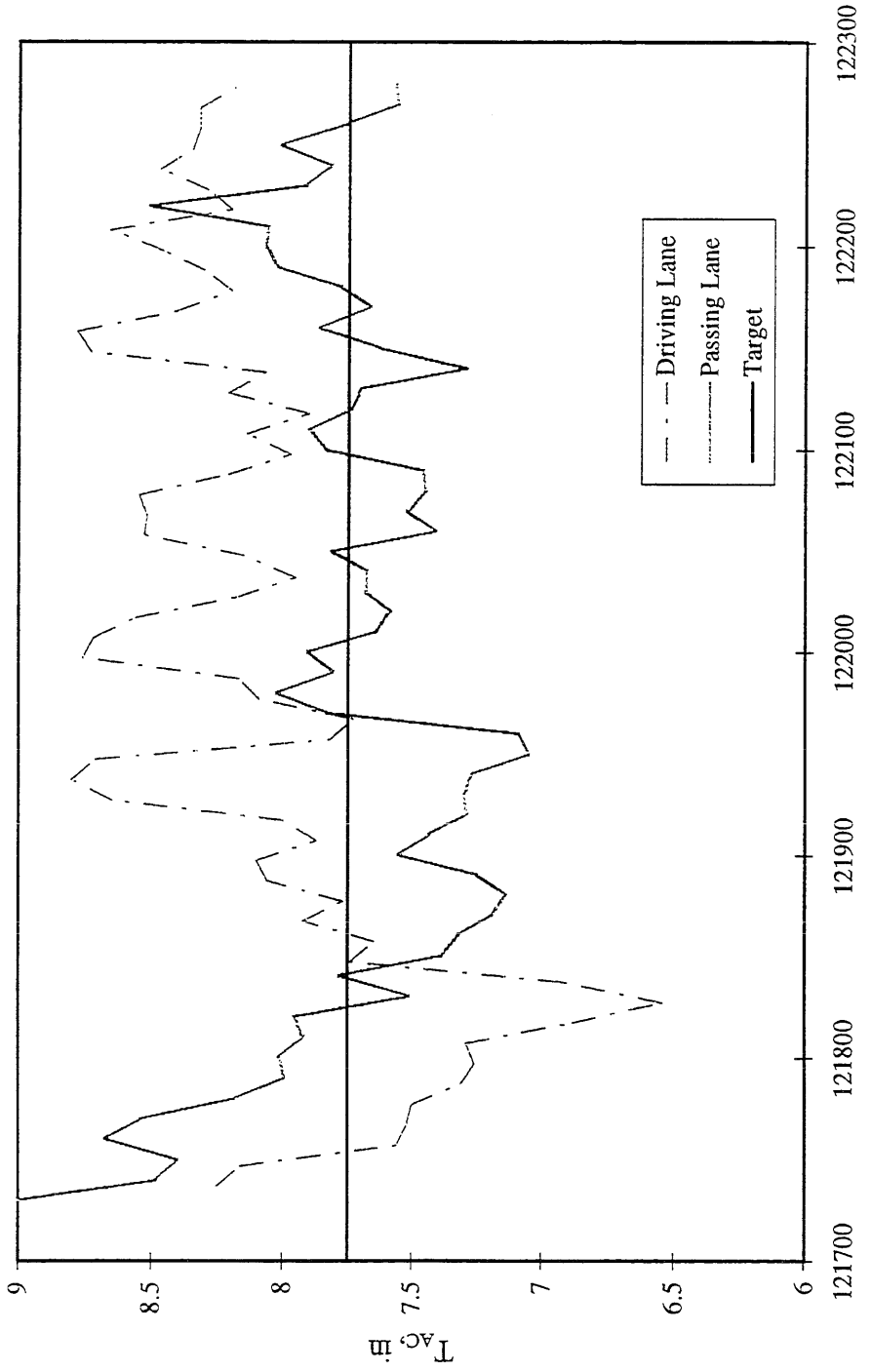

Figure B.10. AC Thickness Variation for Cell 19

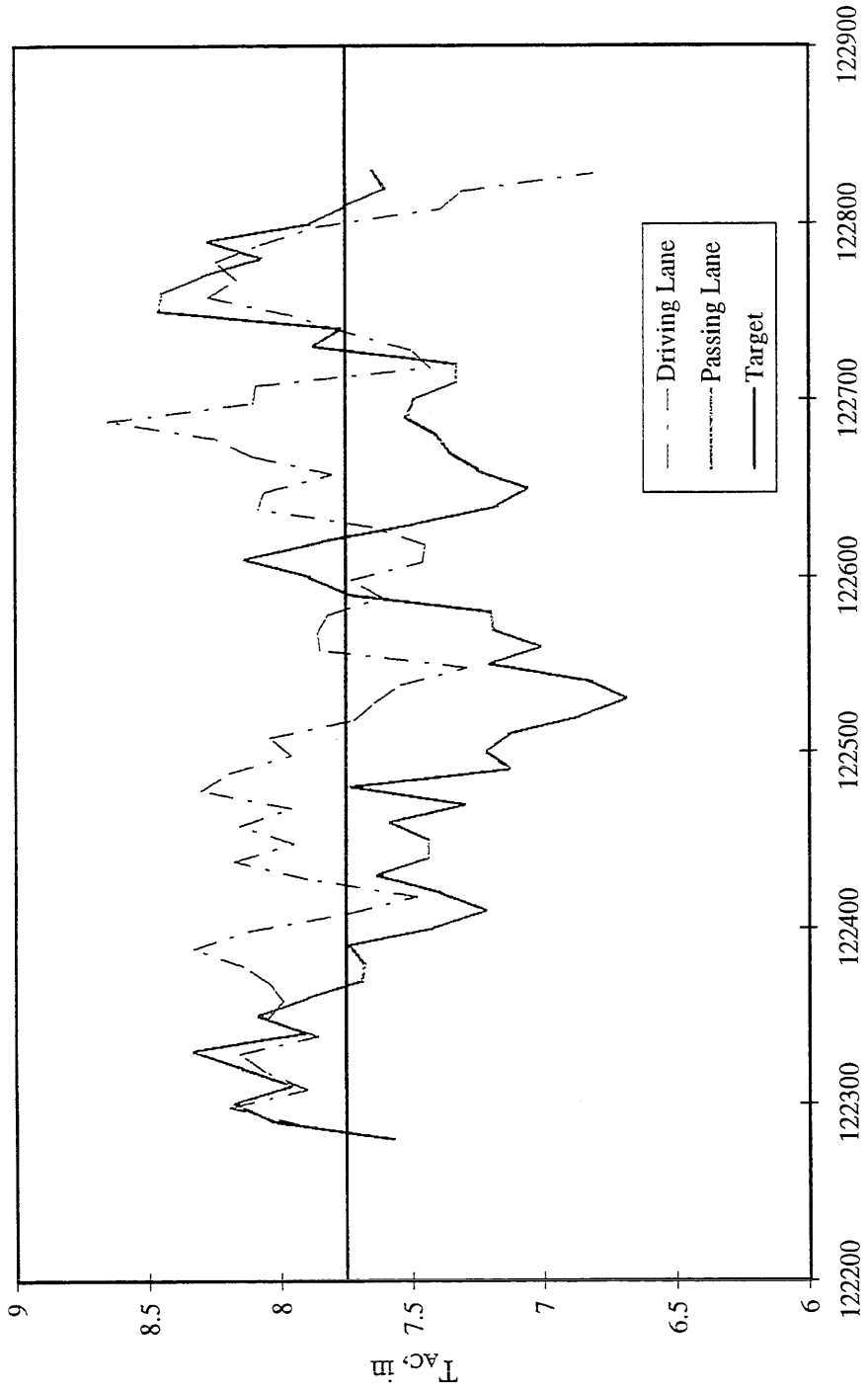

Figure B.11. AC Thickness Variation for Cell 20

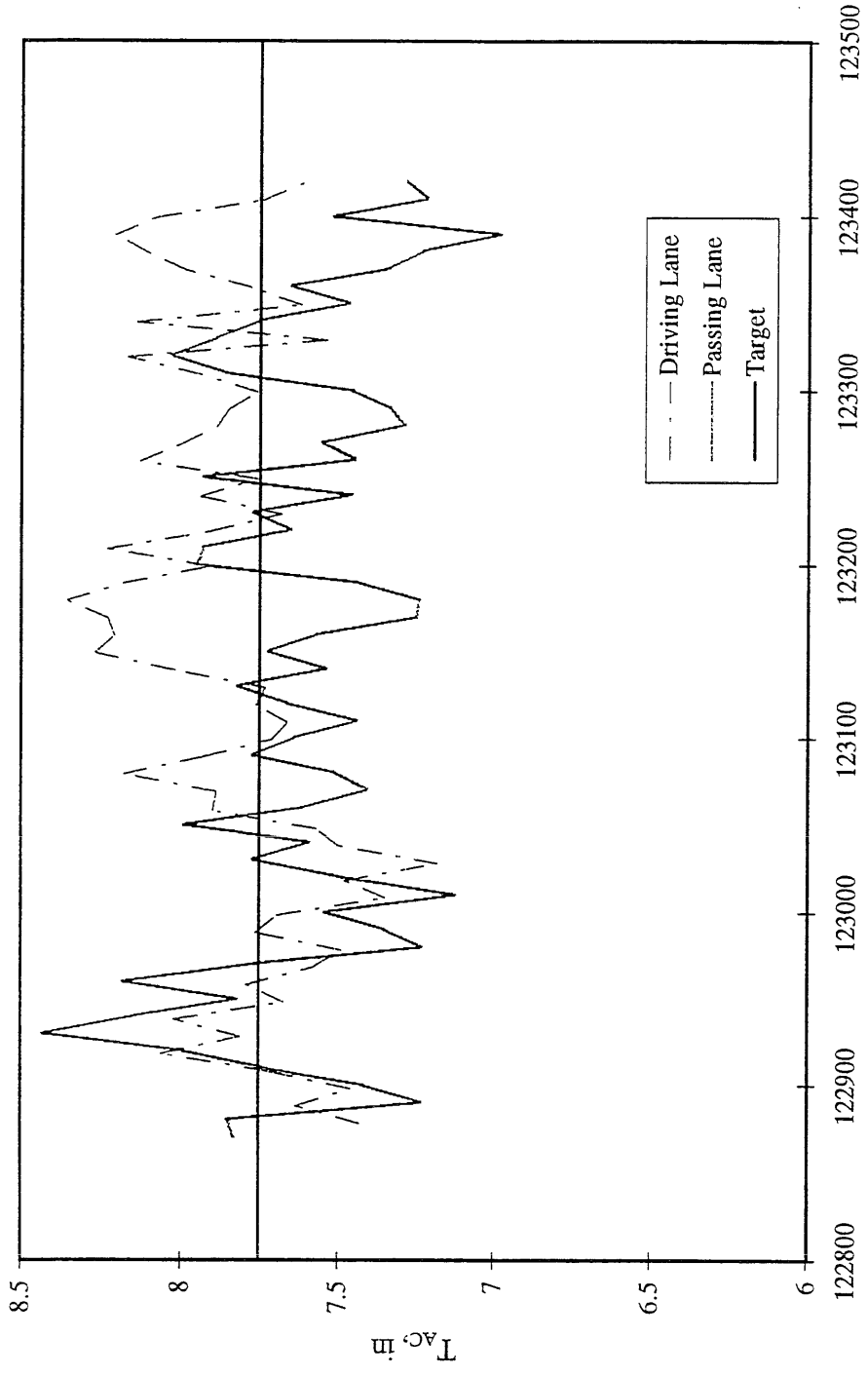

Figure B.12. AC Thickness Variation for Cell 21

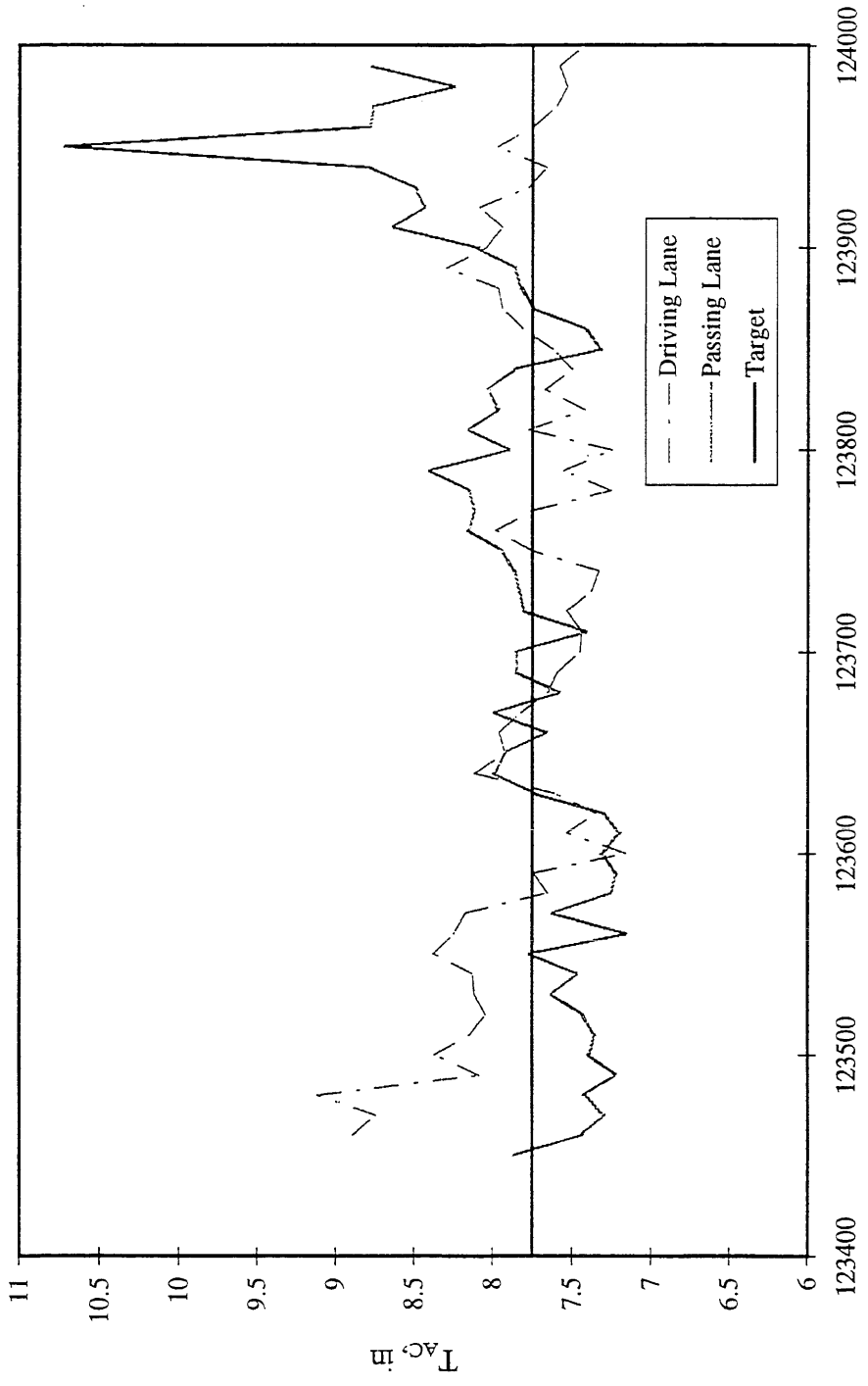

Figure B.13. AC Thickness Variation for Cell 22

Appendix C

Full-Depth Asphalt Concrete Algorithms

Introduction

Full depth asphalt concrete (FDAC) algorithms have been developed in earlier ILLI-PAVE studies (1, 2, 3). The purpose of this study was to increase the sensitivity of the algorithms by reducing the range of thickness included in the database.

The "new" algorithms have been developed to be used specifically in the backcalculation of the Minnesota Road Research Project FDAC test sections.

There are three FDAC sections in Mn/ROAD. The AC layer thickness for each section is as follows:

Cell Number	AC thickness, in.
4	8.75
14	10.75
15	10.75

Falling Weight Deflectometer

Falling Weight Deflectometer (FWD) tests are widely used to assess pavement layer moduli in a nondestructive manner. An FWD test is performed by applying an impulse load to the pavement. This simulates the application of a moving wheel load. When the load is applied, pavement surface sensors measure deflections under the center of the load (D0) and 12 (D1), 24 (D2) and 36 (D3) inches from the center of the load. These four deflections and AREA characterize a deflection basin profile. The AREA concept was initially proposed by Hoffman and Thompson (1).

The pavement layer moduli are then backcalculated from these experimentally determined basins. This is usually accomplished by matching the theoretically determined basin to the experimental one. FWD provides general material characterization, performance criteria and seasonal variation of the properties.

FWD testing has been performed on the Mn/ROAD FDAC sections since construction began in 1991. The algorithms presented in this documented are been used in the analysis of the Mn/ROAD FWD data.

ILLI-PAVE, a finite element program was used to develop the database. In ILLI-PAVE, the pavement is considered an axisymmetric solid of revolution. Nonlinear, stress dependent resilient modulus material models and failure criteria for granular materials and fine-grained soils are incorporated into ILLI-PAVE. The principal stresses in the granular and subgrade layers are modified at the end of each iteration so that they do not exceed the strength of the material as defined by the Mohr-Coulomb theory of failure.

Data Base Development

The analyses performed are based on 9000 lb. circular load (80 psi pressure) as a representation of the dual wheels of the standard 18-kip. (18,000 lb.) single axle load. The depth of the finite element mesh is 50 radii (300 in) .

The data base includes a broad range of AC moduli. The thickness ranged between 7.75 in. and 11.75 in (one inch above and below the range of thickness of the Mn/ROAD FDAC sections). Four fine-grained soil modulus stress level relations were incorporated in the analysis. The range for each pavement parameter is presented in Table C.1.

PARAMETER	LEVELS	NUMBER
Load	9,000 lb.	1
E_{ri}	1, 3.02, 7.68 and 12.34 ksi	4
E_{AC}	200, 500, 1000 and 2000 ksi.	4
Thickness	7.75, 8.75, 9.75, 10.75 and 11.75 in.	4

Table C.1. Pavement parameters ranges.

A factorial of runs using the four different factors and their respective levels were used in developing the database. The AC layer was modeled as a constant modulus material. The stress-softening characteristic of fine-grained soils were included in ILLI-PAVE. Table C.2 presents the properties of the AC and subgrade used in the database development.

	ASPHALT CONCRETE				SUBGRADE			
	Very Hard	**Hard**	**Medium**	**Low**	**Stiff**	**Medium**	**Soft**	**Very Soft**
Unit Weight, psf	145.00	145.00	145.00	145.00	125.00	120.00	115.00	110.00
Lateral Pressure Coefficient at Rest	0.20	0.50	0.67	0.80	0.82	0.82	0.82	0.82
Poisson's Ratio	0.30	0.35	0.40	0.46	0.45	0.45	0.45	0.45
Unconfined Compressive Strength (q_u), psi					32.80	22.85	12.90	6.21
Deviator Stress:								
Upper Limit, psi					32.80	22.85	12.90	6.21
Lower Limit, psi					2.00	2.00	2.00	2.00
Resilient Modulus:								
E_{Ri}, *ksi*					12.34	7.68	3.02	1.00
E-failure, ksi					7.61	4.72	1.83	1.00
E-Constant Modulus, ksi	2000	1000	500	200				
Friction Angle, °					0.00	0.00	0.00	0.00
Cohesion, psi					16.40	11.43	6.45	3.11

Table C.2. ILLI-PAVE Input Material Properties.

FDAC Algorithms

The algorithms developed are presented in Table C.3. Plots were prepared to show the effect of the different variables. Figures C.1 through C.4 show the influence of thickness and AC modulus on D0 and AREA. The projection on the XZ plane indicates that as the thickness increases the AREA also increases. In addition, as the AC modulus increases the AREA term also increases. The projection on the YZ plane shows a decrease in D0 as the thickness and/or the AC modulus increases.

ALGORITHMS	R^2	SEE
$Log(E_{AC}) = 6.778 + 0.123 * AREA - 4.911 * Log(AREA) + 0.315 * (AREA/T_{AC}) - 1.05 * Log(D0)$	0.9902	0.0378 or 9%
$Log(E_{AC}) = 0.633 - 1.056 * Log(D0-D1) + 0.413 * (AREA/T_{AC}) + 0.672 * (D2/D3) + 0.050 * T_{AC}$	0.9938	0.0301 or 7%
$Log(E_{AC}) = 0.741 - 8.5181 * Log(D0-D1) + 10.6040 * (D0-D2) - 3.1328 * (D1-D3)$	0.9988	0.0132 or 3%
$E_{ri} = 25.559 - 5.531* D3 + 0.312 * (D3)^2$	0.9880	0.4729 ksi
$Log\ \varepsilon_{AC} = 1.073 + 0.980 * Log(AUPP)$	0.9880	0.0333 or 8%
$Log(E_{AC}*(T_{AC})^3) = 7.005 - 1.336 * Log(AUPP)$	0.9585	0.0859 or 22%

Table C. 3. ILLI-PAVE Based Full-Depth Asphalt Concrete Algorithms.

Symbols

ε_{AC} Strain at the bottom of the AC layer, microstrains.

$AUPP$ = 1/12 (Area Under Pavement Profile)

= 1/2(5D0 - 2D1 - 2D2 - D3)

E_{AC} Asphalt Concrete Modulus, ksi

T_{AC} Asphalt Concrete thickness, in

$AREA$ = 6(1 + 2(D1/D2) + 2(D2/D0) + (D3/D0)), in

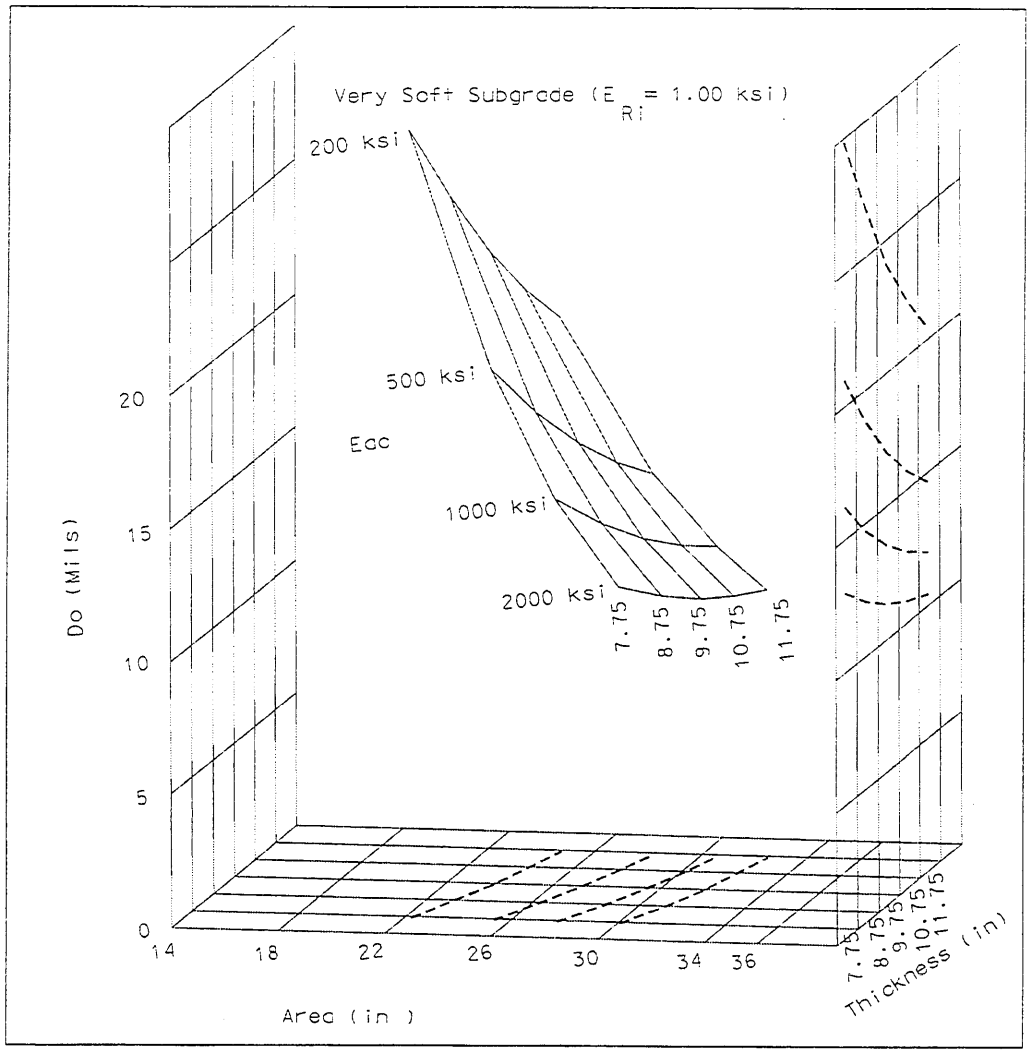

Figure C.1. D0 - AREA - T_{AC} Relationship for Full-Depth Asphalt Concrete Pavement (E_{ri} = 1.00 ksi).

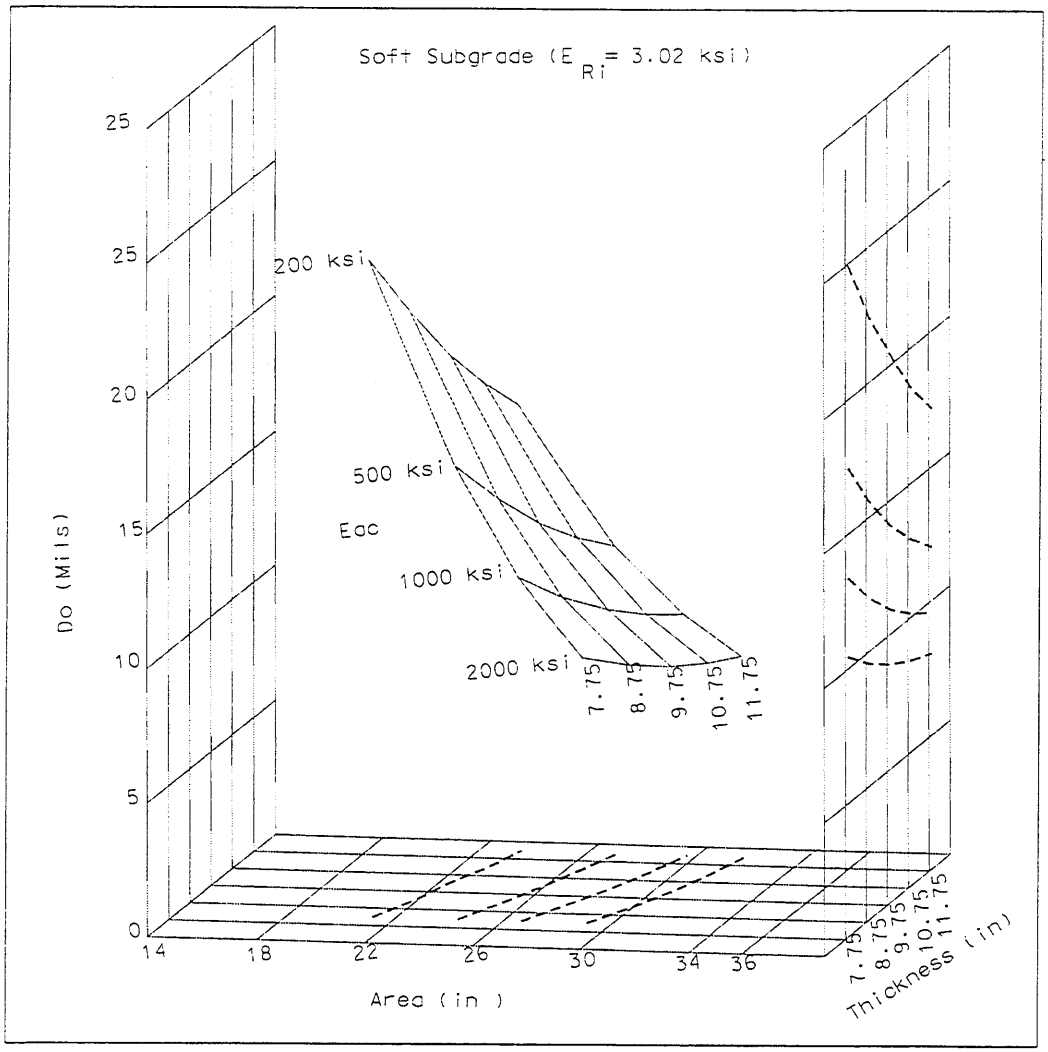

Figure C.2. D0 - AREA - T_{AC} Relationship for Full-Depth Asphalt Concrete Pavement (E_{ri} = 3.02 ksi).

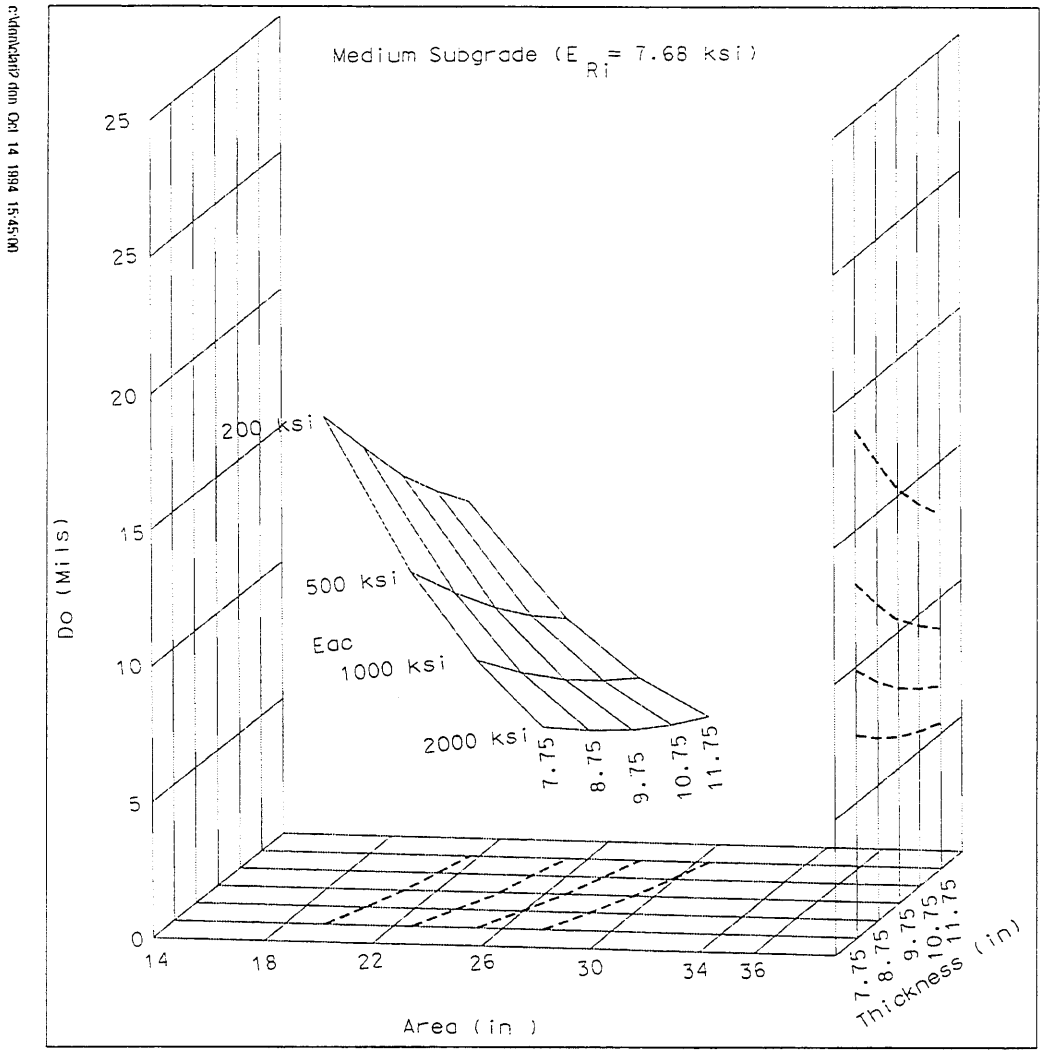

Figure C.3. D0 - AREA - T_{AC} Relationship for Full-Depth Asphalt Concrete Pavement (E_{ri} = 7.68 ksi).

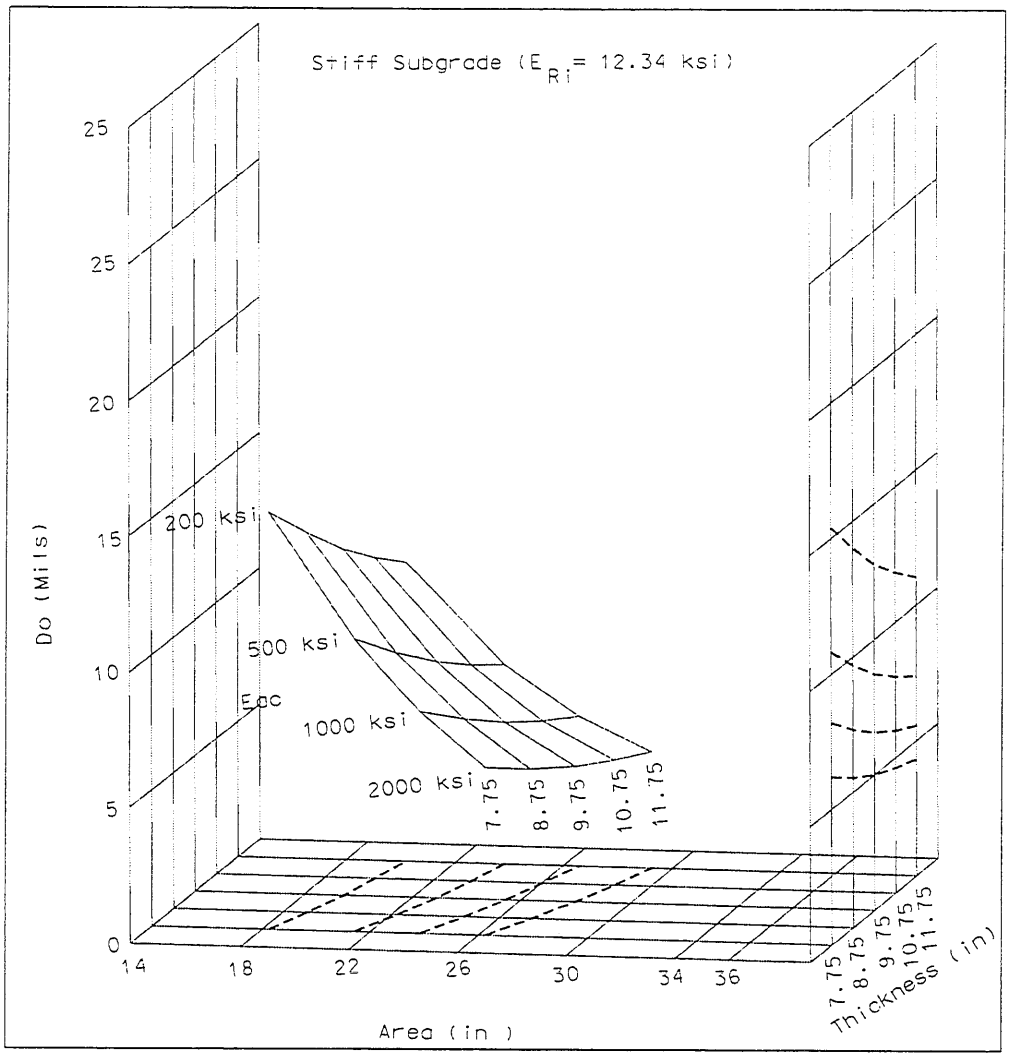

Figure C.4. D0 - AREA - T_{AC} Relationship for Full-Depth Asphalt Concrete Pavement (E_{ri} = 12.34 ksi).

References

1. Hoffman, M.S. and Thompson, M.R. "Mechanistic Design Concepts for Full-Depth Asphalt Concrete Pavements." Civil Engineering Studies, Transportation series 41. University of Illinois at Urbana - Champaign, Aug., 1981.

2. Thompson, M.R., "ILLI-PAVE Based NDT Analysis Procedures," Nondestructive Testing of Pavements and Backcalculation of Moduli, ASTM STP 1026, A.J. Bush III and G.Y. Baladi, Eds., American Society for Testing and Materials, Philadelphia, 1989, pp. 487-501.

3. Gomez-Achecar, M. and Thompson, Marshall R., "ILLI-PAVE-Based Response Algorithms for Full-Depth Asphalt Concrete Flexible Pavements," In Transportation Research Records 1095, TRB, National Research Council, Washington D.C., 1986, pp.11-18.

Appendix D

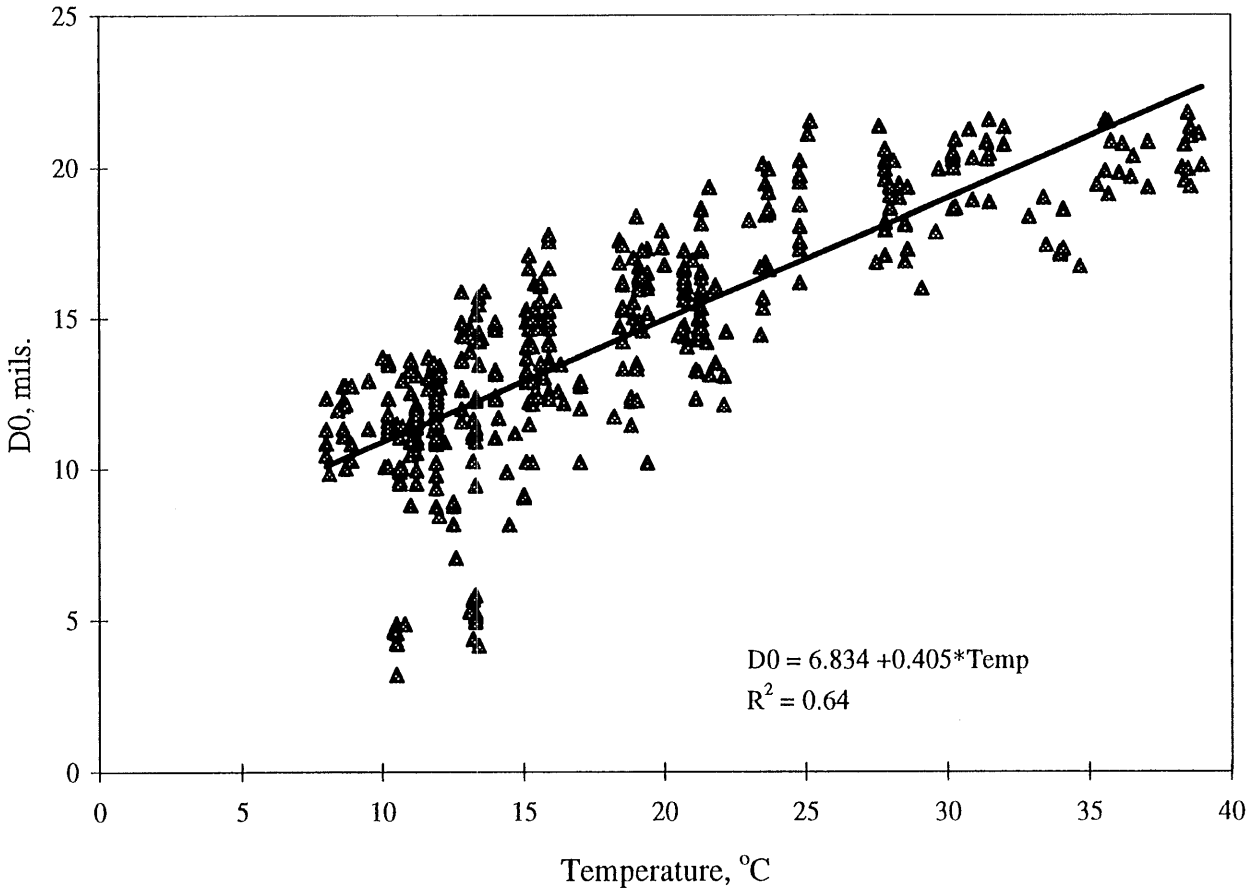

Figure D.1 Variation of D0 with Temperature for Cell 1

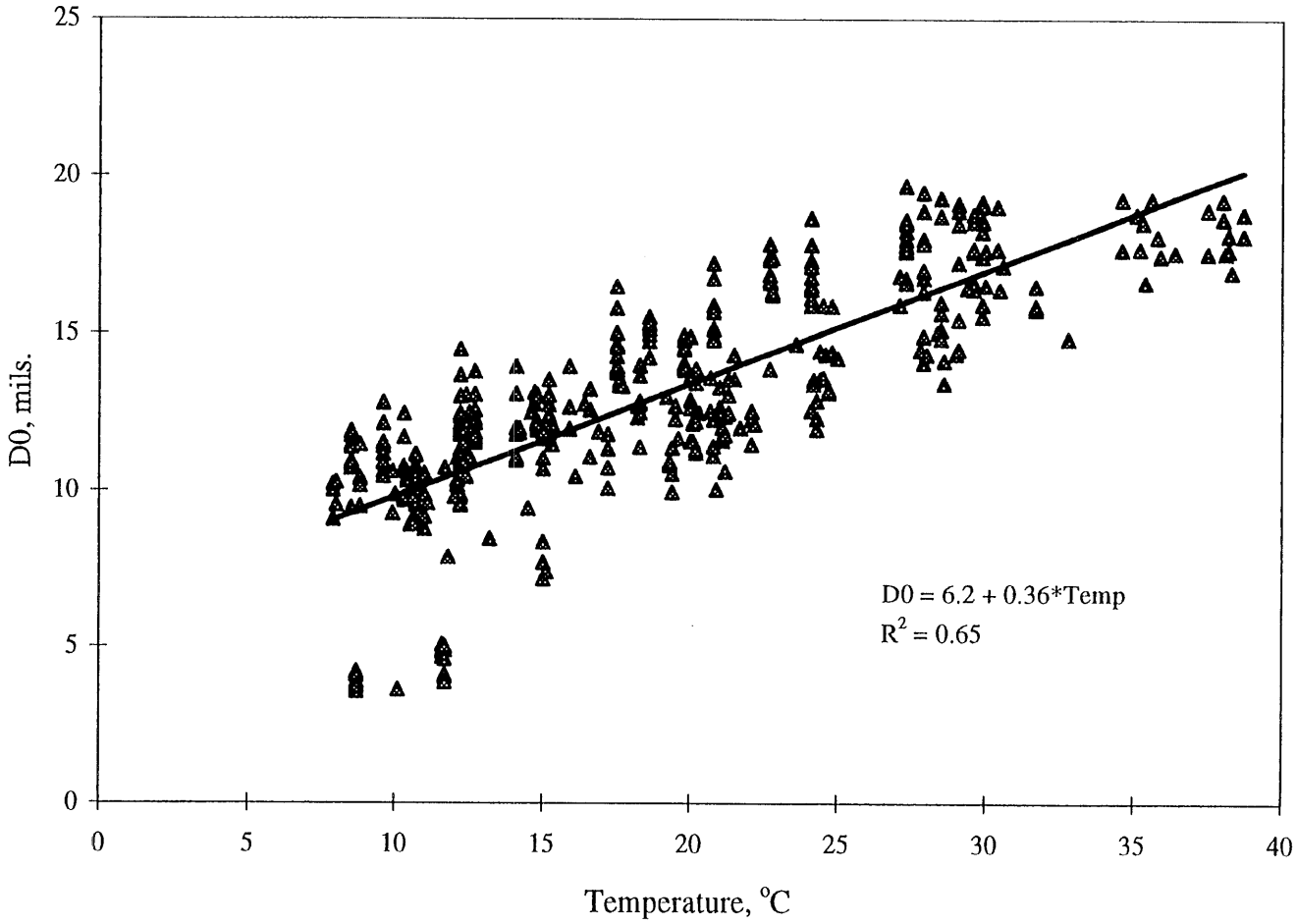

Figure D.2 Variation of D0 with Temperature for Cell 2

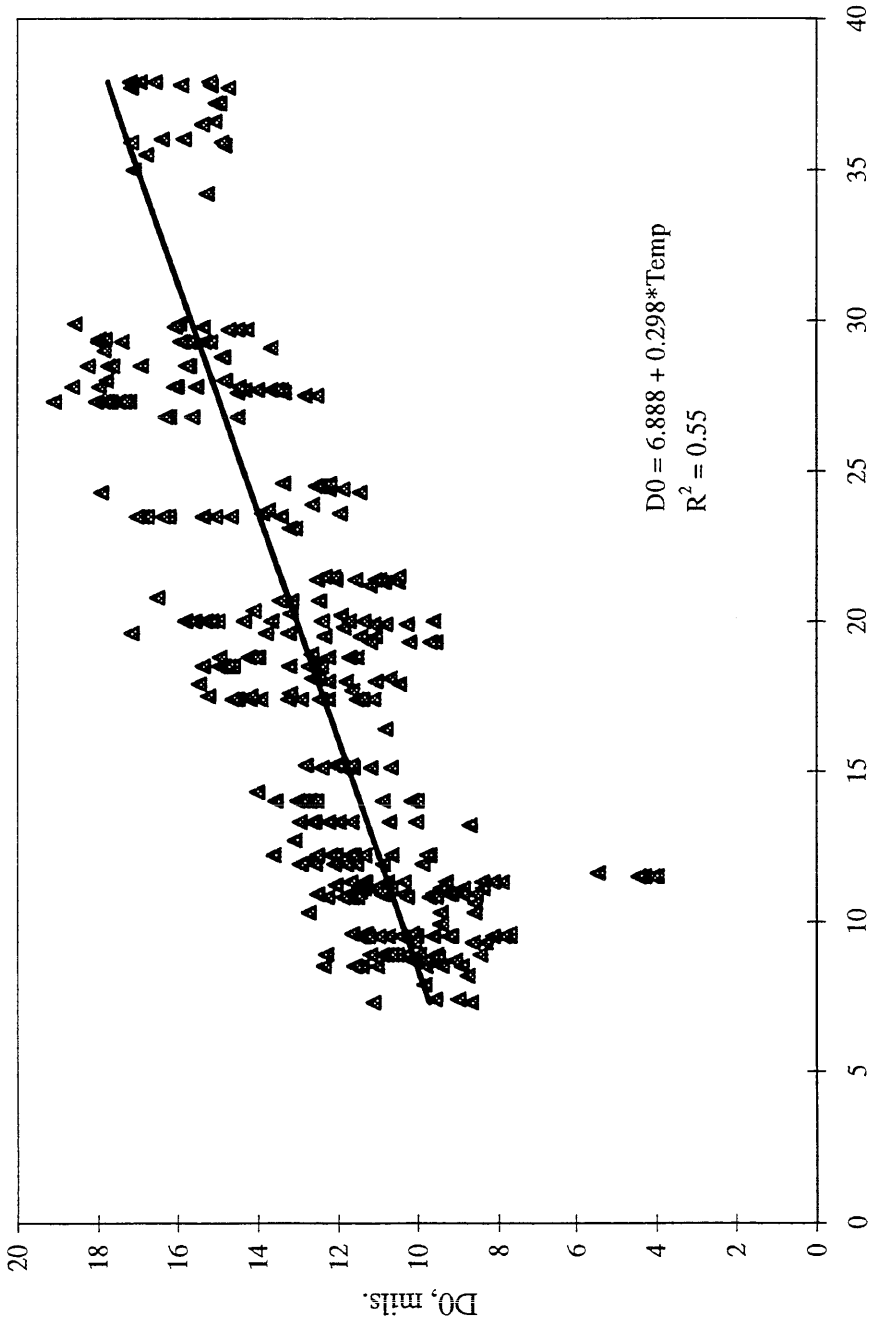

Figure D.3 Variation of D0 with Temperature for Cell 3

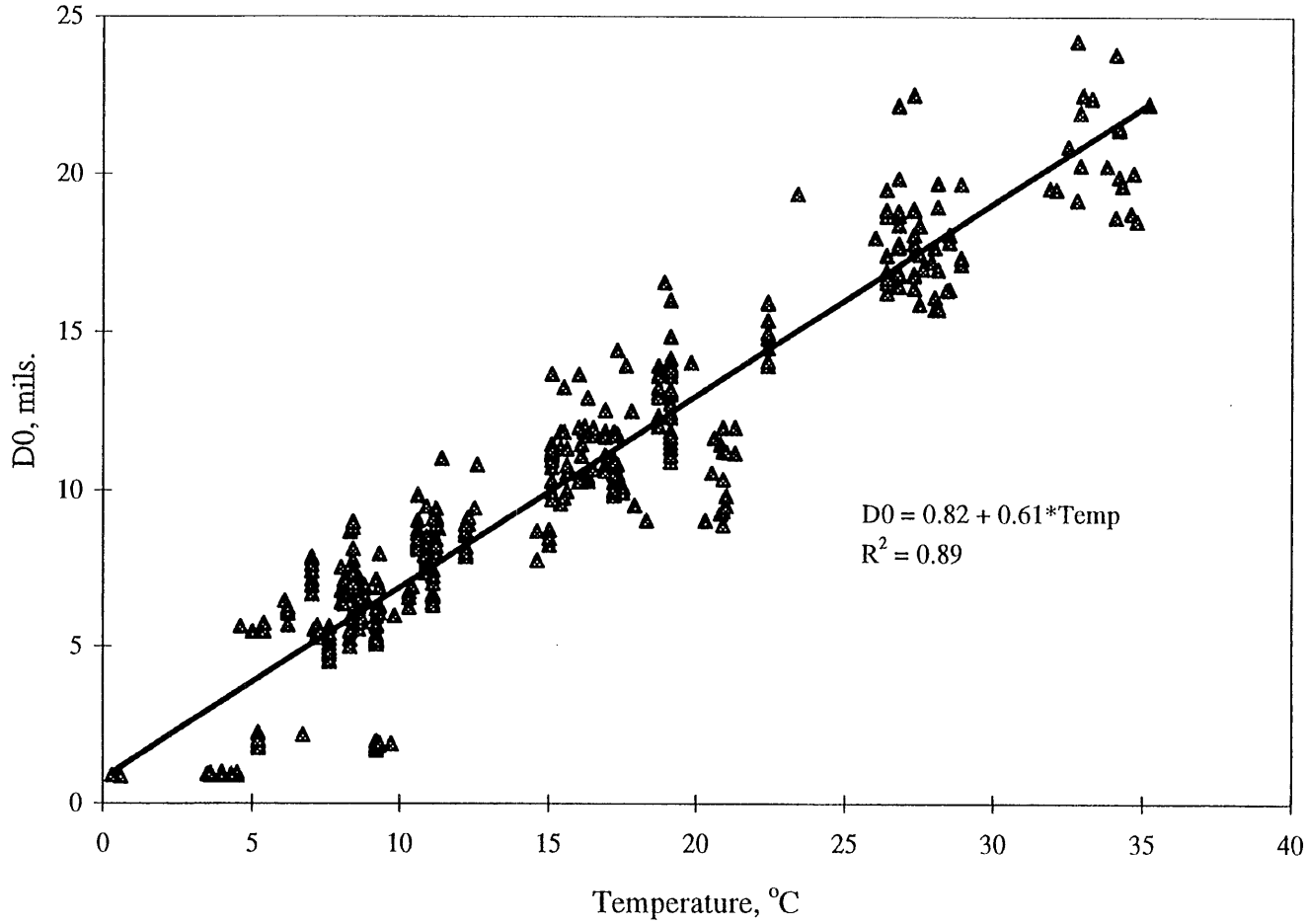

Figure D.4 Variation of D0 with Temperature for Cell 4

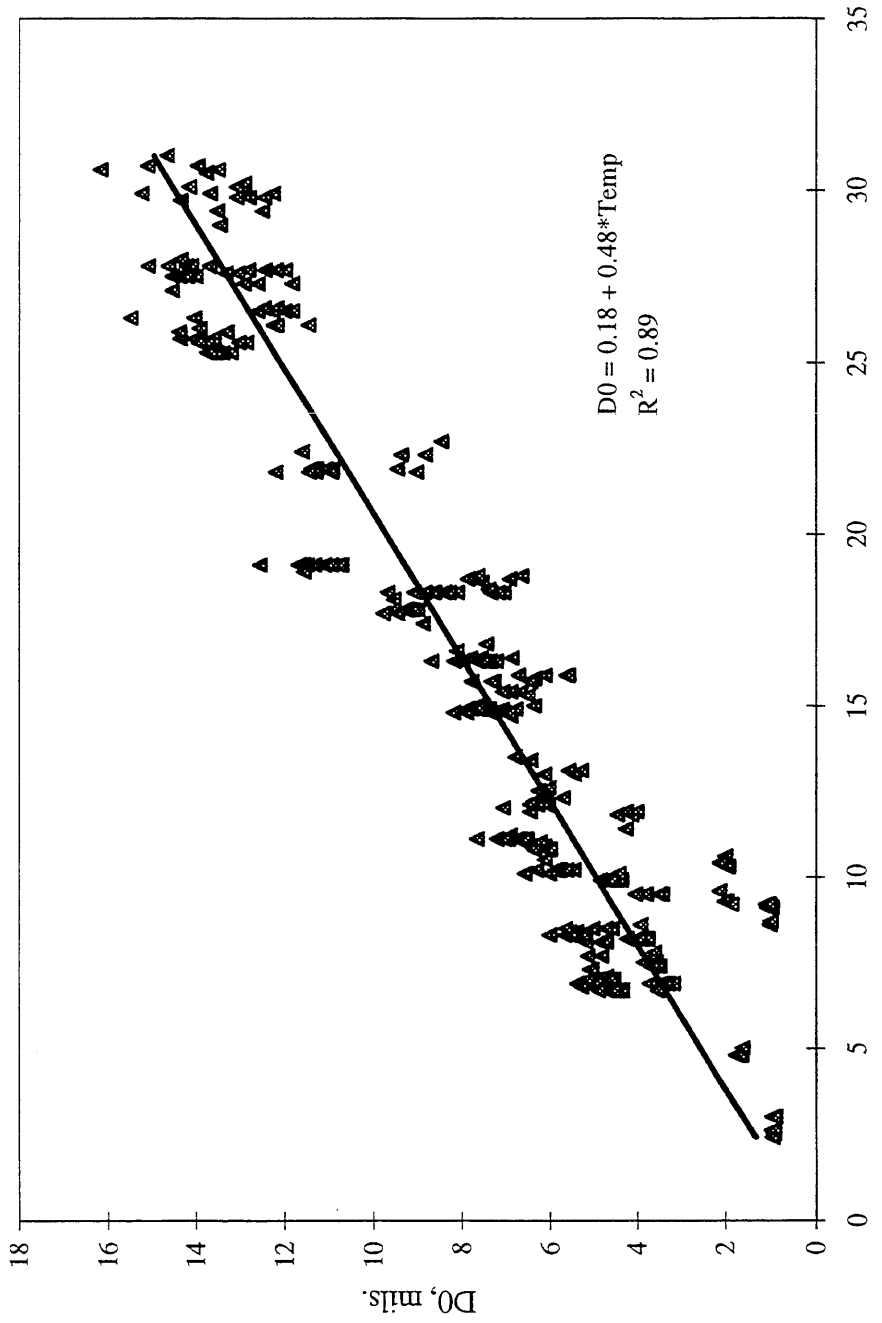

Figure D.5 Variation of D0 with Temperature for Cell 14

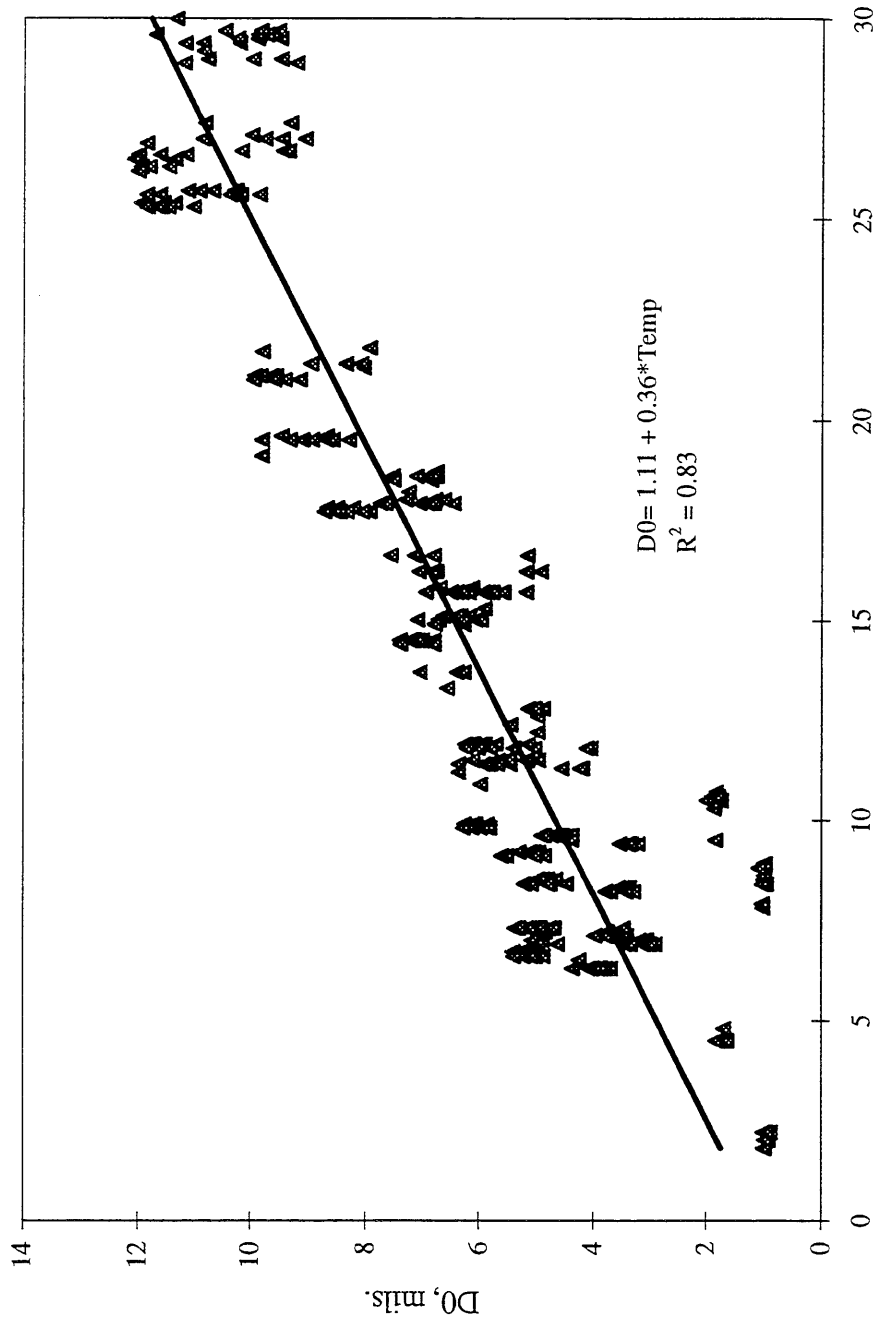

Figure D.6 Variation of D0 with Temperature for Cell 15

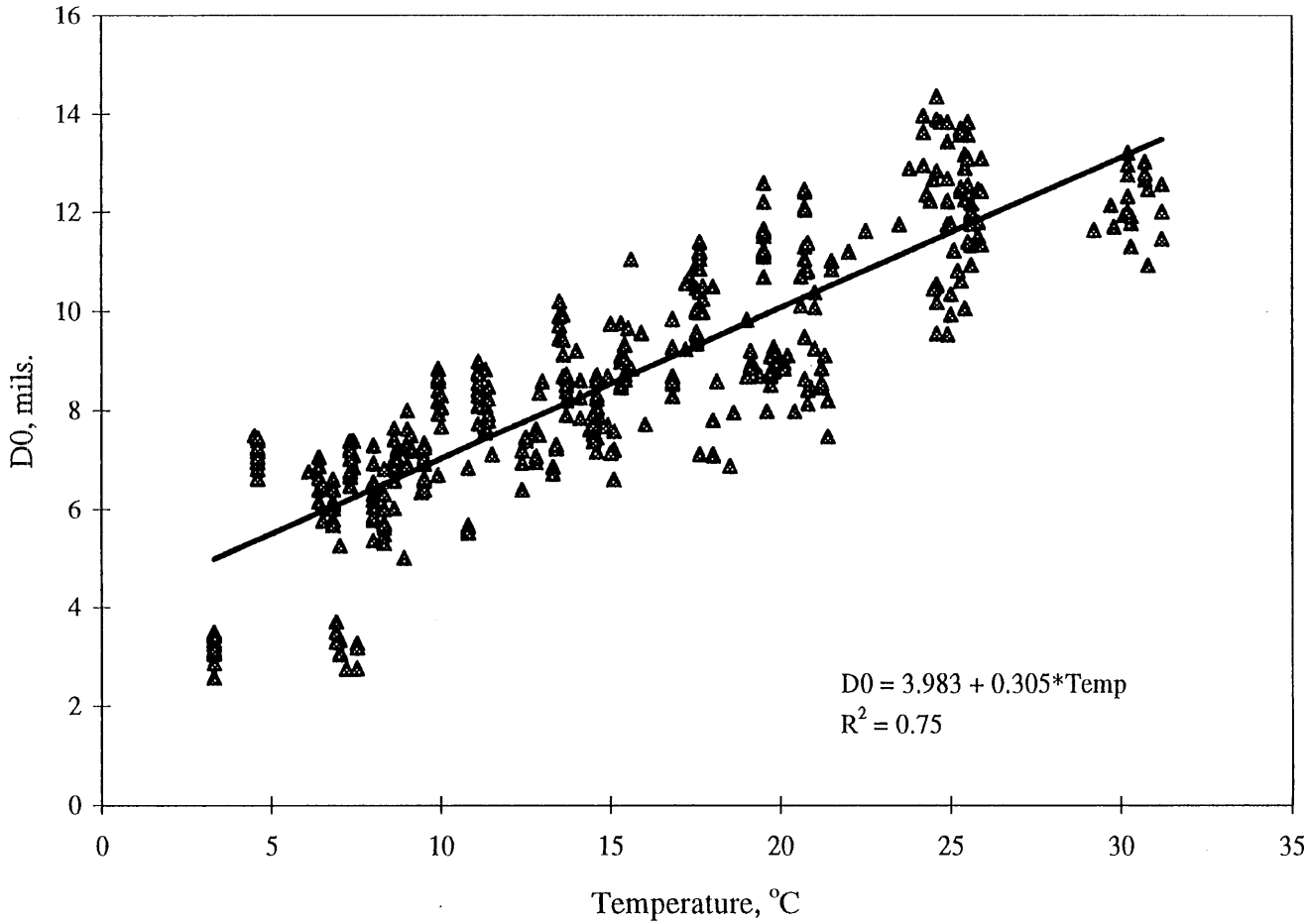

Figure D.7 Variation of D0 with Temperature for Cell 16

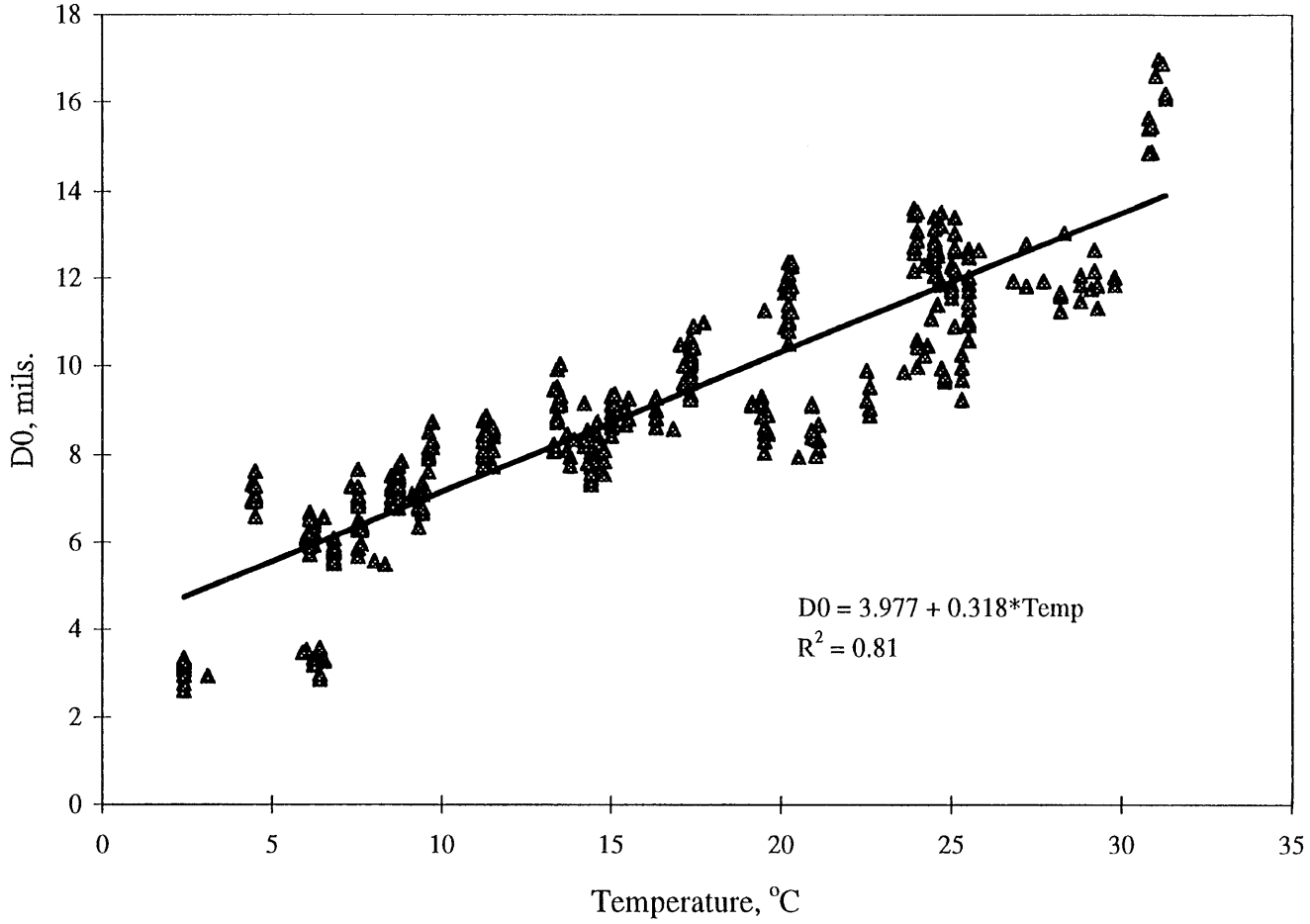

Figure D.8 Variation of D0 with Temperature for Cell 17

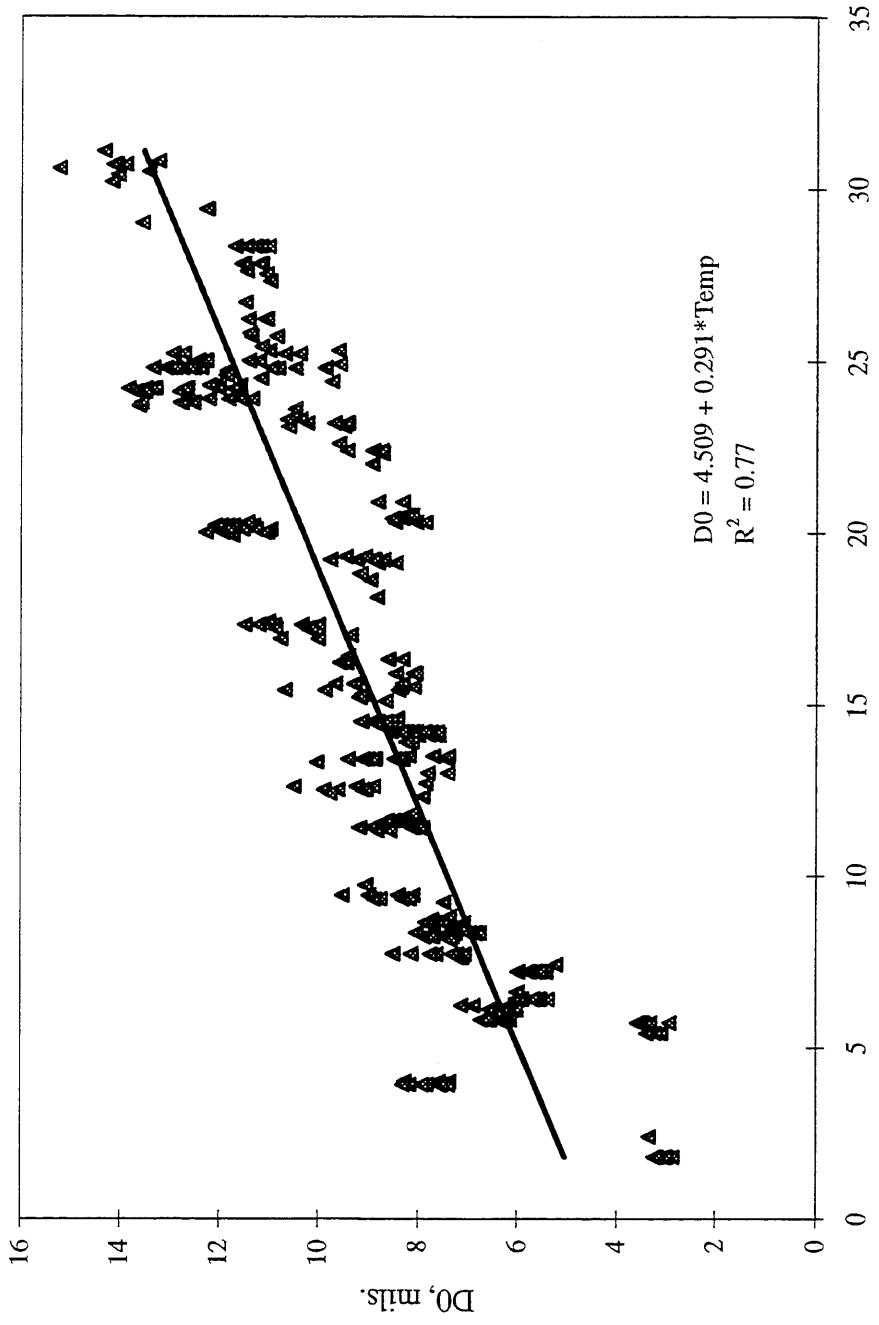

Figure D.9 Variation of D0 with Temperature for Cell 18

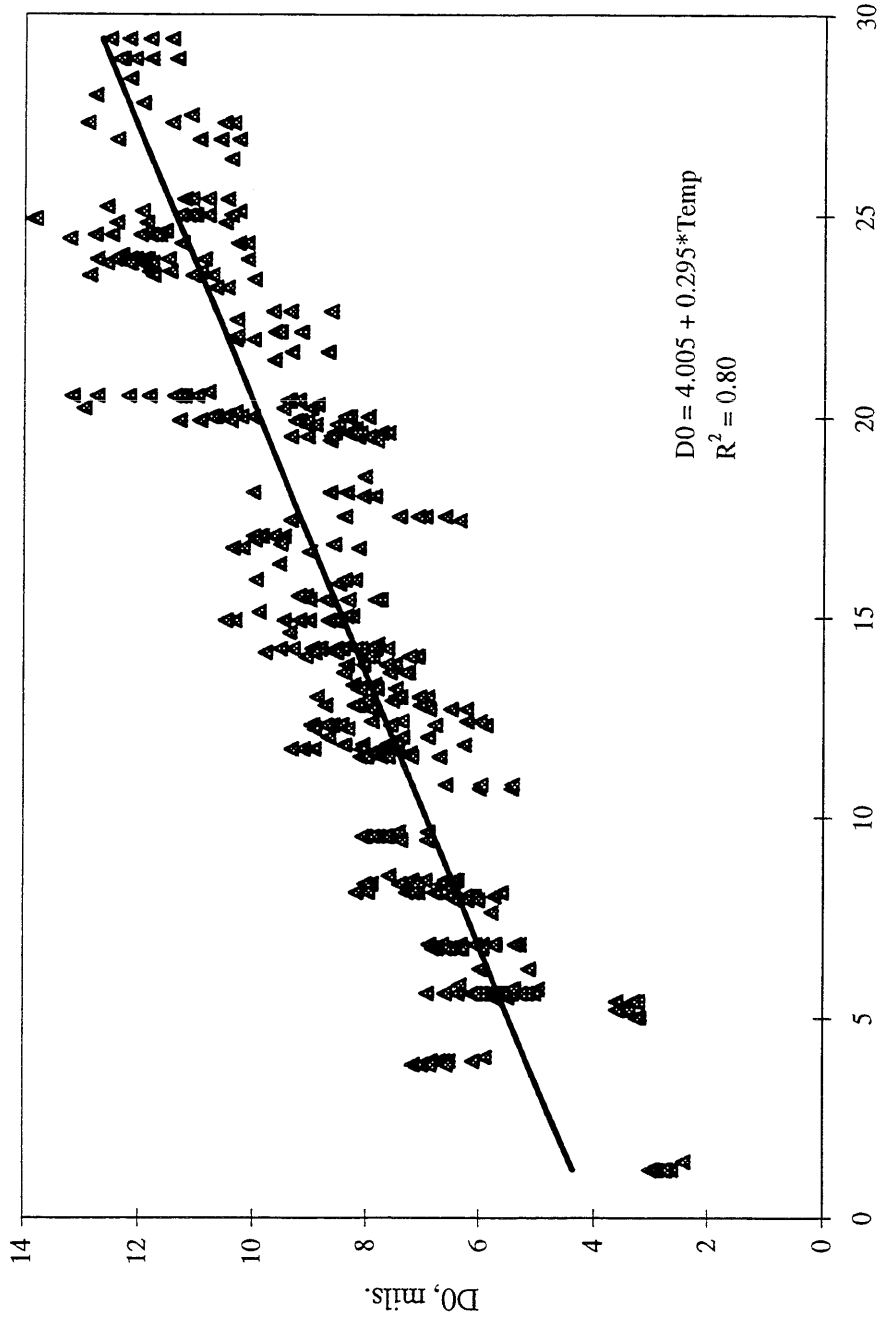

Figure D.10 Variation of D0 with Temperature for Cell 19

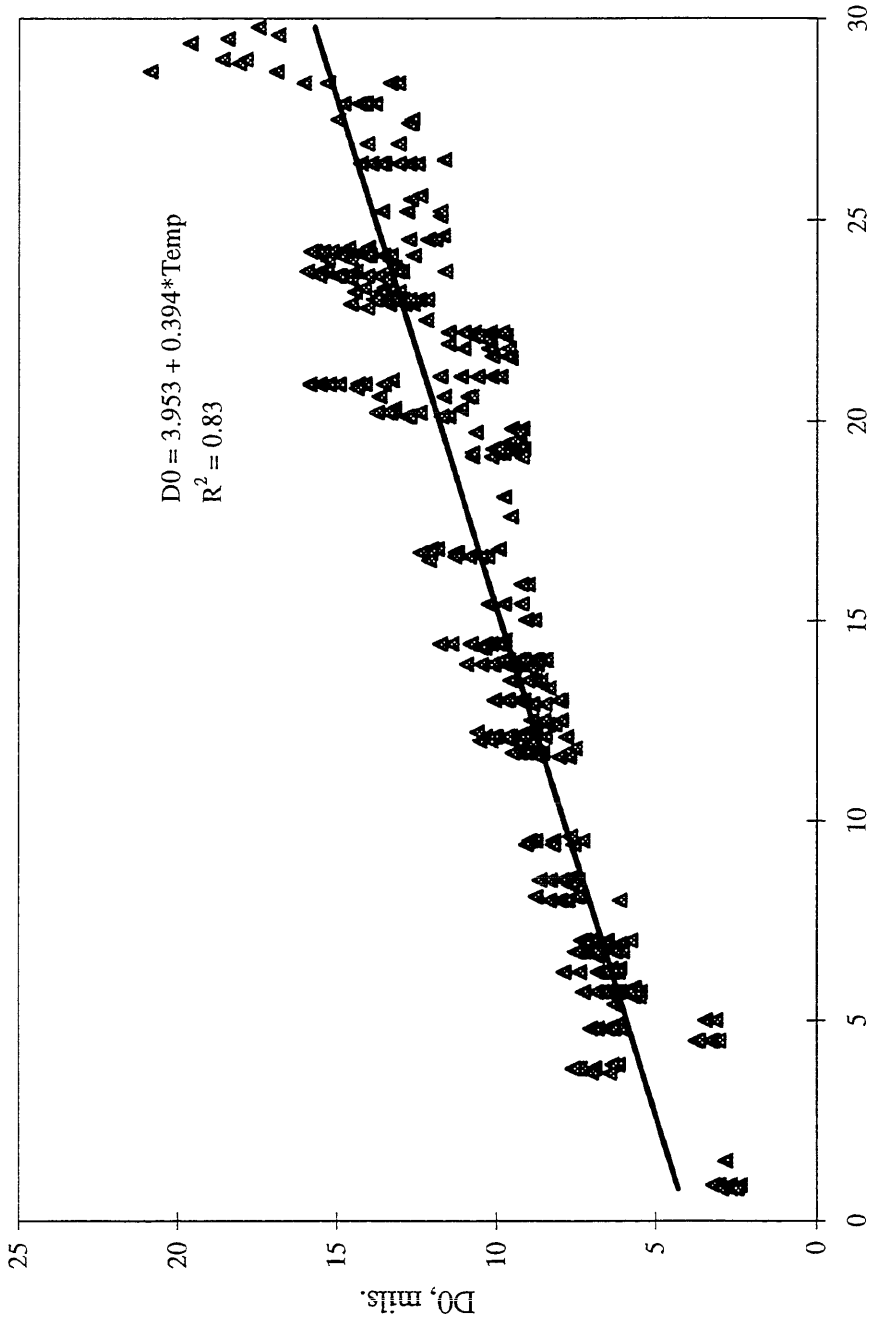

Figure D.11 Variation of D0 with Temperature for Cell 20

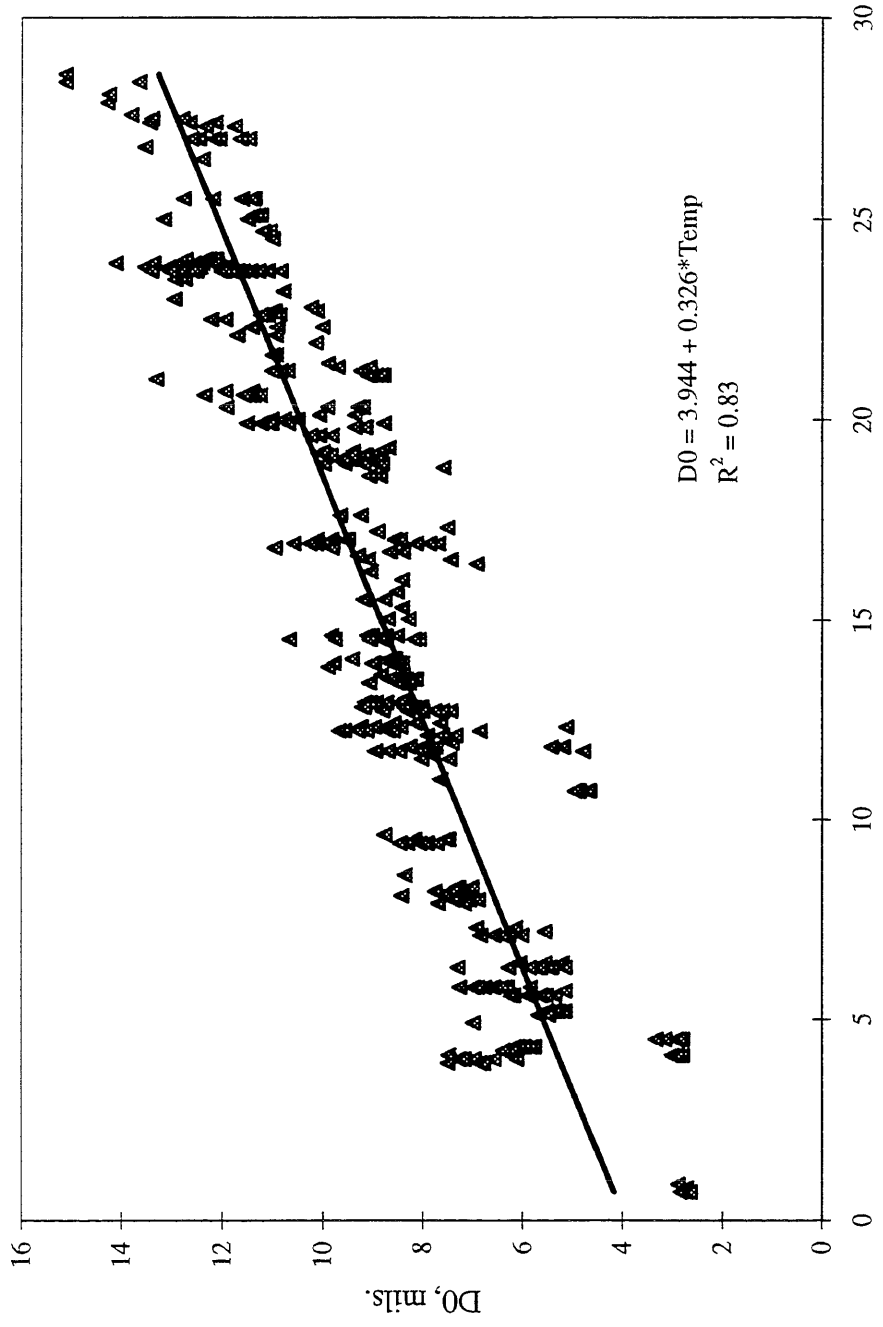

Figure D.12 Variation of D0 with Temperature for Cell 21

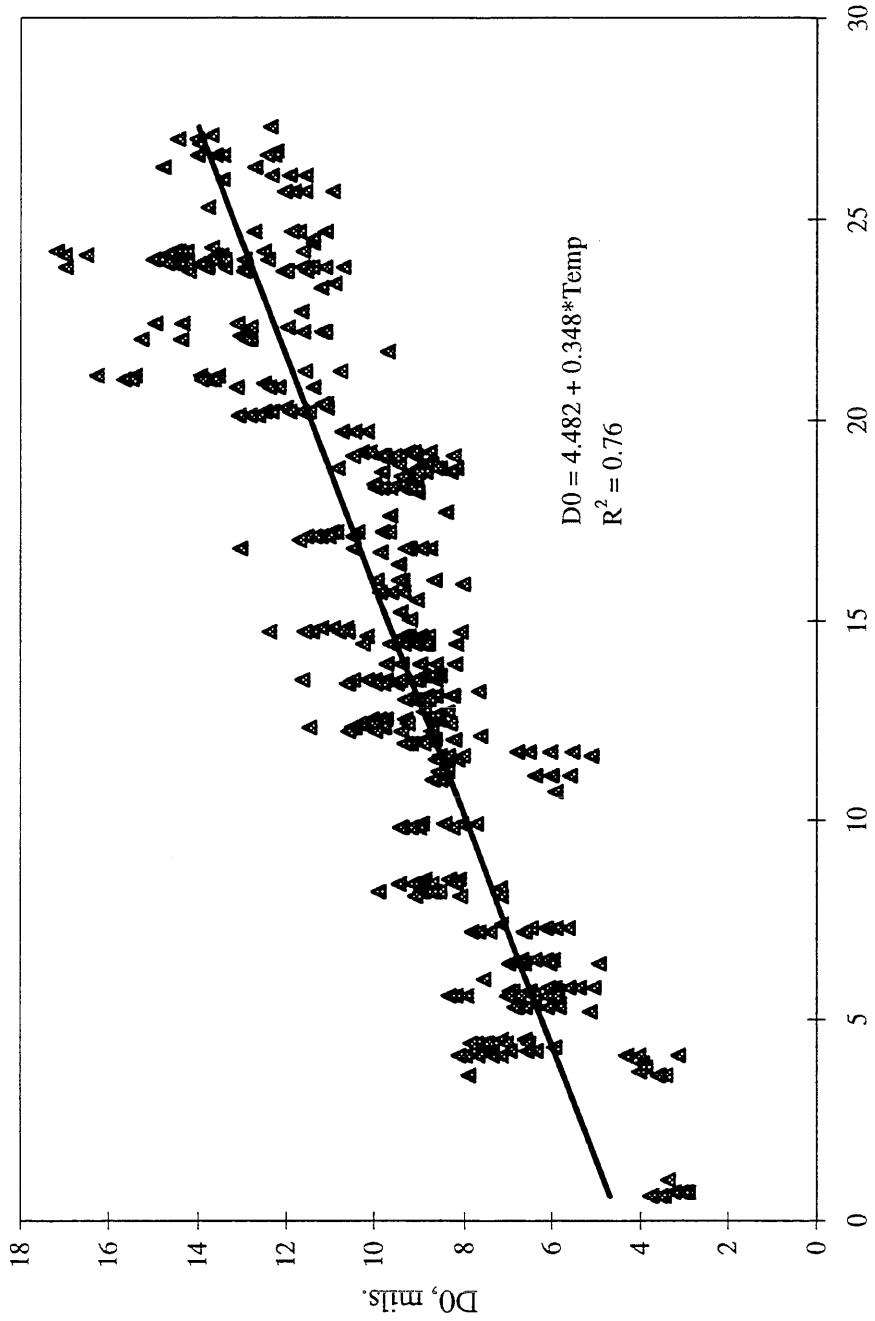

Figure D.13 Variation of D0 with Temperature for Cell 22

Appendix E

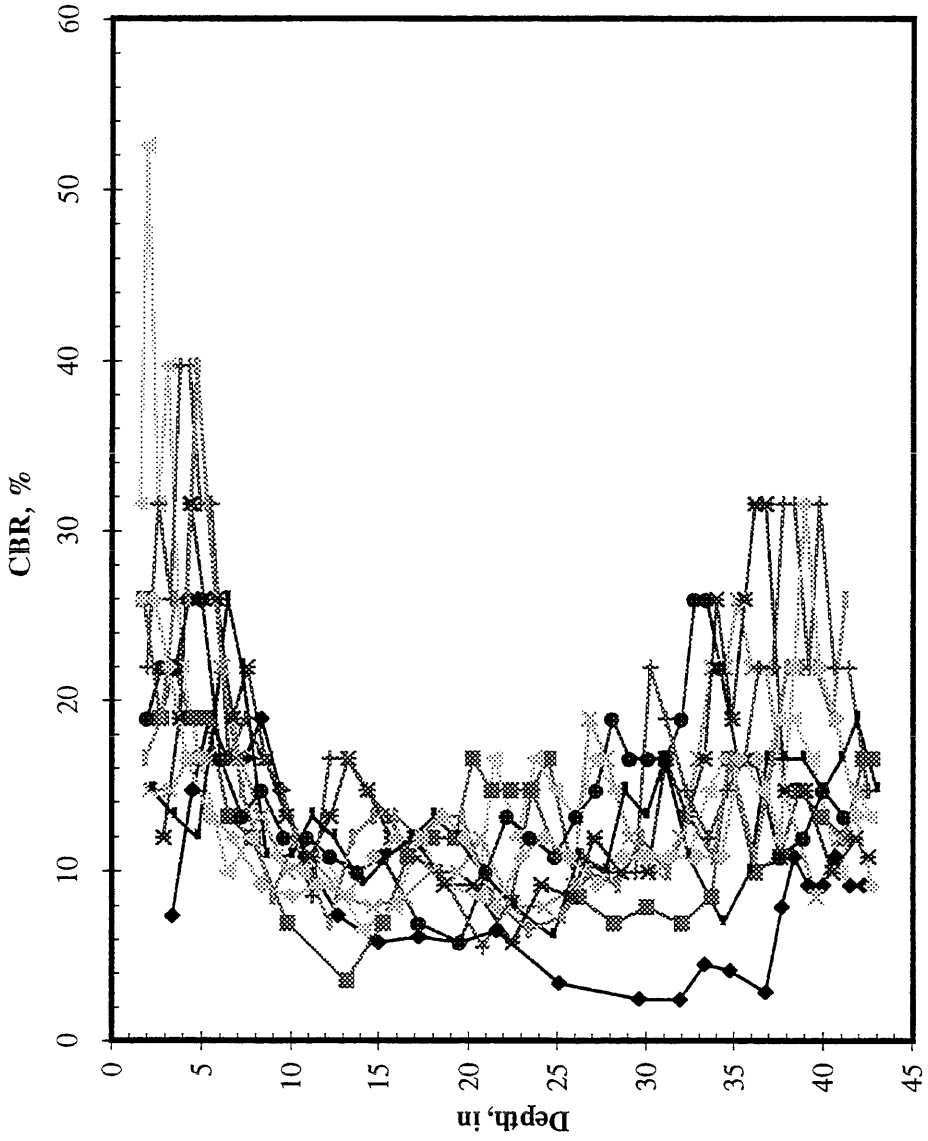

Figure E.1 DCP Results for Cell 4, June 1992.

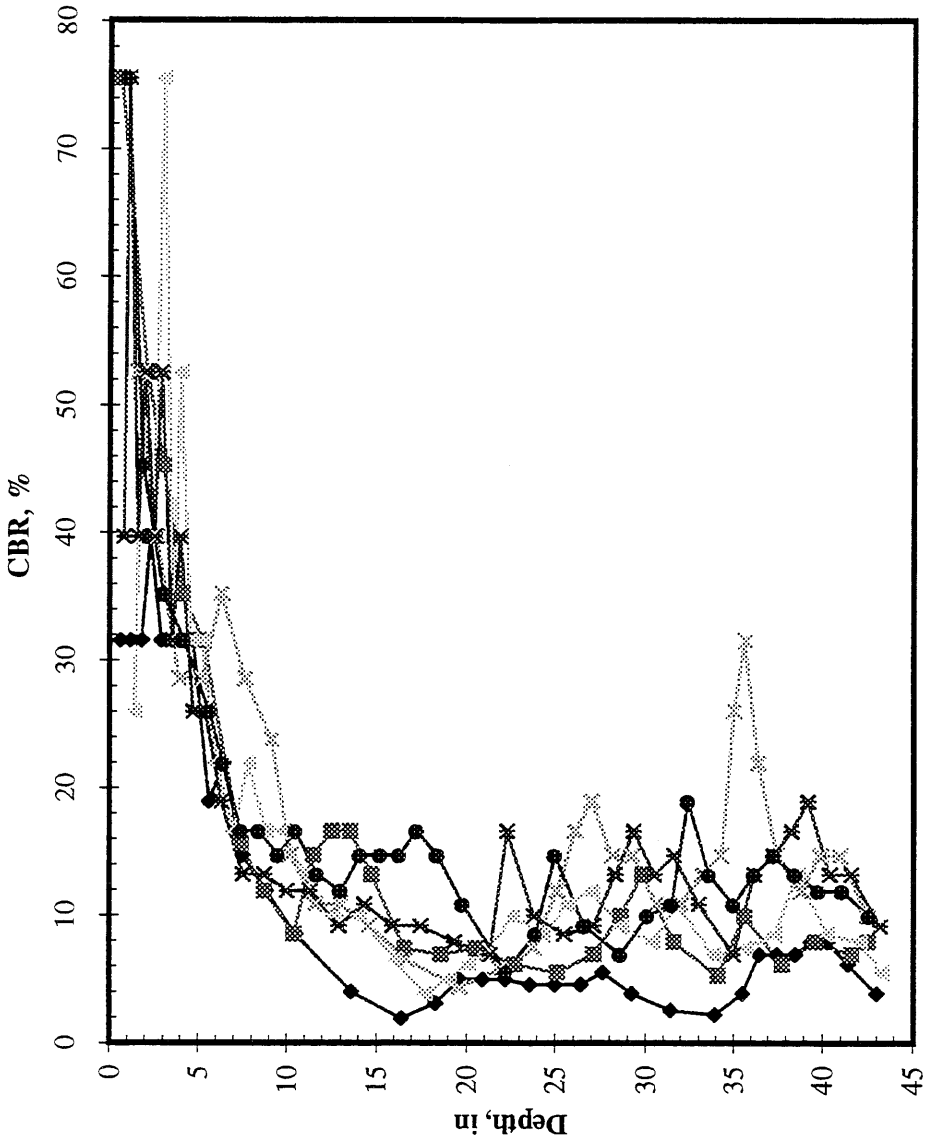

Figure E.2 DCP Results for Cell 4, August 1992.

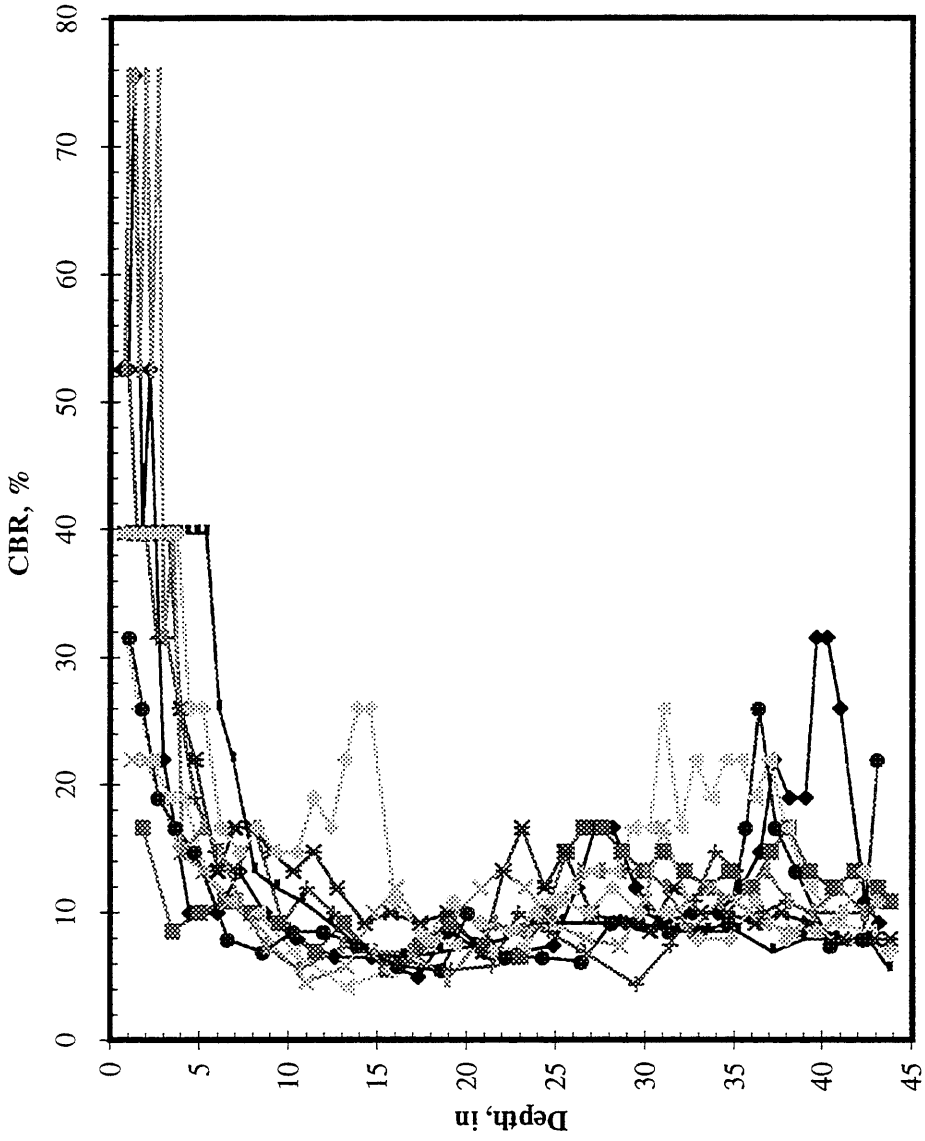

Figure E.3 DCP Results for Cell 14, June 1992.

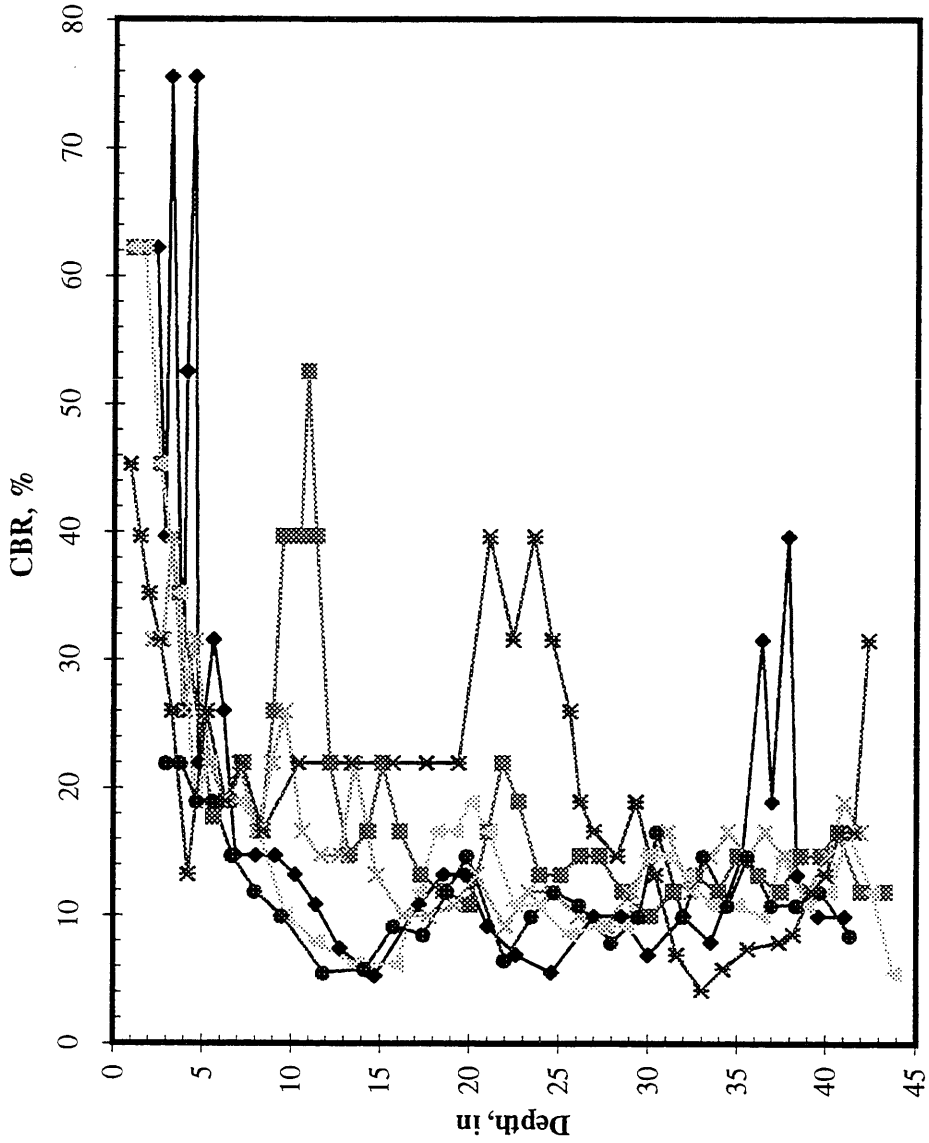

Figure E.4 DCP Results for Cell 14, August 1992.

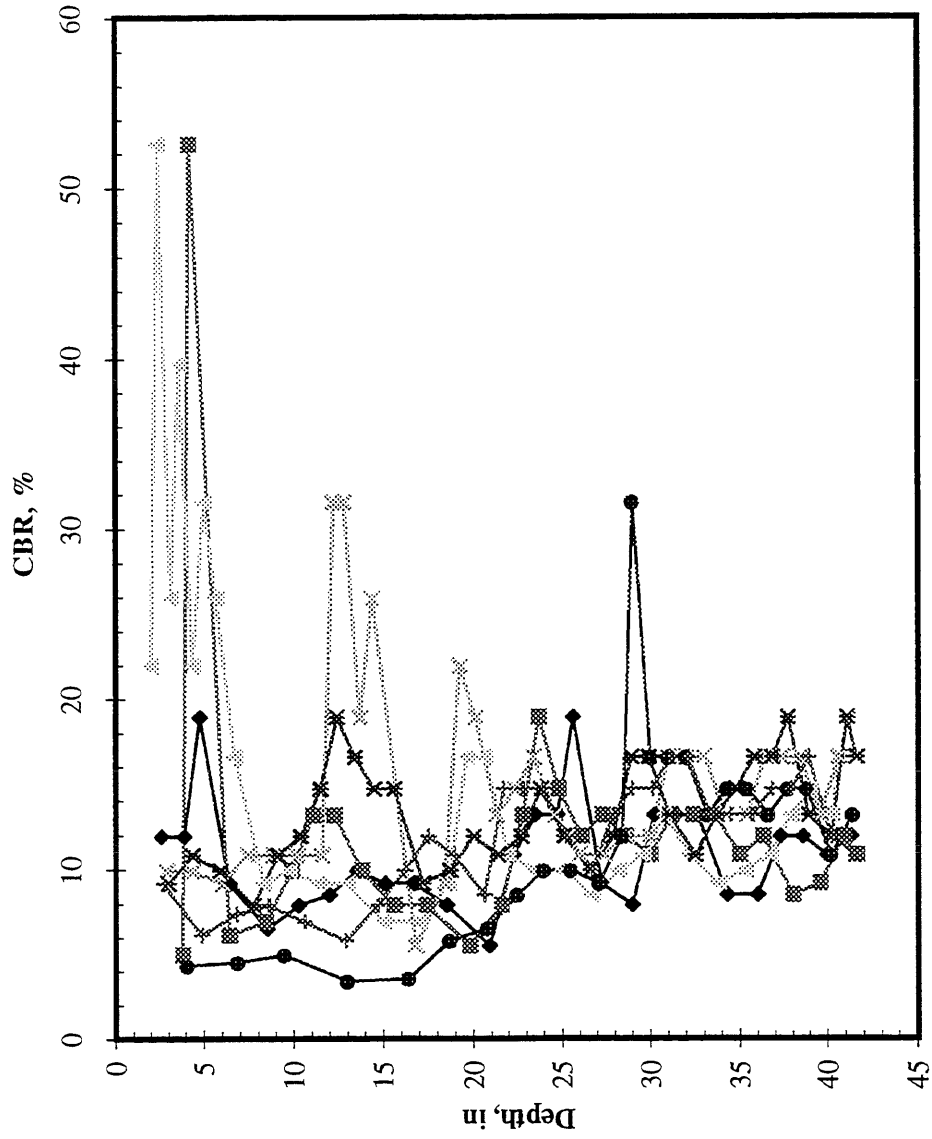

Figure E.5 DCP Results for Cell 14, July 1993.

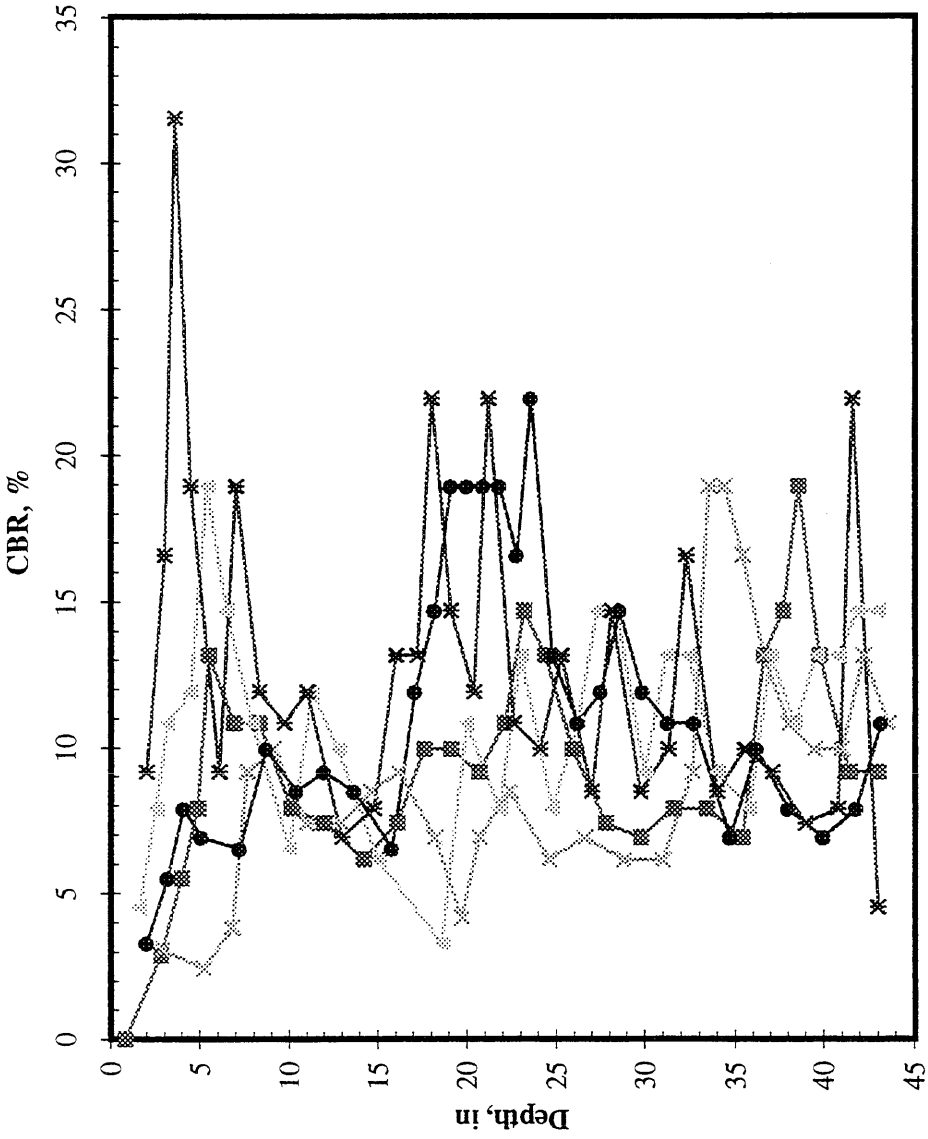

Figure E.6 DCP Results for Cell 15, May 1992

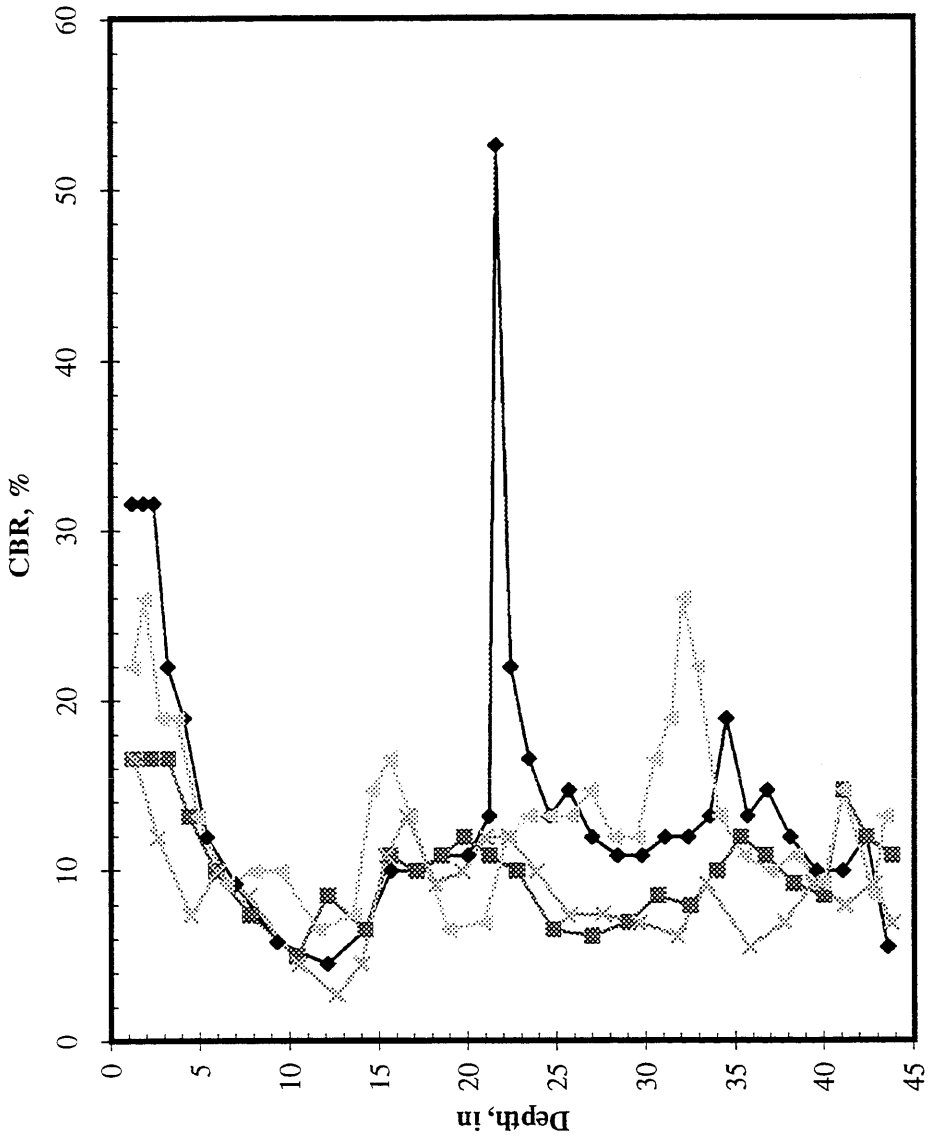

Figure E.7 DCP Results for Cell 15, June 1992

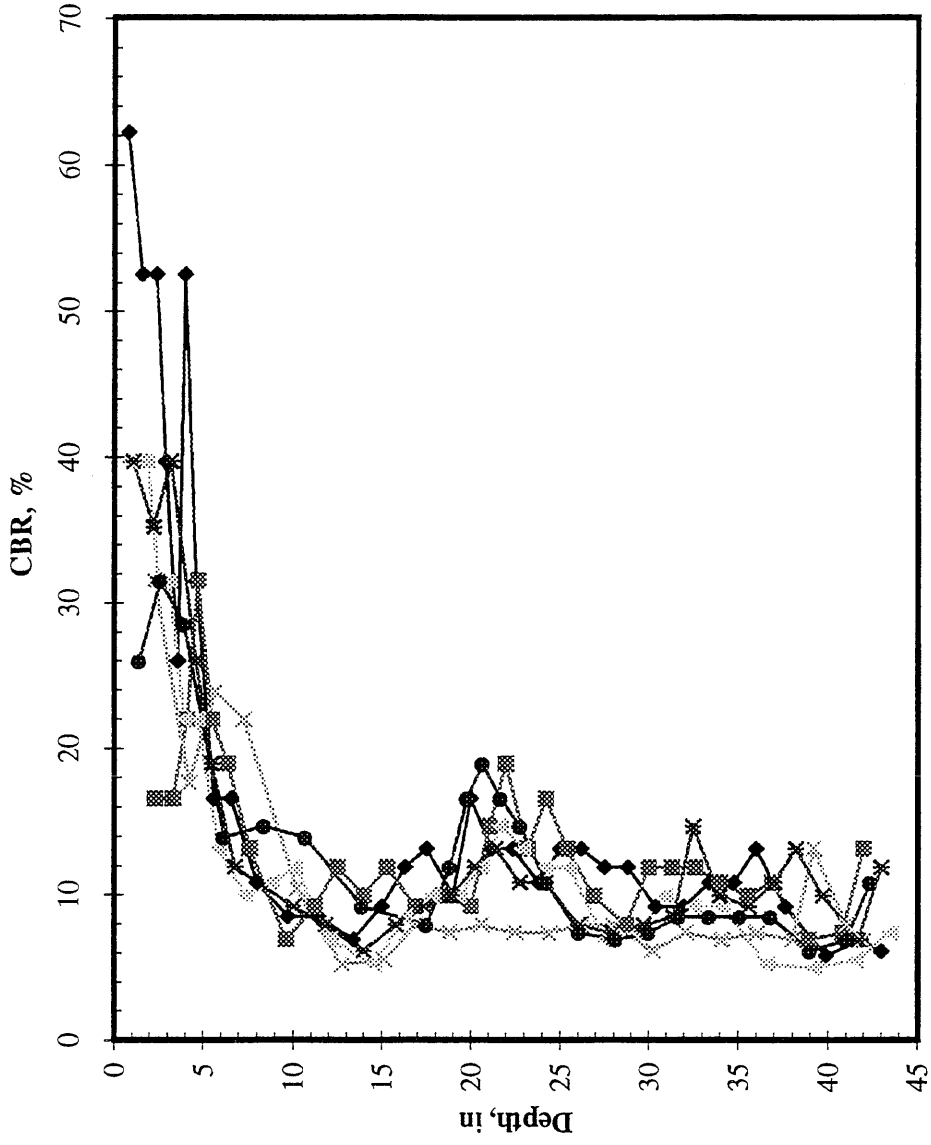

Figure E.8 DCP Results for Cell 15, August 1992

REFERENCES

1. Federal Highway Administration (FHWA), "Transportation Data Sampler 3 CD-ROM" Transportation Research Board, TRB, January, 1996.
2. Thompson, M.R., Elliot, R.P, "ILLI-PAVE-Based Response Algorithms for Design of Conventional Flexible Pavements," In Transportation Research Record 1043, TRB, National Research Council, Washington DC, 1985.
3. Gomez-Achecar, M., Thompson, M.R., "ILLI-PAVE-Based Response Algorithms for Full-Depth Asphalt Concrete Flexible Pavements," In Transportation Research Record 1095, TRB, National Research Council, Washington DC, 1986.
4. Thompson, M.R., "ILLI-PAVE Based NDT Procedures," Nondestructive Testing of Pavement and Backcalculation of Moduli, ASTM STP 1026, A.J. Bush and G.Y. Baladi. E. S., American Society for Testing and Materials, Philadelphia, 1989, pp. 487-501.
5. National Asphalt Pavement Association, " Hot Mix Asphalt Materials, Mixture Design and Construction," Second edition, 1996.
6. "Calibrated Mechanistic Structural Analysis Procedures for Pavements," Phase 1, Volume II-Appendices, National Cooperative Highway Research Program (NCHRP), Project 1-26, Transportation Research Board, December 1990.
7. Van der Poel, C., " A General System Describing the Visco-Elastic Properties of Bitumens and its Relation to Routine Test Data," Journal of Applied Chemistry, London, Vol. 4, 1954.
8. Shahin, M.Y., and McCullough, B.F., "Stiffness History of Asphalt Concrete Surfaces in Roads," Research Record No. 466, Transportation Research Board, 1973.
9. Ullidtz, P., "Pavement Analysis," Developments in Civil Engineering, Vol. 19, Elsevier, 1987.
10. "Shell Pavement Design Manual," Shell International Petroleum Co. Ltd., London, 1978.

11. "Research and Development of The Asphalt Institute's Thickness Design Manual (MS-1) Ninth Edition," Research Report No. 82-2, The Asphalt Institute, August, 1982.

12. Hill, H.J., "Early Life Study of the FA 409 Full-Depth Asphalt Concrete Pavement Sections," Ph.D. thesis directed by M.R. Thompson, Department of Civil Engineering, University of Illinois @ Urbana-Champaign, June 1988.

13. Von Quintus, H. L., et al., "Asphalt-Aggregate Mixture Analysis System: AAMAS," Report 338, National Cooperative Highway Research Program, Transportation Research Board, 1991.

14. Dempsey, B.J., Herlache, W. A., Patel, A. J., "Climatic-Materials-Structural Pavement Analysis Program," In Transportation Research Record 1095, TRB, National Research Council, Washington DC, 1986.

15. Dempsey, B.J., Herlache, W. A., Patel, A. J., "Climatic-Materials-Structural Pavement Analysis Program, Environmental Effects on Pavements-Theory Manual," FHWA/RD-84-115, Vol. 3, FHWA, US Department of Transportation, 1985.

16. Thompson, M.R., and Cation, K., "A Proposed Full-Depth asphalt Concrete Thickness Design and Procedure," Civil engineering Studies, Transportation Engineering Series No. 41, University of Illinois @ Urbana-Champaign, 1984.

17. Elliot, R.P., and Thompson, M.R., "Mechanistic Design Concepts for Conventional Flexible Pavements," Civil Engineering Series No. 42, University of Illinois @ Urbana-Champaign, 1985.

18. Thompson, M.R., and LaGrow, T., "A Proposed Conventional Flexible Pavement Thickness Design Procedure," Civil Engineering Studies, Transportation Engineering Series No. 55, University of Illinois at Urbana-Champaign, 1988.

19. Thompson, M. R., "ILLI-PAVE Based Conventional Flexible Pavement Design Procedure," 7th International Conference on Asphalt Pavements, Nottingham, UK , 1994.

20. Pell, P.S., "Keynote Lecture - Pavement Materials," 6th International Conference on Asphalt Pavements, Ann Arbor, MI, 1987.

21. Finn, F., et al., "Development of Pavement Structural Subsystems," NCHRP Report 291, National Cooperative Highway Research Program, Transportation Research Board, 1986.

22. Pell, P.S., Cooper, K.E., "The Effect of Testing and Mix Variables on the Fatigue Performance of Bituminous Materials," Proceedings, The association of Asphalt Paving Technologists, Vol. 44, 1975.

23. Epps, J., "Influence of Mixture Variables on flexural fatigue and Tensile Properties of asphalt Concrete," Ph.D. Dissertation, University of California, Berkeley, 1968.

24. "ILLI-PAVE Based Full-Depth Flexible Pavement Design Procedure," 6th International Conference on Asphalt Pavements, Ann Arbor, MI, 1987.

25. "Asphalt Pavement design Manual for the U. K.," Mobil Oil Company Ltd., London, 1985.

26. Brunton, J. M., Brown, S.F., and Pell, P. S., "Developments to the Nottingham Analytical Design Method for Asphalt Pavements," 6th International Conference on Asphalt Pavements, Ann Arbor, MI, 1987.

27. Tayebali, A.A., Deacon, J.A., Monismith, C.L., "Development and Evaluation of Surrogate Fatigue Models for SHRP A-003A Abridge Mix Design Procedure," Proceedings, Association of Asphalt Paving Technologists, Vol. 64, 1995.

28. Deacon, J., J. Coplantz, A. Tayebali, and C. Monismith, "Temperature Considerations in Asphalt-Aggregate Mixture Analysis and Design," In Transportation Research Record 1454, TRB, National Research Council, Washington DC, 1994.

29. Harvey, J.T., Deacon, J., Tsai, B., Monismith, C. "Fatigue Performance of Asphalt Concrete Mixes and its Relationship to Asphalt Concrete Pavement Performance in California," Institute of Transportation Studies, University of California, Berkeley, 1995.

30. Harvey, J.T., Deacon, J., Tayebali, A., Leahy, R., Monismith, C. "A Reliability-Cased Mix Design and Analysis System for Mitigating Fatigue Distress," 8th International Conference on Asphalt Pavements, Seattle, WA, 1997.

31. Deacon, J., A. Tayebali , J. Coplantz, F. Finn, and C. Monismith, "Fatigue Response of asphalt-Aggregate Mixes, Part III -Mix Design and Analysis Considerations in Asphalt-Aggregate Mixture Design and Analysis," Strategic Highway Research Program Report No. A-404, National Research Council, Washington DC, 1994.

32. "Standard specifications for Transportation Materials and Methods of sampling and Testing - Part II," AASHTO, 1995.

33. Boateng-Poku, Y., and Drumm, E. C., "Hyperbolic Model for the Resilient Modulus Response of Fine-Grained Soils," Geothecnical Special Publication No. 24, American Society of Civil Engineers, 1989.

34. Thompson, M.R., and Robnett, Q. L., "Resilient Properties of Subgrade Soils," Transportation Engineering Journal, ASCE, Vol. 105, No. TE1, January, 1979.

35. Elliot, R. P., and Thornton, S. I., "Simplification of Subgrade Resilient Modulus Testing," In Transportation Research Record 1192, TRB, National Research Council, Washington DC, 1988.

36. Elliot, R. P. et al., "Resilient Properties of Arkansas Subgrades," Final Report, TRC - 94, Arkansas Highway and Transportation Research Center, Department of Civil Engineering, University of Arkansas, Fayetteville, AR, 1988.

37. Chamberlain, E. J., "A Model for Predicting the Influence of Closed System Freeze-Thaw on Strengths of Thawed Clays," Symposium on Frost Action on Roads, Report Volume III, Organization on Economic Cooperation and Development, Oslo, Norway, 1973.

38. Bergan, A.T., and Monismith, C., "Characterization of Subgrade Soils in Cold Regions for Pavement Design Purposes," Highway Research Record 431, Highway Research Board, 1973.

39. Robnett, Q. L., Thompson, M.R., "Effect of Lime Treatment on the Resilient Behavior of Fine-Grained Soils," Record 560, Transportation Research Board, 1976.

40. TuTumluer, E., "Predicting Behavior of Flexible Pavements with Granular Bases," Ph.D. Thesis, Georgia Institute of Technology, 1995.

41. Monismith, C. L., Ogawa, N., and Freeme, C.R., "Permanent Deformations Characteristics of Subgrade Soils Due to Repeated Loading," In Transportation Research Record 537, TRB, National Research Council, Washington DC, 1975.

42. Knutson, R.M., Thompson, M.R., Mullin, T., Tayabji, S. D., "Materials Evaluation Study - Ballast and Foundation Materials Research Program," FRA - OR&D - 77-02, Federal Railroad Administration, 1977.

43. Knutson, R.M., Thompson, M.R., "Permanent-Deformation Behavior of Railway Ballast," In Transportation Research Record 694, TRB, National Research Council, Washington DC, 1978.

44. Majidzadeh, K., et al., "Implementation of a Pavement Design System," Volumes 1 and 2, Final Report, Research Project EES 579, Ohio State University, 1981.

45. Thompson, M.R., and Nauman, D., "Rutting Rate Analyses of the AASHTO Road Test Flexible Pavements," In Transportation Research Record 1384, TRB, National Research Council, Washington DC, 1993.

46. Theyse, H. L., de Beer, M., Rust, F.C, "Overview of the South African Pavement Design Analysis Method" Paper No. 961294 for Publication In Transportation Research Record, TRB, National Research Council, Washington DC, 1996.

47. StataCorp. 1997. Stata Statistical Software: Release 5.0 College Station, TX, Stata Corporation.

48. Burnham, T. R. and Pirkl, W. M. (1997), "Application of Empirical and Mechanistic-Empirical Pavement Design Procedures to Mn/ROAD Concrete Pavement Test Sections," Report Number 97-14, Minnesota Department of Transportation, Maplewood, MN, 96 pp.

49. Newcomb, D. A., Chadbourn, B. A., and Van Deusen, D., "Relationship Between Statistical Distributions of Traffic Loads and Pavement Responses," Journal of Testing and Evaluation, JTEVA, Vol. 25, No. 2, March 1997, pp. 190-196.

50. Palmquist, D. Research Engineer, Office of Minnesota Road Research. "Memos with the Mn/ROAD Mainline Distress Condition".

51. Paterson, W.D., "Road Deterioration and Maintenance Effects," The World Bank, 1987.

52. Garg, N. "Mechanistic-Empirical Evaluation of Mn/ROAD Mainline Test Sections" Ph.D. Thesis, University of Illinois at Urbana-Champaign, 1997.

53. Rada, G., and Witczak, M. W., "Comprehensive Evaluation of Resilient Moduli Results for Granular Materials," In Transportation Research Record 810, TRB, National Research Council, Washington DC, 1981.

54. Kleyn, E., Maree, j. and Savage, P., " The Application of a portable Pavement Dynamic Cone Penetrometer to Determine In Situ Bearing Properties of Road Pavement Layers and Subgrades in South Africa," Proc. of the Second European Symposium on Penetration Testing, Amsterdam, May, 1982.

55. Burnham, T. R., "Subgrade and Base Material Sampling and Testing Guide -Final Report," Minnesota Department of Transportation, Dec. 1994.

56. Berg, R. L., Bigl, S. R., Stark, J. and Durell, G., "Resilient Modulus Testing of Materials from Mn/ROAD - Phase I," Report No. MN/RC-96/21. Minnesota Department of Transportation, Sept. 1996.

57. Maser, Kenneth, Ground Penetrating Radar Survey for Pavement Thickness Evaluation at Mn/ROAD-Final Report, Mn/ROAD, November, 1994.

58. Stubstad, R.N., Baltzer, S., Lukanen, E.O., and Ertman-Larsen, H.J. "Prediction of AC Mat Temperature for Routine Load/Deflection Measurements" 4th International Conference on Bearing Capacity of Airfields, Minnesota, 1994.

59. Hwang, D., and Witczak, M. W., "Program DAMA (Chevron), User's Manual," Department of Civil Engineering, University of Maryland, 1979.

60. Stroup-Gradiner, M., Newcomb, D. E., "Investigation of Hot Mix Asphalt Mixtures at Mn/ROAD - Final Report," Report No. 97-06, University of Minnesota, Center for Transportation Studies, Feb. 1997.

61. Burnham, T and Johnson, D. "In situ characterization Using the Dynamic Cone Penetrometer," Minnesota Department of Transportation, Physical Research Section. Report No. 93-05, May 1993.

62. Harison, J.A., "Correlation Between California Bearing Ratio and Dynamic Cone Penetrometer Strength Measurement of Soils," Proc. Instn. Civ. Engrs., Part 2, Dec., 1987, pp. 833 - 844.

63. Universal Testing Machines, Feed Back Controlled Beam Fatigue Test, Operating Manual. Stephen King Industrial Process Controls Ltd. Copyright 1993, Revision 6-96. Boronia Vic Australia

64. Carpenter, S. H., Jansen, M., "Fatigue Behavior Under New Aircraft Loading Conditions". Proceedings, 1997 Airfield Pavement Conference in Seattle, WA ASCE, August, 1997.

65. Myre, J. "Fatigue of Asphalt Pavements", Proceedings, Third International Conference on Bearing Capacity of Roads and Airfields, The Norwegian Institute of Technology, Trondheim Norway, 1990.

66. Rauhut, J.B., Lytton, R.L., and Darter, M. I., "Pavement Damage Functions for Cost Allocation -Vol. 2 Description of Detailed Studies" Report FHWA/RD-84/019, Federal Highway Administration, June, 1984.

67. Road Engineering and Geotechnology (VTT) Report. Huhtala, M., Spoof, H., Saarinen, L. and Halonen, P. "Asphalt Mixture Laboratory Tests" Minnesota Road Research Project (Mn/ROAD), 1996.

68. "Calibrated Mechanistic Structural Analysis Procedures for Pavements," Phase 2, Volume II-Appendices, National Cooperative Highway Research Program (NCHRP), Project 1-26, Transportation Research Board, March 1992.

69. Thompson, M.R. "High-Strength Stabilized Base Thickness design Procedure" In Transportation Research Record 1440, TRB, National Research Council, Washington DC.

70. Khedr, S.A., "Deformation Characteristics of Granular Base Course in Flexible Pavement," In Transportation Research Record 1043, TRB, National Research Council, Washington DC, 1985.

71. Maree, J. H., "Design Parameters for Crushed Stone in Pavements" (Afrikaans) M Eng. Thesis, Department of Civil Engineering, Faculty of Engineering, University of Pretoria, South Africa, 1978.

72. Theyse H. L., De Beer, M., Prozzi, J., and Semmelink, C. J., "TRH4 Revision 1995, Phase I: Updating the Transfer Functions for the South African Mechanistic Design Method," National Service Contract NSC24/1, Division for Roads and Transport Technology, CSIR, Pretoria, South Africa, 1995.